frontiers | Research Topics

Pathogenomics of the genus Brucella and beyond, volume II

Edited by
Axel Cloeckaert, Roy Martin Roop II, Holger C. Scholz, Adrian Whatmore and Michel Stanislas Zygmunt

Published in
Frontiers in Microbiology

ISSN 1664-8714
ISBN 978-2-8325-4436-5
DOI 10.3389/978-2-8325-4436-5

About Frontiers

Frontiers is more than just an open access publisher of scholarly articles: it is a pioneering approach to the world of academia, radically improving the way scholarly research is managed. The grand vision of Frontiers is a world where all people have an equal opportunity to seek, share and generate knowledge. Frontiers provides immediate and permanent online open access to all its publications, but this alone is not enough to realize our grand goals.

Frontiers journal series

The Frontiers journal series is a multi-tier and interdisciplinary set of open-access, online journals, promising a paradigm shift from the current review, selection and dissemination processes in academic publishing. All Frontiers journals are driven by researchers for researchers; therefore, they constitute a service to the scholarly community. At the same time, the *Frontiers journal series* operates on a revolutionary invention, the tiered publishing system, initially addressing specific communities of scholars, and gradually climbing up to broader public understanding, thus serving the interests of the lay society, too.

Dedication to quality

Each Frontiers article is a landmark of the highest quality, thanks to genuinely collaborative interactions between authors and review editors, who include some of the world's best academicians. Research must be certified by peers before entering a stream of knowledge that may eventually reach the public - and shape society; therefore, Frontiers only applies the most rigorous and unbiased reviews. Frontiers revolutionizes research publishing by freely delivering the most outstanding research, evaluated with no bias from both the academic and social point of view. By applying the most advanced information technologies, Frontiers is catapulting scholarly publishing into a new generation.

What are Frontiers Research Topics?

Frontiers Research Topics are very popular trademarks of the *Frontiers journals series*: they are collections of at least ten articles, all centered on a particular subject. With their unique mix of varied contributions from Original Research to Review Articles, Frontiers Research Topics unify the most influential researchers, the latest key findings and historical advances in a hot research area.

Find out more on how to host your own Frontiers Research Topic or contribute to one as an author by contacting the Frontiers editorial office: frontiersin.org/about/contact

Pathogenomics of the genus Brucella and beyond, volume II

Topic editors

Axel Cloeckaert — Institut National de recherche pour l'agriculture, l'alimentation et l'environnement (INRAE), France

Roy Martin Roop II — East Carolina University, United States

Holger C. Scholz — Center for Biological Hazards and Special Pathogens, Robert Koch Institute (RKI), Germany

Adrian Whatmore — Animal and Plant Health Agency, United Kingdom

Michel Stanislas Zygmunt — Institut National de recherche pour l'agriculture, l'alimentation et l'environnement (INRAE), France

Citation

Cloeckaert, A., Roop, R. M. II., Scholz, H. C., Whatmore, A., Zygmunt, M. S., eds. (2024). *Pathogenomics of the genus Brucella and beyond, volume II*. Lausanne: Frontiers Media SA. doi: 10.3389/978-2-8325-4436-5

Table of contents

frontiers | Frontiers in Microbiology

TYPE Editorial
PUBLISHED 25 January 2024
DOI 10.3389/fmicb.2024.1370330

OPEN ACCESS

EDITED AND REVIEWED BY
Rustam Aminov,
University of Aberdeen, United Kingdom

*CORRESPONDENCE
Axel Cloeckaert
✉ axel.cloeckaert@inrae.fr

RECEIVED 14 January 2024
ACCEPTED 15 January 2024
PUBLISHED 25 January 2024

CITATION
Cloeckaert A, Roop RM II, Scholz HC, Whatmore AM and Zygmunt MS (2024) Editorial: Pathogenomics of the genus *Brucella* and beyond, volume II. *Front. Microbiol.* 15:1370330. doi: 10.3389/fmicb.2024.1370330

Editorial: Pathogenomics of the genus *Brucella* and beyond, volume II

Axel Cloeckaert[1]*, R. Martin Roop II[2], Holger C. Scholz[3], Adrian M. Whatmore[4] and Michel S. Zygmunt[1]

[1]INRAE, Université de Tours, UMR, ISP, Nouzilly, France, [2]Department of Microbiology and Immunology, Brody School of Medicine, East Carolina University, Greenville, NC, United States, [3]Centre for Biological Threats and Special Pathogens, Highly Pathogenic Microorganisms (ZBS 2), Robert Koch Institute, Berlin, Germany, [4]Department of Bacteriology, Animal and Plant Health Agency, Weybridge, United Kingdom

KEYWORDS

***Brucellaceae*, *Brucella*, *Ochrobactrum*, genetics/genomics, diversity, evolution, cell envelope, virulence**

Editorial on the Research Topic
Pathogenomics of the genus *Brucella* and beyond, volume II

Brucellae are Gram-negative, facultative, intracellular bacteria that can infect humans and many species of animals. Brucellosis is an economically important disease in production animals worldwide causing abortion and infertility. Human brucellosis has usually been associated with an animal reservoir of *Brucella* spp. and transmission occurs mainly via the food chain, in particular through dairy products, or via direct contact with diseased animals. The genus *Brucella* has historically been classified into six species, according to their preferential animal host, of which the most pathogenic for humans are *B. melitensis*, *B. suis*, and *B. abortus*. The genus *Brucella* has been further expanded with a set of new species discovered from the 1990's mainly from wildlife, including marine mammal and amphibian species. Comparative genomics has provided insight into the evolutionary history of species belonging to the genus *Brucella* but has not yet facilitated identification of the underlying mechanisms involved in host preference or diseases caused in their respective hosts.

Following up on the success of the Research Topic *Pathogenomics of the genus Brucella and beyond* we have launched a volume II of the Research Topic. The current Research Topic consisted of 11 Original Research articles and one Opinion article.

Three articles focused on diversity, molecular epidemiology, and evolutionary history of *B. abortus*. The first characterized Ethiopian *B. abortus* isolates from an outbreak in cattle. By comparative genomic analysis with other *B. abortus* sequences available in public databases, Edao et al. reported that the Ethiopian isolates formed a unique cluster within the *B. abortus* phylogeny closely related to a small number of isolates previously described in sub-Saharan Africa, and further analysis suggested a potential evolutionary origin for the *B. abortus* species in East Africa. The second *B. abortus* study by Shevtsov et al. reported the population structure of *B. abortus* in Kazakhstan and its comparison with worldwide genetic diversity of this species. A Bayesian phylodynamic approach suggested that *B. abortus* lineages currently circulating in Kazakhstan were introduced in the nineteenth–twentieth centuries from Europe, mainly from Russia (North Caucasia). The topology of the observed comparative phylogeny of *B. abortus* genome sequences combined with

human history pointed also to East Africa as the current most parsimonious scenario for the origin of *B. abortus*. Finally, Janke et al., in a more comprehensive study, reported the global phylogenomic diversity of *B. abortus*. The authors confirmed 4 major *B. abortus* clades, named A to D. Two of these clades, clade A (median estimate date 972 CE; range 781–1,142 CE) and clade B (median date 150 BCE; range 515 BCE−164 CE), were exceptionally diverse for this species and are exclusively of African origin. The third clade, clade C (median date 949 CE; range 766–1,102 CE), had most isolates coming from a broad swath of the Middle East, Europe, and Asia, also had relatively high diversity. Finally, the fourth and most recent major clade, clade D (median date 1,467 CE; range 1,367–1,553 CE) comprises the large majority of genomes in a dominant but relatively monomorphic group that predominantly infects cattle in Europe and the Americas.

In addition to the above *B. abortus* studies, Xue et al. characterized native circulating *B. melitensis* lineages causing a brucellosis epidemic in Qinghai, China. A global-scale phylogenetic analysis indicated that 54 strains, mostly human, sorted into six subclades, four of which formed independent lineages, suggesting that the increase in the incidence rate of human brucellosis may be caused by local circulating lineages.

The *Brucella* genus also comprises novel species isolated from amphibians. Scholz et al. reported for the first time the isolation of *B. inopinata* from a White's tree frog (*Litoria caerulea*). The species *B. inopinata* was initially reported from a human case and its animal or environmental origin, or any other contaminating source, was not yet identified. Genomic analyses unequivocally classified the exotic frog isolate as belonging to *B. inopinata*. The isolation of *B. inopinata* from a frog, along with other reports of human infection by atypical *Brucella,* raises further the question of whether atypical *Brucella* could pose a risk to human health.

Four articles dealt with pathogenic or immune mechanisms involved in *B. abortus* infection. The first Opinion article by Oliveira and Guimarães raised the question on how the crosstalk between innate immune sensors and metabolic pathways can affect the outcome of *B. abortus* infection. The authors discussed recent developments in the metabolic reprogramming of macrophages and speculate on the prospect of targeting immunometabolism in an effort to develop novel therapeutics to treat *Brucella* and other bacterial infections. A second Original Research article by Muruaga et al. reported the biochemical and functional characterization of *B. abortus* cyclophilins. Cyclophilins of *Brucella* (CypA and CypB) are enzymes encoded by genes that are upregulated within the intraphagosomal replicative niche and required for stress adaptation and host intracellular survival and virulence. In the present study, the authors characterized these cyclophilins from a biochemical standpoint by studying their PPIase activity, chaperone activity, and oligomer formation. In summary, according to the authors *Brucella* cyclophilins come in two different "flavors:" eukaryotic and prokaryotic. CypA and CypB differ in various immunological and biochemical properties, despite their high degree of sequence similarity and conserved functional features. The importance of dimer formation and PPIase activity of CypB for a progressive infection were highlighted in an animal model. These findings shed some light on the potential novel functions of *Brucella* Cyps, some of them could be due to the putative role of CypB as an effector bacterial protein. Regarding innate immunity mechanisms, Santos et al. reported that caspase-8 but not caspase-7 influences inflammasome activation acting in the control of *B. abortus* infection. Programmed cell death (PCD) is an important mechanism of innate immunity against bacterial pathogens. The innate immune PCD pathway involves the molecules caspase-7 and caspase-8, among others. By several *in vivo* experimental approaches, the authors showed the important role of caspase-8 in inflammasome activation and innate immunity against *B. abortus* infection. Finally, regarding *B. abortus* virulence regulation, Castillo-Zeledón et al. showed that the two-component system response regulator BvrR binds to three DNA regulatory boxes in the upstream region of *omp25* encoding a major outer membrane protein. The two-component regulatory system BvrR/BvrS modulates the expression of genes required to transition from extracellular to intracellular lifestyles. Among the genes regulated, *omp25* is positively regulated by this regulatory system. The authors propose that BvrR binds directly to up to three regulatory boxes and probably interacts with other transcription factors to regulate *omp25* expression.

Three articles of the Research Topic focused on means to combat brucellosis, with the development of improved vaccines and of *in vivo* experimental infection models. Mena-Bueno et al. developed and characterized a *wzm*-mutant *B. melitensis* Rev1 vaccine candidate, altered in its cell envelope, and showing improved vaccine properties in a mouse model of infection. The lipopolysaccharide (LPS) O-polysaccharide (O-PS) is a major virulence factor in *Brucella*. After synthesis in the cytoplasmic membrane, O-PS is exported to the periplasm by the Wzm/Wzt system, where it is assembled into a LPS. The *wzm* gene deletion in the Rev1 vaccine strain resulted in lack of external O-PS production as expected, but in addition triggered changes in genetic transcription and in phenotypic properties associated with the outer membrane and cell wall. This highly attenuated mutant strain proved to excel also as an immunogenic and effective vaccine against *B. melitensis* and *B. ovis* in mice, revealing that low persistence is not at odds with efficacy. Overall, these attributes, and the minimal serological interference induced in sheep, make Rev1Δ*wzm* a highly promising vaccine candidate. Nandini et al. performed immuno-profiling of *Brucella* proteins for developing improved vaccines and DIVA (Differentiating Infected from Vaccinated Animals) capable serodiagnostic assays for brucellosis. Several immunodominant proteins were identified in this study by high throughput immunoprofiling of *B. melitensis* protein microarray using brucellosis-positive human and animal serum samples. Among the seroreactive proteins, the Dps protein, strongly reacted with brucellosis-positive serum samples, but it did not react with sera from *B. abortus* S19-vaccinated cattle, indicating DIVA capability. A prototype lateral flow assay and indirect ELISA based on Dps protein exhibited high sensitivity, specificity, and DIVA capability. Finally, Hensel et al. assessed the guinea pig model of infection in comparison to the mouse model of infection, together with intratracheal inoculation, as a model for male reproductive brucellosis. Strains tested were the *B. melitensis* 16M virulent strain and the derived vaccine candidate 16 MΔ*vjbR*. Due to the ability to evaluate for both colonization and inflammation, the authors concluded that guinea pigs seemed the better model relative to the mouse model, not only for assessing host-pathogen interactions but also for future vaccine development efforts.

In summary, the current volume II Research Topic on *Brucella* pathogenomics, contributed to increase our knowledge in (i) the global spread and evolutionary history of pathogenic *Brucella* species, (ii) the pathogenic or immune mechanisms involved in *B. abortus* infection, and (iii) novel approaches and vaccine candidates to combat brucellosis.

Author contributions

AC: Writing – original draft, Writing – review & editing. RR: Writing – original draft, Writing – review & editing. HS: Writing – original draft, Writing – review & editing. AW: Writing – original draft, Writing – review & editing. MZ: Writing – original draft, Writing – review & editing.

Funding

The author(s) declare that no financial support was received for the research, authorship, and/or publication of this article.

Conflict of interest

The authors declare that the research was conducted in the absence of any commercial or financial relationships that could be construed as a potential conflict of interest.

The author(s) declared that they were an editorial board member of Frontiers, at the time of submission. This had no impact on the peer review process and the final decision.

Publisher's note

frontiers | Frontiers in Microbiology

ORIGINAL RESEARCH
published: 04 July 2022
doi: 10.3389/fmicb.2022.908495

Brucella melitensis Wzm/Wzt System: Changes in the Bacterial Envelope Lead to Improved Rev1Δ*wzm* Vaccine Properties

*Sara Mena-Bueno[1,2], Irati Poveda-Urkixo[1], Oihane Irazoki[3], Leyre Palacios[1], Felipe Cava[3], Ana Zabalza-Baranguá[1] and María Jesús Grilló[1]**

[1] Animal Health Department, Instituto de Agrobiotecnología (IdAB, CSIC-Gobierno de Navarra), Pamplona, Spain, [2] Agronomy, Biotecnology and Food Department, Universidad Pública de Navarra (UPNA), Pamplona, Spain, [3] Laboratory for Molecular Infection Medicine Sweden, Department of Molecular Biology, Umeå Centre for Microbial Research, Umeå University, Umeå, Sweden

The lipopolysaccharide (LPS) O-polysaccharide (O-PS) is the main virulence factor in *Brucella*. After synthesis in the cytoplasmic membrane, O-PS is exported to the periplasm by the Wzm/Wzt system, where it is assembled into a LPS. This translocation also engages a bactoprenol carrier required for further biosynthesis pathways, such as cell wall biogenesis. Targeting O-PS export by blockage holds great potential for vaccine development, but little is known about the biological implications of each Wzm/Wzt moiety. To improve this knowledge and to elucidate its potential application as a vaccine, we constructed and studied *wzm/wzt* single- and double-deletion mutants, using the attenuated strain *Brucella melitensis* Rev1 as the parental strain. This allowed us to describe the composition of *Brucella* peptidoglycan for the first time. We observed that these mutants lack external O-PS yet trigger changes in genetic transcription and in phenotypic properties associated with the outer membrane and cell wall. The three mutants are highly attenuated; unexpectedly, Rev1Δ*wzm* also excels as an immunogenic and effective vaccine against *B. melitensis* and *Brucella ovis* in mice, revealing that low persistence is not at odds with efficacy. Rev1Δ*wzm* is attenuated in BeWo trophoblasts, does not infect mouse placentas, and is safe in pregnant ewes. Overall, these attributes and the minimal serological interference induced in sheep make Rev1Δ*wzm* a highly promising vaccine candidate.

Keywords: lipopolysaccharide, Wzm/Wzt system, Rev1Δ*wzm* vaccine, *Brucella* envelope, pregnant sheep, pregnant mice

OPEN ACCESS

Edited by:
Roy Martin Roop II, East Carolina University, United States

Reviewed by:
Jerod Skyberg, University of Missouri, United States
David O'Callaghan, Université de Montpellier, France

***Correspondence:**
María Jesús Grilló
mj.grillo@csic.es

Specialty section:
This article was submitted to Infectious Agents and Disease, a section of the journal Frontiers in Microbiology

Received: *30 March 2022*
Accepted: *26 May 2022*
Published: *04 July 2022*

Citation:
Mena-Bueno S, Poveda-Urkixo I, Irazoki O, Palacios L, Cava F, Zabalza-Baranguá A and Grilló MJ (2022) Brucella melitensis Wzm/Wzt System: Changes in the Bacterial Envelope Lead to Improved Rev1Δwzm Vaccine Properties. Front. Microbiol. 13:908495. doi: 10.3389/fmicb.2022.908495

INTRODUCTION

Brucellosis is one of the most relevant zoonosis worldwide and is caused by bacteria of the genus *Brucella*. These pathogens infect a wide range of domestic and wild animals. *Brucella melitensis* infects predominantly small ruminants and is also the most frequent *Brucella* species in humans in endemic regions. To date, there are no safe vaccines for humans, and antibiotic treatments are onerous with frequent relapses so that the most rational strategy is to control and eradicate animal infections (Blasco, 1997). In small ruminants, Rev1 is the only vaccine recommended (OIE, 2018). However, although

attenuated, Rev1 can be pathogenic for animals (for instance, it induces abortions in pregnant ewes; Blasco, 1997) and can infect humans (Spink et al., 1962; Blasco and Díaz, 1993). Thus, finding a safer alternative vaccine is a priority worldwide.[1] To this end, much research effort has focused on lipopolysaccharide (LPS) modifications and, more specifically, on removing the *N*-formyl-perosamine homopolymer O-polysaccharide (O-PS) (Zhao et al., 2018). Besides being a main virulence factor, O-PS is the immunodominant antigen in *Brucella* (Spink and Anderson, 1954), which is necessary to elicit a protective adaptive immune-response (Montaraz et al., 1986; Grilló et al., 2006b).

Pathways involved in O-PS biosynthesis have been explored as potential targets for vaccine developments (Whitfield, 1995; Schurig et al., 2002; Moriyón et al., 2004; González et al., 2008). In *Brucella*, this molecule is formed in the inner side of the cytoplasmic membrane. It is then translocated to the periplasm by an ATP-binding cassette (ABC) transport system that comprises two essential proteins, Wzt and Wzm, whereby the hydrophilic ATP-binding Wzt is coupled by a unique interface (Bi et al., 2018) to the transmembrane ring-shaped Wzm (Cuthbertson et al., 2007; Mohammad et al., 2016; Caffalette and Zimmer, 2021). This system is broadly conserved among gram-negative bacteria (Whitfield, 1995; Lerouge et al., 2001; Hug and Feldman, 2011; Caffalette et al., 2020), whereby Wzm is strongly conserved, while Wzt has a C-terminal domain (C-Wzt), with a unique structural element that determines the specificity of the O-PS transporter (Izquierdo et al., 2003; Cuthbertson et al., 2005, 2007). Truncation of *wzm/wzt* genes leads to rough (R) mutants carrying O-PS molecules unlinked to the R-LPS rather than smooth (S)-LPS; however, little is known about the effect of each component on *Brucella*. O-PS export further involves the undecaprenol pyro-phosphate (also known as bactoprenol), which is a universal lipid carrier to which sugar precursors attach to initiate O-PS synthesis and export the whole complex to the periplasm (Valvano, 2003). Once O-PS is linked to the LPS, the bactoprenol needs to be released back to the inner membrane, where it can participate other polymerization pathways, such as peptidoglycan (PG) recycling (Valvano, 2015; Vassen, 2018). Thus, we hypothesized that *wzm*/*wzt* truncation and blockage of the O-PS export could alter other bacterial structures and/or functions.

Most *B. melitensis* R mutants were developed from the 16M or H38 virulent strain (Godfroid et al., 2000; González et al., 2008; Wang Z. et al., 2014). However, the background of the parental strain can be crucial for the biological properties of the R derivatives (Barrio et al., 2009). In this work, we built the *wzm*/*wzt* single- and double-mutants from a *B. melitensis* Rev1 attenuated strain, with the objective of understanding how to increase the structural and functional impact derived from disrupting the O-PS export. For this, we analyzed transcriptional changes and features associated with envelope remodeling of Rev1 Wzm/Wzt mutants vs. 16MΔ*wzm* (Zabalza Baranguá, 2017), using state-of-the-art techniques, including transmission electron microscopy (TEM) and ultra-performance liquid chromatography-mass spectrometry (UPLC-MS), as well as *in vivo* experiments in laboratory animals (mice) and in the natural host most susceptible to *B. melitensis* infection (pregnant ewes).

[1]https://brucellosisvaccine.org

RESULTS AND DISCUSSION

Deletion of *wzm* and/or *wzt* Induces *wbkB* and *wbkC* Transcriptional Upregulation, but Only Rev1Δ*wzm* Induces a Marked *wzt* Upregulation

After assessing the expected genotypes by sequencing for the Rev1Δ*wzm*, Rev1Δ*wzt*, and Rev1Δ*wzm*Δ*wzt* mutants (**Figure 1A**; **Supplementary Figures 1, 2**, **Supplementary Table 3**), we studied variations by qRT-PCR (**Supplementary Table 4**) for the relative expression of the genes *wzm*/*wzt*, *wbk*, and *wbo* O-PS biosynthesis clusters (Godfroid et al., 2000; González et al., 2008), as well as for *cgs* and *cgt*, which code for the synthesis and export to the periplasm of cyclic glucans. Of note, these sugars, together with the LPS, are envelope components involved in *Brucella* virulence (Haag et al., 2010; Guidolin et al., 2015). No transcription of *wzm* and/or*wzt* was detectable in the corresponding single- or double-deletion mutants (**Figure 1B**). As both genes are sequentially located in the chromosome (Godfroid et al., 2000), it is generally assumed that *wzm*/*wzt* mutations should cause an analogous effect and that the deletion of *wzm* would hinder *wzt* expression. Strikingly, however, Rev1Δ*wzm* showed significant ($p < 0.001$) overexpression of *wzt*, but Rev1Δ*wzt* showed unchanged expression of *wzm* (e.g., similar to the parental). In agreement with this, the *in silico* study revealed that the start codon of *wzt* overlaps the stop codon by one nucleotide. This overlap suggests the existence of a multiple reading frame, a feature conserved across microbial genomes and a common regulation mechanism (Johnson and Chisholm, 2004). Additionally, it has been proposed that these two genes could constitute a sole operon for other gram-negative bacteria (Rocchetta and Lam, 1997; Goldberg, 1999). Thus, it seems reasonable that a deletion upstream of *wzm* not only maintains but also alters the expression of *wzt*. In sum, we demonstrate that *wzm* deletion allows the transcription of *wzt* and causes its overexpression in Rev1Δ*wzm*.

Additionally, the three Rev1 *wzm*/*wzt* mutants showed enhanced expression ($p < 0.05$) of *wbkB* and *wbkC* with respect to Rev1 (note that *wbkB* encodes an enzyme of unconfirmed function, and, *wbkC*, a formyltransferase; Godfroid et al., 2000). This finding opens the possibility of antigenic changes in the nascent O-PS, although shortening would not be expected, as no signs of repressed expression were detected. Comparatively, 16M*wzm* showed not only overexpression of these three genes (e.g., *wbkB, wbkC, and wzt*) but also upregulation of *gmd* vs. the 16M parental strain, and this was not reproduced in Rev1*wzm*. With respect to the parental strains, Rev1 showed significant upregulation of *gmd* and downregulation of *wbkA*, *wbkD*, *wbkE*, *wbkF*, *cgs*, and *cgt* genes. Of note, *cgs* and *cgt* encode for cyclic glucans, which are involved in evading host immune response (Briones et al., 2001; Arellano-Reynoso et al., 2005;

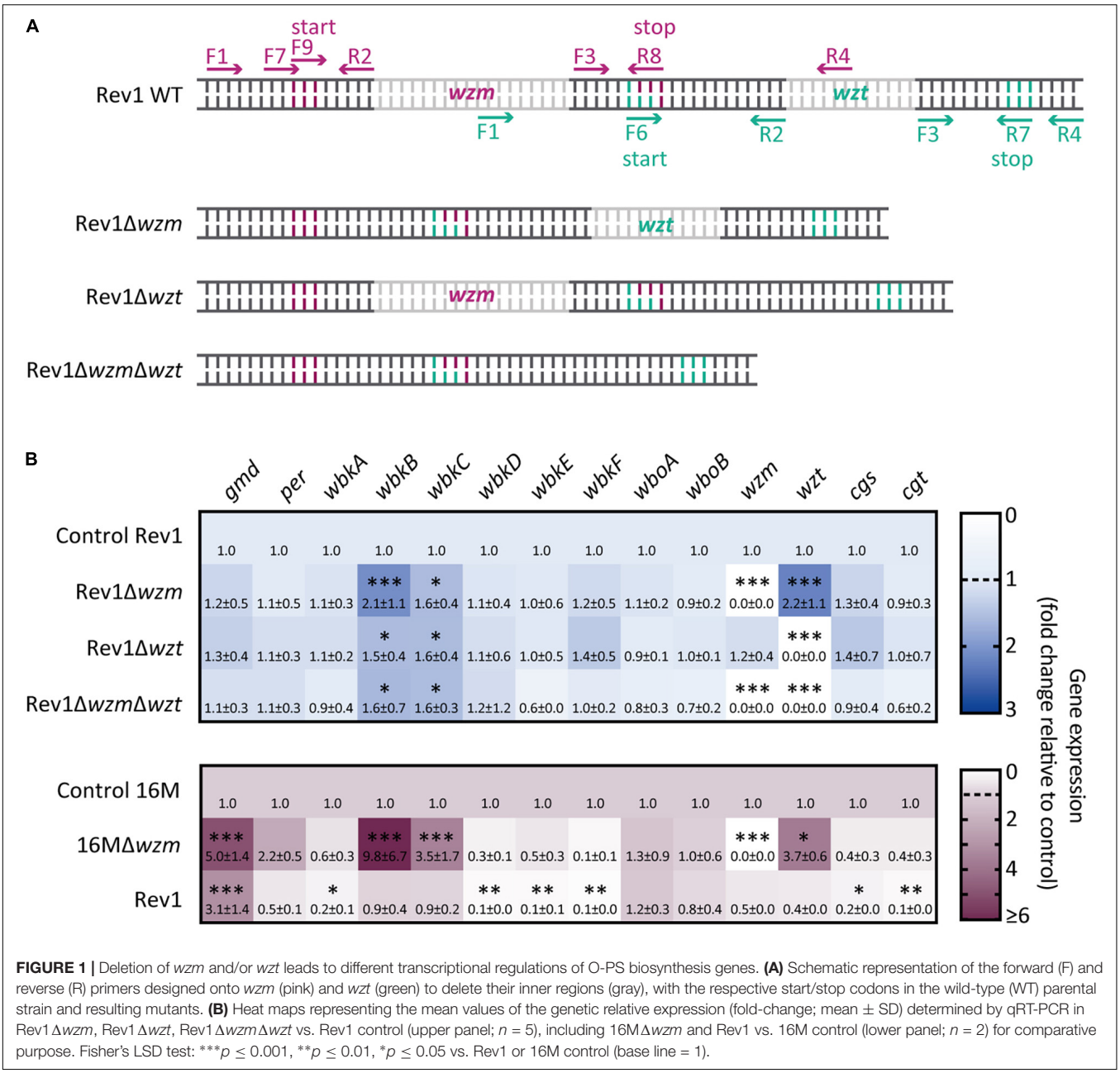

FIGURE 1 | Deletion of *wzm* and/or *wzt* leads to different transcriptional regulations of O-PS biosynthesis genes. **(A)** Schematic representation of the forward (F) and reverse (R) primers designed onto *wzm* (pink) and *wzt* (green) to delete their inner regions (gray), with the respective start/stop codons in the wild-type (WT) parental strain and resulting mutants. **(B)** Heat maps representing the mean values of the genetic relative expression (fold-change; mean ± SD) determined by qRT-PCR in Rev1 Δ*wzm*, Rev1 Δ*wzt*, Rev1 Δ*wzm* Δ*wzt* vs. Rev1 control (upper panel; $n = 5$), including 16M Δ*wzm* and Rev1 vs. 16M control (lower panel; $n = 2$) for comparative purpose. Fisher's LSD test: ***$p \leq 0.001$, **$p \leq 0.01$, *$p \leq 0.05$ vs. Rev1 or 16M control (base line = 1).

Haag et al., 2010; Roset et al., 2014), osmotic resistance (Roset et al., 2014), and oxidative and detergent pressure resistance (Mirabella et al., 2013). Thus, this result is consistent with the attenuation of Rev1.

The Cytoplasmic O-Polysaccharide of Rev1 *wzm/wzt* Mutants Shows Antigenic Features

In standard tests for *Brucella* typing (Alton et al., 1988), the three mutants showed the expected R-LPS phenotype, the typical small colonial size of Rev1 (Grilló et al., 2000) and Rev1 inhibition by penicillin G (P_5) and safranin O (Saf_{100}) (**Supplementary Table 5**). The complete core and the presence of O-PS in *wzm/wzt* mutants were evidenced by alkaline silver staining and Western blot with anti-M monospecific serum, respectively, in whole-cell inactivated bacteria (**Figure 2A**). We confirmed that the O-PS was not exposed at the mutant outer membrane (OM), since it was not detected using purified LPS samples (**Figure 2B**), as reported for other gram-negative bacteria (Guo et al., 2017; Moosavian et al., 2020). Using an anti-M monospecific serum for Western blotting (**Figure 2A**) revealed a faint, smeared band at 35–48 kDa in Rev1 mutants that were absent in BmH38R$manB_{core}$ (control) and were very strong (25–75 kDa) in Rev1 and complemented strains. Further analysis with anti-C/Y 33H8 and 42D2mAbs showed O-PS in

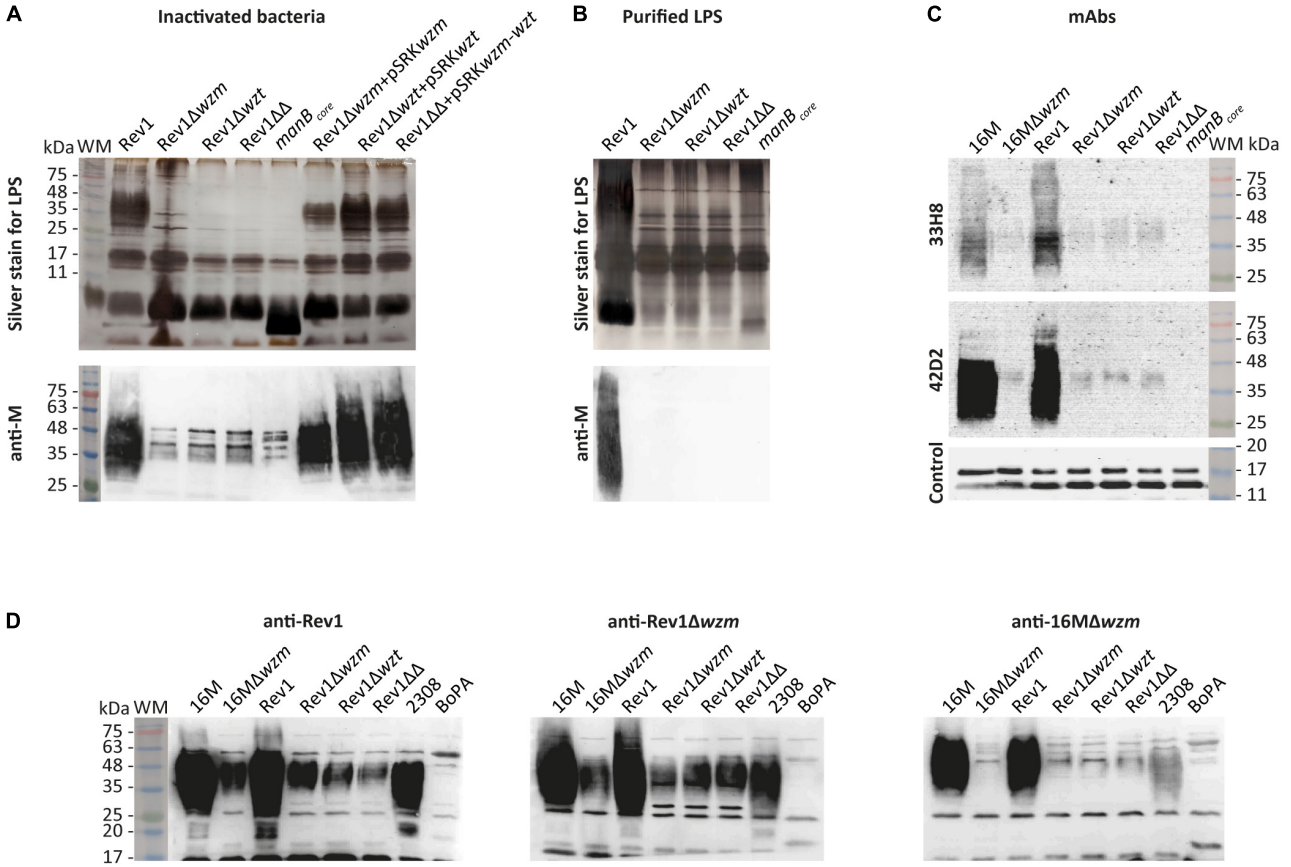

FIGURE 2 | Rev1 *wzm/wzt* mutants express R-LPS with a complete core and a cytoplasmic O-PS reacting with mAbs. **(A)** Whole-cell phenol-inactivated bacteria or **(B)** purified LPS profiles detected by modified periodate-alkaline silver staining (upper panels) or by WB with anti-M monospecific serum (lower panels). **(C)** O-PS epitopes of whole bacteria recognized by the mAbs 33H8 for 20 min of exposure (the upper panel) or 42D2 for 6 min (the middle panel); anti-*B. ovis* serum was run as loading control on the same 42D2 blot (the lower panel). **(D)** Western blot with anti-Rev1, anti-Rev1Δ*wzm*, or anti-16MΔ*wzm* immune sheep sera. The images presented in the same groups were processed in parallel, and the results are representative of reproducible experiments. WM, pre-stained weight Marker VI (PanReac AppliChem, Castellar del Vallés, Barcelona, Spain).

wzm/*wzt* mutants but at lower reactivity than in Rev1 and 16M (**Figure 2C**). As O-PS biosynthesis was not downregulated, differences in reactivity could be due to low amounts of O-PS in the mutants. This hypothesis is compatible with a capture of bactoprenol by the nascent non-translocated O-PS (Rocchetta and Lam, 1997), making it unavailable for further biosynthesis. Both *B. melitensis* S-LPS strains were less reactive with 33H8 than with 42D2 (which is evident even after extended exposure time), and Rev1 systematically exhibited stronger signals with 33H8 than with 16M (**Figure 2C**), evidencing different O-PS epitope compositions.

Rev1 mutants reacted strongly with sera from sheep infected with Rev1Δ*wzm*, showing a ≈35–48 kDa O-PS-smeared band as well as a distinct band at ≈29 kDa, which was also detected (faintly) by anti-Rev1 but not by anti-16MΔ*wzm* sheep sera (**Figure 2D**). This 29 kDa band was absent in 16M parental and mutant strains but observed in Rev1 by a Western blot with heat-treated anti-Rev1Δ*wzm* serum (data not shown). This result suggests the presence of an Omp that is unlinked in Rev1 and covalently bound to PG in 16M, as reported for *Brucella abortus* Omp2b and Omp25 (Godessart et al., 2021).

Rev1 *wzm/wzt* Mutants Exhibit High Sensitivity to Antibiotics and Cationic Dyes

The presence of 10% CO_2 inhibited the growth of 16MΔ*wzm*, as previously reported (Zabalza Baranguá, 2017), but not the growth of the Rev1 mutants. Also, the Rev1 mutants were more susceptible than Rev1 to streptomycin ($Str_{2.5}$), polymyxin B ($PxB_{1.5}$), and colistin (Col_4), with no differences between mutants (**Supplementary Table 6**). Regarding the susceptibility to the antibiotics of choice for treating human brucellosis (Ariza et al., 1986), the three mutants were more susceptible than Rev1 to streptomycin and rifampicin in MIC and MBC_{90}; furthermore, a synergistic effect with doxycycline was detected in a solid medium, particularly for streptomycin ($p \leq 0.001$), leading to almost complete inhibition of mutant growth (**Supplementary Table 7**). These results suggest that, in case of accidental human

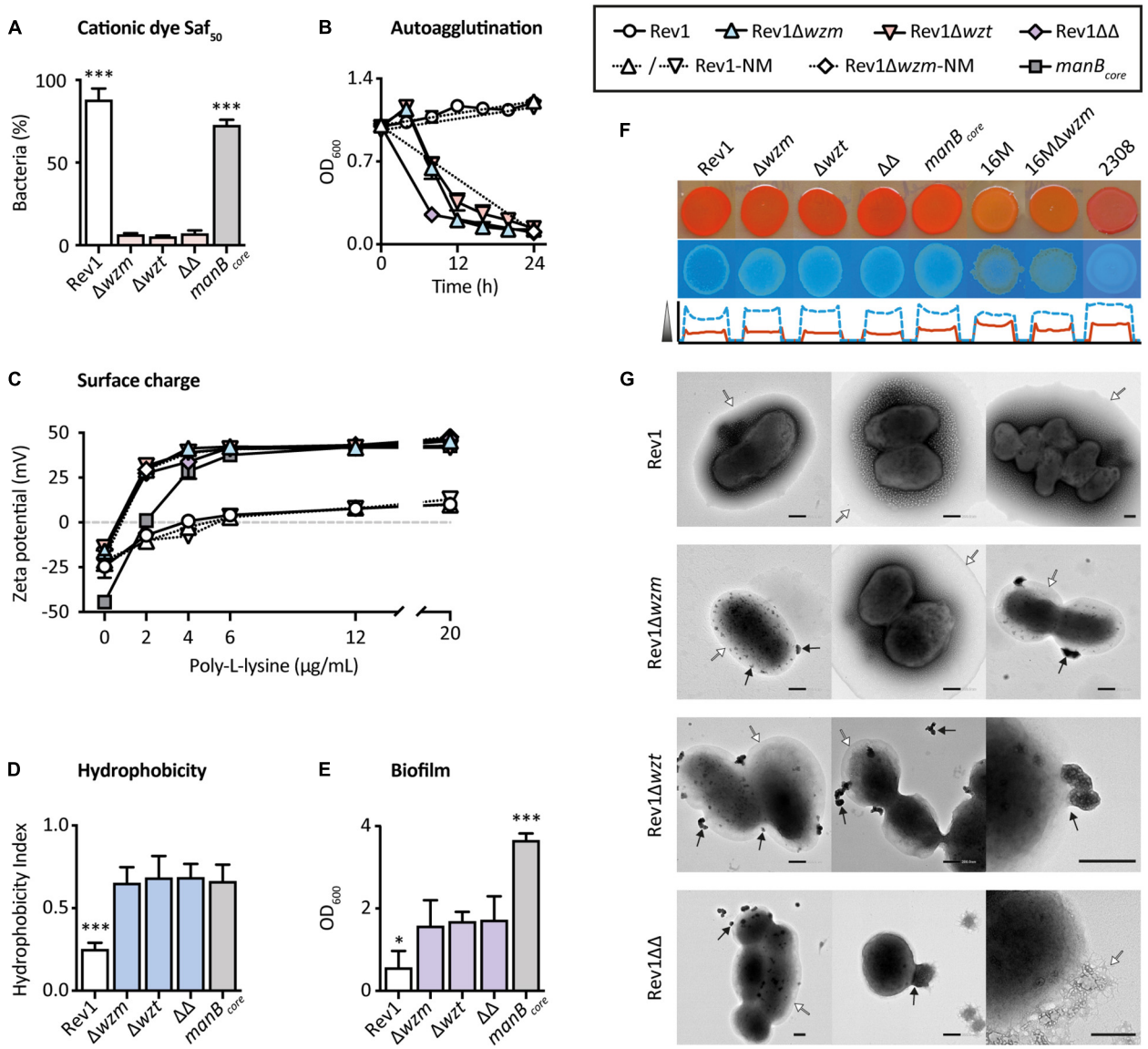

FIGURE 3 | Outer membrane properties of *wzm/wzt* mutants are modified in comparison with Rev1. **(A)** Inhibition by the cationic dye safranin O at 50 μg/ml (Saf_{50}) in BAB-S and 10% CO_2 represented as surviving bacteria (%; mean ± SD; $n = 3$) vs. the standard growth condition. **(B)** Autoagglutination in static culture determined by spectrophotometry (mean ± SD; $n = 2$; representative result). **(C)** Surface charge measured by Zeta-potential (mean ± SD) in absence ($n = 4$) or presence ($n = 2$) of poly-L-lysine. **(D)** Hydrophobicity based on differential partitioning in aqueous-hydrocarbon solution (mean ± SD; $n = 3$). **(E)** Biofilm formation quantified by crystal violet staining (mean ± SD; $n = 3$). **(F)** EPS analysis by the intensity of Congo Red (upper row; red line) or Calcofluor (the low row; the discontinuous blue line). **(G)** Representative TEM images with negative stain in which EPS and OMVs are indicated by white and black arrows, respectively; scale bars = 200 nm. Fisher's LSD test; $^{***}p \leq 0.001$, $^{*}p \leq 0.05$ vs. the other groups.

inoculation, conventional treatment would be successful, in contrast to that reported for Rev1 (Blasco and Díaz, 1993; Grilló et al., 2006a).

The inhibition observed with Saf_{100}, a basic monovalent cationic dye largely adsorbed by hydrophobic surfaces (Atun et al., 1998) as described for crystal violet-oxalate (Popescu and Doyle, 1996), could represent changes in the OM and cell walls (Jankowski et al., 2005). Thus, we quantified the susceptibility of the mutants to a lower concentration of this dye (Saf_{50}), which gave only a 6% viability of mutants, in contrast to ($p \leq 0.001$) the 87.8% of Rev1 parental strains (**Figure 3A**). Rev1 survival could be explained by the hydrophilic hindrance of the S-LPS (Nikaido and Vaara, 1985; Godfroid et al., 2000) and/or by buffering of the free radicals generated by this dye by CO_2 (Jankowski et al., 2005). However, since BmH38R*manB*$_{core}$ survived (72.5%) more than *wzm/wzt* mutants, safranin O susceptibility suggests that the OM undergoes a particular reorganization, resulting in more exposed lipid A and core moieties in the mutants (Vaara, 1992; Perevoshchikova et al., 2009; Clifton et al., 2016; Fontana et al., 2016).

Blocking O-Polysaccharide Transport Causes Pleiotropic Changes Associated With the Outer Membrane and Cell Wall

Lipopolysaccharide biosynthesis is generally related to other cellular components involved in bacterial integrity (Morè et al., 2019). For instance, R-LPS and O-PS deficiencies have been associated with interrelated properties, such as spontaneous autoagglutination (Caro-Hernández et al., 2007), adhesion to solid layers (Nakao et al., 2012), increased hydrophobicity, and negative surface charge (González et al., 2008). Indeed, surface adhesion is dependent on the bacterial charge and the hydrophobic nature of the substrate, e.g., polystyrene (Fletcher and Loeb, 1979). Accordingly, these properties were found in the three mutants (**Figures 3B–E**).

Extracellular polymeric substances (EPS) are heterogeneous components typical of biofilm and stain differently by Congo Red or by Calcofluor (Wood, 1980). We found that both dyes bound moderately to Rev1 and its mutants, but only minimally to 16M and 16MΔ*wzm* (**Figure 3F**); these differences seem to be

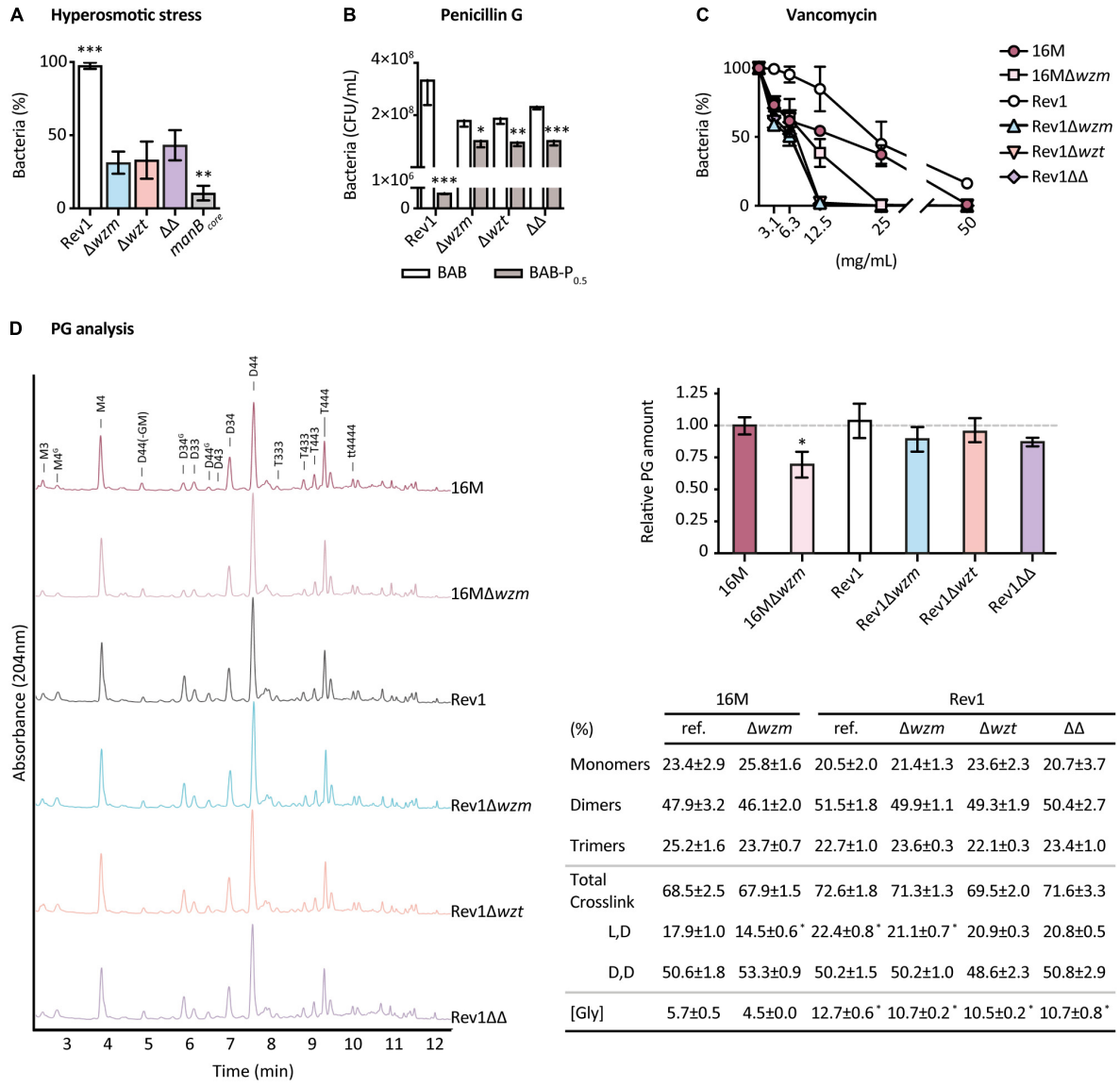

	16M		Rev1			
(%)	ref.	Δ*wzm*	ref.	Δ*wzm*	Δ*wzt*	ΔΔ
Monomers	23.4±2.9	25.8±1.6	20.5±2.0	21.4±1.3	23.6±2.3	20.7±3.7
Dimers	47.9±3.2	46.1±2.0	51.5±1.8	49.9±1.1	49.3±1.9	50.4±2.7
Trimers	25.2±1.6	23.7±0.7	22.7±1.0	23.6±0.3	22.1±0.3	23.4±1.0
Total Crosslink	68.5±2.5	67.9±1.5	72.6±1.8	71.3±1.3	69.5±2.0	71.6±3.3
L,D	17.9±1.0	14.5±0.6*	22.4±0.8*	21.1±0.7*	20.9±0.3	20.8±0.5
D,D	50.6±1.8	53.3±0.9	50.2±1.5	50.2±1.0	48.6±2.3	50.8±2.9
[Gly]	5.7±0.5	4.5±0.0	12.7±0.6*	10.7±0.2*	10.5±0.2*	10.7±0.8*

FIGURE 4 | Rev1*wzm/wzt* mutants exhibit differences in cell-wall properties. Susceptibility to: **(A)** Hyperosmotic stress, expressed as the percentage of bacteria survival after incubation (37°C, 48 h) of 10^4 CFU/ml in 0.5 M NaCl, plated in BAB; **(B)** Penicillin G expressed as the number of CFU/ml obtained after triplicate culturing (37°C, 8 days) of serial 10-fold dilutions from 10^9 to 10^4 CFU/ml in 0.5 IU/ml of penicillin G vs. BAB plates ($P_{0.5}$); and **(C)** Vancomycin, expressed as the percentage of bacteria survival after incubation (37°C, 1 h) of 10^4 CFU/ml in twofold serial dilutions (50–3.125 mg/ml) of the antibiotic and triplicate plating in BAB; all results represent the mean ± SD (n = 3) of 2 or 3 independent experiments. **(D)** PG analysis as representative normalized chromatograms of three independent cultures of each strain, showing the relative PG amount and percentage of composition (mean ± SD; n = 3) of 16M and Rev1 reference and *wzm/wzt* mutant strains. Non-labeled peaks correspond to unknown muropeptides. Fisher's LSD or t-tests; ***$p \leq 0.001$, **$p \leq 0.01$, *$p \leq 0.05$ vs. the other groups or vs. 16M in panel **D**.

associated with the nature of the parental strain, as revealed by BmH38R*manB*$_{core}$ and *B. abortus*2308 controls, and have been previously related to host preference and virulence (Uzureau et al., 2007). Although the acquisition of fine images of the native EPS is a major challenge due to its low contrast and tendency to collapse (Dohnalkova et al., 2011), we successfully detected the presence of EPS in Rev1 and its mutants by transmission electron microscopy (TEM), which revealed it to be a globular structure surrounding both fibrous and hydrated shapes (**Figure 3G**).

Other interesting structures promoting adhesiveness to solid surfaces in *Brucella* are the OM vesicles (OMVs), commonly called blebs (Godefroid et al., 2010). Blebs are nanovesicles released from the OM whose composition (Gamazo and Moriyón, 1987; Avila-Calderón et al., 2020; Ruiz-Palma et al., 2021) and amount (Solanki et al., 2021) have been associated with the lack of O-PS, and they are overproduced in strains that auto-agglutinate (Godefroid et al., 2010). As shown by TEM (**Figure 3G**), the mutants showed abundant OMVs as outward bulges protruding from the surface or as already detached vesicles, while the OM maintained its integrity. In stark contrast, we did not find even a single OMV in Rev1. These structural changes could indicate a rearrangement of cell envelope components.

The OM and the cell wall are covalently linked (Godessart et al., 2021), and their consistency is directly responsible for bacterial osmotic protection (Morè et al., 2019). In our studies, all strains grew well in sucrose hyperosmotic and hypoosmotic conditions; however, fewer than 50% of *wzm*/*wzt* mutants, and 10% of BmH38R*manB*$_{core}$ survived in a hyperosmotic.5-M NaCl medium, while the growth of Rev1 was unaltered (**Figure 4A**), highlighting the importance of the selected osmolyte to be used (Cheung et al., 2009; Shabala et al., 2009; Pilizota and Shaevitz, 2013; Schuster et al., 2020). Even though EPS is involved in protecting against osmotic stress and antimicrobials (Dohnalkova et al., 2011), its presence did not mitigate NaCl stress in Rev1 *wzm*/*wzt* mutants.

Susceptibility to penicillin G can provide information about cell wall rearrangements, since this ß-lactam targets the penicillin-binding proteins (PBPs) involved in PG assembly (Kohanski et al., 2010), leading to the inhibition of PG transpeptidation and subsequent cell-wall destabilization (Wolter and Lister, 2013). We observed a total inhibition at P_5 of 10^9 CFU/ml for Rev1 as well as for its derivatives (**Supplementary Table 5**). Thus, we next sought to determine whether using lower concentrations could detect differences between Rev1 and its derivatives. All strains were significantly inhibited in a solid medium at $P_{0.5}$, but, surprisingly, the mutants were less inhibited than Rev1 (**Figure 4B**) and also showed higher MBC_{90} (0.84 vs. 42 IU/ml). As target modification is relatively unlikely, the increased resistance of mutants could be due: (i) to PBP being shielded—by its own substrate (Lepage et al., 1995) and/or by other cell products or structures (Livermore, 1987); or (ii) to reduced PBP activity, leading to PG remodeling (Peters et al., 2018; Morè et al., 2019). To further elucidate the PG structure, we studied the susceptibility of the mutants to vancomycin, a non-β-lactam glycopeptide that hinders PG assembly by blocking its precursors (Kohanski et al., 2010). Rev1 *wzm*/*wzt* mutants were more susceptible than the parental Rev1, showing total inhibition at 12.5 mg/ml (**Figure 4C**); this could indicate changes in the amount and/or composition of the PG that, in absence of the S-LPS building machinery in the periplasm, could facilitate vancomycin activity.

We therefore analyzed the PG of *B. melitensis* 16M and Rev1 and their derivatives by UPLC-MS (**Figure 4D**). For PG quantification, Rev1 *wzm*/*wzt* mutants presented lower amounts of PG (10–15% less) than the parental lines; reduction was even more remarkable (30%) for 16MΔ*wzm* vs. 16 M, in line with previous studies (Kreutzer et al., 1977). The fact that these mutants showed decreased PG confirms the hypothesis that truncating the Wzm/Wzt system impairs cell wall biogenesis, presumably due to sequestering the complex bactoprenol–O-PS when the transport is blocked. Furthermore, it would explain the higher susceptibility of the mutants to vancomycin. For the PG structure, we report for the first time the basic PG building block in *B. melitensis*, consisting of GlcNAc-MurNAc-L-Ala-D-Glu-mDAP-D-Ala-D-Ala, which is similar to that of other gram-negative bacteria (Vassen, 2018). *B. melitensis* PG included the presence of glycine (Gly) rather than Ala at Position 4 of the stem in a relatively small percentage of the muropeptides. For PG composition, we observed significant differences ($p \leq 0.05$) between Rev1 and 16M parentals, as well as a general increase of L,D-crosslink and Gly in Rev1, suggesting a more active incorporation of glycine by L,D-transpeptidases (Ldts) than in 16M. Interestingly, 16MΔ*wzm* had a significant reduction ($p \leq 0.05$) of the L,D-crosslink vs. 16M, a trend also observed for Rev1 *wzm*/*wzt* mutants vs. Rev1. These compensations underscore the essential, versatile, and functional coupling of LPS, OM, and cell wall biosynthesis, and strongly suggest that a block of O-PS transport causes pleiotropic effects on *Brucella*.

Rev1 *wzm*/*wzt* Mutants Are Highly Attenuated in BALB/c Mice, Highlighting the Immunity Induced by Rev1Δ*wzm*

Resistance of virulent *Brucella* to soluble factors of the host immune system is essential for their survival *in vivo*. We therefore used *in vitro* models of susceptibility to polymyxins as antimicrobial cationic polypeptides, targeting the LPS phosphate groups (Martínez de Tejada et al., 1995), as well as to normal sheep serum as a source of complement. As previously reported (Stranahan and Arenas-Gamboa, 2021), R-LPS mutants were highly inhibited by PxB, Col, and serum complements (**Figures 5A,B**). Moreover, sera from Rev1Δ*wzm*-immunized sheep showed a marked killing effect on *Brucella ovis* rather than on *B. melitensis* (**Figure 5C**), a finding that could be explained by the natural absence of O-PS in *B. ovis* that makes their OM proteins more readily accessible to antibodies (Monreal et al., 2003).

In the BALB/c mice, the three mutants evidenced extreme attenuation. The vaccinated mice had high levels of spleen colonization at 1 week post-inoculation (PI) but were completely cleared of the mutants by 3–4 weeks (**Figure 5D**), in contrast to the longer persistence of Rev1 (**Supplementary Figure 1**). Furthermore, we reproducibly observed a peak

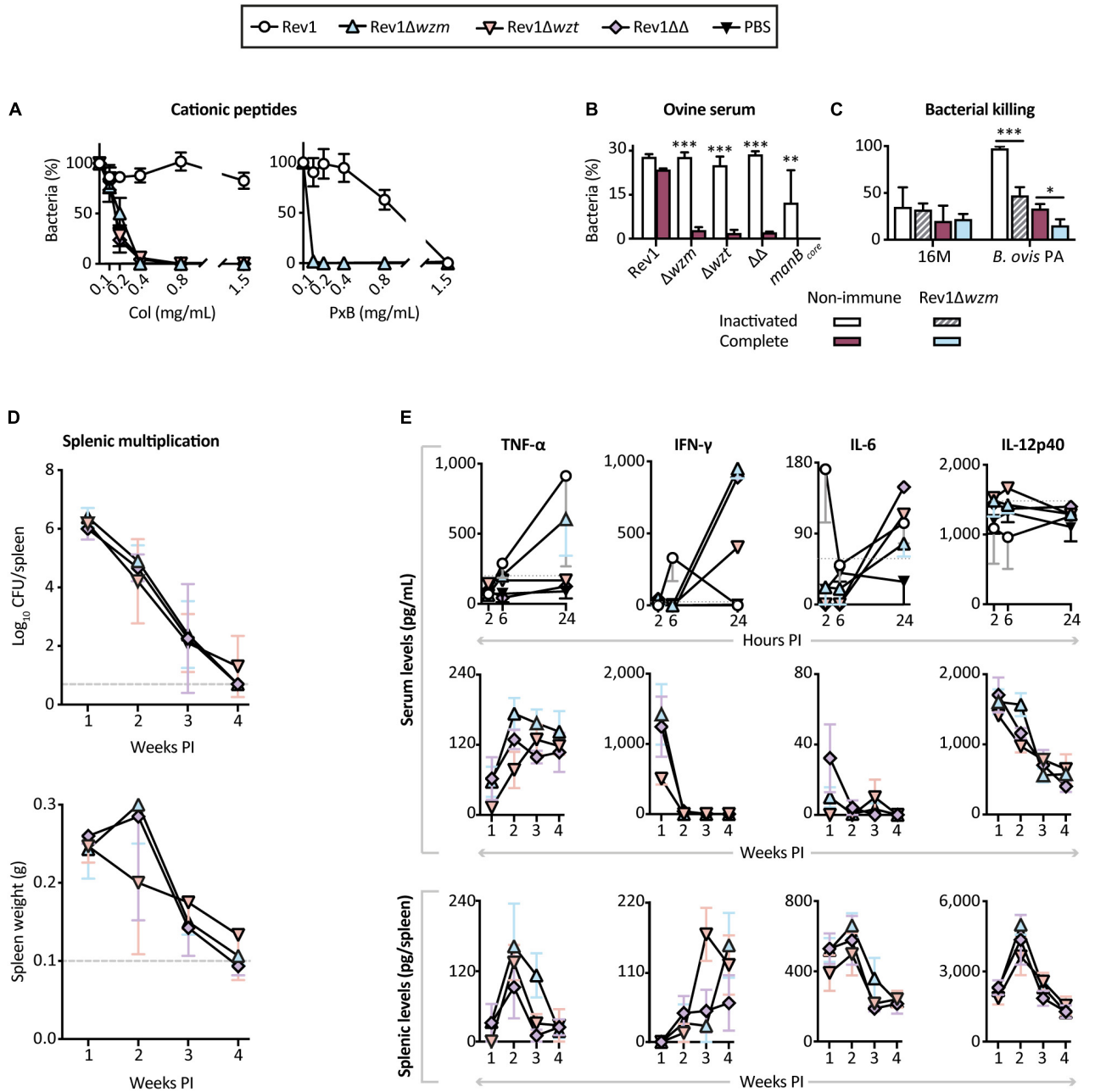

FIGURE 5 | Rev1Δ*wzm* is highly attenuated and triggers a stronger adaptive immune response than Rev1Δ*wzt* or Rev1Δ*wzm*Δ*wzt* in the BALB/c mice. Susceptibility is shown for: **(A)** Polymyxin B (PxB) or colistin (Col), as models of cationic bactericidal peptides of the innate immune system (mean ± SD; $n = 2$); and **(B)** complement-mediated killing by conventional non-immune ovine serum, either complete or heat inactivated (mean ± SD; $n = 2$). **(C)** Bacterial killing activity of sera from sheep immunized with Rev1Δ*wzm* against *B. melitensis* 16M and *B. ovis* PA (BoPA) virulent strains (mean ± SD; $n = 4$). **(D)** Kinetics of spleen infections and weights (mean ± SD; $n = 3$ at 1 and 4 weeks PI, $n = 4$ at 2 and 3 weeks PI) of the BALB/c mice inoculated IP with 10^8 CFU/mouse of the correspondent mutant; the dashed lines indicate the detection limit ($\log_{10}$ 5 CFU/spleen = 0.70) and normal splenic weight (0.1 g) in the BALB/c mice. **(E)** Cytokine profiles in blood sera and splenocytes supernatants from the same mice at selected intervals; sera collected at 2, 6, and 24 h PI ($n = 5$) were processed as pools, including two independent experiments for Rev1Δ*wzm*, Rev1, and PBS groups; dotted lines represent PBS's maximum value; blood sera and splenocytes supernatants collected at 1, 2, 3, and 4 weeks PI were processed individually for each necropsied group (mean ± SEM). Fisher's LSD test; ***$p \leq 0.001$, **$p \leq 0.01$, *$p \leq 0.05$ immune vs. non-immune sera for a given strain.

of splenomegaly at 2 weeks PI in the mice vaccinated with Rev1Δ*wzm*, a less pronounced peak in the mice vaccinated with Rev1Δ*wzm*Δ*wzt*, and no peak in those vaccinated with Rev1Δ*wzt* (**Supplementary Figure 1**). This inflammatory response could be associated with an enhanced adaptive immune response mediated by cytokines, which are crucial in protective

immunity against *Brucella* (Grilló et al., 2012; Sancho et al., 2014). We next analyzed cytokine production in both blood and spleen supernatants at early (≤24 h) and late (≤4 weeks) PI intervals (**Figure 5E**). Notably, the Rev1Δ*wzm* mice displayed high serum levels of circulating TNF-α and IFN-γ at 24 h PI, and of TNF-α and IL-12 at 2 weeks PI; likewise, the peak of splenomegaly at 2 weeks PI correlated with high levels of proinflammatory TNF-α, IL-6, and IL-12 in these spleens, and a peak of IFN-γ at 4 weeks PI, which was delayed with respect to that described for Rev1 (Sancho et al., 2014). This cytokine relation triggered by Rev1Δ*wzm* plays a critical role in limiting intracellular replication and quick clearance of the mutant as well as in triggering a protective Th1 immune response (Baldwin and Goenka, 2006; Dorneles et al., 2015; Jain-Gupta et al., 2019). Thus, we demonstrate that Rev1Δ*wzm* does not require long-lasting persistence to induce protective immunity, in contrast to what is generally accepted for *Brucella*, where Rev1 immunogenicity is dependent on its persistence in mice spleens (Bosseray and Plommet, 1990; Grilló et al., 2000; Moriyón et al., 2004; Barrio et al., 2009; OIE, 2018).

Rev1Δ*wzm* Is as Effective as Rev1 Against *Brucella melitensis* and *Brucella ovis* in BALB/c Mice

On the basis of its immunogenicity, we studied whether the splenomegaly induced by Rev1Δ*wzm* and the subsequent adaptive immune responses were dose dependent (**Supplementary Figure 1**). Immunization with 10^6 to 10^8 CFU/mouse of Rev1Δ*wzm* induced equivalent spleen infections, but only 10^8 CFU achieved a homogeneous intragroup infection and splenomegaly, similar to that induced by Rev1 in standard conditions. This confirmed that the immune response to Rev1Δ*wzm* was dose dependent.

Efficacy studies on mice use intraperitoneal (IP) or subcutaneous (SC) vaccinations as screening or more exigent models for R-*Brucella* strains, using Rev1 in standard conditions and PBS as efficacy and non-vaccinated controls, respectively (González et al., 2008). Accordingly, we used both routes to evaluate Rev1 *wzm*/*wzt* mutants in the BALB/c mice. Against a *B. melitensis* H38 (S-LPS) challenge, Rev1Δ*wzm* was as protective as Rev1, while Rev1Δ*wzt* failed by the SC route and Rev1Δ*wzm*Δ*wzt* induced heterogeneous responses (**Figure 6A**). Against a *B. ovis* PA (R-LPS) challenge, Rev1Δ*wzm* administered *via* SC was also as effective as Rev1, and IP improved the protection conferred by the standard Rev1 vaccine control (**Figure 6B**).

Differences in the immunogenic properties of Rev1 *wzm*/*wzt* mutants could be attributable to a differential presence of Wzm or Wzt, supporting the hypothesis that Wzt has a crucial role in conferring immunity (Wang et al., 2014b). Indeed, we detected *wzt* overexpressed in Rev1Δ*wzm*. Although the overlap of the start/stop codons could lead to a coupled translation of both proteins, an increase at the translational level could be relevant to O-PS antigenicity. Since Wzt is incorporated into the cytoplasm when Wzm is missing (Singh et al., 2013; Mohammad et al., 2016), the accumulation of nascent O-PS molecules in Rev1Δ*wzm*, presumably attached to the cytoplasmic membrane by the lipid carrier, might have positive feedback on Wzt molecules. Additionally, as Wzt is responsible for O-PS terminal recognition (Valvano, 2003, 2015; Clarke et al., 2004; Cuthbertson et al., 2005, 2007; Hagelueken et al., 2015; Williams et al., 2017; Bi and Zimmer, 2020), its binding to the O-PS could be necessary to provide the antigen with its final conformation and thus with its immunogenic properties.

Rev1Δ*wzm* Has a Similar Growth Pattern as Rev1 and Is Stable After *in vitro* and *in vivo* Subculturing

Having selected Rev1Δ*wzm* as a promising vaccine candidate, we sought possible *in vitro* defects that could affect the bacterial viability and/or scale-up production properties. We determined that Rev1Δ*wzm* resembled the growth curve of Rev1 yet provided higher turbidity and larger particle size (**Figures 7A,B**), probably due to the presence of OMVs protruding from the mutant, as evidenced by TEM (**Figure 3G**). Additionally, Rev1Δ*wzm* had a similar susceptibility as Rev1 to desiccation, detergents, oxidative stress, and acidic environment (**Figures 7C–F**), as well as to lyophilization. These environmental susceptibilities of Rev1 (which have not previously been reported) and its mutant agreed with the detected downregulation of cyclic glucan genes as compared to the virulent strain 16M (**Figure 1B**). Furthermore, we detected unaltered genotypical [*wzm* deletion and GI-2/*wbk* regions integrity (Mancilla et al., 2013)] and phenotypical (including inner O-PS production) features after 20 *in vitro* passages as well as after 5 consecutive passages in mice spleens. In contrast, Rev1 viability was significantly reduced after 15 *in vitro* passages, supporting the recommendation of minimizing *in vitro* propagation for quality control (Grilló et al., 2012). These described results (data not shown) suggested that Rev1Δ*wzm* is not likely to have antigenic drift.

Rev1Δ*wzm* Is Attenuated in BeWo Cells and Safe in Pregnant Mice

Brucella infection, including Rev1 (Jiménez de Bagüés et al., 1989), targets the reproductive tract, starting in trophoblast giant cells, disseminating to placenta and fetuses and ending in spontaneous abortion. As preclinical models, we studied the ability of Rev1Δ*wzm* to infect BeWo cells (a trophoblast-derived, choriocarcinoma cell line) and mouse placentas/fetuses as compared to the ability of Rev1. In BeWo cells, Rev1Δ*wzm* was more adherent but was internalized less efficiently after adherence and replicated less than Rev1 (**Figure 8A**). In turn, Rev1Δ*wzm* was not found in mouse placentas/fetuses, even after inoculation at a 10-fold higher dose than Rev1, although both strains resulted in similar spleen infections (**Figure 8B**). Histologically, Rev1Δ*wzm* enabled normal placentas with minimal neutrophilic infiltration and normal fetus viability, differing from Rev1 by its marked macroscopic edema, destruction of placental epithelium, and leukocyte infiltration in yolk sac. This mouse model has been successfully used as screening of pathogenicity (Grilló et al., 2012; Poveda-Urkixo et al., 2022), indicating that Rev1Δ*wzm* might be safer than

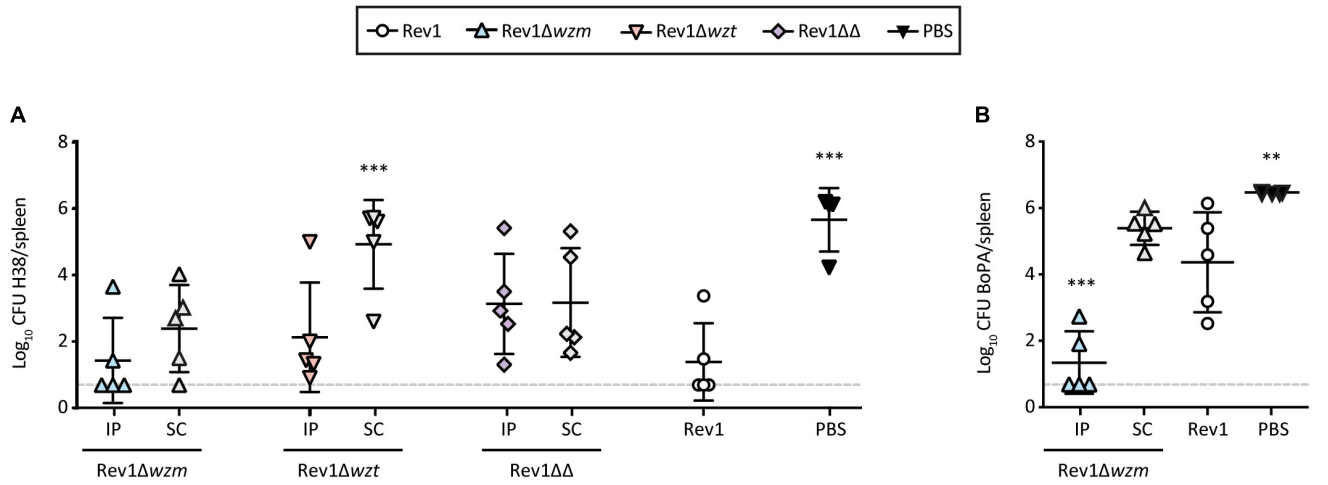

FIGURE 6 | Rev1Δ*wzm* protects against virulent *B. melitensis* and *B. ovis* challenges in the BALB/c mice. Efficacy in the BALB/c mice (n = 5) IP or SC vaccinated with Rev1 *wzm/wzt* mutants (10^8 CFU/animal) or with Rev1 reference vaccine (10^5 CFU/animal, SC) or PBS as controls; after 4 weeks, the mice were IP challenged with **(A)** 1×10^4 of *B. melitensis* H38:Gm^r (H38) or **(B)** 5×10^5 of *B. ovis* PA:Gm^r (BoPA:Gm^r). After 2 or 3 weeks, respectively, the mean ± SD (n = 5) $\log_{10}$ CFU of the challenge strain in spleens was determined. Detection limit ($\log_{10}$ 5 CFU/spleen = 0.70) is indicated with a discontinuous line. Fisher's LSD test; $^{***}p \leq 0.001$, $^{**}p \leq 0.01$ vs. Rev1 control.

Rev1 in pregnant animals and justifying further experiments in the natural host.

Rev1Δ*wzm* Is Safe in Pregnant Ewes and Their Offsprings, and Induces Minimal Serological Interference

All ewes vaccinated with a high dose of Rev1Δ*wzm* at mid-pregnancy (n = 6) showed normal clinical parameters, mild and transient local reactions at the inoculation site, with no shedding the mutant through vagina or milk, during pregnancy or lactation, and had normal parturitions at 144 ± 3.3 days of pregnancy. Likewise, at necropsy, the mutant was not found in any ewe or offspring. These results contrasted with those reported for Rev1 (i.e., shedding by vagina during pregnancy, bacteria in placentas at parturition and in milk, placental necrosis, abortions, and vertical transmission to lambs) (Jiménez de Bagüés et al., 1989; Blasco, 1997; Hensel et al., 2020).

Serologically, all ewes reacted in ELISA-R/LPS after vaccination and turned negative before 8 weeks PI; a 66.7% also reacted in RBT (16.7% CFT positive), a percentage that decreased progressively until turning all ewes negative before 5 weeks PI (**Figure 8C**). These reactions were significantly less interferent than those reported for Rev1 (Barrio et al., 2009).

The Impact of the Rev1 Background on Rev1Δ*wzm* Vaccine Properties Was Unpredictable

It is commonly assumed that vaccine candidates should retain some residual virulence to be efficient (Grilló et al., 2000). Indeed, just those 16M *wzm* mutants that show an attenuation pattern similar to Rev1 are as protective as Rev1 against a *B. melitensis* virulent challenge (Zabalza Baranguá, 2017), while 16MΔ*wzt* is less persistent and less protective than Rev1 (Wang Z. et al., 2014). On this basis, the high attenuation of Rev1Δ*wzm* should have led to failed efficacy; however, and, unpredictably, Rev1Δ*wzm* (but not Rev1Δ*wzt*) triggered a splenomegaly associated with a particular Th1 cytokine balance, as well as to a protective efficacy against virulent challenges. Besides the genetic and phenotypic divergences described between the Rev1 and 16M parentals related to virulence attenuation (Issa and Ashhab, 2016; Salmon-Divon et al., 2018, 2019; Kornspan et al., 2020), we have now described additional differences in genetic transcription, antigenicity evidenced by Western blot, and susceptibility to antibiotics and environmental stress factors. Indeed, when *wzm*/*wzt* mutations were applied to other brucellae (Wang et al., 2014a; Grilló et al., 2017; Aragón-Aranda et al., 2020; Lalsiamthara et al., 2020), neither mutant was as immunogenic as Rev1Δ*wzm*. All these findings demonstrate the relevance of the background in vaccine properties, as well as the unpredictable efficacy results obtained with Rev1Δ*wzm*.

CONCLUSION

The Wzm/Wzt system is broadly conserved among gram-negative bacteria, and its inactivation in Rev1 not only restrains the export, quantity, and availability of O-PS but also triggers phenotypic changes of the OM and cell wall. Despite similarities *in vitro*, deletion of Wzm or Wzt transporter moieties elicited different immune responses and efficacies against *Brucella*-virulent infections. Indeed, Rev1Δ*wzm* displays superior vaccine properties: attenuation, immunogenicity, efficacy against a virulent infection in mice, safety in pregnant mice, high susceptibility to diverse stresses and antimicrobials, and safety and minimal serological interference in pregnant ewes. These results (summarized in **Supplementary Figure 2**) thus highlight

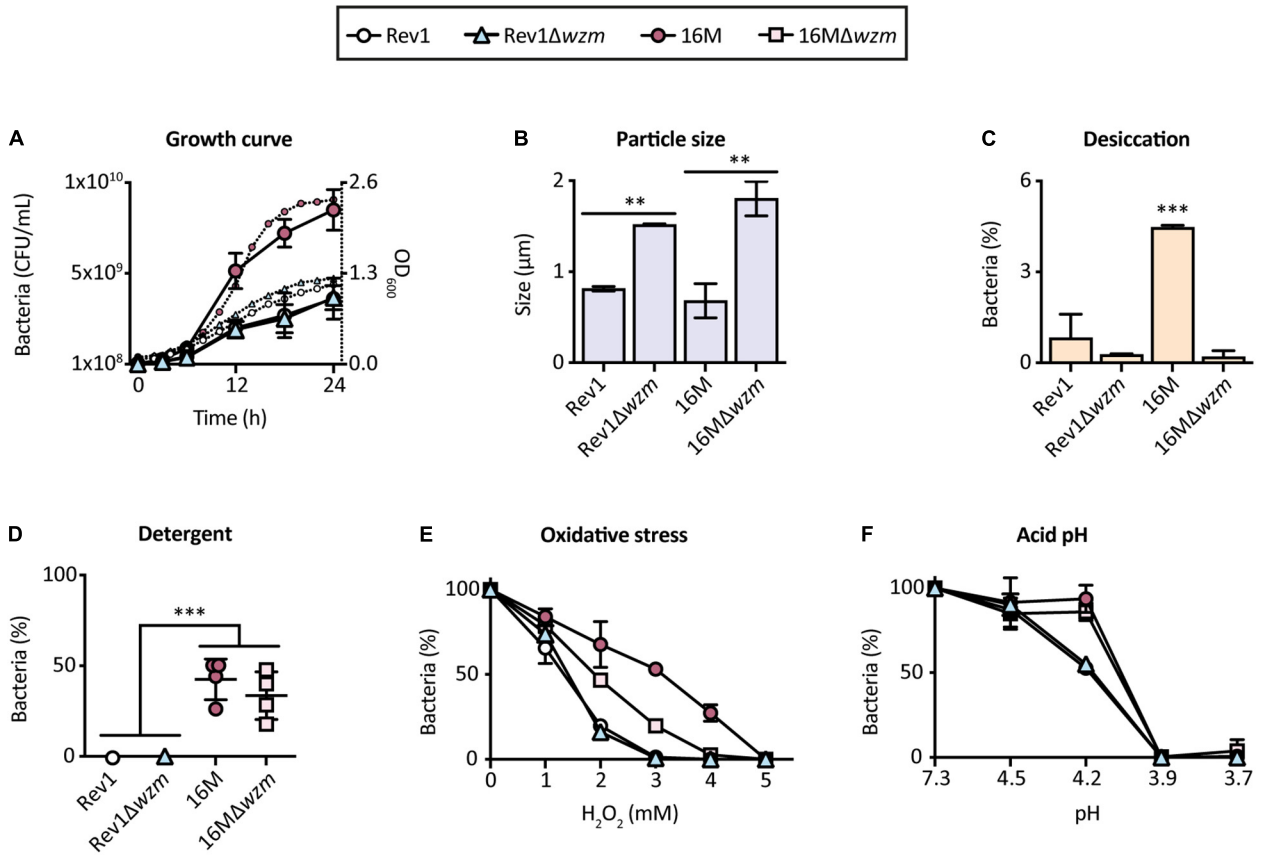

FIGURE 7 | Rev1 Δ*wzm* has larger particle size than Rev1, but both perform similarly in the *in vitro* growth curves and environmental susceptibility. **(A)** Bacterial growth curves determined by the number of viable cells (CFU/ml; the left axe, large symbols) and medium absorbance (OD_{600}; the right axe, small symbols). **(B)** Particle size values measured by Zetasizer (μm). Percentage of bacterial inhibition by: **(C)** Desiccation, **(D)** Detergents (0.1% Triton X-100), **(E)** Oxidative (H_2O_2), and **(F)** Acidic pH pressures, as models of stress encountered by *Brucella* in the natural environment and in the host niche. All results are expressed as the mean ± SD of at least three measures; strains Rev1, 16M, and 16MΔ*wzm* were included as controls in all the experiments; the percentages of surviving bacteria (%) were determined with respect to the initial suspension. Fisher's LSD test; ***$p \leq 0.001$, **$p \leq 0.01$ vs. the indicated groups.

a new concept that is essential in vaccine development, i.e., that a low persistence is not at odds with efficacy.

MATERIALS AND METHODS

Strains and Culture Conditions

Bacterial strains (**Supplementary Table 1**) were stored at −20°C in 10% skimmed milk with 3% lactose (PanReac AppliChem, Castellar del Vallés, Barcelona, Spain) and routinely cultured at 37°C in normal atmosphere (air), using Trypticase Soy Broth (TSB; Condalab) at 150 rpm, or in plates of TSB supplemented with 1.5% bacteriological agar (TSA; Pronadisa) for *Escherichia coli* strains, or Blood Agar Base No. 2 (BAB; Oxoid) for *Brucella* spp., either plain or supplemented with 5% newborn calf serum (S; Gibco), 5% sucrose (Suc_5; VWR Chemicals, Radnor, PA, United States), and/or antibiotics (Sigma-Aldrich, San Luis, MO, United States), such as kanamycin (50 μg/ml; Km_{50}), polymyxin B (1.5 μg/ml; $PxB_{1.5}$), colistin (4 μg/ml; Col_4), gentamycin (15 μg/ml; Gm_{15}), streptomycin (2.5 μg/ml; $Str_{2.5}$), doxycycline (0.02 μg/ml; $Dx_{0.02}$), rifampicin (0.4 μg/ml; $Rf_{0.4}$), and penicillin G at (5 IU/ml; P_5) or (0.5 IU/ml; $P_{0.5}$), as needed. Suspensions were adjusted by spectrophotometry (SmartSpec Plus; Bio-Rad, Hercules, CA, United States) in sterile TSB or PBS (pH, 7.2; VWR Chemicals, Radnor, PA, United States), as described elsewhere (González et al., 2008). The exact number of viable counts was determined retrospectively by serial dilutions in PBS and plating (0.1 ml, done in triplicate).

Sequence Analysis and DNA Manipulation

In silico studies were performed with BLAST (Altschul et al., 1990), NCBI (Sayers et al., 2022), and KEGG (Kanehisa and Goto, 2000) databases. PCR primers (**Supplementary Table 2**) were synthesized by Sigma-Aldrich Química SL (Madrid, Spain). Vector sequences were obtained from Addgene (Kamens, 2015). Vector or chromosomal DNA purifications were performed by *miniprep* with E.Z.N.A. Plasmid Mini Kit I (Omega Bio-tek, Norcross, Georgia) or DNeasyUltraClean Microbial

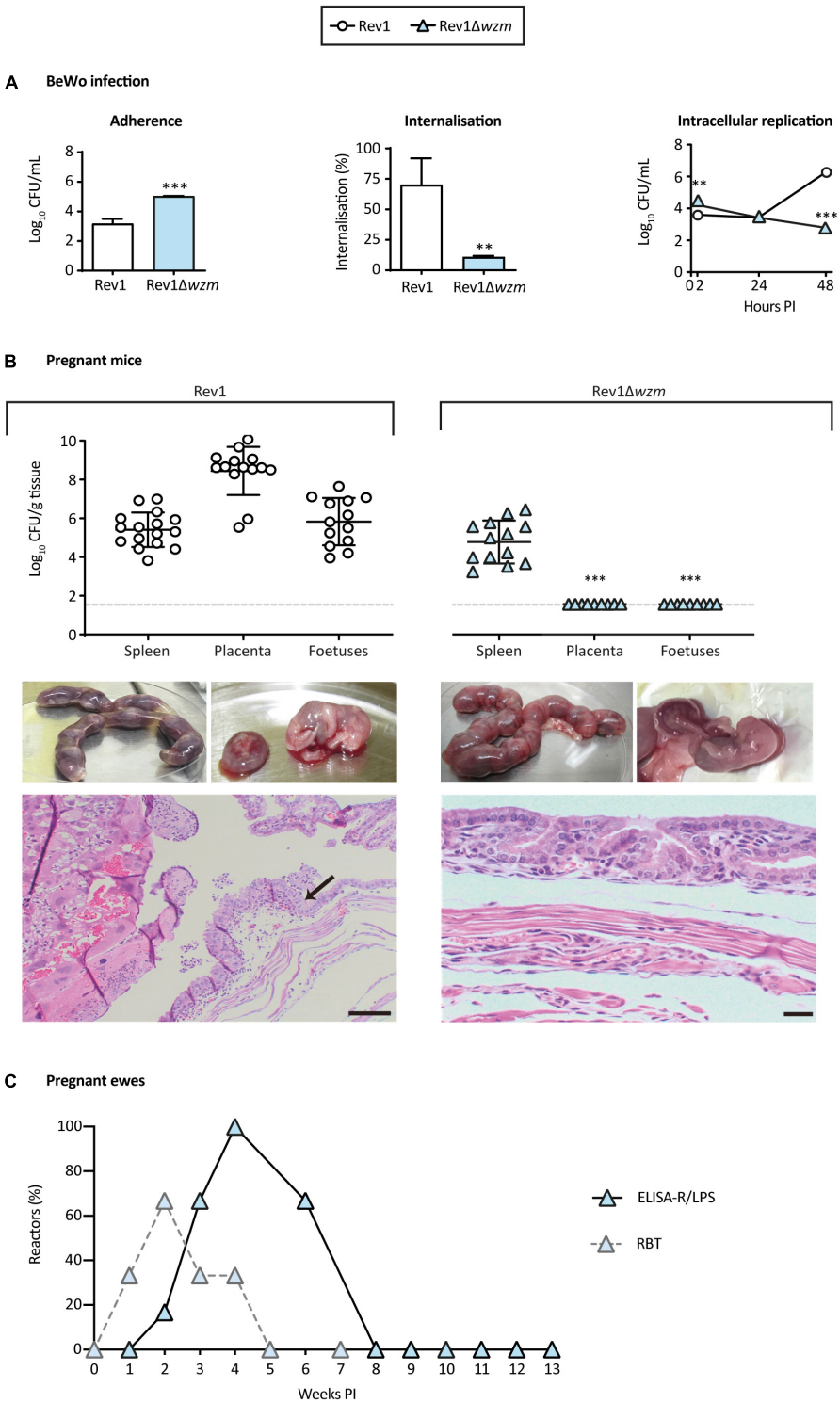

FIGURE 8 | Rev1 Δ*wzm* is attenuated in BeWo cells, safe in pregnant mice, and induces minimal serological interference in ewes vaccinated at mid-pregnancy. **(A)** Adherence, internalization, and intracellular multiplication in BeWo cells (n = 3). **(B)** Bacteriology of spleens (upper panel), as well as macroscopic and microscopic representative images of placentas and fetuses from the pregnant CD1 mice, analyzed at 14 days after IP inoculation with 1×10^7 CFU of Rev1 Δ*wzm* (n = 14; the right column) or 1×10^6 CFU of Rev1 (n = 16; the left column). The arrow indicates leukocyte infiltration; scale bars = 100 μm. Detection limit ($\log_{10}$ 33 CFU/g tissue = 1.52) is indicated with a discontinuous line. In panels **A,B**, results are presented as mean ± SD of the correspondent n value. **(C)** Serological response (% reactors) in ewes vaccinated SC with 1.8×10^{10} CFU of Rev1 Δ*wzm* at mid-pregnancy, developing antibodies in ELISA-R/LPS and RBT. Fisher's LSD or t-tests; ***$p \leq 0.001$, **$p \leq 0.01$ vs. Rev1 control.

Kit (Qiagen, Düsseldorf, Germany). Single-colony DNA was extracted by boiling and centrifugation. PCR products were purified using the ATP Gel/PCR DNA Fragment Extraction Kit (ATP Biotech Inc., Taipei, China). DNA was quantified with a NanoDrop Spectrophotometer (Thermo Fisher Scientific, Waltham, MA, United States) and sequenced by STAB VIDA (Caparica, Portugal).

Construction and Complementation of Single and Double *wzm*/*wzt* Rev1 Mutants

In-frame deletion mutants were obtained as previously described (Conde-Álvarez et al., 2012), using the suicide plasmids pJQKmΔ*wzm* (Zabalza Baranguá, 2017) and/or pJQKmΔ*wzt*. The latter was constructed using 16M genomic DNA and the designed primers (**Supplementary Table 2**) to amplify 198 bp upstream and *wzt* 1-66 codons with F1-R2, and *wzt* 209–253 codons and 193 bp downstream with F3-R4 *wzt*. These fragments were fused by overlap PCR with F1-R4 *wzt*, cloned in pCR2.1 (TOPO®TA Cloning, ThermoFisher Scientific) and sequenced. After using pCR2.1Δ*wzt* to transform *E. coli* TOP10F', Δ*wzt* was subcloned into pJQKm (Quandt and Hynes, 1993; Scupham and Triplett, 1997) *Bam*HI and *Xba*I sites. Clones were screened by PCR (**Supplementary Table 2**), and representative non-mutated (NM) ones from each mutagenesis were kept as controls. For complementation, transconjugants, including the pSRK vector with *wzm* (Zabalza Baranguá, 2017), *wzt* or *wzm-wzt* (subcloning of BMEI1415 or BMEI1415-BMEI1416 into *Spe*I and *Xho*I sites) were selected in Km_{50} plates and, for pSRK*wzm-wzt*, 0.1-mM IPTG (Invitrogen, Waltham, MA, United States), and checked by PCR.

Transcriptional Analysis

Genetic expression was analyzed from five independent extractions of Rev1 and derivatives, or 2 of 16M and 16MΔ*wzm* for comparative purposes. Total RNA from exponential cultures was extracted by lysozyme (Sigma-Aldrich, San Luis, MO, United States), proteinase K (Merck, Darmstadt, Germany), Zwittergent (Merck, Darmstadt, Germany), RNeasy Mini kit (Qiagen, Düsseldorf, Germany), and DNase [Ambion, Austin, TX, United states (ThermoFisher)] treatments, and its quality checked with Gel Loading Buffer II [Ambion, Austin, TX, United states (ThermoFisher)], in an agarose gel by confirming that the intensity ratio of 23S:16S proteins was 2:1, obtaining the cDNA with PrimeScript RT kit (Takara, Saint-Germain-en-Laye, France). The qRT-PCR was performed with SYBR Premix Ex Taq (Takara, Saint-Germain-en-Laye, France) in duplicate in an AriaMx real-time PCR system (Agilent) using 96-well microplates (Axygen, New York, NY, United States) as follows: 10 min at 95°C, 45 cycles of 15 s at 95°C, and 1 min at 60°C. Primers (**Supplementary Table 4**) efficiency (0.9–1.1) was assessed as $10^{(-1/\text{slope of Ct vs. DNA dilutions})}-1$. Data were analyzed with Agilent AriaMx v. 1.2 software (Santa Clara, CA, United States) and relative transcription normalized by the $2^{-\Delta\Delta Ct}$ method using *IF-1* gene and representing the fold-change over Rev1 or 16M controls.

Characterization of Rev1 *wzm*/*wzt* Mutants

Conventional *Brucella* biotyping was performed following the standard protocols (Alton et al., 1988). Briefly, the mutants were submitted to tests of catalase, oxidase, urease, agglutination with acriflavine, agglutination with anti-A/anti-M/anti-R monospecific sera, lysis by bacteriophages Tb, Wb, Iz, and R/C, susceptibility to thionine, fuchsine, and safranin O dyes. Also, we analyzed purity and homogeneity of colony size and the LPS phase by the crystal violet-oxalate test (Grilló et al., 2000). The *in vitro* growth curves were assessed by duplicate as turbidity and CFU/ml from suspensions adjusted to OD_{600} = 0.1 (TSB, 37°C, 150 rpm) at the selected intervals.

MIC/MBC_{90} to the selected antibiotics were determined in the cation-adjusted Müller–Hinton medium (M-H; BD) by the standard broth microdilutions method (EUCAST: European Committee for Antimicrobial Susceptibility Testing, 2003), using Rev1 and *E. coli* K12 as controls. Susceptibility to $Dx_{0.02}$, $Gm_{0.125}$, $Rf_{0.4}$, $Str_{2.5}$, $PxB_{1.5}$, Col_4, $P_{0.5}$, and Saf_{50} was quantified by seeding suspensions between 10^9 and 10^4 CFU/ml by triplicate in BAB or BAB-S plates incubated (37°C, 8 days) under normal air or 10% CO_2 atmosphere. Results were expressed as the% of bacterial survival vs. the standard culture (BAB, air). Resistance to vancomycin (Sigma-Aldrich, San Luis, MO, United States) was determined by incubating a suspension of 10^4 CFU/ml in PBS with twofold serial dilutions (50–3.125 mg/ml) of the antibiotic (37°C, 1 h, 100 μL each, by duplicate) and plating in BAB to determine the% of surviving bacteria vs. control.

Analyses of the R-LPS and internal O-PS were performed with ≈10^{10} CFU/ml of whole bacteria inactivated by 0.5% phenol (72 h, 37°C, 150 rpm) or purified LPS by an extraction kit (Intron Biotechnology, Seongnam, South Korea's) in SDS-PAGE and further modified periodate-alkaline silver staining or WB (Tsai and Frasch, 1982; Monreal et al., 2003). The latter was revealed with primary antibodies: (i) mAbs (1:2,000) anti-C/Y 33H8 or 42D2 (batch No. 051119 or 300502, Ingenasa), (ii) anti-M monospecific polyclonal rabbit serum (1:100; IdAB collection), or (iii) anti- *B. ovis*, Rev1, Rev1Δ*wzm* (either normal or heat treated 1 h, 56°C) or 16MΔ*wzm* sera from sheep experimentally infected (1:400; IdAB collection); and secondary HRP-conjugated antibodies: (i) an anti-mouse at 1:3,000 (Bio-Rad, Hercules, CA, United States cat. No. 170-6516), (ii) an anti-rabbit at 1:2,500 (Bio-Rad, Hercules, CA, United States cat. No. 170-6515), or (iii) protein G at 1:1,000 (Pierce cat. No. 21193), all diluted in 1% milk PBST. The images were acquired with ECL Kit (Bio-Rad, Hercules, CA, United States) in a ChemiDocSyngene with GeneSnap 7 (Frederick, MD, United States) or Bio-Rad with Quantity One (Hercules, CA, United States) software. Brightness and contrast adjustments were applied uniformly using GNU Image Manipulation Program v. 2.10 (open source[2]).

To assess the lack of spontaneous mechanisms of dissociation described for Rev1 (Mancilla et al., 2013), the integrity of GI-2 and *wbk* regions was determined after serial subcultures in BAB under normal or 10% CO_2 atmospheres by conventional

[2]www.gimp.org

PCR with the primers presented in **Supplementary Table 2**; the amplified products were 353 bp (P1–P3) and 1,016 bp (P5–P7) in case of gene integrity, or 586 bp (P1–P2) and ≈1,400 bp (P5–P6) in case of excision.

Study of Envelope-Related Properties

Autoagglutination was assessed by OD_{600} readings as described (Caro-Hernández et al., 2007) in at least two independent experiments. Bacterial particle size and surface charge of phenol-inactivated bacteria (37°C, 150 rpm, 24 h) adjusted to OD_{600} = 0.2 (7,000 × *g*, 4°C, 15 min) were measured in CsCl/HEPES as elsewhere (González et al., 2008) in absence or presence of poly-L-lysine (P6516; Sigma-Aldrich, San Luis, MO, United States) in a Zetasizer Ultra (Malvern Panalytical, Malvern, United Kingdom) at 25°C, using the ZS-XPLORER v. 2.01 software (United Kingdom).

Hydrophobicity was determined by measuring bacterial adherence, using a hydrocarbons method (Rosenberg et al., 1980), modified to avoid cell degradation due to xylene toxicity (Czerwonka et al., 2016). Phenol-inactivated cultures were centrifuged (6,000 × *g*, 4°C, 10 min) and washed with a PUM buffer; then, 2 mL adjusted to OD_{470} = 1 was mixed with an equal volume of xylene (PanReac AppliChem, Castellar del Vallés, Barcelona, Spain) by triplicate. After a vortex (5 s)-incubation (37°C, 10 min)-vortex (30 s)-incubation (room temperature; RT, 2 h) step, the absorbance of the low phase was measured to determine the hydrophobicity index as: 1 – (OD_{470}/1).

Biofilm formation was studied by bacterial adhesion to polystyrene, cellular viability, and Calcofluor and Congo Red assays. Briefly, 200 μL with 5 × 10^8 CFU/ml in TSB was incubated (37°C, 3 weeks) in 96-well plates (Sarstedt) by triplicate and, after PBS washings, was stained with crystal violet (PanReac AppliChem, Castellar del Vallés, Barcelona, Spain; 0.05% in water, RT, 15 min). The stain was washed with distilled water and dissolved in ethanol (Merck, Darmstadt, Germany) to measure adhesion as OD_{600}. The viability of the attached bacteria was assessed by swabbing and culturing in BAB. EPS production was evaluated by seeding 20 μL of 10^9 CFU/ml in BAB with 0.1% Calcofluor White M2R (Sigma-Aldrich, San Luis, MO, United States) or 4% Congo Red (Merck, Darmstadt, Germany); after 3 weeks, at 37°C, the intensity of Calcofluor's fluorescence measured in a UV transilluminator (UVP) and color shift to intense red/black were visualized and quantified with ImageJ/Fiji v. 2.1 software (Schindelin et al., 2012).

The osmotic resistance was studied by incubating (37°C, 48 h) 10^4 CFU/ml in TSB: water (1:5; hypoosmotic) or in 0.5 M NaCl (Dong et al., 2015) or 0.34-M Suc (Roset et al., 2006) (VWR Chemicals, Radnor, PA, United States; hyperosmotic) by triplicate. The CFU/ml was determined in BAB to calculate the % of bacterial survival vs. the initial suspension in two independent experiments.

Susceptibility to Environmental Factors

Tolerance to desiccation was studied by keeping (RT, 6 days) a suspension (200 μL/well, 10^9 CFU/ml, TSB) completely dried by evaporation into 12-well plates (Sarstedt) by triplicate and rehydrating the pellet in PBS to determine the viable CFU/ml in BAB. Susceptibility to detergents was firstly evaluated with SDS (Merck, Darmstadt, Germany), since this surfactant inactivated all the *Brucella* tested at 0.06%; bacterial suspensions (10^4 CFU/ml, 100 μL, by triplicate) were cultured in BAB with 0.1% Triton X-100 (Sigma-Aldrich, San Luis, MO, United States). Oxidative stress and acid pH resistances were analyzed by incubating (37°C, 1 h) a 10^4 CFU/ml suspension in TSB with an equal volume (100 μL) of H_2O_2 at increasing concentrations up to 5 mM or with acidified TSB at a final pH from 7.3 to 2.3 by duplicate. Results were expressed as bacteria (%) vs. control.

Transmission Electron Microscopy

Massive *Brucella* cultures (37°C, 24 h) were harvested, washed (7,000 × *g*, 10 min) two times with sterile Sorenson's phosphate buffer pH 7.4 (Kuo, 2007) and fixed (4°C, overnight) with 2.5% glutaraldehyde (Grade I, 70%; Sigma-Aldrich San, Luis, MO, United States) and 2% paraformaldehyde (powder, Sigma-Aldrich, San Luis, MO, United States) in a buffer. Samples were adsorbed (1:200 dilution, 3 μL, 1 min) in hydrophilized carbon-coated copper grids (glow discharge 5 mA, 20 s, Leica EM ACE200). After negative staining (1% uranyl acetate, 10 s, two times), representative images were acquired (JEOL JEM 1400 Plus).

Ultra-Performance Liquid Chromatography-Mass Spectrometry

Peptidoglycan was purified from three biological replicas normalized to OD_{600} = 1 and analyzed, using 16M as control, as described elsewhere (Desmarais et al., 2013; Alvarez et al., 2016, 2020) on a Waters UPLC system (Waters Corporation, Milford, MA, United States) equipped with an ACQUITY UPLC BEH C18 Column, 130 Å, 1.7 μm, 2.1 mm × 150 mm (Waters, United States) and a dual wavelength absorbance detector. Muropeptide identity was confirmed by MS/MS analysis, using Xevo G2-XS QT of system (Waters Corporation, Milford, MA, United States). Quantification of muropeptides was based on their relative abundances normalized to the total amount of PG. Unidentified muropeptides and minor peaks with a relative abundance lower than 0.5% were excluded from further analysis.

Susceptibility to Soluble Factors of the Immune System

Susceptibility to polymyxins B and E (colistin) as a model of cationic peptides and to normal ovine serum (IdAB collection) as a source of complement after 18 h of incubation was determined by duplicate as reported (Martínez de Tejada et al., 1995; González et al., 2008). Likewise, the *in vitro* bacterial killing properties of serum from sheep immunized with Rev1Δ*wzm* (IdAB collection) were studied against *B. melitensis* 16M (S-LPS) or *B. ovis* PA (R-LPS) virulent strains; normal sheep serum and PBS or PBS-S for *B. ovis* PA were used as controls to determine survival (%) in two independent experiments.

BeWo Cells Studies

Bacterial adhesion, internalization, and intracellular multiplication in the BeWo (ATCC CCL-98; Sigma-Aldrich,

San Luis, MO, United States) trophoblast-like cell line were determined as described previously (Castañeda-Roldán et al., 2004; Salcedo et al., 2013; Poveda-Urkixo et al., 2022). Briefly, 5×10^4 cells/well were cultured in 12-well microtiter plates (Sarstedt) with an enriched F-12K medium (Kaighn's Modification) supplemented with 10% of inactivated FBS and 2-mM L-glutamine (Glutamax 100×) (Gibco). The cells were infected at an MOI of 100, and, after 30 min of incubation, the adhered bacteria were killed with Gm_{50} (1.5-h exposure). After cells lysis with 0.1% Triton X-100 (Sigma-Aldrich, San Luis, MO, United States), the number of CFU/ml was determined in both treated (intracellular) and untreated (total) wells by plating in BAB to calculate (i) adhesion as $\log_{10}$ CFU/ml = total CFU-intracellular CFU; (ii)% of internalization = (intracellular CFU/total CFU) × 100; and (iii) intracellular multiplication as $\log_{10}$ CFU/ml found at 2, 24, and 48 h.

Animal Experiments

Biosafety and Ethics Statements

Brucella and GMOs were used in the registered BSL3 facilities (code A/ES/15/I-05) of the Instituto de Agrobiotecnologìa (IdAB), previous authorization of the Spanish Consejo Interministerial de Organismos Modificados Genéticamente (CIOMG) (A/ES/16/39). BALB/c 7-week-old female or CD1 4-week-old male and female mice were purchased from Charles River (Elbeuf, France) and accommodated for 2 weeks in the authorized IdAB animal facilities (ES/31-2016-000002-CR-SU-US) before experimental proceedings. The animals were kept in biosafety cages with water and food *ad libitum* and manipulations carried out following FELASA (Rehbinder et al., 2000) and ARRIVE (Percie du Sert et al., 2020) guidelines. Procedures were based on brucellosis standards (Grilló et al., 2012) and authorized by Gobierno de Navarra (PI-025-14) in compliance with the current Spanish (RD 53/2013; ECC/566/2015) and European (Directive UE 2010/63) legislations. Churra ewes were purchased from *B. melitensis* and *B. ovis* free herds of Castilla y León, Spain, and kept in the authorized BSL2 and BSL3 facilities of the Universidad Complutense de Madrid (UCM; ES/281200000147 and ES/280790000154). Before starting the experiment, all ewes were serologically assessed as free from the main reproductive infections (i.e., *Chlamydia abortus*, *Coxiellaburnetii*, *Salmonella* Abortusovis, *Toxoplama gondii*, and Maedi-Visna). The GMOs and animal experiments were evaluated by the ethics and biosecurity committee of UCM [OH (CEA)-UCM-32-2018], CIOMG (B/ES/18/31; A/ES/20/83), and Agencia Española de Medicamentos y Productos Sanitarios (AEMPS; 194/PIV and 432/ECV). Eventual authorizations were granted by Gobierno de la Comunidad de Madrid (PROEX 187/18). Note that the use of *Brucella* Gm^R strains is no longer under restricted use since 2014, as it does not compromise the control of disease in humans or animals (Smith et al., 2015).

Spleen Infection and Cytokine Profiles in Mice

In general, the mice were inoculated IP or SC with 0.1 ml of bacterial suspension and killed by cervical dislocation at selected intervals to determine the number of viable CFU/spleen (expressed as $\log_{10}$ CFU/spleen), and the spleens weight (grams/spleen), as reported (Grilló et al., 2006b). The mice inoculated with Rev1 in standard conditions (10^5 CFU, IP or SC) or with PBS were used as controls.

A dose-response experiment was performed in the BALB/c mice inoculated IP with 10^5, 10^6, 10^7 or 10^8 CFU/mouse of Rev1Δ*wzm*, and the spleen counts/weights (n = 5) were determined at 2 weeks PI. Thereafter, with the two selected doses (10^6 and 10^8 CFU/mouse), we performed an experiment of persistence by determining the spleen counts and weights at 1, 2, 4, and/or 6 weeks PI.

For the three mutants, the kinetics of infection, weights, and cytokines in spleens were studied in groups of 14 BALB/c mice IP, inoculated with 10^8 CFU/animal (selected as optimal dose) and weekly killed (n = 3 at 1 and 4 weeks PI; n = 4 at 2 and 3 weeks PI). For cytokines, individual supernatants were obtained (1,000 × *g*, 10 min) in Hanks balanced salt solution (Gibco) treated (1 h, 4°C) with 1% CHAPS (Sigma-Aldrich, San Luis, MO, United States) and filtrated (0.20 μm, Millipore). Moreover, blood samples were collected at 2, 6, and 24 h PI (n = 5) by retro-orbital plexus puncture in mice anesthetized (ISOFLO, Ecuphar) and processed as a pool (by mixing equal volume of serum from each mouse) by analyzing each pool in duplicate; Rev1Δ*wzm*, Rev1, and PBS groups (n = 5) were analyzed in two independent experiments. Similarly, the blood samples were obtained one time a week directly prior to each necropsy and processed individually (n = 5). Sera samples and splenocytes supernatants were used to determine IL-6, IL-12p40, TNF-α, and IFN-γ using commercial ELISA kits (BD OptEIA) in two technical replicates/sample. The results were expressed as pg/spleen and pg/ml of serum.

The *in vivo* stability of Rev1Δ*wzm* was evaluated after 5 serial passages in the mice (Schurig et al., 1991). Groups of 3 CD1 mice were inoculated IP at 10^8 CFU/animal and necropsied at 3 days PI to determine the CFU/spleens. The bacteria recovered in each passage were subcultured to prepare the inocula of the next one. The genetic and phenotypic stability of the bacteria recovered from the last passage was assessed as described for the *in vitro* stability.

Vaccine Efficacy Studies

The efficacy of Rev1 *wzm*/*wzt* mutants to protect against *B. melitensis* or *B. ovis* virulent infections was analyzed in the BALB/c mice (n = 5), as reported (González et al., 2008; Soler-Lloréns et al., 2014). The mice (n = 5) were vaccinated IP or SC with 10^8 CFU of the mutant and, 4 weeks later, were challenged IP with 10^4 CFU of *B. melitensis* H38:Gm or with 5×10^5 CFU of *B. ovis* PA:Gm. Additional groups (n = 5) of Rev1 in standard conditions (10^5 CFU/animal, SC) and PBS were included as controls. The $\log_{10}$ CFU/spleen of the challenge strain was determined in BAB-Gm_{15}, or in BAB-S-Gm_{15} with incubation in 10% CO_2 at 2 or 3 weeks after challenging with H38 or *B. ovis* PA, respectively.

Safety in Pregnant Mice

Pregnancies were synchronized in the CD1 mice by light/darkness control and naturally mating for 2 days. On the day of pregnancy 4.5 ± 1, the mice were inoculated

IP with 1×10^7 CFU/mouse of Rev1Δ*wzm* (n = 14), or 1×10^6 CFU/mouse of Rev1 (n = 16) as control; 14 days later, all were necropsied to individually collect spleens, placentas, and fetuses. The CFU/g was determined by plating serial 10-fold PBS dilutions in BAB, applying external ethanol to avoid fetus-placenta cross contamination. For histopathological studies, placental tissues were fixed with 10% neutral buffered formaldehyde and stained with hematoxylin-eosin (H-E) (PanReac AppliChem, Castellar del Vallés, Barcelona, Spain).

Safety in Pregnant Ewes

Churra ewes (n = 6) were SC vaccinated on the day of gestation 75 ± 2 (DG75) with 1.8×10^{10} CFU of Rev1Δ*wzm*, including a PBS group of pregnant ewes (n = 4) as control. Clinical symptoms, rectal temperature, and local reactions were assessed during the first 2 weeks PI. Vaginal shedding was weekly monitored along the pregnancy by double-swab sampling and at parturition by collecting cotyledons and milk. The swabs were analyzed by (i) direct DNA extract and qRT-PCR of the IS*711* (Pérez-Sancho et al., 2013) and (ii) duplicate culturing in a CITA-selective medium (De Miguel et al., 2011) standard or modified by halving vancomycin and colistin concentrations, and incubation at 37°C for 7–14 days; presumptive colonies were confirmed by over-colony PCR with F1-R4*wzm* (**Supplementary Table 2**). Cotyledons homogenized in sterile PBS (1:10, w:v) and the milk samples were cultured (1 ml/plate) in these media. Within 4 weeks after delivery, all ewes and lambs were necropsied to determine bacterial presence in organs (spleen, liver, uterus, and mammary gland) and lymph nodes (pre-scapular, parotid, retropharyngeal, submaxillary, crural, iliac, and supra-mammary) by homogenization. Serological responses were weekly monitored in serum by an INgezim *B. ovis* kit (ELISA-R/LPS; Ingenasa), standard Rose Bengal test (RBT), and those reacting in RBT by S-LPS Complement Fixation test (CFT) at the officially accredited Laboratorio de Calidad Agroalimentaria de Navarra (Villava, Navarra, Spain), as recommended (OIE, 2018).

Statistical Analysis

Statistical analysis and graphical representations were performed with GraphPad Prism 8 software (Inc., San Diego, CA, United States). *P*-values were determined by unpaired two-tailed Student's *t*-test or by one- or two-way ANOVA, followed by Fisher's least significant difference (LSD) test, with 95% confidence intervals, according to data classification. For PG analysis, only variations higher than 10% were considered as significant. The final figures were assembled using Adobe Illustrator 2020 (San José, CA, United States).

DATA AVAILABILITY STATEMENT

The original contributions presented in this study are included in the article/**Supplementary Material**, further inquiries can be directed to the corresponding author.

ETHICS STATEMENT

Mice studies were reviewed and approved by Comité de Ética, Experimentación Animal y Bioseguridad (CEEAB) of Public University of Navarra (UPNA), Comité de Ética of CSIC, and the competent authority of Navarra Government; and sheep experiments were approved by the Ethics and Biosecurity Committee of Universidad Complutense de Madrid (UCM) and the competent authority of Comunidad de Madrid.

AUTHOR CONTRIBUTIONS

MG conceived, led, and supervised the study. SM-B designed and performed experiments. IP-U performed experiments in cells and pregnant mice. SM-B and MG carried out other mice experiments, and wrote the draft and the final manuscript. SM-B, IP-U, and MG participated in the sheep assay. SM-B, AZ-B, and LP contributed to mutants' construction and to design some *in vitro* experiments. OI and FC performed UPLC-MS, and analyzed and discussed the results. SM-B, IP-U, AZ-B, and MG analyzed, discussed, and interpreted all results. All the authors revised and approved the final document for publication.

FUNDING

This work was funded by Agencia Estatal de Investigación of the Ministerio de Ciencia, Innovación y Universidades (AGL2014-58795-C4-2-R and RTI2018-098658-B-C21), Gobierno de Navarra (PT040-2018 and PT007-2019) projects. SM-B contracts were granted by the FEDER 2016–2018 program of Garantía Juvenil and by an UPNA pre-doctoral fellowship 2018–2022. IP-U Doctorados Industriales contract was cofounded by Gobierno de Navarra and CSIC. Research in the FC lab was supported by The Swedish Research Council (VR), The Knut and Alice Wallenberg Foundation (KAW), The Laboratory of Molecular Infection Medicine Sweden (MIMS), and The Kempe Foundation. The funders had no role in study design, data collection and analysis, decision to publish, or preparation of the manuscript.

ACKNOWLEDGMENTS

We thank the technical support provided by Itziar Alkorta, Ricardo Andrade, and Loli Martín (SGIker, Universidad del País Vasco, Spain), the NED research group of VISAVET (Universidad Complutense de Madrid, Spain), Montse Barberán (Universidad de Zaragoza, Spain), Manuel Barrón (Laboratorio de Calidad Alimentaria de Navarra, Villava, Spain), and Goizeder Almagro (IdAB-CSIC staff). We also thank John Wild for the English revision of the manuscript.

SUPPLEMENTARY MATERIAL

The Supplementary Material for this article can be found online at: https://www.frontiersin.org/articles/10.3389/fmicb.2022.908495/full#supplementary-material

REFERENCES

Alton, G. G., Jones, L., Angus, R., and Verger, J. (1988). *Techniques for the Brucellosis Laboratory*. Paris: Institut National de la Recherche Agronomique.

Altschul, S. F., Gish, W., Miller, W., Myers, E. W., and Lipman, D. J. (1990). Basic local alignment search tool. *J. Mol. Biol.* 215, 403–10. doi: 10.1016/S0022-2836(05)80360-2

Alvarez, L., Cordier, B., van Teeffelen, S., and Cava, F. (2020). Analysis of Gram-negative bacteria peptidoglycan by ultra-performance liquid chromatography. *Bio-Protocol* 10, 1–14. doi: 10.21769/bioprotoc.3780

Alvarez, L., Hernandez, S. B., De Pedro, M. A., and Cava, F. (2016). Ultra-sensitive, high-resolution liquid chromatography methods for the high-throughput quantitative analysis of bacterial cell wall chemistry and structure. *Methods Mol. Biol.* 1440, 11–27. doi: 10.1007/978-1-4939-3676-2_2

Aragón-Aranda, B., De Miguel, M. J., Lázaro-Antón, L., Salvador-Bescós, M., Zúñiga-Ripa, A., Moriyón, I., et al. (2020). Development of attenuated live vaccine candidates against swine brucellosis in a non-zoonotic *B. suis* biovar 2 background. *Vet. Res.* 51:8. doi: 10.1186/s13567-020-00815-8

Arellano-Reynoso, B., Lapaque, N., Salcedo, S., Briones, G., Ciocchini, A. E., Ugalde, R., et al. (2005). Cyclic β-1,2-glucan is a *Brucella* virulence factor required for intracellular survival. *Nat. Immunol.* 6, 618–25. doi: 10.1038/ni1202

Ariza, J., Bosch, J., Gudiol, F., Liñares, J., Viladrich, P. F., and Martín, R. (1986). Relevance of *in vitro* antimicrobial susceptibility of *Brucella melitensis* to relapse rate in human brucellosis. *Antimicrob. Agents Chemother.* 30, 958–60. doi: 10.1128/AAC.30.6.958

Atun, G., Hisarli, G., and Tunçay, M. (1998). Adsorption of safranine-O on hydrophilic and hydrophobic glass surfaces. *Colloids Surfaces A Physicochem. Eng. Asp.* 143, 27–33. doi: 10.1016/S0927-7757(98)00494-4

Avila-Calderón, E. D., Medina-Chávez, O., Flores-Romo, L., Hernández-Hernández, J. M., Donis-Maturano, L., López-Merino, A., et al. (2020). Outer membrane vesicles from *Brucella melitensis* modulate immune response and induce cytoskeleton rearrangement in peripheral blood mononuclear cells. *Front. Microbiol.* 11:1–18. doi: 10.3389/fmicb.2020.556795

Baldwin, C. L., and Goenka, R. (2006). Host immune responses to the intracellular bacteria *Brucella*: does the bacteria instruct the host to facilitate chronic infection? *Crit. Rev. Immunol.* 26, 407–42. doi: 10.1615/CritRevImmunol.v26.i5.30

Barrio, M. B., Grilló, M. J., Muñoz, P. M., Jacques, I., González, D., De Miguel, M. J., et al. (2009). Rough mutants defective in core and O-polysaccharide synthesis and export induce antibodies reacting in an indirect ELISA with smooth lipopolysaccharide and are less effective than Rev 1 vaccine against *Brucella melitensis* infection of sheep. *Vaccine* 27, 1741–9. doi: 10.1016/j.vaccine.2009.01.025

Bi, Y., and Zimmer, J. (2020). Structure and ligand-binding properties of the O antigen ABC transporter carbohydrate-binding domain. *Structure* 28, 252.e–8.e. doi: 10.1016/j.str.2019.11.020

Bi, Y., Mann, E., Whitfield, C., and Zimmer, J. (2018). Architecture of a channel-forming O-antigen polysaccharide ABC transporter. *Nature* 553, 361–5. doi: 10.1038/nature25190

Blasco, J. M. (1997). A review of the use of *B. melitensis* Rev 1 vaccine in adult sheep and goats. *Prev. Vet. Med.* 31, 275–83. doi: 10.1016/s0167-5877(96)01110-5

Blasco, J. M., and Díaz, R. (1993). *Brucella melitensis* Rev-1 vaccine as a cause of human brucellosis. *Lancet* 342:805. doi: 10.1016/0140-6736(93)91571-3

Bosseray, N., and Plommet, M. (1990). *Brucella suis* S2, *Brucella melitensis* Rev. 1 and *Brucella abortus* S19 living vaccines: residual virulence and immunity induced against three *Brucella* species challenge strains in mice. *Vaccine* 8, 462–8. doi: 10.1016/0264-410X(90)90247-J

Briones, G., Iñón de Iannino, N., Roset, M., Vigliocco, A., Silva Paulo, P., and Ugalde, R. A. (2001). *Brucella abortus* cyclic β-1,2-glucan mutants have reduced virulence in mice and are defective in intracellular replication in HeLa cells. *Infect. Immun.* 69, 4528–35. doi: 10.1128/IAI.69.7.4528-4535.2001

Caffalette, C. A., and Zimmer, J. (2021). Cryo-EM structure of the full-length Wzm/Wzt ABC transporter required for lipid-linked O antigen transport. *Proc. Natl. Acad. Sci. U S A.* 118, 1–10. doi: 10.1073/pnas.2016144118

Caffalette, C. A., Kuklewicz, J., Spellmon, N., and Zimmer, J. (2020). Biosynthesis and export of bacterial glycolipids. *Annu. Rev. Biochem.* 89, 741–68. doi: 10.1146/annurev-biochem-011520-104707

Caro-Hernández, P., Fernández-Lago, L., De Miguel, M. J., Martín-Martín, A. I., Cloeckaert, A., Grilló, M. J., et al. (2007). Role of the Omp25/Omp31 family in outer membrane properties and virulence of *Brucella ovis*. *Infect. Immun.* 75, 4050–61. doi: 10.1128/IAI.00486-07

Castañeda-Roldán, E. I., Avelino-Flores, F., Dall'Agnol, M., Freer, E., Cedillo, L., Dornand, J., et al. (2004). Adherence of *Brucella* to human epithelial cells and macrophages is mediated by sialic acid residues. *Cell. Microbiol.* 6, 435–45. doi: 10.1111/j.1462-5822.2004.00372.x

Cheung, C., Lee, J., Lee, J., and Shevchuk, O. (2009). The effect of ionic (NaCl) and non-ionic (sucrose) osmotic stress on the expression of β-galactosidase in wild type *E.coli* BW25993 and in the isogenic BW25993Δ*lacI* mutant. *J. Exp. Microbiol. Immunol.* 13, 1–6.

Clarke, B. R., Cuthbertson, L., and Whitfield, C. (2004). Nonreducing terminal modifications determine the chain length of polymannose O antigens of *Escherichia coli* and couple chain termination to polymer export *via* an ATP-binding cassette transporter. *J. Biol. Chem.* 279, 35709–18. doi: 10.1074/jbc.M404738200

Clifton, L. A., Ciesielski, F., Skoda, M. W. A., Paracini, N., Holt, S. A., and Lakey, J. H. (2016). The effect of lipopolysaccharide core oligosaccharide size on the electrostatic binding of antimicrobial proteins to models of the Gram-negative bacterial outer membrane. *Langmuir* 32, 3485–94. doi: 10.1021/acs.langmuir.6b00240

Conde-Álvarez, R., Arce-Gorvel, V., Iriarte, M., Manček-Keber, M., Barquero-Calvo, E., Palacios-Chaves, L., et al. (2012). The lipopolysaccharide core of *Brucella abortus* acts as a shield against innate immunity recognition. *PLoS Pathog.* 8:e1002675. doi: 10.1371/journal.ppat.1002675

Cuthbertson, L., Kimber, M. S., and Whitfield, C. (2007). Substrate binding by a bacterial ABC transporter involved in polysaccharide export. *Proc. Natl. Acad. Sci.* 104, 19529–34. doi: 10.1073/pnas.0705709104

Cuthbertson, L., Powers, J., and Whitfield, C. (2005). The C-terminal domain of the nucleotide-binding domain protein Wzt determines substrate specificity in the ATP-binding cassette transporter for the lipopolysaccharide O-antigens in *Escherichia coli* serotypes O8 and O9a. *J. Biol. Chem.* 280, 30310–9. doi: 10.1074/jbc.M504371200

Czerwonka, G., Guzy, A., Kałuża, K., Grosicka, M., Dańczuk, M., Lechowicz, Ł., et al. (2016). The role of *Proteus mirabilis* cell wall features in biofilm formation. *Arch. Microbiol.* 198, 877–84. doi: 10.1007/s00203-016-1249-x

De Miguel, M. J., Marín, C. M., Muñoz, P. M., Dieste, L., Grilló, M. J., and Blasco, J. M. (2011). Development of a selective culture medium for primary isolation of the main *Brucella* species. *J. Clin. Microbiol.* 49, 1458–63. doi: 10.1128/JCM.02301-10

Desmarais, S. M., De Pedro, M. A., Cava, F., and Huang, K. C. (2013). Peptidoglycan at its peaks: how chromatographic analyses can reveal bacterial cell wall structure and assembly. *Mol. Microbiol.* 89, 1–13. doi: 10.1111/mmi.12266

Dohnalkova, A. C., Marshall, M. J., Arey, B. W., Williams, K. H., Buck, E. C., and Fredrickson, J. K. (2011). Imaging hydrated microbial extracellular polymers: comparative analysis by electron microscopy. *Appl. Environ. Microbiol.* 77, 1254–62. doi: 10.1128/AEM.02001-10

Dong, H., Liu, W., Peng, X., and Wu, Q. (2015). The effects of RegM on stress responses in *Brucella melitensis*. *Curr. Microbiol.* 70, 730–4. doi: 10.1007/s00284-015-0782-1

Dorneles, E. M. S., Teixeira-Carvalho, A., Araújo, M. S. S., Sriranganathan, N., and Lage, A. P. (2015). Immune response triggered by *Brucella abortus* following infection or vaccination. *Vaccine* 33, 3659–66. doi: 10.1016/j.vaccine.2015.05.057

EUCAST: European Committee for Antimicrobial Susceptibility Testing. (2003). *Determination of Minimum Inhibitory Concentrations (MICs) of Antibacterial Agents by Broth Dilution*. Central Hospital Växjö: EUCAST.

Fletcher, M., and Loeb, G. I. (1979). Influence of substratum characteristics on the attachment of a marine *Pseudomonas* to solid surfaces. *Appl. Environ. Microbiol.* 37, 67–72. doi: 10.1128/aem.37.1.67-72.1979

Fontana, C., Conde-Álvarez, R., Ståhle, J., Holst, O., Iriarte, M., Zhao, Y., et al. (2016). Structural studies of lipopolysaccharide-defective mutants from *Brucella melitensis* identify a core oligosaccharide critical in virulence. *J. Biol. Chem.* 291, 7727–41. doi: 10.1074/jbc.M115.701540

Gamazo, C., and Moriyón, I. (1987). Release of outer membrane fragments by exponentially growing *Brucella melitensis* cells. *Infect. Immun.* 55, 609–15. doi: 10.1128/iai.55.3.609-615.1987

Godefroid, M., Svensson, M. V., Cambier, P., Uzureau, S., Mirabella, A., De Bolle, X., et al. (2010). *Brucella melitensis* 16M produces a mannan and other extracellular matrix components typical of a biofilm. *FEMS Immunol. Med. Microbiol.* 59, 364–77. doi: 10.1111/j.1574-695X.2010.00689.x

Godessart, P., Lannoy, A., Dieu, M., Van der Verren, S. E., Soumillion, P., Collet, J. F., et al. (2021). β-barrels covalently link peptidoglycan and the outer membrane in the α-proteobacterium *Brucella abortus*. *Nat. Microbiol.* 6, 27–33. doi: 10.1038/s41564-020-00799-3

Godfroid, F., Cloeckaert, A., Taminiau, B., Danese, I., Tibor, A., De Bolle, X., et al. (2000). Genetic organisation of the lipopolysaccharide O-antigen biosynthesis region of *Brucella melitensis* 16M (*wbk*). *Res. Microbiol.* 151, 655–68. doi: 10.1016/s0923-2508(00)90130-x

Goldberg, J. B. (1999). *Genetics of Bacterial Polysaccharides*, 1st Edn. Boca Raton, FL: CRC Press LLC, doi: 10.1201/9781420074413

González, D., Grilló, M. J., De Miguel, M. J., Ali, T., Arce-Gorvel, V., Delrue, R. M., et al. (2008). Brucellosis vaccines: assessment of *Brucella melitensis* lipopolysaccharide rough mutants defective in core and O-polysaccharide synthesis and export. *PLoS One* 3:e2760. doi: 10.1371/journal.pone.0002760

Grilló, M. J., Blasco, J. M., Gorvel, J., Moriyón, I., and Moreno, E. (2012). What have we learned from brucellosis in the mouse model? *Vet. Res.* 43, 1–35. doi: 10.1186/1297-9716-43-29

Grilló, M. J., Bosseray, N., and Blasco, J. M. (2000). *In vitro* markers and biological activity in mice of seed lot strains and commercial *Brucella melitensis* Rev 1 and *Brucella abortus* B19 vaccines. *Biologicals* 28, 119–27. doi: 10.1006/biol.2000.0249

Grilló, M. J., Manterola, L., De Miguel, M. J., Muñoz, P. M., Blasco, J. M., Moriyón, I., et al. (2006b). Increases of efficacy as vaccine against *Brucella abortus* infection in mice by simultaneous inoculation with avirulent smooth *bvrS*/*bvrR* and rough *wbkA* mutants. *Vaccine* 24, 2910–6. doi: 10.1016/j.vaccine.2005.12.038

Grilló, M. J., De Miguel, M. J., Muñoz, P. M., Marín, C. M., Ariza, J., and Blasco, J. M. (2006a). Efficacy of several antibiotic combinations against *Brucella melitensis* Rev 1 experimental infection in BALB/c mice. *J. Antimicrob. Chemother.* 58, 622–6. doi: 10.1093/jac/dkl289

Grilló, M. J., San Román Aberasturi, B., Palacios Chaves, L., Mena Bueno, S., and Zabalza Baranguá, A. (2017). *A Modified Brucella Vaccine Strain for the Treatment of Brucellosis*. Madrid: Consejo Superior de Investigaciones Científicas.

Guidolin, L. S., Morrone Seijo, S. M., Guaimas, F. F., Comerci, D. J., and Ciocchinia, A. E. (2015). Interaction network and localization of *Brucella abortus* membrane proteins involved in the synthesis, transport, and succinylation of cyclic β-1,2-glucans. *J. Bacteriol.* 197, 1640–8. doi: 10.1128/JB.00068-15

Guo, R., Jiao, Y., Li, Z., Zhu, S., Fei, X., Geng, S., et al. (2017). Safety, protective immunity, and DIVA capability of a rough mutant *Salmonella* Pullorum vaccine candidate in broilers. *Front. Microbiol.* 8:1–10. doi: 10.3389/fmicb.2017.00547

Haag, A. F., Myka, K. K., Arnold, M. F. F., Caro-Hernández, P., and Ferguson, G. P. (2010). Importance of lipopolysaccharide and cyclic β-1,2-glucans in *Brucella*-mammalian infections. *Int. J. Microbiol.* 2010, 1–12. doi: 10.1155/2010/124509

Hagelueken, G., Clarke, B. R., Huang, H., Tuukkanen, A., Danciu, I., Svergun, D. I., et al. (2015). A coiled-coil domain acts as a molecular ruler to regulate O-antigen chain length in lipopolysaccharide. *Nat. Struct. Mol. Biol.* 22, 50–6. doi: 10.1038/nsmb.2935

Hensel, M. E., Garcia-Gonzalez, D. G., Chaki, S. P., Hartwig, A., Gordy, P. W., Bowen, R., et al. (2020). Vaccine candidate *Brucella melitensis* 16MΔ*vjbR* is safe in a pregnant sheep model and confers protection. *mSphere* 5:20. doi: 10.1128/msphere.00120-20

Hug, I., and Feldman, M. F. (2011). Analogies and homologies in lipopolysaccharide and glycoprotein biosynthesis in bacteria. *Glycobiology* 21, 138–51. doi: 10.1093/glycob/cwq148

Issa, M. N., and Ashhab, Y. (2016). Identification of *Brucella melitensis* Rev.1 vaccine-strain genetic markers: towards understanding the molecular mechanism behind virulence attenuation. *Vaccine* 34, 4884–91. doi: 10.1016/j.vaccine.2016.08.059

Izquierdo, L., Merino, S., Regué, M., Rodriguez, F., and Tomás, J. M. (2003). Synthesis of a *Klebsiella pneumoniae* O-antigen heteropolysaccharide (O12) requires an ABC 2 transporter. *J. Bacteriol.* 185, 1634–41. doi: 10.1128/JB.185.5.1634-1641.2003

Jain-Gupta, N., Waldrop, S. G., Tenpenny, N. M., Witonsky, S. G., Boyle, S. M., and Sriranganathan, N. (2019). Rough *Brucella neotomae* provides protection against *Brucella suis* challenge in mice. *Vet. Microbiol.* 239:108447. doi: 10.1016/j.vetmic.2019.108447

Jankowski, A., Jankowski, S., Mirończyk, A., and Niedbach, J. (2005). The action of photosensitizers and serum in a bactericidal process. II. The effects of dyes: hypericin, eosin Y and saphranine O. *Polish J. Microbiol.* 54, 323–30.

Jiménez de Bagüés, M. P., Marín, C. M., Barberán, M., and Blasco, J. M. (1989). Responses of ewes to *B. melitensis* Rev1 vaccine administered by subcutaneous or conjunctival routes at different stages of pregnancy. *Ann. Rech. Vet.* 20, 205–13.

Johnson, Z. I., and Chisholm, S. W. (2004). Properties of overlapping genes are conserved across microbial genomes. *Genome Res.* 14, 2268–72. doi: 10.1101/gr.2433104

Kamens, J. (2015). The Addgene repository: an international nonprofit plasmid and data resource. *Nucleic Acids Res.* 43, D1152–7. doi: 10.1093/nar/gku893

Kanehisa, M., and Goto, S. (2000). KEGG: kyoto encyclopedia of genes and genomes. *Nucleic Acids Res.* 28, 27–30. doi: 10.1093/nar/28.1.27

Kohanski, M. A., Dwyer, D. J., and Collins, J. J. (2010). How antibiotics kill bacteria: from targets to networks. *Nat. Rev. Microbiol.* 8, 423–35. doi: 10.1038/nrmicro2333

Kornspan, D., Lubkovskaia, R., Mathur, S., Yeheskel, A., and Salmon-Divon, M. (2020). Genomic analysis of natural rough *Brucella melitensis* Rev.1 vaccine strains: identification and characterization of mutations in key genes associated with bacterial lps biosynthesis and virulence. *Int. J. Mol. Sci.* 21, 1–15. doi: 10.3390/ijms21249341

Kreutzer, D. L., Scheffel, J. W., Draper, L. R., and Robertson, D. C. (1977). Mitogenic activity of cell wall components from smooth and rough strains of *Brucella abortus*. *Infect. Immun.* 15, 842–5. doi: 10.1128/iai.15.3.842-845.1977

Kuo, J. (2007). *Electron Microscopy: Methods and Protocols*, 2nd Edn. Totowa,NJ: Humana Press Inc, doi: 10.1007/978-1-62703-776-1

Lalsiamthara, J., Kaur, G., Gogia, N., Ali, S. A., Goswami, T. K., and Chaudhuri, P. (2020). *Brucella abortus* S19 *rfbD* mutant is highly attenuated, DIVA enable and confers protection against virulent challenge in mice. *Biologicals* 63, 62–7. doi: 10.1016/j.biologicals.2019.11.005

Lepage, S., Lakaye, B., Galleni, M., Thamm, I., Crine, M., Groslambert, S., et al. (1995). Saturation of penicillin-binding protein 1 by β—lactam antibiotics in growing cells of *Bacillus licheniformis*. *Mol. Microbiol.* 16, 365–72. doi: 10.1111/j.1365-2958.1995.tb02308.x

Lerouge, I., Laeremans, T., Verreth, C., Vanderleyden, J., Van Soom, C., Tobin, A., et al. (2001). Identification of an ATP-binding cassette transporter for export of the O-antigen across the inner membrane in *Rhizobium etli* based on the genetic, functional, and structural analysis of an LPS mutant deficient in O-antigen. *J. Biol. Chem.* 276, 17190–8. doi: 10.1074/jbc.M101129200

Livermore, D. M. (1987). Mechanisms of resistance to cephalosporin antibiotics. *Drugs* 34, 64–88. doi: 10.2165/00003495-198700342-00007

Mancilla, M., Grilló, M. J., De Miguel, M. J., López-Goñi, I., San-Román, B., Zabalza-Baranguá, A., et al. (2013). Deletion of the GI-2 integrase and the *wbkA* flanking transposase improves the stability of *Brucella melitensis* Rev 1 vaccine. *Vet. Res.* 44, 1–12. doi: 10.1186/1297-9716-44-105

Martínez de Tejada, G., Pizarro-Cerdá, J., Moreno, E., and Moriyón, I. (1995). The outer membranes of *Brucella* spp. are resistant to bactericidal cationic peptides. *Infect. Immun.* 63, 3054–61. doi: 10.1128/iai.63.8.3054-3061

Mirabella, A., Terwagne, M., Zygmunt, M. S., Cloeckaert, A., De Bolle, X., and Letesson, J. J. (2013). *Brucella melitensis* MucR, an orthologue of *Sinorhizobium meliloti* MucR, is involved in resistance to oxidative, detergent, and saline stresses and cell envelope modifications. *J. Bacteriol.* 195, 453–65. doi: 10.1128/JB.01336-12

Mohammad, M. M., Tomita, N., Ohta, M., and Movileanu, L. (2016). The transmembrane domain of a bicomponent ABC transporter exhibits channel-forming activity. *ACS Chem. Biol.* 11, 2506–18. doi: 10.1021/acschembio.6b00383

Monreal, D., Grilló, M. J., González, D., Marín, C. M., De Miguel, M. J., López-Goñi, I., et al. (2003). Characterization of *Brucella abortus* O-polysaccharide

and core lipopolysaccharide mutants and demonstration that a complete core is required for rough vaccines to be efficient against *Brucella abortus* and *Brucella ovis* in the mouse model. *Infect. Immun.* 71, 3261–71. doi: 10.1128/IAI.71.6.3261-3271.2003

Montaraz, J. A., Winter, A. J., Hunter, D. M., Sowa, B. A., Wu, A. M., and Adams, L. G. (1986). Protection against *Brucella abortus* in mice with O-polysaccharide-specific monoclonal antibodies. *Infect. Immun.* 51, 961–3. doi: 10.1128/iai.51.3.961-963.1986

Moosavian, M., Emam, N., Pletzer, D., and Savari, M. (2020). Rough-type and loss of the LPS due to *lpx* genes deletions are associated with colistin resistance in multidrug-resistant clinical *Escherichia coli* isolates not harbouring *mcr* genes. *PLoS One* 15:1–14. doi: 10.1371/journal.pone.0233518

Morè, N., Martorana, A. M., Biboy, J., Otten, C., Winkle, M., Gurnani Serrano, C. K., et al. (2019). Peptidoglycan remodeling enables *Escherichia coli* to survive severe outer membrane assembly defect. *MBio* 10, e2729–2718.

Moriyón, I., Grilló, M. J., Monreal, D., González, D., Marín, C., López-Goñi, I., et al. (2004). Rough vaccines in animal brucellosis: structural and genetic basis and present status. *Vet. Res.* 35, 1–38. doi: 10.1051/vetres:2003037

Nakao, R., Ramstedt, M., Wai, S. N., and Uhlin, B. E. (2012). Enhanced biofilm formation by *Escherichia coli* LPS mutants defective in Hep biosynthesis. *PLoS One* 7:1–13. doi: 10.1371/journal.pone.0051241

Nikaido, H., and Vaara, M. (1985). Molecular basis of bacterial outer membrane permeability. *N Y. State J. Med.* 49, 1–32. doi: 10.1128/mr.49.1.1-32.1985

OIE (2018). "Chapter 3.1.4: Brucellosis (*Brucella abortus*, *B. melitensis* and *B. suis*) (Infection with *B. abortus*, *B. melitensis* and *B. suis*)," in *Office International of Epizooties, World Organisation for Animal Health. Manual of Diagnostic Tests and Vaccines for Terrestrial Animals*. (Paris: World Organisation for Animal Health).

Percie du Sert, N., Hurst, V., Ahluwalia, A., Alam, S., Avey, M. T., Baker, M., et al. (2020). The ARRIVE guidelines 2.0: updated guidelines for reporting animal research. *PLoS Biol.* 18:e3000410. doi: 10.1371/journal.pbio.3000410

Perevoshchikova, I. V., Sorochkina, A. I., Zorov, D. B., and Antonenko, Y. N. (2009). Safranine O as a fluorescent probe for mitochondrial membrane potential studied on the single particle level and in suspension. *Biochem* 74, 663–71. doi: 10.1134/s000629790906011x

Pérez-Sancho, M., García-Seco, T., Arrogante, L., García, N., Martínez, I., Diez-Guerrier, A., et al. (2013). Development and evaluation of an IS*711*-based loop mediated isothermal amplification method (LAMP) for detection of *Brucella* spp. on clinical samples. *Res. Vet. Sci.* 95, 489–94. doi: 10.1016/j.rvsc.2013.05.002

Peters, K., Pazos, M., Edoo, Z., Hugonnet, J. E., Martorana, A. M., Polissi, A., et al. (2018). Copper inhibits peptidoglycan LD-transpeptidases suppressing β-lactam resistance due to bypass of penicillin-binding proteins. *Proc. Natl. Acad. Sci. U S A.* 115, 10786–91. doi: 10.1073/pnas.1809285115

Pilizota, T., and Shaevitz, J. W. (2013). Plasmolysis and cell shape depend on solute outer-membrane permeability during hyperosmotic shock in *E. coli*. *Biophys. J.* 104, 2733–42. doi: 10.1016/j.bpj.2013.05.011

Popescu, A., and Doyle, R. (1996). The Gram stain after more than a century. *Biotech. Histochem.* 71, 145–51. doi: 10.1016/S0246-0343(10)19912-2

Poveda-Urkixo, I., Ramírez, G. A., and Grilló, M.-J. (2022). Kinetics of placental infection by different smooth *Brucella* strains in mice. *Pathogens* 11, 1–17. doi: 10.3390/PATHOGENS11030279

Quandt, J., and Hynes, M. F. (1993). Versatile suicide vectors which allow direct selection for gene replacement in Gram-negative bacteria. *Gene* 127, 15–21. doi: 10.1016/0378-1119(93)90611-6

Rehbinder, C., Alenius, S., Bures, J., De las Heras, M., Greko, C., Kroon, P. S., et al. (2000). FELASA recommendations for the health monitoring of experimental units of calves, sheep and goats - Report of the federation of European Laboratory Animal Science Associations (FELASA) Working Group on Animal Health. *Lab. Anim.* 34, 329–50. doi: 10.1258/002367700780387723

Rocchetta, H. L., and Lam, J. S. (1997). Identification and functional characterization of an ABC transport system involved in polysaccharide export of A-band lipopolysaccharide in *Pseudomonas aeruginosa*. *J. Bacteriol.* 179, 4713–24. doi: 10.1128/jb.179.15.4713-4724.1997

Rosenberg, M., Gutnick, D., and Rosenberg, E. (1980). Adherence of bacteria to hydrocarbons: a simple method for measuring cell-surface hydrophobicity. *FEMS Microbiol. Lett.* 9, 29–33. doi: 10.1111/j.1574-6968.1980.tb05599.x

Roset, M. S., Ciocchini, A. E., Ugalde, R. A., and Iñón de Iannino, N. (2006). The *Brucella abortus*cyclic β-1,2-glucan virulence factor is substituted with O-ester-linked succinyl residues. *J. Bacteriol.* 188, 5003–13. doi: 10.1128/JB.00086-06

Roset, M. S., Ibañez, A. E., De Souza Filho, J. A., Spera, J. M., Minatel, L., Oliveira, S. C., et al. (2014). *Brucella* cyclic B-1,2-glucan plays a critical role in the induction of splenomegaly in mice. *PLoS One* 9:1–9. doi: 10.1371/journal.pone.0101279

Ruiz-Palma, M., del, S., Avila-Calderón, E. D., Aguilera-Arreola, M. G., López-Merino, A., Ruiz, E. A., et al. (2021). Comparative proteomic analysis of outer membrane vesicles from *Brucella suis*, *Brucella ovis*, *Brucella canis* and *Brucella neotomae*. *Arch. Microbiol.* 203, 1611–26. doi: 10.1007/s00203-020-02170-w

Salcedo, S. P., Chevrier, N., Lacerda, T. L. S., Ben Amara, A., Gerart, S., Gorvel, V. A., et al. (2013). Pathogenic brucellae replicate in human trophoblasts. *J. Infect. Dis.* 207, 1075–83. doi: 10.1093/infdis/jit007

Salmon-Divon, M., Yeheskel, A., and Kornspan, D. (2018). Genomic analysis of the original Elberg *Brucella melitensis* Rev.1 vaccine strain reveals insights into virulence attenuation. *Lab. Anim.* 9, 1436–48. doi: 10.1080/21505594.2018.1511677

Salmon-Divon, M., Zahavi, T., and Kornspan, D. (2019). Transcriptomic analysis of the *Brucella melitensis* Rev.1 vaccine strain in an acidic environment: insights into virulence attenuation. *Front. Microbiol.* 10:1–12. doi: 10.3389/fmicb.2019.00250

Sancho, P., Tejedor, C., Sidhu-Muñoz, R. S., Fernández-Lago, L., and Vizcaíno, N. (2014). Evaluation in mice of *Brucella ovis* attenuated mutants for use as live vaccines against *B. ovis* infection. *Vet. Res.* 45, 1–10. doi: 10.1186/1297-9716-45-61

Sayers, E. W., Bolton, E. E., Brister, J. R., Canese, K., Chan, J., Comeau, D. C., et al. (2022). Database resources of the National Center for Biotechnology Information (NCBI). *Nucleic Acids Res.* 50, D20–6. doi: 10.1093/nar/gkab1112

Schindelin, J., Arganda-Carreras, I., Frise, E., Kaynig, V., Longair, M., Pietzsch, T., et al. (2012). Fiji: an open-source platform for biological-image analysis. *Nat. Methods* 9, 676–82. doi: 10.1038/nmeth.2019

Schurig, G. G., Roop, R. M., Bagchi, T., Boyle, S., Buhrman, D., and Sriranganathan, N. (1991). Biological properties of RB51; a stable rough strain of *Brucella abortus*. *Vet. Microbiol.* 28, 171–88. doi: 10.1016/0378-1135(91)90091-S

Schurig, G. G., Sriranganathan, N., and Corbel, M. J. (2002). Brucellosis vaccines: past, present and future. *Vet. Microbiol.* 90, 479–96. doi: 10.1016/S0378-1135(02)00255-9

Schuster, C. F., Wiedemann, D. M., Kirsebom, F. C. M., Santiago, M., Walker, S., and Gründling, A. (2020). High-throughput transposon sequencing highlights the cell wall as an important barrier for osmotic stress in methicillin resistant *Staphylococcus aureus* and underlines a tailored response to different osmotic stressors. *Mol. Microbiol.* 113, 699–717. doi: 10.1111/mmi.14433

Scupham, A. J., and Triplett, E. W. (1997). Isolation and characterization of the UDP-glucose 4'-epimerase-encoding gene, *galE*, from *Brucella abortus* 2308. *Gene* 202, 53–9. doi: 10.1016/s0378-1119(97)00453-8

Shabala, L., Bowman, J., Brown, J., Ross, T., McMeekin, T., and Shabala, S. (2009). Ion transport and osmotic adjustment in *Escherichia coli* in response to ionic and non-ionic osmotica. *Environ. Microbiol.* 11, 137–48. doi: 10.1111/j.1462-2920.2008.01748.x

Singh, D. R., Mohammad, M. M., Patowary, S., Stoneman, M. R., Oliver, J. A., Movileanu, L., et al. (2013). Determination of the quaternary structure of a bacterial ATP-binding cassette (ABC) transporter in living cells. *Integr. Biol.* 5, 312–23. doi: 10.1039/C2IB20218B

Smith, J., Gangadharan, D., and Weyant, R. (2015). Review of restricted experiment requests, division of select agents and toxins, centers for disease control and prevention, 2006-2013. *Health Secur.* 13, 307–16. doi: 10.1089/hs.2015.0021

Solanki, K. S., Varshney, R., Qureshi, S., Thomas, P., Singh, R., Agrawal, A., et al. (2021). Non-infectious outer membrane vesicles derived from *Brucella abortus* S19Δ*per* as an alternative acellular vaccine protects mice against virulent challenge. *Int. Immunopharmacol.* 90:107148. doi: 10.1016/j.intimp.2020.107148

Soler-Lloréns, P., Gil-Ramírez, Y., Zabalza-Baranguá, A., Iriarte, M., Conde-Álvarez, R., Zúñiga-Ripa, A., et al. (2014). Mutants in the lipopolysaccharide of *Brucella ovis* are attenuated and protect against *B. ovis* infection in mice. *Vet. Res.* 45, 1–11. doi: 10.1186/s13567-014-0072-0

Spink, W. W., and Anderson, D. (1954). Experimental studies on the significance of endotoxin in the pathogenesis of brucellosis. *J. Clin. Invest.* 33, 540–8. doi: 10.1172/JCI102924

Spink, W. W., Hall, J. W., Finstad, J., and Mallet, E. (1962). Immunization with viable *Brucella* organisms. Results of a safety test in humans. *Bull. World Health Organ.* 26, 409–19.

Stranahan, L. W., and Arenas-Gamboa, A. M. (2021). When the going gets rough: the significance of *Brucella* lipopolysaccharide phenotype in host-pathogen interactions. *Front. Microbiol.* 12:713157. doi: 10.3389/fmicb.2021.713157

Tsai, C. M., and Frasch, C. E. (1982). A sensitive silver stain for detecting lipopolysaccharides in polyacrylamide gels. *Anal. Biochem.* 119, 115–9. doi: 10.1016/0003-2697(82)90673-X

Uzureau, S., Godefroid, M., Deschamps, C., Lemaire, J., De Bolle, X., and Letesson, J. J. (2007). Mutations of the quorum sensing-dependent regulator VjbR lead to drastic surface modifications in *Brucella melitensis*. *J. Bacteriol.* 189, 6035–47. doi: 10.1128/JB.00265-07

Vaara, M. (1992). Agents that increase the permeability of the outer membrane. *Microbiol. Rev.* 56, 395–411. doi: 10.1093/jac/dkq040

Valvano, M. A. (2003). Export of O-specific lipopolysaccharide. *Front. Biosci.* 8:452–71. doi: 10.2741/1079

Valvano, M. A. (2015). "Chapter 4. Genetics and biosynthesis of lipopolysaccharide," in *Molecular Medical Microbiology*, 2nd Edn. (Amsterdam: Elsevier Ltd), 55–89. doi: 10.1016/B978-0-12-397169-2.00004-4

Vassen, V. (2018). *Polarity of Envelope Growth and Heterogeneity of the Outer Membrane of Brucella Abortus*. Ph. D. Thesis. Namur: University of Namur.

Wang, X., Wang, L., Lu, T., Yang, Y., Chen, S., Zhang, R., et al. (2014a). Effects of partial deletion of the *wzm* and *wzt* genes on lipopolysaccharide synthesis and virulence of *Brucella abortus* S19. *Mol. Med. Rep.* 9, 2521–7. doi: 10.3892/mmr.2014.2104

Wang, X., Yan, G. M., Zhang, R., Lang, X. L., Yang, Y. L., Li, X. Y., et al. (2014b). Immunogenic response induced by *wzm* and *wzt* gene deletion mutants from *Brucella abortus* S19. *Mol. Med. Rep.* 9, 653–8. doi: 10.3892/mmr.2013.1810

Wang, Z., Niu, J. R., Wang, X. L., Wu, T. L., Cheng, J., Lu, L., et al. (2014). Evaluation of a *Brucella melitensis* mutant deficient in O-polysaccharide export system ATP-binding protein as a rough vaccine candidate. *Microbes Infect.* 16, 633–9. doi: 10.1016/j.micinf.2014.06.013

Whitfield, C. (1995). Biosynthesis of lipopolysaccharide O antigens. *Trends Microbiol.* 3, 178–85. doi: 10.1016/s0966-842x(00)88917-9

Williams, D. M., Ovchinnikova, O. G., Koizumi, A., Mainprize, I. L., Kimber, M. S., Lowary, T. L., et al. (2017). Single polysaccharide assembly protein that integrates polymerization, termination, and chain-length quality control. *Proc. Natl. Acad. Sci. U S A.* 114, E1215–23. doi: 10.1073/pnas.1613609114

Wolter, D. J., and Lister, P. D. (2013). Mechanisms of β-lactam resistance among *Pseudomonas aeruginosa*. *Curr. Pharm. Des.* 19, 209–22. doi: 10.2174/1381612811306020209

Wood, P. J. (1980). Specificity in the interaction of direct dyes with polysaccharides. *Carbohydr. Res.* 85, 271–87. doi: 10.1016/S0008-6215(00)84676-5

Zabalza Baranguá, A. (2017). *Desarrollo De Vacunas Marcadas con GFP Frente a la Brucelosis Ovina y Tests Diagnósticos Asociados*. Ph. D. Thesis. Navarre: Public University of Navarre.

Zhao, Y., Arce-Gorvel, V., Conde-Álvarez, R., Moriyón, I., and Gorvel, J. P. (2018). Vaccine development targeting lipopolysaccharide structure modification. *Microbes Infect.* 20, 455–60. doi: 10.1016/j.micinf.2017.11.006

Conflict of Interest: We would like to state that Rev1Δ*wzm* is protected by the patent WO/2019/101993 (PCT/EP2018/082539) belonging to CSIC and UPNA.

The authors declare that the research was conducted in the absence of any commercial or financial relationships that could be construed as a potential conflict of interest.

Publisher's Note: All claims expressed in this article are solely those of the authors and do not necessarily represent those of their affiliated organizations, or those of the publisher, the editors and the reviewers. Any product that may be evaluated in this article, or claim that may be made by its manufacturer, is not guaranteed or endorsed by the publisher.

frontiers | Frontiers in Microbiology

TYPE Opinion
PUBLISHED 11 August 2022
DOI 10.3389/fmicb.2022.995219

OPEN ACCESS

EDITED BY
Michel Stanislas Zygmunt,
Institut National de recherche pour l'agriculture, l'alimentation et l'environnement (INRAE), France

REVIEWED BY
Clayton Caswell,
Virginia Tech, United States
Gary Splitter,
University of Wisconsin-Madison, United States

*CORRESPONDENCE
Sergio C. Oliveira
scozeus1@gmail.com

SPECIALTY SECTION
This article was submitted to Infectious Agents and Disease, a section of the journal Frontiers in Microbiology

RECEIVED 15 July 2022
ACCEPTED 29 July 2022
PUBLISHED 11 August 2022

CITATION
Oliveira SC and Guimarães ES (2022) How the crosstalk between innate immune sensors and metabolic pathways affect the outcome of *Brucella abortus* infection? *Front. Microbiol.* 13:995219. doi: 10.3389/fmicb.2022.995219

How the crosstalk between innate immune sensors and metabolic pathways affect the outcome of *Brucella abortus* infection?

Sergio C. Oliveira[1]* and Erika S. Guimarães[1,2]

[1]Departamento de Bioquímica e Imunologia, Instituto de Ciências Biológicas, Universidade Federal de Minas Gerais, Belo Horizonte, Minas Gerais, Brazil, [2]Departamento de Genética, Ecologia e Evolução, Programa de Pós-Graduação, Instituto de Ciências Biológicas, Universidade Federal de Minas Gerais, Belo Horizonte, Minas Gerais, Brazil

KEYWORDS

innate immunity, immunometabolism, *Brucella*, STING, AIM2, MyD88

Introduction

Brucella is an important human and animal bacterial pathogen that can survive in macrophages causing chronic infections (Roop et al., 2009). Innate immunity is the first line of defense against pathogens such as *Brucella.* TLR9, AIM2, MyD88, and STING are important receptors and adaptor molecules that are involved in protective responses against *Brucella* infection (Macedo et al., 2008; Gomes et al., 2016; Costa Franco et al., 2018, 2019). Microbial pathogens such as *Brucella* use different host cell energy sources to replicate intracellularly. Erythritol, glutamic acid, and glucose are efficiently metabolized by *Brucella* (Anderson and Smith, 1965). Macrophages are central population of cells of innate immunity; however, it is clear that macrophage phenotypes are difficult to categorize. They can be oversimplified into two major profiles, a pro-inflammatory (M1) and an anti-inflammatory (M2) subsets (Viola et al., 2019). Previously, it was reported that *Brucella abortus* survives and replicates preferentially in anti-inflammatory (M2), which are more abundant during chronic infection (Xavier et al., 2013). Glucose uptake was involved in *B. abortus* replication in M2 macrophages during chronic infection. Inactivation of *Brucella* glucose transporter gluP lead to reduced bacterial survival in macrophages and mouse susceptibility to infection. Additionally, stimulation of peroxisome proliferator-activated receptor γ (PPARγ) results in enhanced availability of glucose for *Brucella* in M2 macrophages augmenting bacterial replication (Xavier et al., 2013).

Macrophages and dendritic cells can undergo a change in energy metabolism by shutting down oxidative phosphorylation and increasing the rate of aerobic glycolysis in a pathway termed as the Warburg effect (Kelly and O'Neill, 2015). Macrophages from humans infected with *Brucella abortus* undergo a Warburg-effect metabolic change to an aerobic glycolytic profile (Czyz et al., 2017). Czyz et al. (2017) demonstrate that inhibition of host glycolysis and lactate production by using 3-BPA and NHI-2 reduced bacterial replication intracellularly without affecting *Brucella* growth.

Metabolic reactions such as glycolysis, the Krebs cycle, fatty acid metabolism, and nitrogen metabolism are critical pathways that host cells undergo to combat several pathogens (Escoll and Buchrieser, 2018). In this opinion article, we connected the interplay of host innate immune recognition of the intracellular bacteria *Brucella* with recent findings in immunemetabolism and how this findings can impact on the outcome of infection.

TLRs and immunometabolism

TLR activation by microbial products can provide signal for metabolic shift in immune cells. TLR signaling activates the NF-κB and HIF-1α transcription factors inducing transcriptional reprogramming toward the glycolytic gene expression profile in macrophages (Krawczyk et al., 2010). It is already established that LPS binding to TLR4 activate multiple downstream metabolic pathways in different Gram-negative bacterial infections (Pan et al., 2022). However, in the case of *Brucella* infection, TLR9 is the most single TLR associated with host protection against infection, suggesting the bacterial DNA as an important bacterial agonist (Gomes et al., 2016). *B. abortus* or its DNA induced activation of MAPK/NF-κB pathways and production of IL-12 and TNF-α by macrophages partially dependent on TLR9 (Gomes et al., 2016). Bacterial LPS leads to HIF-1α and PI3K-AKT-mTOR activation leading to glycolysis and an inflammatory macrophage state (Pan et al., 2022; Figure 1A). However, if *Brucella* DNA *via* TLR9 induces this metabolic shift in macrophages yet to be determined. All TLRs except TLR3, signal through the adaptor molecule myeloid

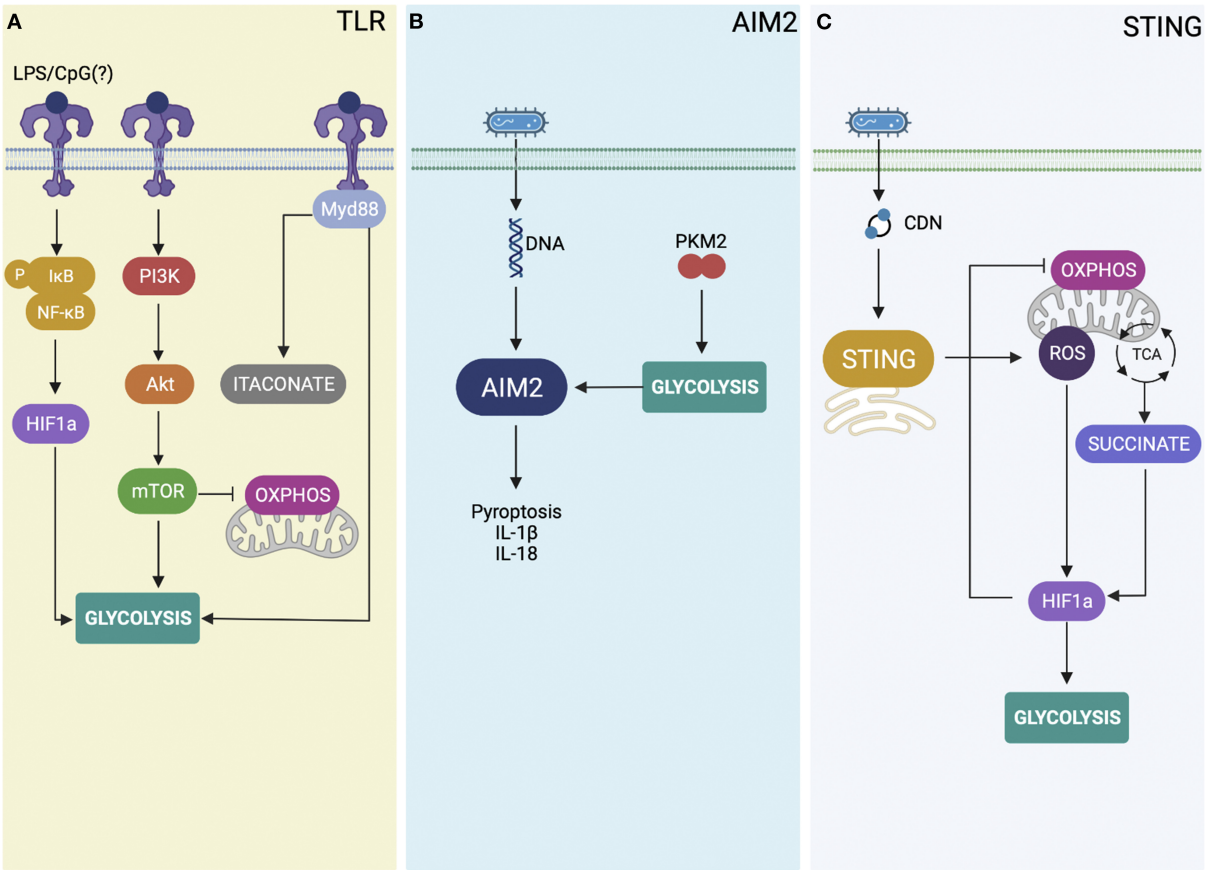

FIGURE 1
Overview of the role of innate immune receptors in immunometabolism. **(A)** TLR (toll-like receptors) stimulation activates the NF-κB (nuclear factor kappa B) pathway and the transcription factor HIF-1α (hypoxia-inducible factor-1α), thereby inducting the metabolic reprogramming toward glycolysis. Additionally, TLR stimulation also activates the PI3K-AKT-mTOR (phosphatidylinositol 3-kinase-protein kinase B-mechanistic target of rapamycin) pathway, a signaling pathway that plays a critical role in inducing the metabolic reprogramming and glycolysis. Further, *Brucella* activates TLRs signaling through MyD88-dependent glycolysis that results in itaconate production and restriction of *Brucella* infection. **(B)** Bacterial DNA and the M2 isoform of pyruvate kinase muscle 2 (PKM2)-dependent aerobic glycolysis activates AIM2 leading to IL-β secretion and pyroptosis. **(C)** During *B. abortus* infection, STING activation increases intracellular succinate levels and mROS (mitochondrial reactive oxygen species) production that contributes to HIF-1α stabilization. HIF-1α drives the metabolic reprogramming in infected macrophages, increasing glycolysis and reducing OXPHOS (mitochondrial oxidative phosphorylation).

differentiation factor 88 (MyD88; Adachi et al., 1998). Activation of the TLR/MyD88 axis in host cells can promote glycolysis and glucose consumption (Lachmandas et al., 2016). Previously, our group has demonstrated that MyD88-dependent signaling is critical to *Brucella* control in mice leading to dendritic cell maturation and IL-12 production (Macedo et al., 2008). Others have shown that enhanced replication of *B. abortus* in M2 macrophages require the function of *Brucella* glucose transporter gluP metabolizing host glucose (Xavier et al., 2013). More recently, Lacey et al. determined whether MyD88-dependent host glycolysis could be involved in control of *B. melitensis* infection (Lacey et al., 2021). Their findings suggest that glucose restriction induced by MyD88 signaling pathway was important for control of *B. melitensis* infection *in vivo*. Additionally, they found that itaconate production is dependent on MyD88 and this metabolite can reduce *Brucella* replication and modulate pro-inflammatory cytokine responses. It would be interest to see whether the activation of a single TLR, such as TLR9 would be able to trigger glycolysis and itaconate production in host cells infected with *Brucella*.

AIM2 inflammasome and glycolysis

AIM2 was identified as the receptor involved in inflammasome activation in response to the recognition of cytosolic DNA during bacterial infections (Rathinam et al., 2010) leading to the production of IL-1β and IL-18, and pyroptosis (Hornung et al., 2009). Previously, our group has demonstrated that AIM2 senses *Brucella* DNA in dendritic cells to induce pyroptosis (Costa Franco et al., 2019). Dendritic cells from AIM2-deficient animals infected with *B. abortus* showed reduced caspase-1 processing and diminished IL-1β secretion. AIM2-deficient animals also displayed reduced resistance to *B. abortus* infection, and this susceptibility was associated with defective IL-1β secretion and reduced IFN-γ T cell responses. However, the influence of AIM2 activation on host cell immunometabolism during *Brucella* infection is unknown.

The M2 isoform of pyruvate kinase muscle 2 (PKM2)-dependent aerobic glycolysis induces IL-1β secretion in LPS-activated macrophages (Palsson-McDermott et al., 2015). However, still to be determined whether PKM2-induced glycolysis regulates IL-1β secretion by modulating inflammasome activation. Studies by Xie et al. showed that PKM2-induced glycolysis promotes AIM2 inflammasome activation by producing lactose to modulate eukaryotic translation initiation factor 2 alpha kinase 2 (EIF2AK2, also termed PKR) phosphorylation in macrophages during sepsis (Xie et al., 2016). The authors also showed that blocking the PKM2-EIF2AK2 hub using target inhibitors can reduce inflammasome activation and protect mice from sepsis. Furthermore, genetic deletion of PKM2 in myeloid cells reduces inflammasome activation and protects animals against death by septic shock. Besides AIM2 activation induced by PKM2-mediated glycolysis, Cho et al. demonstrated a novel mechanism that links glucose transporter 1 (GLUT1)-mediated glycolysis and AIM2 to modulate lung fibrogenesis caused by *Streptococcus* infection (Cho et al., 2020). Glut1-deficient mice showed reduced morbidity and collagen levels in bleomycin-induced lung fibrosis upon *Streptococcus pneumoniae* infection. Reduced AIM2 inflammasome activation by poly(dA:dT) was also observed in Glut1-KO macrophages. It is possible that glycolysis and enhanced expression of GLUT1 marker observed in *Brucella*-infected macrophages (Gomes et al., 2021) triggers AIM2-inflammasome activation and IL-1β secretion and helps to control bacterial infection as presented in Figure 1B. However, this hypothesis has to be proven by further experiments.

STING paving the way to inflammatory macrophages

STING is an adaptor molecule that together with cGAS is critical to sense cytosolic DNA from different pathogens (Ishikawa and Barber, 2008). During intracellular bacterial infection such as *Brucella*, activation of STING can be accomplished by two different pathways. STING can directly recognize bacterial cyclic dinucleotides (CDNs; Burdette et al., 2011), or senses DNA *via* cGAS triggering cGAMP synthesis and then activating STING as a secondary receptor (Sun et al., 2013). Previously, we have demonstrated that STING is important to control *Brucella* infection in macrophages and *in vivo* but not the receptor cGAS (Costa Franco et al., 2018). More recently, we reveal the mechanisms by which STING induces an inflammatory macrophage profile following *Brucella* infection (Gomes et al., 2021). This metabolic shift induced by STING helps to stabilize the hypoxia-inducible factor-1 alpha (HIF-1α), a transcription factor involved in cellular metabolism and innate immune functions. HIF-1α stabilization reduced oxidative phosphorylation and increases glycolysis during infection with *B. abortus*. This metabolic reprogramming leads to augmented nitric oxide production, inflammasome activation, and IL-1β release in bacterial infected macrophages (Gomes et al., 2021). In addition, this inflammatory profile induced by STING is associated with the control of *Brucella* persistence since HIF-1α-deficient animals are more susceptible to bacterial infection (Gomes et al., 2021). HIF-1α stabilization induced by STING during *B. abortus* infection is influenced by mitochondrial reactive oxygen species (mROS) production. Additionally, STING elicits the production of the metabolite succinate in infected macrophages. Succinate leads to HIF-1α stabilization and IL-1β secretion as shown in Figure 1C. Our findings demonstrate the mechanisms by which STING induces

metabolic reprogramming in infected macrophages *via* the HIF-1α pathway.

The mitochondrial enzyme aconitate decarboxylase 1 (ACOD1, also termed as IRG1) is involved in itaconate production and function as potential modulator of cell metabolism. Bacterial LPS induces *ACOD1* gene expression in macrophages (Lee et al., 1995). In turn, ACOD1-activaded macrophages produces itaconate with potential anti-inflammatory activity (Bambouskova et al., 2021). Chen et al. (2022) studies using the sepsis model reported that STING mediates LPS-induced ACOD1 expression by binding to MyD88. They showed that the STING-MyD88 pathway mediates inducible ACOD1 expression in macrophages activated by TLR1, TRL2, TRL4, TRL5, or TLR6 ligands. Overall, activated STING in monocytes and macrophages interacts with MyD88 leading to LPS-induced ACOD1 expression and itaconate production that will result in septic death in host cells. So, far this connection between STING and MyD88 signaling pathway during *Brucella* infection is not yet understood. However, it is possible that STING-MyD88 hub is important to drive host cells to a metabolic state sufficient to trigger inflammatory responses and bacterial infection control.

Final considerations

Recently, studies have connected cell metabolism to innate immune activation. Metabolic shift in immune cells can occur to drive inflammatory or anti-inflammatory profiles. Inflammatory signals will lead to a metabolic switch in innate immune cells resulting in aerobic glycolysis. A landmark of pharmaceutical intervention has arisen with a concept of reprogramming immune cells by changing the metabolic profile using small molecules and metabolites. In this opinion article, we tried to connect innate immune sensors responsible for *Brucella* recognition and host protection and how the activation of these receptors and adaptor molecules result in metabolic shift in macrophages. More data are reported for TLR-MyD88 and STING pathways; however, scarce information is available for the AIM2 inflammasome association with metabolic reprogramming of host cells. The findings reported here highlight the potential use of metabolites such as succinate and itaconate to combat bacterial infections like Brucellosis. More pre-clinical and clinical investigation are required to determine the role of metabolites during the crosstalk between innate immune cells and metabolic pathways. In summary, we discussed here the recent developments in the metabolic reprogramming of macrophages and speculate on the prospect of targeting immunometabolism in the effort to develop novel therapeutics to treat *Brucella* and other bacterial infections.

Author contributions

SO and EG drafted, critically revised the manuscript, and agree to be accountable for the content of the work. All authors contributed to the article and approved the submitted version.

Funding

This work was funded by Conselho Nacional de Desenvolvimento Científico e Tecnológico (grant#303044/2020-9), Fundacão de Amparo a Pesquisa do Estado de Minas Gerais (grants# APQ #01945/17 and Rede #00140-16), and National Institutes of Health (grant# R01 AI116453).

Conflict of interest

The authors declare that the research was conducted in the absence of any commercial or financial relationships that could be construed as a potential conflict of interest.

Publisher's note

All claims expressed in this article are solely those of the authors and do not necessarily represent those of their affiliated organizations, or those of the publisher, the editors and the reviewers. Any product that may be evaluated in this article, or claim that may be made by its manufacturer, is not guaranteed or endorsed by the publisher.

References

Adachi, O., Kawai, T., Takeda, K., Matsumoto, M., Tsutsui, H., Sakagami, M., et al. (1998). Targeted disruption of the MyD88 gene results in loss of IL-1- and IL-18-mediated function. *Immunity* 9, 143–150. doi: 10.1016/S1074-7613(00)80596-8

Anderson, J. D., and Smith, H. (1965). The metabolism of erythritol by *Brucella abortus*. *J. Gen. Microbiol.* 38, 109–124. doi: 10.1099/00221287-38-1-109

Bambouskova, M., Potuckova, L., Paulenda, T., Kerndl, M., Mogilenko, D. A., Lizotte, K., et al. (2021). Itaconate confers tolerance to late NLRP3 inflammasome activation. *Cell Rep.* 34, 108756. doi: 10.1016/j.celrep.2021.108756

Burdette, D. L., Monroe, K. M., Sotelo-Troha, K., Iwig, J. S., Eckert, B., Hyodo, M., et al. (2011). STING is a direct innate immune sensor of cyclic di-GMP. *Nature* 478, 515–518. doi: 10.1038/nature10429

Chen, F., Wu, R., Liu, J., Kang, R., Li, J., Tang, D., et al. (2022). The STING1-MYD88 complex drives ACOD1/IRG1 expression and function in lethal innate immunity. *iScience* 25, 104561. doi: 10.1016/j.isci.2022.104561

Cho, S. J., Moon, J. S., Nikahira, K., Yun, H. S., Harris, R., Hong, K. S., et al. (2020). GLUT1-dependent glycolysis regulates exacerbation of fibrosis *via* AIM2

inflammasome activation. *Thorax* 75, 227–236. doi: 10.1136/thoraxjnl-2019-213571

Costa Franco, M. M., Marim, F., Guimaraes, E. S., Assis, N. R. G., Cerqueira, D. M., Alves-Silva, J., et al. (2018). *Brucella abortus* triggers a cGAS-independent STING pathway to induce host protection that involves guanylate-binding proteins and inflammasome activation. *J. Immunol.* 200, 607–622. doi: 10.4049/jimmunol.1700725

Costa Franco, M. M. S., Marim, F. M., Alves-Silva, J., Cerqueira, D., Rungue, M., Tavares, I. P., et al. (2019). AIM2 senses *Brucella abortus* DNA in dendritic cells to induce IL-1beta secretion, pyroptosis and resistance to bacterial infection in mice. *Microbes Infect.* 21, 85–93. doi: 10.1016/j.micinf.2018.09.001

Czyz, D. M., Willett, J. W., and Crosson, S. (2017). *Brucella abortus* induces a warburg shift in host metabolism that is linked to enhanced intracellular survival of the pathogen. *J. Bacteriol.* 199, 17. doi: 10.1128/JB.00227-17

Escoll, P., and Buchrieser, C. (2018). Metabolic reprogramming of host cells upon bacterial infection: why shift to a Warburg-like metabolism? *FEBS J.* 285, 2146–2160. doi: 10.1111/febs.14446

Gomes, M. T., Campos, P. C., Pereira Gde, S., Bartholomeu, D. C., Splitter, G., Oliveira, S. C., et al. (2016). TLR9 is required for MAPK/NF-kappaB activation but does not cooperate with TLR2 or TLR6 to induce host resistance to *Brucella abortus*. *J. Leukoc. Biol.* 99, 771–780. doi: 10.1189/jlb.4A0815-346R

Gomes, M. T. R., Guimaraes, E. S., Marinho, F. V., Macedo, I., Aguiar, E., Barber, G. N., et al. (2021). STING regulates metabolic reprogramming in macrophages *via* HIF-1alpha during *Brucella* infection. *PLoS Pathog.* 17, e1009597. doi: 10.1371/journal.ppat.1009597

Hornung, V., Ablasser, A., Charrel-Dennis, M., Bauernfeind, F., Horvath, G., Caffrey, D. R., et al. (2009). AIM2 recognizes cytosolic dsDNA and forms a caspase-1-activating inflammasome with ASC. *Nature* 458, 514–518. doi: 10.1038/nature07725

Ishikawa, H., and Barber, G. N. (2008). STING is an endoplasmic reticulum adaptor that facilitates innate immune signalling. *Nature* 455, 674–678. doi: 10.1038/nature07317

Kelly, B., and O'Neill, L. A. (2015). Metabolic reprogramming in macrophages and dendritic cells in innate immunity. *Cell Res.* 25, 771–784. doi: 10.1038/cr.2015.68

Krawczyk, C. M., Holowka, T., Sun, J., Blagih, J., Amiel, E., DeBerardinis, R. J., et al. (2010). Toll-like receptor-induced changes in glycolytic metabolism regulate dendritic cell activation. *Blood* 115, 4742–4749. doi: 10.1182/blood-2009-10-249540

Lacey, C. A., Ponzilacqua-Silva, B., Chambers, C. A., Dadelahi, A. S., and Skyberg, J. A. (2021). MyD88-dependent glucose restriction and itaconate production control *Brucella* infection. *Infect. Immun.* 89, e0015621. doi: 10.1128/IAI.00156-21

Lachmandas, E., Boutens, L., Ratter, J. M., Hijmans, A., Hooiveld, G. J., Joosten, L. A., et al. (2016). Microbial stimulation of different Toll-like receptor signalling pathways induces diverse metabolic programmes in human monocytes. *Nat. Microbiol.* 2, 16246. doi: 10.1038/nmicrobiol.2016.246

Lee, C. G., Jenkins, N. A., Gilbert, D. J., Copeland, N. G., and O'Brien, W. E. (1995). Cloning and analysis of gene regulation of a novel LPS-inducible cDNA. *Immunogenetics* 41, 263–270. doi: 10.1007/BF00172150

Macedo, G. C., Magnani, D. M., Carvalho, N. B., Bruna-Romero, O., Gazzinelli, R. T., Oliveira, S. C., et al. (2008). Central role of MyD88-dependent dendritic cell maturation and proinflammatory cytokine production to control *Brucella abortus* infection. *J. Immunol.* 180, 1080–1087. doi: 10.4049/jimmunol.180.2.1080

Palsson-McDermott, E. M., Curtis, A. M., Goel, G., Lauterbach, M. A. R., Sheedy, F. J., Gleeson, L. E., et al. (2015). Pyruvate kinase M2 regulates Hif-1alpha activity and IL-1beta induction and is a critical determinant of the Warburg effect in LPS-activated macrophages. *Cell Metab.* 21, 347. doi: 10.1016/j.cmet.2014.12.005

Pan, T., Sun, S., Chen, Y., Tian, R., Chen, E., Tan, R., et al. (2022). Immune effects of PI3K/Akt/HIF-1alpha-regulated glycolysis in polymorphonuclear neutrophils during sepsis. *Crit. Care* 26, 29. doi: 10.1186/s13054-022-03893-6

Rathinam, V. A., Jiang, Z., Waggoner, S. N., Sharma, S., Cole, L. E., Waggoner, L., et al. (2010). The AIM2 inflammasome is essential for host defense against cytosolic bacteria and DNA viruses. *Nat. Immunol.* 11, 395–402. doi: 10.1038/ni.1864

Roop, R. M., Gaines, J. M., Anderson, E. S., Caswell, C. C., and Martin, D. W. (2009). Survival of the fittest: how *Brucella* strains adapt to their intracellular niche in the host. *Med. Microbiol. Immunol.* 198, 221–238. doi: 10.1007/s00430-009-0123-8

Sun, L., Wu, J., Du, F., Chen, X., and Chen, Z. J. (2013). Cyclic GMP-AMP synthase is a cytosolic DNA sensor that activates the type I interferon pathway. *Science* 339, 786–791. doi: 10.1126/science.1232458

Viola, A., Munari, F., Sanchez-Rodriguez, R., Scolaro, T., and Castegna, A. (2019). The metabolic signature of macrophage responses. *Front. Immunol.* 10, 1462. doi: 10.3389/fimmu.2019.01462

Xavier, M. N., Winter, M. G., Spees, A. M., den Hartigh, A. B., Nguyen, K., Roux, C. M., et al. (2013). PPARgamma-mediated increase in glucose availability sustains chronic *Brucella abortus* infection in alternatively activated macrophages. *Cell Host Microbe* 14, 159–170. doi: 10.1016/j.chom.2013.07.009

Xie, M., Yu, Y., Kang, R., Zhu, S., Yang, L., Zeng, L., et al. (2016). PKM2-dependent glycolysis promotes NLRP3 and AIM2 inflammasome activation. *Nat. Commun.* 7, 13280. doi: 10.1038/ncomms13280

frontiers | Frontiers in Microbiology

TYPE Original Research
PUBLISHED 19 October 2022
DOI 10.3389/fmicb.2022.1029199

OPEN ACCESS

EDITED BY
Michel Stanislas Zygmunt,
Institut National de recherche pour l'agriculture, l'alimentation et l'environnement (INRAE), France

REVIEWED BY
María-Pilar Jiménez de Bagüés,
Aragon Agrifood Research and Technology Center (CITA), Spain
Jonathan Lalsiamthara,
Oregon Health and Science University, United States

*CORRESPONDENCE
Angela M. Arenas-Gamboa
aarenas@cvm.tamu.edu

SPECIALTY SECTION
This article was submitted to Infectious Agents and Disease, a section of the journal Frontiers in Microbiology

RECEIVED 31 August 2022
ACCEPTED 26 September 2022
PUBLISHED 19 October 2022

CITATION
Hensel ME, Stranahan LW, Edwards JF and Arenas-Gamboa AM (2022) Intratracheal inoculation results in Brucella-associated reproductive disease in male mouse and guinea pig models of infection. *Front. Microbiol.* 13:1029199. doi: 10.3389/fmicb.2022.1029199

Intratracheal inoculation results in Brucella-associated reproductive disease in male mouse and guinea pig models of infection

Martha E. Hensel[1,2], Lauren W. Stranahan[1], John F. Edwards[1] and Angela M. Arenas-Gamboa[1]*

[1]Department of Veterinary Pathobiology, Texas A&M University, College Station, TX, United States, [2]MD Anderson Cancer Center, Michale E. Keeling Center for Comparative Medicine and Research, Bastrop, TX, United States

Brucella species are considered a significant cause of reproductive pathology in male and female animals. Importantly, *Brucella melitensis* can induce reproductive disease in humans. Reproductive pathogenesis and evaluation of newly developed countermeasures against brucellosis studies have traditionally utilized female animal models. However, any potential, new intervention for use in humans would need to be evaluated in both sexes. Therefore, animal models for male reproductive brucellosis are desperately needed to understand disease progression. Accordingly, we evaluated guinea pigs and mice using *B. melitensis* 16M in an intratracheal model of inoculation at different stages of infection (peracute, acute, and chronic) with an emphasis on determining the effect to the male reproductive organs. Aerosol inoculation resulted in colonization of the reproductive organs (testicle, epididymis, prostate) in both species. Infection peaked during the peracute (1-week post-infection [p.i.]) and acute (2-weeks p.i.) stages of infection in the mouse in spleen, epididymis, prostate, and testicle, but colonization was poorly associated with inflammation. In the guinea pig, peak infection was during the acute stage (4-weeks p.i.) and resulted in inflammation that disrupted spermatogenesis chronically. To determine if vaccine efficacy could be evaluated using these models, males were vaccinated using subcutaneous injection with vaccine candidate 16MΔ*vjbR* at 10^9 CFU/100μl followed by intratracheal challenge with 16M at 10^7. Interestingly, vaccination efficacy varied between species and reproductive organs demonstrating the value of evaluating vaccine candidates in multiple models and sexes. Vaccination resulted in a significant reduction in colonization in the mouse, but this could not be correlated with a decrease in inflammation. Due to the ability to evaluate for both colonization and inflammation, guinea pigs seemed the better model not only for assessing host-pathogen interactions but also for future vaccine development efforts.

KEYWORDS

***Brucella melitensis*, male, reproductive tract, vaccine, intratracheal inoculation**

Introduction

Reproductive disease is a well-known consequence of brucellosis in animals. In small ruminants (sheep and goats), cattle, and dogs, infection during pregnancy typically results in abortions, stillbirths, and vertical transmission to the offspring (Garin-Bastuji and Blasco, 2016). Male animals of the same species may develop epididymitis and testicular degeneration, which can negatively impact fertility (Picard-Hagen et al., 2015; Garin-Bastuji and Blasco, 2016).

Brucella species can be divided into two groups based on structure of the lipopolysaccharide O chain: smooth or rough (Huddleson, 1943). While rough strains such as *B. canis* and *B. ovis* cause reproductive disease in dogs and sheep, respectively, only smooth strains (*B. melitensis* and *B. abortus*) have been documented to cause reproductive disease in both animals and men (Young, 1983, 1995; Corbel, 2006). *B. abortus* and *B. melitensis* infection in men may cause orchitis, epididymitis, and prostatitis (Young, 1983; Khan et al., 1989; Colmenero et al., 2007; Savasci et al., 2014).

Brucellosis is often spread from animals to humans through either direct contact with infected animals, inhalation of infectious aerosols, or indirectly through ingestion of unpasteurized milk (Corbel, 2006). Common symptoms regardless of sex are fever, inappetence, malaise, and joint pain (Young, 1995). Reproductive disease is a less common manifestation of disease, but retrospective studies in endemic areas estimate a range of 6.8–9.1% of genito-urinary issues in men are due to brucellosis (Yetkin et al., 2005; Colmenero et al., 2007; Gul et al., 2009).

It is important to assess the impact of the disease on both sexes and to understand potential differences associated with disease pathogenesis that may affect vaccine safety and efficacy and treatment performance in males. Historically, a majority of the comparative *in vivo* studies have been conducted in females with less known about the impact of brucellosis on the male reproductive tract (García-Carrillo, 1990; Grillo et al., 2012). While several studies in animal models for human disease (rhesus macaques, guinea pigs, and mice) have investigated the impact of smooth *Brucella* spp. on the male reproductive tract, these studies fail to fully characterize the kinetics or pathologic changes associated with infection (Hillaert et al., 1950; Mense et al., 2004; Izadjoo et al., 2008; Yingst et al., 2010).

The first step towards the goal of evaluating vaccines or therapeutics in males is to better characterize the effect of wild-type *Brucella* spp. on the male reproductive tract in commonly utilized animal models. For these studies, we elected to evaluate an aerosol exposure route, which is an important occupational hazard for certain professions including veterinarians, microbiological laboratorians, or abattoir workers (Young, 1983; Traxler et al., 2013). In order to deliver a targeted aerosol dose, an intratracheal route of inoculation using the PennCentury MicroSprayer™ was applied. This device has previously been used to inoculate guinea pigs and mice and generates a particle size that produces lower airway disease (Hensel et al., 2019, 2020). The benefit of intratracheal inoculation includes delivering a small particle size that is evenly distributed to the lower airways, and this route allows for a known infectious dose since it does not depend on the individual animal's respiratory physiology such as respiratory rate and depth. Dose titration and kinetics of this route of inoculation for *B. melitensis* were previously characterized in female guinea pigs, which resulted in colonization and pathologic changes in the uterus and placenta (Gregory et al., 2019; Hensel et al., 2019, 2020). Therefore, the objective of this study was to first characterize the kinetics of *B. melitensis* 16 M infection with an emphasis on impact to the male reproductive tract following intratracheal inoculation in two of the most commonly used animal models, C57Bl/6 mice and Hartley guinea pigs. Following that, our objective was to compare the models in a practical application: evaluating vaccine efficacy in males.

Materials and methods

Bacterial strains

B. melitensis 16 M (originally isolated from an aborted goat fetus lung) was used in this study (Kahl-McDonagh et al., 2006). Vaccine candidate *B. melitensis 16MΔvjbR* is a targeted gene deletion mutant derived from our laboratory stock (Arenas-Gamboa et al., 2008, 2012). The vjbR gene is a transcriptional regulator that influences expression of the type IV secretion system and contributes to virulence (Weeks et al., 2010). Bacteria were cultured on tryptic soy agar (TSA; Difco, Becton, Dickinson) at 37°C with 5% (vol/vol) CO_2 for 72 h and harvested from plates with phosphate-buffered saline (PBS; Gibco). Using a Klett colorimeter to determine optical density, inoculums of either 1×10^7 CFU/50 µl (guinea pig) or 1×10^7 CFU/25 µl (mouse) were prepared. The inoculum dose was retrospectively verified through serial dilution and plating onto TSA medium in duplicate.

Animal research ethics statement

All studies were performed with the approval of the Texas A&M University's Institutional Animal Care and Use Committee (protocol: 2021–0038). Texas A&M University is fully accredited by the Association for Assessment and Accreditation of Laboratory Animal Care (AAALAC).

Guinea pig infection with *Brucella melitensis* 16M

Eighteen, 300–500 g (approximately 5 months old), male Hartley guinea pigs were obtained from Charles River (Wilmington, MA). Males were first assessed for reproductive capacity during an in-house breeding program and were then transferred to an ABSL-3 facility at Texas A&M University and

housed individually in microisolator cages during experimental infection. After an acclimation period, animals were randomly divided into three inoculation groups (peracute, acute, chronic): 12 guinea pigs ($n = 4$/time point), which received *B. melitensis via* intratracheal inoculation, and 6 guinea pigs received sterile, endotoxin-free PBS as uninfected controls ($n = 2$/time point). Guinea pigs were anesthetized *via* intraperitoneal injection (i.p.) with a cocktail of ketamine (50 mg/kg) and xylazine (5 mg/kg). Once a surgical plane of anesthesia was achieved, animals were inoculated with 1×10^7 CFU *B. melitensis* 16 M in 50 µl *via* intratracheal inoculation (IT) using the PennCentury MicroSprayer™ Aerosolizer (Wyndmoor, PA) as previously described (Gregory et al., 2019; Hensel et al., 2019, 2020). In brief, the guinea pig was placed in ventral-dorsal recumbency, and the larynx visualized using a small animal laryngoscope. The tip of the device was then placed in the proximal trachea. Negative control animals ($n = 2$ per time point) were sham inoculated with 50 µl of sterile, endotoxin-free PBS IT.

At peracute (2-weeks post-infection [p.i.]), acute (4-weeks p.i.), or chronic (8-weeks p.i.) time points, guinea pigs were euthanized i.p. with sodium pentobarbital (100 mg/kg) followed by cardiac exsanguination. One gram each of spleen, liver, lung, testicle, epididymis, and prostate were collected into pre-sterilized 2 ml collection tubes containing 1 ml PBS and 1.47 g of ceramic beads (Omni International). Tissues were homogenized as previously described using a Bead Ruptor Elite Bead Mill Homogenizer (Omni International), and homogenates were serially diluted and cultured on Farrell's media. (Hensel et al., 2020) Following incubation for a minimum of 72 h, colonies were counted to determine CFU/g.

Intratracheal inoculation of male C57Bl/6 mice

Twenty-eight, 8-10-week old, male C57BL/6 mice that had previously been used for an in-house breeding program were obtained from the Texas A&M Institute for Genomic Medicine. Males were transferred to an ABSL-3 facility at Texas A&M University and housed individually in microisolator cages during experimental infection. After an acclimation period, animals were randomly divided into four groups (peracute [1 and 2-weeks p.i.], acute [4-weeks p.i.], and chronic [8-weeks p.i.]): 20 mice ($n = 5$/time point) received *B. melitensis via* intratracheal inoculation, and 8 mice received sterile, endotoxin-free PBS as uninfected controls ($n = 2$/time point). Mice were anesthetized i.p. with ketamine (50 mg/kg) and xylazine (5 mg/kg) diluted in PBS, placed on a Mouse Intubation Platform (Penn-Century) in dorsoventral recumbency, and a small animal laryngoscope (Penn-Century) was used to visualize the larynx. The PennCentury MicroSprayer™ Aerosolizer was inserted into the proximal trachea and used to inoculate mice with 1×10^7 CFU *B. melitensis* 16 M in 25 µl IT. Negative control animals ($n = 2$ per time point) were sham inoculated with 25 µl of sterile, endotoxin-free PBS IT.

At peracute (1 and 2-weeks p.i.), acute (4-weeks p.i.), or chronic (8-weeks p.i.) time points, mice were euthanized *via* carbon dioxide asphyxiation followed by cervical dislocation. Spleen, liver, lung, prostate, testicle, and epididymis were collected into 1 ml PBS. Tissues were weighed, homogenized, serially diluted, and plated as previously described (Stranahan et al., 2019). Following incubation for a minimum of 72 h, colonies were counted to determine CFU/g.

Evaluation of histopathological changes in mice and guinea pigs

Testicle and epididymis from mice, and testicle, epididymis, and prostate from guinea pigs were collected at the aforementioned peracute, acute and chronic time points and fixed in 10% neutral buffered formalin (NBF; ThermoScientific) for a minimum of 48 h. Tissues were routinely processed, embedded in paraffin, sectioned at 5 µm, and stained with hematoxylin and eosin (H&E). Histologic changes of the testicle, epididymis, and prostate were scored for severity of inflammation (0–4), edema, necrosis, and tissue architecture changes by a board-certified anatomic veterinary pathologist as described in Supplementary Table S1.

Immunohistochemistry to detect *Brucella* antigen

Five micrometer tissue sections of testicle/epididymis (mouse and guinea pig) and prostate (guinea pig only) were adhered to positively charged glass slides for immunohistochemistry. Slides were routinely processed, and antigen retrieval was performed as previously described using a 2,100 Antigen Retriever (Aptum Biologics Ltd. Southampton, UK; Hensel et al., 2019). Slides were blocked as previously described with Bloxall Blocking Solution (Vector Laboratories, Burlingame, CA) and normal goat serum (Vector Laboratories; Hensel et al., 2019). Primary incubation was performed overnight at 4° C with a *Brucella* polyclonal rabbit antibody (Bioss Antibodies, Boston, MA) at dilution of 1:500. A Vectastain Elite® ABC HRP Kit (Vector Laboratories) with an avidin/biotinylated anti-rabbit secondary antibody was used according to the manufacturer's instructions. Antigen was visualized with a Betazoid DAB chromagen kit (Biocare Medical, Pachecho, CA). The slides were counterstained with Gills's hematoxylin III and cover slipped.

Comparison of the mouse and guinea pig as models to assess vaccine efficacy

Five, 6–8 week old, male C57BL/6 mice and four, 400 g male Hartley guinea pigs were vaccinated subcutaneously with 16 M*ΔvjbR* at 1×10^9 CFU/100 µl and then rested for 6-weeks. Vaccinated animals were then moved to an ABSL-3 and housed

as a group (mice) or individually (guinea pigs) in microisolator cages. Challenge inoculum of 1×10^7 CFU 16 M *B. melitensis* was prepared, and animals were anesthetized and inoculated IT as described above. At 1-week post-challenge, mice were euthanized *via* CO_2 asphyxiation followed by cervical dislocation, and spleen, liver, lung, testicle, epididymis, and prostate were collected for culture. At 2-weeks post-challenge, guinea pigs were euthanized as previously described, and the same tissues were collected for culture on Farrell's media. Spleen, liver, lung, testicle, and epididymis were also collected for histopathology.

Statistical analysis

Statistical analysis of infection kinetics in the mouse and guinea pig was performed using two-way analysis of variance (ANOVA) followed by Šídák's multiple comparisons to evaluate differences in organ colonization by time point. The limit of detection using standard culture methods is 10 CFU/g; as such, several tissues were reported as 0 indicating colonization was less than 10 CFU/g. Therefore, to evaluate the normality of the data, Q-Q plots were assessed following 2-way ANOVA. The sum of the histologic lesion scores between time points and negative controls were evaluated by the Kruskal–Wallis test followed by Dunn's multiple comparisons. Analysis of vaccine efficacy was performed using multiple Mann Whitney U Test with Šídák-Bonferroni correction to compare colonization following challenge in vaccinated and unvaccinated mice and guinea pigs. All tests were performed using GraphPad Prism v9 (GraphPad Software, San Diego, CA).

Results

The first objective was to characterize intratracheal inoculation with *B. melitensis* 16 M in male C57BL/6 mice and Hartley guinea pigs and characterize the effects of infection, not only on the lung and hematopoietic targets, but most importantly in the reproductive tract. Infertility, orchitis, and epididymitis in males has been reported in naturally infected males, both human and animal, but efforts to develop a small animal laboratory model for reproductive disease have been sporadic (Young, 1983; Corbel, 2006; Izadjoo et al., 2008). Aerosol inoculation is an important route of natural transmission in people, but this inoculation route has not been evaluated for male reproductive disease (Pappas et al., 2003, 2006). To assess common milestones of disease, male animals were euthanized at peracute (1 to 2-weeks p.i.), acute (4-weeks p.i.), or chronic (8-weeks p.i.) phases of infection. In humans, these stages are characterized by the onset of fever and flu-like symptoms during the peracute and acute stages while reproductive disease is often identified in the chronic stages when clinical signs such as scrotal swelling and pain develop (Young, 1983).

To determine if IT inoculation resulted in systemic infection, the spleen, liver, and lung were cultured. In the 2-week mouse group, an anesthetic death occurred during intratracheal inoculation. Organ colonization of the spleen was detected in 100% of mice at the peracute time points of 1-week p.i. (5/5) and 2-weeks p.i. (4/4) and 100% of guinea pigs (4/4) by 2-weeks p.i. (Figures 1A,B). At 1-week p.i., 100% of mice and guinea pigs had colonization of the lungs confirming intratracheal inoculation resulted in infection of the lung. Colonization of the spleen, liver, and lung peaked at 1-week p.i. in the mice and was significantly increased at 1-week p.i. compared to 2-,4-, and 8-weeks p.i. (Figure 1A). No significant differences were detected between 2- and 4-weeks p.i. in mice in the spleen, but colonization of the liver ($p<0.05$) and lung ($p<0.001$) at 4-weeks p.i. were significantly decreased compared to 2-weeks p.i. The kinetics of colonization mimics that seen in other aerosol models with *Brucella melitensis* in mice in which colonization peaks during peracute infection and declines by 4-weeks p.i. (Mense et al., 2001; Kahl-McDonagh et al., 2007).

Guinea pigs were evaluated at 2-, 4-, and 8-weeks p.i. since previous experiments utilizing IT inoculation of guinea pigs have demonstrated that infection required at least 2-weeks to become established (Hensel et al., 2019, 2020). At the peracute stage of infection (2-weeks p.i.), 100% of the guinea pigs had colonization of the spleen, liver, and lung (Figure 1B). Colonization of male guinea pigs is similar to that seen in non-pregnant and pregnant female guinea pigs when dosed with 10^7 IT, where colonization of the spleen, liver, and lung occurs in 91.6% of the animals during the peracute stage of infection and 100% by the acute stage (Hensel et al., 2019, 2020). When the kinetics of colonization in guinea pigs was explored, colonization of the liver ($p<0.01$), spleen ($p<0.05$), and lung ($p<0.05$) was significantly increased at 4-weeks compared to 8-weeks p.i. In contrast to mice, infection in the guinea pigs required 4-weeks p.i. to peak in the spleen and liver. Whereas colonization in lung peaks in mice at 1-week p.i. and declines exponentially thereafter, colonization in the guinea pig was stable with no significant difference in mean CFU/g between 2- and 4-weeks p.i. (Figure 1B). However, colonization of lung ($p<0.05$) significantly decreased from 4- to 8-weeks p.i. (Figure 1B).

Several studies have been conducted in male guinea pigs and mice using aerosol routes of inoculation, but the reproductive organs were not evaluated (Elberg and Henderson, 1948; Druett et al., 1956; Henning et al., 2012). Therefore, a second objective was to determine if IT inoculation would generate reproductive disease in males. Interestingly, the reproductive organs (prostate, testicle, epididymis) in both mice and guinea pigs were colonized following IT inoculation with 10^7 CFU *B. melitensis* (Figures 1C,D). Like the pattern seen in the other organs, infection peaked at 1-week p.i. in the mouse and at 4-weeks p.i. in the guinea pig. Colonization did not persist in the mouse beyond the acute stage of infection (4-weeks p.i.); however, colonization of the epididymis, testicle, and prostate persisted in 50% of the guinea pigs through 4-weeks, and in the epididymis and prostate of 50%

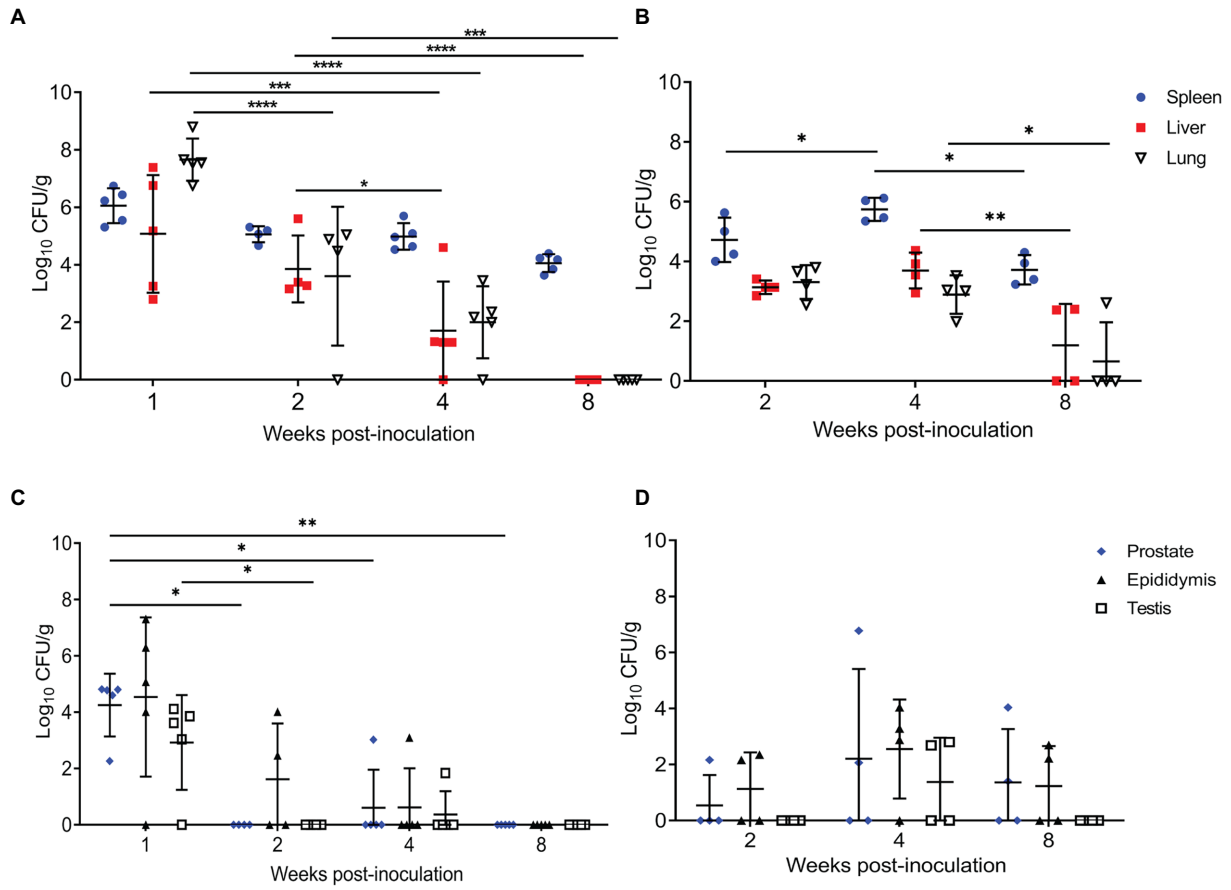

FIGURE 1
Intratracheal inoculation results in colonization of the spleen, liver, lung, and reproductive organs in mice and guinea pigs. **(A)** Spleen, liver, and lung were collected from mice (n=5/time point) inoculated with 1×10^7 CFU/25µl *via* intratracheal inoculation and euthanized at 1-,2-,4-, and 8-weeks post-challenge. **(B)** Spleen, liver, and lung were collected from guinea pigs (n=4/time point) inoculated with 1×10^7 CFU/50µl *via* intratracheal inoculation and euthanized at 2-,4-, and 8-weeks post-challenge. Epididymis, testicle, and prostate were collected at the same time points in mice **(C)** and guinea pigs **(D)**. Differences in mean colonization between time points analyzed by 2-way ANOVA followed by Šídák's multiple comparison test. Horizontal bar indicates mean colonization. Results reported as $\log_{10}$ CFU/g with S.D. **p<0.01, ***p<0.001, ****p<0.0001.

(2/4) at 8-weeks p.i. (Figures 1C,D). While colonization was not significantly different when compared to controls or by time points in the guinea pigs, these results suggest that IT inoculation can induce chronic disease of the reproductive organs.

Culture results do not provide the full picture of the impact of infection upon the reproductive organs; therefore, testicle, epididymis, and prostate from guinea pigs and testicle and epididymis from mice were evaluated for changes in tissue architecture, inflammation, and effect on spermatogenesis (Supplementary Table S1). *B. melitensis* causes epididymitis, prostatitis, and testicular swelling in naturally infected small ruminants and in humans (Boyd, 1938; Young, 1983; Khan et al., 1989; Yetkin et al., 2005; Corbel, 2006; Savasci et al., 2014). Epididymitis is a common lesion that results from infection; therefore, histologic sections of epididymis were examined to correlate colonization with microscopic evidence of disease (Khan et al., 1989; Gul et al., 2009; Savasci et al., 2014). During the peracute stage of infection, 25% (1/4) of the mice had epididymitis characterized by degeneration and rupture of the epididymal duct which generated an intense histiocytic reaction to the extra-tubular spermatids (Figure 2A). Degeneration and rupture of the epididymal duct was presumably due to infection with *B. melitensis* as macrophages in the lesion contained abundant, intracytoplasmic bacteria that stained positively with a polyclonal *Brucella* antibody (Figure 2A). Despite a level of colonization considered to be too low to be detected by culture (<10 CFU/g) in the mouse, the epididymis had evidence of an inflammatory infiltrate of macrophages in the epididymal duct interstitium at 2-weeks p.i. (Figure 2A). By 4-weeks p.i., the epididymis had no detectable lesions, but cross-sections of the epididymal duct subjectively appeared to have fewer spermatids (Figure 2A). In the mouse, the mean histologic score was not statistically increased compared to uninfected controls (Figure 3A).

Colonization and lesion development were delayed in guinea pigs, but the histologic lesions were more pronounced. At 4-weeks p.i., mean colonization in the epididymis was 2.6 logs with a mean

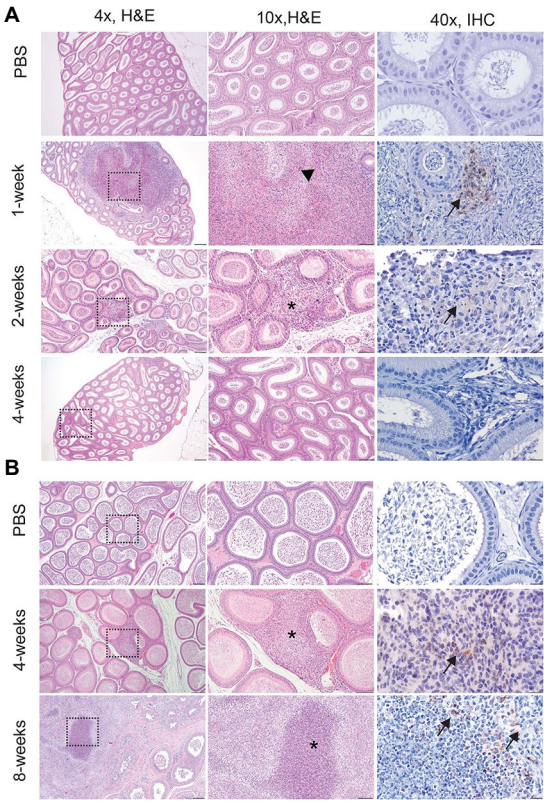

FIGURE 2
Infection with *Brucella melitensis* results in epididymitis at the peracute stage of infection in mice and the acute and chronic stages in guinea pigs. Mice **(A)** and guinea pigs **(B)** were inoculated with 10^7 *B. melitensis via* IT inoculation, and the epididymis was collected for histology. Representative images for the mouse **(A)** at the peracute (1- and 2-week p.i.) and acute (4-week p.i.) and guinea pig **(B)** at the acute (4-week p.i.) and chronic (8-weeks p.i.) stages of infection. A single mouse had rupture of the epididymal duct with intense inflammatory infiltrate (arrowhead). Macrophages in this region had abundant intracytoplasmic bacteria (IHC, arrows). The lesion in mice at 2-weeks and guinea pigs at 4-weeks consisted of a focally extensive infiltrate of histiocytes and neutrophils (*) in the interstitium of the epididymal duct. Scant macrophages were positive for *Brucella* antigen by IHC (arrows). By 8-weeks p.i., guinea pigs developed spermatic granulomas from rupture of the epididymal duct, and macrophages in the lesion contained abundant intracytoplasmic and extracellular *Brucella* antigen (IHC, arrows). Tissues were stained with hematoxylin and eosin (H&E) and a polyclonal *Brucella* antibody (IHC) at 1:500 with Gill's hematoxylin counterstain. Dashed box of 4x image indicates area highlighted for the 10x and 40x images. 4x, scale bar=100μm; 10x, scale bar=50μm; 40x, scale bar=10μm.

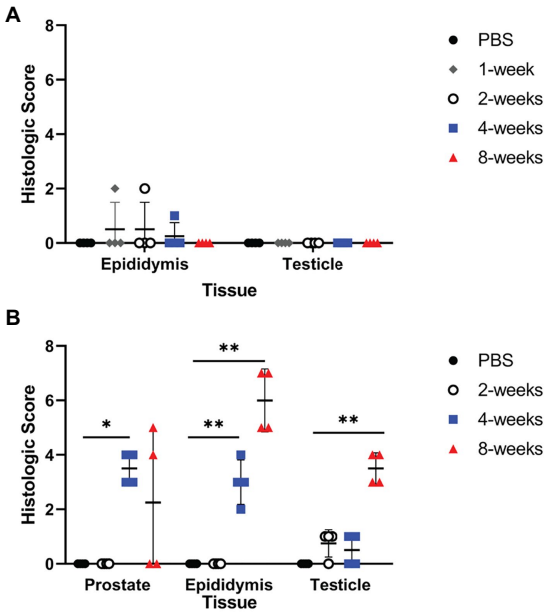

FIGURE 3
Infection resulted in significant inflammation in the epididymis and prostate of guinea pigs. Histologic changes of the testicle, epididymis, and prostate were scored for inflammation, edema, necrosis, and tissue architecture changes in the mouse **(A)** and guinea pig **(B)**. Prostate from the mouse was not available for histologic examination. Histologic scores between PBS controls and infected animals at each time point were compared using the Kruskal-Wallis test followed by Dunn's multiple comparisons. Horizontal line indicates median. Statistical significance compared to controls *p<0.05; **p<0.01.

histologic score of 3 ($p<0.01$) compared to uninfected controls (Figure 3B). Similar to the mouse during the acute stage of infection, the histologic lesions at 4-weeks consisted of multifocal inflammatory infiltrates of macrophages and neutrophils in the interstitial tissue of the epididymal duct (Figure 2B). However, by 8-weeks p.i., colonization was 1.1 logs, but the mean histologic score was significantly increased ($p<0.01$) compared to 4-weeks p.i. and PBS controls ($p<0.01$; Figure 3B). At 8-weeks p.i., the epididymal changes consisted of multifocal to coalescing necrotizing and histiocytic epididymitis with no mature spermatids in the epididymal duct which suggests spermiostasis (Figure 2B). The lack of spermatids within the epididymal duct was likely secondary to disordered spermatogenesis in the testicle. When a polyclonal anti-*Brucella* antibody was applied to sections, epididymal lesions at 4- and 8-weeks p.i. had abundant intralesional *Brucella* antigen within foci of necrosis, and macrophages contained intracytoplasmic antigen (Figure 2B).

Orchitis (inflammation of the testicle) is less common in animals than epididymitis, but the literature reporting disease in men does not often distinguish between primary testicular or epididymal infection and instead describes the lesion as epididymo-orchitis (Khan et al., 1989; Colmenero et al., 2007; Gul et al., 2009). Despite colonization of testicle in the mouse, no histologic evidence of disease was detected at any time point (Figure 4A). In guinea pigs, the earliest lesion was high-protein edema that expanded the interstitium and separated the seminiferous tubules (Figure 4B). This lesion did not appear to impact spermatogenesis because maturation of spermatogonia was orderly and mature spermatids were in the epididymal duct. Colonization did not correlate with inflammation in the testicle in either species. Although no bacteria were recovered at 8-weeks p.i. from the testicle, guinea pigs had evidence of diminished and disordered spermatogenesis at the chronic stage of infection (Figure 4B). A single guinea pig had evidence of on-going

inflammation characterized by focal necrosis of the seminiferous tubules surrounded by an intense inflammatory reaction composed of neutrophils and macrophages (Figure 4B). It is likely that infection at an earlier time point led to necrosis of the tubules and a localized inflammatory reaction to the release of "foreign" material of immature spermatozoa.

The prostate is an accessory sex organ responsible for producing part of the seminal fluid (Foley, 2001; Motrich et al., 2018). In men, prostatitis is reported to occur with infection (Boyd, 1938; Young, 1983). Due to the small organ size of the prostate in the mouse, culture was prioritized over histology, which prevented any correlation of colonization in this species. Culture was prioritized as it is the gold standard of determining infection and can be used to quantify viable organisms. Colonization of the prostate was detected in 2 of 4 (50%) guinea pigs at the acute stage of infection (4-weeks p.i.), and chronic time point (8-weeks p.i.). Inflammatory lesions were noted in the prostate at 4-weeks p.i. and 8-weeks p.i. which is reflected by a significant increase in mean histologic score (Figure 3B). The lesion was characterized by necrosis of the epithelium of the prostate acini with intense neutrophil and histiocyte coagulum replacing the normal seminal fluid (Figure 5). Acini were surrounded and separated by thick bands of fibrosis indicating chronic inflammation and tissue remodeling (Figure 5). *Brucella* antigen was detected by IHC within the foci of necrosis and intracellularly within macrophages (Figure 5). The lack of detectable colonization suggests the positive IHC response was due to dead bacteria contained within areas of necrosis and macrophages. The mismatch between colonization and histologic score in the epididymis and prostate suggests that *B. melitensis* can induce an intense inflammatory response in the absence of significant colonization.

After establishing that IT inoculation results in male reproductive disease in both species, the next objective was to evaluate a vaccine candidate to compare efficiency of the models. Since the goal was to establish the relative usefulness of the model rather than to evaluate the vaccine candidate, a reference strain was not used for comparison. In the vaccinated mouse group, an anesthetic death occurred during intratracheal inoculation. When vaccinated mice were challenged with 16 M *B. melitensis*, only the lung had a statistically significant reduction in mean colonization compared to unvaccinated animals challenged with 16 M (Figure 6A). While not statistically significant, vaccination reduced colonization in the epididymis and prostate to below the limit of detection by culture (<10 CFU/g). Unexpectedly, vaccination did not reduce colonization in the guinea pigs (Figure 6B). This contrasts with a previous experiment in which pregnant guinea pigs vaccinated with 16 M*ΔvjbR* were protected following challenge. (Hensel et al., 2020) It is possible that 16 M*ΔvjbR* requires an adjuvant to increase the efficacy; in the pregnant guinea pig challenge model, the vaccine was administered with Quil-A (Hensel et al., 2020). The contrasting results in male mice and guinea pigs and between female and male guinea pig stresses the value of evaluating novel vaccine candidates in more than one model and using both sexes.

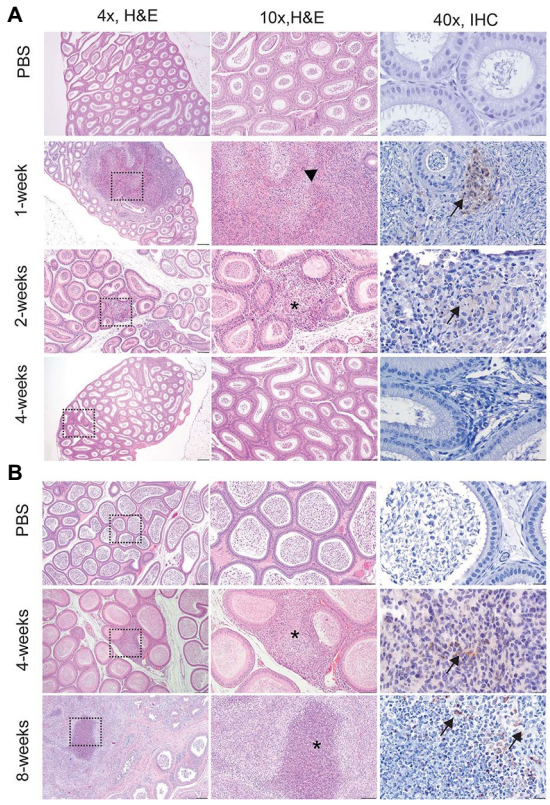

FIGURE 4
Infection with 16M *B. melitensis* disrupts spermatogenesis in the guinea pig. Testicle from mice **(A)** at the peracute (1- and 2-week p.i.) and acute (4-week p.i.) and guinea pigs **(B)** at the acute (4-week p.i.) and chronic (8-weeks p.i.) stages of infection following IT inoculation with 10^7 *B. melitensis*. No lesions were detected in the mouse at any stage of infection. The lesion in guinea pigs at 8-weeks consisted of a focally extensive area of necrosis with macrophages and neutrophils (yellow arrow). Adjacent seminiferous tubules were degenerate (*) with disrupted spermatogenesis. Macrophages were positive for *Brucella* antigen by IHC (black arrow). Tissues were stained with hematoxylin and eosin (H&E) and a polyclonal *Brucella* antibody (IHC) at 1:500 with Gill's hematoxylin counterstain. Dashed box of 4x image indicates area highlighted for the 10x and 40x images. 4x, scale bar=100μm; 10x, scale bar=50μm; 40x, scale bar=10μm.

Discussion

B. abortus and *B. melitensis* cause reproductive disease in both males and females, making it critical to be able to model disease in both sexes to better understand disease pathogenesis underlying reproductive disease as well as to evaluate newly developed countermeasures (i.e., vaccines and therapeutics) for use in humans.

Brucella-associated reproductive disease has been evaluated in female mice and more recently in female guinea pigs (Tobias et al., 1993; Kim et al., 2005; Grillo et al., 2012; Byndloss et al., 2019; Hensel et al., 2019, 2020). While vaccination strategies in production animals focus on vaccinating female animals to prevent the spread of disease to other animals and humans, any vaccine for

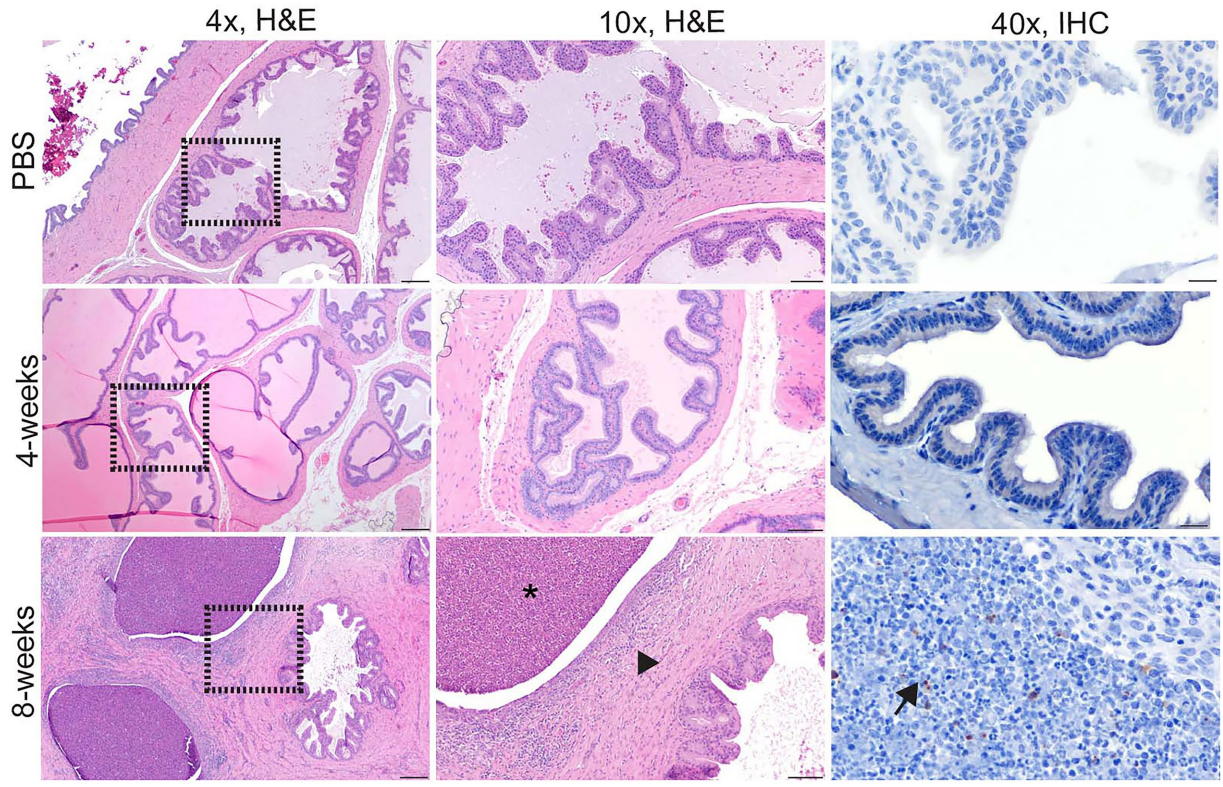

FIGURE 5
Intratracheal inoculation with 16M *B. melitensis* in the guinea pig results in prostatitis at the chronic time point. Prostate from guinea pigs at the acute (4-week p.i.) and chronic (8-weeks p.i.) stages of infection following IT inoculation with 10^7 *B. melitensis*. Two guinea pigs in the chronic group had abundant fibrosis separating the glands (arrowhead) with infiltrates of lymphocytes and plasma cells. The prostatic glands were dilated and contained abundant degenerate neutrophils and cellular debris (*). IHC of the prostate lesion revealed extracellular *Brucella* antigen within the area of cellular debris (arrow). Tissues were stained with hematoxylin and eosin (H&E) and a polyclonal *Brucella* antibody (IHC) at 1:500 with Gill's hematoxylin counterstain. Dashed box of 4x image indicates area highlighted for the 10x and 40x images. 4x, scale bar=100μm; 10x, scale bar=50μm; 40x, scale bar=10μm.

use in humans would need to be safe and efficacious in both sexes to be useful in preventing disease. In endemic regions, infection with *B. melitensis* results in scrotal swelling, pain, epididymitis, and orchitis in men (Khan et al., 1989; Yetkin et al., 2005; Colmenero et al., 2007; Gul et al., 2009). This study aimed to provide a foundation for exploring reproductive brucellosis in men through comparative animal models: mice and guinea pigs.

Hartley guinea pigs and C57BL/6 mice have both been used extensively in *Brucella* spp. vaccination and pathogenesis studies (García-Carrillo, 1990; Grillo et al., 2012). Guinea pigs were previously the model of choice to assess virulence and commercially available vaccines for brucellosis were tested in guinea pigs (Huddleson, 1943; García-Carrillo, 1990). Previous studies in male mice and guinea pigs have utilized intraperitoneal, intratesticular, or intra-gastric (oral) routes of inoculation to evaluate the impact of the male reproductive organs (Meyer et al., 1922; Hillaert et al., 1950; Moulton and Meyer, 1958; Jimenez de Bagues et al., 1993; Izadjoo et al., 2008). When considering a route of inoculation for experimental use, it is important to consider the relevance to natural transmission pathways as well as the anatomy and physiology of the animal. I.p. inoculation is artificial route of inoculation and is especially challenging for studies investigating the impact on the male reproductive system because the scrotum and peritoneal cavity are continuous; therefore, the inoculum can move directly to the reproductive tissues without first generating systemic disease/bacteremia (Knoblaugh et al., 2018a). Aerosol or oral routes of inoculation are most applicable for studies investigating natural transmission methods for *Brucella* spp. in humans (Young, 1983; Corbel, 2006).

For this study, intratracheal inoculation was utilized as it mimics a natural transmission route, and IT intratracheal inoculation with 10^7 16 M has been shown to reliably produce reproductive disease in female guinea pigs (Hensel et al., 2019, 2020). Although a dose of 10–100 CFU reportedly results in clinical symptoms in humans, occupational exposures such as handling aborted placentas or unknown microbial cultures on an open bench could result in a much higher aerosolized dose (Pappas et al., 2003, 2006). Furthermore, previous work using IT inoculation in guinea pigs and an aerosolization study in rhesus macaques both demonstrated that 10^3 CFU was the minimum dose required to generate disease; however, in both rhesus macaques and guinea pigs, higher doses (10^5 to 10^6 CFU,

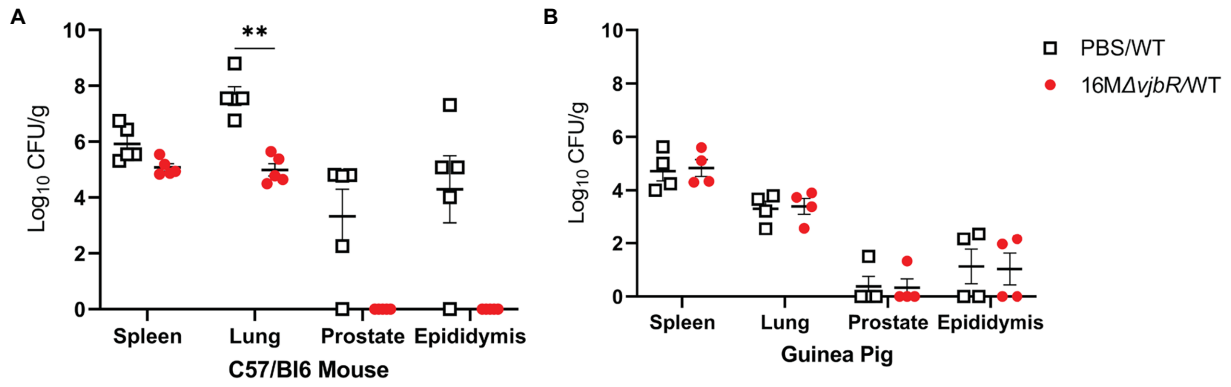

FIGURE 6
Vaccination in mice reduced colonization in the spleen, lung, and reproductive tissues. Mice and guinea pigs were vaccinated with 1×10^9 CFU/100µl *B. melitensis* 16MΔ*vjbR* (16MΔ*vjbR*/WT) subcutaneously or sham vaccinated with 100µl endotoxin-free PBS (PBS/WT) and were challenged IT with 1×10^7 CFU 16M *B. melitensis*. **(A)** Mice (n=5) were euthanized 1-week post challenge and spleen, lung, epididymis, and prostate were cultured on Farrell's media. **(B)** Spleen, lung, epididymis, and prostate were collected from guinea pigs (n=4) at 2-weeks post-challenge and cultured on Farrell's. Differences in colonization between groups analyzed by multiple Mann Whitney U Test with Sidak-Bonferroni correction. Horizontal bar indicates mean. Results reported as $\log_{10}$ CFU/g with S.D. **p<0.01.

respectively) resulted in a higher percentage of infected animals and generated reproductive disease (Mense et al., 2004; Hensel et al., 2019). Therefore, a higher dose was administered *via* IT inoculation in mice and guinea pigs to determine the impact on the reproductive organs.

In the male mice, colonization initially occurred in the reproductive tissues at higher levels than that seen in the guinea pigs, but inflammation was more severe in the guinea pigs. This suggests that guinea pigs are better at replicating the natural course of infection because they develop lesions in the epididymis and testes, which impact spermatogenesis. A study by Izadjoo et al. in C57BL/6 male mice found that oral inoculation with 10^{11} *B. melitensis* resulted in low levels of infection in the testicle starting 2-weeks p.i. through 8-weeks p.i.(Izadjoo et al., 2008). This infection was accompanied by perivascular inflammation of the epididymis, but no lesions were reported in the parenchyma of the testicle or epididymis (Izadjoo et al., 2008). Taken together, the Izadjoo study and our current results suggest that male mice do not develop inflammation in the reproductive organs following oral or aerosol inoculation with *B. melitensis* despite evidence of colonization (Izadjoo et al., 2008). These results also stress the importance of correlating colonization with histologic evidence of disease.

Early studies utilizing artificial routes of intraperitoneal or intratesticular inoculation demonstrated that guinea pigs develop abscesses of the testicle and epididymis when infected with *B. suis, abortus,* and *melitensis* (Meyer et al., 1922; Hillaert et al., 1950; Braude, 1951; Moulton and Meyer, 1958). When male guinea pigs were used in the early aerosol exposure research, these studies did not characterize the effect on the male reproductive tract (Elberg and Henderson, 1948; Harper, 1955; Druett et al., 1956). Therefore, it was unknown if aerosol transmission would generate reproductive pathology in the guinea pig model. Interestingly, guinea pigs inoculated intratracheally developed lesions in the parenchyma of the reproductive organs even with limited colonization at the chronic stage of infection. In this study, evidence indicates an intratracheal dose of 10^7 generates acute and chronic infection accompanied by significant inflammation.

B. melitensis and *B. suis* have been used in aerosol studies in rhesus macaques as a model for human brucellosis, which have demonstrated that an aerosol dose of 10^5 CFU *B. melitensis* and 10^7 CFU *B. suis* could induce orchitis and epididymitis in a small number of animals (Mense et al., 2004; Yingst et al., 2010). Mense et al. detected histologic lesions of infection in a single animal 63-days post-inoculation with 10^5 which resemble the lesions described in guinea pigs of this report. The study by Yingst et al. confirmed infection by polymerase chain reaction (PCR) rather than culture. Therefore, the reported lesion in this case may not have been due to active colonization. The lesions reported in the macaques are like those we describe in the guinea pig. Thus, it may be possible to have active inflammation in the absence of positive culture from the tissue. Additional studies are required to elucidate this seeming contradiction of active inflammation without a detectable agent.

In natural hosts such as bulls, rams, bucks, and dogs the histologic lesion is characterized by necrosis, fibrosis, and atrophy of the testicle and epididymis, which is replicated in both the mouse and guinea pig (Lambert et al., 1963; Greene and Carmichael, 2012; Foster, 2016). In humans, the diagnosis is often by serology and response to antibiotic therapy rather than histologic evaluation. Therefore, we cannot definitively know if the guinea pig or mouse reflect the underlying pathology (Young, 1983; Colmenero et al., 2007). However, the severity of the clinical symptoms in infected men (testicular swelling/pain) suggests that the underlying pathology is marked (Young, 1983; Khan et al., 1989).

The organs of the reproductive tract are considered immune privileged but do have a resident population of immune cells in the subepithelium of the epididymal duct and submucosa of the prostate acini (Foster, 2016). Infection with *B. melitensis* may stimulate an inflammatory response in these resident populations

that leads to necrosis of the epididymal duct between 4 to 8-weeks post-infection. Spermatids contain unique genetic material which is recognized as "foreign" to immune cells; spermatids not contained within the lumen of the epididymal duct incite a strong inflammatory reaction (spermatic granuloma; Foster, 2016). Thus, inflammation of the reproductive tract associated with *B. melitensis* may not be correlated with current levels of colonization. Instead, it may indicate infection at an earlier time point. Intense inflammation in the epididymis can create an outflow obstruction, leading to spermiostasis and degeneration of the seminiferous tubules. Since the spermatic cycle in guinea pigs takes 2-weeks, infection with *B. melitensis* produced on-going spermiostasis in the guinea pig resulting in a paucity of mature spermatids and decreased fertility (Cleland, 1951). This suggests that fertility of infected men may still be negatively impacted in the absence of active infection.

Humans, mice, and guinea pigs have similar accessory sex glands (prostate, seminal vesicle) that contribute components of the seminal fluid to nourish the spermatozoa (Hargaden and Singer, 2012; Knoblaugh et al., 2018b). The prostate is a potential reservoir of *Brucella* spp., and infection of this organ in man can lead to abscesses and urinary tract infections (Boyd, 1938; Young, 1983). While a reservoir function cannot be appreciated due to the lack of detectable colonization at 8-weeks post-inoculation, previous infection of this organ in the guinea pig is reflected by an inflammatory response within the prostate which is similar to the lesions described in case reports of men with prostatitis (Savasci et al., 2014).

The stark contrast in protection afforded by the same vaccine in mice and guinea pigs emphasizes the necessity of evaluating candidates in more than one model. Several vaccine candidates have shown promising results in mice but have diminished efficacy when introduced into target species, like small ruminants (Carvalho et al., 2016). Guinea pigs are outbred animals and therefore may be more representative of vaccine efficacy than mouse models, which are often genetically homogeneous. An additional advantage of the guinea pig is the ability to evaluate both microbiological and histopathological results due to the larger size of the reproductive organs. Future experiments are required to determine optimal study end-points for vaccine efficacy in the guinea pig, but the results presented herein make a compelling case that guinea pigs are an appropriate animal model for evaluating the impact on the male reproductive tract.

Conclusion

This study characterizes reproductive disease in two commonly available animal models. Understanding the pathogenesis of reproductive disease and evaluating potential vaccines for use in men requires an animal model that mimics the manifestation of human disease. This study demonstrates that infectious aerosols can generate reproductive disease in male guinea pigs and highlights the potential of intratracheal inoculation in guinea pigs to serve as a model for reproductive disease. Further studies are needed to evaluate vaccines in male animals and determine if the results presented herein are typical of vaccine efficacy in males.

Data availability statement

The raw data supporting the conclusions of this article will be made available by the authors, without undue reservation.

Ethics statement

The animal study was reviewed and approved by Institutional Animal Care and Use Committee Texas A&M University.

Author contributions

MH, JE, and AA-G: conceptualized the project and performed data analysis. MH and LS: performed the experiments. MH: wrote the manuscript. All authors participated in manuscript review and approved the manuscript.

Funding

Student stipend support was provided by the National Institutes of Health Institutional Training Grant T32 OD 11057 (MH).

Conflict of interest

The authors declare that the research was conducted in the absence of any commercial or financial relationships that could be construed as a potential conflict of interest.

Publisher's note

All claims expressed in this article are solely those of the authors and do not necessarily represent those of their affiliated organizations, or those of the publisher, the editors and the reviewers. Any product that may be evaluated in this article, or claim that may be made by its manufacturer, is not guaranteed or endorsed by the publisher.

Supplementary material

The Supplementary material for this article can be found online at: https://www.frontiersin.org/articles/10.3389/fmicb.2022.1029199/full#supplementary-material

References

Arenas-Gamboa, A. M., Ficht, T. A., Kahl-McDonagh, M. M., and Rice-Ficht, A. C. (2008). Immunization with a single dose of a microencapsulated Brucella melitensis mutant enhances protection against wild-type challenge. *Infect. Immun.* 76, 2448–2455. doi: 10.1128/IAI.00767-07

Arenas-Gamboa, A. M., Rice-Ficht, A. C., Fan, Y., Kahl-Mcdonagh, M. M., and Ficht, T. A. (2012). Extended safety and efficacy studies of the attenuated Brucella vaccine candidates 16 M(Delta)vjbR and S19(Delta)vjbR in the immunocompromised IRF-1−/− mouse model. *Clin. Vaccine Immunol.* 19, 249–260. doi: 10.1128/CVI.05321-11

Boyd, M. L. (1938). Human prostatic infection with Brucella abortus (Alcaligenes Abortus). *J. Urol.* 39, 717–721. doi: 10.1016/S0022-5347(17)71908-8

Braude, A. I. (1951). Studies in the pathology and pathogenesis of experimental brucellosis. I. a comparison of the pathogenicity of Brucella abortus, Brucella melitensis, and Brucella suis for Guinea pigs. *J. Infect. Dis.* 89, 76–86. doi: 10.1093/infdis/89.1.76

Byndloss, M. X., Tsai, A. Y., Walker, G. T., Miller, C. N., Young, B. M., English, B. C., et al. (2019). Brucella abortus infection of placental Trophoblasts triggers endoplasmic reticulum stress-mediated cell death and fetal loss via type IV secretion system-dependent activation of CHOP. *MBio* 10:e01538–19. doi: 10.1128/mBio.01538-19

Carvalho, T. F., Haddad, J. P., Paixao, T. A., and Santos, R. L. (2016). Meta-analysis and advancement of brucellosis Vaccinology. *PLoS One* 11:e0166582. doi: 10.1371/journal.pone.0166582

Cleland, K. W. (1951). The spermatogenic cycle of the Guinea pig. *Aust. J. Sci. Res. B* 4, 344–369. doi: 10.1071/BI9510344

Colmenero, J. D., Munoz-Roca, N. L., Bermudez, P., Plata, A., Villalobos, A., and Reguera, J. M. (2007). Clinical findings, diagnostic approach, and outcome of Brucella melitensis epididymo-orchitis. *Diagn. Microbiol. Infect. Dis.* 57, 367–372. doi: 10.1016/j.diagmicrobio.2006.09.008

Corbel, M. J. (2006). Brucellosis in humans and animals. World Health Organization. Available at: https://apps.who.int/iris/handle/10665/43597 (Accessed September 22, 2016).

Druett, H. A., Henderson, D. W., and Peacock, S. (1956). Studies on respiratory infection. III Experiments with Brucella suis. *J. Hyg. (Lond.)* 54, 49–57. doi: 10.1017/S0022172400044296

Elberg, S. S., and Henderson, D. W. (1948). Respiratory pathogenicity of Brucella. *J. Infect. Dis.* 82, 302–306. doi: 10.1093/infdis/82.3.302

Foley, G. L. (2001). Overview of male reproductive pathology. *Toxicol. Pathol.* 29, 49–63. doi: 10.1080/019262301301418856

Foster, R. A. (2016). "Chapter 5-Male genital system" in *Jubb, Kennedy and Palmer's Pathology of Domestic Animals*. ed. M. G. Maxie. *6th* ed (St. Louis, MO: W.B. Saunders), 465–510. doi: 10.1016/B978-0-7020-5319-1.00016-5

García-Carrillo, C. (1990). *Laboratory Animal Models for Brucellosis Studies*. Boca Raton, FL: CRC Press.

Garin-Bastuji, B., and Blasco, J. M. (2016). Brucellosis (infection with Brucella abortus, B. melitensis, and B. suis) [online]. Available at: http://www.oie.int/en/international-standard-setting/terrestrial-manual/access-online/ (Accessed August 10, 2016).

Greene, C. E., and Carmichael, L.E. (2012). *Infectious Diseases of the Dog and Cat. 4th Edn.* (London: Elsevier Health Sciences).

Gregory, A. E., Van Schaik, E. J., Russell-Lodrigue, K. E., Fratzke, A. P., and Samuel, J. E. (2019). Coxiella burnetii Intratracheal aerosol infection model in mice, Guinea pigs, and nonhuman primates. *Infect. Immun.* 87:e00178–19. doi: 10.1128/IAI.00178-19

Grillo, M. J., Blasco, J. M., Gorvel, J. P., Moriyon, I., and Moreno, E. (2012). What have we learned from brucellosis in the mouse model? *Vet. Res.* 43:29. doi: 10.1186/1297-9716-43-29

Gul, H. C., Akyol, I., Sen, B., Adayener, C., and Haholu, A. (2009). Epididymoorchitis due to Brucella melitensis: review of 19 patients. *Urol. Int.* 82, 158–161. doi: 10.1159/000200791

Hargaden, M., and Singer, L. (2012). "Chapter 20-Anatomy, physiology, and behavior," in *The Laboratory Rabbit, Guinea Pig, Hamster, and Other Rodents*. eds. M. A. Suckow, K. Stevens and R. Wilson (Amsterdam, Netherlands: Academic Press).

Harper, G. J. (1955). Brucella suis infection of Guinea-pigs by the respiratory route. *Br. J. Exp. Pathol.* 36, 60–70. PMID: 14351638

Henning, L. N., Gillum, K. T., Fisher, D. A., Barnewall, R. E., Krile, R. T., Anderson, M. S., et al. (2012). The pathophysiology of inhalational brucellosis in BALB/c mice. *Sci. Rep.* 2:495. doi: 10.1038/srep00495

Hensel, M. E., Chaki, S. P., Stranahan, L., Gregory, A. E., Van Schaik, E. J., Garcia-Gonzalez, D. G., et al. (2020). Intratracheal inoculation with Brucella melitensis in the pregnant Guinea pig is an improved model for reproductive pathogenesis and vaccine studies. *Infect. Immun.* 88:e00204–20. doi: 10.1128/IAI.00204-20

Hensel, M. E., Garcia-Gonzalez, D. G., Chaki, S. P., Samuel, J., and Arenas-Gamboa, A. M. (2019). Characterization of an intratracheal aerosol challenge model of Brucella melitensis in Guinea pigs. *PLoS One* 14:e0212457. doi: 10.1371/journal.pone.0212457

Hillaert, E. L., Hutchings, L. M., and Andrews, F. N. (1950). Brucellosis in male guinea pigs. *Am. J. Vet. Res.* 11, 84–88.

Huddleson, I.F. (1943). *Brucellosis in Man and Animals*. New York: The Commonwealth Fund.

Izadjoo, M. J., Mense, M. G., Bhattacharjee, A. K., Hadfield, T. L., Crawford, R. M., and Hoover, D. L. (2008). A study on the use of male animal models for developing a live vaccine for brucellosis. *Transbound. Emerg. Dis.* 55, 145–151. doi: 10.1111/j.1865-1682.2008.01019.x

Jimenez de Bagues, M. P., Marin, C. M., Barberan, M., and Blasco, J. M. (1993). Evaluation of vaccines and of antigen therapy in a mouse model for Brucella ovis. *Vaccine* 11, 61–66. doi: 10.1016/0264-410X(93)90340-4

Kahl-McDonagh, M. M., Arenas-Gamboa, A. M., and Ficht, T. A. (2007). Aerosol infection of BALB/c mice with Brucella melitensis and Brucella abortus and protective efficacy against aerosol challenge. *Infect. Immun.* 75, 4923–4932. doi: 10.1128/IAI.00451-07

Kahl-McDonagh, M. M., Elzer, P. H., Hagius, S. D., Walker, J. V., Perry, Q. L., Seabury, C. M., et al. (2006). Evaluation of novel Brucella melitensis unmarked deletion mutants for safety and efficacy in the goat model of brucellosis. *Vaccine* 24, 5169–5177. doi: 10.1016/j.vaccine.2006.04.005

Khan, M. S., Humayoon, M. S., and Al Manee, M. S. (1989). Epididymo-orchitis and brucellosis. *Br. J. Urol.* 63, 87–89. doi: 10.1111/j.1464-410X.1989.tb05131.x

Kim, S., Lee, D. S., Watanabe, K., Furuoka, H., Suzuki, H., and Watarai, M. (2005). Interferon-gamma promotes abortion due to Brucella infection in pregnant mice. *BMC Microbiol.* 5:22. doi: 10.1186/1471-2180-5-22

Knoblaugh, S. E., True, L., Tretiakova, M., and Hukkanen, R. R. (2018a). "Chapter 18-Male reproductive system," in *Comparative Anatomy and Histology*. eds. P. M. Treuting, S. M. Dintzis and K.S. Montine (Cambridge, MA: Academic Press).

Knoblaugh, S. E., True, L., Tretiakova, M., and Hukkanen, R. R. (2018b). "Chapter 18-Male reproductive system," in *Comparative Anatomy and Histology: A Mouse, Rat and Human Atlas. 2nd Edn.* eds. P. M. Treuting, S. M. Dintzis and K. S. Montine (Academic Press).

Lambert, G. M., Manthei, C. A., and Deyoe, B. L. (1963). Studies on Brucella abortus infection in bulls. *Am. J. Vet. Res.* 24, 1152–1157. PMID: 14081449

Mense, M. G., Borschel, R. H., Wilhelmsen, C. L., Pitt, M. L., and Hoover, D. L. (2004). Pathologic changes associated with brucellosis experimentally induced by aerosol exposure in rhesus macaques (Macaca mulatta). *Am. J. Vet. Res.* 65, 644–652. doi: 10.2460/ajvr.2004.65.644

Mense, M. G., Van De Verg, L. L., Bhattacharjee, A. K., Garrett, J. L., Hart, J. A., Lindler, L. E., et al. (2001). Bacteriologic and histologic features in mice after intranasal inoculation of Brucella melitensis. *Am. J. Vet. Res.* 62, 398–405. doi: 10.2460/ajvr.2001.62.398

Meyer, K. F., Shaw, E. B., and Fleischner, E. C. (1922). The pathogenicity of B. melitensis and B. abortus for Guinea-pigs: studies on the genus Brucella Nov Gen. IV. *J. Infect. Dis.* 31, 159–197. doi: 10.1093/infdis/31.2.159

Motrich, R. D., Salazar, F. C., Breser, M. L., Mackern-Oberti, J. P., Godoy, G. J., Olivera, C., et al. (2018). Implications of prostate inflammation on male fertility. *Andrologia* 50:e13093. doi: 10.1111/and.13093

Moulton, J. E., and Meyer, M. E. (1958). The pathogenesis of Brucella suis infection in Guinea pigs: lesions of the spleen, liver, testis, and articulations. *Cornell Vet.* 48, 165–195. PMID: 13537582

Pappas, G., Bosilkovski, M., Akritidis, N., Mastora, M., Krteva, L., and Tsianos, E. (2003). Brucellosis and the respiratory system. *Clin. Infect. Dis.* 37, e95–e99. doi: 10.1086/378125

Pappas, G., Panagopoulou, P., Christou, L., and Akritidis, N. (2006). Biological weapons. *Cell. Mol. Life Sci. CMLS* 63, 2229–2236. doi: 10.1007/s00018-006-6311-4

Picard-Hagen, N., Berthelot, X., Champion, J. L., Eon, L., Lyazrhi, F., Marois, M., et al. (2015). Contagious epididymitis due to Brucella ovis: relationship between sexual function, serology and bacterial shedding in semen. *BMC Vet. Res.* 11:125. doi: 10.1186/s12917-015-0440-7

Savasci, U., Zor, M., Karakas, A., Aydin, E., Kocaaslan, R., Oren, N. C., et al. (2014). Brucellar epididymo-orchitis: a retrospective multicenter study of 28 cases and review of the literature. *Travel Med. Infect. Dis.* 12, 667–672. doi: 10.1016/j.tmaid.2014.10.005

Stranahan, L. W., Khalaf, O. H., Garcia-Gonzalez, D. G., and Arenas-Gamboa, A. M. (2019). Characterization of Brucella canis infection in mice. *PLoS One* 14:e0218809. doi: 10.1371/journal.pone.0218809

Tobias, L., Cordes, D. O., and Schurig, G. G. (1993). Placental pathology of the pregnant mouse inoculated with Brucella abortus strain 2308. *Vet. Pathol.* 30, 119–129. doi: 10.1177/030098589303000204

Traxler, R. M., Lehman, M. W., Bosserman, E. A., Guerra, M. A., and Smith, T. L. (2013). A literature review of laboratory-acquired brucellosis. *J. Clin. Microbiol.* 51, 3055–3062. doi: 10.1128/JCM.00135-13

Weeks, J. N., Galindo, C. L., Drake, K. L., Adams, G. L., Garner, H. R., and Ficht, T. A. (2010). Brucella melitensis VjbR and C12-HSL regulons: contributions of the N-dodecanoyl homoserine lactone signaling molecule and LuxR homologue VjbR to gene expression. *BMC Microbiol.* 10:167. doi: 10.1186/1471-2180-10-167

Yetkin, M. A., Erdinc, F. S., Bulut, C., and Tulek, N. (2005). Epididymoorchitis due to brucellosis in Central Anatolia, Turkey. *Urol. Int.* 75, 235–238. doi: 10.1159/000087801

Yingst, S. L., Huzella, L. M., Chuvala, L., and Wolcott, M. (2010). A rhesus macaque (Macaca mulatta) model of aerosol-exposure brucellosis (Brucella suis): pathology and diagnostic implications. *J. Med. Microbiol.* 59, 724–730. doi: 10.1099/jmm.0.017285-0

Young, E. J. (1983). Human brucellosis. *Rev. Infect. Dis.* 5, 821–842. doi: 10.1093/clinids/5.5.821

Young, E. J. (1995). An overview of human brucellosis. *Clin. Infect. Dis.* 21, 283–290. doi: 10.1093/clinids/21.2.283

frontiers | Frontiers in Microbiology

TYPE Original Research
PUBLISHED 31 October 2022
DOI 10.3389/fmicb.2022.1046640

OPEN ACCESS

EDITED BY
Roy Martin Roop II,
East Carolina University,
United States

REVIEWED BY
Clayton Caswell,
Virginia Tech,
United States
Myron Christodoulides,
University of Southampton,
United Kingdom
Alessia Ruggiero,
Institute of Biostructure and Bioimaging (CNR), Italy

*CORRESPONDENCE
Mara S. Roset
mroset@iib.unsam.edu.ar
Gabriel Briones
gbriones@iib.unsam.edu.ar

SPECIALTY SECTION
This article was submitted to Infectious Agents and Disease, a section of the Journal Frontiers in Microbiology

RECEIVED 17 September 2022
ACCEPTED 13 October 2022
PUBLISHED 31 October 2022

CITATION
Muruaga EJ, Briones G and Roset MS (2022) Biochemical and functional characterization of *Brucella abortus* cyclophilins: So similar, yet so different.
Front. Microbiol. 13:1046640.
doi: 10.3389/fmicb.2022.1046640

Biochemical and functional characterization of *Brucella abortus* cyclophilins: So similar, yet so different

Emanuel J. Muruaga[1,2], Gabriel Briones[1,2]* and Mara S. Roset[1,2]*

[1]Instituto de Investigaciones Biotecnológicas, Universidad Nacional de San Martín (UNSAM)-Consejo Nacional de Investigaciones Científicas y Técnicas (CONICET), Buenos Aires, Argentina, [2]Escuela de Bio y Nanotecnologías (EByN), Universidad Nacional de San Martín, Buenos Aires, Argentina

Brucella spp. are the etiological agent of animal and human brucellosis. We have reported previously that cyclophilins of *Brucella* (CypA and CypB) are upregulated within the intraphagosomal replicative niche and required for stress adaptation and host intracellular survival and virulence. Here, we characterize *B. abortus* cyclophilins, CypA, and CypB from a biochemical standpoint by studying their PPIase activity, chaperone activity, and oligomer formation. Even though CypA and CypB are very similar in sequence and share identical chaperone and PPIase activities, we were able to identify outstanding differential features between them. A series of differential peptide loops were predicted when comparing CypA and CypB, differences that might explain why specific antibodies (anti-CypA or anti-CypB) were able to discriminate between both cyclophilins without cross-reactivity. In addition, we identified the presence of critical amino acids in CypB, such as the Trp^{134} which is responsible for the cyclosporin A inhibition, and the Cys^{128} that leads to CypB homodimer formation by establishing a disulfide bond. Here, we demonstrated that CypB dimer formation was fully required for stress adaptation, survival within HeLa cells, and mouse infection in *B. abortus*. The presence of Trp^{134} and the Cys^{128} in CypB, which are not present in CypA, suggested that two different kinds of cyclophilins have evolved in *Brucella*, one with eukaryotic features (CypB), another (CypA) with similar features to Gram-negative cyclophilins.

KEYWORDS

brucellosis, *Brucella abortus*, Cyclophilins, virulence, PPIase activity, dimeric CypB, Brucella-host interaction, stress adaptation

Introduction

Cyclophilins are enzymes that belong to the superfamily of peptidyl-prolyl cis/trans isomerases (PPIases: EC 5.2.1.8). These enzymes act as biological catalysts speeding up the rate-limiting cis/trans or trans/cis conformational changes at Xaa-Pro bonds during protein folding in both eukaryotes and prokaryotes. The spontaneous isomerization of the peptidyl proline bonds is a slow reaction and consequently requires the assistance of PPIases that accelerates this step during protein folding. In addition to the cyclophilins, the superfamily of PPIases, also includes the FK506-binding proteins (FKBPs) and the parvulins, a classification that is based on their structure and specific inhibitor compound. Thus, while cyclophilins are inhibited by the immunosuppressive cyclosporin A (CsA), the FKBPs and parvulins are inhibited by the compounds FK506, and rapamycin, respectively (Galat, 2003; Fanghanel and Fischer, 2004).

Cyclophilins are either small single-domain proteins or large multi-domain ones (Pemberton, 2006; Krucken et al., 2009). In the case of the multi-domain cyclophilins, it has been described that additionally to the cyclophilin domain there are also protein domains that act as chaperones or promote the oligomerization state of the protein. Interestingly, even though single-domain cyclophilins are devoid of a canonical chaperone protein domain they can still present certain chaperone activity, which in some cases it has been shown to be independent of the PPIase catalytic activity (Dimou et al., 2011; Zhang et al., 2013; Pandey et al., 2016). Moreover, it has been described that some of the single-domain cyclophilins are still able to oligomerize (Zhang et al., 2011; Jakob et al., 2016).

Of relevance, the over-expression of many cyclophilin-encoding genes is triggered in response to a variety of stressors, suggesting a possible function of cyclophilins (Cyps) in stress adaptation. In agreement with this, microbial Cyps have been described to improve microbial survival under stress conditions and to be upregulated upon host-cell internalization, suggesting a possible function of these proteins in microbial-host interaction (Dimou et al., 2017). Interestingly, the critical role of PPIases in stress tolerance and pathogenesis of bacteria has been demonstrated in *Yersinia pseudotuberculosis* (Obi et al., 2011), *Streptococcus pneumoniae* (Hermans et al., 2006), *Enterococcus faecalis* (Reffuveille et al., 2012), *Streptococcus gordoni* (Cho et al., 2013), *Mycobacterium tuberculosis* (Pandey et al., 2017), *Staphylococcus aureus* (Wiemels et al., 2017; Keogh et al., 2018), *Legionella pneumophila* (Rasch et al., 2019), *Burkholderia pseudomallei* (Bzdyl et al., 2019), and *Salmonella* Typhimurium (Kumawat et al., 2020).

Brucellosis is a worldwide zoonotic disease caused by the intracellular bacterial pathogen, *Brucella* spp. *Brucella* spp. are Gram-negative bacteria that belongs to the α-2 group of *Proteobacteria*, a bacterial group characterized for living in close association with eukaryotic hosts such as plants or mammals (Corbel, 1997). *Brucella* infection causes abortion and sterility in animals, and undulating fever and debilitating disorders in humans, resulting in a serious public health problem and economic losses (de Figueiredo et al., 2015). *Brucella* virulence relies on its ability to adapt to an intracellular lifestyle within the host cells. To gain insight into the molecular mechanisms involved in intracellular adaptation and virulence of *Brucella*, we performed a comparative proteome analysis of *Brucella* grown in culture media or recovered from *Brucella* infected macrophages using two complementary technologies: 2D gel (Roset et al., 2013) and iTraq isobaric tag (Roset et al., 2017). We demonstrated through 2D gel analysis, that, upon intracellular localization, *B. abortus* over-expresses two PPIases (BAB1_1117 and BAB1_1118), belonging to the cyclophilin family (COG0652), referred to as CypB and CypA, respectively. Analysis of their function by mutagenesis and subsequent characterization showed that they are involved in stress adaptation, intracellular survival, and *Brucella* virulence (Roset et al., 2013). In this report, we characterized CypA and CypB from a biochemical and functional standpoint exploring the role of the cyclophilins in *Brucella*-host cell interaction.

Materials and methods

Bacterial strains and growth conditions

Bacterial strains and plasmids used are shown in Table 1. *Escherichia coli* strains were grown in Luria-Bertani (LB) media at 37°C on a rotatory shaker (250 rpm) or in LB agar for 16–24 h. *Brucella abortus* strains were grown in tryptic soy agar (TSA) or tryptic soy broth (TSB) media at 37°C on a rotatory shaker (250 rpm) for 16–24 h. When necessary, media were supplemented with the following antibiotics: kanamycin (km), 50 μg/ml, ampicillin 100 μg/ml, or nalidixic acid 5 μg/ml. Experiments involving live *Brucella* were performed in a Biosafety level 3 (BSL3) facility at the University of San Martín, Buenos Aires, Argentina.

Cloning

cypB and *cypB*$^{R59A/F64A}$ genes were amplified from *Brucella* genomic DNA or p*cypB*$^{R55A/F60A}$ plasmid, respectively, by PCR using the oligonucleotides (pFWCypBBamHI CGGGATCCGACC CAGAAAATACGCTCG and pRVCypBXhoI CCCTCGAGTCA GTCGGCGGCGATACG). Amplicons were digested with *BamH*I and *Xho*I restriction enzymes and cloned in pET-28a(+) vector from Novagen.

Synthetic genes, synthesized by Gene Universal Inc. (United States), *cypA*, *cypB*^{C128M}, *cypB*^{W134F}, *cypB*(*L2cypA*), *cypB*(*L3cypA*), *cypB*(*L2-L3cypA*), and *cypA*(*L1cypB*) were cloned in pET-28a (+). Genes *cypA3flag*, *3flagcypB*, *3flagcypB*$^{R59A/F64A}$, and *3flagcypB*^{C128M} were cloned in pBlueScript II SK(+) and then digested with *BamH*I and *Sac*II and subcloned in pDCyaA plasmid.

10.3389/fmicb.2022.1046640

TABLE 1 Bacterial strains and plasmids used in this study.

Strain or plasmid	Genotype or phenotype	Reference or source
Strains		
Escherichia coli		
BL21 DE3	F- ompT hsdSB (rBmB-) gal dcm (DE3)	Stratagen
TOP10	F-*mcrA* Δ(mrr-hsdRMS-mcrBC) Φ80*lacZ*ΔM15-Δ *lac*X74 *rec*A1 *ara*D139Δ(*araleu*)7697 *gal*U *gal*K *rps*L (StrR) *end*A1 *nup*G	Invitrogen
DH5α F'IQ	F′ Φ80d*lacZ*ΔM15 Δ(*lacZYA-argF*) *U169 deoR recA1 endA1 hsdR17*(r_K^+ m_K^+) *phoA*$^+$ *supE44* λ$^-$ *thi-1 gyrA96 relA1*/F′ *proAB*$^+$ *lacI*^{q}*Z*ΔM15 *zzf*::Tn*5* (Km^r)	Invitrogen
S17.1 (λ pir)	λ lysogenic S17-1 derivative producing π protein for replication of plasmids carrying oriR6K, Nal^S	Herrero et al. (1990)
Brucella abortus		
Wild type 2,308	Wild, smooth, virulent strain, Nal^r	Laboratory stock
2,308 (p*fcypB*)	*B. abortus* 2,308 with plasmid p*fcypB*, Amp^r	This study
2,308 (p*fcypB*$^{R59A/F64A}$)	*B. abortus* 2,308 with plasmid p*fcypB*$^{R59A/F64A}$, Amp^r	This study
Δ*cypAB* mutant	*B. abortus* 2,308 double mutant by deletion of the *cypA* and *cypB* genes	Roset et al. (2013)
Δ*cypAB*(p*cypAf*)	*B. abortus* Δ*cypAB* mutant with plasmid p*cypAf*, Amp^r	This study
Δ*cypAB*(p*fcypB*)	*B. abortus* Δ*cypAB* mutant with plasmid p*fcypB*, Amp^r	This study
Δ*cypAB*(p*fcypB*$^{R59A/F64A}$)	*B. abortus* Δ*cypAB* mutant with plasmid p*fcypB*$^{R59A/F64A}$, Amp^r	This study
Δ*cypAB*(p*fcypB*^{C128M})	*B. abortus* Δ*cypAB* mutant with plasmid p*fcypB*^{C128M}, Amp^r	This study
Plasmids		
pET-28a(+)	Bacterial cloning vector with T7lac promoter that carries in the N-terminal a His-Tag / thrombin / T7-Tag configuration, an optional His-Tag sequence in the C-terminal and kanamycin resistance gene.	EMD Biosciences
pET-28-*cypA*	510 pb *BamHI*/*Xho*I fragment containing the *B. abortus* 2,308 *cypA* gene starting at position 82 bp, cloned into pET-28a(+), Km^r.	This study
pET-28-*cypB*	492 pb *BamHI*/*Xho*I fragment containing the *B. abortus* 2,308 *cypB* gene starting at position 37 bp, cloned into pET-28a(+), Km^r.	This study
pET-28-*cypB*$^{R59A/F64A}$	492 pb *BamHI*/*Xho*I fragment containing the *B. abortus* 2,308 *cypB*$^{R55A/F60A}$ mutant gene starting at position 37 bp, cloned into pET-28a(+), Km^r.	This study
pET-28-*cypB*^{W134F}	492 pb *BamHI*/*Xho*I fragment containing the *B. abortus* 2,308 *cypB*^{W134F} mutant gene starting at position 37 bp, cloned into pET-28a(+), Km^r	This study
pET-28-*cypB*^{C128M}	492 pb *BamHI*/*Xho*I fragment containing the *B. abortus* 2,308 *cypB*^{C128M} mutant gene starting at position 37 bp, cloned into pET-28a(+), Km^r.	This study
pET-28-*cypB*(*L2cypA*)	534 bp *Nhe*I/*Xho*I fragment containing the *B. abortus* 2,308 *cypB* gene starting at position 37 bp, where loop-2 from *cypB* (289–294 bp) was replaced by loop-2 of *cypA* (310–336 bp), cloned into pET-28a(+), Km^r.	This study
pET-28-*cypB*(*L3cypA*)	525 bp *Nhe*I/*Xho*I fragment containing the *B. abortus* 2,308 *cypB* gene starting at position 37 bp, where loop-3 from *cypB* (478–489 bp) was replaced by loop-3 of *cypA* (523–546 bp), cloned into pET-28a(+), Km^r.	This study
pET-28-*cypB*(*L2-L3cypA*)	534 bp *Nhe*I/*Xho*I fragment containing the *B. abortus* 2,308 *cypB* gene starting at position 37 bp, where loop-2 (289–294 bp) and loop-3 from *cypB* (478–489 bp) were replaced by loop-2 (310–336 bp) and loop-3 (523–546 bp) of *cypA* respectively, cloned into pET-28a(+), Km^r.	This study
pET-28-*cypA*(*L1cypB*)	552 bp *Nhe*I/*Xho*I fragment containing the *B. abortus* 2,308 *cypA* gene starting at position 82 bp, where loop-1 from *cypA* (268–297 bp) was replaced by loop-1 of *cypB* (223–276 bp), cloned into pET-28a(+), Km^r.	This study
p*cypB*$^{R55A/F60A}$	*B. abortus cypB*$^{K55A/F60A}$ gene cloned into pDK51, Amp^r	Roset et al. (2013)
pET-21-eGFP	Derived from pET21b, expresses eGFP fusion protein, Km^r.	Fina Martin et al. (2019)
pDCyaA	Cloning vector for C-terminus fusion to CyaA under bcsp31 gene promoter, Amp^r	Marchesini et al. (2011)
p*cypAf*	657-bp *BamHI*/*Sac*II synthetic fragment containing full-length *B. abortus cypA* gene and 3flag, cloned into pDCyaA, Amp^r	This study
p*fcypB*	0.6-kb *BamHI*/*Sac*II synthetic fragment containing 3flag and the *B. abortus 2,308* full-length *cypB* gene, cloned into pDCyaA, Amp^r	This study
p*fcypB*$^{R59A/F64A}$	0.6-kb *BamHI*/*Sac*II synthetic fragment containing 3flag and the *B. abortus 2,308* full-length *cypB* gene where Arg^{59} and Phe^{64} were replaced by Ala, cloned into pDCyaA, Amp^r	This study
p*fcypB*^{C128M}	0.6-kb *BamHI*/*Sac*II synthetic fragment containing 3flag and the *B. abortus 2,308* full-length *cypB* gene where Cys^{128} was replaced by Met, cloned into pDCyaA, Amp^r	This study

Amp^r, ampicillin resistance; Nal^r, nalidixic acid resistance; Km^r, kanamycin resistance.

Electroporation of the *E. coli* strain was performed with the Pulser-BioRad electroporator according to the manufacturer's protocol.

Brucella abortus complementation

Brucella abortus ΔcypAB mutant was genetically complemented by introducing p*3flagcypA*, p*3flagcypB*, p*3flagcypB*$^{R59A/F64A}$, and p*3flagcypB*^{C128M} plasmids by biparental mating using *E. coli* S17.1 as donor strain (Ditta et al., 1980). *Brucella* complemented strains were selected in ampicillin and nalidixic acid TSA plates, and the presence of different cyclophilins were confirmed by PCR and Western blot analysis (anti-CypA and anti-CypB antibodies).

Brucella abortus 2,308 was genetically transformed by introducing p*3flagcypB* or p*3flagcypB*$^{R59A/F64A}$ plasmids by biparental mating using *E. coli* S17.1 as donor strain (Ditta et al., 1980). *Brucella* transformed strains were selected in ampicillin and nalidixic acid TSA plates, and the presence of different cyclophilins were confirmed by PCR and Western blot analysis (anti-3FLAG antibody).

Purification of recombinant proteins

His-tagged recombinant proteins (CypA, CypB, CypB$^{R59A/F64A}$, CypB^{C128M}, CypB^{W134F} CypA(L1CypB), CypB(L2CypA), CypB(L3CypA), CypB(L2-L3CypA), and GFP) were expressed in *E. coli* and purified using nickel affinity chromatography. Briefly, *E. coli* strains were grown at 37°C at 200 rpm and the expression was induced with 0.1 mM IPTG at A600 = 0.5. Two hours post-induction cells were harvested at 7000 X *g* and lysed by sonication. Recombinant proteins were purified from soluble fractions with the HisTrap™ HP column (GE Healthcare). Elution was performed with an imidazole gradient (20 to 500 mM). Fractions with recombinant proteins were dialyzed and quantified with NanoDrop One Microvolume UV–Vis Spectrophotometer (Thermo Fischer). Expression was confirmed by Western blotting. The predicted molecular weight of the recombinant proteins are: 21.5 kDa (CypA), 21.1 kDa (CypB), 21.0 kDa (CypB$^{R59A/F64A}$), 20.2 kDa (CypB^{C128M}), 20.1 kDa (CypB^{W134F}), 21.0 kDa (CypA(L1CypB)), 20.9 kDa (CypB(L2CypA)), 20.5 kDa (CypB(L3CypA)), 21.3 kDa (CypB(L2-L3CypA)), and 46.6 kDa (GFP).

Protein analysis

Protein samples were suspended in cracking buffer (2% SDS, 10% Glycerol, 60 mM Tris-Cl pH 6.8, 0.01% Bromophenol Blue, and 100 mM DTT) and incubated for 5 min at 100°C. Protein electrophoresis was performed at 120 V on a 12% SDS-PAGE gel. Gels were stained in Coomassie-Blue solution (20% methanol, 10% acetic acid).

For Western Blot analysis, proteins were transferred to a nitrocellulose membrane (Immobilon – Merck Millipore Ltd) for 55 min at 15 V using a semi-dry electroblotting transfer unit (Bio-Rad, Hercules, CA, USA). Membranes were incubated for 1 h with blocking buffer (1% dry skim milk, 0.1% Tween in PBS) and then incubated for 1 h with primary antibody diluted in blocking buffer (1/500). After washing with PBS-0.1%Tween, membranes were incubated for 1 h with secondary antibody labeled with IRDye fluorophores (LI-COR, Lincoln, NE, United States) diluted in blocking buffer (1/20,000). Finally, the membranes were scanned using the Odyssey Imaging System (LI-COR).

Proteins were quantified with the UV–Vis NanoDrop One spectrometer (Thermo Scientific).

Antibodies generation

BALB/c mice were immunized intraperitoneally with a volume of 200 µl containing 10 µg of the different purified recombinant proteins (CypA or CypB) using aluminum hydroxide as an adjuvant. Boosters with 5 µg of protein were further performed at 2 and 4 weeks. One week after the last immunization, the mice were bled, and the serum was stored at −20°C for later use.

PPIase activity measurement

Determination of the PPIase activity of recombinant cyclophilins was performed as described (Mares et al., 2011). Briefly, a 5 µM acid denatured Green Fluorescent Protein (GFP) solution was prepared by diluting 10 µM GFP solution in denaturation buffer (150 mM NaCl, 50 mM Tris–HCl, pH 7.5) with an equal volume of 125 mM HCl solution. The mixture was incubated for 1 min at room temperature verifying the denaturation with fluorescence measurements. Then, the 2.5 µM denatured GFP solution was diluted 1:100 in refolding buffer (25 mM $MgCl_2$, 100 mM KCl, 50 mM Tris–HCl, pH 7.5) in the absence or presence of cyclophilins in different concentrations. The reaction was carried out in a final volume of 200 µl at room temperature measuring the fluorescence for 20 min on the FilterMax F5 spectrometer at 485 nm excitation and 538 nm emission wavelengths.

PPIase inhibition assay was performed as it was described for activity measurement but with the addition of different concentrations of CsA (0, 5, 10, 15, and 20 µM) to the reaction mix in the presence of 2 µM of cyclophilin.

To estimate change percentage in GFP refolding assay, fluorescence value corresponding to 15-min reaction was compared. Signal corresponding to the basal control (spontaneous refolding of GFP) was considered as 0% of PPIase activity. PPIase activity of CypB (that was the highest activity in our assay) was selected as 100%.

Chaperone activity assay: residual activity of denatured *Nde*I

The optimal denaturation temperature for the restriction enzyme *Nde*I was determined. For this, 1 U of enzyme in NEB 3.1 buffer was heated at different temperatures in the range of interest for 20 min. Then, 150 ng of pET28a (+) plasmid were added and incubated for 1 h at 37°C to digest. Restriction digestion of pET28a (+) plasmid was analyzed by 1% agarose gel electrophoresis.

To analyze the chaperone activity of the recombinant proteins, the method already described was adapted (Pandey et al., 2016). Briefly, 1, 2.5, and 5 μg of CypA, CypB, $CypB^{R59A/F64A}$, $CypB^{C128M}$, or 5 μg of BSA (control) were mixed with 1 U of enzyme *Nde*I in NEB 3.1 buffer and heated at 53.8°C for 20 min (optimal denaturation temperature). The residual *Nde*I activity was measured by digesting 150 ng of pET28a (+) plasmid for 1 h at 37°C. The result of the digestion was analyzed by electrophoresis on 1% agarose gel, stained with ethidium bromide, and subsequent UV visualization.

Cell culture and infection assay

HeLa cells were maintained at 37°C in a 5% CO2 atmosphere in Dulbecco modified Eagle medium (DMEM) supplemented with 5% fetal bovine serum and streptomycin (50 μg/ml)-penicillin (50 U/ml). 5×10^4 cells per well were seeded on 24-well plates and kept for 24 h in antibiotic-free DMEM. Infection with *B. abortus* was carried out with a multiplicity of infection (MOI) of 1,000: 1.

First, cells were incubated for 60 min with the bacteria. Then, to eliminate non-internalized bacteria, wells were washed five times with phosphate-buffered saline (PBS) and incubated with a fresh medium supplemented with 50 μg/ml gentamicin and 100 μg/ml streptomycin. Finally, infected cells at 4 h post-infection were washed with PBS five times and lysed with 500 μl 0.1% Triton X-100. Intracellular CFU was determined by plating serial dilutions in TSA with the corresponding antibiotics.

Sensitivity to deoxycholate assay (DOC)

Brucella abortus cultures were adjusted to a standardized optical density at $\lambda = 600$ nm (OD_{600}) and suspended in 1 ml of PBS. Immediately, cultures were serially diluted in PBS and plated in TSA plates containing 1,000 μg/ml deoxycholate. Plates were incubated for 3 days at 37°C.

Mouse infection assay

Before inoculation, 0.1 ml of 10% sodium bicarbonate was administrated to groups of five female BALB/c mice. Oral infection was performed with a volume of 200 μl containing 10^9 CFU of *Brucella*. Mice were euthanized at 6 weeks after infection and bacteria were recovered from the spleens. Spleens were homogenized in 2 ml of PBS, and serial dilutions were plated on TSA.

ELISA assay

Enzyme-linked immunosorbent assay was performed as published (Uriza et al., 2020). Briefly, wells were coated with 125 ng of recombinant proteins in 50 μl of buffer (0.5 M carbonate–bicarbonate pH 9.6). Wells were washed four times (0.1% Tween 20 in PBS buffer). Then, 50 μl of primary antibodies α-CypA or α-CypB per well (1:500) were incubated for 1 h. After that, wells were washed again four times and incubated for 1 h with HRP-anti-mouse IgG (1, 1,000). Finally, wells were washed and incubated for 10 min with 50 μl of substrate solution containing 3, 3′,5,5’ Tetramethylbenzidine (Sigma) and 50 μl of stopping solution for 10 min. Absorbance was measured in the FilterMax F5 Microplate Reader at 450 nm.

Protein structure modeling

Protein structure modeling and comparison between CypA and CypB protein structures were conducted by SWISS-MODEL[1] and UCSF Chimera 1.14 software, respectively (Meng et al., 2006).

Sequences alignment

Sequences alignment comparison of CypA and CypB was done with UCSF Chimera 1.14 (Meng et al., 2006).

Statistical analysis

GraphPad Prism 5 software was used to perform graphs and statistical analyses. One-way analysis of variance (ANOVA) with Bonferroni post-hoc test and Two-way ANOVA-Tukey’s multiple comparison test (within each row, compare columns) were used to analyze statistical significance.

Results

Brucella’s Cyps have in common a typical core domain of the cyclophilin fold but present different structural characteristics

A three-dimensional structural model of the cyclophilins CypA and CypB from *B. abortus* was built, showing that both

1 https://swissmodel.expasy.org/

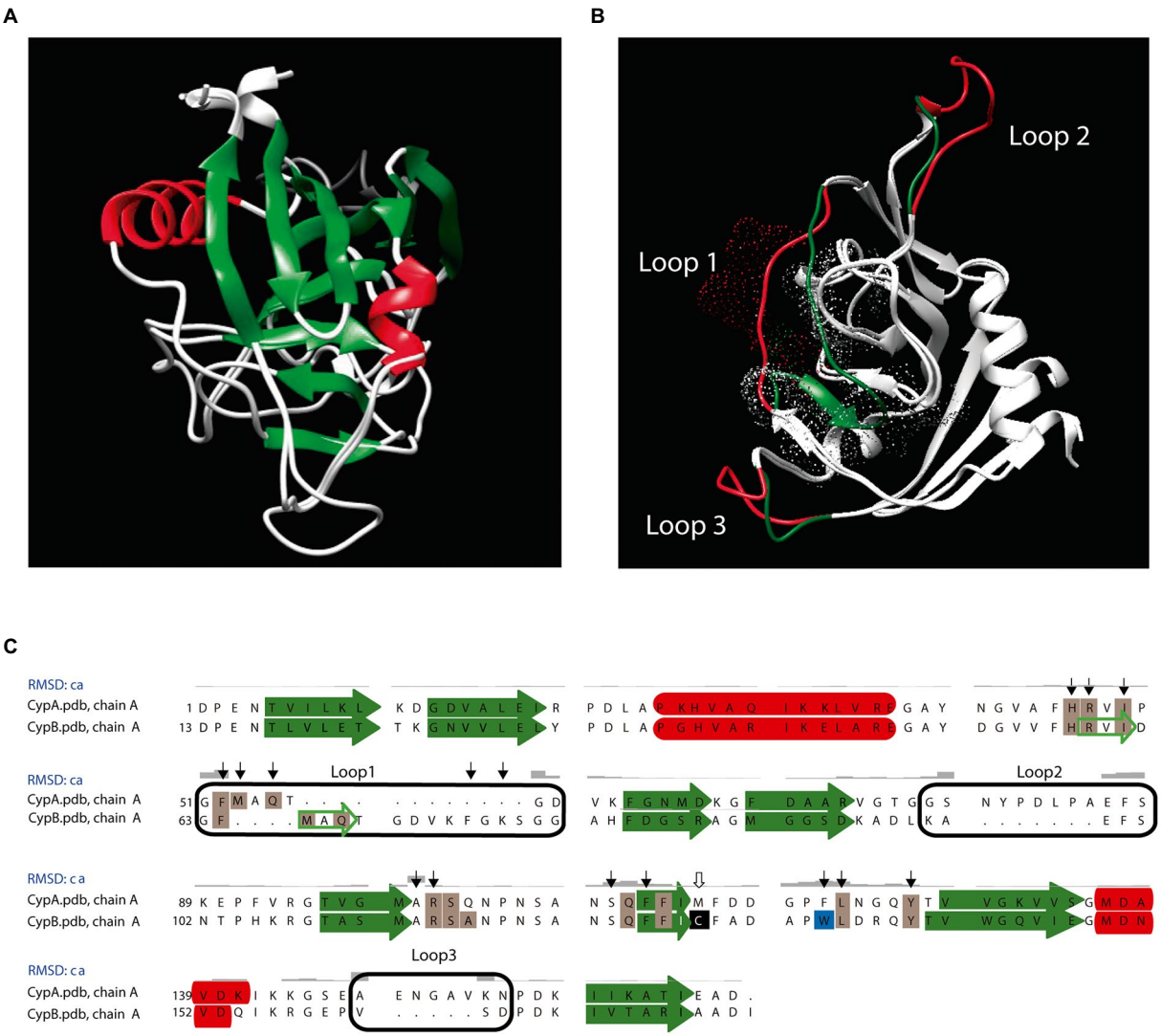

FIGURE 1
Comparison of the three-dimensional structural model of *Brucella abortus* cyclophilins. **(A)** Comparison of the three-dimensional structural model for *B. abortus* cyclophilins CypA and CypB. Swiss-model and Chimera 1.14 programs were used for the model and to compare three-dimensional structural, respectively. The Swiss-model program selected the structure of AquaCyp293 (PDB ID: 5ex2.1A) as a template for CypA and CypB. The predicted general protein structure consists of eight antiparallel beta sheets (green) and two alpha-helices (red). **(B)** Differential loops detected between CypA and CypB were indicated in red and green, respectively. Dot clouds highlighted the PPIase active site areas **(C)** Sequence alignment of *B. abortus* cyclophilins. Amino acid residues involved in cyclosporin (CsA) binding are indicated by black arrows, and those involved in peptidyl-prolyl *cis*/*trans* isomerase (PPIase) activity are highlighted in gray. Cysteine is indicated by a white arrow and highlighted in black and conserved tryptophan is highlighted in light blue. Secondary structures are indicated in green arrows (beta sheets) and red boxes (alpha-helices). Differential peptide loops are marked with black boxes. The alignment was performed with the Chimera 1.4 program.

Cyps have in common several secondary structural features. As shown in Figure 1A, the cyclophilin domain of both CypA and CypB share eight stranded antiparallel β-barrel with two α-helix covering the top and the bottom of the barrel, which is consistent with other structures from the cyclophilin family, such as the human PpiA and the *E. coli* EcCypB (Ke et al., 1991; Ke, 1992; Edwards et al., 1997). However, the 3D structure modeling of both cyclophilins was also able to reveal some differences in their structure over three peptide loops (Figures 1B,C). As shown in Figures 1B,C and Figure 2, catalytic active sites of both Cyps are completely conserved suggesting that both cyclophilins can potentially recognize similar protein substrates. Sequence alignment and 3D models also highlighted the presence of a critical tryptophan at position 134 of the CypB sequence (Trp^{134}) which is absent in *Brucella* CypA and replaced by a phenylalanine in the equivalent position (Phe^{121}). As shown in Figure 2, this critical tryptophan is also present within the active site of the human hCyp18 and absent in the *E. coli* EcCypB, where it is also replaced by phenylalanine. Of particular interest, it has been reported that this conserved tryptophan is critical for the interaction with the immunosuppressor compound cyclosporin A (CsA) in all the described eukaryotic Cyps (Bossard et al., 1991;

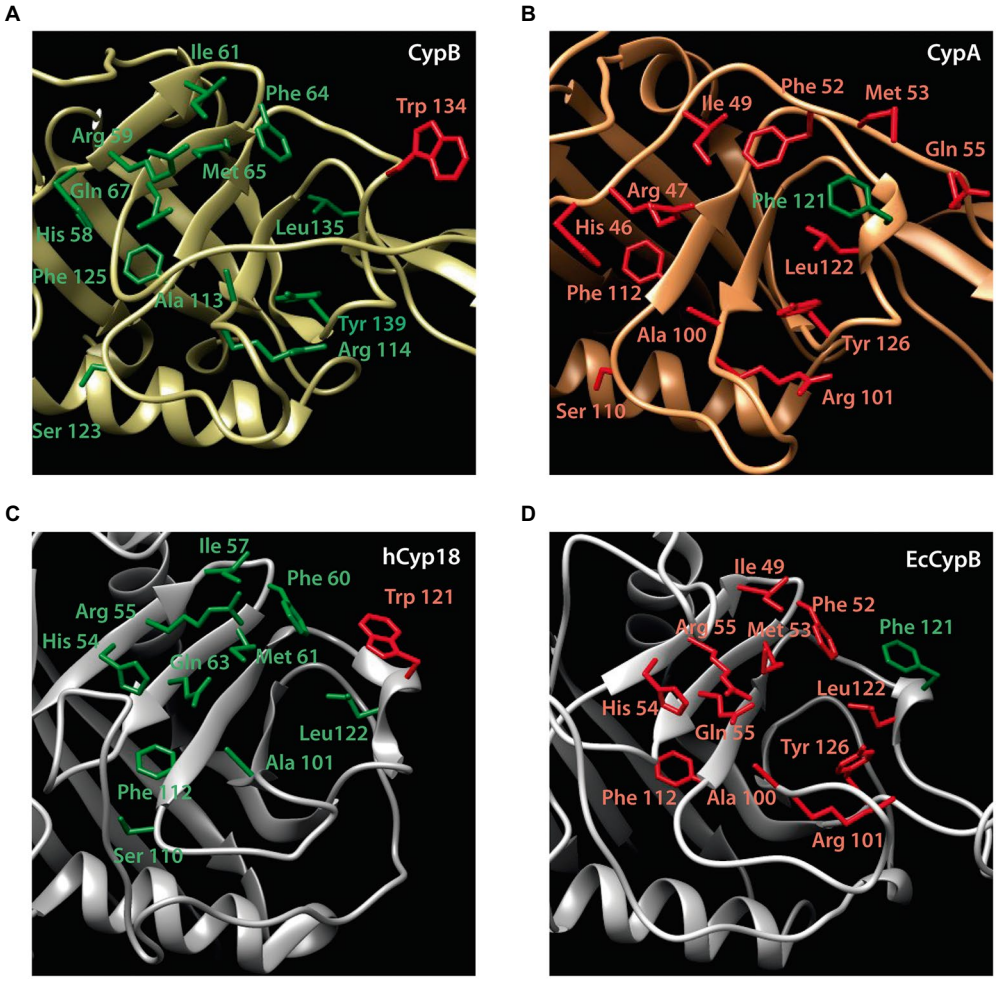

FIGURE 2
Active site structure of *Brucella abortus* cyclophilins CypB **(A)** and CypA **(B)** [in comparison with hCyp18 (2cpl.pdb) **(C)** and EcCypB (1Lop.pdb) **(D)**]. Residues that contribute to the active site of the cyclophilin family are labeled and shown in stick representation. The tryptophan involved in CsA inhibition is highlighted in red for CypB (Trp^{134}) and hCyp18 (Trp^{121}). Phe^{121} is highlighted in green for CypA and EcCypB.

Liu et al., 1991). Differently, in cyclophilins derived from gram negative-bacteria, this critical tryptophan is absent, a modification that correlates with the CsA-insensitivity observed for these Cyps (Liu and Walsh, 1990; Liu et al., 1991). Another feature, which is characteristic of eukaryotic cyclophilins (eCyps), is the presence of cysteines along their amino acid sequence (Liu et al., 1990) that in some cases have been reported to modulate the PPIase activity (Motohashi et al., 2003; Gourlay et al., 2007). Interestingly, *Brucella* CypB has a single cysteine in its sequence which is not conserved in *Brucella* CypA (Figure 1C).

Considering that differences between *Brucella* CypA and CypB might reflect diverse physiological functions we decided to characterize both Cyps from a biochemical and functional standpoint. With that in mind, genes encoding CypA or CypB were recombinantly expressed in *E. coli* BL21 (DE3) and further purified using Ni-NTA chromatography as described in Materials and Methods (Figure 3A). These recombinant proteins were used for the characterization of biochemical activities.

Brucella cyclophilins CypA and CypB exhibit PPIase activity, but only CypB is inhibited By cyclosporin A

The *B. abortus* cyclophilins CypA and CypB present a typical isomerase domain, containing residues involved in PPIase activity (Figures 1C, 2). To confirm if *Brucella* CypA and CypB are functional PPIases, their enzymatic determination was performed with purified recombinant cyclophilins, as described by Mares et al. (2011). To test cyclophilin enzymatic activity, refolding of acid-denatured GFP was adapted for PPIase determination since proline isomerization is the limiting step in the refolding process of GFP (Andrews et al., 2007). As shown in Figure 3B, the addition of CypA or CypB resulted in a highly significant improvement ($p < 0.0001$) in the refolding of the acid-denatured GFP confirming their true enzymatic activity. Interestingly, results from the GFP refolding assay showed that CypB presented a higher rate of reaction compared with CypA that presented an activity reduction

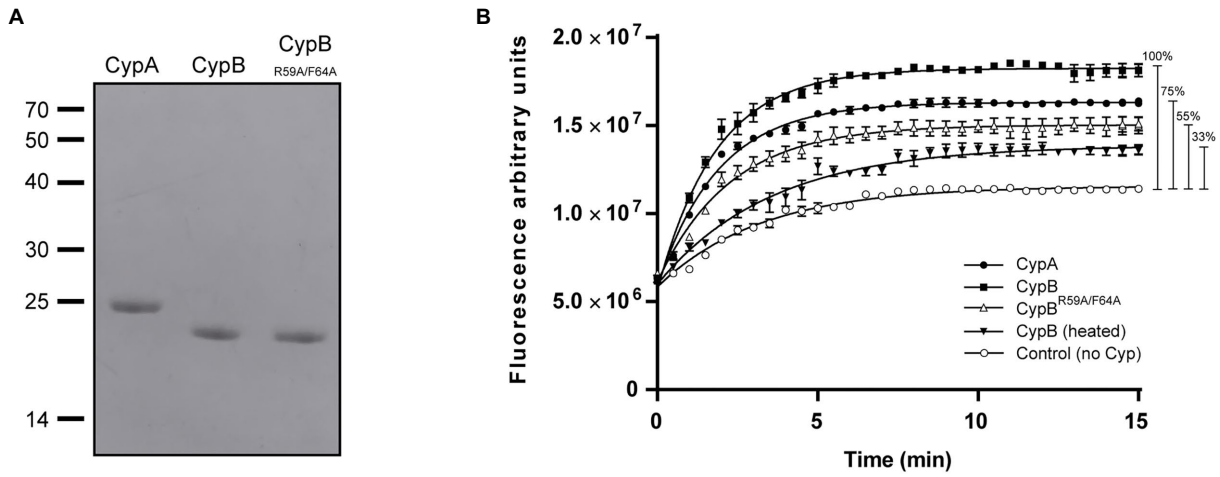

FIGURE 3
PPIase activity determination of recombinant CypA, CypB, and CypB$^{R59A/F64A}$ proteins. **(A)** SDS-PAGE of purified recombinant cyclophilins stained with Coomassie blue. **(B)** GFP PPIase activity assay with 2μM of CypA, CypB, and with the point mutant in the active site CypB$^{R59A/F64A}$. The figure shows the mean and standard deviation of the triplicate experiment and is representative of three independent experiments. Two-way ANOVA and Tukey's multiple comparison test (within each row, compare columns) were used to analyze the statistical significance of the results, ****p<0.0001.

of 25% (Figure 3B). To confirm PPIase activity, a double point mutation was performed in CypB to replace two amino acids reported to be critical for PPIase activity (R59A and F64A; Zydowsky et al., 1992). The resulting recombinant protein CypB$^{R59A/F64A}$ was expressed and purified (Figure 3A) and used in the GFP refolding assay. As shown in Figure 3B, CypB$^{R59A/F64A}$ displayed a 45% diminished PPIase activity compared with CypB.

As shown in Figures 1C, 2, a comparative analysis of the amino acid sequence between CypA and CypB revealed the presence of some features in CypB which are characteristic of eukaryotic cyclophilins like the presence of a critical tryptophan (Trp^{134}), an amino acid predicted to be involved in the CsA interaction (Bossard et al., 1991; Liu et al., 1991). Thus, we explored the inhibition effect of CsA on the enzymatic activity of CypA and CypB of *B. abortus*. After the preincubation with increasing concentrations of CsA, the PPIase activity was highly significantly inhibited (p < 0.0001) in a dose-dependent manner in the case of CypB (more than 50% inhibition with 15 μM; Figure 4A), but not in CypA (Figure 4B). CsA inhibition of CypB was abolished in the case of CypB^{W134F} mutant, where tryptophan, was replaced for phenylalanine (Figures 4C,D). Altogether, these results are in accordance with the *in-silico* prediction that CypB behaves in terms of CsA inhibition like a eukaryotic cyclophilin.

Brucella abortus cyclophilins CypA and CypB protect *Nde*I from thermal inactivation

It has been described that some cyclophilins, in addition to their PPIase activity, also have chaperone activity (Dimou et al., 2011; Zhang et al., 2013; Pandey et al., 2016). Therefore, we investigated whether CypA and CypB recombinant proteins of *B. abortus* were able to prevent the thermal denaturation of the restriction enzyme *Nde*I, an assay used to determine chaperone activity. The ability of *Nde*I to digest the pET-28a(+) plasmid in 1 h at 37°C after thermal denaturation (53.8°C for 20 min), was evaluated in the presence or absence of cyclophilins. As shown in Figure 5, pET-28a(+) plasmid (lane 1) when was incubated with native *Nde*I was fully digested (lane 2). In absence of cyclophilins or in presence of BSA as a control, *Nde*I enzyme activity was completely inactivated by the heat treatment and therefore was not able to cut and linearize the pET-28a(+) plasmid (Figure 5, lane 3–4). Interestingly, the addition of increasing concentrations of CypA or CypB during the heat treatment protected *Nde*I from thermal inactivation (Figure 5, lanes 5–10). These results demonstrated that both cyclophilins have chaperone-like activity. To determine if this chaperone-like activity was dependent on PPIase activity, the double point mutant CypB$^{R59A/F64A}$ was also analyzed. As shown in Figure 5, lanes 11–13, CypB$^{R59A/F64A}$ protects against thermal denaturation to the same extent as CypB, indicating that chaperone-like activity is independent of the PPIase activity.

Brucella abortus cyclophilins CypA and CypB present different immunodominant loops in their structure

To generate molecular tools for this research, recombinant proteins CypA and CypB were used as antigens to produce antibodies in mice. As shown in Figure 6A, when evaluating mouse sera, we found that antibodies raised against CypA were not able to recognize the recombinant CypB and vice versa. As

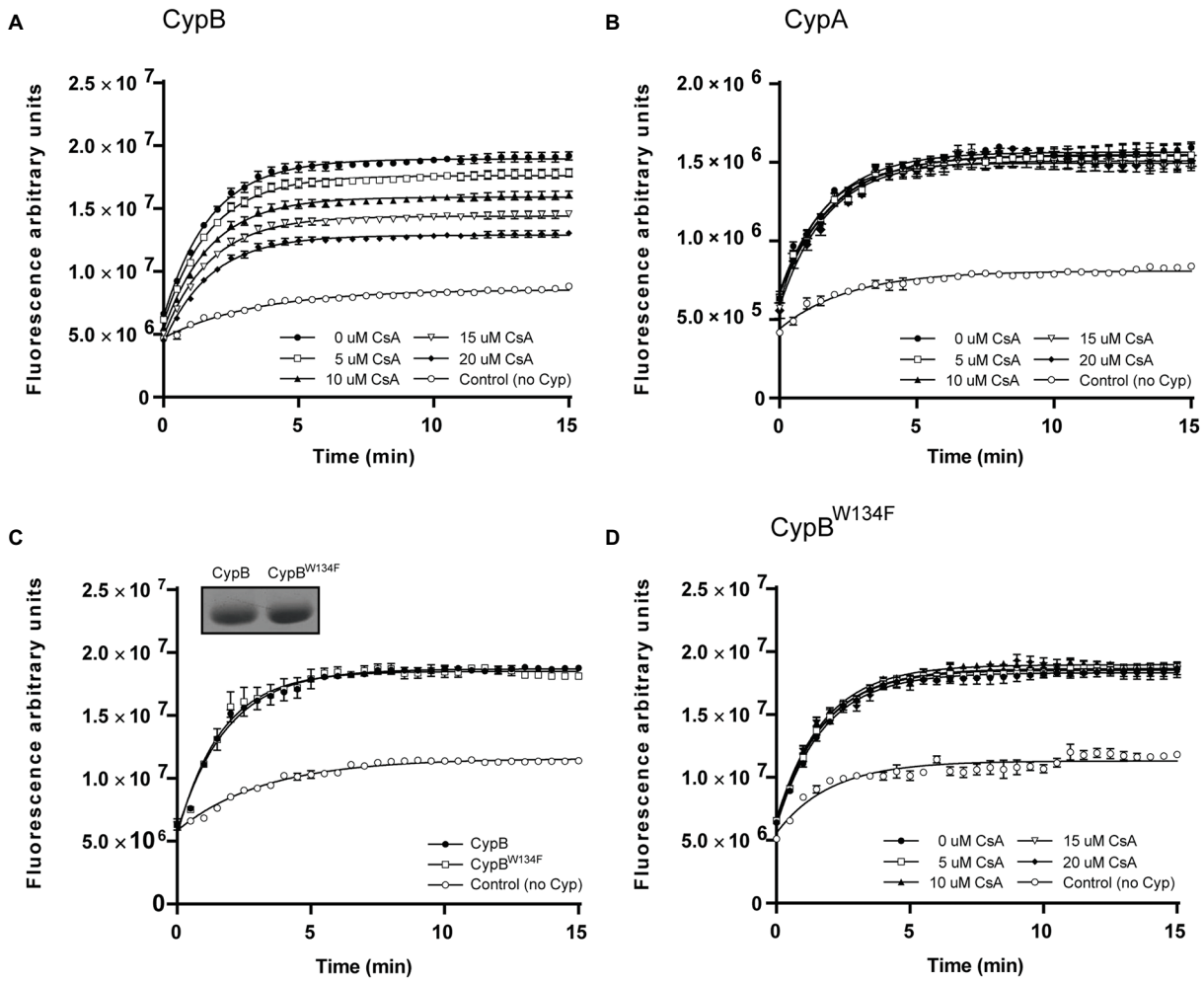

FIGURE 4
Inhibition of enzyme activity by cyclosporin A. CypB **(A)**, CypA **(B)**, or CypB^{W134F} **(D)** were preincubated with increasing concentrations of CsA and the remaining PPIase activity was analyzed with the GFP PPIase activity assay. **(C)** GFP PPIase activity assay with 2μM of CypB^{W134F}. In inset Coomassie blue of purified CypB^{W134F}. The figures show the mean and standard deviation of triplicate experiments and are representative of three independent experiments. Two-way ANOVA and Tukey's multiple comparison test (within each row, compare columns) were used to analyze the statistical significance of the results, ****p<0.0001.

shown in Figure 6B, the same was also observed in whole-cell lysates of *B. abortus* 2,308, *B. abortus* Δ*cypAB (pcypA)*, and *B. abortus* Δ*cypAB(pcypB)*. As expected, no signal was detected for the whole-cell lysate of *B. abortus* Δ*cypAB* mutant either with α-CypA or α-CypB antibodies. These results are remarkable because, although CypA and CypB share a 63% of identity in the amino acid sequence, the immune system still was able to reveal structural differences existing between both cyclophilins. As shown in Figure 6C,D, these antigenic differences can be potentially mapped on three differential amino acid loops. Interestingly, analysis of CypA and CypB sequences by the BepiPred-2.0 algorithm predicted a series of differential linear epitopes that can be located within these differential loops (Figures 6C,D). To pinpoint which peptide loop is contributing to the antibody differential recognition, an experimental approach of swapping loops between CypA and CypB was performed (Figure 6E). Based on the 3D structure prediction, it was observed that formation of loop-1 was determined by the interloop (i-Loop) region (Figures 6D,E). Consequently, we swapped loop1 + i-Loop either of CypA or CypB. To analyze linear and conformational epitopes of CypA, CypB, and their derived chimeras, Western blot analysis, and ELISA tests were carried out (Figure 6E). Thus, the replacement of loop-1 of CypA by the loop-1 from CypB (see CypA(L1CypB) in Figure 6E) determined the lack of recognition of α-CypA antibody and the gain of recognition of α-CypB antibody indicating that loop-1 contained a major determinant of the differential immunogenicity of *B. abortus* Cyps. In addition, loop-2 of CypA was also important for the recognition of α-CypA antibody since CypB(L2CypA) and CypB(L2-L3CypA) were recognized by α-CypA antibodies. Analysis of CypB(L3CypA) immunogenicity suggested that loop-3 of both Cyps is devoid of immunodominant epitopes. Altogether these immunological

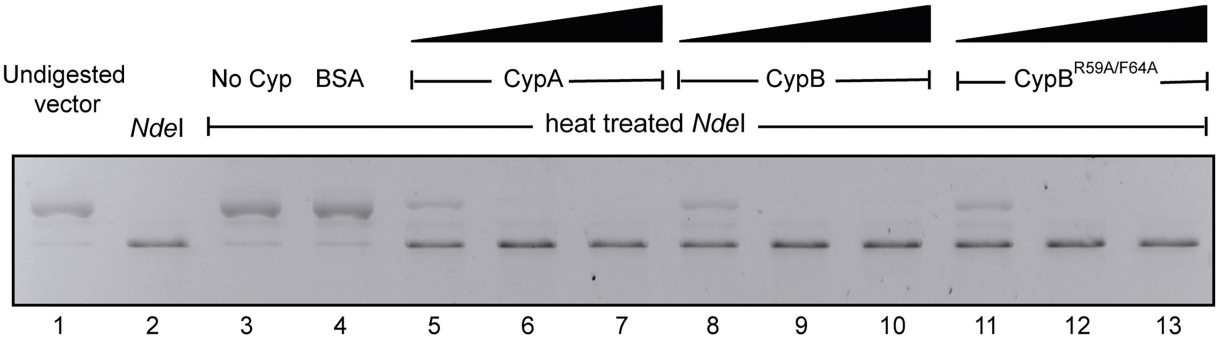

FIGURE 5
CypA and CypB of *B. abortus* prevent thermal inactivation of *Nde*I activity. Enzymatic activity of thermal-denatured *Nde*1 (53.8°C for 20min) in the absence or presence of CypA, CypB, CypB$^{R59A/F64A}$, or BSA as a control protein. Lane 1, uncut pET28 plasmid; lane 2, pET28 plasmid incubated with native *Nde*I; Lane 3, pET28 plasmid incubated with heat-inactivated *Nde*I; Lane 4, pET28 plasmid incubated with heat-inactivated *Nde*I in the presence of BSA (5μg); Lane 5, 6, and 7, pET28 plasmid incubated with heat-inactivated *Nde*I in the presence of increasing concentrations of CypA protein (1, 2.5, and 5μg); Lane 8, 9, and 10, pET28 plasmid incubated with heat-inactivated *Nde*I in the presence of increasing concentrations of CypB protein (1, 2.5, and 5μg); Lane 11, 12, and 13, pET28 plasmid incubated with heat-inactivated *Nde*I in the presence of increasing concentrations of CypB$^{R59A/F64A}$ protein (1, 2.5, and 5μg). The gel is representative of three independent experiments.

results confirmed structural differences predicted by the *in-silico* analysis between CypA and CypB.

CypB forms homodimers that are sensitive to reduction

Since it was reported that PPIases can form homo-oligomers (Budiman et al., 2009; Zhang et al., 2011; Jakob et al., 2016; Polley et al., 2016) we studied the possibility that CypA and CypB were able to oligomerize. As shown in Figure 7A, when we subjected CypA or CypB to SDS-PAGE and Western blot analysis, a single protein band corresponding to the recombinant CypA or CypB was detected as expected for the monomeric form of these cyclophilins. However, when samples were treated in a non-reducing condition (without DTT in the loading sample) in addition to the monomeric band of CypB or CypB$^{R59A/F64A}$, a larger band compatible with the formation of a homodimer of CypB or CypB^{R59AF64A} was observed (Figure 7A). Interestingly, CypA either in the presence or absence of DTT was observed like a single band, as expected for a monomeric CypA (Figure 7A). These results indicate that CypB but not CypA was able to interact to form homodimers in solution, a process that was independent of the PPIase activity.

As shown above, a comparison between both cyclophilin sequences showed that CypB has a unique cysteine residue which is absent in the CypA sequence (Figure 1C). To study the potential role of this conserved cysteine residue in dimer formation, a point mutant CypB^{C128M} was constructed, where the Cys^{128} was replaced by methionine (Figure 7B). The resulting recombinant protein CypB^{C128M} was expressed and purified and its ability to form homodimers was evaluated. As shown in Figure 7B, CypB^{C128M} was not able to form homodimers in non-reducing conditions indicating that cysteine was responsible for CypB dimerization. In addition, it was interesting to investigate if Cys^{128} was also important for PPIase or chaperone activities of CypB. As shown in Figure 7C, the PPIase activity of CypB^{C128M} was not different from CypB. In addition, results shown in Figure 7D indicated that CypB^{C128M} was also able to protect *Nde*I from thermal denaturation as efficiently as CypB. Altogether these results showed that the loss of the ability to form homodimers does not affect the *in vitro* activities of CypB analyzed in this study.

Homodimeric CypB is important for stress survival and virulence of *Brucella abortus*

Although the loss of CypB ability to form homodimers showed no effect on the *in vitro* PPIase or chaperone activities, we explored if CypB oligomerization can affect *in vivo* functions of CypB in *B. abortus* related to stress and intracellular host-cell adaptation. For that, the plasmid p*fcypB*^{C128M} was introduced into *B. abortus* Δ*cypAB* mutant strain and the stress adaptation, intracellular survival, and virulence in mice were examined (Figure 8). The expression of CypB^{C128M} protein in *B. abortus* was confirmed by Western blot analysis (Figure 8A). As described previously in Roset et al. (2013) Δ*cypAB* deletion generates a phenotype in *B. abortus* characterized by an increased sensitivity to a set of different stressors such as deoxycholate acid (DOC). As shown in Figure 8B, the plasmid p*fcypB*^{C128M} was unable to complement the DOC sensitivity of *B. abortus* Δ*cypAB* mutant. These results indicated that CypB homodimer formation is necessary for *Brucella* stress adaptation.

To examine if the homodimeric formation of CypB is required for *B. abortus* intracellular survival, Hela cells were infected with *B. abortus* 2,308 wild-type strain, *B. abortus*

10.3389/fmicb.2022.1046640

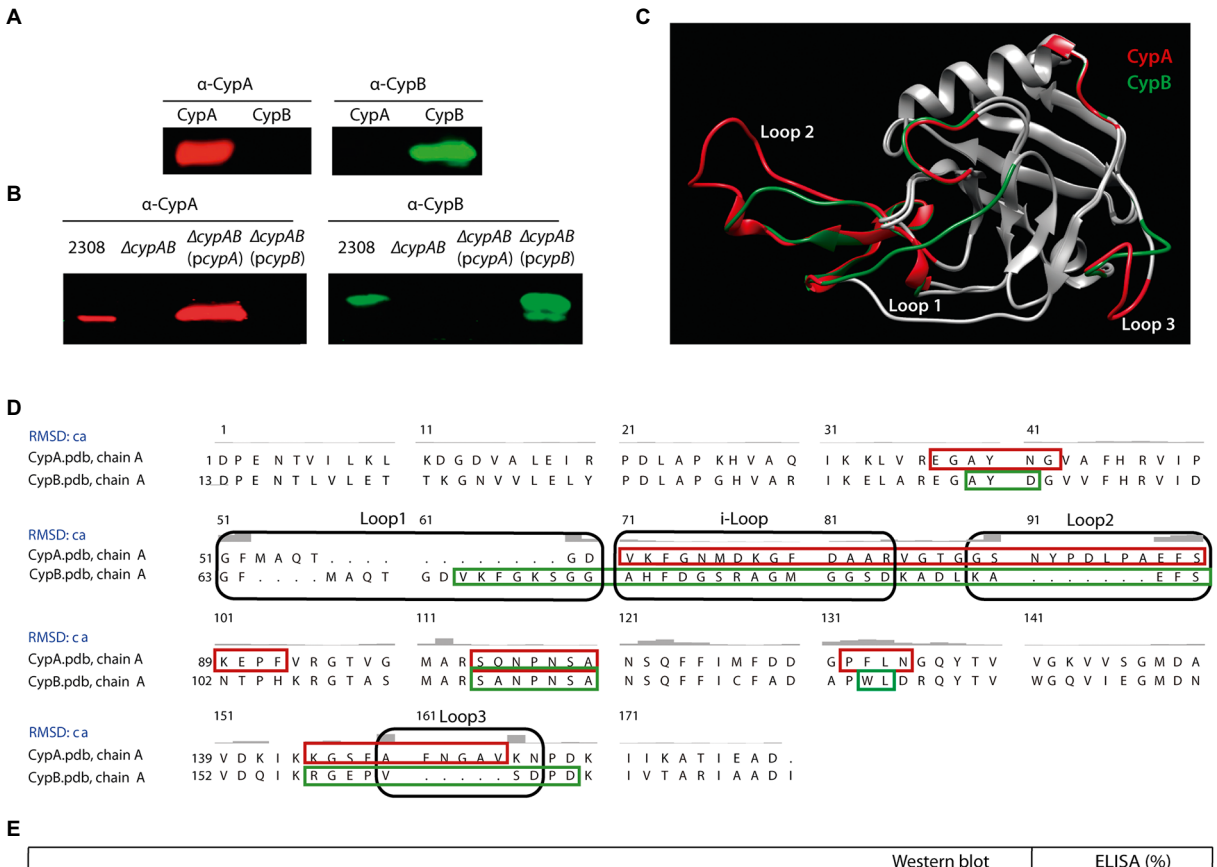

FIGURE 6
Differential immunodominant loops between CypA and CypB. Western blot analysis of **(A)** CypA and CypB recombinant proteins and **(B)** different *Brucella* whole-cell lysates probed with mouse antibodies produced against CypA or CypB. **(C)** Overlap of the three-dimensional structural model for *B. abortus* cyclophilins CypA and CypB. Swiss-model and Chimera 1.14 programs were used for modeling and the comparison of the predicted three-dimensional structure, respectively. The BepiPred-2.0 algorithm was used to predict linear epitopes. Immunodominant epitopes of CypA and CypB are marked in red and green, respectively. **(D)** Sequence alignment of *B. abortus* cyclophilins. Loops and i-Loop are indicated in a black open box. Linear epitopes are indicated in green open boxes for CypA or red open boxes for CypB. **(E)** Western blot analysis and indirect ELISA of different recombinant chimeras of CypA and CypB were revealed with anti-CypA or anti-CypB antibodies. The results are representative of three independent experiments.

Δ*cypAB* mutant, *B. abortus* Δ*cypAB*(p*fcypB*), *B. abortus* Δ*cypAB*(p*fcypB*$^{R59A/F64A}$) and, *B. abortus* Δ*cypAB*(p*fcypB*^{C128M}) (Figure 8C). Results showed that at 4 h post-infection *B. abortus* Δ*cypAB*(p*fcypB*^{C128M}) showed a 10-fold reduction in intracellular survival, like what was observed in *B. abortus* Δ*cypAB* mutant suggesting that the dimeric form of CypB was also necessary for intracellular survival in Hela cells. Since *B. abortus* Δ*cypAB*(p*fcypB*^{C128M}) was affected in intracellular adaptation it was interesting to investigate if this mutant was also affected in the mouse infection model. As shown in Figure 8D, orally infected mice had a reduced number (more than hundred-fold decrease) of *B. abortus* Δ*cypAB*(p*fcypB*^{C128M}) in spleen at 6 weeks post-infection compared with those infected with *B. abortus* Δ*cypAB*(p*fcypB*) and like *B. abortus* Δ*cypAB* mutant. These results also showed that the dimeric form of *Brucella* CypB was fully required to establish a persistent infection in mice. All these results showed that homodimer formation was necessary for the *in vivo* functions of CypB.

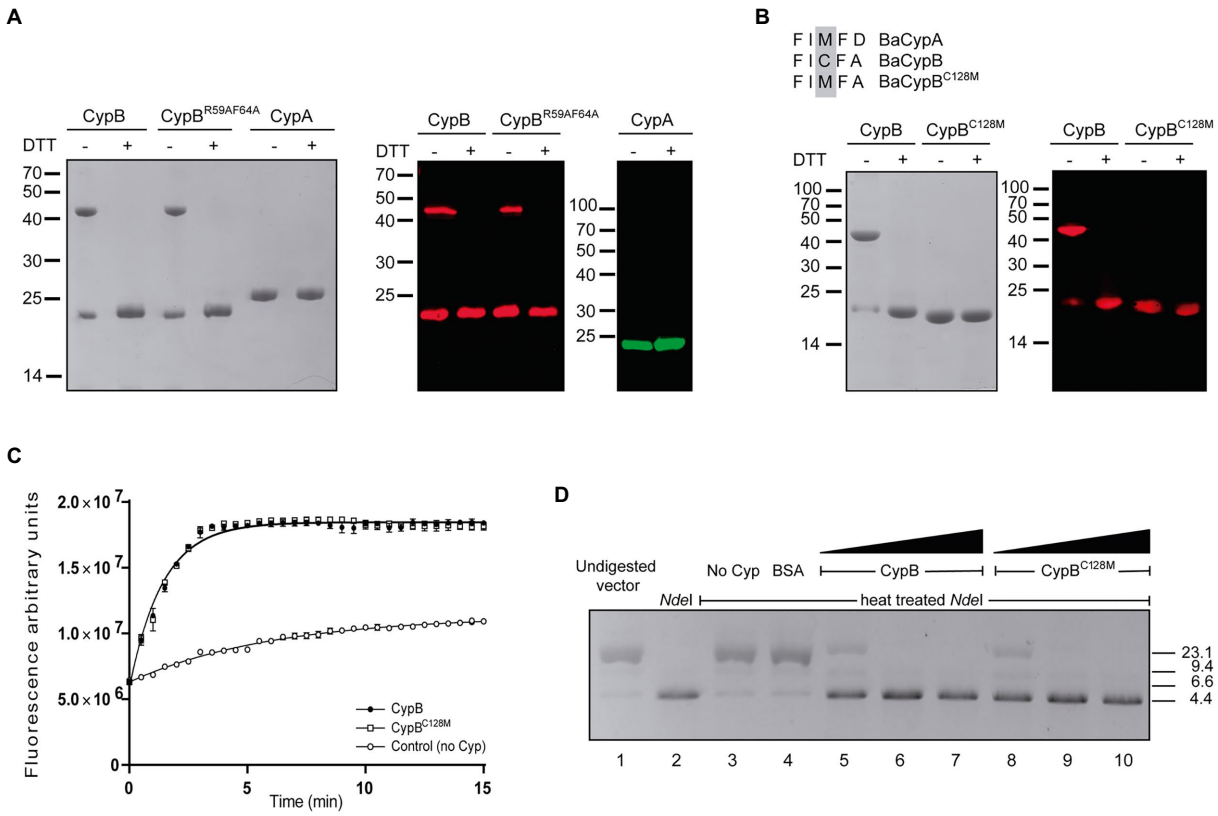

FIGURE 7
CypB is a homodimeric protein. Coomassie blue staining and Western blot analysis of protein samples incubated in the presence or absence of DTT. **(A)** CypB, CypB$^{R59A/F64A}$, CypA, **(B)** CypB and CypB^{C128M}. **(C)** GFP PPIase activity assay with 2μM of CypB, CypB^{C128M}, or without CypB. **(D)** Enzymatic activity of thermal-denatured *Nde*1 (53.8°C for 20min) in the presence of CypB, CypB^{C128M}, or control protein BSA. Lane 1, uncut pET28 plasmid; Lane 2, pET28 plasmid incubated with native *Nde*I; Lane 3, pET28 plasmid incubated with heat-inactivated *Nde*I; Lane 4, pET28 plasmid incubated with heat-inactivated *Nde*I in the presence of BSA (5μg), Lane 5, 6, and 7, pET28 plasmid incubated with heat-inactivated *Nde*I in the presence of increasing concentrations of CypB protein (1, 2.5, and 5μg); Lane 8, 9, and 10, pET28 plasmid incubated with heat-inactivated *Nde*I in the presence of increasing concentrations of CypB^{C128M} protein (1, 2.5, and 5μg). The results are representative of three independent experiments.

PPIase activity of CypB is required for full virulence of *Brucella abortus* in the mouse model

As we described previously (Roset et al., 2013), the plasmid p*cypB*$^{R59A/F64A}$ partially rescued the *B. abortus* Δ*cypAB* mutant for DOC sensitivity (Figure 8B). Intermediate results observed in complementation assays with p*cypB*$^{R59A/F64A}$ can be explained by the existence of certain residual PPIase activity in the cyclophilin mutant CypB$^{R59A/F64A}$ (Figure 3B). This CypB$^{R59A/F64A}$ residual activity was sufficient to complement intracellular survival of the *B. abortus* Δ*cypAB* mutant to the wild-type level (Figure 8C; Roset et al., 2013). To understand if the residual cyclophilin activity present in the mutant protein CypB$^{R59A/F64A}$ was also sufficient to complement the *B. abortus* Δ*cypAB* mutant in the mouse model, an infection experiment was performed. As shown in Figure 8D, after 6 weeks post-infection *B. abortus* Δ*cypAB*(p*fcypB*$^{R59A/F64A}$) was 66-fold less efficient in spleen colonization in BALB/c mice than *B. abortus* Δ*cypAB*(p*fcypB*) and similar to *B. abortus* Δ*cypAB* mutant. It is possible to speculate that the discrepancies observed can be explained by the different requirements of CypB activity dependent on the chosen experimental model. Thus, mouse oral infection is predicted to be the most demanding assay since *B. abortus* Δ*cypAB* mutant had to face a variety of sequential stressors when progressing in the intestinal tract (pH, bile salts, proteases, etc). Consequently, the mouse experiment highlighted the critical importance of CypB PPIase activity in *Brucella* intracellular survival and virulence.

The *cypB*$^{R59A/F64A}$ gene functions as a dominant-negative mutant

To explore if the loss-of-function mutation of CypB (*cypB*$^{R59A/F64A}$) can exert a dominant-negative effect on *B. abortus* 2,308 wild-type strain, the plasmid p*fcypB*^{R59AF64A} was introduced into this strain by biparental mating and ectopic expression of CypB$^{R59A/F64A}$ was confirmed by Western blot analysis (Figure 9A). As shown in

10.3389/fmicb.2022.1046640

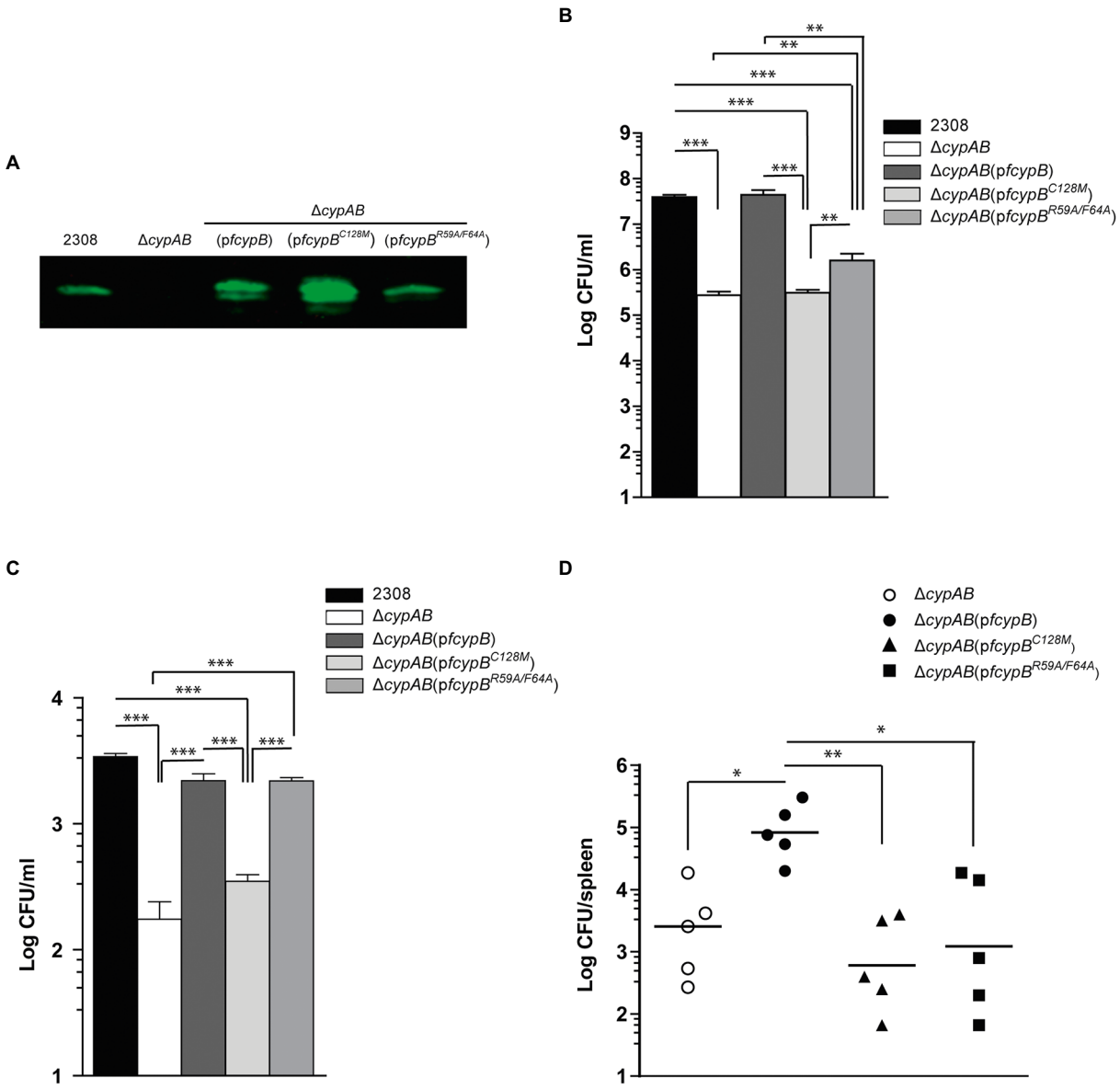

FIGURE 8
Dimeric form of CypB is required for survival and virulence of *B. abortus*. **(A)** Western blot analysis of whole-cell lysates of *B. abortus* strains expressing wild-type CypB, the monomeric form CypB^{C128M}, and the active site mutant CypB$^{R59A/F64A}$ detected by a mouse antibody against CypB. **(B)** Detergent sensitivity assay using serial dilutions of different *B. abortus* strains plated in triplicate onto TSB agar plates containing deoxycholate (DOC) (1,000μg/ml). Plates were incubated for 72h, and the number of CFU was scored. **(C)** Intracellular survival of the *B. abortus* strains in HeLa cells. Numbers of CFU of intracellular bacteria were determined after lysis of infected cells at 4h post-infection. Each determination was performed in triplicate, and values are shown as the mean with its respective standard deviation and are representative of three independent experiments. **(D)** BALB/c mice were infected orally (1×10^9CFU) with different *B. abortus* strains. At 6 weeks post-infection, the numbers of CFU recovered from spleens were determined by serial dilutions and plating onto TSA. Five animals were used for each determination. One-way ANOVA and Bonferroni's Multiple Comparison Test were used to analyze the statistical significance of the results. *, $p<0.05$, **, $p<0.01$, *** $p<0.001$.

Figure 9, the expression of CypB$^{R59A/F64A}$ impaired the ability of *Brucella* to survive in DOC sensitivity assay (Figure 9B) and reduced 70-fold the ability to survive within HeLa cells (Figure 9C). Considering that CypB$^{R59A/F64A}$ still can interact with CypB wild type to form dimers, these results might suggest that CypB requires dimer formation for full activity, having both monomers a fully intact active site.

Discussion

Cyclophilins are a family of highly conserved enzymes that catalyze the process of cis-trans isomerization of the Xaa-proline bonds, which is the rate-limiting step in protein folding. This activity is critical for many biological processes including bacterial virulence (Dimou et al., 2017). We have previously reported that

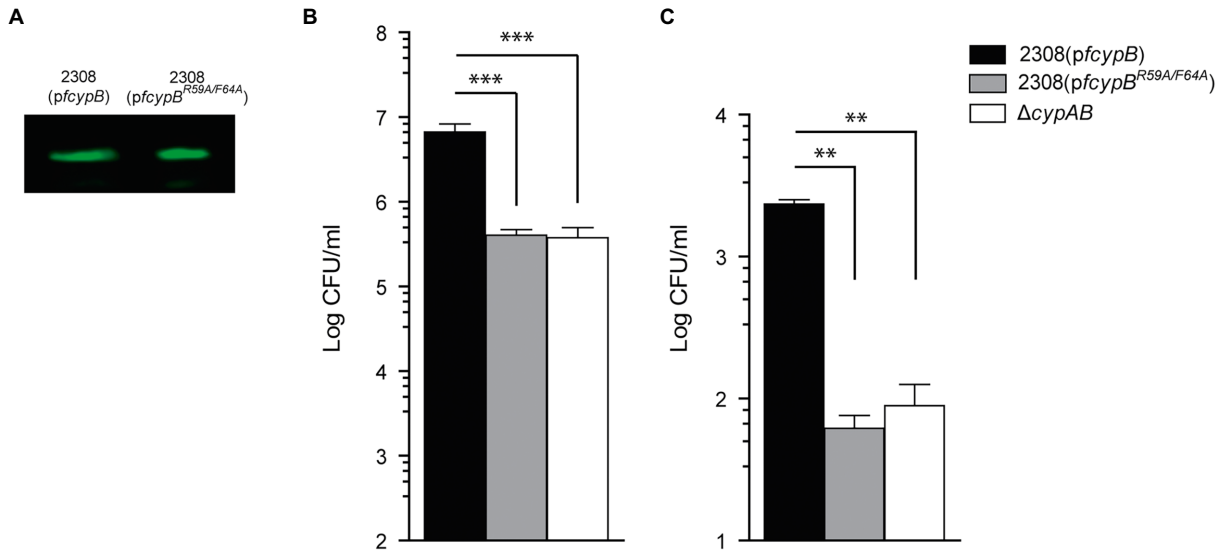

FIGURE 9
Dominant-negative mutation. **(A)** Western blot analysis of whole-cell lysates of *B. abortus* 2,308 strain expressing wild-type CypB, or CypB$^{R59A/F64A}$ detected by an anti-flag antibody. The strains were assayed for detergent sensitivity (DOC) **(B)**, and survival in HeLa cells **(C)** as described in "Materials and methods." One-way ANOVA and Bonferroni's Multiple Comparison Test were used to analyze the statistical significance of the results. The results shown are representative of three independent experiments, $^{**}p<0.01$, $^{***}p<0.001$.

B. abortus has two cyclophilins, named cyclophilin A (CypA) and cyclophilin B (CypB) that are upregulated within the intraphagosomal replicative niche during *B. abortus* infection (Roset et al., 2013). In addition, we have also demonstrated that both cyclophilins play an important role in stress adaptation, intracellular survival, and virulence. Interestingly, defective phenotypes for stress and intracellular survival can be complemented either with CypA or CypB alone, suggesting that both Cyps show certain redundancy in their functions (Roset et al., 2013). In this report, we have also identified a group of differential features by comparing CypA with CypB. For instance, although both *B. abortus* cyclophilins share a conserved secondary structure, we have identified structural differences over three immunodominant loops identified by an *in-silico* approach and by different immunoassays. Cyclophilins are enzymes that can interact with different protein targets to help them in their folding process allowing them to acquire their functional protein structure. It would be interesting to hypothesize if differences observed in structure and antigenicity of CypA and CypB might also be reflecting differences in their preferred protein targets that can reveal novel functions for these cyclophilins.

We demonstrated here that unlike CypA, CypB presents a Trp^{134} which is involved in CsA inhibition, like in all characterized Cyps from eukaryotic origin (Bossard et al., 1991; Liu et al., 1991). On the other hand, CypA shares homology with Cyps of Gram-negative bacteria, presenting a replacement of the Trp^{134} by a Phe residue, a modification that correlates with CsA insensitivity observed for this kind of Cyps (Liu and Walsh, 1990; Liu et al., 1991). Interestingly, the replacement of Trp^{134} in CypB (CypB^{W134F}) does not modify the PPIase activity either in the presence or absence of CsA indicating that Trp^{134} is not required for peptidyl-prolyl cis-trans isomerization. As mentioned above, another characteristic feature that has been described in eukaryotic cyclophilins is the presence of cysteines in their sequences (Liu et al., 1990; Motohashi et al., 2003; Gourlay et al., 2007). *Brucella* CypB has a single cysteine residue in its sequence (Cys^{128}) which is absent in CypA. As shown here, *Brucella* CypB has the capacity to self-associate to form homodimers. This interaction was reversed by the addition of the reducing agent DTT indicating that Cys^{128} is the amino acid responsible for dimer formation. Thus, CypB^{C128M} mutant was unable to form homodimers showing the same behavior as CypA which is only present in a monomeric state.

It has been reported that PPIases can form homo-oligomers (Zhang et al., 2011; Jakob et al., 2016; Polley et al., 2016) although, in the family of cyclophilins, only a few cases have been reported: the human hCypA (Zhang et al., 2011) and the *Trichomonas vaginalis* cyclophilin 1 (Martin et al., 2018). In addition, in the case of dimeric PPIases, no homodimer formation has been reported dependent on disulfide bonds. Hence, *Brucella* CypB is the first example of a dimeric PPIase stabilized by disulfide bridges.

Interestingly, it has been also reported that oligomerization of enzymes modulates their activities (Kropp et al., 2022). We showed here that CypB dimer formation was fully required to complement the defective phenotype of *Brucella* Δ*cypAB* mutant in stress survival, intracellular adaptation, and virulence in mice but not required for the *in vitro* PPIase activity. This apparent discrepancy can be explained because the *in vitro* PPIase substrate, the acid-denatured GFP, is not expected to be a physiological protein target. Similar results to those described here were reported for

Legionella protein MIP, a PPIase belonging to the FKB family (Kohler et al., 2003).

As shown here, the defective phenotype of *B. abortus* Δ*cypAB* mutant cannot be complemented by $CypB^{C128M}$ indicating that the formation of homodimers is critical for PPIase activity of CypB.

To understand in more detail how *Brucella* cyclophilins participate in the process of stress adaptation and intracellular survival, a dominant-negative experiment was performed. As shown here, the over-expression of $CypB^{R59A/F64A}$ interfered with bacterial ability to survive to stressors and within the host cell resembling what is observed in the *B. abortus* Δ*cypAB* mutant. Interpretations of these results suggested that for the fully enzymatic activity of the dimeric CypB, both monomers must present functional active sites. As we mentioned before and it was shown previously (Roset et al., 2013), CypA and CypB are equivalent when complemented the *B. abortus* Δ*cypAB* mutant indicating a functional redundancy. Interestingly, in the dominant-negative experiment, the wild-type activity of CypA was also surprisingly inhibited, although CypA is not expected to form heterodimers with $CypB^{R59A/F64A}$. An explanation for these results can be that homodimers formed by $CypB^{R59A/F64A}$ or heterodimers formed by CypB-$CypB^{R59A/F64A}$ were able to trap also the protein targets of CypA preventing their folding.

It has been reported that there is a general link between cyclophilins and cellular stress response (Dimou et al., 2017). We have described that *Brucella's* Cyps participate in survival to diverse types of stresses which is dependent on the PPIase activity (Roset et al., 2013). Proteins involved in oxidative stress such as OxyR and Hsp33 are regulated by redox activity and activated by the formation of intramolecular disulfide bridges (Zheng et al., 1998; Graumann et al., 2001). Moreover, evidence for redox regulation of PPIase activity of cyclophilins has been reported for hCypA from T lymphocytes (Ghezzi et al., 2006), Chloroplast CypA from *Arabidopsis thaliana* (Motohashi et al., 2003), and CypA from *Schistosoma mansoni* (Gourlay et al., 2007), suggesting that redox regulation involving cysteine residues must be a common mechanism of cyclophilin regulation. In all the mentioned cases, activity regulation is mediated by the formation of intramolecular disulfide bridges. It is conceivable that in the case of *Brucella,* upon exposure to an oxidative stress condition (for instance when the bacterium enters its host cell) the intermolecular formation of disulfide bridges between two monomers of CypB can be triggered to obtain fully functional PPIase activity. Thus, the dimerization of CypB might function as a regulatory switch to respond to oxidative stress in *Brucella*.

Bacterial pathogens that have co-evolved with their host have acquired mechanisms to modulate the host cell physiology for their own benefit. Thus, pathogenic bacteria can translocate virulence proteins (known as effector proteins) into the host cell, using specialized secretion systems to hijack different processes, such as the acquisition of nutrients, vesicle trafficking, and modulation of the immune system to allow adequate time for bacterial replication. To accomplish these functions, some effector proteins use "eukaryotic-like" protein domains to mimic the structure or the function of host proteins, promoting the manipulation of a particular host cell pathway (Ke et al., 2015). In the light of, *i*) *Brucella* Cyps are overexpressed during *B. abortus* intracellular life, *ii*) *Brucella* Cyps are required for stress adaptation, intracellular survival, and virulence in BALB/c mice, *iii*) *Brucella* CypA and CypB differ in immunodominant loops that may be reflecting differential functions as well, *iv*) *Brucella* CypB has structural and functional eukaryotic characteristics, it is possible to hypothesize that CypB might function as an effector protein. Further studies to understand if CypB can function as an effector bacterial protein are still in progress.

Conclusion

Remarkably, we have shown here that *Brucella* cyclophilins come in two different "flavors": eukaryotic and prokaryotic. In addition, we reported here that *Brucella* cyclophilins CypA and CypB differ in various immunological and biochemical properties, despite their high degree of sequence similarity and conserved functional features. Also, we highlighted the importance of dimer formation and PPIase activity of CypB for a progressive infection in an animal model. These findings shed some light on the potential novel functions of *Brucella* Cyps, some of them could be due to the putative role of CypB as an effector bacterial protein.

Data availability statement

The original contributions presented in the study are included in the article/supplementary material, further inquiries can be directed to the corresponding authors.

Ethics statement

The animal study was reviewed and approved by The experimental procedure of this study (permit number CICUAE UNSAM 15/2018) was approved by the Committee on the Ethics of Animal Experiments of the Universidad Nacional de San Martín (UNSAM), under the recommendations for animal experimentation (Helsinki Declaration and its amendments, Amsterdam Protocol of welfare and animal protection and National Institutes of Health, USA NIH, guidelines: Guide for the Care and Use of Laboratory Animals).

Author contributions

MR and GB conceived and design the experiments. EM and MR performed experiments. EM, MR, and GB analyzed the data. MR and GB wrote the paper. All authors contributed to the article and approved the submitted version.

Funding

This work was supported by grants from the Agencia Nacional de Promoción Científica y Tecnológica, Buenos Aires, Argentina (PICT-2018-0778, PICT-2016-0412) and CONICET (PUE-0086, PIP-11220200102517CO).

Acknowledgments

We would like to thank Dr. Rodrigo Sieira for his careful and critical reading of this manuscript. EM is doctoral fellow from CONICET. MR and GB are members of the Research Career of CONICET.

Conflict of interest

The authors declare that the research was conducted in the absence of any commercial or financial relationships that could be construed as a potential conflict of interest.

Publisher's note

All claims expressed in this article are solely those of the authors and do not necessarily represent those of their affiliated organizations, or those of the publisher, the editors and the reviewers. Any product that may be evaluated in this article, or claim that may be made by its manufacturer, is not guaranteed or endorsed by the publisher.

References

Andrews, B. T., Schoenfish, A. R., Roy, M., Waldo, G., and Jennings, P. A. (2007). The rough energy landscape of superfolder GFP is linked to the chromophore. *J. Mol. Biol.* 373, 476–490. doi: 10.1016/j.jmb.2007.07.071

Bossard, M. J., Koser, P. L., Brandt, M., Bergsma, D. J., and Levy, M. A. (1991). A single Trp121 to Ala121 mutation in human cyclophilin alters cyclosporin a affinity and peptidyl-prolyl isomerase activity. *Biochem. Biophys. Res. Commun.* 176, 1142–1148. doi: 10.1016/0006-291X(91)90404-U

Budiman, C., Bando, K., Angkawidjaja, C., Koga, Y., Takano, K., and Kanaya, S. (2009). Engineering of monomeric FK506-binding protein 22 with peptidyl prolyl cis-trans isomerase. Importance of a V-shaped dimeric structure for binding to protein substrate. *FEBS J.* 276, 4091–4101. doi: 10.1111/j.1742-4658.2009.07116.x

Bzdyl, N. M., Scott, N. E., Norville, I. H., Scott, A. E., Atkins, T., Pang, S., et al. (2019). Peptidyl-prolyl isomerase ppiB is essential for proteome homeostasis and virulence in *Burkholderia pseudomallei*. *Infect. Immun.* 87. doi: 10.1128/IAI.00528-19

Cho, K., Arimoto, T., Igarashi, T., and Yamamoto, M. (2013). Involvement of lipoprotein PpiA of *Streptococcus gordonii* in evasion of phagocytosis by macrophages. *Mol. Oral Microbiol.* 28, 379–391. doi: 10.1111/omi.12031

Corbel, M. J. (1997). Brucellosis: an overview. *Emerg. Infect. Dis.* 3, 213–221. doi: 10.3201/eid0302.970219

De Figueiredo, P., Ficht, T. A., Rice-Ficht, A., Rossetti, C. A., and Adams, L. G. (2015). Pathogenesis and immunobiology of brucellosis: review of Brucella-host interactions. *Am. J. Pathol.* 185, 1505–1517. doi: 10.1016/j.ajpath.2015.03.003

Dimou, M., Venieraki, A., and Katinakis, P. (2017). Microbial cyclophilins: specialized functions in virulence and beyond. *World J. Microbiol. Biotechnol.* 33:164. doi: 10.1007/s11274-017-2330-6

Dimou, M., Venieraki, A., Liakopoulos, G., Kouri, E. D., Tampakaki, A., and Katinakis, P. (2011). Gene expression and biochemical characterization of *Azotobacter vinelandii* cyclophilins and protein interaction studies of the cytoplasmic isoform with dnaK and lpxH. *J. Mol. Microbiol. Biotechnol.* 20, 176–190. doi: 10.1159/000329486

Ditta, G., Stanfield, S., Corbin, D., and Helinski, D. R. (1980). Broad host range DNA cloning system for gram-negative bacteria: construction of a gene bank of rhizobium meliloti. *Proc. Natl. Acad. Sci. U. S. A.* 77, 7347–7351. doi: 10.1073/pnas.77.12.7347

Edwards, K. J., Ollis, D. L., and Dixon, N. E. (1997). Crystal structure of cytoplasmic *Escherichia coli* peptidyl-prolyl isomerase: evidence for decreased mobility of loops upon complexation. *J. Mol. Biol.* 271, 258–265. doi: 10.1006/jmbi.1997.1151

Fanghanel, J., and Fischer, G. (2004). Insights into the catalytic mechanism of peptidyl prolyl cis/trans isomerases. *Front. Biosci.* 9, 3453–3478. doi: 10.2741/1494

Fina Martin, J., Palomino, M. M., Cutine, A. M., Modenutti, C. P., Fernandez Do Porto, D. A., Allievi, M. C., et al. (2019). Exploring lectin-like activity of the S-layer protein of *Lactobacillus acidophilus* ATCC 4356. *Appl. Microbiol. Biotechnol.* 103, 4839–4857. doi: 10.1007/s00253-019-09795-y

Galat, A. (2003). Peptidylprolyl cis/trans isomerases (immunophilins): biological diversity--targets--functions. *Curr. Top. Med. Chem.* 3, 1315–1347. doi: 10.2174/1568026033451862

Ghezzi, P., Casagrande, S., Massignan, T., Basso, M., Bellacchio, E., Mollica, L., et al. (2006). Redox regulation of cyclophilin A by glutathionylation. *Proteomics* 6, 817–825. doi: 10.1002/pmic.200500177

Gourlay, L. J., Angelucci, F., Baiocco, P., Boumis, G., Brunori, M., Bellelli, A., et al. (2007). The three-dimensional structure of two redox states of cyclophilin A from *Schistosoma mansoni*. Evidence for redox regulation of peptidyl-prolyl cis-trans isomerase activity. *J. Biol. Chem.* 282, 24851–24857. doi: 10.1074/jbc.M702714200

Graumann, J., Lilie, H., Tang, X., Tucker, K. A., Hoffmann, J. H., Vijayalakshmi, J., et al. (2001). Activation of the redox-regulated molecular chaperone Hsp33--a two-step mechanism. *Structure* 9, 377–387. doi: 10.1016/S0969-2126(01)00599-8

Hermans, P. W., Adrian, P. V., Albert, C., Estevao, S., Hoogenboezem, T., Luijendijk, I. H., et al. (2006). The streptococcal lipoprotein rotamase a (SlrA) is a functional peptidyl-prolyl isomerase involved in pneumococcal colonization. *J. Biol. Chem.* 281, 968–976. doi: 10.1074/jbc.M510014200

Herrero, M., De Lorenzo, V., and Timmis, K. N. (1990). Transposon vectors containing non-antibiotic resistance selection markers for cloning and stable chromosomal insertion of foreign genes in gram-negative bacteria. *J. Bacteriol.* 172, 6557–6567. doi: 10.1128/jb.172.11.6557-6567.1990

Jakob, R. P., Schmidpeter, P. A., Koch, J. R., Schmid, F. X., and Maier, T. (2016). Structural and functional characterization of a novel family of Cyclophilins, the AquaCyps. *PLoS One* 11:e0157070. doi: 10.1371/journal.pone.0157070

Ke, H. (1992). Similarities and differences between human cyclophilin A and other beta-barrel structures. Structural refinement at 1.63 A resolution. *J. Mol. Biol.* 228, 539–550. doi: 10.1016/0022-2836(92)90841-7

Ke, Y., Wang, Y., Li, W., and Chen, Z. (2015). Type IV secretion system of *Brucella* spp. and its effectors. *Front. Cell. Infect. Microbiol.* 5:72. doi: 10.3389/fcimb.2015.00072

Ke, H. M., Zydowsky, L. D., Liu, J., and Walsh, C. T. (1991). Crystal structure of recombinant human T-cell cyclophilin A at 2.5 a resolution. *Proc. Natl. Acad. Sci. U. S. A.* 88, 9483–9487. doi: 10.1073/pnas.88.21.9483

Keogh, R. A., Zapf, R. L., Wiemels, R. E., Wittekind, M. A., and Carroll, R. K. (2018). The intracellular Cyclophilin PpiB contributes to the virulence of Staphylococcus aureus independently of its peptidyl-prolyl cis/trans isomerase activity. *Infect. Immun.* 86. doi: 10.1128/IAI.00379-18

Kohler, R., Fanghanel, J., Konig, B., Luneberg, E., Frosch, M., Rahfeld, J. U., et al. (2003). Biochemical and functional analyses of the Mip protein: influence of the N-terminal half and of peptidylprolyl isomerase activity on the virulence of legionella pneumophila. *Infect. Immun.* 71, 4389–4397. doi: 10.1128/IAI.71.8.4389-4397.2003

Kropp, C., Bruckmann, A., and Babinger, P. (2022). Controlling enzymatic activity by modulating the Oligomerization state via chemical rescue and optical control. *Chembiochem* 23:e202100490. doi: 10.1002/cbic.202100490

Krucken, J., Greif, G., and Von Samson-Himmelstjerna, G. (2009). In silico analysis of the cyclophilin repertoire of apicomplexan parasites. *Parasit. Vectors* 2:27. doi: 10.1186/1756-3305-2-27

Kumawat, M., Singh, P. K., Rananaware, S. R., and Ahlawat, S. (2020). Comparative evaluation of structure and characteristic of peptidyl-prolyl cis-trans isomerase proteins and their function in Salmonella Typhimurium stress responses and virulence. *Folia Microbiol. (Praha)* 65, 161–171. doi: 10.1007/s12223-019-00717-z

Liu, J., Albers, M. W., Chen, C. M., Schreiber, S. L., and Walsh, C. T. (1990). Cloning, expression, and purification of human cyclophilin in *Escherichia coli* and assessment of the catalytic role of cysteines by site-directed mutagenesis. *Proc. Natl. Acad. Sci. U. S. A.* 87, 2304–2308. doi: 10.1073/pnas.87.6.2304

Liu, J., Chen, C. M., and Walsh, C. T. (1991). Human and *Escherichia coli* cyclophilins: sensitivity to inhibition by the immunosuppressant cyclosporin A correlates with a specific tryptophan residue. *Biochemistry* 30, 2306–2310. doi: 10.1021/bi00223a003

Liu, J., and Walsh, C. T. (1990). Peptidyl-prolyl cis-trans-isomerase from *Escherichia coli*: a periplasmic homolog of cyclophilin that is not inhibited by cyclosporin A. *Proc. Natl. Acad. Sci. U. S. A.* 87, 4028–4032. doi: 10.1073/pnas.87.11.4028

Marchesini, M. I., Herrmann, C. K., Salcedo, S. P., Gorvel, J. P., and Comerci, D. J. (2011). In search of *Brucella abortus* type IV secretion substrates: screening and identification of four proteins translocated into host cells through VirB system. *Cell. Microbiol.* 13, 1261–1274. doi: 10.1111/j.1462-5822.2011.01618.x

Mares, R. E., Melendez-Lopez, S. G., and Ramos, M. A. (2011). Acid-denatured green fluorescent protein (GFP) as model substrate to study the chaperone activity of protein disulfide isomerase. *Int. J. Mol. Sci.* 12, 4625–4636. doi: 10.3390/ijms12074625

Martin, T., Lou, Y. C., Chou, C. C., Wei, S. Y., Sadotra, S., Cho, C. C., et al. (2018). Structural basis of interaction between dimeric cyclophilin 1 and Myb1 transcription factor in trichomonas vaginalis. *Sci. Rep.* 8:5410. doi: 10.1038/s41598-018-23821-5

Meng, E. C., Pettersen, E. F., Couch, G. S., Huang, C. C., and Ferrin, T. E. (2006). Tools for integrated sequence-structure analysis with UCSF chimera. *BMC Bioinformatics* 7:339. doi: 10.1186/1471-2105-7-339

Motohashi, K., Koyama, F., Nakanishi, Y., Ueoka-Nakanishi, H., and Hisabori, T. (2003). Chloroplast cyclophilin is a target protein of thioredoxin. Thiol modulation of the peptidyl-prolyl cis-trans isomerase activity. *J. Biol. Chem.* 278, 31848–31852. doi: 10.1074/jbc.M304258200

Obi, I. R., Nordfelth, R., and Francis, M. S. (2011). Varying dependency of periplasmic peptidylprolyl cis-trans isomerases in promoting *Yersinia pseudotuberculosis* stress tolerance and pathogenicity. *Biochem. J.* 439, 321–332. doi: 10.1042/BJ20110767

Pandey, S., Sharma, A., Tripathi, D., Kumar, A., Khubaib, M., Bhuwan, M., et al. (2016). *Mycobacterium tuberculosis* peptidyl-prolyl isomerases also exhibit chaperone like activity in-vitro and in-vivo. *PLoS One* 11:e0150288. doi: 10.1371/journal.pone.0150288

Pandey, S., Tripathi, D., Khubaib, M., Kumar, A., Sheikh, J. A., Sumanlatha, G., et al. (2017). *Mycobacterium tuberculosis* peptidyl-prolyl isomerases are immunogenic, alter cytokine profile and aid in intracellular survival. *Front. Cell. Infect. Microbiol.* 7:38. doi: 10.3389/fcimb.2017.00038

Pemberton, T. J. (2006). Identification and comparative analysis of sixteen fungal peptidyl-prolyl cis/trans isomerase repertoires. *BMC Genomics* 7:244. doi: 10.1186/1471-2164-7-244

Polley, S., Chakravarty, D., Chakrabarti, G., and Sau, S. (2016). Determining the roles of a conserved tyrosine residue in a Mip-like peptidyl-prolyl cis-trans isomerase. *Int. J. Biol. Macromol.* 87, 273–280. doi: 10.1016/j.ijbiomac.2016.02.070

Rasch, J., Unal, C. M., Klages, A., Karsli, U., Heinsohn, N., Brouwer, R., et al. (2019). Peptidyl-prolyl-cis/trans-isomerases Mip and PpiB of legionella pneumophila contribute to surface translocation, growth at suboptimal temperature, and infection. *Infect. Immun.* 87. doi: 10.1128/IAI.00939-17

Reffuveille, F., Connil, N., Sanguinetti, M., Posteraro, B., Chevalier, S., Auffray, Y., et al. (2012). Involvement of peptidylprolyl cis/trans isomerases in *Enterococcus faecalis* virulence. *Infect. Immun.* 80, 1728–1735. doi: 10.1128/IAI.06251-11

Roset, M. S., Alefantis, T. G., Delvecchio, V. G., and Briones, G. (2017). Iron-dependent reconfiguration of the proteome underlies the intracellular lifestyle of *Brucella abortus*. *Sci. Rep.* 7:10637. doi: 10.1038/s41598-017-11283-0

Roset, M. S., Garcia Fernandez, L., Delvecchio, V. G., and Briones, G. (2013). Intracellularly induced cyclophilins play an important role in stress adaptation and virulence of *Brucella abortus*. *Infect. Immun.* 81, 521–530. doi: 10.1128/IAI.01125-12

Uriza, P. J., Trautman, C., Palomino, M. M., Fina Martin, J., Ruzal, S. M., Roset, M. S., et al. (2020). Development of an antigen delivery platform using *Lactobacillus acidophilus* decorated with heterologous proteins: a sheep in Wolf's clothing story. *Front. Microbiol.* 11:509380. doi: 10.3389/fmicb.2020.509380

Wiemels, R. E., Cech, S. M., Meyer, N. M., Burke, C. A., Weiss, A., Parks, A. R., et al. (2017). An intracellular peptidyl-prolyl cis/trans isomerase is required for folding and activity of the *Staphylococcus aureus* secreted virulence factor nuclease. *J. Bacteriol.* 199. doi: 10.1128/JB.00453-16

Zhang, X. C., Wang, W. D., Wang, J. S., and Pan, J. C. (2013). PPIase independent chaperone-like function of recombinant human Cyclophilin A during arginine kinase refolding. *FEBS Lett.* 587, 666–672. doi: 10.1016/j.febslet.2013.01.028

Zhang, X. C., Wang, W. D., Wang, J. S., Pan, J. C., and Zou, G. L. (2011). Evidences of monomer, dimer and trimer of recombinant human cyclophilin A. *Protein Pept. Lett.* 18, 1188–1193. doi: 10.2174/092986611797642670

Zheng, M., Aslund, F., and Storz, G. (1998). Activation of the OxyR transcription factor by reversible disulfide bond formation. *Science* 279, 1718–1722. doi: 10.1126/science.279.5357.1718

Zydowsky, L. D., Etzkorn, F. A., Chang, H. Y., Ferguson, S. B., Stolz, L. A., Ho, S. I., et al. (1992). Active site mutants of human cyclophilin A separate peptidyl-prolyl isomerase activity from cyclosporin A binding and calcineurin inhibition. *Protein Sci.* 1, 1092–1099. doi: 10.1002/pro.5560010903

frontiers | Frontiers in Microbiology

TYPE Original Research
PUBLISHED 01 December 2022
DOI 10.3389/fmicb.2022.1086925

OPEN ACCESS

EDITED BY
Axel Cloeckaert,
Institut National de recherche pour l'agriculture, l'alimentation et l'environnement (INRAE), France

REVIEWED BY
Clayton Caswell,
Virginia Tech,
United States
Juan Esteban Ugalde,
Universidad Nacional de San Martin,
Argentina
Gary Splitter,
University of Wisconsin-Madison,
United States

*CORRESPONDENCE
Sergio C. Oliveira
scozeus@icb.ufmg.br

SPECIALTY SECTION
This article was submitted to Infectious Agents and Disease, a section of the journal Frontiers in Microbiology

RECEIVED 01 November 2022
ACCEPTED 15 November 2022
PUBLISHED 01 December 2022

CITATION
Santos RA, Cerqueira DM, Zamboni DS and Oliveira SC (2022) Caspase-8 but not caspase-7 influences inflammasome activation to act in control of *Brucella abortus* infection.
Front. Microbiol. 13:1086925.
doi: 10.3389/fmicb.2022.1086925

Caspase-8 but not caspase-7 influences inflammasome activation to act in control of *Brucella abortus* infection

Raiany A. Santos[1], Daiane M. Cerqueira[2], Dario S. Zamboni[3] and Sergio C. Oliveira[1,2,4]*

[1]Departamento de Genética, Ecologia e Evolução, Programa de Pós-Graduação em Genética, Instituto de Ciências Biológicas, Universidade Federal de Minas Gerais, Belo Horizonte, Minas Gerais, Brazil, [2]Departamento de Bioquímica e Imunologia, Instituto de Ciências Biológicas, Universidade Federal de Minas Gerais, Belo Horizonte, Minas Gerais, Brazil, [3]Departamento de Biologia Celular e Molecular e Bioagentes Patogênicos, Faculdade de Medicina de Ribeirão Preto, Universidade de São Paulo, Ribeirão Preto, Brazil, [4] Departamento de Imunologia, Instituto de Ciências Biomédicas, Universidade de São Paulo, São Paulo, Brazil

Programmed cell death (PCD) is an important mechanism of innate immunity against bacterial pathogens. The innate immune PCD pathway involves the molecules caspase-7 and caspase-8, among others. *Brucella abortus* is a gram-negative bacterium that causes a zoonotic disease termed brucellosis. The innate immune response against this pathogen involves activation of inflammasome components and induction of pyroptosis. However, no studies so far have revealed the role of caspase-7 or caspase-8 during this bacterial infection. Herein, we demonstrate that caspase-7 is dispensable for caspase-1 processing, IL-1β secretion and cell death in macrophages. Additionally, caspase-7 deficient animals control *B. abortus* infection as well as the wild type mice. Furthermore, we addressed the role of caspase-8 in inflammasome activation and pyroptosis during this bacterial infection. Macrophages deficient in caspase-8 secreted reduced amounts of IL-1β that parallels with diminished caspase-1 activity when compared to wild type cells. Additionally, caspase-8 KO macrophages showed reduced LDH release when compared to wild type, suggesting that caspase-8 may play an important role in pyroptosis in response to *B. abortus*. Finally, caspase-8 KO animals were more susceptible to *Brucella* infection when compared to wild type mice. Overall, this study contributes to a better understanding of the involvement of caspase-7 and caspase-8 in innate immunity against *B. abortus* infection.

KEYWORDS

caspase-8, caspase-7, *Brucella abortus*, inflammasome, pyroptosis, innate immunity

Introduction

Brucellosis is a zoonosis caused by bacteria of the genus *Brucella* of worldwide distribution. Great advance has been made in the control of brucellosis in recent years. However, in many regions of the world, *Brucella* infection in domestic animals still persists, leading to frequent transmission to the human population. In regions such as the

Mediterranean countries of Europe, like Portugal, Italy and Greece, brucellosis is still considered an important human disease and it is often neglected (Corbel, 1997).

Innate immunity is an important arm of the immune system involved in the control of *Brucella* infection. In previous studies performed by our research group, we demonstrated that receptors and adaptor molecules such as TLR9, AIM2, MyD88, and STING are important components in the protective response against *Brucella* infection (Macedo et al., 2008; Gomes et al., 2016; Costa Franco et al., 2018, 2019). In addition, we and others have shown that pyroptosis triggered upon activation of inflammasomes, is also an important mechanism in restricting *in vivo* infection against *Brucella abortus* (Cerqueira et al., 2018; Lacey et al., 2018). In recent study, we showed that caspase-11/GSDMD-dependent pyroptosis process triggered by *B. abortus* contributed to the restriction of infection *in vivo* by assisting in the recruitment and activation of immune cells such as neutrophils, macrophages, and dendritic cells (Cerqueira et al., 2018).

Programmed cell death (PCD) is a intricate circuit that involves the cross-talk among different caspases, and their substrates. Caspase-3 and caspase-7 are considered executioner molecules triggering host cell apoptosis (Kim et al., 2005). Recent study demonstrated that *Brucella* inhibited the PCD in early stage of infection to allow bacterial replication in host cells and promoted apoptosis in the later stage during infection in macrophages (Zhang et al., 2022). In the literature, there are some controversies in the role of caspase-7 during bacterial infections. Caspase-7 has been implicated in resistance to *L. pneumophila* through the NLRC4 inflammasome (Akhter et al., 2009). In contrast, Gonçalves et al. (Goncalves et al., 2019) demonstrated that mice with a single deletion in caspase-7 are not fully susceptible to *L. pneumophila*. The *Casp7*$^{-/-}$ did not phenocopy the susceptibility to *L. pneumophila* infection as observed in *Nlrc4*$^{-/-}$ animals.

Caspase-8, early on classified as an apoptotic caspase, has lately been shown to have a role in several inflammatory processes. Caspase-8 is involved in the inflammasome pathway and can be activated by NLRP3, AIM2 and NLRC4 in macrophages (Man et al., 2013; Sagulenko et al., 2013) and NLRP3 inflammasome in dendritic cells (Antonopoulos et al., 2015). Caspase-8 can act by controlling NF-kB signaling, influencing the positive regulation of components of the inflammasome, such as the NLRP3 and pro-IL-1β (Weng et al., 2014). It can also activate the inflammasome pathway in response to *C. albicans* β-glucans (Ganesan et al., 2014). Interestingly, upon TLR or death receptor activation, active caspase-8 can cleave the IL-1β precursor into its bioactive fragment at the same site as caspase-1 (Shenderov et al., 2014), and can directly cleave GSDMD into its N-terminal fragment, triggering pyroptosis during *Yersinia* infection (Sarhan et al., 2018). In addition, once the inflammasome is activated, but pyroptosis is impaired, caspase-8 can act leading to a cell death program. This has been demonstrated in studies with intracellular bacteria such as *L. pneumophila* and *S. Typhimurium* in the absence of caspase-1 or GSDMD (Mascarenhas et al., 2017; Lee et al., 2018).

To the best of our knowledge, the role of caspase-7 and caspase-8 in *Brucella* infection has not been addressed so far. Therefore, in order to expand the understanding of the mechanisms involved in the innate immune response and inflammatory cell death, we investigated the participation of the caspase-7 and caspase-8 molecules during *B. abortus* infection.

Materials and methods

Mice

Wild-type C57BL/6 (WT) mice were purchased from the Federal University of Minas Gerais (UFMG) and, *Casp7*$^{-/-}$, *Casp7/1/11*$^{-/-}$, *Casp7/Gsdmd*$^{-/-}$, *Gsdmd*$^{-/-}$, *Casp8*$^{+/+}$*/RIPK3*$^{-/-}$, and *Casp8/RIPK3*$^{-/-}$ were kindly provided by Dr. Prof. Dario Simões Zamboni, Department of Cell and Molecular Biology and Pathogenic Bioagents, Ribeirão Preto Medical School, University of Sao Paulo, Brazil. Genetically deficient and control mice were maintained at our facilities and used at 6–8 weeks of age. Mice were housed in filter top cages and provided with sterile water and food *ad libitum*. Groups of 5–7 animals were used to perform all experiments. The procedures for animal experimentation were approved by the Ethics Committee for the Use of Animals of the Federal University of Minas Gerais-CEUA/UFMG under protocol number 69/2020.

Bacteria and culture conditions

Brucella abortus virulent strain 2,308 was used in this study. To prepare the inoculum, the bacteria were grown in BB (*Brucella Broth*) medium (BD Biosciences, United States) for 24 h at 37°C under 180 rpm shaking, washed in PBS for 10 min, 5,000 rpm at 4°C, and resuspended in sterile PBS. The OD of the culture was measured at 600 nm in a spectrophotometer to determine the bacterial number in the solution.

Mice infection with *Brucella abortus*

Five to seven mice from each group were infected intraperitoneally (i.p.) with 1×10^6 *B. abortus* in 100 µl of PBS and the animals sacrificed at 14 days post-infection. The spleens were harvested and macerated in 10 ml saline (NaCl 0.9%), serially diluted, and plated in duplicated on *Brucella Broth* agar. Plates were incubated for 3 days at 37°C and the CFU number was determined.

Bone marrow-derived macrophages

BMDMs were differentiated *in vitro* from bone marrow cells extracted from mouse femurs. Cultures were differentiated for

7 days in an incubator at 37°C, 5% CO2 in DMEM medium supplemented with 1% HEPES, 20% fetal bovine serum (FBS), 30% L929 cell-conditioned medium (LCCM) source of M-CSF (important for differentiation of progenitor cells into macrophages), 100 U/ml penicillin and 100 μg/ml streptomycin (Thermo Fischer Scientific). After differentiation, macrophages were collected by washing the monolayers with ice-cold PBS, distributed on culture plates, and cultured in DMEM medium containing 1% SFB and 1% HEPES or 10% SFB and 1% HEPES and they were ready for use.

Lactate dehydrogenase release assay

For the lactate dehydrogenase (LDH) release assay, BMDMs were plated at 5×10^5 cells/well in 24-well plates and infected with *B. abortus* (MOI 100) for 8 h. RPMI 1640 medium without phenol red, with 1% glutamine, 1% FBS was used. Supernatants were collected, and LDH was quantified using the Cytotox96 LDH kit (Promega, Madison, WI) according to the manufacturer's instructions. During infection, bacteria were opsonized with a polyclonal mouse antibody (anti-*B.abortus*, dilution 1:1,000) to ensure more efficient bacterial phagocytosis. This polyclonal antibody was generated by injecting 1×10^6 heat-killed bacteria/mouse. The animals were injected three times during a 15-day interval, and after this period, serum from each mouse was tested for the presence of the specific antibody and stored at −80°C.

Cytokine measurement

For cytokine determination, BMDMs were plated at a concentration of 5×10^5 cells/well in 24-well plates and the cells were infected with *B. abortus* at an MOI of 100 for 17 h. Supernatants were collected and cytokines were measured with the mouse IL-1β, ELISA kit (R&D systems, Minneapolis, MN) according to the manufacturer's instructions.

Western blot analysis

BMDMs were cultured at 5×10^5 cells/well in 24-well plates. The cells were infected with *B. abortus* for 17 h as described above. After 17 h of infection, culture supernatants were harvested and cells were lysed with M-PER Mammalian Protein Extraction Reagent (Thermo Fisher Scientific) supplemented with 1:100 protease inhibitor mixture (Sigma-Aldrich). Cell lysates and supernatants were subjected to SDS-PAGE analysis as already described in previous studies by our research group (Cerqueira et al., 2018). The primary Abs used included a mouse monoclonal against the p20 subunit of caspase-1 (Adipogen, San Diego, CA, United States) at a dilution of 1:1,000. Loading control was performed using anti-β-actin mAb (Cell Signaling Technology, Danvers, MA) at a dilution of 1:1,000.

Statistical analysis

Statistical analysis was performed using Prism 5.0 software (GraphPad Software, San Diego, CA). The unpaired Student *t*-test was used to compare two groups. One-way ANOVA followed by multiple comparisons according to Tukey procedure was used to compare three or more groups. Unless otherwise stated, data are expressed as the mean ± SD. Differences were considered statistically significant at a p-value <0.05.

Results

Il-1β secretion in response to *Brucella abortus* occurs in a caspase-7-independent manner

The classical executioner caspases (caspase-7 and -3) are activated to initiate the process that culminate in the classical cell death signals (Nagata, 2018). Previous studies demonstrate that caspase-7 activation requires caspase-1 processing under inflammatory conditions (Lamkanfi and Kanneganti, 2010). To investigate whether caspase-7 participates in caspase-1 cleavage and IL-1β secretion during *Brucella abortus* infection, we infected BMDMs of C57BL/6 (WT), *Casp7*$^{-/-}$, *Casp7/1/11*$^{-/-}$, *Casp7/Gsdmd*$^{-/-}$, and *Gsdmd*$^{-/-}$ with *Brucella*. After 17 h of infection, we evaluated IL-1β secretion in the supernatant of the cells (Figure 1A) and the lysate was properly prepared for the assay of caspase-1 processing by Western blot analysis (Figure 1B). In all assays, C57BL/6 and *Gsdmd*$^{-/-}$ animals were used as controls, since the importance of gasdermin-D (GSDMD) for the control of *B.abortus* infection had been demonstrated previously by our research group (Cerqueira et al., 2018). We observed that BMDMs from *Casp7*$^{-/-}$ mice secreted similar amounts of IL-1β as WT animals. In macrophages from *Casp7/1/11*$^{-/-}$, *Casp7/Gsdmd*$^{-/-}$, and *Gsdmd*$^{-/-}$ animals the amount of IL-1β secreted was dramatically reduced compared to C57BL/6. Caspase-1 cleavage was observed only in the C57BL/6 and *Casp7*$^{-/-}$ strains, corroborating with the IL-1β cytokine secretion profile. Collectively, these data suggest that caspase-7 has no significant impact in IL-1β secretion and caspase-1 cleavage in response to *B. abortus* infection.

Caspase-7 does not participate in macrophage pyroptosis during *Brucella abortus* infection

Next, we addressed the role of caspase-7 in *B. abortus* induced cell death by quantifying LDH release in cell culture supernatants (Figure 2). BMDMs from C57BL/6, *Casp7*$^{-/-}$, *Casp7/1/11*$^{-/-}$, *Casp7/Gsdmd*$^{-/-}$, and *Gsdmd*$^{-/-}$ mice were infected with *B.abortus* and after 8 h of infection, LDH was quantified in the supernatant. *B. abortus* infection triggered higher LDH release in BMDMs of C57BL6 and *Casp7*$^{-/-}$ strains when compared to *Casp7/1/11*$^{-/-}$,

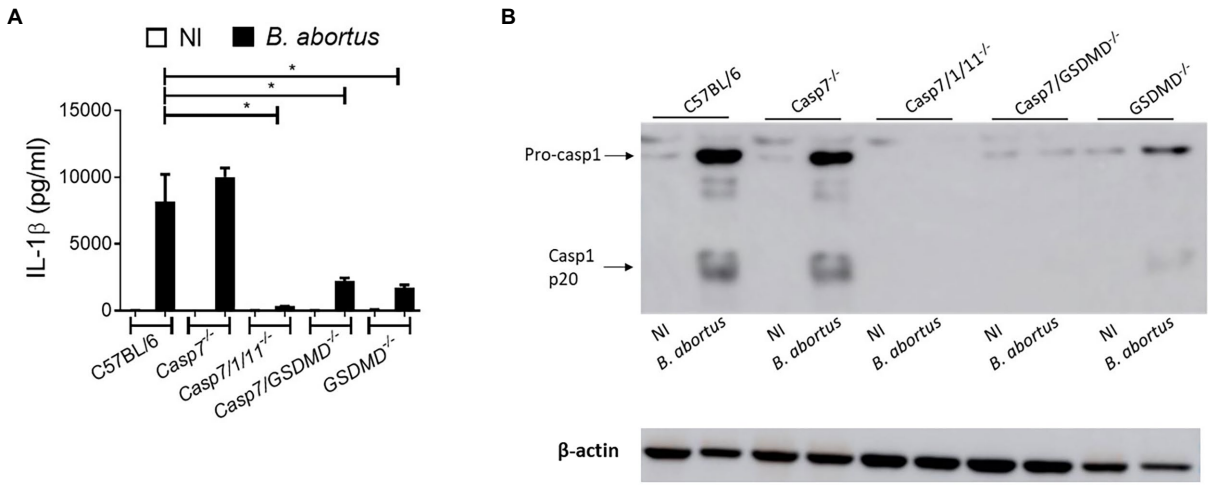

FIGURE 1
IL-1β production in response to *Brucella abortus* occurs in a caspase-7-independent manner. BMDMs were infected with *B. abortus* MOI: 100 for 17h. **(A)** IL-1β measurement in the supernatant by ELISA. **(B)** Immunoblot analysis of caspase-1 processing. Data show the mean±standard deviation of triplicates. The data are representative of three independent experiments. One-way ANOVA, *p<0.05 compared to C57BL/6.

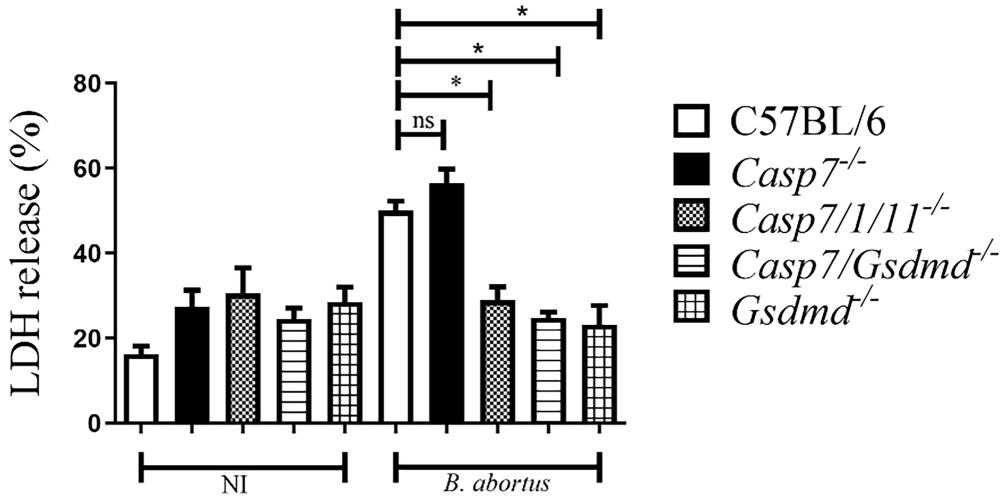

FIGURE 2
Caspase-7 does not participate in macrophage pyroptosis during *B. abortus* infection. BMDMs were infected with *Brucella abortus* MOI: 100 for 8h and LDH quantification was performed in the cell supernatant. Values represent the percentage of LDH released compared to control cells lysed with Triton X-100. The data show the mean±standard deviation representative of three independent experiments. One-way ANOVA, *p<0.05 compared to C57BL/6.

Casp7/Gsdmd$^{-/-}$, and *Gsdmd*$^{-/-}$ cells. This finding suggests that caspase-7 does not have a role in the induction of programmed cell death in response to *B. abortus* infection.

Caspase-7 plays no role in *Brucella abortus* infection *in vivo*

To determine whether the absence of caspase-7 influences the control of *Brucella* infection *in vivo*, we infected C57BL/6, *Casp7*$^{-/-}$, *Casp7/1/11*$^{-/-}$, *Casp7/Gsdmd*$^{-/-}$, and *Gsdmd*$^{-/-}$ mouse strains intraperitoneally and after 2 weeks the animals were sacrificed and the spleens were removed for quantification of the number of bacterial CFU. As shown in Figure 3, the bacterial burden measured in *Casp7*$^{-/-}$ animals showed no difference compared to the C57BL/6 controls. Higher bacterial numbers were observed in *Casp7/1/11*$^{-/-}$, *Casp7/Gsdmd*$^{-/-}$, and *Gsdmd*$^{-/-}$ mice. This result demonstrates that this susceptibility profile to infection occurred not because the lack of caspase-7, but rather, because of the deletion of *Casp1/11* or *Gsdmd*.

Caspase-8 participates in caspase-1 cleavage and IL-1β secretion in response to *Brucella abortus*

Further, we addressed the role of caspase-8 in regulating the inflammatory response during *B.abortus* infection. Deletion of caspase-8 results in RIPK3-dependent embryonic lethality. To rescue this viability, additional deletion of the RIPK3 kinase *via* the CRISPR/Cas9 technique was required (Wang et al., 2013). Therefore, the animals used in this study deficient for caspase-8 possess the additional deletion of RIPK3. We infected BMDMs of C57BL/6, *Gsdmd*$^{-/-}$, *Casp8/RIPK3*$^{-/-}$, and *Casp8*$^{+/+}$*/RIPK3*$^{-/-}$ mouse strains with *B. abortus*, and after 17 h of infection, we evaluated the secretion of IL-1β in the supernatant of the cells. Additionally, cell lysates were properly prepared for caspase-1 processing by Western blot analysis. BMDMs of *Casp8/RIPK3*$^{-/-}$ secreted reduced amounts of IL-1β compared to the WT and *Casp8*$^{+/+}$*/RIPK3*$^{-/-}$ controls, similar to the profile observed in *Gsdmd*$^{-/-}$ macrophages (Figure 4A). Further, the immunoblot data corroborate with the IL-1β secretion profile, where caspase-1 cleavage was detected only in the C57BL/6 and *Casp8*$^{+/+}$*/RIPK3*$^{-/-}$ cells (Figure 4B). These data suggest an important role of caspase-8 in caspase-1 cleavage and consequent IL-1β secretion during *B. abortus* infection.

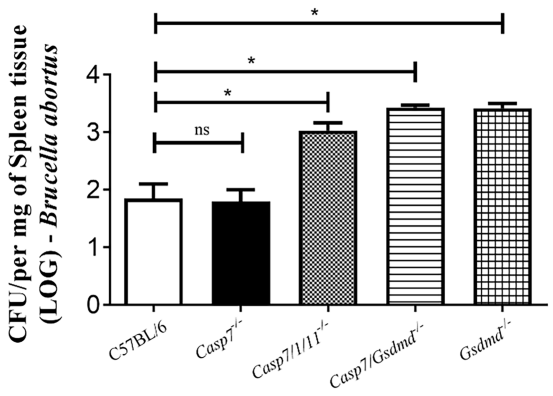

FIGURE 3
The role of caspase-7 in controlling *Brucella abortus* infection *in vivo*. Mice were infected intraperitoneally with 1x10^6 CFU of *B. abortus* and sacrificed after 2weeks of infection, and spleen homogenates were seeded onto plates containing BB agar medium for CFU determination. Data shown are the mean±standard deviation of five mice/group. The data are representative of three independent experiments. One-way ANOVA, *p<0.05, compared to wild-type mice.

Lack of caspase-8 interferes with cell death induced by *Brucella abortus* infection

Our results demonstrate that caspase-8 influences inflammasome activation induced by *Brucella*, since caspase-1 activation and IL-1β secretion occurs in a caspase-8-dependent manner. Thus, we sought to investigate whether caspase-8 is involved in pyroptosis induced by *B.abortus*. Macrophages from

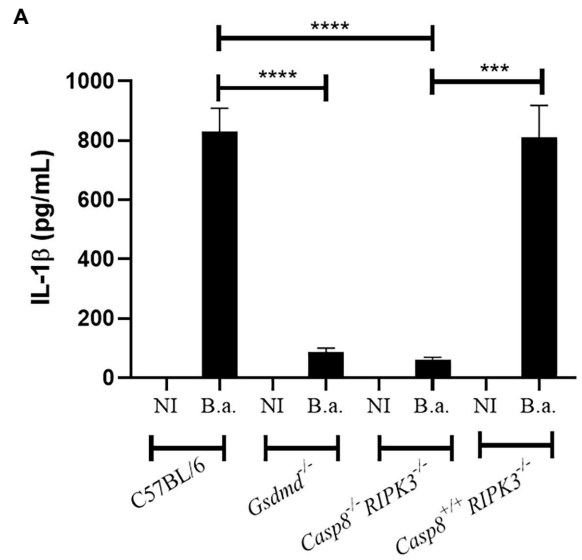

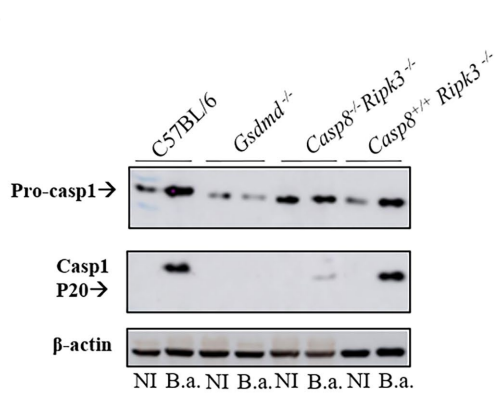

FIGURE 4
Caspase-8 participates in caspase-1 cleavage and IL-1β secretion in response to *B. abortus*. BMDMs obtained from C57BL/6, *Gsdmd*$^{-/-}$, *Casp8/RIPK3*$^{-/-}$ and *Casp8*$^{+/+}$*/RIPK3*$^{-/-}$ mice were uninfected (NI) or infected with *B. abortus* S2308 with MOI 100 for 17h. The supernatant was collected and subjected to ELISA assay to estimate the concentration of IL-1β **(A)**. The supernatant was labeled with anti-caspase-1 p20 monoclonal antibody **(B)**. Data show the mean±the standard deviation of triplicates. The data are representative of three independent experiments. Student *t*-test, ****p<0.0001 compared to C57BL/6 or *Casp8*$^{+/+}$*/RIPK3*$^{-/-}$. ***p<0.001.

C57BL/6, *Gsdmd*$^{-/-}$, and *Casp8/RIPK3*$^{-/-}$ strains were infected with *B.abortus* for 8 h. After this period, we performed the quantification of LDH release in cell culture supernatants (Figure 5). LDH release was greatly reduced in cells from animals deficient for caspase-8 and GSDMD, suggesting a potential role of caspase-8 in the induction of cell death in response to *B.abortus*.

Absence of caspase-8 enhances susceptibility to *Brucella abortus* infection *in vivo*

Since BMDMs deficient in caspase-8 showed reduced caspase-1 activation and secretion of IL-1β levels, we finally evaluated whether caspase-8 also played a role in restricting *Brucella* infection in mice. First, C57BL/6, *Gsdmd*$^{-/-}$, and *Casp8/RIPK3*$^{-/-}$ mice were infected intraperitoneally with *B. abortus*. After 2 weeks of infection, bacterial colony forming units (CFU) were determined from spleen homogenates. The recovery of bacteria in the spleen of *Casp8/RIPK3*$^{-/-}$ animals was higher than the WT control group, in a manner very similar to that observed in *Gsdmd*$^{-/-}$ animals (Figure 6). Collectively, these data suggest that caspase-8 is involved in an inflammatory response and in the control of *B. abortus in vivo*.

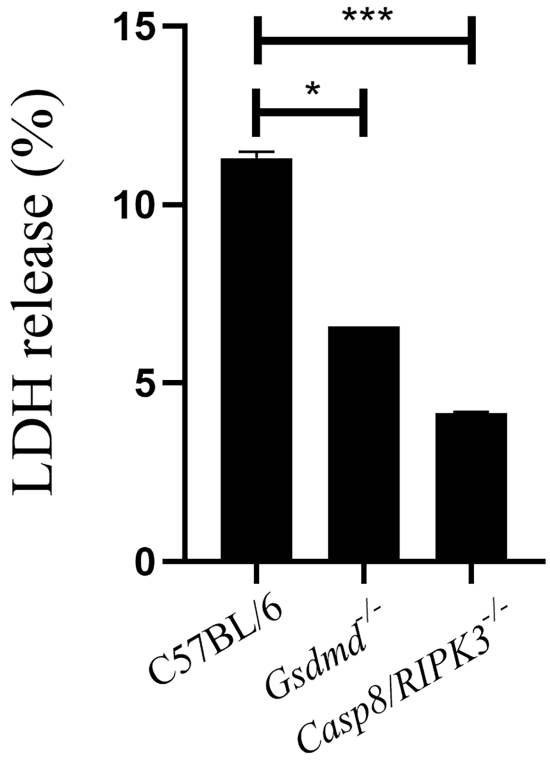

FIGURE 5
Caspase-8 is important to induce cell death during *B.abortus* infection. BMDMs of C57BL/6, *Gsdmd*$^{-/-}$ and *Casp8/RIPK3*$^{-/-}$ were infected with *B. abortus* with MOI 100 for 8hs and LDH quantification was performed in the cell supernatant. Values represent the percentage of LDH released compared to control cells lysed with Triton X-100. Data show the mean±the representative standard deviation of triplicates. The data are representative of three independent experiments. Student *t*-test, **p*<0.05, ****p*<0.001 compared to C57BL/6.

Discussion

Programmed cell death (PCD) can be activated in response to different stimuli (Nagata, 2018). Apoptosis, necroptosis and pyroptosis are three types of cell death that have major involvement in immune response and disease control (Schwarzer et al., 2020). Apoptosis helps in the destruction and removal of infected cells during bacterial infections (Speir et al., 2016). In the case of *Brucella*, some studies have already established that a virulent strain inhibits cell death in macrophages to allow bacterial replication (Chen et al., 2011). In contrast, in dendritic cells, astrocytes and T lymphocytes, the smooth strain induced apoptotic cell death (Garcia Samartino et al., 2010; Velasquez et al., 2012). Caspase-7, like caspase-3, is an executing caspase, both of which are activated by caspases-8 and -9 during death receptor-induced apoptosis, under certain conditions (Lamkanfi et al., 2002). Recently, some studies show that caspase-7 has a distinct role from caspase-3 during activation of apoptosis and also has a role in the inflammatory response against bacterial pathogens (Slee et al., 2001). Studies using *Salmonella typhymurium* infection of macrophages or cells stimulated with LPS and ATP, showed that caspase-7 activation was caspase-1-dependent.

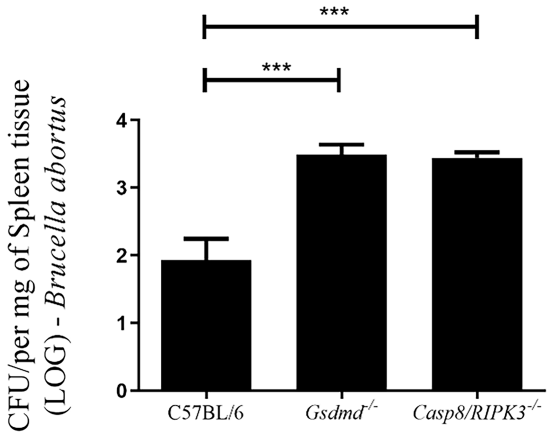

FIGURE 6
Caspase-8 influences the resistance to *Brucella* infection *in vivo*. C57BL/6, *Gsdmd*$^{-/-}$ and *Casp8/RIPK3*$^{-/-}$ m ice were infected intraperitoneally with 1x10^{6} CFU of *B. abortus*. Animals were sacrificed 2weeks after infection and diluted spleen homogenates were plated on agar plates containing BB medium for CFU determination. Data shown are the mean±standard deviation of five mice/group. The graph is representative of three independent experiments. One-way ANOVA, ****p*<0.001 compared to C57BL/6.

Additionally, Akhter et al. have observed in the absence of caspase-7 impaired ability of macrophages to restrict intracellular replication of *Legionella pneumophila* (Akhter et al., 2009). In contrast, Gonçalves et al. (Goncalves et al., 2019) demonstrated that lack of caspase-7 is not required to control *L. pneumophila* replication *in vitro* and *in vivo*. In another study, using an *in vivo* septic shock model, caspase-7-deficient mice were shown to be resistant to lethality induced by intraperitoneal injections of LPS (Lamkanfi et al., 2009). However, in our study caspase-7 does not appear to participate in the control of *B.abortus* infection. Inflammasome activation with cleavage of caspase-1 and secretion of IL-1β is not affected in the absence of caspase-7, as well as induction of cell death and *in vivo* susceptibility to infection. We have previously shown the participation of caspase-1, caspase-11 and GSDMD in controlling *B. abortus* (Cerqueira et al., 2018). Therefore, susceptibility to *Brucella* infection observed in *Casp7/1/11*$^{-/-}$ and *Casp7/Gsdmd*$^{-/-}$ animals is not due to lack of caspase-7 but rather the absence of caspase-1/11 and GSDMD.

Necroptosis is a programmed cell death pathway, with inflammatory features, that involves the kinases RIPK1 and RIPK3 and the pore-forming pseudokinase MLKL. When RIPK3 is phosphorylated, oligomerization of MLKL is initiated and subsequently inserts into the plasma membrane of the cell, leading to pore formation and cell rupture (Tummers and Green, 2017). Caspase-8 is involved in apoptosis and pyroptosis mechanisms of cell death, and when caspase-8 is inhibited RIPK1 interacts with RIPK3 leading to necroptosis (Pandian and Kanneganti, 2022). Pyroptosis is another type of inflammatory programmed cell death triggered by inflammasome activation, and for a long time, it was considered to be caspase-1-mediated in response to bacterial challenge. However, when caspase-11 was shown to detect intracellular LPS and also serve as a trigger to pyroptosis, the role of pyroptosis expanded widely (Kayagaki et al., 2011). Herein, we observed that in WT infected cells LDH release occurs, corroborating with data from our previous study where we showed that *B. abortus* infection triggers pyroptosis, and this phenomenon is GSDMD-dependent (Cerqueira et al., 2018). Additionally, in this study, we demonstrated that cell death induced by *Brucella* was also shown to be caspase-8-dependent. Caspase-8 contributes to activation of canonical and noncanonical inflammasomes. During *Salmonella* infection, caspase-8 can be recruited to the NLRC4 inflammasome regulating IL-1β secretion, but not playing a role in cell death (Man et al., 2013). In contrast, in *Yersinia* infection model, like we observed in this study, caspase-8 activates GSDMD to induce cell death (Sarhan et al., 2018). Furthermore, we observed here that mice deficient for caspase-8 and GSDMD are more susceptible to *Brucella* infection *in vivo* compared to wild type animals, suggesting that pyroptosis triggered during *B. abortus* infection is an important mechanism to control infection.

Several studies have already identified cellular functions for the GSDMD-mediated pore, such as secretion of molecules such as IL-1β and IL-1α and eicosanoids, which are important for recruiting neutrophils to the site of infection and promoting phagocytosis of infected cells and contributing to infection restriction (Jorgensen et al., 2016). Herein, reduced IL-1β secretion and pyroptosis observed in *Casp8/RIPK3*$^{-/-}$ mice are possible mechanisms that may contribute to increased susceptibility to infection. Although we did not investigate cell recruitment in this study, we hypothesize that innate cells recruitment to the site of infection may be impaired by the absence of pyroptosis in caspase-8 deficient animals, which could in part explain the increased bacterial load observed in these animals. Recently, caspase-8 was involved in *Aspergillus fumigatus* keratitis being critical in the recruitment of inflammatory cells and the clearance of the fungus (Wang et al., 2022). In summary, we suggest that caspase-8 plays an important role in cell death induced during *B.abortus* infection, contributing to inflammation and infection control in mice.

Data availability statement

The raw data supporting the conclusions of this article will be made available by the authors, without undue reservation.

Ethics statement

The animal study was reviewed and approved by the procedures for animal experimentation were approved by the Ethics Committee for the Use of Animals of the Federal University of Minas Gerais-CEUA/UFMG under protocol number 69/2020.

Author contributions

RS performed all the experiments and wrote the manuscript. DC participated in the design of this study, provided assistance with data acquisition, data analysis, and statistical analysis. DZ participated in the design of this study and provided reagents to perform the experiments. SO participated in the design of this study, provided assistance with data acquisition and wrote and reviewed the manuscript. All authors contributed to the article and approved the submitted version.

Funding

This work was supported by grants from the Conselho Nacional de Desenvolvimento Científico e Tecnológico to SO (CNPq, www.cnpq.br; grant# 303044/2020-9), Fundação de Amparo a Pesquisa do Estado de Minas Gerais to SO (FAPEMIG, www.fapemig.br; grants# APQ #01945/17 and Rede Mineira de

Imunobiológicos #00140-16), National Institutes of Health to SO (NIH, www.nih.gov; grant# R01 AI116453).

Conflict of interest

The authors declare that the research was conducted in the absence of any commercial or financial relationships that could be construed as a potential conflict of interest.

Publisher's note

References

Akhter, A., Gavrilin, M. A., Frantz, L., Washington, S., Ditty, C., Limoli, D., et al. (2009). Caspase-7 activation by the Nlrc 4/Ipaf inflammasome restricts legionella pneumophila infection. *PLoS Pathog.* 5:e1000361. doi: 10.1371/journal.ppat.1000361

Antonopoulos, C., Russo, H. M., El Sanadi, C., Martin, B. N., Li, X., Kaiser, W. J., et al. (2015). Caspase-8 as an effector and regulator of NLRP3 Inflammasome signaling. *J. Biol. Chem.* 290, 20167–20184. doi: 10.1074/jbc.M115.652321

Cerqueira, D. M., Gomes, M. T. R., Silva, A. L. N., Rungue, M., Assis, N. R. G., Guimaraes, E. S., et al. (2018). Guanylate-binding protein 5 licenses caspase-11 for Gasdermin-D mediated host resistance to *Brucella abortus* infection. *PLoS Pathog.* 14:e1007519. doi: 10.1371/journal.ppat.1007519

Chen, F., Ding, X., Ding, Y., Xiang, Z., Li, X., Ghosh, D., et al. (2011). Proinflammatory caspase-2-mediated macrophage cell death induced by a rough attenuated *Brucella* suis strain. *Infect. Immun.* 79, 2460–2469. doi: 10.1128/IAI.00050-11

Corbel, M. J. (1997). Brucellosis: an overview. *Emerg. Infect. Dis.* 3, 213–221. doi: 10.3201/eid0302.970219

Costa Franco, M. M. S., Marim, F. M., Alves-Silva, J., Cerqueira, D., Rungue, M., Tavares, I. P., et al. (2019). AIM2 senses *Brucella abortus* DNA in dendritic cells to induce IL-1beta secretion, pyroptosis and resistance to bacterial infection in mice. *Microbes Infect.* 21, 85–93. doi: 10.1016/j.micinf.2018.09.001

Costa Franco, M. M., Marim, F., Guimaraes, E. S., Assis, N. R. G., Cerqueira, D. M., Alves-Silva, J., et al. (2018). *Brucella abortus* triggers a cGAS-independent STING pathway to induce host protection that involves guanylate-binding proteins and Inflammasome activation. *J. Immunol.* 200, 607–622. doi: 10.4049/jimmunol.1700725

Ganesan, S., Rathinam, V. A. K., Bossaller, L., Army, K., Kaiser, W. J., Mocarski, E. S., et al. (2014). Caspase-8 modulates dectin-1 and complement receptor 3-driven IL-1beta production in response to beta-glucans and the fungal pathogen, *Candida albicans*. *J Immunol* 193, 2519–2530. doi: 10.4049/jimmunol.1400276

Garcia Samartino, C., Delpino, M. V., Pott Godoy, C., Di Genaro, M. S., Pasquevich, K. A., Zwerdling, A., et al. (2010). *Brucella abortus* induces the secretion of proinflammatory mediators from glial cells leading to astrocyte apoptosis. *Am. J. Pathol.* 176, 1323–1338. doi: 10.2353/ajpath.2010.090503

Gomes, M. T., Campos, P. C., Pereira Gde, S., Bartholomeu, D. C., Splitter, G., and Oliveira, S. C. (2016). TLR9 is required for MAPK/NF-kappa B activation but does not cooperate with TLR2 or TLR6 to induce host resistance to *Brucella abortus*. *J. Leukoc. Biol.* 99, 771–780. doi: 10.1189/jlb.4A0815-346R

Goncalves, A. V., Margolis, S. R., Quirino, G. F. S., Mascarenhas, D. P. A., Rauch, I., Nichols, R. D., et al. (2019). Gasdermin-D and Caspase-7 are the key Caspase-1/8 substrates downstream of the NAIP5/NLRC4 inflammasome required for restriction of legionella pneumophila. *PLoS Pathog.* 15:e1007886. doi: 10.1371/journal.ppat.1007886

Jorgensen, I., Zhang, Y., Krantz, B. A., and Miao, E. A. (2016). Pyroptosis triggers pore-induced intracellular traps (PITs) that capture bacteria and lead to their clearance by efferocytosis. *J. Exp. Med.* 213, 2113–2128. doi: 10.1084/jem.20151613

Kayagaki, N., Warming, S., Lamkanfi, M., Vande Walle, L., Louie, S., Dong, J., et al. (2011). Non-canonical inflammasome activation targets caspase-11. *Nature* 479, 117–121. doi: 10.1038/nature10558

Kim, H. E., Du, F., Fang, M., and Wang, X. (2005). Formation of apoptosome is initiated by cytochrome c-induced dATP hydrolysis and subsequent nucleotide exchange on Apaf-1. *Proc. Natl. Acad. Sci. U. S. A.* 102, 17545–17550. doi: 10.1073/pnas.0507900102

Lacey, C. A., Mitchell, W. J., Dadelahi, A. S., and Skyberg, J. A. (2018). Caspase-1 and Caspase-11 mediate Pyroptosis, inflammation, and control of *Brucella* joint infection. *Infect. Immun.* 86, e00361–18. doi: 10.1128/IAI.00361-18

Lamkanfi, M., Declercq, W., Kalai, M., Saelens, X., and Vandenabeele, P. (2002). Alice in caspase land. A phylogenetic analysis of caspases from worm to man. *Cell Death Differ.* 9, 358–361. doi: 10.1038/sj.cdd.4400989

Lamkanfi, M., and Kanneganti, T. D. (2010). Caspase-7: a protease involved in apoptosis and inflammation. *Int. J. Biochem. Cell Biol.* 42, 21–24. doi: 10.1016/j.biocel.2009.09.013

Lamkanfi, M., Moreira, L. O., Makena, P., Spierings, D. C., Boyd, K., Murray, P. J., et al. (2009). Caspase-7 deficiency protects from endotoxin-induced lymphocyte apoptosis and improves survival. *Blood* 113, 2742–2745. doi: 10.1182/blood-2008-09-178038

Lee, B. L., Mirrashidi, K. M., Stowe, I. B., Kummerfeld, S. K., Watanabe, C., Haley, B., et al. (2018). ASC- and caspase-8-dependent apoptotic pathway diverges from the NLRC4 inflammasome in macrophages. *Sci. Rep.* 8:3788. doi: 10.1038/s41598-018-21998-3

Macedo, G. C., Magnani, D. M., Carvalho, N. B., Bruna-Romero, O., Gazzinelli, R. T., and Oliveira, S. C. (2008). Central role of MyD88-dependent dendritic cell maturation and proinflammatory cytokine production to control *Brucella abortus* infection. *J. Immunol.* 180, 1080–1087. doi: 10.4049/jimmunol.180.2.1080

Man, S. M., Tourlomousis, P., Hopkins, L., Monie, T. P., Fitzgerald, K. A., and Bryant, C. E. (2013). Salmonella infection induces recruitment of Caspase-8 to the inflammasome to modulate IL-1beta production. *J. Immunol.* 191, 5239–5246. doi: 10.4049/jimmunol.1301581

Mascarenhas, D. P. A., Cerqueira, D. M., Pereira, M. S. F., Castanheira, F. V. S., Fernandes, T. D., Manin, G. Z., et al. (2017). Inhibition of caspase-1 or gasdermin-D enable caspase-8 activation in the Naip 5/NLRC4/ASC inflammasome. *PLoS Pathog.* 13:e1006502. doi: 10.1371/journal.ppat.1006502

Nagata, S. (2018). Apoptosis and clearance of apoptotic cells. *Annu. Rev. Immunol.* 36, 489–517. doi: 10.1146/annurev-immunol-042617-053010

Pandian, N., and Kanneganti, T. D. (2022). PANoptosis: a unique innate immune inflammatory cell death modality. *J. Immunol.* 209, 1625–1633. doi: 10.4049/jimmunol.2200508

Sagulenko, V., Thygesen, S. J., Sester, D. P., Idris, A., Cridland, J. A., Vajjhala, P. R., et al. (2013). AIM2 and NLRP3 inflammasomes activate both apoptotic and pyroptotic death pathways via ASC. *Cell Death Differ.* 20, 1149–1160. doi: 10.1038/cdd.2013.37

Sarhan, J., Liu, B. C., Muendlein, H. I., Li, P., Nilson, R., Tang, A. Y., et al. (2018). Caspase-8 induces cleavage of gasdermin D to elicit pyroptosis during Yersinia infection. *Proc. Natl. Acad. Sci. U. S. A.* 115, E10888–E10897. doi: 10.1073/pnas.1809548115

Schwarzer, R., Laurien, L., and Pasparakis, M. (2020). New insights into the regulation of apoptosis, necroptosis, and pyroptosis by receptor interacting protein kinase 1 and caspase-8. *Curr. Opin. Cell Biol.* 63, 186–193. doi: 10.1016/j.ceb.2020.02.004

Shenderov, K., Riteau, N., Yip, R., Mayer-Barber, K. D., Oland, S., Hieny, S., et al. (2014). Cutting edge: endoplasmic reticulum stress licenses macrophages to produce mature IL-1beta in response to TLR4 stimulation through a caspase-8- and TRIF-dependent pathway. *J. Immunol.* 192, 2029–2033. doi: 10.4049/jimmunol.1302549

Slee, E. A., Adrain, C., and Martin, S. J. (2001). Executioner caspase-3, -6, and -7 perform distinct, non-redundant roles during the demolition phase of apoptosis. *J. Biol. Chem.* 276, 7320–7326. doi: 10.1074/jbc.M008363200

Speir, M., Lawlor, K. E., Glaser, S. P., Abraham, G., Chow, S., Vogrin, A., et al. (2016). Eliminating legionella by inhibiting BCL-XL to induce macrophage apoptosis. *Nat. Microbiol.* 1:15034. doi: 10.1038/nmicrobiol.2015.34

Tummers, B., and Green, D. R. (2017). Caspase-8: regulating life and death. *Immunol. Rev.* 277, 76–89. doi: 10.1111/imr.12541

Velasquez, L. N., Delpino, M. V., Ibanez, A. E., Coria, L. M., Miraglia, M. C., Scian, R., et al. (2012). *Brucella abortus* induces apoptosis of human T lymphocytes. *Microbes Infect.* 14, 639–650. doi: 10.1016/j.micinf.2012.02.004

Wang, L., Yan, H., Chen, X., Lee, J., Sun, J., Liu, G., et al. (2022). Caspase-8 is involved in pyroptosis, necroptosis and the maturation and release of IL-1beta in aspergillus fumigatus keratitis. *Int. Immunopharmacol.* 113:109275. doi: 10.1016/j.intimp.2022.109275

Wang, H., Yang, H., Shivalila, C. S., Dawlaty, M. M., Cheng, A. W., Zhang, F., et al. (2013). One-step generation of mice carrying mutations in multiple genes by CRISPR/Cas-mediated genome engineering. *Cells* 153, 910–918. doi: 10.1016/j.cell.2013.04.025

Weng, D., Marty-Roix, R., Ganesan, S., Proulx, M. K., Vladimer, G. I., Kaiser, W. J., et al. (2014). Caspase-8 and RIP kinases regulate bacteria-induced innate immune responses and cell death. *Proc. Natl. Acad. Sci. U. S. A.* 111, 7391–7396. doi: 10.1073/pnas.1403477111

Zhang, L., Yu, S., Ning, X., Fang, H., Li, J., Zhi, F., et al. (2022). A Lys R transcriptional regulator manipulates macrophage autophagy flux during *Brucella* infection. *Front. Cell. Infect. Microbiol.* 12:858173. doi: 10.3389/fcimb.2022.858173

frontiers | Frontiers in Microbiology

TYPE Original Research
PUBLISHED 22 March 2023
DOI 10.3389/fmicb.2023.1106994

OPEN ACCESS

EDITED BY
Jens Andre Hammerl,
Bundesinstitut für Risikobewertung,
Germany

REVIEWED BY
Jiabo Ding,
Institute of Animal Sciences,
Chinese Academy of Agricultural Sciences,
China
Mostafa Y. Abdel-Glil,
Friedrich Loeffler Institut,
Germany

*CORRESPONDENCE
Alexandr Shevtsov
ncbshevtsov@gmail.com
Gilles Vergnaud
gilles.vergnaud@universite-paris-saclay.fr

†These authors have contributed equally to this work and share first authorship

SPECIALTY SECTION
This article was submitted to Infectious Agents and Disease, a section of the journal Frontiers in Microbiology

RECEIVED 24 November 2022
ACCEPTED 01 March 2023
PUBLISHED 22 March 2023

CITATION
Shevtsov A, Cloeckaert A, Berdimuratova K, Shevtsova E, Shustov AV, Amirgazin A, Karibayev T, Kamalova D, Zygmunt MS, Ramanculov Y and Vergnaud G (2023) *Brucella abortus* in Kazakhstan, population structure and comparison with worldwide genetic diversity.
Front. Microbiol. 14:1106994.
doi: 10.3389/fmicb.2023.1106994

Brucella abortus in Kazakhstan, population structure and comparison with worldwide genetic diversity

Alexandr Shevtsov[1*†], Axel Cloeckaert[2†], Kalysh Berdimuratova[1], Elena Shevtsova[1], Alexandr V. Shustov[1], Asylulan Amirgazin[1], Talgat Karibayev[3], Dinara Kamalova[1], Michel S. Zygmunt[2], Yerlan Ramanculov[1,4] and Gilles Vergnaud[5*]

[1]National Center for Biotechnology, Astana, Kazakhstan, [2]INRAE, UMR ISP, Université de Tours, Nouzilly, France, [3]National Reference Center for Veterinary, Astana, Kazakhstan, [4]School of Sciences and Humanities, Nazarbayev University, Astana, Kazakhstan, [5]Université Paris-Saclay, CEA, CNRS, Institute for Integrative Biology of the Cell (I2BC), Gif-sur-Yvette, France

Brucella abortus is the main causative agent of brucellosis in cattle, leading to severe economic consequences in agriculture and affecting public health. The zoonotic nature of the infection increases the need to control the spread and dynamics of outbreaks in animals with the incorporation of high resolution genotyping techniques. Based on such methods, *B. abortus* is currently divided into three clades, A, B, and C. The latter includes subclades C1 and C2. This study presents the results of whole-genome sequencing of 49 *B. abortus* strains isolated in Kazakhstan between 1947 and 2015 and of 36 *B. abortus* strains of various geographic origins isolated from 1940 to 2004. *In silico* Multiple Locus Sequence Typing (MLST) allowed to assign strains from Kazakhstan to subclades C1 and to a much lower extend C2. Whole-genome Single-Nucleotide Polymorphism (wgSNP) analysis of the 46 strains of subclade C1 with strains of worldwide origins showed clustering with strains from neighboring countries, mostly North Caucasia, Western Russia, but also Siberia, China, and Mongolia. One of the three Kazakhstan strains assigned to subclade C2 matched the *B. abortus* S19 vaccine strain used in cattle, the other two were genetically close to the 104M vaccine strain. Bayesian phylodynamic analysis dated the introduction of *B. abortus* subclade C1 into Kazakhstan to the 19th and early 20th centuries. We discuss this observation in view of the history of population migrations from Russia to the Kazakhstan steppes.

KEYWORDS

***Brucella abortus*, genetic diversity, WGS, SNP, genotyping, epidemiology**

1. Introduction

Brucellosis is a bacterial zoonotic disease caused by species belonging to the genus *Brucella* and results in high economic impact (McDermott et al., 2013). *Brucella* spp. may be transmitted to humans resulting in a severe disease requiring a specific and long-term antibiotic treatment with significant burden to public health systems (Franc et al., 2018). The genus *Brucella* currently contains 12 validly published species (Olsen and Palmer, 2014; Whatmore and Foster, 2021; Occhialini et al., 2022). *Brucella melitensis*, *Brucella abortus*, *B. suis*, *B. ovis*, *B. neotomae*, and

B. canis are often referred to as "classical" *Brucella* species in the literature. These have been identified between 1887 and 1968 and were differentiated on the basis of phenotypic traits and host preference (Buddle, 1956; Stoenner and Lackman, 1957; Carmichael and Bruner, 1968; Moreno et al., 2002). Since 2007, the wider use of genetic methods of identification and differentiation has led to the identification of *B. ceti*, *B. pinnipedialis*, *B. microti*, *B. inopinata*, *B. papionis,* and *B. vulpis*, which also preserve the tradition of naming the species in accordance with their original host (with the exception of *B. inopinata* isolated from a breast implant; Foster et al., 2007; Scholz et al., 2008, 2010; Whatmore et al., 2014; Scholz et al., 2016). The use of molecular methods made it possible to identify other potential new species recovered not only from mammals but also from amphibians, reptiles, and fish (Soler-Llorens et al., 2016; Al Dahouk et al., 2017; Eisenberg et al., 2017; Mühldorfer et al., 2017; Eisenberg et al., 2020), leading to further expansion of our knowledge of the genus *Brucella*. Based on whole-genome comparisons, a merge of the *Ochrobactrum* and *Brucella* genus was recently proposed (Hordt et al., 2020; Leclercq et al., 2020). Nonetheless, the greatest impact on public health and livestock infections around the globe have to date only been caused by *B. melitensis, B. abortus* and *B. suis* (Godfroid et al., 2011; Franc et al., 2018). An increase of human cases due to *B. canis* is currently suspected (Hensel et al., 2018; Zhou et al., 2020).

The majority of brucellosis cases are reported in the Mediterranean countries, South and Central America, Africa, Asia, Arabian Peninsula, Indian subcontinent, Eastern Europe, and the Middle East (Pappas et al., 2006; Nicoletti, 2010). Over the past decade, there has been a decline in incidence in many regions previously considered to be highly endemic, but also new reservoirs have been identified, such as in Africa and the Middle East, possibly resulting from a better implementation of diagnostic methods (Wang and Jiang, 2020). The real incidence of the disease in the mentioned regions is most probably largely underestimated because registration is based on passively collected data (Dean et al., 2012).

In Kazakhstan, brucellosis remains a major livestock and public health problem. More than 1,300 cases of human brucellosis are registered annually corresponding to an incidence of 7.6 per 100,000 inhabitants. Seropositivity to *Brucella* antigens in cattle and small cattle is 0.6% and 0.4%, respectively (Charypkhan and Ruegg, 2022).

The high zoonotic potential, re-emergence of the infection in previously disease-free regions, and identification of new reservoirs underscore the need for modern molecular epidemiology approaches such as genotyping to trace source reservoirs and paths of introduction. For *Brucella* genotyping at subspecies level, two methods are most widely used, Multilocus Sequence Typing (MLST) and Multiple Loci VNTR polymorphisms (Variable Number of Tandem Repeats, MLVA; Whatmore et al., 2016; Vergnaud et al., 2018). Robust phylogenetic relationships can be obtained from nucleotide sequencing data owing to the strictly clonal evolution of classical *Brucella* spp. (Whatmore and Foster, 2021). The first MLST scheme included nine loci, seven housekeeping genes, the outer membrane protein gene *omp25* and int-hyp. Six *B. abortus* MLST9 sequence types (STs) were initially described (Whatmore et al., 2007). Twenty-six *B. abortus* MLST9 STs are recorded in the current version of the *Brucella* spp. MLST database.[1] Including 12 housekeeping genes in the genotyping resulted in the more discriminatory MLST21. Thirty MLST21 STs were initially described in 172 *B. abortus* strains defining three clades (A, B, C including C1 and C2; Whatmore et al., 2016) and 43 STs are recorded in the current version of the *Brucella* spp. MLST database (see text footnote 1). The rare clades A and B include strains originating almost exclusively from Africa and allow defining the most ancestral nodes within the *B. abortus* phylogeny. Clades C1 and C2 are found on five continents and their presence in Africa seem to result from livestock importation (Whatmore et al., 2016; Vergnaud et al., 2018). Several MLVA genotyping schemes have been proposed for *Brucella*, one most commonly used scheme is MLVA16 (Scholz and Vergnaud, 2013). MLVA16 combines two panels of markers: one VNTR panel with a low discriminatory ability allows determining the species and main genetic lineages, and the other VNTR panel with a high discriminatory ability but low phylogenetic value allows differentiating strains in local outbreaks (Scholz and Vergnaud, 2013; Whatmore and Foster, 2021). The current version (Brucella v4_6_5) of the Brucella MLVA data hosted by MLVAbank[2] contains *in vitro* data derived from more than 1,400 *B. abortus* strains. The eight VNTR loci with the low discriminatory power (MLVA8) cluster *B. abortus* into 28 genotypes represented by at least two entries. MLVA alone is not suitable for phylogenetic reconstructions because of the high homoplasy at VNTR loci (Keim et al., 2004), but interestingly, MLVA using the low discriminatory markers (MLVA8, MLVA10 or MLVA11) and MLST clustering are highly congruent allowing to indirectly deduce phylogenetic signal from MLVA data (Vergnaud et al., 2018). Consequently, MLVA may constitute a first-line assay with low phylogenetic resolution until whole-genome sequencing (WGS) becomes sufficiently low-cost to be directly used as first line assay. MLVA genotypes can be readily deduced from WGS data with sequencing reads longer than 200 bp so that the highly discriminatory MLVA loci can also constitute a strain identity control tool (Vergnaud et al., 2018; Holzer et al., 2021; Pelerito et al., 2021).

The availability of whole-genome sequence (WGS) data opened the way to whole-genome and core genome MLST assays (wgMLST and cgMLST, respectively) with much higher resolution and phylogenetic value than these classical genotyping tools (Janowicz et al., 2018; Abdel-Glil et al., 2022). Genome-scale MLST assays as well as genome-wide SNP-genotyping confirmed the presence of the four major clusters A, B, C1, C2 in a collection of *B. abortus* with strains collected at a global scale (Whatmore and Foster, 2021; Abdel-Glil et al., 2022).

The current knowledge on the genetic diversity of *B. abortus* circulating in Kazakhstan is limited to MLVA-typing data. Interestingly, the MLVA genotyping investigations demonstrated low genetic diversity among strains circulating in Kazakhstan (Shevtsov et al., 2015; Daugaliyeva et al., 2018). Inclusion in the analysis of strains deposited since 1935 made it possible to describe the predominance of *B. abortus* clade C1, with genetic proximity of the majority of strains to Russian, Chinese and European strains. A few strains were assigned to *B. abortus* clade C2 (Shevtsova et al., 2016; Daugaliyeva et al., 2018). In order to better understand the population structure and origins of *B. abortus* in Kazakhstan, we selected 49 representative strains from Kazakhstan for whole-genome sequencing.

1 https://pubmlst.org/organisms/brucella-spp/ (Accessed January 24, 2023).

2 https://microbesgenotyping.i2bc.paris-saclay.fr/

We also selected 36 *B. abortus* strains representing the genetic diversity previously uncovered by MLVA within the historical collection maintained by Inrae, Nouzilly, France (Vergnaud et al., 2018) to determine phylogenic relations among *B. abortus* strains and to evaluate the usefulness of genomic data in the epidemiological control of the infection in a highly endemic region, such as Kazakhstan.

2. Materials and methods

2.1. *Brucella abortus* DNA and selection of strains for WGS

DNA analyzed were selected among 213 *B. abortus* strains isolated in Kazakhstan between 1943 and 2015 from bovine clinical material (aborted fetuses, lymph nodes, or whole blood). The strains were previously characterized by MLVA genotyping (Shevtsov et al., 2015; Shevtsova et al., 2016). The full MLVA assay (MLVA16) resolved 28 genotypes, 12 of which were represented by individual strains, the remaining genotypes were represented by up to 86 strains. The choice of strains for WGS was based on MLVA data, year and geographic origin. We selected 49 strains representing the 28 genotypes (up to eight strains per MLVA16 genotype). The selected strains originated from eight regions of Kazakhstan (Supplementary Table S1; Supplementary Figure S1).

Similarly, 212 *B. abortus* representative strains from the Inrae BCCN (Brucella Culture Collection Nouzilly) collected worldwide during the period 1976–2006 were previously characterized by MLVA (Vergnaud et al., 2018). Clade B and clade C represented 197 and 15 strains, respectively. A representative subset of 36 strains was selected for WGS (Supplementary Table S1).

2.2. Whole-genome sequencing

Kazakhstan strain sequencing was performed on the MiSeq platform (Illumina) as recommended by the manufacturer (Illumina, CA, United States). Nextera XT DNA Library preparation Kit (Illumina, CA, United States) was used to prepare libraries with double barcoding. Paired-end libraries were sequenced using MiSeq Reagent Kit v3 (600 cycles or 300 bp read length). *De novo* assemblies were produced using SKESA version 2.3.0 (Souvorov et al., 2018). The assemblies had an average of 49 contigs (range 33 to 88), an average N50 value of 171 kb (range 75 to 260 kb) and an average total assembly length of 3.25 Mb (range 3.229–3.256 Mb).

BCCN strains were sequenced by Genoscreen (Lille, France) using the MiSeq platform (Illumina). Read length was 250 bp. Sequencing reads were assembled using SPAdes version 3.13 (Bankevich et al., 2012). The assemblies had an average of 25 contigs (range 18 to 60), an average N50 value of 417 kb (range 251 to 884 kb) and an average total assembly length of 3.27 Mb (range 3.260–3.327 Mb).

Whole-genome MLST was run on genome assemblies using the BioNumerics "MLST for WGS" and "WGS tools" plugin and associated *Brucella* spp. scheme (Applied-Maths, Sint-Martens-Latem, Belgium). The plugins were also used to recover the MLST9 and MLST21 assignments (Whatmore et al., 2007, 2016) defined in the *Brucella* spp. database hosted by PubMLST (Jolley et al., 2018; Supplementary Table S1).

Raw reads were deposited in the European Nucleotide Archive BioProject PRJNA892249 (Kazakhstan collection) and PRJNA901374 (BCCN collection, France). Individual sequence reads archives (SRA), bioproject and biosample accessions are indicated in Supplementary Table S1.

2.3. Whole-genome single-nucleotide polymorphism analysis

All publicly available *Brucella* assemblies, sequence reads archive, and associated metadata, were downloaded from EBI ENA (read archives) or NCBI (assemblies) (last updated 2022-09-10). Sequence read archives were *de novo* assembled with SKESA. All assemblies were imported into BioNumerics version 8.1 (Applied-Maths, Sint-Martens-Latem, Belgium). The assemblies were used to produce artificial reads data sets (50 bp long, 10x coverage) for SNP calling by read mapping using genome assembly GCA_000740155 (*B. abortus* strain Tulya) as reference genome (Blouin et al., 2012; Vergnaud et al., 2018). The BioNumerics parameters for reads mapping were 95% minimum sequence identity, minimum inter-SNP distance 12 base-pairs. Maximum parsimony trees were drawn within BioNumerics. The list of all public datasets evaluated is presented in Supplementary Table S2. Supplementary Table S2 includes comments facilitating the selection of strains, including "duplicates" (more than one dataset available for the same strain), "redundant" (coincident wgSNP genotype). Some datasets provided poor coverage or induced topological issues, due to sample mix or inappropriate assembly procedure.

For input in BEAST version 1.10.4 (Suchard et al., 2018), a table of SNP positions from selected strains was exported from BioNumerics and SNPs were concatenated as fasta files. BEAST was run under a general time-reversible model of nucleotide substitution with a gamma distribution between sites, a relaxed molecular clock, Bayesian skyline plot (BSP) demographic model, lognormal distribution for population sizes as previously described (Kamath et al., 2016). The convergence of 20 independent runs with a chain length of 150 million was examined using Tracer v1.7 (Rambaut et al., 2018). The selected runs were merged with a burning of 15 million using LogCombiner and TreeAnnotator (Suchard et al., 2018). The resulting trees were visualized using FigTree v1.4.4 (Rambaut, 2018).

2.4. Analysis of homoplasia in MLVA profiles

The previously published MLVA16 profiles of 49 strains from Kazakhstan were used within BioNumerics for clustering based on categorical data distance measure and unweighted paired group with arithmetic means method (UPGMA). MLVA homoplasia was recognized when MLVA clustering was not congruent with the phylogeny deduced from wgSNP analysis.

3. Results

3.1. MLST assignment of the 49 *Brucella abortus* strains from Kazakhstan

Four MLST9 STs were present, ST1 (two strains) ST2 (45 strains), ST5 (one strain), and ST119 (new MLST9 genotype, represented by

one strain). ST2 and the closely related ST119 belong to subclade C1 whereas ST1 and ST5 belong to subclade C2 (Whatmore et al., 2007). MLST21 resolves one additional genotype, as subclade C1 strain Kaz041 defined a new allele at MLST21 locus csdb due to a single-nucleotide variation (Supplementary Table S2). Using the wgMLST analysis assay, alleles could be called at 3,312 up to 3,345 loci in the 46 clade C1 strains. Seven hundred and three loci were called in all 46 strains and were polymorphic. Supplementary Figure S1 shows the clustering derived from the corresponding wgMLST character dataset of the 46 clade C1 strains.

3.2. Wgsnp based phylogenetic analysis of the 46 *Brucella abortus* subclade C1 strains from Kazakhstan

Figure 1 shows the phylogeny of 46 *B. abortus* subclade C1 strains from Kazakhstan deduced from wgSNP analysis. The maximum distance between two strains was 208 SNPs. Distances from root (blue star) to tips varied from 76 up to 117 SNPs. The analyzed Kazakhstan strains partitioned into six main branches labeled A to F. The topology obtained with wgSNP and wgMLST (Supplementary Figure S1) were identical. Branches A to D are defined by one to three different wgSNP genotypes corresponding to "historical" strains mainly collected in the Almaty region during the 1948–1970 period. All strains isolated from 2007 to 2015 were assigned to branches E and F. Whereas branch F was defined by a single strain, Kaz021, branch E could be further subdivided into four sub lineages labeled I to IV. Each one contained one or two historical strains in addition to recent strains. Lineage E-I is geographically associated with the Eastern and Northern parts of Kazakhstan (Figure 2). Lineages E-II to E-IV are predominantly associated with strains collected in 2015 in six settlements of the West Kazakhstan region (WKR).

3.3. Congruence between WGS phylogeny and MLVA clustering

The wgSNP analysis grouped 31 strains from Kazakhstan into 8 clusters labeled WGS_1 to WGS_8 in Figure 1; Supplementary Figure S1, which show a difference within each cluster of no more than 7 SNPs. Cluster WGS_1 comprised six "historical" strains lacking accompanying epizootological data, isolated in WKR, Akmola and Almaty regions between 1948 and 1970. The four strains identical by wgSNP from WGS_1 were also identical by MLVA16, while Kaz049 and Kaz046 differed at the highly variable Bruce07 locus. In spite of their very high wgSNP similarity, the strains were collected over a period of 13 years in three regions of Kazakhstan. Previous reports described similar long term maintenance of highly similar wgSNP or wgMLST genotypes (Garofolo et al., 2017; Janowicz et al., 2018; Allen et al., 2020; Holzer et al., 2021). Cluster WGS_2 was formed by ten strains isolated from Kostanay region in the 2008–2011 period and strain a_1 isolated in Almaty region in 2007. According to epidemiological data, nine out of ten strains from the Kostanay region represented four independent outbreaks. These strains represented three MLVA16 genotypes with a difference in the Bruce09 hypervariable locus. Cluster WGS_3 included two epidemiologically unrelated strains from EKR and Almaty regions, differing from each other by one SNPs, and by MLVA16 at the Bruce09 locus. Cluster WGS_4 was represented by two strains from the Kostanay region from two independent outbreaks which are identical in wgSNP and MLVA16. Cluster WGS_5 cluster was represented by two "historical" epidemiologically independent strains from WKR and Almaty regions identical in MLVA16 analysis and separated by two SNPs. Cluster WGS-6 combined two epidemiologically unrelated strains which are identical in their MLVA16 profiles and differ by three SNPs. Cluster WGS_7 combined two strains from the same outbreak in WKR, with an identical wgSNP genotype and differing in MLVA16 at locus Bruce07. Cluster WGS_8 combined four strains isolated in 2015 in the Akmola region, all from the same settlement and representing a single outbreak. The maximum difference between these strains is two SNPs, with all having an individual MLVA16 profile that differs in Bruce07 or Bruce09.

According to clustering on the basis of MLVA data, 10 MLVA16 genotypes (out of 28 genotypes) combined two to eight strains (Supplementary Figure S2). Homoplasia was suspected in five genotypes: MLVA_6 genotype includes two historical strains from Almaty (Kaz030 and Kaz041) and one recent strain from WKR (Kaz086). Kaz041 belongs to branch C, whereas Kaz086 and Kaz030 belong to E-III and E-IV, respectively, (Figure 1; Supplementary Figure S1). Genotype MLVA_7 included two strains, Kaz052 and Kaz070 isolated from Akmola and WKR regions in 2015, and belonging to E-IV and E-II, respectively. Genotype MLVA_14 combined four historical strains isolated from WKR and Akmola part of cluster WGS_1 from branch C and strain a_112 isolated in Kostanay in 2011 from branch E-I. Genotype MLVA_16 combined seven strains from cluster WGS_2 in branch E-I isolated in Almaty and Kostanay between 2007 and 2011, and also historical strain Kaz046 isolated in Almaty in 1957, belonging to cluster WGS_1 branch C. The MLVA_19 genotype combined strain Kaz020 (branch E-I, isolated in 2015, EKR region) and historical strain Kaz029 from Atyrau region from branch E-III. These lack of congruence between MLVA16 typing and wgSNP phylogeny are due to minor variations in the most variable loci constituting panel2B, in agreement with previous observations regarding the instability of these loci (Garcia-Yoldi et al., 2007; Maquart et al., 2009; Allen et al., 2020).

3.4. Comparison of the 46 *Brucella abortus* subclade C1 strains from Kazakhstan with public datasets

For comparison, we recovered 148 public WGS datasets, and eight *B. abortus* subclade C1 WGS datasets from the BCCN collection (Supplementary Table S2). Fifty-three duplicate datasets were removed (WGS data available as assembly and sequence reads archives, or identical strains sequenced by different institutions). Datasets contributing terminal branches shorter than five SNPs were also removed. Figure 3 shows the result of wgSNP analysis of the 46 *B. abortus* subclade C1 strains from Kazakhstan together with 77 selected WGS datasets of worldwide origins. Starting from the root, four main lineages were defined. Branch length from root to tip vary from 280 up to 309 SNPs. All 46 Kazakhstan strains clustered in one of these four clade C1 sub-lineages. Most Kazakhstan strains were closest to strains from neighboring countries, Russia and to a lower extend, China. About 10 independent introductions from these neighbors would be sufficient to explain the observed topology of the tree. Figure 4 shows an enlarged view of the subclade C1 lineages containing the Kazakhstan strains,

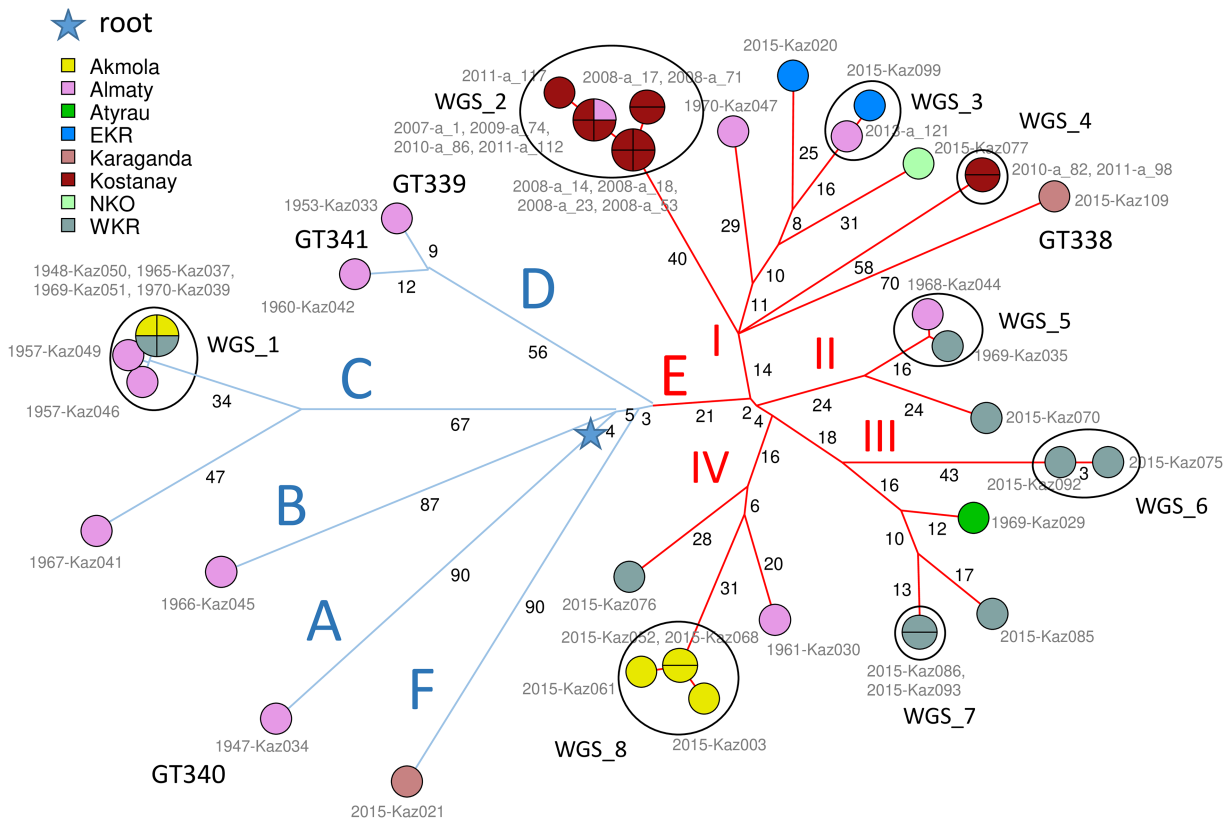

FIGURE 1
Brucella abortus subclade C1, 46 strains from Kazakhstan. Maximum parsimony tree based on core genome SNPs. 1,146 SNPs were called by mapping on genome accession GCA_000740155 (*B. abortus* clade B strain Tulya). The size of the resulting tree is 1,151 SNPs (homoplasia 0.44%). Thirty-three whole-genome SNP (wgSNP) genotypes are resolved. Branch lengths of two SNPs and more are indicated by black numbers. Strains are labeled in gray with collection year and strain Ids and colored according to region of origin as indicated. The MLVA11 genotype is indicated for new lineages distinct from GT72 (GT338 to GT341). The blue star indicates the root of the phylogeny (branching point toward *B. melitensis* type strain 16M used as outgroup). From the blue star, early splits define six branches, labeled A to F. Blue branches A to D are defined by a few ancient strains isolated between 1947 and 1970. Blue branch F is defined by one recent strain, KAZ021 isolated in 2015. Red branch E with 34 strains (24 wgSNP genotypes) is remarkable by its diversity (24 wgSNP genotypes) and high number of associated strains (34 out of 46). It contains all but one of the recent strains (isolated in 2007–2015) together with five ancient strains. The E branch is structured into four subbranches labeled I to IV in red. Strains closely related or coincident in terms of wgSNP genotype define eight clusters labeled WGS_1 to WGS_8.

together with the region of origin of the strains. Most strains from Kazakhstan appeared to be closest to strains from neighboring Russia and Georgia (Sidamonidze et al., 2017; Kovalev et al., 2021). For instance, the unique branch F representative from Kazakhstan, Kaz021 isolated in 2015, is surrounded in Figure 4 by multiple strains from Russia (North Caucasus) and Georgia. Branches A and D showed interesting features. In branch D, a split created a sublineage populated by seven strains collected in Western Europe, and one from Egypt. Branch A comprised only one strain from Kazakhstan and one from Italy.

3.5. Comparison of the three *Brucella abortus* clade C2 strains from Kazakhstan with public datasets

Public databases contain 880 *B. abortus* subclade C2 WGS datasets including assemblies and sequence read archives (Supplementary Table S2). After removal of datasets achieving a poor coverage of the reference genome, 870 datasets were available for comparison. Strain Kaz031 from Kazakhstan clustered in a tight group of approximately 100 strains, including representatives of strains 2308, RB51, S19, and *B. abortus* reference strain 544. RB51 is used as a vaccine, and was derived from 2308 (Schurig et al., 1991). Of note, Kaz031 differs by two SNPs from *Brucella* vaccine strain A19 (assembly accession GCA_003290345). The two other subclade C2 strains from Kazakhstan clustered together with vaccine strain 104M. A total of 80 and 87 SNPs separated strains Kaz027 and Kaz025 from the vaccine strain *B. abortus* 104M (assembly accession GCA_001296965). The two strains are also separated by three up to 18 SNPs from assembly accessions GCA_000250835 (an entry incorrectly labeled as a derivative of *B. melitensis* type strain 16M, strain 16M13W), GCA_000292025 and GCA_000298635 (Supplementary Figure S3).

3.6. Global view of *Brucella abortus* phylogeny based on currently available WGS datasets

A total of 1,169 *B. abortus* WGS datasets could be investigated including public datasets (Supplementary Table S2) and the 85

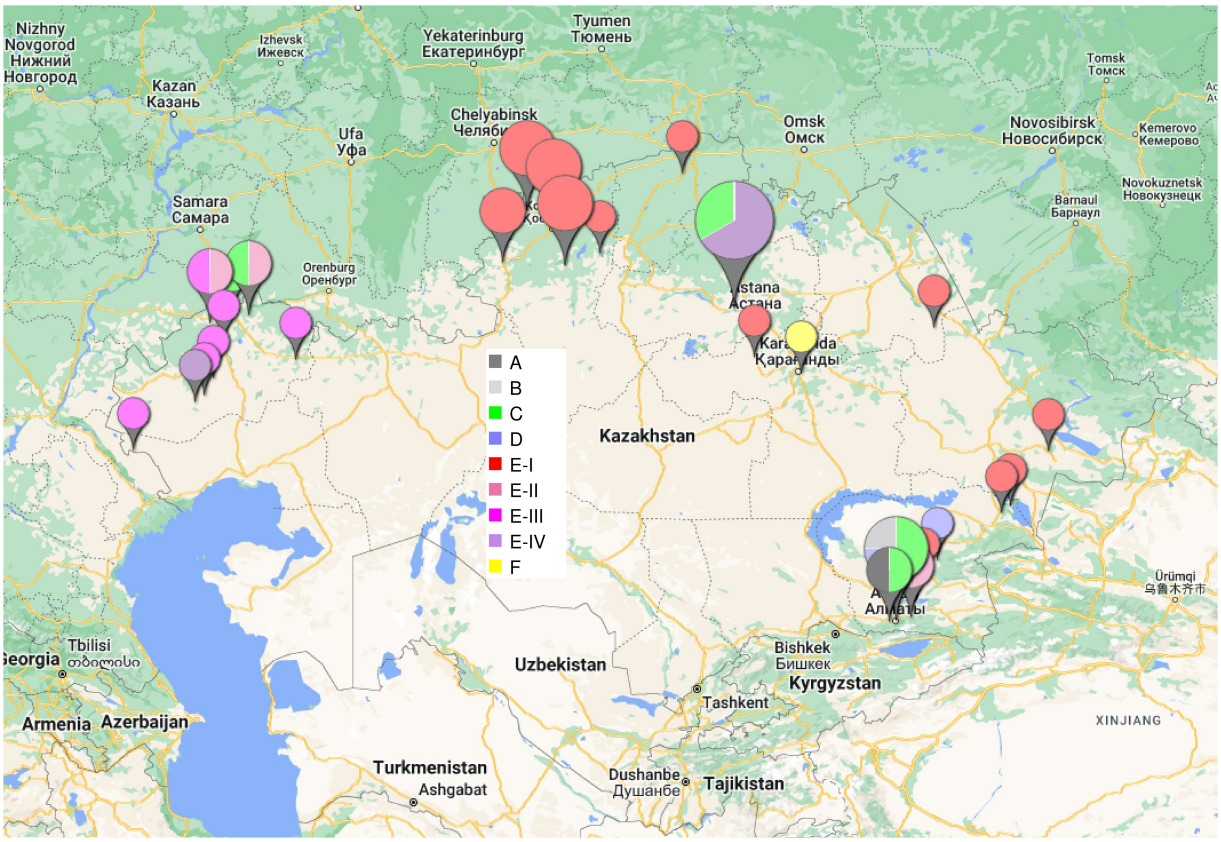

FIGURE 2
Geographic origin of the *B. abortus* clade C1 strains from Kazakhstan. The size of the labels reflect the number of strains (from 1 to 10) in the corresponding location. The color code shown in the central inset reflects the phylogenetic position (branch assignment) indicated in Figures 1, 3.

datasets produced for this report. Two hundred and thirty-six datasets were kept after removal of duplicates, redundant datasets, poor datasets, and closely related strains contributing terminal branches shorter than 5 SNPs. Figure 5 shows a global view of the phylogeny of *B. abortus* deduced from this dataset. The three clades, A, B, and C, were clearly resolved. Clades A and B showed a strong geographic association, clade A with East Africa, and clade B with West Africa. Clade C subclade C1 was predominantly associated with the eastern part of Eurasia, and subclade C2 with the western part of Eurasia as well as North and South America. Estimated divergence dates of the most ancestral nodes are shown. Supplementary Figure S4 shows the same phylogeny with more detailed metadata information.

3.7. Tentative dating of *Brucella abortus* introduction events in Kazakhstan

As a preliminary attempt to date these introduction events, we applied BEAST to the previous selection of 236 *B. abortus* and to 193 *B. melitensis* strains (Supplementary Table S2). *B. melitensis* and *B. abortus* are closest relatives within genus *Brucella*. They share the same mutation inactivating the Entner–Doudoroff pathway (EDP) for hexose catabolism, suggesting that their most recent common ancestor was already an obligate animal pathogen (Machelart et al., 2020). The inclusion of *B. melitensis* allowed to take advantage of the WGS sequence data recovered from a well-dated Medieval sample (Sardinia, *circa* year 1,375 CE), thus providing a key time point (Kay et al., 2014). SNPs were called by mapping on genome accession GCA_000740155 from *B. abortus* strain Tulya (23,086 SNPs were identified). Representative dating estimates are included in Figures 3–5. The analysis suggested that currently circulating *B. abortus* strains in Kazakhstan originated from imports in the 19th and 20th century. The split toward the European sublineage in branch D would have occurred in year 1759–1842. The Italian and Kazakhstan strains constituting branch A would share a most recent common ancestor *circa* year 1,641–1762. The estimated molecular evolution rate is 0.3 SNP per year per genome (95% HPD—highest probability density—range 0.24–0.45). A higher evolution rate of 0.46 SNP per year per genome (95% HPD range 0.30–0.74) was previously proposed (Kamath et al., 2016). The main differences in the two investigations were the collection of strains used (both *B. abortus* and *B. melitensis* in the present investigation versus North American *B. abortus* clade C2 only in Kamath et al.) and the inclusion in the present investigation of the Medieval sample.

4. Discussion

Brucellosis in cattle remains a major problem for cattle breeders in Kazakhstan. Genetic monitoring of genotypic dynamics is not included in the infection control strategy at the state level, but is

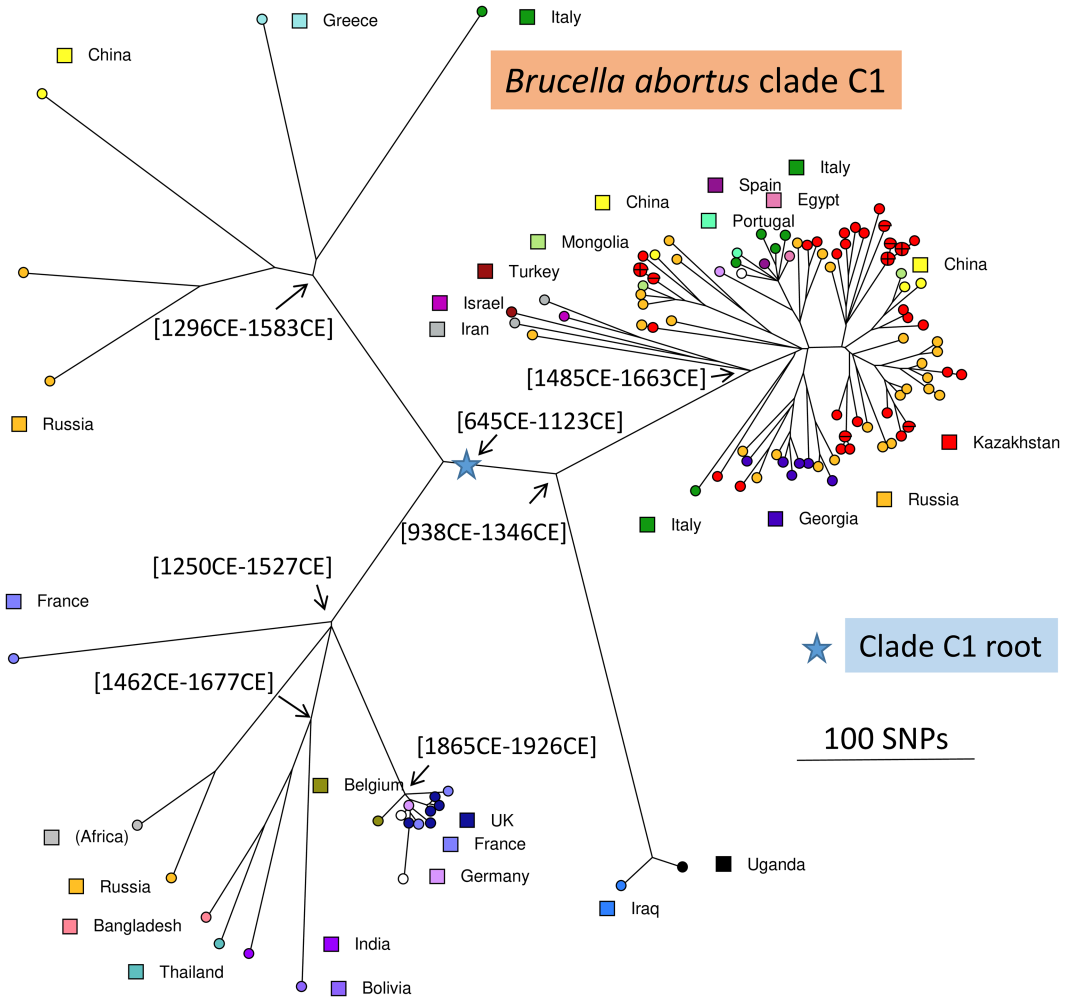

FIGURE 3
Brucella abortus subclade C1, position of the Kazakhstan strains within the global subclade C1 phylogeny. Maximum parsimony tree based on core genome SNPs. A total of 123 strains was used, including 77 selected strains of worldwide origins in addition to the 46 Kazakhstan strains. 5,446 SNPs were called by mapping on genome accession GCA_000740155 (*B. abortus* strain Tulya). The size of the resulting tree is 5,487 SNPs (homoplasia 0.75%). Strains are colored according to country of origin as indicated. The blue star indicates the root of the phylogeny (branching point toward *B. abortus* clade B strain Tulya used as outgroup). Representative estimated divergence dates are indicated (CE, common era).

implemented in the country through scientific grants and is mainly based on MLVA technology. This is the first study to describe the genetic diversity of *B. abortus* isolated between 1947 and 2015 in the territory of Kazakhstan using genome-wide sequence data that confirmed the presence of the two major subclades C1 and C2. Clades A and B were absent, in agreement with the previously published MLVA clustering analysis (Shevtsova et al., 2016; Daugaliyeva et al., 2018) and well established very strong geographic association of clades A and B with East and West Africa, respectively, (Whatmore et al., 2016; Vergnaud et al., 2018).

In this study, in five among the 10 MLVA16 genotypes represented by at least two strains, unrelated wgSNP genotypes were observed. The high percentage of homoplasia in the VNTR analysis is primarily due to the targeted selection of strains with identical MLVA16 from outbreaks which are unrelated by epidemiological data, and to the high level of homoplasia associated with the most variable VNTR loci. Four out of five cases of MLVA16 homoplasia involved combinations of the "historical" and currently circulating strains. Therefore, MLVA16 homoplasia seems higher in strains collected over an extended period of time. Eight wgSNP clusters were identical in MLVA16 or differed only in one or two hypervariable loci (Bruce07 or Bruce09), generally supporting the MLVA clustering. Previous studies of *B. abortus* strains using whole-genome SNP analysis and MLVA demonstrated similar results in outbreak differentiation and detection of imported strains, with a conclusion of a need to use genome-wide SNPs for reliable phylogenetic inference (Garofolo et al., 2017; Allen et al., 2020; Suárez-Esquivel et al., 2020; Holzer et al., 2021). Comparable strain clustering for MLVA11 and wgSNP allows MLVA in combination with epidemiological data to be considered as a first choice of methods to select strains for WGS in highly endemic regions, but only WGS analyzes will provide sufficiently precise phylogenetic information and might progressively become the first choice methods if global sequencing costs keep decreasing.

The identification of very closely related wgSNP genotypes in different regions with a difference of isolation by several years indicates a long-term circulation of *B. abortus* genotypes in

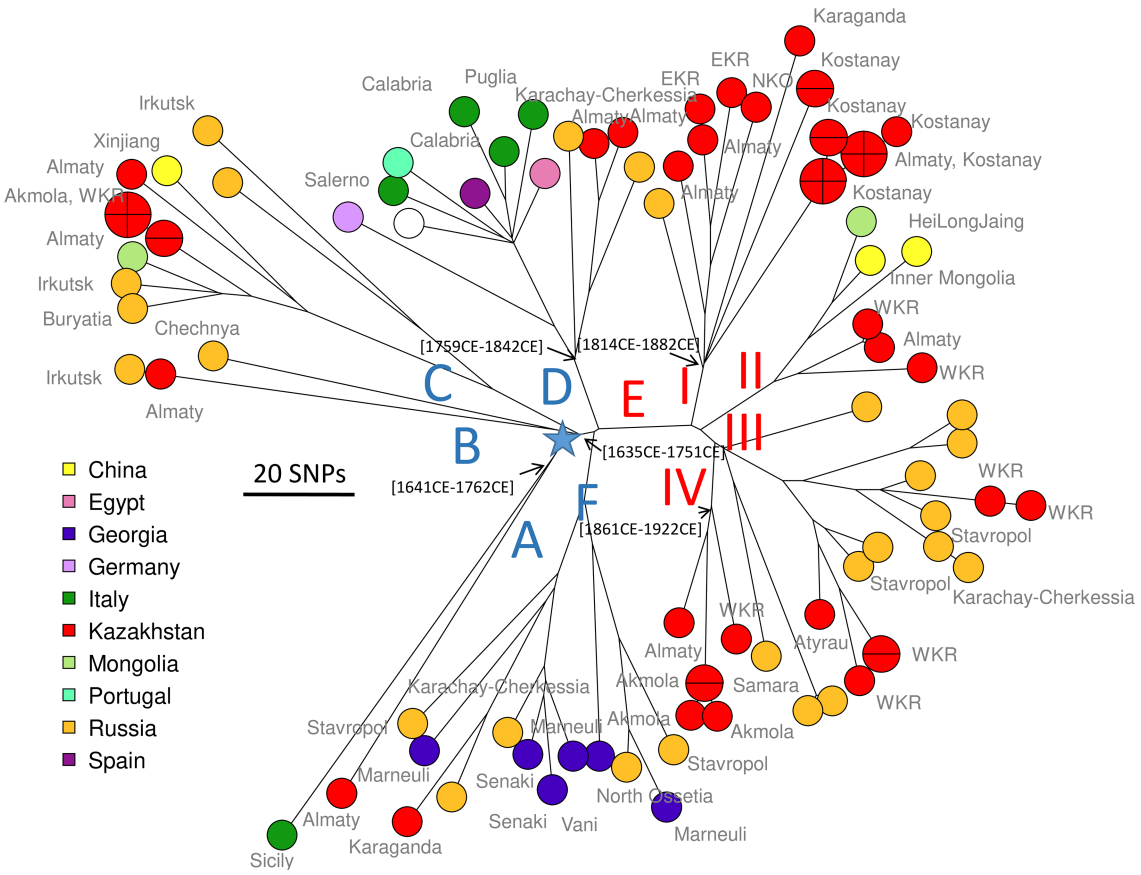

FIGURE 4
Zoom on *B. abortus* subclade C1, position of the Kazakhstan strains within the global subclade C1 phylogeny. Close-up on Figure 3. Strains are colored according to country of origin as indicated and labeled with region of origin when known. The blue star indicates the root of the phylogeny (branching point toward *B. abortus* clade B strain Tulya used as outgroup). Branch names A to F defined in Figure 1 are shown. Representative estimated divergence dates are indicated (CE, common era).

Kazakhstan. Also, identification of the same wgSNP genotype cluster in unrelated outbreaks in the same region, such as Kostanay, indicates circulation of infected animals between farms. Thus, uncontrolled cattle trade and movement, as well as keeping animals from different farms on the same pastures, is postulated to be among main factors in the spread of the cattle brucellosis infection in Kazakhstan (Syzdykov et al., 2014; Charypkhan et al., 2019).

The Bayesian phylodynamic approach suggested that *B. abortus* lineages currently circulating in Kazakhstan were introduced in the 19th-20th centuries from Europe, mainly from Russia (North Caucasia). It may be interesting to note that evolution of subclades C1 and C2 showed similarities in this respect. The import of clade C2 into the United States was dated to the end of the 17th century (Kamath et al., 2016), with closest neighbor lineages corresponding to strains isolated in Western Europe.

The introduction of *B. abortus* clade C1 in Kazakhstan might have happened during periods of human migration and because of the importation of numerous livestock for breeding with native breeds of cattle. Migration processes to Kazakhstan from the territory of the Russian Empire, and later the USSR, began with the accession of the northern territories of Kazakhstan in the Russian Empire in the 1730s and continued until the 1970s (Qazaqstan_tarihy, 2018; Presidential_Library_RF, 2022). The imperial period was characterized by mass migration of peasants, whose migration had an impact on the livestock breeding system of the nomadic people. Migrations had a wave-like character and were associated with the abolition of serfdom and the resettlement of free peasants from the European part of Russia since 1861. In 1889 the law on resettlement provided land plots and loans to peasant settlers. Crop failure and famine in European Russia and the Stolypin reforms of 1906–1911 further stimulated these migrations (Rather and Abdullah, 2018). In 1897 Russians made up 12 percent of the total population of Kazakhstan, i.e., 600,000 inhabitants. From the end of the 19th century to 1916, about 1,400,000 European Russians arrived in the Kazakh steppes, making up 40% of the population of the steppe regions of Kazakhstan (Bell-Fialloff, 2016). There are no exact data on imported livestock for that period, however, there are some data indicating that people moved with their livestock, and original Kalmyk-cattle-breeds appeared in Kazakhstan along with immigrants from Voronezh, Stavropol, Astrakhan, and other provinces of southern Russia (Belmont, 1960). During this period, many Kazakhs were forced to rebuild their traditional way of life with the transition to agriculture and a semi-nomadic lifestyle due to the seizure of land in favor of settlers for farming and taking rangelands to graze Russian riches' cattle (Sailaukyzy et al., 2018). In the structure of Kazakhs herds, the number of cattle had increased because of greater demand for cattle meat. At the end of the 19th and the beginning of the 20th

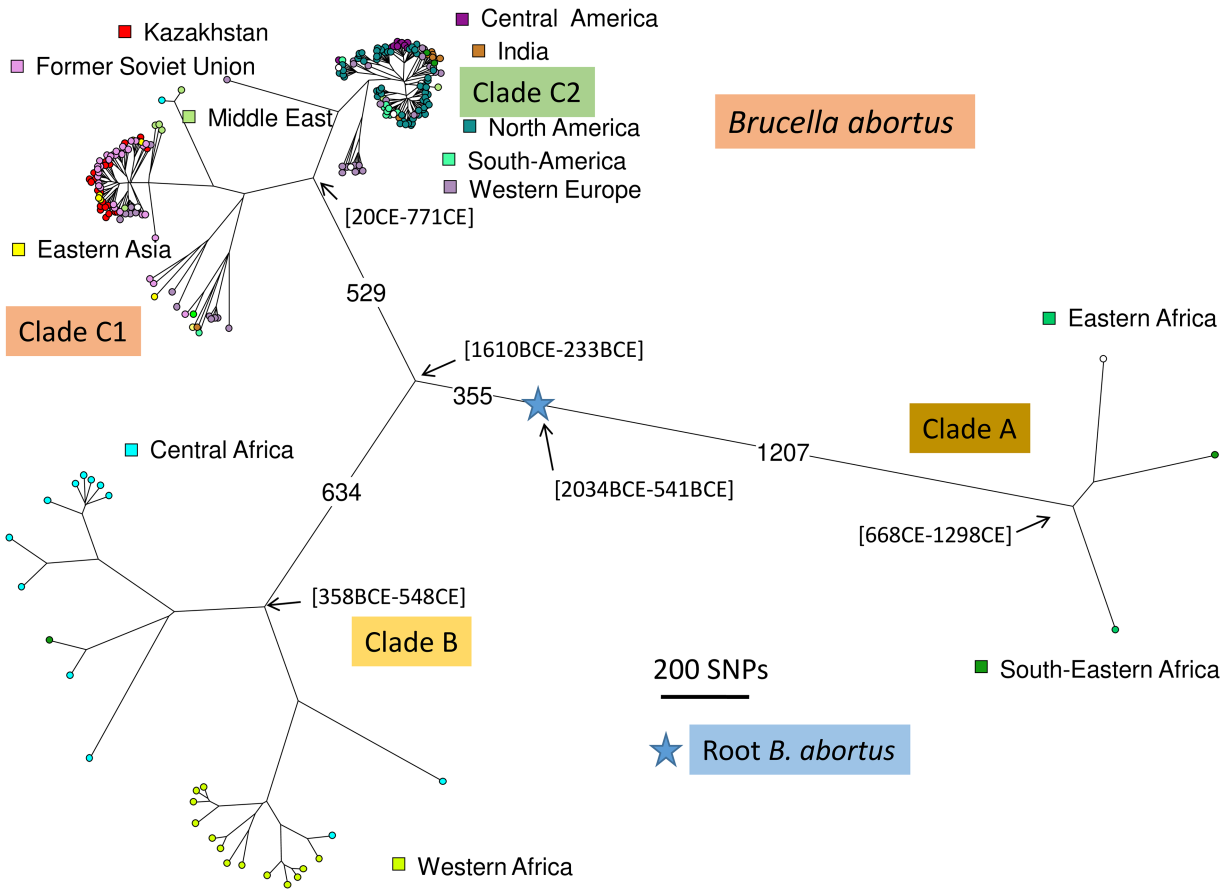

FIGURE 5
Global *B. abortus* phylogeny. Maximum parsimony tree based on core genome SNPs. A total of 236 representative strains was used and 16,987 SNPs were called by mapping on genome accession GCA_000740155 (*B. abortus* strain Tulya). The size of the resulting tree is 17,178 SNPs (homoplasia 1.12%). Nodes are colored according to geographic origin as indicated. The blue star indicates the root of the phylogeny (branching point toward the *B. melitensis* type strain 16M). The largest branch lengths and the scale are shown. Representative estimated divergence dates are indicated (CE, common era; BCE, before common era).

century, selective transformation of aboriginal cattle began, for which a massive import of cattle from various regions of Russia was carried out. For example, to create the Alatau breed from 1904 to 1940, Swiss and Kostroma cattle were brought to Kazakhstan and Kyrgyzstan from the Smolensk, Sumy and Kostroma regions (Soldatov, 2001). The Aulieatinskaya cattle breed has been developed since 1885 by crossing the Dutch Black Pied breed with aboriginal cattle and subsequent improvement in the 1930s of the 20th century by East Friesian bulls (Dmitriev and Ernst, 1989). All these processes might have constituted opportunities for a wide distribution of European strains of *B. abortus* in Kazakhstan, but it is important to note that essentially subclade C1 strains contaminate Kazakhstan whereas Western Europe is associated with subclade C2. Subclade C1 is common in North Caucasus (Kovalev et al., 2021). At the same time, the disastrous large-scale collectivization carried out in 1929–1933 resulted in a four-fold reduction in the local cattle population (Zhumasultanova, 2021), which could lead to a reduction in the historically circulating strains of *B. abortus*. The observed reduction in the genetic diversity of *B. abortus* strains in Kazakhstan in the 21st century is possibly associated with the successful implementation of epidemic-control activities similar to methods implemented in the 1970–1980s. During 4 years, from 1981 to 1985, the incidence of brucellosis in cattle decreased from 3.5 to 2.2% and a reduction in the most affected areas was as high as 30% (Shablov et al., 1988). Another factor for consideration is a two-fold reduction in the cattle population from 1991 to 2000.

The isolation of two *B. abortus* subclade C2 strains Kaz025 and Kaz027 genetically closest to the *B. abortus* 104 M vaccine strain is intriguing. We could not find records of the use of this vaccine in Kazakhstan. The *B. abortus* 104 M strain was first isolated from an aborted fetus of cattle in the central European Russia in 1929, selected and proposed as a vaccine strain for human vaccination by Kh. S. Kotlyarova in 1950 (Kotlyarova, 1950; Shumilov et al., 1983). Despite proven immunogenicity, strain 104 M did not find wide application in the USSR and was used in experimental vaccination of cattle and in limited production trials on small cattle. In this connection, the probability of importation of a vaccinated animal is low. We are more inclined toward the introduction of genetically close pathogenic strains. Expanding the results of genome-wide data on *B. abortus* strains isolated in the central European Russia will improve understanding of the origin of strains Kaz025 and Kaz027.

5. Concluding remarks

The new data of various origins contributed in this report strengthen the strong association of clades A and B with East and West Africa, respectively. The topology of the observed phylogeny combined with human history is pointing to East Africa as current most parsimonious scenario for the origin of *B. abortus*. The WGS data analysis of *B. abortus* strains from Kazakhstan shows that currently circulating lineages were introduced only recently in Kazakhstan, most of them during the 19th or 20th century. The closest currently known lineages are present in Caucasia, in agreement with the history of recent population migrations. This recent introduction is reminiscent of the situation described in Costa Rica, in which WGS data analysis allowed to identify five independent introductions responsible for the current population structure of *B. abortus* in Costa Rica (Suárez-Esquivel et al., 2020). Costa Rica was contaminated by *B. abortus* subclade C2 strains, imported from neighboring countries, whereas Kazakhstan was contaminated essentially by subclade C1 strains. This reflects the progressive spread of *Brucella* worldwide.

Data availability statement

The datasets presented in this study can be found in online repositories. The names of the repository/repositories and accession number(s) can be found below: Bioproject PRJNA892249 and PRJNA901374.

Author contributions

GV editing of the original manuscript. GV, AC, and AShe conceptualization, designed the experiments, and analyzed the data. AShe and AC wrote the first draft of the manuscript. KB, MZ, ES, AShu, AA, DK, and YR genotyping and wrote sections of the manuscript. TK bacteriological researches and wrote sections of the manuscript. All authors contributed to the article and approved the submitted version.

Funding

This study was supported by the Ministry of Education and Science of the Republic of Kazakhstan (grant no. AP08052352) and by the french «Agence Nationale de la Recherche» grant ASTRID430 Maturation ANR-14-ASMA-0002-02.

Conflict of interest

The authors declare that the research was conducted in the absence of any commercial or financial relationships that could be construed as a potential conflict of interest.

Publisher's note

All claims expressed in this article are solely those of the authors and do not necessarily represent those of their affiliated organizations, or those of the publisher, the editors and the reviewers. Any product that may be evaluated in this article, or claim that may be made by its manufacturer, is not guaranteed or endorsed by the publisher.

Supplementary material

The Supplementary material for this article can be found online at: https://www.frontiersin.org/articles/10.3389/fmicb.2023.1106994/full#supplementary-material

References

Abdel-Glil, M. Y., Thomas, P., Brandt, C., Melzer, F., Subbaiyan, A., Chaudhuri, P., et al. (2022). Core genome multilocus sequence typing scheme for improved characterization and epidemiological surveillance of pathogenic *Brucella*. *J. Clin. Microbiol.* 60:e0031122. doi: 10.1128/jcm.00311-22

Al Dahouk, S., Kohler, S., Occhialini, A., Jimenez de Bagues, M. P., Hammerl, J. A., Eisenberg, T., et al. (2017). *Brucella* spp. of amphibians comprise genomically diverse motile strains competent for replication in macrophages and survival in mammalian hosts. *Sci. Rep.* 7:44420. doi: 10.1038/srep44420

Allen, A. R., Milne, G., Drees, K., Presho, E., Graham, J., McAdam, P., et al. (2020). Genomic epizootiology of a *Brucella abortus* outbreak in Northern Ireland (1997-2012). *Infect. Genet. Evol.* 81:104235. doi: 10.1016/j.meegid.2020.104235

Bankevich, A., Nurk, S., Antipov, D., Gurevich, A. A., Dvorkin, M., Kulikov, A. S., et al. (2012). SPAdes: a new genome assembly algorithm and its applications to single-cell sequencing. *J. Comput. Biol.* 19, 455–477. doi: 10.1089/cmb.2012.0021

Bell-Fialloff, A. (2016). *The Role of Migration in the History of the Eurasian Steppe: Sedentary Civilization vs.'Barbarian'and Nomad* Houndmills, Basingstoke, Hampshire and London: MacMillan Press LTD.

Belmont, V. (1960). *Breeds of Farm Animals Bred in Kazakhstan. [Porody Selskohozyajstvennyh Zhivotnyh, Vyvedennye v Kazahstane]*. Alma-Ata: Kazakh state publishing house Alma-Ata.

Blouin, Y., Hauck, Y., Soler, C., Fabre, M., Vong, R., Dehan, C., et al. (2012). Significance of the identification in the horn of Africa of an exceptionally deep branching *mycobacterium tuberculosis* clade. *PLoS One* 7:e52841. doi: 10.1371/journal.pone.0052841 PONE-D-12-22563 [pii]

Buddle, M. B. (1956). Studies on *Brucella ovis* (n.sp.), a cause of genital disease of sheep in New Zealand and Australia. *J. Hyg. (Lond)* 54, 351–364. doi: 10.1017/s0022172400044612

Carmichael, L. E., and Bruner, D. W. (1968). Characteristics of a newly-recognized species of *Brucella* responsible for infectious canine abortions. *Cornell Vet.* 48, 579–592. PMID: 5693645

Charypkhan, D., and Ruegg, S. R. (2022). One health evaluation of brucellosis control in Kazakhstan. *PLoS One* 17:e0277118. doi: 10.1371/journal.pone.0277118

Charypkhan, D., Sultanov, A. A., Ivanov, N. P., Baramova, S. A., Taitubayev, M. K., and Torgerson, P. R. (2019). Economic and health burden of brucellosis in Kazakhstan. *Zoonoses Public Health* 66, 487–494. doi: 10.1111/zph.12582

Daugaliyeva, A., Sultanov, A., Usserbayev, B., Baramova, S., Modesto, P., Adambayeva, A., et al. (2018). Genotyping of *Brucella melitensis* and *Brucella abortus* strains in Kazakhstan using MLVA-15. *Infect. Genet. Evol.* 58, 135–144. doi: 10.1016/j.meegid.2017.12.022

Dean, A. S., Crump, L., Greter, H., Schelling, E., and Zinsstag, J. (2012). Global burden of human brucellosis: a systematic review of disease frequency. *PLoS Negl. Trop. Dis.* 6:e1865. doi: 10.1371/journal.pntd.0001865

Dmitriev, N., and Ernst, L. *Animal Genetic Resources of the USSR; FAO and UNEP*: Rome, Italy: Food and Agriculture Organization of the United Nations and United Nations Environment Programme. (1989).

Eisenberg, T., Risse, K., Schauerte, N., Geiger, C., Blom, J., and Scholz, H. C. (2017). Isolation of a novel 'atypical' *Brucella* strain from a bluespotted ribbontail ray (*Taeniura lymma*). *Antonie Van Leeuwenhoek* 110, 221–234. doi: 10.1007/s10482-016-0792-4

Eisenberg, T., Schlez, K., Fawzy, A., Völker, I., Hechinger, S., Curic, M., et al. (2020). Expanding the host range: infection of a reptilian host (*Furcifer pardalis*) by an atypical *Brucella* strain. *Antonie Van Leeuwenhoek* 113, 1531–1537. doi: 10.1007/s10482-020-01448-9

Foster, G., Osterman, B. R., Godfroid, J., Jacques, I., and Cloeckaert, A. (2007). *Brucella ceti* sp. nov. and *Brucella pinnipedialis* sp. nov. for *Brucella* strains with cetaceans and seals as their preferred hosts 57, 2688–2693. doi: 10.1099/ijs.0.65269-0,

Franc, K. A., Krecek, R. C., Hasler, B. N., and Arenas-Gamboa, A. M. (2018). Brucellosis remains a neglected disease in the developing world: a call for interdisciplinary action. *BMC Public Health* 18:125. doi: 10.1186/s12889-017-5016-y

Garcia-Yoldi, D., Le Fleche, P., Marin, C. M., De Miguel, M. J., Munoz, P. M., Vergnaud, G., et al. (2007). Assessment of genetic stability of *Brucella melitensis* rev 1 vaccine strain by multiple-locus variable-number tandem repeat analysis. *Vaccine* 25, 2858–2862. doi: 10.1016/j.vaccine.2006.09.063

Garofolo, G., Di Giannatale, E., Platone, I., Zilli, K., Sacchini, L., Abass, A., et al. (2017). Origins and global context of *Brucella abortus* in Italy. *BMC Microbiol.* 17:28. doi: 10.1186/s12866-017-0939-0

Godfroid, J., Scholz, H. C., Barbier, T., Nicolas, C., Wattiau, P., Fretin, D., et al. (2011). Brucellosis at the animal/ecosystem/human interface at the beginning of the 21st century. *Prev. Vet. Med.* 102, 118–131. doi: 10.1016/j.prevetmed.2011.04.007

Hensel, M. E., Negron, M., and Arenas-Gamboa, A. M. (2018). Brucellosis in dogs and public health risk. *Emerg. Infect. Dis.* 24, 1401–1406. doi: 10.3201/eid2408.171171

Holzer, K., El-Diasty, M., Wareth, G., Abdel-Hamid, N. H., Hamdy, M. E. R., Moustafa, S. A., et al. (2021). Tracking the distribution of *Brucella abortus* in Egypt based on Core genome SNP analysis and in silico MLVA-16. *Microorganisms* 9:1942. doi: 10.3390/microorganisms9091942

Hordt, A., Lopez, M. G., Meier-Kolthoff, J. P., Schleuning, M., Weinhold, L. M., Tindall, B. J., et al. (2020). Analysis of 1,000+type-strain genomes substantially improves taxonomic classification of Alphaproteobacteria. *Front. Microbiol.* 11:468. doi: 10.3389/fmicb.2020.00468

Janowicz, A., De Massis, F., Ancora, M., Camma, C., Patavino, C., Battisti, A., et al. (2018). Core genome multilocus sequence typing and single nucleotide polymorphism analysis in the epidemiology of *Brucella melitensis* infections. *J. Clin. Microbiol.* 56, e00517–e00518. doi: 10.1128/JCM.00517-18

Jolley, K. A., Bray, J. E., and Maiden, M. C. J. (2018). Open-access bacterial population genomics: BIGSdb software, the PubMLST.org website and their applications. *Wellcome Open Res* 3:124. doi: 10.12688/wellcomeopenres.14826.1

Kamath, P. L., Foster, J. T., Drees, K. P., Luikart, G., Quance, C., Anderson, N. J., et al. (2016). Genomics reveals historic and contemporary transmission dynamics of a bacterial disease among wildlife and livestock. *Nat. Commun.* 7:11448. doi: 10.1038/ncomms11448

Kay, G. L., Sergeant, M. J., Giuffra, V., Bandiera, P., Milanese, M., Bramanti, B., et al. (2014). Recovery of a medieval *Brucella melitensis* genome using shotgun metagenomics. *MBio* 5, e01337–e01314. doi: 10.1128/mBio.01337-14

Keim, P., Van Ert, M. N., Pearson, T., Vogler, A. J., Huynh, L. Y., and Wagner, D. M. (2004). Anthrax molecular epidemiology and forensics: using the appropriate marker for different evolutionary scales. *Infect. Gene. Evol.* 4, 205–213. doi: 10.1016/j.meegid.2004.02.005

Kotlyarova, H. (1950). Comparative data on vaccine strains of brucella bovine type in experiments on Guinea pigs [Sravnitelnye dannye o vakcinnyh shtammah brucell korovego tipa v opytah na morskih svinkah]. *J. Microbiol. Epidemiol. Immunobiol.* 6, 13–19.

Kovalev, D. A., Ponomarenko, D. G., Pisarenko, S. V., Shapakov, N. A., Khachaturova, A. A., Serdyuk, N. S., et al. (2021). Phylogeny of *Brucella abortus* strains isolated in the Russian Federation. *Asian Pac. J. Trop. Med.* 14, 323–329. doi: 10.4103/1995-7645.320523

Leclercq, S. O., Cloeckaert, A., and Zygmunt, M. S. (2020). Taxonomic Organization of the Family Brucellaceae Based on a Phylogenomic approach. *Front. Microbiol.* 10:3083. doi: 10.3389/fmicb.2019.03083

Machelart, A., Willemart, K., Zúñiga-Ripa, A., Godard, T., Plovier, H., Wittmann, C., et al. (2020). Convergent evolution of zoonotic *Brucella* species toward the selective use of the pentose phosphate pathway. *Proc. Natl. Acad. Sci. U. S. A.* 117, 26374–26381. doi: 10.1073/pnas.2008939117

Maquart, M., Le Flèche, P., Foster, G., Tryland, M., Ramisse, F., Djonne, B., et al. (2009). MLVA-16 typing of 295 marine mammal *Brucella* isolates from different animal and geographic origins identifies 7 major groups within *Brucella ceti* and *Brucella pinnipedialis*. *BMC Microbiol.* 9:145. doi: 10.1186/1471-2180-9-145

McDermott, J., Grace, D., and Zinsstag, J. (2013). Economics of brucellosis impact and control in low-income countries. *Rev. Sci. Tech.* 32, 249–261. doi: 10.20506/rst.32.1.2197

Moreno, E., Cloeckaert, A., and Moriyon, I. (2002). *Brucella* evolution and taxonomy. *Vet. Microbiol.* 90, 209–227. doi: 10.1016/s0378-1135(02)00210-9

Mühldorfer, K., Wibbelt, G., Szentiks, C. A., Fischer, D., Scholz, H. C., Zschöck, M., et al. (2017). The role of 'atypical' *Brucella* in amphibians: are we facing novel emerging pathogens? *J. Appl. Microbiol.* 122, 40–53. doi: 10.1111/jam.13326

Nicoletti, P. (2010). Brucellosis: past, present and future. *Prilozi* 31, 21–32.

Occhialini, A., Hofreuter, D., Ufermann, C. M., Al Dahouk, S., and Kohler, S. (2022). The retrospective on atypical *Brucella* species leads to novel definitions. *Microorganisms* 10:813. doi: 10.3390/microorganisms10040813

Olsen, S. C., and Palmer, M. V. (2014). Advancement of knowledge of *Brucella* over the past 50 years. *Vet. Pathol.* 51, 1076–1089. doi: 10.1177/0300985814540545

Pappas, G., Papadimitriou, P., Akritidis, N., Christou, L., and Tsianos, E. V. (2006). The new global map of human brucellosis. *Lancet Infect. Dis.* 6, 91–99. doi: 10.1016/S1473-3099(06)70382-6

Pelerito, A., Nunes, A., Grilo, T., Isidro, J., Silva, C., Ferreira, A. C., et al. (2021). Genetic characterization of *Brucella* spp.: whole genome sequencing-based approach for the determination of multiple locus variable number tandem repeat profiles. *Front. Microbiol.* 12:740068. doi: 10.3389/fmicb.2021.740068

Presidential_Library_RF (2022). *Incorporation of Kazakh khanate into Russia was launched [online]*. Available at: https://www.prlib.ru/en/history/619652 (Accessed).

Qazaqstan_tarihy (2018). Beginning of accession of Kazakhstan to the Russian empire [online]. Available at: https://e-history.kz/en/history-of-kazakhstan/show/9565.

Rambaut, A. (2018). FigTree v1.4.4 [Online]. Available at: https://github.com/rambaut/figtree (Accessed February 02, 2023).

Rambaut, A., Drummond, A. J., Xie, D., Baele, G., and Suchard, M. A. (2018). Tracer v1.7 [online]. Available at: http://beast.community/tracer (Accessed February 02, 2023).

Rather, Z., and Abdullah, D. (2018). Russian migration and structural change in Kazakh SSR with special reference to agricultural developments (1917-1991). *J. Central Asian Stud.* 25, 25–43.

Sailaukyzy, A., Shakuova, R., Sak, K., and Lebedeva, T. (2018). Contemporary view to the history of Kazakhstan's democratic journalism and publicism. *Opción* 34, 774–799.

Scholz, H. C., Hubalek, Z., Sedlacek, I., Vergnaud, G., Tomaso, H., Al Dahouk, S., et al. (2008). *Brucella microti* sp. nov., isolated from the common vole Microtus arvalis. *Int. J. Syst. Evol. Microbiol.* 58, 375–382. doi: 10.1099/ijs.0.65356-0

Scholz, H. C., Nockler, K., Gollner, C., Bahn, P., Vergnaud, G., Tomaso, H., et al. (2010). *Brucella inopinata* sp. nov., isolated from a breast implant infection. *Int. J. Syst. Evol. Microbiol.* 60, 801–808. doi: 10.1099/ijs.0.011148-0

Scholz, H. C., Revilla-Fernandez, S., Dahouk, S. A., Hammerl, J. A., Zygmunt, M. S., Cloeckaert, A., et al. (2016). *Brucella vulpis* sp. nov., isolated from mandibular lymph nodes of red foxes (*Vulpes vulpes*). *Int. J. Syst. Evol. Microbiol.* 66, 2090–2098. doi: 10.1099/ijsem.0.000998

Scholz, H. C., and Vergnaud, G. (2013). Molecular characterisation of *Brucella* species. *Rev. Sci. Tech.* 32, 149–162. doi: 10.20506/rst.32.1.2189

Schurig, G. G., Roop, R. M. 2nd, Bagchi, T., Boyle, S., Buhrman, D., and Sriranganathan, N. (1991). Biological properties of RB51; a stable rough strain of *Brucella abortus*. *Vet. Microbiol.* 28, 171–188. doi: 10.1016/0378-1135(91)90091-s

Shablov, V., Ivanov, N., and Zadorozhnyj, I. (1988). "Features of the regional epizootology of brucellosis and their impact on the course and spread of infection [Osobennosti kraevoj epizootologii brucelleza i ih vliyanie na techenie i rasprostranenie infekcii]" in *Improving Measures to Combat Brucellosis and Tuberculosis in Farm Animals [Sovershenstvovanie mer borby s Brucellezom i Tuberkulezom Selskohozyajstvennyh Zhivotnyh]*. ed. Z. K. Kozhebekov. (Alma-Ata: Eastern Branch of VASKhNIL, Kazakh Research Veterinary Institute).

Shevtsov, A., Ramanculov, E., Shevtsova, E., Kairzhanova, A., Tarlykov, P., Filipenko, M., et al. (2015). Genetic diversity of *Brucella abortus* and *Brucella melitensis* in Kazakhstan using MLVA-16. *Infect. Genet. Evol.* 34, 173–180. doi: 10.1016/j.meegid.2015.07.008

Shevtsova, E., Shevtsov, A., Mukanov, K., Filipenko, M., Kamalova, D., Sytnik, I., et al. (2016). Epidemiology of brucellosis and genetic diversity of *Brucella abortus* in Kazakhstan. *PLoS One* 11:e0167496. doi: 10.1371/journal.pone.0167496

Shumilov, K., Albertyan, M., Klochkov, A., and Romahov, V. (1983). Immunization of heifers with a low dose of vaccine from the strain *B. abortus* 104-M [Immunizaciya telok maloj dozoj vakciny iz shtama Br.Abortus 104-M]. *Trudi VIEV* 51, 71–74.

Sidamonidze, K., Hang, J., Yang, Y., Dzavashvili, G., Zhgenti, E., Trapaidze, N., et al. (2017). Genome sequences of human and livestock isolates of *Brucella melitensis* and *Brucella abortus* from the country of Georgia. *Genome Announc.* 5, e01518–e01516. doi: 10.1128/genomeA.01518-16

Soldatov, A. (2001). "Complete catalog of breeds of farm animals in Russia" in *Pets [Polnyj katalog Porod Selskohozyajstvennyh Zhivotnyh Rossii. Domashnie Zhivotnye]* (Moscow: Eksmo-Press, Lik-Press)

Soler-Llorens, P. F., Quance, C. R., Lawhon, S. D., Stuber, T. P., Edwards, J. F., Ficht, T. A., et al. (2016). A *Brucella* spp. isolate from a Pac-man frog (*Ceratophrys ornata*) reveals characteristics departing from classical Brucellae. *Front. Cell. Infect. Microbiol.* 6:116. doi: 10.3389/fcimb.2016.00116

Souvorov, A., Agarwala, R., and Lipman, D. J. (2018). SKESA: strategic k-mer extension for scrupulous assemblies. *Genome Biol.* 19:153. doi: 10.1186/s13059-018-1540-z

Stoenner, H. G., and Lackman, D. B. (1957). A new species of *Brucella* isolated from the desert wood rat, *Neotoma lepida* Thomas. *Am. J. Vet. Res.* 18, 947–951. PMID: 13470254

Suárez-Esquivel, M., Hernández-Mora, G., Ruiz-Villalobos, N., Barquero-Calvo, E., Chacón-Díaz, C., Ladner, J. T., et al. (2020). Persistence of *Brucella abortus* lineages revealed by genomic characterization and phylodynamic analysis. *PLoS Negl. Trop. Dis.* 14:e0008235. doi: 10.1371/journal.pntd.0008235

Suchard, M. A., Lemey, P., Baele, G., Ayres, D. L., Drummond, A. J., and Rambaut, A. (2018). Bayesian phylogenetic and phylodynamic data integration using BEAST 1.10. *Virus Evol.* 4:vey016. doi: 10.1093/ve/vey016

Syzdykov, M., Kuznetsov, A., Kazakov, S., Daulbayeva, S., Duysenova, A., Berezovskiy, D., et al. (2014). Analiz prostranstvenno-vremennogo raspredeleniya

brutselloza cheloveka i zhivotnykh s ispol'zovaniyem Geograficheskikh informatsionnykh tekhnologiy—[analysis of the spatial and temporal distribution of human and animal brucellosis using geographic information technology]. *Gig., Epidemiol. immunobiol. -[Hyg. Epidemiol. Immunbiol.]* 72, 24–26.

Vergnaud, G., Hauck, Y., Christiany, D., Daoud, B., Pourcel, C., Jacques, I., et al. (2018). Genotypic expansion within the population structure of classical *Brucella* species revealed by MLVA16 typing of 1404 *Brucella* isolates from different animal and geographic origins, 1974-2006. *Front. Microbiol.* 9:1545. doi: 10.3389/fmicb.2018.01545

Wang, X. H., and Jiang, H. (2020). Global prevalence of human brucellosis. *Zhonghua Liu Xing Bing Xue Za Zhi* 41, 1717–1722. doi: 10.3760/cma.j.cn112338-20191022-00751

Whatmore, A. M., Davison, N., Cloeckaert, A., Al Dahouk, S., Zygmunt, M. S., Brew, S. D., et al. (2014). *Brucella papionis* sp. nov., isolated from baboons (*Papio* spp.). *Int. J. Syst. Evol. Microbiol.* 64, 4120–4128. doi: 10.1099/ijs.0.065482-0

Whatmore, A. M., and Foster, J. T. (2021). Emerging diversity and ongoing expansion of the genus *Brucella*. *Infect. Genet. Evol.* 92:104865. doi: 10.1016/j.meegid.2021.104865

Whatmore, A. M., Koylass, M. S., Muchowski, J., Edwards-Smallbone, J., Gopaul, K. K., and Perrett, L. L. (2016). Extended multilocus sequence analysis to describe the global population structure of the genus *Brucella*: Phylogeography and relationship to Biovars. *Front. Microbiol.* 7:2049. doi: 10.3389/fmicb.2016.02049

Whatmore, A. M., Perrett, L. L., and MacMillan, A. P. (2007). Characterisation of the genetic diversity of *Brucella* by multilocus sequencing. *BMC Microbiol.* 7:34. doi: 10.1186/1471-2180-7-34

Zhou, K., Wu, B. B., Pan, H., Paudyal, N., Jiang, J. Z., Zhang, L., et al. (2020). ONE health approach to address zoonotic brucellosis: a spatiotemporal associations study between animals and humans. *Front. Vet. Sci.* 7:521. doi: 10.3389/fvets.2020.00521

Zhumasultanova, G. (2021). Political repression in the context of complete collectivization of agriculture in Kazakhstan as a way to strengthen the Stalinist regime. *J. Int. scientific rev. (LXXX)*, 42–49. doi: 10.24411/2542-0798-2021-18004

frontiers | Frontiers in Microbiology

TYPE Original Research
PUBLISHED 04 May 2023
DOI 10.3389/fmicb.2023.1128966

OPEN ACCESS

EDITED BY
Antonio Battisti,
Institute of Experimental Zooprophylactic of the Lazio and Tuscany Regions (IZSLT), Italy

REVIEWED BY
Zhiguo Liu,
Chinese Center For Disease Control and Prevention, China
Gamal Wareth,
Institut für bakterielle Infektionen und Zoonosen, Friedrich Loeffler Institut, Germany
Henriette Van Heerden,
University of Pretoria, South Africa
Mikeljon P. Nikolich,
Walter Reed Army Institute of Research, United States

*CORRESPONDENCE
Roland T. Ashford
roland.ashford@apha.gov.uk

†PRESENT ADDRESS
Stefan Berg,
Bernhard Nocht Institute for Tropical Medicine, Hamburg, Germany

‡These authors share senior authorship

SPECIALTY SECTION
This article was submitted to Infectious Agents and Disease, a section of the journal Frontiers in Microbiology

RECEIVED 21 December 2022
ACCEPTED 23 February 2023
PUBLISHED 04 May 2023

CITATION
Edao BM, Ameni G, Berg S, Tekle M, Whatmore AM, Wood JLN, van Tonder AJ and Ashford RT (2023) Whole genome sequencing of Ethiopian *Brucella abortus* isolates expands the known diversity of an early branching sub-Saharan African lineage. *Front. Microbiol.* 14:1128966. doi: 10.3389/fmicb.2023.1128966

Whole genome sequencing of Ethiopian *Brucella abortus* isolates expands the known diversity of an early branching sub-Saharan African lineage

Bedaso Mammo Edao[1,2], Gobena Ameni[3,4], Stefan Berg[5†], Muluken Tekle[2], Adrian M. Whatmore[5], James L. N. Wood[1], Andries J. van Tonder[1‡] and Roland T. Ashford[5*‡]

[1]Department of Veterinary Medicine, University of Cambridge, Cambridge, United Kingdom, [2]College of Veterinary Medicine, Addis Ababa University, Bishoftu, Ethiopia, [3]Aklilu Lemma Institute of Pathobiology, Addis Ababa University, Addis Ababa, Ethiopia, [4]Department of Veterinary Medicine, College of Food and Agriculture, United Arab Emirates University, Al Ain, United Arab Emirates, [5]Department of Bacteriology, Animal and Plant Health Agency, Weybridge, United Kingdom

Brucellosis remains one of the most significant zoonotic diseases globally, responsible for both considerable human morbidity and economic losses due to its impacts on livestock productivity. Despite this, there remain significant evidence gaps in many low- and middle-income countries, including those of sub-Saharan Africa. Here we report the first molecular characterisation of *Brucella* sp. from Ethiopia. Fifteen *Brucella* sp. isolates from an outbreak in cattle from a herd in central Ethiopia were identified as *Brucella abortus*, using bacterial culture and molecular methods. Sequencing of the Ethiopian *B. abortus* isolates allowed their phylogenetic comparison with 411 *B. abortus* strains of diverse geographical origins, using whole genome single nucleotide polymorphisms (wgSNP). The Ethiopian isolates belonged to an early-branching lineage (Lineage A) previously only represented by data from two strains, both of sub-Saharan African origin (Kenya and Mozambique). A second *B. abortus* lineage (Lineage B), also comprised solely of strains originating from sub-Saharan Africa, was identified. The majority of strains belonged to one of two lineages of strains originating from a much broader geographical range. Further analyses based on multi-locus sequence typing (MLST) and multi-locus variable-number tandem repeat analysis (MLVA) expanded the number of *B. abortus* strains available for comparison with the Ethiopian isolates and were consistent with the findings from wgSNP analysis. MLST profiles of the Ethiopian isolates expanded the sequence type (ST) diversity of the early branching lineage of *B. abortus*, equivalent to wgSNP Lineage A. A more diverse cluster of STs, equivalent to wgSNP Lineage B, was comprised solely of strains originating from sub-Saharan Africa. Similarly, analysis of *B. abortus* MLVA profiles (n=1891) confirmed that the Ethiopian isolates formed a unique cluster, similar to only two existing strains, and distinct from the majority of other strains of sub-Saharan African origin. These findings expand the known diversity of an under-represented lineage of *B. abortus* and suggest a potential evolutionary origin for the species in East Africa. In addition to providing information concerning *Brucella* species extant within Ethiopia this work serves as the basis for further studies on the global population structure and evolutionary history of a major zoonotic pathogen.

KEYWORDS

***Brucella abortus*, sub-Saharan Africa, lineage, whole genome sequencing, molecular typing**

1. Introduction

Brucellosis is a zoonotic infection caused by bacteria of the genus *Brucella*, which affects domestic livestock and a wide range of wild mammals (Ducrotoy et al., 2017). The disease is amongst the most common zoonotic infections globally, with an estimated 500,000 human cases annually (Pappas et al., 2006), though this figure is likely to be a significant under-estimate of the burden of disease (Moreno et al., 2022). Brucellosis remains endemic in much of Africa, South America, the Middle East and the Mediterranean region of Europe (Pappas et al., 2006; McDermott et al., 2013). However, there is a notable lack of evidence concerning endemic brucellosis in many low-income countries of Africa and Asia (McDermott et al., 2013).

Infection in humans occurs primarily as a result of direct contact with infected animals (in particular their products of conception), or ingestion of unpasteurised dairy products from infected animals (Corbel, 2006). Human brucellosis is characterized by febrile illness which can lead to debilitating chronic conditions if left untreated (Dean et al., 2012). In addition, brucellosis has indirect health consequences, especially for livestock-keeping populations in resource-limited settings, which depend on livestock for food security and income (McDermott et al., 2013; Lokamar et al., 2020).

The majority of human brucellosis infections are caused by two *Brucella* species, *Brucella melitensis* and *Brucella abortus*, which exhibit marked livestock host preferences (Corbel, 2006). Brucellosis in small ruminants (sheep and goats) is primarily caused by *B. melitensis*, whilst in cattle the infection is most commonly caused by *B. abortus*. However, in areas where cattle are kept in close association with sheep or goats, as is common in many mixed-livestock keeping populations, infection in cattle may also be caused by *B. melitensis*, and in small ruminants by *B. abortus* (e.g., Akoko et al., 2021).

Developments in molecular typing have contributed to current understanding of the global population structure of *Brucella* spp. organisms and of local disease epidemiology (Whatmore and Foster, 2021; Ashford and Whatmore, 2022). Two methods, in particular, have been applied to explore genetic relationships between *Brucella* species, and relate these to the geographic origin of strains; multi-locus sequence typing (MLST) and multi-locus variable number tandem repeat analysis (MLVA). Whatmore et al. (2016) used a 21-locus MLST scheme (extending the existing 9-locus scheme; Whatmore et al., 2007) to identify three major clades within *B. abortus* (referred to as A, B and C). In this dataset clades A and B were comprised entirely of isolates of sub-Saharan African origin (Chad, Kenya, Mozambique, Nigeria, Sudan, Uganda and Zimbabwe), whilst clade C (further sub-divided into C1 and C2) originated from a broad geographical range and contained the majority of isolates for which data were available. Clade A, the most basal in the *B. abortus* MLST phylogeny, was represented by just two historical strains, isolated from Kenya and Mozambique in 1963 and 1988, respectively. It was suggested that these findings indicate the existence of substantial diversity yet to be characterised in *B. abortus* isolates from Africa, which are significantly under-represented in molecular typing databases.

Multi-locus variable-number tandem repeat analysis loci are not typically employed for inferring ancestral phylogenetic relationships, due to their higher mutation rates and greater risk of homoplasy (e.g., Keim et al., 2004). Nonetheless, global analyses of *B. abortus* population structure based on MLVA have supported findings from MLST studies. For example, a large analysis by Vergnaud et al. (2018) described three *B. abortus* clades which correspond broadly with the clades B, C1 and C2 described above. Clade B was comprised solely of isolates originating in Africa, with the majority of these isolated in West Africa (Cameroon, Guinea, Guinea-Bissau, Mauritania, Niger, Senegal, Togo) and a smaller number from the east of the continent (Rwanda and Sudan). Clade A was absent from this analysis, which did not include data from the two basally located strains reported by Whatmore et al. (2016).

Whole genome sequencing (WGS) methods are increasingly being applied to describe relationships between *Brucella* strains, either replacing established molecular typing techniques or augmenting studies based on existing approaches (e.g., MLST) and extracting these data *in silico* (Whatmore and Foster, 2021; Ashford and Whatmore, 2022). Ledwaba et al. (2021) reported *B. abortus* isolates from various regions of South Africa, using whole-genome single nucleotide polymorphisms (wgSNPs) to describe relationships with publicly available genomes. Consistent with previous results, three major lineages (referred to as A, B and C) were identified, with the South African isolates clustering in lineage C, with isolates from a broad geographic range, including Africa (Mozambique and Zimbabwe), Europe, Asia and America. Other recent studies reporting whole genome sequencing of *B. abortus* from North Africa have focused primarily on local disease epidemiology rather than broader population structure (Holzer et al., 2021; Khan et al., 2021).

In Ethiopia, studies from various regions of the country have reported individual-level brucellosis prevalence ranging from 0.06% in commercial intensive dairy production (Edao et al., 2018) to 9.7% in an extensive production system at the livestock-wildlife interface (Chaka et al., 2018). A recent systematic review and meta-analysis reported an estimated seroprevalence of 2.6% (95% CI: 2.2–3.0) in cattle, which increased to 16.3% (95% CI: 12.9–20.5) when herd-level prevalence was estimated (Sibhat et al., 2022). However, only two studies have reported the isolation of *Brucella* sp. strains from Ethiopia. Tekle et al. (2019) reported the isolation of *B. melitensis* from goats in the Afar region of eastern Ethiopia, and Geresu et al. (2016) reported the isolation of *B. abortus* from dairy cattle in central Ethiopia. To date there have been no studies reporting the molecular typing of *Brucella* sp. from Ethiopia.

There remains a dearth of *B. abortus* strains originating from sub-Saharan Africa (SSA), and WGS data from this region are consequently significantly under-represented in public sequence databases. To date there have been no published global analyses of *B. abortus* integrating data from both WGS and existing molecular typing methods (MLST and MLVA). In this study, we report the first isolation and molecular characterisation of Ethiopian *B. abortus* strains. We apply existing molecular typing approaches and whole genome sequence data analysis in order to characterise the strains and their phylogenetic placement relative to the global diversity of this important zoonotic pathogen.

2. Materials and methods

2.1. Study location, animals and sample collection

Adami Tullu Agricultural Research Centre (ATARC) is located in the mid Rift Valley, central Ethiopia, 167 km south of Addis Ababa in

Oromia National Regional State (Figure 1). It lies at latitude 7°9'N and longitude 38°7′E at an elevation of 1,650 m above sea level. The study population included a total of 547 Jersey or Holstein Friesian (*Bos taurus*), Arsi zebu (*Bos indicus*) and crossbred (*Bos indicus* × *Bos taurus*) dairy cattle, which were reared semi-intensively at ATARC. A high number of abortions within the ATARC herd were reported to the Assela Veterinary Regional Laboratory in March 2018, and consequently an investigation of the outbreak was conducted (Edao, 2020).

Seropositive animals were identified using serial testing by Rose Bengal test (RBT) and competitive ELISA (cELISA; Table 1), performed according to standard protocols (WOAH, 2018). Of 547 animals in the ATARC herd 125 (22.85%) were identified as seropositive by both RBT and cELISA (Table 1). A sub-sample of seropositive animals with a history of abortion were opportunistically selected during culling for *post mortem* sample collection. From these 30 animals, 66 samples were collected for bacteriological culture, comprising 28 vaginal swabs, 24 uterine tissue samples, 13 mammary gland lymph node samples and a single placental sample. A vaginal swab was available for 28 animals; 23 also had a uterine tissue sample, ten additionally had a mammary gland lymph node sample and in two cases a mammary gland lymph node sample was available but uterine tissue was absent. The two animals missing swab samples had, respectively, one (placenta) and two (mammary gland lymph node and uterine tissue) other samples.

Tissue samples (uterus, mammary gland lymph nodes and placenta) were collected into 20 ml sterile centrifuge tubes with sterile saline. Vaginal swabs were collected using Amies sterile media swabs (Deltalab, Spain). Thereafter, all samples were transported with ice packs to the Aklilu Lemma Institute of Pathobiology, Addis Ababa University (ALIPB-AAU) where they were stored at −20°C until shipped to the WOAH Brucellosis Reference Laboratory and FAO Reference Centre for Brucellosis at the Animal and Plant Health Agency (APHA) in the United Kingdom.

2.2. *Brucella* isolation and culture

Bacteriological confirmation was performed using standard protocols (Alton et al., 1975), at the Animal and Plant Health Agency (APHA), United Kingdom, between August 2018 and October 2018. A total of 66 samples consisting of 28 vaginal swabs and 38 tissue samples were cultured. The tissue samples were manually trimmed then macerated using a mechanical homogeniser (Stomacher Bagmixer 100 MiniMix, Seward Ltd, United Kingdom). The tissue suspensions and swab samples were inoculated directly onto both Farrell's and serum dextrose agar (SDA) media plates. All plates were incubated with 10% CO_2 at 37°C for three to five days. One colony was selected for sub-culture on Farrell's media for further molecular identification and typing. Pure colonies were harvested in 500 µL

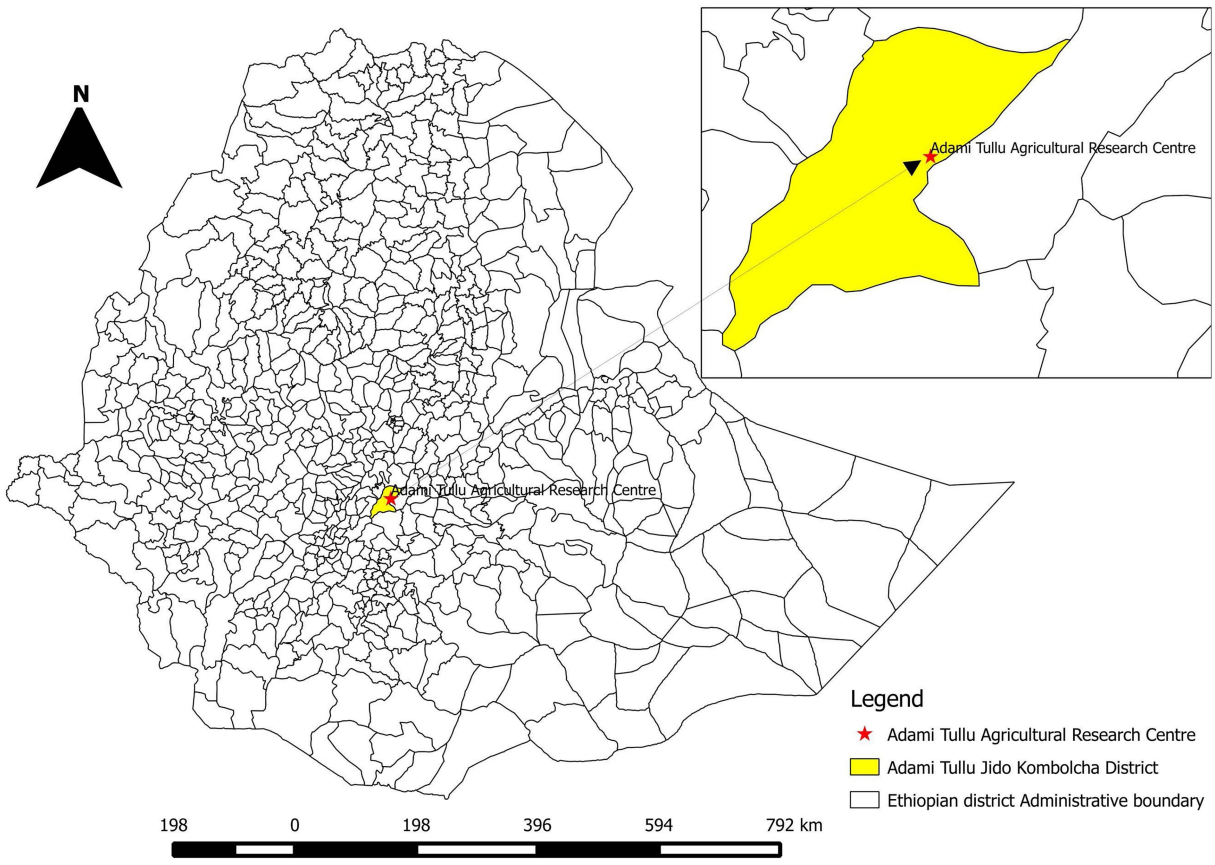

FIGURE 1
Map of Ethiopia, showing Adami Tullu Jido Kombolcha District and the location of Adami Tullu Agricultural Research Centre (ATARC).

TABLE 1 Summary data for 125 seropositive cattle identified by Rose Bengal test (RBT) and competitive ELISA (cELISA) during the suspected brucellosis outbreak investigation at Adami Tullu Agricultural Research Centre (ATARC), central Ethiopia.

	Category	Number of animals
Breed	Jersey	1
	Jersey × Arsi	1
	Holstein Friesian × Arsi	15
	Arsi	108
Age	≤ 3 years	25
	> 3 years	100
Number of pregnancies	≤ 2	108
	> 2	17
Reproductive status	Pregnant	50
	Not pregnant	75
Breeding	Natural	6
	Artificial insemination	119
Number of abortions recorded	One	63
	Two	62

nuclease-free water and inactivated at 100°C for 10 min, to produce thermo-lysates.

2.3. Molecular identification of isolates

The identity of isolates was initially confirmed using *Brucella* spp. specific quantitative PCR (qPCR) assays based on insertion sequence IS*711* and *bcsp*31 targets (Probert et al., 2004; Matero et al., 2011, respectively). The qPCR assays were considered positive when amplification was observed at cycle threshold (Ct) values of ≤ 35 for IS*711* and ≤ 40 for *bcsp*31. Identification to species level was performed using the Bruceladder multiplex PCR (Mayer-Scholl et al., 2010; López-Goñi et al., 2011) and qPCR-based single nucleotide polymorphism (SNP) typing (Gopaul et al., 2008). For all assays, thermo-lysates, prepared as described above, were used.

2.4. Whole genome sequencing

Brucella sp. cultures identified as described above were subsequently submitted for whole genome sequencing. Thermo-lysates were pelleted by centrifugation (10,000 *g* for 10 min), prior to DNA extraction using the Qiagen DNeasy Blood and Tissue Kit (Qiagen, United Kingdom) following the manufacturer's protocol for Gram-negative bacteria. DNA concentrations were quantified using the Qubit 2.0 fluorometer and Qubit dsDNA HS (High Sensitivity) Assay Kit (Thermo Fisher Scientific, United Kingdom). Genomic libraries were constructed using the NEBNext Ultra II DNA Library Prep Kit for Illumina (New England Biolabs Inc., United Kingdom) according to the manufacturer's instructions. The library size selection was 550 base pairs (bp) and a 250 bp paired-end (PE) sequencing strategy was employed using the MiSeq platform and MiSeq Reagent Kit V2 (Illumina Inc., San Diego, CA, United States), following the manufacturer's recommended protocol. Basic quality control metrics for the raw sequence data were generated using FastQC[1] and the reads were trimmed using fastp (Chen et al., 2018) to remove low quality reads and adapter sequences.

2.5. Whole genome sequencing data collection and quality assessment

Genome data downloaded from NCBI[2] and ENA[3] were manually checked and duplicate entries removed. This included reference and vaccine strains sequenced by multiple institutions, as well as strains present in both assembly and short-read data formats. Sequence reads with similarity to *Brucella* species were identified using Kraken 2 (Wood et al., 2019) and Bracken (Lu et al., 2017) and samples with < 70% reads assigned to *B. abortus* were excluded from further analyses.

2.6. Whole genome SNP (wgSNP) analysis

The *B. abortus* biovar 1 reference strain 9-941 (RefSeq accession number: GCF_000008145.1) was used as the reference genome for mapping of the Ethiopian sequences and NCBI/ENA data. *B. abortus* 9-941 is a well characterised reference strain which was the first published genome sequence for the species (Halling et al., 2005). The genome is a complete assembly (NCBI accession numbers NC_006932 and NC_006933 for chromosome I and II respectively) which has previously been used as a reference in several published whole genome sequencing studies (e.g., Suarez-Esquivel et al., 2020). The bactmap pipeline[4] was used for mapping and variant calling. Briefly, sequence data were mapped to the reference with BWA mem (Li and Durbin, 2009), variants were called and filtered with BCFtools (Li, 2011) and consensus fasta sequences were generated for each sample using a python script. The consensus fasta sequences and the reference sequence were then used to create a multiple sequence alignment from which the variant sites were extracted using SNP-sites (Page et al., 2016). Samples that mapped to < 75% of the reference genome were omitted from further analyses. The resulting alignment of variable SNP sites was then used to construct a maximum likelihood phylogeny with IQ-TREE (Nguyen et al., 2014) using the model finder (MFP) and 1,000 fast bootstraps. The phylogeny was rooted using *B. melitensis* type strain 16M^T (GCF_000007125.1) and visualised and annotated using the R library ggtree (Yu et al., 2017; R Core Team, 2022). Pairwise SNP distances for all genomes were calculated using pairsnp.[5]

2.7. *In silico* MLST and MLVA

Ethiopian *B. abortus* isolates and *B. abortus* fastq files downloaded from the ENA were *de novo* assembled using SPAdes v3.13.1

1 https://github.com/s-andrews/FastQC
2 https://www.ncbi.nlm.nih.gov/assembly
3 https://www.ebi.ac.uk/ena/browser/home
4 https://nf-co.re/bactmap
5 https://github.com/gtonkinhill/pairsnp

(Bankevich et al., 2012). The quality of the final assemblies was assessed using Quast (Gurevich et al., 2013).

Assembled genomes of the Ethiopian *Brucella* isolates underwent *in silico* multi-locus sequence typing (mlst)[6] to retrieve both nine and 21 locus allelic profiles (Whatmore et al., 2007, 2016). *In silico* MLST was also performed on *B. abortus* genome assemblies retrieved from NCBI and short-read data from ENA (following *de novo* assembly). Additionally, *B. abortus* allelic profiles from the *Brucella* PubMLST database[7] were downloaded for inclusion in the analysis. This database includes MLST profiles generated using both Sanger sequencing and *in silico* MLST typing from WGS data.

In silico 16-locus MLVA (MLVA16: Le Fleche et al., 2006) typing was undertaken using a purpose-written script (MLVA_finder)[8] applied to genome assemblies, as described by Vergnaud et al. (2018). Genotypes obtained by *in silico* MLVA16 analysis were compared with entries for *B. abortus* accessed via the publicly accessible *Brucella* MLVA database[9] (Brucella v4_6_3). This database includes MLVA profiles generated using both traditional fragment sizing approaches and *in silico* MLVA typing from WGS data (Vergnaud et al., 2018). The Hunter-Gaston diversity index (HGDI) was used to describe the discriminatory capacity of MLVA loci for Ethiopian isolates (Hunter and Gaston, 1988).

Molecular typing data downloaded from PubMLST and MLVA databases, respectively, were manually checked and duplicate entries removed. This included reference and vaccine strains sequenced by multiple institutions, as well as field isolates for which both conventional (Sanger sequencing) data and *in silico* typing data were present. Allelic profiles and associated metadata for both MLST and MLVA were visualised with minimum spanning trees, using GrapeTree (Zhou et al., 2018).

3. Results

3.1. *Brucella* culture and molecular identification

Of 66 bovine tissue and swab samples processed for isolation of *Brucella* spp., 15 samples (22.7%) were culture positive (nine mammary gland lymph nodes, three uterine tissues and three vaginal swabs). Table 2 summarises the samples from which putative *Brucella* sp. cultures were recovered. Thermo-lysates from cultures generated Ct values between 13.05 and 14.36 for IS*711* and 15.44 and 17.04 for *bcsp*31, confirming that all isolates belong to the genus *Brucella* (see Supplementary Table S1). Bruceladder multiplex PCR identified all 15 isolates as *B. abortus* based on the pattern of amplified products observed following electrophoresis (products corresponding to 1,682, 794, 587, 450 and 152 bp in length; see Supplementary Table S1). Similarly, qPCR-based SNP assays identified all isolates as *B. abortus* (see Supplementary Table S1).

TABLE 2 Details of *Brucella abortus* isolates from Ethiopian cattle included in the current study, with NCBI SRA accession numbers.

Isolate ID	Sequence ID	Animal ID	Sample type	Accession #
F5/18-T8	1_S1_L001	1968	Mammary gland LN	ERS5240204
F5/18-T6	2_S2_L001	1678	Mammary gland LN	ERS5240211
F5/18-T5	3_S3_L001	2016	Mammary gland LN	ERS5240212
F5/18-T10	4_S4_L001	1966	Mammary gland LN	ERS5240213
F5/18-T7	5_S5_L001	2034	Mammary gland LN	ERS5240214
F5/18-T4	6_S6_L001	2079	Mammary gland LN	ERS5240215
F5/18-T3	7_S7_L001	1681	Mammary gland LN	ERS5240216
F5/18-S35	8_S8_L001	2133	Vaginal swab	ERS5240217
F5/18-S14	9_S9_L001	1540	Vaginal swab	ERS5240218
F5/18-T18	10_S10_L001	2115	Uterine tissue	ERS5240205
F5/18-T15	11_S11_L001	2032	Mammary gland LN	ERS5240206
F5/18-T21	12_S12_L001	2108	Uterine tissue	ERS5240207
F5/18-T16	13_S13_L001	1672	Uterine tissue	ERS5240208
F5/18-S36[1]	14_S14_L001	2144	Vaginal swab	ERS5240209
F5/18-T12[1]	15_S15_L001	2144	Mammary gland LN	ERS5240210

LN = lymph node. [1]Isolates F5/18-S36 and F5/18-T12 from vaginal swab and mammary gland lymph node from the same animal.

3.2. Whole genome sequencing, *de novo* assembly and quality assessment

An average of 2,787,993 reads per sample were generated by Illumina sequencing of the Ethiopian *B. abortus* isolates. Summary statistics for Illumina sequencing and mapping for each isolate are provided in Supplementary Table S2. *De novo* assembly of the Ethiopian sequence data resulted in an average of 38 contigs per genome, an average total genome length of 3,273,080 bp, an average GC content of 57.23% and an average N50 of 389,770. Summary statistics for each *de novo* genome assembly are provided in Supplementary Table S2.

Five NCBI genome assemblies were removed from further analysis following identity assessment by Kraken/Bracken, due to the low proportion of reads identified as originating from *B. abortus* (< 70%). For two of these assemblies the majority of reads were identified as *Brucella suis* (strains BCB013 [GCA_000292205] and B104M [GCA_000292045]), whilst for three the majority of reads were identified as *B. melitensis* (strains S-586 [GCA_016091965], 2308 [GCA_018604785] and BCB027 [GCA_000292145]). Following mapping, 84 SRA datasets were removed due to the relatively low proportion of the reference genome mapped by the reads (< 75%). These SRA datasets included 72 from the United States, seven from Costa Rica and five from Egypt.

6 https://github.com/tseemann/mlst

7 https://pubmlst.org/brucella/

8 https://github.com/dpchris/MLVA

9 http://microbesgenotyping.i2bc.paris-saclay.fr

3.3. Whole genome SNP (wgSNP) analysis

Phylogenetic analysis was undertaken using a total of 426 *B. abortus* whole genome sequences. In addition to data from 15 Ethiopian isolates this included 153 assembled genomes and 258 short read datasets, downloaded from NCBI and ENA, respectively. Accession numbers for all downloaded sequences can be found in Supplementary Table S3. Mapping of Ethiopian *B. abortus* sequence data against reference strain 9–941 demonstrated that all Ethiopian *B. abortus* isolates differed by at least 3,749 SNPs from the chosen reference strain. Within the Ethiopian *B. abortus* isolates there was relatively little diversity evident in wgSNP analysis, with no more than five SNPs identified between any two strains within the panel (0–5). A matrix of pairwise SNP distances between all strains incorporated in the wgSNP analysis is provided in Supplementary Table S4.

Phylogenetic analysis based on wgSNPs demonstrated that *B. abortus* from Ethiopia clustered with *B. abortus* strains from Mozambique (strain 88/217) and Kenya (strain 63/294; Figure 2; Lineage A). These two strains, along with the 15 Ethiopian isolates, formed a distinct lineage, basal to all other *B. abortus* strains included in the current analysis. Strains 88/217 and 63/294 differed from the Ethiopian isolates by 828 to 834 and 802 to 808 SNPs respectively, and by 698 SNPs from each other.

Outside of this basally branching lineage, a second lineage contained a larger number of isolates, also of exclusively sub-Saharan African origin (Figure 2; Lineage B), though a single strain in this lineage did not have a geographic origin recorded in the available metadata. Within Lineage B three isolates formed a basal cluster (Figure 2; Lineage B1). These three strains originated from Nigeria (strain 80/101), Senegal (strain 78/32) and an unknown location (strain 78/36). Outside of Lineage B1 a second lineage was identified, also consisting of just three isolates (Figure 2; Lineage B2). These originated from Zimbabwe (strain F1/06-B21), Sudan (strain F6/05–3) and Uganda (strain Tulya). This latter strain is the *B. abortus* biovar 3 reference (NCTC 10502), though the other two strains in this cluster are described as belonging to biovar 1 in the available metadata. The remaining isolates from Lineage B fell into a larger grouping of 13 strains in total (Figure 2; Lineage B3), which consisted of two lineages (Lineage B3i and B3ii). Lineage B3i was made up of six strains from several locations across SSA, namely Chad (strain 78/14), Nigeria (strain 65/110) and Sudan (strains 87/28, F6/05-2, F6/05-4 and F6/05-9). Clade B3ii consisted of seven strains including a further strain from Chad (strain 80/28) and six from Nigeria (strains babNG1, babNG2, babNG9, babNG15, babNG19, babNG20; described by Suarez-Esquivel et al. (2020)).

The majority of strains included in the wgSNP phylogenetic analysis (390/426; 91.5%) fell within a large clade comprised of two main lineages (Figure 2; Lineage C1 and Lineage C2). Strains included within lineage C1 originated from a broad geographic range across Europe and Asia, covering China ($n = 9$), Georgia ($n = 7$), Greece ($n = 1$), Israel ($n = 1$), Italy ($n = 8$), Netherlands ($n = 1$), Russia ($n = 23$), Spain ($n = 4$) and the United Kingdom ($n = 3$). Clade C1 included biovar reference strains for biovars 5 (strain B3196), 6 (strain 870) and 9 (strain C68; Figure 2; Lineage C1).

The second group within this lineage (Lineage C2) contained the greatest number of strains (331/426; 77.7%) yet was characterised by a relatively low level of diversity, relative to other lineages (Figure 2; Lineage C2). Strains within this clade originated from a broad geographic range across Africa (Egypt, Mozambique and Zimbabwe), Asia (Bangladesh, China, India, Israel, Saudi Arabia and South Korea), Europe (Italy, Kosovo, Poland, Portugal, Republic of Ireland, Russia, Spain and United Kingdom), North America (Costa Rica, United States), Oceania (New Zealand) and South America (Argentina, Bolivia and Columbia). Lineage C2 included the *B. abortus* type strain and biovar 1 reference strain 544^{T} (= NCTC 10093^{T}), biovar 2 reference strain 86/8/59 and biovar 4 reference strain 292, as well as *B. abortus* vaccine strains RB51 and S19.

3.4. *In silico* multi-locus sequence typing

Multi-locus sequence typing profiles retrieved *in silico* from Ethiopian isolates and other whole genome data (genome assemblies and *de novo* assembled short reads), and profiles retrieved from the PubMLST database, provided a total 650 records for which 9-locus MLST profiles were available, and 628 records for which 21-locus allelic profiles were available. Seven and 38 isolates were not assigned a 9- and 21-locus MLST ST, respectively. Full MLST profiles and metadata are provided in Supplementary Table S5.

3.4.1. 9-locus MLST

All Ethiopian isolates were identified as ST72 by 9-locus MLST, an ST which was shared by only a single other strain within the dataset (strain 88/218), isolated from a bovine sample from Mozambique. The two strains identified as belonging to Lineage A by wgSNP (strains 88/217 and 63/294) belonged to 9-locus MLST ST37 and ST38, respectively (Figure 2). Nine-locus MLST profile ST37 was represented by just three strains (88/217, 88/219 and 88/220), all of which arise from the same study in Mozambique, whilst ST38 was represented by only a single strain (63/294), from Kenya. Sequence types ST37, ST38 and ST72 clustered together on a minimum spanning tree based on all 9-locus MLST data (Figure 3). MLST-9 ST72, containing the 15 Ethiopian isolates, branched from ST1 but differed at six of nine alleles.

A second cluster of STs, which also consisted of strains exclusively of sub-Saharan African origin, was evident in minimum spanning tree analysis of 9-locus MLST data (Figure 3). This cluster of STs branched from ST1 but differed by at least four of nine alleles. This cluster consisted of nine separate STs (plus one unassigned ST) from a broad geographic distribution across SSA, including ST6 (Sudan, Uganda and Zimbabwe), ST32 (Cameroon, Chad, Kenya, Nigeria, Rwanda and Tanzania), ST33 (Sudan), ST34 (Chad, Nigeria and Sudan), ST35 (represented by a single isolate of unknown geographic origin [78/36]), ST36 (Nigeria, Senegal, Togo), ST82 (Senegal), ST83 (Niger), ST84 (Senegal). As can be seen in Figure 2, this cluster of STs corresponds to Lineage B in wgSNP analysis.

The majority of strains included in the 9-locus MLST analysis, including all others of sub-Saharan African origin, belonged to three clusters of STs (ST1, ST2 and ST5, and single allele variants of these) which exhibited a broad geographical distribution. The ST1 cluster contained the largest number of strains ($n = 331$), including a large proportion from North America ($n = 179$) and smaller numbers from Europe ($n = 59$), South America ($n = 60$), Asia ($n = 18$), Africa ($n = 9$; Egypt, Mozambique, Zambia, Zimbabwe), Oceania ($n = 4$) and two strains of unknown geographic origin. The ST2 cluster ($n = 132$) was similarly geographically diverse, including strains from Europe

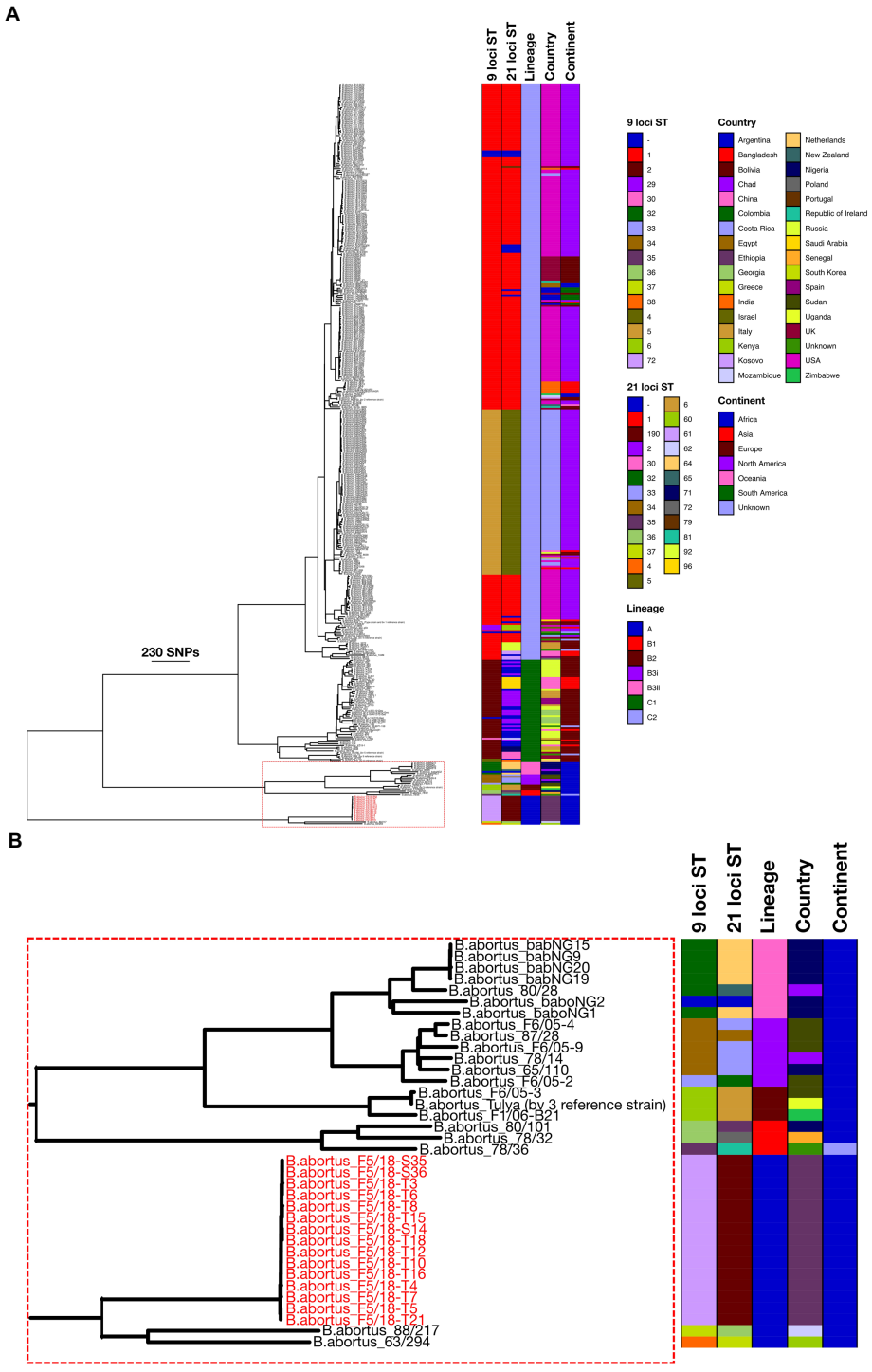

FIGURE 2
Maximum likelihood phylogeny of *Brucella abortus* strains (n=426), including 15 Ethiopian isolates from the present study (tip labels highlighted in red), based on wgSNPs. Colour-coded keys give 9- and 21-locus sequence type (ST), continent and country of origin, and lineage. The scale bar shows number of SNPs. *B. melitensis* (16M^T) was used to root the phylogenetic tree (not shown). Figure 2B shows the section of the phylogeny containing the Ethiopian isolates and other strains in Lineages A and B.

(n=80), Asia (n=36), South America (n=10), Africa (n=4; Chad, Egypt, Sudan, Uganda) and two strains of unknown geographic origin. Finally, ST5 (n=112) included strains from North America (n=96), Asia (n=9), Europe (n=4), Africa (n=2; Zimbabwe) and South America (n=1).

3.4.2. 21-locus MLST

Analysis of 21-locus MLST data revealed essentially the same pattern as that described above, with the inclusion of additional loci increasing the number of distinct STs identified. Two distinct clusters of STs consisting solely of strains of sub-Saharan African origin were

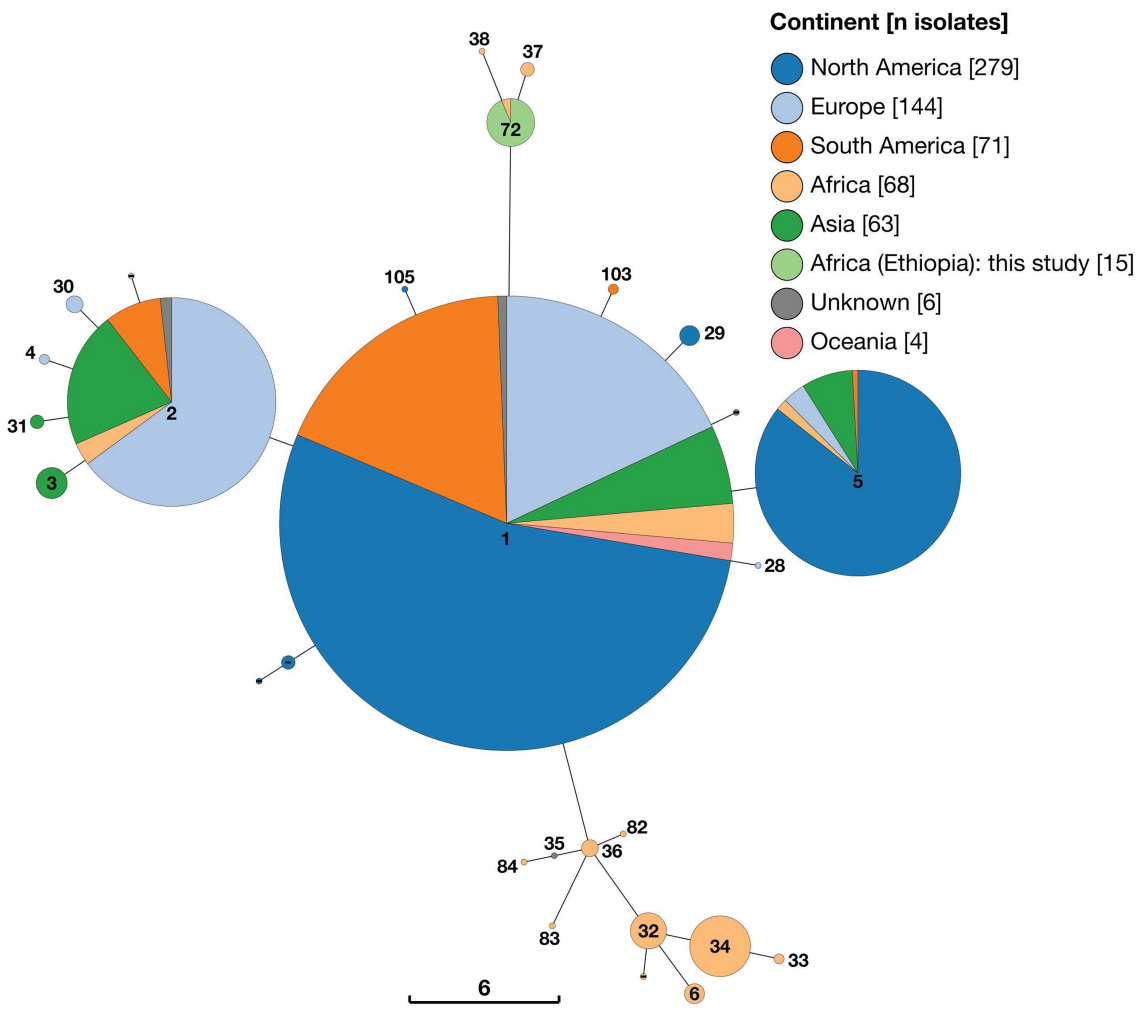

FIGURE 3
Minimum spaning tree of 650 *Brucella abortus* strains, including 15 Ethiopian isolates, based on 9-locus MLST profiles derived *in silico* from whole genome sequences and downloaded from PubMLST *Brucella* database. Node labels give the assigned sequence type (ST), and node colours give the continent of origin (Ethiopian isolates=ST72). The scale bar gives the number of differing loci.

identified, with the majority of strains, including some also from SSA, falling within three larger clusters (Figure 4). The 15 Ethiopian *B. abortus* isolates were assigned to a single ST (ST190), of which they were the only representatives. ST190 clustered with two other STs (ST36 and ST37), each of which was represented by only a single strain (88/217 isolated from Mozambique and 63/294 from Kenya, respectively). These two strains were those identified as belonging to Lineage A by wgSNP (Figure 2). The cluster of 21-locus STs containing the 15 Ethiopian isolates and related strains branched from ST1 but differed at 11 of 21 alleles.

A second cluster of strains ($n = 46$) also originating from SSA was composed of 15 individual sequence types (ST6, ST32, ST33, ST34, ST35, ST64, ST65, ST72, ST81, ST110 ST123, ST124, ST129, ST130 and ST133 plus one isolate with no ST assigned; Figure 4). This cluster of STs corresponded to Lineage B in wgSNP analysis (Figure 2) and originated from 11 countries across SSA (Sudan ($n = 21$), Nigeria ($n = 8$), Senegal ($n = 4$), Chad ($n = 3$), Zimbabwe ($n = 3$), Cameroon ($n = 1$), Kenya ($n = 1$), Niger ($n = 1$), Rwanda ($n = 1$), Togo ($n = 1$) and Uganda ($n = 1$), plus one of unknown origin). This cluster of strains branched from ST2 but differed by at least seven of 21 alleles.

The remaining strains included in 21-locus MLST analysis were assigned to three broad clusters of STs (referred to as ST1, ST2 and ST5 clusters) by minimum spanning tree analysis (Figure 4). In the case of the ST1 cluster, this included 313 strains which were either ST1 (n = 292) or single allele variants of this ST (ST28, ST59, ST60, ST79, ST80, ST92 and ST152), plus a single ST differing by two alleles (ST61). Strains belonging to the ST1 cluster exhibited a broad geographical distribution, originating from North America ($n = 171$), Europe ($n = 58$), South America ($n = 51$), Asia ($n = 17$), Africa ($n = 9$) and Oceania ($n = 4$), plus three from unknown locations. In the case of the ST5 cluster ($n = 112$), the majority of isolates originated from North America ($n = 96$), with smaller numbers of isolates from Asia ($n = 9$), Europe ($n = 4$), Africa ($n = 2$) and South America ($n = 1$). Finally, the ST2 cluster ($n = 102$) consisted of 10 distinct STs, which were either single or double allele variants of ST2 or ST30. These originated from Europe ($n = 58$), Asia ($n = 28$), South America ($n = 10$) and Africa ($n = 4$), plus two isolates from unknown locations.

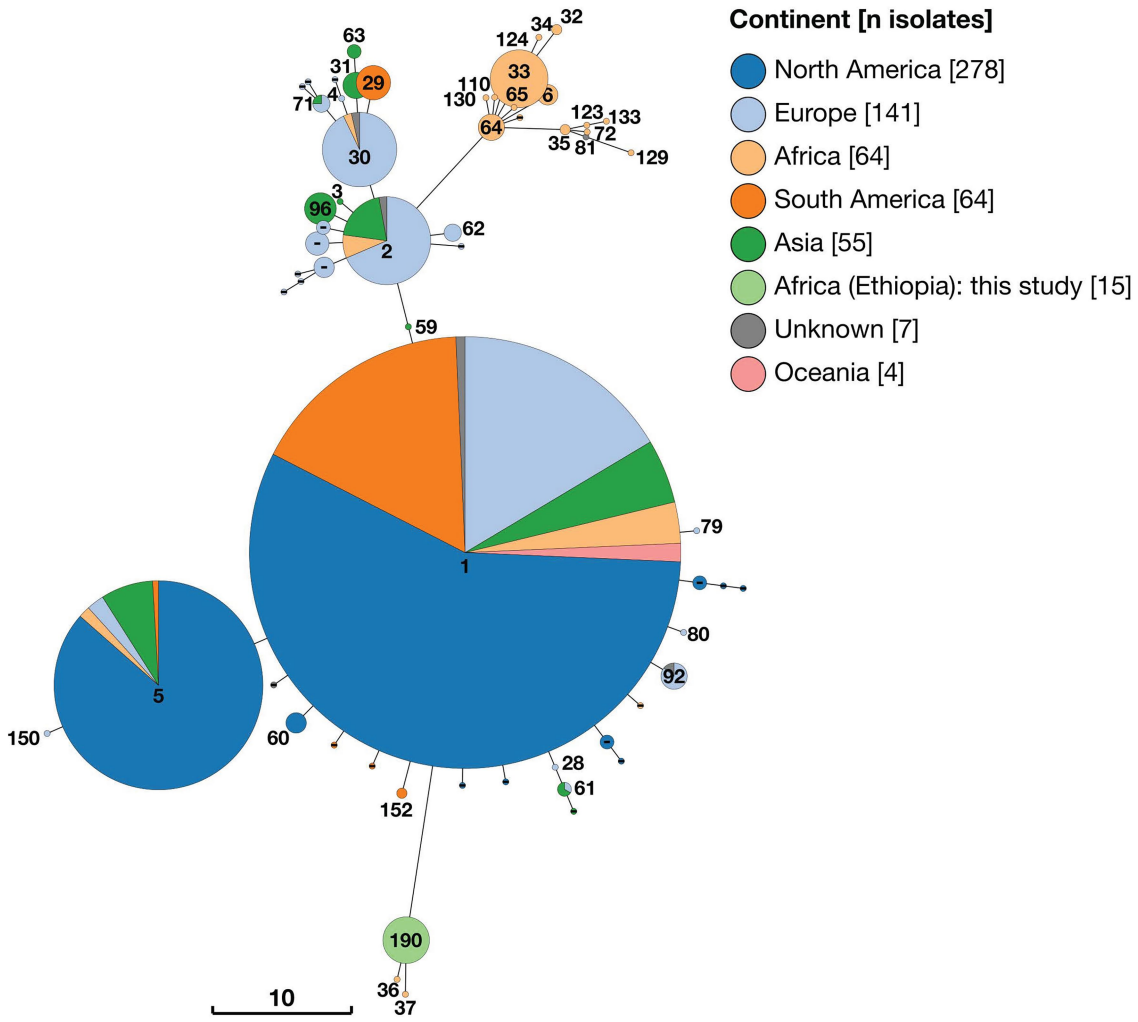

FIGURE 4
Minimum spaning tree of 628 *Brucella abortus* strains, including 15 Ethiopian isolates, based on 21-locus MLST profiles derived *in silico* from whole genome sequences and downloaded from PubMLST *Brucella* database. Node labels give the assigned sequence type (ST), and node colours give the continent of origin (Ethiopian isolates=ST190). The scale bar gives the number of differing loci.

3.5. *In silico* multi-locus VNTR analysis

In silico MLVA typing of *B. abortus* from Ethiopia identified heterogeneity amongst the isolates in three of 16 MLVA loci; Bruce04, Bruce 16 and Bruce30 exhibited HGDI estimates of 0.50, 0.73 and 0.50, respectively. These markers are highly-variable micro-satellite loci located in Panel 2B of the MLVA16 scheme (Le Fleche et al., 2006). All other loci were homogeneous within the Ethiopian isolates. Full MLVA profiles and metadata are provided in Supplementary Table S6.

Minimum spanning tree analysis was undertaken using a total of 1891 MLVA profiles. In addition to data from 15 Ethiopian isolates this included 147 genome assemblies and 416 short read datasets, downloaded from NCBI and ENA, respectively. Additionally, 1,313 existing *B. abortus* profiles were obtained via the *Brucella* MLVA database. Minimum spanning trees constructed with 11 (excluding Panel 2B) and 16 MLVA loci were broadly consistent in the clustering of isolates (see Figure 5 and Supplementary Figure S1 for MLVA11 and MLVA16 minimum spanning trees, respectively).

MLVA11 minimum spanning tree analysis revealed that the 15 Ethiopian isolates from the current study formed a distinct cluster with two other strains, from Mozambique (strain 88/217) and Kenya (strain 63/294; Figure 5). The Ethiopian cluster was otherwise distinct from its nearest neighbouring cluster by four loci (Bruce08; Bruce11, Bruce42 and Bruce 18). Strains 88/217 and 63/294 were those previously identified as belonging to Lineage A by wgSNP analysis (Figure 2), 9-locus MLST STs 37/38 (Figure 3) and 21-locus MLST STs 36/37 (Figure 4).

The majority of African isolates included within the MLVA11 dataset (230/313, 73.5%) were contained within a second, larger, cluster, comprised of strains originating almost exclusively from SSA. Only a single strain within this cluster was not recorded as originating from the African continent (one isolate of unknown origin [78/36]). African isolates contained within this cluster originated from a broad geographical range across the continent, with significant numbers from West Africa (notably, Senegal [$n = 139$] and Togo [$n = 28$]). The other sub-Saharan African counties represented in this cluster were Cameroon ($n = 3$), Chad ($n = 4$), Guinea ($n = 2$),

Guinea-Bissau ($n = 6$), Kenya ($n = 10$), Mauritania ($n = 1$), Niger ($n = 3$), Nigeria ($n = 8$), Rwanda ($n = 14$), Sudan ($n = 8$), Uganda ($n = 3$) and Zimbabwe ($n = 1$). This grouping included the *B. abortus* biovar 3 reference strain (Tulya) which was identified as belonging to wgSNP Lineage B and 9- and 21-locus MLST ST6 (Figures 2–4).

Outside of these two predominantly African groupings, the majority of strains fell within two much larger clusters of related MLVA11 types (Figure 5). The first of these was dominated by a single node of 559 strains sharing the same MLVA11 type, in which North American strains from Costa Rica and the United States formed the majority of isolates ($n = 291$). Within this node 39 strains from the African continent were present, with the majority of these originating from Egypt ($n = 35$) and smaller numbers from Mozambique ($n = 1$) and Zimbabwe ($n = 3$). MLVA11 genotypes associated with this major node ($n = 429$ strains) included 22 strains of African origin, with the majority of these from Egypt ($n = 19$) and a smaller number from Zimbabwe ($n = 3$).

The second major cluster was dominated by a single node of 400 strains, in which strains from Asia comprised the majority of isolates ($n = 257$), but also with a significant number of strains originating from Europe ($n = 141$). MLVA11 genotypes associated with this major node ($n = 255$ strains) included only five strains of African origin.

4. Discussion

In the present study we have reported the isolation and first molecular characterisation of *Brucella abortus* from Ethiopia and undertaken a comprehensive analysis of the relationship of these isolates to existing strains. In doing so we have applied a number of molecular typing approaches, in order to maximise the value of existing molecular typing datasets. Despite using different numbers of informative loci, and employing loci with different mechanisms of mutation, the molecular typing approaches applied have generated broadly consistent results. We have shown that the Ethiopian isolates described in the present study expand the known diversity of an early-branching *B. abortus* lineage which previously consisted of only two fully sequenced strains, both of sub-Saharan African origin. A second early branching lineage was also shown to consist solely of strains isolated in sub-Saharan Africa.

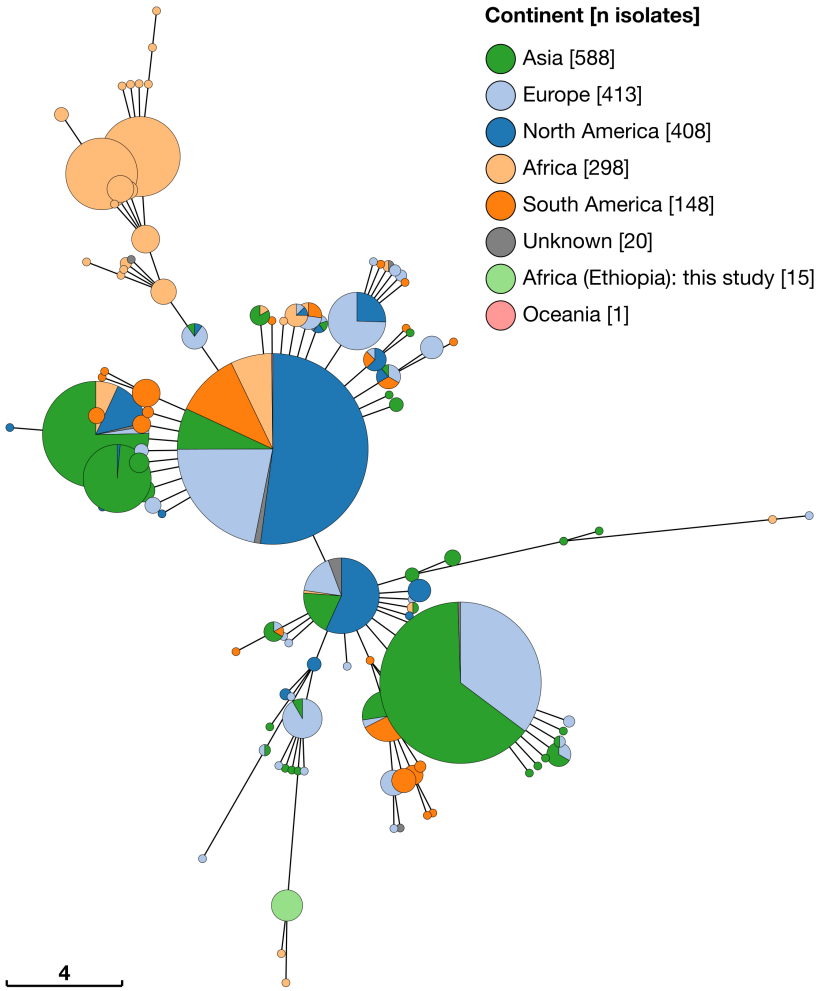

FIGURE 5
Minimum spaning tree of 1,891 *Brucella abortus* strains, including 15 Ethiopian isolates, based on MLVA11 profiles derived *in silico* from whole genome sequences and downloaded from MLVA-NET *Brucella* database. Node colours give the continent of origin, whilst the scale bar gives the number of differing loci.

Phylogenetic analysis based on wgSNPs identified that Ethiopian *B. abortus* isolates from the current study form a distinct lineage with two previously described strains (88/217 and 63/294 isolated in Mozambique and Kenya, respectively), branching basally to all other isolates included within the analysis. The existence of a basally branching *B. abortus* clade has been previously described, using an expanded 21-locus MLST scheme applied to a comprehensive panel of over 500 *Brucella* isolates (Whatmore et al., 2016). Similarly, Ledwaba et al. (2021) employed wgSNP analysis to describe a similar structure using 175 publicly available *B. abortus* genomes and 13 South African strains. These authors identified major lineages A and B, both of which are described as containing solely African isolates. More recently, Abdel-Glil et al. (2022) presented the results of analyses based on a core genome MLST (cgMLST) scheme for *Brucella*, using 1,764 genes, which also identified three *B. abortus* lineages, with the two most basal lineages represented by strains of African origin.

These results suggest that the ancestral lineage of *B. abortus* may have originated in East Africa, based on currently available information, with the relatively fewer strains of African origin found within the more numerous wgSNP Lineages C1 and C2 potentially reflecting historical re-importation to the continent. A comparable evolutionary scenario has been described for *Mycobacterium bovis*, another zoonotic bacterial pathogen, primarily of cattle. Phylogenetic analyses using whole genome data have indicated that *M. bovis* is likely to have originated in East Africa, and that whilst specific lineages have remained restricted to East and West Africa, others have become globally widely dispersed by cattle movements (Smith et al., 2011; Inlamea et al., 2020; Loiseau et al., 2020). Studies concerning the genetic diversity of *M. bovis* strains present in cattle populations in Ethiopia have demonstrated that two distinct clonal complexes are present, with one of African origin (African 2), and the other reflecting more recent importation of a derived European *M. bovis* lineage (European 3; Almaw et al., 2021).

The present analyses do not allow us to definitively conclude that *B. abortus* Lineage A is ancestral to all other lineages, with an origin in East Africa. It remains possible that more basal lineages exist, and that Lineage A, as currently described, forms part of a larger monophyletic clade. This is particularly true given the relative sparsity of *B. abortus* genome data from Ethiopia, East Africa and the wider continent. It is clear that there is considerable genomic diversity of *B. abortus* within sub-Saharan Africa, and that further sampling across the continent may help to reveal the underlying phylogenetic structure of the species. Future work could also seek to investigate the most likely geographical origin of *B. abortus* lineages using methods to infer ancestral states (e.g., Coscolla et al., 2021). Additionally, phylodynamic analyses, making use of known dates of isolation, may help to infer most recent common ancestors for specific lineages (e.g., Almaw et al., 2021).

The population of Ethiopia has increased markedly in recent decades, with a parallel expansion of the country's agricultural sector (Firdessa et al., 2012). Ethiopia now has the largest livestock population in Africa, including approximately 65 million cattle, with 70% of the Ethiopian population directly involved in the agricultural sector (CSA, 2020). In the dairy sector this has been associated with a shift from small-scale extensive cattle farming towards larger more intensively farmed herds in urban and peri-urban settings (Firdessa et al., 2012; Deneke et al., 2022). These have been shown to be associated with an increased risk for transmission of infectious diseases such as bovine tuberculosis (Mekonnen et al., 2019). Indeed, previous studies have demonstrated that larger herd size is significantly associated with brucellosis seropositivity in cattle in Ethiopia (Edao et al., 2020). Whilst the present study provides no data regarding prevalence of *B. abortus* in dairy cattle in the Oromia region or in Ethiopia, the isolation of the same strain from multiple animals on a single farm suggests that bovine brucellosis may be a significant problem in similar settings. To date, no brucellosis control strategy, including vaccination, has been implemented in cattle or other livestock species in Ethiopia. As the national herd-level seroprevalence in cattle has been estimated to be 16.3% (Sibhat et al., 2022) it is likely that bovine brucellosis represents an endemic veterinary and public health priority issue in other geographic areas of the country. The successful isolation of *Brucella* from lymph nodes of the mammary glands highlights the potentially significant public health risk from *Brucella abortus* infection in cattle, if milk or dairy products are consumed without pasteurisation. One recent study indicated that the consumption of raw milk was a relatively common practice in Ethiopia, including in the Oromia region, with 20.4% of interviewees consuming raw milk with varying degrees of frequency (Deneke et al., 2022). Furthermore, a much larger proportion of respondents in this study (82%) reporting drinking fermented milk, which is usually made from non-pasteurised or unboiled milk, and which may continue to represent a microbiological hazard despite fermentation (e.g., Zúñiga Estrada et al., 2005).

There are a number of limitations to the present study, which impact the scope of the conclusions which can be drawn. The samples analysed in this work arose from opportunistic sampling of a brucellosis outbreak in a single location in central Ethiopia. As such, it is not possible to draw any conclusions regarding the prevalence of infection within the geographical region (Oromia regional state) or the wider Ethiopian cattle sector. Similarly, the available dataset does not allow us to draw any conclusions regarding the predominant *Brucella* species circulating within the country, and the relative importance of these for livestock and human infections. Appropriately designed prospective epidemiological studies would be required to address these evidence gaps. Furthermore, it is not possible to make any inferences concerning the within-species genetic diversity of other strains of *B. abortus* circulating within Ethiopia. Additional work would be required to characterise diversity within *Brucella* species present in Ethiopia, including sampling of a wider range of livestock hosts and broader geographical coverage across the country.

A methodological issue encountered during the current study was the presence of incorrectly identified genome sequences in open-access genomic databases. A number of recent studies have identified basal clades using *Brucella* sp. genomes which have been incorrectly identified as "*B. abortus*" in public sequence databases. For example, Islam et al., (2019) present a whole genome phylogeny for *B. abortus*, in which strain BCB013 (GCF_000292205.1) is presented as basal to all other *B. abortus* genomes. However, further inspection (e.g., NCBIs Taxonomy Check; Ciufo et al., 2018) reveal that this whole genome sequence is likely to be mis-identified. This is supported by the identification of this assembly, amongst others, for exclusion from the current analysis. Such anomalies highlight the importance of careful curation of datasets downloaded from public repositories, as well as reliable identification of bacteriological isolates, in order to avoid erroneous conclusions from being drawn regarding within-species phylogenetic relationships.

A related methodological issue is the high degree of duplication present in publicly available molecular typing databases. Publicly available databases of both MLST and MLVA data incorporate profiles retrieved *in silico* from genome assembly and short-read datasets (Jolley et al., 2018; Vergnaud et al., 2018). This has resulted in data from individual strains being duplicated, where existing profiles were present from "conventional" (e.g., capillary sequencing based) typing and *in silico* profiles have subsequently been added. This has the potential to artificially inflate the representation of certain strains, potentially skewing the relative composition of specific lineages. Again, this highlights the need for careful curation of datasets downloaded from public repositories.

5. Conclusion

The work presented here provides a comprehensive analysis of the phylogenetic structure of *Brucella abortus*, a zoonotic pathogen of global significance. We describe the first detailed characterisation of *B. abortus* isolates from Ethiopia and demonstrate that these isolates expand the known diversity of a basal lineage within the species, which was previously only represented by two isolates from sub-Saharan Africa. By combining analyses based on whole genome sequencing data and existing molecular typing methods (MLST and MLVA) we provide further support for the existence of two basal *B. abortus* lineages, both comprised solely of isolates of sub-Saharan African origin. This work will serve as the basis for further studies concerning the global population structure and evolutionary history of a major zoonotic pathogen which continues to impact the populations of many low- and middle-income countries.

Data availability statement

The datasets presented in this study can be found in online repositories. The names of the repository/repositories and accession number(s) can be found in the article/Supplementary material.

Author contributions

BE undertook experimental work, bioinformatic analyses, and contributed to the manuscript. MT supported *post mortem* examinations and sample collection. JW, GA, SB, and AW conceived of and designed the study and contributed to the manuscript. AT performed bioinformatic analyses and contributed to the manuscript. RA performed data analysis and drafted the manuscript. All authors contributed to the article and approved the submitted version.

Funding

This work was partially funded by the Biotechnology and Biological Sciences Research Council, the Department for International Development, the Economic and Social Research Council, the Medical Research Council, the Natural Environment Research Council and the Defence Science and Technology Laboratory, under the Zoonoses and Emerging Livestock Systems (ZELS) programme (ref.: BB/L018977/1). *Brucellosis* research activities at APHA are supported by the United Kingdom Department for Environment, Food and Rural Affairs (Defra).

Acknowledgments

We are grateful to Emma-Jane Dale and Amanda Dainty for assistance with *Brucella* culture.

Conflict of interest

The authors declare that the research was conducted in the absence of any commercial or financial relationships that could be construed as a potential conflict of interest.

Publisher's note

All claims expressed in this article are solely those of the authors and do not necessarily represent those of their affiliated organizations, or those of the publisher, the editors and the reviewers. Any product that may be evaluated in this article, or claim that may be made by its manufacturer, is not guaranteed or endorsed by the publisher.

Supplementary material

The Supplementary material for this article can be found online at: https://www.frontiersin.org/articles/10.3389/fmicb.2023.1128966/full#supplementary-material

References

Abdel-Glil, M. Y., Thomas, P., Brandt, C., Melzer, F., Subbaiyan, A., Chaudhuri, P., et al. (2022). Core genome multilocus sequence typing scheme for improved characterization and epidemiological surveillance of pathogenic *Brucella*. *J. Clin. Microbiol.* 60:e0031122. doi: 10.1128/jcm.00311-22

Akoko, J. M., Pelle, R., Lukambagire, A. S., Machuka, E. M., Nthiwa, D., Mathew, C., et al. (2021). Molecular epidemiology of *Brucella* species in mixed livestock-human ecosystems in Kenya. *Sci. Rep.* 11:8881. doi: 10.1038/s41598-021-88327-z

Almaw, G., Mekonnen, G. A., Mihret, A., Aseffa, A., Taye, H., Conlan, A. J. K., et al. (2021). Population structure and transmission of *Mycobacterium bovis* in Ethiopia. *Microb. Genom.* 7:000539. doi: 10.1099/mgen.0.000539

Alton, G. G., Jones, L. M., Pietz, D. E., and World Health Organization (1975). Laboratory Techniques in Brucellosis. World Health Organization.

Ashford, R. T., and Whatmore, A. M. (2022). "*Brucella*." In *Molecular Typing in Bacterial Infections. Vol. II*, (ed.) FilippisI. de. Cham: Springer International Publishing, 217–245.

Bankevich, A., Nurk, S., Antipov, D., Gurevich, A. A., Dvorkin, M., Kulikov, A. S., et al. (2012). SPAdes: a new genome assembly algorithm and its applications to single-cell sequencing. *J. Comput. Biol.* 19, 455–477. doi: 10.1089/cmb.2012.0021

Chaka, H., Aboset, G., Garoma, A., Gumi, B., and Thys, E. (2018). Cross-sectional survey of brucellosis and associated risk factors in the livestock-wildlife interface area of Nechisar National Park, Ethiopia. *Trop. Anim. Health Prod* 50, 1041–1049. doi: 10.1007/s11250-018-1528-4

Chen, S., Zhou, Y., Chen, Y., and Gu, J. (2018). Fastp: an ultra-fast all-in-one FASTQ preprocessor. *Bioinformatics* 34, i884–i890. doi: 10.1093/bioinformatics/bty560

Ciufo, S., Kannan, S., Sharma, S., Badretdin, A., Clark, K., Turner, S., et al. (2018). Using average nucleotide identity to improve taxonomic assignments in prokaryotic genomes at the NCBI. *Int. J. Syst. Evol. Microbiol.* 68, 2386–2392. doi: 10.1099/ijsem.0.002809

Corbel, M. J. (2006). *Brucellosis in Humans and Animals*. Geneva: World Health Organization.

Coscolla, M., Gagneux, S., Menardo, F., Loiseau, C., Ruiz-Rodriguez, P., Borrell, S., et al. (2021). Phylogenomics of *Mycobacterium africanum* reveals a new lineage and a complex evolutionary history. *Microb. Genom.* 7:000477. doi: 10.1099/mgen.0.000477

CSA. (2020) Agricultural Sample Survey 2019/20 [2012 E.C.]. Volume II Report on livestock and livestock characteristics (private peasant holdings). Central statistical agency (CSA): Addis Ababa, Ethiopia.

Dean, A. S., Crump, L., Greter, H., Hattendorf, J., Schelling, E., and Zinsstag, J. (2012). Clinical manifestations of human brucellosis: a systematic review and meta-analysis. *PLoS Negl. Trop. Dis.* 6:e1929. doi: 10.1371/journal.pntd.0001929

Deneke, T. T., Bekele, A., Moore, H. L., Mamo, T., Almaw, G., Mekonnen, G. A., et al. (2022). Milk and meat consumption patterns and the potential risk of zoonotic disease transmission among urban and peri-urban dairy farmers in Ethiopia. *BMC Public Health* 22:222. doi: 10.1186/s12889-022-12665-4

Ducrotoy, M., Bertu, W. J., Matope, G., Cadmus, S., Conde-Álvarez, R., Gusi, A. M., et al. (2017). Brucellosis in sub-Saharan Africa: current challenges for management, diagnosis and control. *Acta Trop.* 165, 179–193. doi: 10.1016/j.actatropica.2015.10.023

Edao, B. M. (2020). Brucellosis in Ethiopia: Epidemiology and public health significance. PhD thesis, University of Cambridge.

Edao, B. M., Ameni, G., Assefa, Z., Berg, S., Whatmore, A. M., and Wood, J. L. N. (2020). Brucellosis in ruminants and pastoralists in Borena, Southern Ethiopia. *PLoS Negl. Trop. Dis.* 14:e0008461. doi: 10.1371/journal.pntd.0008461

Edao, B. M., Hailegebreal, G., Berg, S., Zewude, A., Zeleke, Y., Sori, T., et al. (2018). Brucellosis in the Addis Ababa dairy cattle: the myths and the realities. *BMC Vet. Res.* 14:396. doi: 10.1186/s12917-018-1709-4

Firdessa, R., Tschopp, R., Wubete, A., Sombo, M., Hailu, E., Erenso, G., et al. (2012). High prevalence of bovine tuberculosis in dairy cattle in Central Ethiopia: implications for the dairy industry and public health. *PLoS One* 7:e52851. doi: 10.1371/journal.pone.0052851

Geresu, M. A., Ameni, G., Wubete, A., Arenas-Gamboa, Á. M., and Kassa, G. M. (2016). Isolation and identification of *Brucella* species from dairy cattle by biochemical tests: the first report from Ethiopia. *World Vet. J.* 6, 80–88. doi: 10.5455/wvj.20160471

Gopaul, K. K., Koylass, M. S., Smith, C. J., and Whatmore, A. M. (2008). Rapid identification of *Brucella* isolates to the species level by real time PCR based single nucleotide polymorphism (SNP) analysis. *BMC Microbiol.* 8:1. doi: 10.1186/1471-2180-8-86

Gurevich, A., Saveliev, V., Vyahhi, N., and Tesler, G. (2013). QUAST: quality assessment tool for genome assemblies. *Bioinformatics (Oxford, England)* 29, 1072–1075. doi: 10.1093/bioinformatics/btt086

Halling, S. M., Peterson-Burch, B. D., Bricker, B. J., Zuerner, R. L., Qing, Z., Li, L.-L., et al. (2005). Completion of the genome sequence of *Brucella abortus* and comparison to the highly similar genomes of *Brucella melitensis* and *Brucella suis*. *J. Bacteriol.* 187, 2715–2726. doi: 10.1128/jb.187.8.2715-2726.2005

Holzer, K., El-Diasty, M., Wareth, G., Abdel-Hamid, N. H., Hamdy, M. E. R., Moustafa, S. A., et al. (2021). Tracking the distribution of *Brucella abortus* in Egypt based on Core genome SNP analysis and in silico MLVA-16. *Microorganisms* 9:1942. doi: 10.3390/microorganisms9091942

Hunter, P. R., and Gaston, M. A. (1988). Numerical index of the discriminatory ability of typing systems: an application of Simpson's index of diversity. *J. Clin. Microbiol.* 26, 2465–2466. doi: 10.1128/jcm.26.11.2465-2466.1988

Inlamea, O. F., Soares, P., Ikuta, C. Y., Heinemann, M. B., Achá, S. J., Machado, A., et al. (2020). Evolutionary analysis of *Mycobacterium bovis* genotypes across Africa suggests co-evolution with livestock and humans. *PLoS Negl. Trop. Dis.* 14:e0008081. doi: 10.1371/journal.pntd.0008081

Islam, M. S., Zowalaty, M. E. E., Vliet, A. H. M. V., Thakur, S., Khatun, M. M., Saha, S., et al. (2019). First genome sequence of *Brucella abortus* Biovar 3 strain BAU21/S4023, isolated from a dairy cow in Bangladesh. *Microbiol. Resour. Announc.* 8, e00446–e00419. doi: 10.1128/MRA.00446-19

Jolley, K. A., Bray, J. E., and Maiden, M. C. J. (2018). Open-access bacterial population genomics: BIGSdb software, the PubMLST.org website and their applications. *Wellcome Open Res* 3:124. doi: 10.12688/wellcomeopenres.14826.1

Keim, P., Van Ert, M. N., Pearson, T., Vogler, A. J., Huynh, L. Y., and Wagner, D. M. (2004). Anthrax molecular epidemiology and forensics: using the appropriate marker for different evolutionary scales. *Infect. Genet. Evol.* 4, 205–213. doi: 10.1016/j.meegid.2004.02.005

Khan, A. U., Melzer, F., Sayour, A. E., Shell, W. S., Linde, J., Abdel-Glil, M., et al. (2021). Whole-genome sequencing for tracing the genetic diversity of *Brucella abortus* and *Brucella melitensis* isolated from livestock in Egypt. *Pathogens* 10:759. doi: 10.3390/pathogens10060759

Le Fleche, P., Jacques, I., Grayon, M., Al Dahouk, S., Bouchon, P., Denoeud, F., et al. (2006). Evaluation and selection of tandem repeat loci for a *Brucella* MLVA typing assay. *BMC Microbiol.* 6:9. doi: 10.1186/1471-2180-6-9

Ledwaba, M. B., Glover, B. A., Matle, I., Profiti, G., Martelli, P. L., Casadio, R., et al. (2021). Whole Genome Sequence Analysis of *Brucella abortus* Isolates from Various Regions of South Africa. *Microorganisms* 9:570. doi: 10.3390/microorganisms9030570

Li, H. (2011). A statistical framework for SNP calling, mutation discovery, association mapping and population genetical parameter estimation from sequencing data. *Bioinformatics* 27, 2987–2993. doi: 10.1093/bioinformatics/btr509

Li, H., and Durbin, R. (2009). Fast and accurate short read alignment with burrows–wheeler transform. *Bioinformatics* 25, 1754–1760. doi: 10.1093/bioinformatics/btp324

Loiseau, C., Menardo, F., Aseffa, A., Hailu, E., Gumi, B., Ameni, G., et al. (2020). An African origin for *Mycobacterium bovis*. *Evol. Med. Public Health* 2020, 49–59. doi: 10.1093/emph/eoaa005

Lokamar, P. N., Kutwah, M. A., Atieli, H., Gumo, S., and Ouma, C. (2020). Socio-economic impacts of brucellosis on livestock production and reproduction performance in Koibatek and Marigat regions, Baringo County, Kenya. *BMC Vet. Res.* 16:61. doi: 10.1186/s12917-020-02283-w

López-Goñi, I., García-Yoldi, D., Marín, C. M., de Miguel, M. J., Barquero-Calvo, E., Guzmán-Verri, C., et al. (2011). New Bruce-ladder multiplex PCR assay for the biovar typing of *Brucella suis* and the discrimination of *Brucella suis* and *Brucella canis*. *Vet. Microbiol.* 154, 152, 152–155. doi: 10.1016/j.vetmic.2011.06.035

Lu, J., Breitwieser, F. P., Thielen, P., and Salzberg, S. L. (2017). Bracken: estimating species abundance in metagenomics data. *PeerJ Comput. Sci.* 3:e104. doi: 10.7717/peerj-cs.104

Matero, P., Hemmilä, H., Tomaso, H., Piiparinen, H., Rantakokko-Jalava, K., Nuotio, L., et al. (2011). Rapid field detection assays for *Bacillus anthracis*, *Brucella* spp., *Francisella tularensis* and *Yersinia pestis*. *Clin. Microbiol. Infect.* 17, 34–43. doi: 10.1111/j.1469-0691.2010.03178.x

Mayer-Scholl, A., Draeger, A., Göllner, C., Scholz, H. C., and Nöckler, K. (2010). Advancement of a multiplex PCR for the differentiation of all currently described *Brucella* species. *J. Microbiol. Methods* 80, 112–114. doi: 10.1016/j.mimet.2009.10.015

McDermott, J., Grace, D., and Zinsstag, J. (2013). Economics of brucellosis impact and control in low-income countries. *Rev. Sci. Tech.* 32, 249–261. doi: 10.20506/rst.32.1.2197

Mekonnen, G. A., Conlan, A. J. K., Berg, S., Ayele, B. T., Alemu, A., Guta, S., et al. (2019). Prevalence of bovine tuberculosis and its associated risk factors in the emerging dairy belts of regional cities in Ethiopia. *Prev. Vet. Med.* 168, 81–89. doi: 10.1016/j.prevetmed.2019.04.010

Moreno, E., Blasco, J.-M., and Moriyón, I. (2022). Facing the human and animal brucellosis conundrums: the forgotten lessons. *Microorganisms* 10:942. doi: 10.3390/microorganisms10050942

Nguyen, L.-T., Schmidt, H. A., von Haeseler, A., and Minh, B. Q. (2014). IQ-TREE: a fast and effective stochastic algorithm for estimating maximum-likelihood phylogenies. *Mol. Biol. Evol.* 32, 268–274. doi: 10.1093/molbev/msu300

Page, A. J., Taylor, B., Delaney, A. J., Soares, J., Seemann, T., Keane, J. A., et al. (2016). SNP-sites: rapid efficient extraction of SNPs from multi-FASTA alignments. *Microb. Genom.* 2:e000056. doi: 10.1099/mgen.0.000056

Pappas, G., Papadimitriou, P., Akritidis, N., Christou, L., and Tsianos, E. V. (2006). The new global map of human brucellosis. *Lancet Infect. Dis.* 6, 91–99. doi: 10.1016/S1473-3099(06)70382-6

Probert, W. S., Schrader, K. N., Khuong, N. Y., Bystrom, S. L., and Graves, M. H. (2004). Real-time multiplex PCR assay for detection of *Brucella* spp., *B. abortus*, and *B. melitensis*. *J. Clin. Microbiol.* 42, 1290–1293. doi: 10.1128/jcm.42.3.1290-1293.2004

R Core Team (2022). "*R: A Language and Environment for Statistical Computing*.". R Foundation for Statistical Computing, Vienna, Austria.

Sibhat, B., Tessema, T. S., Nile, E., and Asmare, K. (2022). Brucellosis in Ethiopia: a comprehensive review of literature from the year 2000–2020 and the way forward. *Transboundary and Emerging Diseases.* 69, e1231–e1252. doi: 10.1111/tbed.14495

Smith, N. H., Berg, S., Dale, J., Allen, A., Rodriguez, S., Romero, B., et al. (2011). European 1: a globally important clonal complex of *Mycobacterium bovis*. *Infect. Genet. Evol.* 11, 1340–1351. doi: 10.1016/j.meegid.2011.04.027

Suarez-Esquivel, M., Hernandez-Mora, G., Ruiz-Villalobos, N., Barquero-Calvo, E., Chacon-Diaz, C., Ladner, J. T., et al. (2020). Persistence of *Brucella abortus* lineages revealed by genomic characterization and phylodynamic analysis. *PLoS Negl. Trop. Dis.* 14:e0008235. doi: 10.1371/journal.pntd.0008235

Tekle, M., Legesse, M., Edao, B. M., Ameni, G., and Mamo, G. (2019). Isolation and identification of *Brucella melitensis* using bacteriological and molecular tools from aborted goats in the Afar region of North-Eastern Ethiopia. *BMC Microbiol.* 19:108. doi: 10.1186/s12866-019-1474-y

Vergnaud, G., Hauck, Y., Christiany, D., Daoud, B., Pourcel, C., Jacques, I., et al. (2018). Genotypic expansion within the population structure of classical *Brucella* species revealed by MLVA16 typing of 1404 *Brucella* isolates from different animal and geographic origins, 1974–2006. *Front. Microbiol.* 9:1545. doi: 10.3389/fmicb.2018.01545

Whatmore, A. M., and Foster, J. T. (2021). Emerging diversity and ongoing expansion of the genus *Brucella*. *Infect. Genet. Evol.* 92:104865. doi: 10.1016/j.meegid.2021.104865

Whatmore, A., Koylass, M., Muchowski, J., Edwards-Smallbone, J., Gopaul, K., and Perrett, L. (2016). Extended multilocus sequence analysis to describe the global

population structure of the genus *Brucella*: phylogeography and relationship to biovars. *Front. Microbiol.* 7:2049. doi: 10.3389/fmicb.2016.02049

Whatmore, A. M., Perrett, L. L., and MacMillan, A. P. (2007). Characterisation of the genetic diversity of *Brucella* by multilocus sequencing. *BMC Microbiol.* 7:34. doi: 10.1186/1471-2180-7-34

WOAH (2018). *Brucellosis (infection with Brucella abortus, B. melitensis and B. suis). Chapter 3.1.4. Manual of diagnostic tests and vaccines for terrestrial animals*. World Organisation for Animal Health (WOAH), Paris, France.

Wood, D. E., Lu, J., and Langmead, B. (2019). Improved metagenomic analysis with kraken 2. *Genome Biol.* 20:257. doi: 10.1186/s13059-019-1891-0

Yu, G., Smith, D. K., Zhu, H., Guan, Y., and Lam, T. T.-Y. (2017). Ggtree: an r package for visualization and annotation of phylogenetic trees with their covariates and other associated data. *Methods Ecol. Evol.* 8, 28–36. doi: 10.1111/2041-210X.12628

Zhou, Z., Alikhan, N.-F., Sergeant, M. J., Luhmann, N., Vaz, C., Francisco, A. P., et al. (2018). GrapeTree: visualization of core genomic relationships among 100,000 bacterial pathogens. *Genome Res.* 28, 1395–1404. doi: 10.1101/gr.232397.117

Zúñiga Estrada, A., Mota de la Garza, L., Sánchez Mendoza, M., Santos López, E. M., Filardo Kerstupp, S., and López Merino, A. (2005). Survival of *Brucella abortus* in milk fermented with a yoghurt starter culture. *Rev. Latinoam. Microbiol.* 47, 88–91.

frontiers | Frontiers in Microbiology

TYPE Original Research
PUBLISHED 08 June 2023
DOI 10.3389/fmicb.2023.1173252

OPEN ACCESS

EDITED BY
Antonio Battisti,
Institute of Experimental Zooprophylactic of the Lazio and Tuscany Regions (IZSLT), Italy

REVIEWED BY
Elena Lavinia Diaconu,
Institute of Experimental Zooprophylactic of the Lazio and Tuscany Regions (IZSLT), Italy
Clayton Caswell,
Virginia Tech, United States
Steven Olsen,
Agricultural Research Service (USDA), United States

*CORRESPONDENCE
Holger C. Scholz
✉ scholzh@rki.de

†PRESENT ADDRESS
Holger Scholz,
Centre for Biological Threats and Special Pathogens (ZBS2),
Robert Koch Institute,
Berlin, Germany

RECEIVED 24 February 2023
ACCEPTED 02 May 2023
PUBLISHED 08 June 2023

CITATION
Scholz HC, Heckers KO, Appelt S, Geier-Dömling D, Schlegel P and Wattam AR (2023) Isolation of *Brucella inopinata* from a White's tree frog (*Litoria caerulea*): pose exotic frogs a potential risk to human health?
Front. Microbiol. 14:1173252.
doi: 10.3389/fmicb.2023.1173252

Isolation of *Brucella inopinata* from a White's tree frog (*Litoria caerulea*): pose exotic frogs a potential risk to human health?

Holger C. Scholz[1*†], Kim O. Heckers[2], Sandra Appelt[1], Dorothee Geier-Dömling[2], Patrick Schlegel[3] and Alice R. Wattam[4]

[1]Department of Bacteriology and Toxinology, Bundeswehr Institute of Microbiology, Munich, Germany, [2]LABOklin GmbH and Co KG, Labor für klinische Diagnostik, Bad Kissingen, Germany, [3]Kleintierpraxis Dr. med vet. Patrick Schlegel, Sargans, Switzerland, [4]Biocomplexity Institute, University of Virginia, Charlottesville, VA, United States

Introduction: Cold-blooded hosts, particularly exotic frogs, have become a newly recognized reservoir for atypical *Brucella* species and strains worldwide, but their pathogenicity to humans remains largely unknown. Here we report the isolation and molecular characterization of a *B. inopinata* strain (FO700662) cultured from clinical samples taken from a captive diseased White's Tree Frog (*Litoria caerulea*) in Switzerland. The isolation of *B. inopinata* from a frog along with other reports of human infection by atypical Brucella raises the question of whether atypical Brucella could pose a risk to human health and deserves further attention.

Methods: The investigations included histopathological analysis of the frog, bacterial culture and in-depth molecular characterization of strain FO700662 based on genome sequencing data.

Results and Discussion: Originally identified as *Ochrobactrum* based on its rapid growth and biochemical profile, strain FO700622 was positive for the *Brucella*-specific markers *bcsp31* and *IS711*. It showed the specific banding pattern of *B. inopinata* in conventional Bruce-ladder multiplex PCR and also had identical 16S rRNA and recA gene sequences as *B. inopinata*. Subsequent genome sequencing followed by core genome-based MLST (cgMLST) analysis using 2704 targets (74% of the total chromosome) revealed only 173 allelic differences compared to the type strain of *B. inopinata* BO1^T, while previously considered the closest related strain BO2 differed in 2046 alleles. The overall average nucleotide identity (ANI) between the type strain BO1^T and FO700622 was 99,89%, confirming that both strains were almost identical. In *silico* MLST-21 and MLVA-16 also identified strain FO700662 as *B. inopinata*. The nucleotide and amino acid-based phylogenetic reconstruction and comparative genome analysis again placed the isolate together with *B. inopinata* with 100% support. In conclusion, our data unequivocally classified strain FO700622, isolated from an exotic frog, as belonging to *B. inopinata*.

KEYWORDS

***Brucella inopinata*, atypical *Brucella*, exotic frogs, public health, genomics**

Introduction

Many members of the genus *Brucella* are important zoonotic pathogens that can infect various animal species and humans (Godfroid et al., 2005; Seleem et al., 2010). The resulting disease, brucellosis, is one of the most common bacterial zoonoses worldwide with an estimated incidence of 500,000 human cases annually (Pappas et al., 2006b). The majority of human cases are caused by *B. melitensis*, followed by *B. abortus* and *B. suis*, with other species only rarely causing disease in man. Because of the low infection dose and possible transmission as an aerosol, *B. melitensis* and most other *Brucella* species, including *B. inopinata*, are classified as a risk level 3 (category A) pathogens (Pappas et al., 2006a).

For decades, the genus *Brucella* consisted exclusively of the classical *Brucella* species (*B. melitensis*, *B. abortus*, *B. suis*, *B. canis*, *B. ovis*, and *B. neotomae*). However, in recent years, the genus has expanded rapidly from terrestrial and marine mammals to fish, amphibians, and even reptiles (Godfroid et al., 2005; Foster et al., 2007; De et al., 2008; Scholz et al., 2008c, 2016a,b; Whatmore et al., 2014; Muhldorfer et al., 2017; Eisenberg et al., 2020).

Many of these novel *Brucella* isolates have either atypical biochemical or molecular characteristics compared to the group of closely related classical *Brucella* species (Scholz and Vergnaud, 2013). Consequently, the genus is now divided into the classical species (also referred to as "core *Brucella*"), including strains of marine mammals (*B. ceti* and *B. pinnipedialis*), and the genomes composed of genetically and biochemically more diverse species and isolates (Scholz et al., 2008a; Whatmore, 2009; Whatmore et al., 2016; Ashford et al., 2020). While the pathogenicity of classical species to humans is well documented, these data are largely missing for atypical species.

One of these atypical *Brucella* species is *B. inopinata*, which was unexpectedly isolated in 2008 from a 71-year-old woman in the United States with an endogenous breast implant infection and clinical signs consistent with brucellosis (De et al., 2008; Scholz et al., 2010). At this time, *B. inopinata* was the most genetically diverse *Brucella* species compared to the classical *Brucella* species. While all classical *Brucella* species are identical in their 16S rRNA and *recA* gene sequences, *B. inopinata* was the first to show multiple mutations in these genes (Scholz and Vergnaud, 2013; Scholz et al., 2016a). The comparative genomic analysis identified genomic regions that distinguished *B. inopinata* from the classic *Brucella* genomes, including one *B. inopinata* region comprising several genes coding for proteins associated with l-rhamnose utilization that have been shown to form the O-antigen component of the LPS in some bacteria (Giraud and Naismith, 2000; Wattam et al., 2012). Analysis of *Brucella* isolates from frogs and BO2 found that many of the genes required to generate the LPS in the traditional *Brucella* species (Al Dahouk et al., 2017) are lacking, but some of these strains had four genes associated with L-rhamnose utilization. Specifically, three of the frog isolates (B13-0095, 10RB9215, and 10RB9213) and the BO2 strain lacked many of the original genes but had the L-rhamnose utilization genes. Since that original analysis, these genes have been found in two additional genomes: *Brucella* sp. 141,012,304 (Eisenberg et al., 2017), which was isolated from a bluespotted ribbontail ray, and strain BO3 (Rouzic et al., 2021), a close relative of B13-0095 isolate, which was isolated from a human (Tiller et al., 2010).

In further studies addressing *B. inopinata* virulence, it was shown that *B. inopinata* is able to replicate intracellularly in macrophages and to cause disease and long-term infection in mice (Jimenez de Bagues et al., 2014; Al Dahouk et al., 2017). In contrast to classical *Brucella* species, *B. inopinata* BO1^{T} also caused death in the mouse model, which was not observed with classical *Brucella* species (Jimenez de Bagues et al., 2014).

Until now, *B. inopinata* BO1^{T} was the only existing isolate of this species. Here, we report the molecular characterization of a second *B. inopinata* strain isolated from a White's Tree Frog (*Litoria caerulea*) in Switzerland. Comparative genome analysis clearly showed that strain FO700622 is a true member of *B. inopinata* and does not represent a *B. inopinata*-like organism, as previously reported for other atypical *Brucella* strains by other authors (Fischer et al., 2012; Scholz et al., 2016a). Within the last few years, exotic frogs have been recognized as an important host for atypical *Brucella* species worldwide (Shilton et al., 2008; Eisenberg et al., 2012; Fischer et al., 2012; Whatmore et al., 2015; Soler-Lloréns et al., 2016; Scholz et al., 2016a; Al Dahouk et al., 2017; Muhldorfer et al., 2017). Since exotic frogs are found in many zoos and are kept by exotic animal enthusiasts as terrarium pets and also provide a human food source, we discuss the possible public health implications of this finding.

Materials and methods

Case description

A female, captive White's tree frog (*Litoria caerulea, synonym: Ranoidea caerulea,* natural habitat Australia and Papua New Guinea), with clinical signs of anorexia, fatigue, and a skin mass on its back suspicious of a skin abscess or neoplasia, was presented to a veterinary practice specialized in exotic animals. For 2 weeks, the frog showed progressive loss of appetite and inclined position in the water until it finally avoided swimming. After a general examination, swabs were taken from skin lesions for bacteriologic examination. As a precaution, the frog was given antibiotic treatment with Marbocyl FD (marbofloxacin 10 mg/kg, subcutaneously, daily for 10 days). The frog became increasingly lethargic and was euthanized 1 month after the first presentation and sent for autopsy.

The animal originated from a private breeder in Switzerland and was bought together with a second one of the same species in a pet shop in 2008. Both frogs were exclusively kept in a naturally decorated terrarium for nearly 10 years, from which they were rarely removed. Skin changes were noted on one frog 10 years after the initial purchase. The second frog remained clinically unremarkable and was moved to a second terrarium because of the diagnosis of a *Brucella* infection in the other frog. Both frogs were fed crickets and grasshoppers, and commercial calcium and vitamin powder was added regularly.

Bacterial cultivation and preliminary identification

Following necropsy, bacteria were cultivated from various clinical samples (liver, spleen, lung, heart, kidney, ovary, gut, skin, and, in one case, intraocular fluid) on Columbia sheep blood (COLS COL+^{2SBplus}; Oxoid, Wesel, Germany) and Endo-Agar (Becton Dickinson, Karlsruhe, Germany) at 37°C aerobically and with 5% CO_2 for up to 96 h. For bacterial growth, the tissue samples were immersed in 70% ethanol, air-dried for 5 min, and sectioned with a scalpel. The cut

surface was streaked over the agar plate. Skin swabs and fluids were applied directly to the solid culture media. Initial bacterial identification was done by MALDI-TOF analysis (Microflex LT, Bruker Daltonik GmbH, Bremen, Germany).

Subsequent phenotypic characterization of an isolate isolated from the skin (FO700622), sent to the *Brucella* Reference Laboratory of the Bundeswehr Institute of Microbiology in Munich, Germany, included growth on *Brucella* selective agar, Gram stain morphology, catalase and cytochrome oxidase activity, hydrogen sulfide (H_2S) production, and biochemical characterization using API 20NE and API ZYM (bioMerieux, Nürtingen, Germany). *Brucella*-specific serological reactions with monospecific agglutination A and M antisera (Anses, Maisons-Alfort, France) were performed as described by Alton et al. (1988).

Histo-pathology procedures

Histological examinations were performed according to a standard protocol. Samples were embedded in paraffin wax and stained with hematoxylin and eosin (HE). Periodic acidic Schiff (PAS) staining was performed for fungi and endoparasites, and a Ziehl–Neelsen stain was performed to detect acid-fast bacteria.

Molecular identification by PCR

The detection of the *Brucella*-specific genetic markers *bcsp31* and *IS711* by real-time PCR and species-differentiating multiplex PCR (Bruce-ladder) was performed as described previously (García-Yoldi et al., 2006; Scholz et al., 2008b; López-Goñi et al., 2011). The 16S rRNA and *recA* gene sequences were determined and analyzed as described previously (Scholz et al., 2008a).

Genome sequencing and assembly

High-quality genomic DNA (gDNA) was prepared for whole-genome sequencing by using the Qiagen genomic extraction kit and Qiagen Genomic-tip 20/G (Qiagen, Hilden, Germany) according to the manufacturer's recommendations. DNA concentration was determined by the use of a Qubit® 2.0 Fluorometer (Thermo Fisher Scientific) and the Qubit® dsDNA high-sensitivity assay kit (Thermo Fisher Scientific).

Next, era® XT DNA Library Preparation kit (Illumina) with an input DNA amount of 1 to 3 ng was used for library preparation. Whole-genome sequencing was performed on a MiSeq instrument (Illumina) with corresponding MiSeq Reagent Kit v3 (600 cycles; 300 bp paired end) chemistry. A total of 20,866,712 sequencing reads were generated. Trimming of raw sequencing reads and *de novo* sequence assembly was performed using the software package CLC genomics workbench together with the microbial finishing module (Qiagen, Hilden, Germany). After quality trimming (quality limit 0.05, max ambiguities 2) and adapter removal, 20,865,498 reads remained with an average read length of 288.24 nucleotides, corresponding to an average coverage of approximately 1,900 × relative to the reference genome *B. melitensis* 16M^T. Sequencing reads were down-sampled (reproducible sampling) to 5 M reads (approximately 200x coverage) and assembled *de novo* with a minimum contig length set to 500 bp. *De novo* assembly generated 40 assembled contigs (GC content 57.13%) with maximum and average lengths of 337.887 and 70.713 bp, respectively, and a genome length of 3,333,147 bp.

RAW sequencing reads were submitted to NCBI Sequence Read Archive, BioProject accession number: PRJNA906025. The assembled genome with additional information is publicly available in BV-BRC.[1]

Scaffolding

Each of the 40 contigs produced when assembling *Brucella inopinata* strain FO700662 (Acc. No. JARQXC000000000; BioSample SAMN31890425) was blasted against the *B. suis* 1330 (Acc. No. AE014291, AE014292) genome to determine the order based on this reference. Contigs were manually combined into an artificial scaffold that matched the order in that genome.

Calculating overall genome similarities

The average nucleotide identities between strain FO700622 (Acc. No. JARQXC000000000; BioSample SAMN31890425) and *B. inopinata* BO1^T (Acc. No. ADEZ00000000) as well as its closest relatives, strains BO2 (Acc. No. CP065399, CP065400) and BO3 (Acc. No. CP047232, CP047233), were determined using the online tool (OrthoANIu method; Yoon et al., 2017) form EzBioCloud available from https://www.ezbiocloud.net/tools/ani.

Genome similarities (DDH estimates) between *B. inopinata* BO1^T and strains BO2 and BO3 were also calculated using the genome-to-genome distance calculator[2] (Meier-Kolthoff et al., 2022).

In silico MLVA and MLSA

In silico MLVA-16 analysis (Le Flèche et al., 2006; Al Dahouk et al., 2007) was carried out as described previously using an in-house script (Georgi et al., 2017). Each locus was checked in respect of the expected total length, internal repeat homogeneity, or probability to get collapsed VNTRs during the assembly. The resulting MLVA-16 genotype of strain FO700622 was compared to entries of a public database consisting of more than 6,000 *Brucella* strains of each species that can be assessed online via http://microbesgenotyping.i2bc.paris-saclay.fr/. Extended multilocus sequence analysis (BruMLSA21) based on 21 different markers was carried out as described by Whatmore et al. (2016). The scheme and the database are available at PubMLST.[3] For *in silico* analysis, the scheme was downloaded from the database and a task template was created with SeqSphere+ software, v5.0.90 (Ridom GmbH, Münster, Germany). The required identity for the target scan was set to 90% with the required 99% alignment to the respective reference gene. Automatic allele calling from assembled genomes was done using SeqSphere+.

1 https://www.bv-brc.org/view/Genome/1218315.22
2 https://ggdc.dsmz.de/ggdc.php
3 https://pubmlst.org/organisms/brucella-spp

Phylogeny and comparative analyses

Thirty-three *Brucella* genomes (Supplementary Table 1) were used in a comparison. All genomes, including the new isolate FO700662, were annotated in PATRIC, now known as BV-BRC, the Bacterial and Viral Bioinformatics Resource Center (Wattam et al., 2017, 2018; Davis et al., 2020; Olson et al., 2022) using the RASTtk pipeline (Brettin et al., 2015) which includes annotated genes being automatically assigned into two kmer-based protein families that are genus-specific (PLFams), or are global spanning the genus boundary (PGFams; Davis et al., 2016). The genome of FO700662 is available in BV-BRC under the identifier 1218315.22. Five *Ochrobactrum* reference genomes were also included in the phylogeny and were used to verify *Brucella*-specific genes (Supplementary Table 2).

The phylogenetic trees were generated using the Codon Trees pipeline at BV-BRC. Single-copy PGFams present in each genome were identified, and the protein (amino acid) and gene (nucleotide) sequences were used for each of the selected genes. The tree was generated using MUSCLE (Edgar, 2004; amino acid alignment), Biopython (Cock et al., 2009; codon alignment), and RaxML (Stamatakis et al., 2008; Stamatakis, 2014) for tree generation using the GTRGAMMA model for nucleotides and the LG model for amino acids. Support values were generated using 100 rounds of the "Rapid" bootstrapping option (Stamatakis et al., 2008) of RaxML. The resulting Newick file was visualized using FigTree (Rambaut, 2006).

Both the 40 contigs and the reference-based scaffolded FO70062 genome were compared to the *B. suis* 1330 genome using the Proteome Comparison tool to identify areas within the genomes that were not shared with the comparison genome(s). In addition, protein families were arranged based on the order that they occurred in specific genomes (*B. suis* 1330, *Brucella* sp. 09RB8471, and *Brucella* sp. FO700662) to look for unique regions or regions of potential lateral transfer in the amphibian isolates using the Protein Family Sorter tool (Wattam et al., 2018). Once a potential genomic island was identified, the region of the genome was examined in JBrowse (Skinner et al., 2009), with the flanking regions examined for tRNA genes. Flanking regions were confirmed using the Proteome Comparison tool (Overbeek et al., 2014). Each potential island was visualized in BV-BRC's Compare Region Viewer (Overbeek et al., 2014) to look for conservation of the gene neighborhood across genomes that had a similar region, and the presence or absence in specific genomes was confirmed by BLASTN of the regional sequence against the target genomes with an expected value of 0.0001, sc_match of 1, sc_mismatch of −2, gap_open of 0, gap_extend of 0, and filter of L;m; (Boratyn et al., 2013). Each region was also searched against a database of plasmid genomes in BV-BRC (Wattam et al., 2017) and also against the reference and representative genomes in the genus *Ochrobactrum* to confirm whether novel regions were conserved from a recent ancestor. Genes in these regions that were not annotated as hypothetical were examined to see whether they were present in KEGG pathways (Kanehisa et al., 2023) and subsystems (Overbeek et al., 2005) or were described in the published literature.

Core-genome-based MLST

A previously developed core-genome-based MLST (cgMLST) assay (Janowicz et al., 2018) using SeqSphere+ software, v5.0.90 (Ridom GmbH, Münster, Germany) was used to determine the genetic relationship of strain FO700622 and BO1^T. The cgMLST scheme covers 2,704 genes with a total of 2.441.649 out of 3.294.931 bp (74%) of the reference strain *B. melitensis* 16M^T (NC_003317.1; NC_003318.1) and can be freely downloaded from the cgMLST Nomenclature Server[4] or within the software. The assay uses a required identity for the target scan of 90% with a required 100% alignment to the respective reference genes. For cgMLST analysis, the *de novo* assembly generated by the CLC Genomic Workbench was imported as a FASTA file into SeqSphere+. The type strains of all currently known *Brucella* species as well as a set of biovar reference strains were included in the analysis. Genome accession numbers are given in Supplementary Table 1.

Results

Bacterial cultivation and identification

After 48 h of culture, an almost uniformly mixed bacterial flora of different non-fermenters was observed. In addition, *Brucella*-suspicious colonies were isolated in high grade from the skin but also in small numbers from all clinical specimens tested. Bacteria were positive for cytochrome oxidase and catalase with a rapid urease reaction (5 min). No hemolysis was observed. Bacterial identification using MALDI-TOF revealed *Ochrobactrum* sp. with a high identification score of 2.2. However, with the knowledge of the recent emergence of atypical *Brucella* in exotic frogs resembling *Ochrobactrum*, one sample (FO700622) was sent to the Institute of Microbiology, Munich, for further clarification. Strain FO700622 was highly similar to *B. inopinata* BO1^T (De et al., 2008; Scholz et al., 2016a) in all phenotypic reactions. Similar to *B. inopinata* BO1^T, rapid growth was observed on all media tested in a temperature range of 28°C–40°C. On *Brucella* agar (Merck, Darmstadt), growth became visible within 10 h of incubation at 37°C with or without supplementary CO_2. Single colonies of 1–2 mm were formed within 24 –48 h. Weak agglutination was observed with monospecific anti-M serum up to a dilution of 1:40 but not with anti-A serum. Production of H_2S and Voges–Proskauer reaction is positive. Strains were negative for hydrolysis of esculin, gelatin liquefaction, production of indole, and citrate utilization. Strains tested positive (API ZYM) for acid phosphatase, alkaline phosphatase, trypsin, leucine arylamidase, and naphthol-AS-BI-phosphohydrolase. Strains were negative (API ZYM) for esterase, esterase lipase, lipase, valine arylamidase, cystine arylamidase, α-chymotrypsin, α- and β-galactosidase, β-glucuronidase, α- and β-glucosidase, N-acetyl-β-glucosaminidase, α-mannosidase, and α-fucosidase. Strains tested positive (API 20NE) for d-glucose, maltose, l-arabinose, d-mannose, N-acetylglucosamine, and adipic acid and negative for d-mannitol, citric acid, gluconate, capric acid, malic acid, and phenylacetic acid. In API 20E, Strains tested positive for fermentation of l-arabinose.

Pathological findings

The entire body of the dead White's tree frog (*Litoria caerulea*), with a body size of 11.8 cm and a body weight of 112 g, was submitted

4 https://www.cgmlst.org/ncs

for pathological examination. Gross examination showed a dorsal mass of 3.0 × 3.0 × 1.3 cm cranial to the cloaca (Figure 1A). A 0.6 cm large excoriation was observed on the right front limb. Both thighs were diffusely moderately swollen, and there was a 0.3 cm large excoriation on the right thigh (Figure 1B). The internal organs were macroscopically unremarkable as far as could be evaluated due to their fixation in formalin.

Histopathologically, the skin lesions on the thighs and the mass on the back showed moderate epidermal hyperplasia with multiple ulcerations (Supplementary Figure 1).

A severe multifocal to coalescing granulomatous inflammation with moderate numbers of intralesional acid-fast, rod-shaped bacteria in the macrophages and freely located were seen in the dermis and the underlying musculature (Figure 2).

The musculature contained moderate numbers of cysts of cestodes. The morphology of the parasite was indicative of the sparganum of *Spirometra erinacei* (Supplementary Figure 2). Other organs examined were morphologically unremarkable.

PCR and *in silico* analysis

Strain FO700622, received as *Ochrobactrum* sp. as identified by MALDI-TOF analysis, was positive in PCR for the *Brucella*-specific targets *IS711* and *bcsp*31, suggesting its affiliation to the genus *Brucella* but not to *Ochrobactrum*. The species-differentiating Bruce-ladder-multiplex-PCR revealed the *B. inopinata* BO1^T-specific banding pattern with fragment sizes of 152, 272, 450, 587, 794, and 1,682 base pairs, indicating its affiliation or close relationship to this species. This finding was remarkable because up to that date, all *Brucella* isolates from exotic frogs had a unique banding pattern, different from all other species, consisting of five fragments with sizes of 152, 272, 450, 587, and 794 bp (Eisenberg et al., 2012). We, therefore, genome-sequenced strain FO700622 for further molecular characterization. The *in silico* generated MLST-21 profile of strain FO700622 was identical to the specific profile of *B. inopinata* BO1^T (sequence type 69), confirming that strain FO700622 belongs to this species. In contrast, the profile of the to date closest related strain BO2 differed in all of the given markers (*mviM*-negative, no assigned ST).

With the exception of one VNTR marker (bruce 18), the MLVA profiles of *B. inopinata* BO1^T and strain FO700622 were identical, whereas the closest relative, BO2, differed in six of the sixteen markers. MLVA-16 profiles were as follows: *B. inopinata* BO1^T (2, 5, 9, 13, 3, 2, 5, 4, 8, 40,0, 10, 0 3, 3, and 0); *B. inopinata* FO700662 (2, 5, 9, 13, 3, 2, 5, 4, 9, 40, 0, 10, 0, 3, 3, and 0), and *Brucella* sp. BO2 (1, 5, 3, 13, 4, 2, 5, 3, 12, 37, 8, 19, 5, 3, 5, and 10). When calculating the genome-to-genome distance, the DNA–DNA hybridization (DDH) estimate between strains BO1^T and FO700662 was 99.4%, indicating that these genomes are highly similar. In comparison, the DDH estimate between strain BO1^T and BO2 was 85.8% and 84.9% with strain BO3. This was also reflected in the ANI values obtained (BO1^T/FO700662: 99.86; BO1^T/BO2: 98.31; BO1^T/BO3: 98.25) with genome coverages of 75.14%/74.35, 70.76%/68.97, and 64.89%/64.11%, respectively.

Phylogeny

The phylogenetic tree was built using the Codon Trees pipeline at PATRIC. Both the amino acid and nucleic acid sequences from 901 single-copy orthologous genes included 260,286 amino acids and 780,858 nucleotides that were concatenated together in an alignment and used to generate the tree (Figure 3).

The *B. inopinata* BO1^T strain (De et al., 2008), an isolate from human infection, was closest to the FO700622 strain, with a 100% support value. The closest strain to these two genomes was another human isolate, the BO2 strain (Tiller et al., 2010). The branch containing FO700622 and the two human isolates is found on the same branch as *Brucella* strains that have been recently isolated from the Pacman frog (strain B13-0095) and BO3, a human isolate (Rouzic et al., 2021). The next closest clade includes an isolate from the bluespotted ribbon tail ray (strain 141,012,304; Eisenberg et al., 2017), other African bullfrog isolates (strains 10RB9210, 09RB8471, 09RB8918, and 09RB8913; Al Dahouk et al., 2017), an isolate from a chameleon (strain 191,011,898; Eisenberg et al., 2020), and three isolates from humans in Australia (strains 6,810, 2,280, and 458).

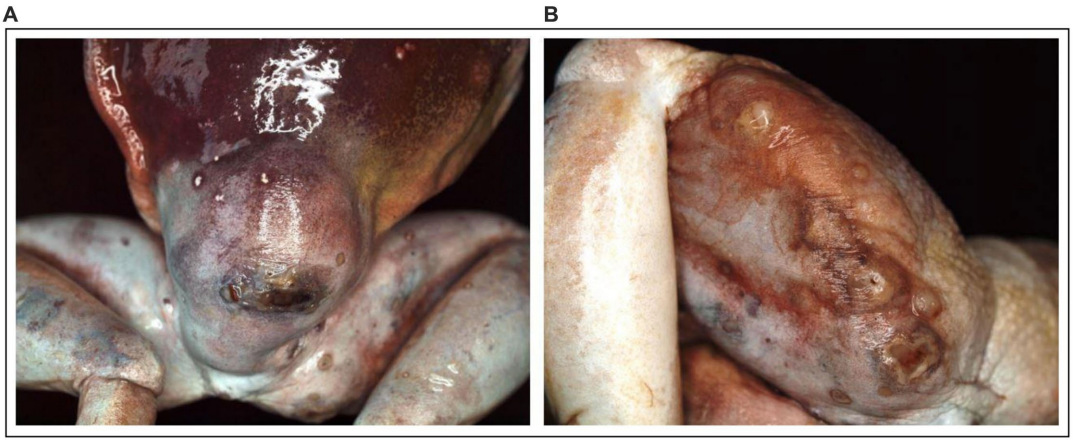

FIGURE 1
(A) Dermal granulomatous inflammation with excoriations of the skin measuring 3.0 × 3.0 × 1.3cm from a 13-year-old White's tree frog after fixation.
(B) Diffuse swelling of the thigh with an excoriation on a 13-year-old White's tree frog after fixation.

Genetic analysis does not suggest a clear distinction between *Brucella* strains isolated from warm- or cold-blooded hosts as isolates from cold-blooded hosts appear in both ancestral and classical clades of the phylogenetic tree. The *Brucella microti*-like genome was isolated from a *Pelophylax ridibundus* in a domestic frog farm in France (Jay et al., 2018) and was found within the classical clade (Figure 3). The addition of *Ochrobactrum* genomes (Supplementary Figure 3) shows that the root of the *Brucella* tree occurs in the middle of the atypical genomes and is not clear between the classical and atypical strains.

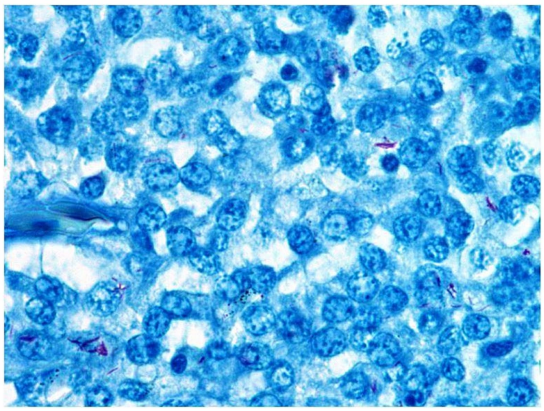

FIGURE 2
Granulomatous inflammation composed of macrophages and single lymphocytes. Moderate numbers of intralesional acid-fast, rod-shaped bacteria phagocytosed by macrophages or freely located (Ziehl–Neelsen, 1,000x magnification).

Core-genome-based MLST

The cgMLST assay was originally optimized for *B. melitensis*; however, the high genetic similarity of all *Brucella* species, including atypical *Brucella*, allows accurate typing of atypical *Brucella*. Only 10% to 15% of the 2,704 target genes cannot be used, thus, there is still an average of 2,300 genes available for cgMLST analysis.

The minimum spanning tree (MST) was generated with the SeqShere+ software. The genomes of genetically atypical *Brucella* species are well separated from the classic *Brucella* species by 1,969 allelic differences with *B. ovis* lying on the path between the two groups (Supplementary Figure 4). The distances among most genetically classical species ranged from 730 (*B. pinnipedialis* / *B. ceti*) to 1,719 alleles (*B. pinnipedialis* / *B. melitensis*). The close genetic relationship between *B. canis* and *B. suis* bv 4 was reflected by a distance of only 308 alleles (lower left). Significantly larger distances (>2,000 alleles) were detected in epidemiologically unrelated isolates of the atypical group, indicating higher genetic diversity in this population compared to the classical *Brucella* species. Only epidemiologically related frog isolates were clustered together with few allelic differences. The distance of 36 alleles between two strains of Australian rodents (NF2651 and 83/13) supports a possible epidemiological link. The two *B. vulpis* strains (F60H and F965) isolated from two different red foxes in Lower Austria differed in only 15 alleles. Only 173 different alleles were detected between *B. inopinata* BO1^{T} and *B. inopinata* strain FO700662, confirming their very close genetic relationship. Interestingly, strain BO2, which until then was considered the closest relative of strain BO1^{T}, differed in 2,046 alleles in a head-to-head comparison (Figure 4). A similarly large distance of 1,948

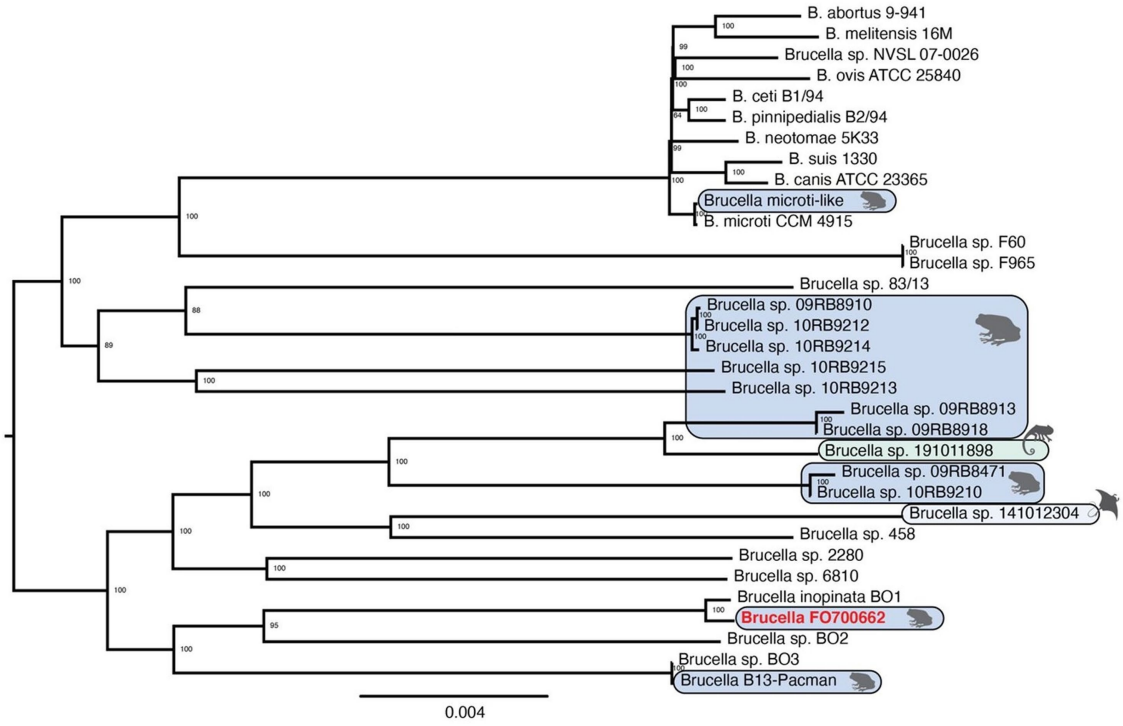

FIGURE 3
Midpoint rooted, maximum likelihood tree for 33 *Brucella* genomes.

alleles was observed between strains BO2 and B130095/BO3. It is noteworthy that strain BO3, a human isolate, differed in only 11 alleles in cgMLST analysis from strain B13-0095 isolated from a Pacman frog. An allelic distance matrix of strains FO700662, BO1^{T}, BO2, BO3, and B130095/BO3 is given in Supplementary Table 3.

Distinctive regions

Seventeen regions of interest were identified when all strains were compared to FO700662 (Table 1). A complete list of the genes in these regions is available (Supplementary Table 4). A BLAST analysis of the genomic sequences of each of these regions showed that they were not present in the genomes associated with the "classical *Brucella*" strains and also were not universally shared across all of the strains found in the non-classical *Brucella* strains that are found in the lower half of the phylogenetic tree (Table 2; Figure 3).

The combined regions include nine tRNA genes and 264 protein-coding sequences, 139 (52.6%) of which are annotated as hypothetical. Seven of the regions (Regions 1, 3, 4, 6, 10, 12, and 14) have at least one phage gene annotated within it. Two of the regions (Regions 7 and 14) were unique to FO700662, but the others are either narrowly (Regions 4, 5, 6, 10, and 12) or widely (Regions 1, 13, and 17) shared across the non-classical strains. Many of these regions (1, 4, 6, 7, 11, 12, 14, and 15) are flanked by tRNA genes, which are known to be associated with horizontal gene transfer (Hacker and Kaper, 2000; Ochman et al., 2000). Other indications of horizontal transfer included the presence of genes annotated as mobile element proteins or transposases, and several of the regions have one or more genes that are identified as such (Regions 1, 2, 4, 6, 7, 10, 12, 13, and 16). Each region was compared to the plasmid database using BLASTN in BV-BRC (Davis et al., 2020). Five regions (Region 8, 9, 11, 16, and 17) had more than a 10% query coverage match against plasmid genomes in that database (Supplementary Tables 4, 5), indicating that they could have been incorporated by lateral transfer. These regions were all on the second chromosome.

BLASTN analysis of the nucleotide sequences of the regions was compared to the five *Ochrobactrum* representative genomes. Region 5 had a query coverage of 87% query coverage to *O. rhizosphaerae* SJY1, and region 14 had 67% to *O. intermedium* LMG 3301, indicating that these two regions were ancestral and did not enter *Brucella* by lateral, or horizontal transfer. Region 11 had 38% query coverage when compared to *O. anthropi* ATCC 49188, but this was one of the plasmids in this genome.

While most of the 272 genes found in these 17 regions are annotated as hypothetical (Supplementary Table 4), several regions contain some notable genes.

Regions 1, 3, 4, 6, 10, 12, and 14 all have bacteriophage genes annotated, with some regions (3, 6, and 14) having a number of these genes present.

All the genes in Region 9 are involved in rhamnose metabolism, with some being potentially active in the KEGG Fructose and Mannose pathway. Four of these genes are predicted to work as a rhamnose transporter (Richardson and Oresnik, 2007). This region had weak homology when compared to *O. intermedium* LMG 3301 (43%) and also in a plasmid found in *Rhizobium topicic* (39%). An examination of the genes found in this region showed that the genes and their orientation were strongly conserved in these particular genomes (Figure 5), with differentiation in the flanking regions. This was the most strongly conserved of the regions with non-*Brucella* genomes.

Region 11 has a toxin/antitoxin HigB/HigA system. These types of systems have been found in many pathogens (Wood and Wood, 2016). Region 16 has three genes (proVWX) that have been identified as the *proU* operon in other bacteria, which encodes a binding

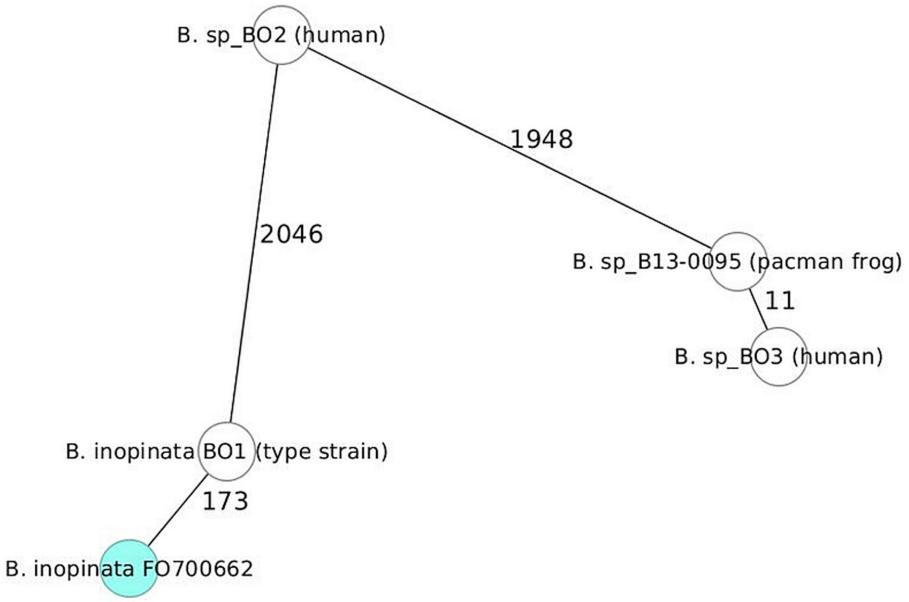

FIGURE 4
cgMLST minimum spanning tree (MST). Direct comparison of strains BO1^{T}, BO2, FO700622, BO3, and B13-0095. Allele distances are shown in numbers.

protein-dependent transport system that is essential for the uptake of osmoprotectants such as glycine betaine and is known to be upregulated in response to osmotic stress (Lucht and Bremer, 1994).

TABLE 1 Genomic regions unique to FO700662 when compared to classical *Brucella* strains.

Region	Contig	Start	Stop	Size	tRNA	Genes
One	Contig 20	193,697	199,385	5,688	Yes	10
Two	Contig 39	247	18,081	17,834	No	19
Three	Contig 16	18,004	21,422	3,418	No	7
Four	Contig 12	109,977	113,564	3,587	Yes	6
Five	Contig 2	196,970	200,851	3,881	No	6
Six	Contig 7	211,494	224,602	13,108	Yes	15
Seven	Contig 2	52	12,378	12,326	Yes	16
	Contig 37	41,518	53,206	11,688	Yes	11
Eight	Contig 15	65,238	72,094	6,856	No	11
Nine	Contig 28	253	26,954	10,795	No	9
Ten	Contig 36	601,007	628,634	26,701	No	26
Eleven	Contig 36	89,967	91,628	1,661	Yes	5
Twelve	Contig 22	123,522	127,301	3,779	Yes	8
Thirteen	Contig 9	205,073	236,210	31,137	No	20
Fourteen	Contig 9	236,212	270,742	34,530	Yes	52
Fifteen	Contig 4	52	16,348	16,296	Yes	8
Sixteen	Contig 4	32,067	63,489	31,422	No	31
Seventeen	Contig 26	36,035	45,309	9,274	No	10

A close examination of the genes that are known or predicted to be involved in lipopolysaccharide (LPS) production was conducted. This included the *wbk* region, *wboA* and *wboB*, and the four genes in BO2 (Wattam et al., 2012) that other bacteria use for making a rhamnose-based O-antigen (Table 3).

Both BO1^T and FO70062 share the 13 genes in the *wbk* region that are essential for lipopolysaccharide (LPS) synthesis (Godfroid et al., 2000; Gonzalez et al., 2008; Al Dahouk et al., 2017), as well as *wboAB*. Both strains are missing the rhamnose genes first identified in BO2. An expanded analysis, using the protein sequences for the BO2 rhamnose genes and WboAB and the Wbk proteins from FO700662, showed that other than BO2, only six of the 19 non-classical strains have the four rhamnose genes (10RB9215, 10RB9213, 1412304, and BO3 and B13 Pacman). WbkF and WbkD are shared across all strains. The other genes in the Wbk region are absent from most strains, except for WbkE, ManA, ManC, and ManB, which are strains 2280 and 6810. Strain 6810 is also a pseudogene that matches WbkA.

Discussion

While our understanding of the *Brucella* genus remained unchanged for decades in the past, several new *Brucella* species and strains of human origin and from various new animal hosts have been described more recently (Godfroid et al., 2005; Foster et al., 2007; Scholz et al., 2008b; Whatmore et al., 2014; Scholz et al., 2016b; Eisenberg et al., 2017). The isolation from cold-blooded hosts, particularly amphibians but also from fish and reptiles, has greatly expanded the host range of this medically

TABLE 2 Genomic regions unique to FO700662 with more than 50% query coverage in the non-classical *Brucella* strains.

Strain	Host	1	2	3	4	5	6	7	8	9	10	11	12	13	14	15	16	17
09RB8910	Amphibian													78.1				
10RB9212	Amphibian				56.7									78.1				
10RB9214	Amphibian													78.1				
10RB9215	Amphibian									100				81.9				100
10RB9213	Amphibian									100				81.8				100
09RB8913	Amphibian	85										100		52.8				
09RB8918	Amphibian	85										100		52.8				
191,011,898	Reptile	85										100		78.1				100
09RB8471	Amphibian	86.5			90.1									81.8				100
10RB9210	Amphibian	86.5			60.7									81.8				100
141,012,304	Ray	69.8								100		90.3		52.8				100
458	Human		100						100	100				88.6		50.4		100
2,280	Human	85.6	100		51.3				100	51		77.2		88.6		50.4	100	
6,810	Human	97.7		70.1	60.8				100			77.2						
BO1	Human	100	100	100		66.2	96.9		100	100	65.7	100	100	86.3		68	50.4	100
FO700662	Amphibian	100	100	100	100	100	100	100	100	100	100	100	100	100	100	100	100	100
BO2	Human	100	100		59.1				100	100				88.6		90.2	90.7	100
BO3	Human	100								100		77.2		78.2				
B13-Pacman	Amphibian	100								100		77.2		78.2				

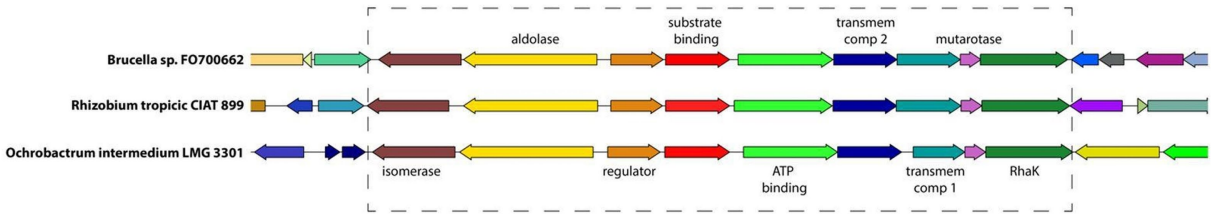

FIGURE 5
Genes from region nine, depicted in the box, showing conservation of gene length and orientation in the FO700662 compared to the *Rhizobium* plasmid and *Ochrobactrum* contig in which they were also found.

important genus. Exotic frogs, in particular, have become an important newly recognized host of *Brucella* in recent years (Shilton et al., 2008; Eisenberg et al., 2012; Fischer et al., 2012; Soler-Lloréns et al., 2016; Muhldorfer et al., 2017). Isolation from different continents indicates a worldwide distribution of atypical *Brucella* in different exotic frog species (Scholz et al., 2016a). The majority of infections induce severe clinical signs in the frogs and frequently lead to death (Muhldorfer et al., 2017). However, it is currently unknown whether the mucous skin of frogs forms a natural reservoir for *Brucella* and whether the disease only occurs after trauma or stress conditions. The infection could also occur through contaminated food or an unknown reservoir in soil or water. Isolates from exotic frogs belong to the so-called atypical *Brucella* which are phenotypically close to *Ochrobactrum* spp., a soil-associated facultative human pathogen, but genetically more closely related to the *Brucella* genus (Lebuhn et al., 2000; Elsaghir and James, 2003; Scholz et al., 2008a). In-depth molecular-biological analyses at the isolate level have shown that brucellae from exotic frogs, in contrast to classic brucellae, have a markedly higher level of genetic diversity and possess genes on their chromosomes from other soil-associated bacteria, indicating horizontal gene transfer (Wattam et al., 2009; Occhialini et al., 2022).

Although most atypical brucellae are currently being isolated from amphibian hosts, the first genetically (and phenotypically) atypical *Brucella* strain BO1, later named *B. inopinata*, was not isolated from a frog but unexpectedly from a 71-year-old woman in 2008 with an endogenous breast implant infection (De et al., 2008). At this point, however, the source of infection was unknown and exotic frogs had not yet been recognized as hosts for atypical *Brucella*. The first isolation of atypical brucellae from wild-caught African bullfrogs (*Pyxicephalus edulis*) from Tanzania was published in 2012 (Eisenberg et al., 2012). Eight-locus MLSA (Whatmore et al., 2007) placed the isolates close to *B. inopinata* BO1^T and other atypical isolates from Australian rodents (Eisenberg et al., 2012) forming a new branch distinct from the classic *Brucella* species but clearly related to *Brucella* and more distantly related to *Ochrobactrum*. To date, the number of atypical brucellae (sometimes referred to as "non-core" brucellae) has increased significantly due to the description of various new atypical isolates from different sources (Al Dahouk et al., 2017; Muhldorfer et al., 2017; Whatmore and Foster, 2021). Because *B. inopinata* was the first atypical species described (Scholz et al., 2010) and was still the only validly published species among the atypical brucellae, members of the atypical clade are often referred to as "*B. inopinata*-like." However, as shown in the cgMLST analysis targeting 2,704 genes (Figure 4; Supplementary Figure 4), even to date most closely related atypical strain BO2, also a human clinical isolate, differs in 2,046 alleles from *B. inopinata* BO1^T, while the strain analyzed in this study (FO700622) differs from *B. inopinata* BO1^T in only 173 alleles. This close and unexpected proximity of *B. inopinata* BO1^T and strain FO700622 prompted us to perform a more detailed comparative genomic analysis of both strains and other atypical members and to investigate whether strain FO700622 is a true member of *B. inopinata*. Since strain BO2 was identified as the genetically most closely related strain compared to BO1^T in several previous studies (Wattam et al., 2012; Al Dahouk et al., 2017), the distinguishing features of both strains were investigated in detail.

Strain FO700622 showed the specific banding pattern of *B. inopinata* BO1^T in the species-differentiating Bruce-Leader PCR. Both MLSA and *in silico* MLVA also confirmed strain FO700622 as a true member of *B. inopinata* with an identical MLSA profile and only one repeat difference in one of the 16 VNTR markers. In contrast, strain BO2 differed significantly from strain BO1^T and differed in all MLST markers and six VNTR markers. The calculated genome-to-genome distance of 99.4% between strains BO1^T and FO700622 showed that both genomes are highly similar while comparing strain BO1^T with BO2 a significantly lower value of 85.8% was obtained.

The phylogenetic tree (Figure 3) clearly shows that FO700622 and *B. inopinata* are most closely related. Strain BO2 is close to both of these strains, but it is also distinctly different. Most notably, it is missing the *wboAB* and the genes in the Wbk region that are essential in producing the O-antigen and, in the same location, has four genes that are involved in the formation of the O-antigen component of the LPS in many gram-negative bacteria (Giraud and Naismith, 2000; Wattam et al., 2012).

While the tree does show that the previously known "classical" strains are united in a clade, the genomes isolated from cold-blooded hosts are not. The *Brucella microti*-like strain is comfortably located within the classic clade, and it was isolated from a frog. When *Ochrobactrum* genomes were included in the phylogeny (Supplementary Figure 3), the root of the *Brucella* genomes is found somewhere within the middle of the atypical genomes. This suggests that early radiation of the *Brucella* had several successful lines, with one particular line being very successful and evolving into the ancestral genome that is the progenitor of the classic clade.

The identification of strain FO700622 as a second *B. inopinata* isolate and its isolation from an exotic frog raises the question of

TABLE 3 BLAST results showing genes with more than 50% identity to LPS amino acid sequences.

Strain	Host	Rhamnose genes				Wbo genes		Wbk genes											
		rfbD	rfbB	rfbC	rfbA	wboB	wboA	wbkE	manA	manC	manB	wbkA	gmd	per	wzm	wzt	wbkB	wbkC	wbkF	wbkD
09RB8910	Amphibian																		97	100
10RB9212	Amphibian																		97	100
10RB9214	Amphibian																		97	100
10RB9215	Amphibian	94	98	98	98														98	99
10RB9213	Amphibian	94	98	98	97														97	100
09RB8913	Amphibian																		96	100
09RB8918	Amphibian																		96	100
191,011,898	Reptile																		96	100
09RB8471	Human																		98	99
10RB9210	Human																		98	99
141,012,304	Ray	96	98	98	99														98	100
458	Human	95	99	99	98														98	99
2,280	Human							99	98	99	92								97	99
6,810	Human							99	99	99	93	pseudo							100	100
BO1	Human					100	100	100	100	100	100	100	100	100	100	100	100	99	100	100
FO700662	Amphibian					100	100	100	100	100	100	100	100	100	100	100	100	100	100	100
BO2	Human	100	100	100	100														97	99
BO3	Human	97	98	98	98														98	99
B13-Pacman	Amphibian	97	98	98	99														98	99

10.3389/fmicb.2023.1173252

whether amphibians may play a role as a potential source of human infection. This could apply to people who keep exotic frogs as pets in a terrarium, or to frogs that are produced for human consumption. Indeed, only recently, another member of the biochemically atypical *Brucella*, *B. microti*, was isolated in large quantities from frogs bred for human consumption at a French frog farm (Jay et al., 2020). While most atypical *Brucella* are not risk classified, *B. inopinata* has been classified in risk group 3. It needs to be clarified how the natural occurrence of a risk group 3 pathogen in exotic frogs kept as pets or housed in zoos is to be assessed.

However, it should be noted that human infections with atypical *Brucella* are extremely rare with only four cases reported to date (Tiller et al., 2010; Soler-Lloréns et al., 2016; Rouzic et al., 2021). In 2010, strain BO2 was isolated from a patient in Australia with severe pneumonia (Tiller et al., 2010), and more recently in 2019, strain BO3 almost identical to strain B13-0095 isolated from a Pacman frog in Texas, United States, was isolated from a French patient with typical signs of severe brucellosis. The patient infected with strain BO3 had close contact with exotic animals including Pacman frogs (Rouzic et al., 2021). In cgMLST analysis (Figure 4; Supplementary Figure 4), strains BO3 and B13-0095 were nearly indistinguishable with a difference of only 11 alleles, which is even closer than the relatedness of strains BO1^T and FO700662. This is remarkable in view of the overall higher genetic diversity among the atypical *Brucella* and no obvious epidemiological connection. Three other clinical isolates of *B.* sp. 2,280 (biosample: SAMN12091575), *B.* sp. 6,810 (Biosample: SAMN15962648), and *B.* sp. 458 (BioSample: SAMN18395631) were recently isolated from human patients in Australia, with no further information available. However, in Australia, atypical *Brucella* have been isolated from rodents and repeatedly from exotic frogs (Tiller et al., 2010; Latheef et al., 2020).

The worldwide occurrence and high genetic diversity of atypical *Brucella* isolated from various exotic frog species indicate that amphibians may play an important role as natural reservoirs and potential vectors of "atypical" *Brucella* species and also may function as a source for human infections. As pointed out previously (Scholz et al., 2016a), we speculate that atypical *Brucella* may have a reservoir in the soil rhizosphere or in yet unknown non-vertebrate hosts occasionally colonizing the skin of amphibians as opportunistic pathogens. Stressful conditions during transport, especially when importing wild-caught animals or after skin injuries that may occur during quarantine or improper animal husbandry, might trigger local and systemic infection.

Data availability statement

The datasets presented in this study can be found in online repositories. The names of the repository/repositories and accession number(s) can be found in the article/Supplementary material.

Ethics statement

Ethical review and approval was not required for the animal study because bacterial isolation from the frog was done as routine diagnostics in a veterinary laboratory. Written informed consent was obtained from the owners for the participation of their animals in this study.

Author contributions

HS and AW conceived and designed the experiments related to molecular strain characterization, analyzed all molecular data, and wrote the original manuscript. SA contributed to conception and design of the study and wrote sections of the manuscript. KH and PS carried out all experiments regarding dissection of the frog, including histo-pathological examinations and initial isolation of bacteria and also wrote the accompanying text in the manuscript. DG-D was involved in the initial strain isolation and further characterization. All authors contributed to the article and approved the submitted version.

Funding

AW was funded in part by Federal funds from the National Institute of Allergy and Infectious Diseases, National Institutes of Health, Department of Health and Human Services, under contract no. 75N93019C0007. The project on which this report is based was partially funded by the Robert Koch Institute with funds from the Federal Ministry of Health under funding number 1369-448.

Acknowledgments

The authors thank Gabriele Echle from the Bundeswehr Institute of Microbiology, Munich, Germany, for excellent technical assistance.

Conflict of interest

KH and DG-D were employed by LABOklin GmbH and Co KG, Bad Kissingen, Germany.

The remaining authors declare that the research was conducted in the absence of any commercial or financial relationships that could be construed as a potential conflict of interest.

Publisher's note

Supplementary material

The Supplementary material for this article can be found online at: https://www.frontiersin.org/articles/10.3389/fmicb.2023.1173252/full#supplementary-material

References

Al Dahouk, S., Kohler, S., Occhialini, A., Jimenez De Bagues, M. P., Hammerl, J. A., Eisenberg, T., et al. (2017). Brucella spp. of amphibians comprise genomically diverse motile strains competent for replication in macrophages and survival in mammalian hosts. *Sci. Rep.* 7:44420. doi: 10.1038/srep44420

Al Dahouk, S., Le Flèche, P., Nöckler, K., Jacques, I., Grayon, M., Scholz, H. C., et al. (2007). Evaluation of Brucella MLVA typing for human brucellosis. *J. Microbiol. Methods* 69, 137–145. doi: 10.1016/j.mimet.2006.12.015

Alton, G. G., Jones, L. M., Angus, R., Verger, J., Plackett, P., Corner, L., et al. (1988). *Techniques for the brucellosis laboratory*. France: Institut National de la recherche Agronomique (INRA).

Ashford, R. T., Muchowski, J., Koylass, M., Scholz, H. C., and Whatmore, A. M. (2020). Application of whole genome sequencing and Pan-family multi-locus sequence analysis to characterize relationships within the family Brucellaceae. *Front. Microbiol.* 11:1329. doi: 10.3389/fmicb.2020.01329

Boratyn, G. M., Camacho, C., Cooper, P. S., Coulouris, G., Fong, A., Ma, N., et al. (2013). BLAST: a more efficient report with usability improvements. *Nucleic Acids Symp. Ser.* 41, W29–W33. doi: 10.1093/nar/gkt282

Brettin, T., Davis, J. J., Disz, T., Edwards, R. A., Gerdes, S., Olsen, G. J., et al. (2015). RASTtk: a modular and extensible implementation of the RAST algorithm for building custom annotation pipelines and annotating batches of genomes. *Sci. Rep.* 5, 1–6. doi: 10.1038/srep08365

Cock, P. J., Antao, T., Chang, J. T., Chapman, B. A., Cox, C. J., Dalke, A., et al. (2009). Biopython: freely available Python tools for computational molecular biology and bioinformatics. *Bioinformatics* 25, 1422–1423. doi: 10.1093/bioinformatics/btp163

Davis, J. J., Gerdes, S., Olsen, G. J., Olson, R., Pusch, G. D., Shukla, M., et al. (2016). PATtyFams: protein families for the microbial genomes in the PATRIC database. *Front. Microbiol.* 7:118. doi: 10.3389/fmicb.2016.00118

Davis, J. J., Wattam, A. R., Aziz, R. K., Brettin, T., Butler, R., Butler, R. M., et al. (2020). The PATRIC bioinformatics resource center: expanding data and analysis capabilities. *Nucleic Acids Res.* 48, D606–D612. doi: 10.1093/nar/gkz943

De, B. K., Stauffer, L., Koylass, M. S., Sharp, S. E., Gee, J. E., Helsel, L. O., et al. (2008). Novel Brucella strain (BO1) associated with a prosthetic breast implant infection. *J. Clin. Microbiol.* 46, 43–49. doi: 10.1128/JCM.01494-07

Edgar, R. C. (2004). MUSCLE: multiple sequence alignment with high accuracy and high throughput. *Nucleic Acids Res.* 32, 1792–1797. doi: 10.1093/nar/gkh340

Eisenberg, T., Hamann, H. P., Kaim, U., Schlez, K., Seeger, H., Schauerte, N., et al. (2012). Isolation of potentially novel Brucella spp. from frogs. *Appl. Environ. Microbiol.* 78, 3753–3755. doi: 10.1128/AEM.07509-11

Eisenberg, T., Risse, K., Schauerte, N., Geiger, C., Blom, J., and Scholz, H. C. (2017). Isolation of a novel 'atypical' Brucella strain from a bluespotted ribbontail ray (*Taeniura lymma*). *Antonie Van Leeuwenhoek* 110, 221–234. doi: 10.1007/s10482-016-0792-4

Eisenberg, T., Schlez, K., Fawzy, A., Volker, I., Hechinger, S., Curic, M., et al. (2020). Expanding the host range: infection of a reptilian host (*Furcifer pardalis*) by an atypical Brucella strain. *Antonie Van Leeuwenhoek* 113, 1531–1537. doi: 10.1007/s10482-020-01448-9

Elsaghir, A. A. F., and James, E. A. (2003). Misidentification of *Brucella melitensis* as *Ochrobactrum anthropi* by API 20NE. *J. Med. Microbiol.* 52, 441–442. doi: 10.1099/jmm.0.05153-0

Fischer, D., Lorenz, N., Heuser, W., Kämpfer, P., Scholz, H. C., and Lierz, M. (2012). Abscesses associated with a *Brucella inopinata*–like bacterium in a big-eyed tree frog (*Leptopelis vermiculatus*). *J. Zoo Wildl. Med.* 43, 625–628. doi: 10.1638/2011-0005R2.1

Foster, G., Osterman, B. S., Godfroid, J., Jacques, I., and Cloeckaert, A. (2007). *Brucella ceti* sp. nov. and *Brucella pinnipedialis* sp. nov. for Brucella strains with cetaceans and seals as their preferred hosts. *Int. J. Syst. Evol. Microbiol.* 57, 2688–2693. doi: 10.1099/ijs.0.65269-0

García-Yoldi, D., MaríN, C. M., De Miguel, M. J., Munoz, P. M., Vizmanos, J. L., and LóPez-GoñI, I. (2006). Multiplex PCR assay for the identification and differentiation of all Brucella species and the vaccine strains *Brucella abortus* S19 and RB51 and *Brucella melitensis* Rev1. *Clin. Chem.* 52, 779–781. doi: 10.1373/clinchem.2005.062596

Georgi, E., Walter, M. C., Pfalzgraf, M. T., Northoff, B. H., Holdt, L. M., Scholz, H. C., et al. (2017). Whole genome sequencing of *Brucella melitensis* isolated from 57 patients in Germany reveals high diversity in strains from Middle East. *PLoS One* 12:e0175425. doi: 10.1371/journal.pone.0175425

Giraud, M. F., and Naismith, J. H. (2000). The rhamnose pathway. *Curr. Opin. Struct. Biol.* 10, 687–696. doi: 10.1016/S0959-440X(00)00145-7

Godfroid, J., Cloeckaert, A., Liautard, J. P., Kohler, S., Fretin, D., Walravens, K., et al. (2005). From the discovery of the Malta fever's agent to the discovery of a marine mammal reservoir, brucellosis has continuously been a re-emerging zoonosis. *Vet. Res.* 36, 313–326. doi: 10.1051/vetres:2005003

Godfroid, F., Cloeckaert, A., Taminiau, B., Danese, I., Tibor, A., De Bolle, X., et al. (2000). Genetic organisation of the lipopolysaccharide O-antigen biosynthesis region of *Brucella melitensis* 16M (wbk). *Res. Microbiol.* 151, 655–668. doi: 10.1016/S0923-2508(00)90130-X

Gonzalez, D., Grilló, M.-J., De Miguel, M.-J., Ali, T., Arce-Gorvel, V., Delrue, R.-M., et al. (2008). Brucellosis vaccines: assessment of *Brucella melitensis* lipopolysaccharide rough mutants defective in core and O-polysaccharide synthesis and export. *PLoS One* 3:e2760. doi: 10.1371/journal.pone.0002760

Hacker, J., and Kaper, J. B. (2000). Pathogenicity islands and the evolution of microbes. *Annu. Rev. Microbiol.* 54, 641–679. doi: 10.1146/annurev.micro.54.1.641

Janowicz, A., De Massis, F., Ancora, M., Camma, C., Patavino, C., Battisti, A., et al. (2018). Core genome multilocus sequence typing and single nucleotide polymorphism analysis in the epidemiology of *Brucella melitensis* infections. *J. Clin. Microbiol.* 56:e00517–18. doi: 10.1128/JCM.00517-18

Jay, M., Freddi, L., Mick, V., Durand, B., Girault, G., Perrot, L., et al. (2020). *Brucella microti*-like prevalence in French farms producing frogs. *Transbound. Emerg. Dis.* 67, 617–625. doi: 10.1111/tbed.13377

Jay, M., Girault, G., Perrot, L., Taunay, B., Vuilmet, T., Rossignol, F., et al. (2018). Phenotypic and molecular characterization of *Brucella microti*-like Bacteria from a domestic marsh frog (*Pelophylax ridibundus*). *Front Vet Sci* 5:283. doi: 10.3389/fvets.2018.00283

Jimenez De Bagues, M. P., Iturralde, M., Arias, M. A., Pardo, J., Cloeckaert, A., and Zygmunt, M. S. (2014). The new strains *Brucella inopinata* BO1 and Brucella species 83-210 behave biologically like classic infectious Brucella species and cause death in murine models of infection. *J Infect Dis* 210, 467–472. doi: 10.1093/infdis/jiu102

Kanehisa, M., Furumichi, M., Sato, Y., Kawashima, M., and Ishiguro-Watanabe, M. (2023). KEGG for taxonomy-based analysis of pathways and genomes. *Nucleic Acids Res.* 51, D587–D592. doi: 10.1093/nar/gkac963

Latheef, S., Keyburn, A., Broz, I., Bagnara, A., Bayley, C., Frith, S., et al. (2020). Atypical Brucella sp in captive Australian green tree frogs (*Litoria caerulea*): clinical features, pathology, culture and molecular characterization. *Aust. Vet. J.* 98, 216–221. doi: 10.1111/avj.12925

Le Flèche, P., Jacques, I., Grayon, M., Al Dahouk, S., Bouchon, P., Denoeud, F., et al. (2006). Evaluation and selection of tandem repeat loci for a Brucella MLVA typing assay. *BMC Microbiol.* 6, 1–14. doi: 10.1186/1471-2180-6-9

Lebuhn, M., Achouak, W., Schloter, M., Berge, O., Meier, H., Barakat, M., et al. (2000). Taxonomic characterization of Ochrobactrum sp. isolates from soil samples and wheat roots, and description of *Ochrobactrum tritici* sp. nov. and *Ochrobactrum grignonense* sp. nov. *Int. J. Syst. Evol. Microbiol.* 50, 2207–2223. doi: 10.1099/00207713-50-6-2207

López-Goñi, I., García-Yoldi, D., Marín, C. M., De Miguel, M. J., Barquero-Calvo, E., Guzmán-Verri, C., et al. (2011). New Bruce-ladder multiplex PCR assay for the biovar typing of Brucella suis and the discrimination of Brucella suis and *Brucella canis*. *Vet. Microbiol.* 154, 152–155. doi: 10.1016/j.vetmic.2011.06.035

Lucht, J. M., and Bremer, E. (1994). Adaptation of *Escherichia coli* to high osmolarity environments: osmoregulation of the high-affinity glycine betaine transport system ProU. *FEMS Microbiol. Rev.* 14, 3–20. doi: 10.1111/j.1574-6976.1994.tb00067.x

Meier-Kolthoff, J. P., Carbasse, J. S., Peinado-Olarte, R. L., and Goker, M. (2022). TYGS and LPSN: a database tandem for fast and reliable genome-based classification and nomenclature of prokaryotes. *Nucleic Acids Res.* 50, D801–D807. doi: 10.1093/nar/gkab902

Muhldorfer, K., Wibbelt, G., Szentiks, C. A., Fischer, D., Scholz, H. C., Zschock, M., et al. (2017). The role of 'atypical' Brucella in amphibians: are we facing novel emerging pathogens? *J. Appl. Microbiol.* 122, 40–53. doi: 10.1111/jam.13326

Occhialini, A., Hofreuter, D., Ufermann, C. M., Al Dahouk, S., and Kohler, S. (2022). The retrospective on atypical Brucella species leads to novel definitions. *Microorganisms* 10, 2–29. doi: 10.3390/microorganisms10040813

Ochman, H., Lawrence, J. G., and Groisman, E. A. (2000). Lateral gene transfer and the nature of bacterial innovation. *Nature* 405, 299–304. doi: 10.1038/35012500

Olson, R. D., Assaf, R., Brettin, T., Conrad, N., Cucinell, C., Davis, J. J., et al. (2022). Introducing the bacterial and viral bioinformatics resource center (BV-BRC): a resource combining PATRIC, IRD and ViPR. *Nucleic Acids Res.* doi: 10.1093/nar/gkz943

Overbeek, R., Begley, T., Butler, R. M., Choudhuri, J. V., Chuang, H. Y., Cohoon, M., et al. (2005). The subsystems approach to genome annotation and its use in the project to annotate 1000 genomes. *Nucleic Acids Res.* 33, 5691–5702. doi: 10.1093/nar/gki866

Overbeek, R., Olson, R., Pusch, G. D., Olsen, G. J., Davis, J. J., Disz, T., et al. (2014). The SEED and the rapid annotation of microbial genomes using subsystems technology (RAST). *Nucleic Acids Res.* 42, D206–D214. doi: 10.1093/nar/gkt1226

Pappas, G., Panagopoulou, P., Christou, L., and Akritidis, N. (2006a). Brucella as a biological weapon. *Cell. Mol. Life Sci.* 63, 2229–2236. doi: 10.1007/s00018-006-6311-4

Pappas, G., Papadimitriou, P., Akritidis, N., Christou, L., and Tsianos, E. V. (2006b). The new global map of human brucellosis. *Lancet Infect. Dis.* 6, 91–99. doi: 10.1016/S1473-3099(06)70382-6

Rambaut, A. (2006). FigTree, a graphical viewer of phylogenetic trees. Available at: http://tree.bio.ed.ac.uk/software/figtree/

Richardson, J. S., and Oresnik, I. J. (2007). L-Rhamnose transport is sugar kinase (RhaK) dependent in *Rhizobium leguminosarum* bv. Trifolii. *J. Bacteriol.* 189, 8437–8446. doi: 10.1128/JB.01032-07

Rouzic, N., Desmier, L., Cariou, M. E., Gay, E., Foster, J. T., Williamson, C. H. D., et al. (2021). First case of brucellosis caused by an amphibian-type Brucella. *Clin. Infect. Dis.* 72, e404–e407. doi: 10.1093/cid/ciaa1082

Scholz, H. C., Al Dahouk, S., Tomaso, H., Neubauer, H., Witte, A., Schloter, M., et al. (2008a). Genetic diversity and phylogenetic relationships of bacteria belonging to the Ochrobactrum-Brucella group by recA and 16S rRNA gene-based comparative sequence analysis. *Syst. Appl. Microbiol.* 31, 1–16. doi: 10.1016/j.syapm.2007.10.004

Scholz, H. C., Hubalek, Z., Nesvadbova, J., Tomaso, H., Vergnaud, G., Le Flèche, P., et al. (2008b). Isolation of *Brucella microti* from soil. *Emerg. Infect. Dis.* 14, 1316–1317. doi: 10.3201/eid1408.080286

Scholz, H. C., Hubalek, Z., Sedlacek, I., Vergnaud, G., Tomaso, H., Al Dahouk, S., et al. (2008c). *Brucella microti* sp. nov., isolated from the common vole *Microtus arvalis*. *Int. J. Syst. Evol. Microbiol.* 58, 375–382. doi: 10.1099/ijs.0.65356-0

Scholz, H. C., Muhldorfer, K., Shilton, C., Benedict, S., Whatmore, A. M., Blom, J., et al. (2016a). The change of a medically important genus: worldwide occurrence of genetically diverse novel Brucella species in exotic frogs. *PLoS One* 11:e0168872. doi: 10.1371/journal.pone.0168872

Scholz, H. C., Nockler, K., Gollner, C., Bahn, P., Vergnaud, G., Tomaso, H., et al. (2010). *Brucella inopinata* sp. nov., isolated from a breast implant infection. *Int. J. Syst. Evol. Microbiol.* 60, 801–808. doi: 10.1099/ijs.0.011148-0

Scholz, H. C., Revilla-Fernandez, S., Dahouk, S. A., Hammerl, J. A., Zygmunt, M. S., Cloeckaert, A., et al. (2016b). Brucella vulpis sp. nov., isolated from mandibular lymph nodes of red foxes (*Vulpes vulpes*). *Int. J. Syst. Evol. Microbiol.* 66, 2090–2098. doi: 10.1099/ijsem.0.000998

Scholz, H. C., and Vergnaud, G. (2013). Molecular characterisation of Brucella species. *Rev. Sci. Tech.* 32, 149–162. doi: 10.20506/rst.32.1.2189

Seleem, M. N., Boyle, S. M., and Sriranganathan, N. (2010). Brucellosis: a re-emerging zoonosis. *Vet. Microbiol.* 140, 392–398. doi: 10.1016/j.vetmic.2009.06.021

Shilton, C. M., Brown, G. P., Benedict, S., and Shine, R. (2008). Spinal arthropathy associated with *Ochrobactrum anthropi* in free-ranging cane toads (Chaunus [Bufo] marinus) in Australia. *Vet. Pathol.* 45, 85–94. doi: 10.1354/vp.45-1-85

Skinner, M. E., Uzilov, A. V., Stein, L. D., Mungall, C. J., and Holmes, I. H. (2009). JBrowse: a next-generation genome browser. *Genome Res.* 19, 1630–1638. doi: 10.1101/gr.094607.109

Soler-Lloréns, P. F., Quance, C. R., Lawhon, S. D., Stuber, T. P., Edwards, J. F., Ficht, T. A., et al. (2016). A Brucella spp. isolate from a Pac-man frog (*Ceratophrys ornata*) reveals characteristics departing from classical Brucellae. *Frontiers in cellular and infection. Microbiology* 6:116. doi: 10.3389/fcimb.2016.00116

Stamatakis, A. (2014). RAxML version 8: a tool for phylogenetic analysis and post-analysis of large phylogenies. *Bioinformatics* 30, 1312–1313. doi: 10.1093/bioinformatics/btu033

Stamatakis, A., Hoover, P., and Rougemont, J. (2008). A rapid bootstrap algorithm for the RAxML web servers. *Syst. Biol.* 57, 758–771. doi: 10.1080/10635150802429642

Tiller, R. V., Gee, J. E., Lonsway, D. R., Gribble, S., Bell, S. C., Jennison, A. V., et al. (2010). Identification of an unusual Brucella strain (BO2) from a lung biopsy in a 52 year-old patient with chronic destructive pneumonia. *BMC Microbiol.* 10:23. doi: 10.1186/1471-2180-10-23

Wattam, A. R., Brettin, T., Davis, J. J., Gerdes, S., Kenyon, R., Machi, D., et al. (2018). "Assembly, annotation, and comparative genomics in PATRIC, the all bacterial bioinformatics resource center" in *Comparative genomics*. (New York, NY: Humana Press), 79–101.

Wattam, A. R., Davis, J. J., Assaf, R., Boisvert, S., Brettin, T., Bun, C., et al. (2017). Improvements to PATRIC, the all-bacterial bioinformatics database and analysis resource center. *Nucleic Acids Res.* 45, D535–D542. doi: 10.1093/nar/gkw1017

Wattam, A. R., Inzana, T. J., Williams, K. P., Mane, S. P., Shukla, M., Almeida, N. F., et al. (2012). Comparative genomics of early-diverging Brucella strains reveals a novel lipopolysaccharide biosynthesis pathway. *MBio* 3, e00246–e00212. doi: 10.1128/mBio.00246-12

Wattam, A. R., Williams, K. P., Snyder, E. E., Almeida, N. F. Jr., Shukla, M., Dickerman, A. W., et al. (2009). Analysis of ten Brucella genomes reveals evidence for horizontal gene transfer despite a preferred intracellular lifestyle. *J. Bacteriol.* 191, 3569–3579. doi: 10.1128/JB.01767-08

Whatmore, A. M. (2009). Current understanding of the genetic diversity of Brucella, an expanding genus of zoonotic pathogens. *Infect. Genet. Evol.* 9, 1168–1184. doi: 10.1016/j.meegid.2009.07.001

Whatmore, A. M., Dale, E. J., Stubberfield, E., Muchowski, J., Koylass, M., Dawson, C., et al. (2015). Isolation of Brucella from a White's tree frog (*Litoria caerulea*). *JMM Case Rep* 2, 1–5. doi: 10.1099/jmmcr.0.000017

Whatmore, A. M., Davison, N., Cloeckaert, A., Al Dahouk, S., Zygmunt, M. S., Brew, S. D., et al. (2014). Brucella papionis sp. nov., isolated from baboons (Papio spp.). *Int. J. Syst. Evol. Microbiol.* 64, 4120–4128. doi: 10.1099/ijs.0.065482-0

Whatmore, A. M., and Foster, J. T. (2021). Emerging diversity and ongoing expansion of the genus Brucella. *Infect. Genet. Evol.* 92:104865. doi: 10.1016/j.meegid.2021.104865

Whatmore, A. M., Koylass, M. S., Muchowski, J., Edwards-Smallbone, J., Gopaul, K. K., and Perrett, L. L. (2016). Extended multilocus sequence analysis to describe the global population structure of the genus Brucella: Phylogeography and relationship to Biovars. *Front. Microbiol.* 7:2049. doi: 10.3389/fmicb.2016.02049

Whatmore, A. M., Perrett, L. L., and Macmillan, A. P. (2007). Characterisation of the genetic diversity of Brucella by multilocus sequencing. *BMC Microbiol.* 7:34. doi: 10.1186/1471-2180-7-34

Wood, T. L., and Wood, T. K. (2016). The HigB/HigA toxin/antitoxin system of *Pseudomonas aeruginosa* influences the virulence factors pyochelin, pyocyanin, and biofilm formation. *Microbiology* 5, 499–511. doi: 10.1002/mbo3.346

Yoon, S. H., Ha, S. M., Lim, J., Kwon, S., and Chun, J. (2017). A large-scale evaluation of algorithms to calculate average nucleotide identity. *Antonie Van Leeuwenhoek* 110, 1281–1286. doi: 10.1007/s10482-017-0844-4

frontiers | Frontiers in Microbiology

TYPE Original Research
PUBLISHED 14 September 2023
DOI 10.3389/fmicb.2023.1241143

OPEN ACCESS

EDITED BY
Axel Cloeckaert,
Institut National de recherche pour l'agriculture, l'alimentation et l'environnement (INRAE), France

REVIEWED BY
Clayton Caswell,
Virginia Tech, United States
Alfonso Mendez Tenorio,
National Polytechnic Institute (IPN), Mexico

*CORRESPONDENCE
Caterina Guzmán-Verri
✉ catguz@una.cr

†PRESENT ADDRESS
Olman Gómez-Espinoza,
Laboratorio de Fisiología y Biología Molecular Vegetal, Instituto de Agroindustria, Departamento de Ciencias Agronómicas y Recursos Naturales, Facultad de Ciencias Agropecuarias y Medioambiente, Universidad de La Frontera, Temuco, Chile

‡These authors have contributed equally to this work and share first authorship

RECEIVED 16 June 2023
ACCEPTED 15 August 2023
PUBLISHED 14 September 2023

CITATION
Castillo-Zeledón A, Rivas-Solano O, Villalta-Romero F, Gómez-Espinoza O, Moreno E, Chaves-Olarte E and Guzmán-Verri C (2023) The *Brucella abortus* two-component system response regulator BvrR binds to three DNA regulatory boxes in the upstream region of *omp25*. *Front. Microbiol.* 14:1241143. doi: 10.3389/fmicb.2023.1241143

The *Brucella abortus* two-component system response regulator BvrR binds to three DNA regulatory boxes in the upstream region of *omp25*

Amanda Castillo-Zeledón[1‡], Olga Rivas-Solano[1,2‡], Fabián Villalta-Romero[2], Olman Gómez-Espinoza[2†], Edgardo Moreno[1], Esteban Chaves-Olarte[3] and Caterina Guzmán-Verri[1*]

[1]Programa de Investigación en Enfermedades Tropicales, Escuela de Medicina Veterinaria, Universidad Nacional de Costa Rica, Heredia, Costa Rica, [2]Centro de Investigación en Biotecnología, Escuela de Biología, Instituto Tecnológico de Costa Rica, Campus Tecnológico Central Cartago, Cartago, Costa Rica, [3]Centro de Investigación en Enfermedades Tropicales, Facultad de Microbiología, Universidad de Costa Rica, San José, Costa Rica

Brucella abortus is a facultative extracellular-intracellular bacterial zoonotic pathogen worldwide. It is also a major cause of abortion in bovines, generating economic losses. The two-component regulatory system BvrR/BvrS modulates the expression of genes required to transition from extracellular to intracellular lifestyles. However, few regulatory regions of BvrR direct target genes have been studied. In this study, we characterized the regulatory region of *omp25*, a gene encoding an outer membrane protein that is positively regulated by TCS BvrR/BvrS. By *omp25-lacZ* reporter fusions and β-galactosidase activity assays, we found that the region between -262 and + 127 is necessary for transcriptional activity, particularly a 111-bp long fragment located from -262 to –152. In addition, we demonstrated the binding of P-BvrR to three sites within the –140 to +1 region. Two of these sites were delimited between –18 to +1 and – 99 to –76 by DNase I footprinting and called DNA regulatory boxes 1 and 2, respectively. The third binding site (box 3) was delimited from –140 to –122 by combining EMSA and fluorescence anisotropy results. A molecular docking analysis with HDOCK predicted BvrR-DNA interactions between 11, 13, and 12 amino acid residue-nucleotide pairs in boxes 1, 2, and 3, respectively. A manual sequence alignment of the three regulatory boxes revealed the presence of inverted and non-inverted repeats of five to eight nucleotides, partially matching DNA binding motifs previously described for BvrR. We propose that P-BvrR binds directly to up to three regulatory boxes and probably interacts with other transcription factors to regulate *omp25* expression. This gene regulation model could apply to other BvrR target genes and to orthologs of the TCS BvrR/BvrS and Omp25 in phylogenetically closed *Rhizobiales*.

KEYWORDS

two-component regulatory system, outer membrane protein (OMP), *Rhizobiales*, *Brucella*, *Brucella abortus*

1. Introduction

Brucella abortus is a facultative extracellular-intracellular Gram-negative pathogen. It belongs to *Rhizobiales*, an order composed of cell-associated pathogens, symbionts, and free-living bacteria (Batut et al., 2004; Moreno, 2021). *B. abortus* causes brucellosis, a widely distributed zoonotic disease. In infected cattle, the disease manifests with abortion and infertility, causing economic losses (Spink, 1957).

The pathogenicity of brucellae resides in their ability to invade, survive, and replicate inside host cells (Roop et al., 2021). In *B. abortus*, the two-component regulatory system (TCS), BvrR/BvrS, is important for the transition from the extracellular to the intracellular milieu (Sola-Landa et al., 1998; Guzman-Verri et al., 2002; López-Goñi et al., 2002; Altamirano-Silva et al., 2018). This TCS comprises a transmembrane sensor protein with histidine kinase activity called BvrS and a cytoplasmic response regulator called BvrR, which has homology to OmpR (López-Goñi et al., 2002; Altamirano-Silva et al., 2018).

Phylogenetic analyses revealed that the TCS BvrR/BvrS is orthologous to other *Rhizobiales* TCSs, including ExoS/ChvI from the plant endosymbiont *Sinorhizobium meliloti*, ChvG/ChvI from the plant pericellular pathogen *Agrobacterium tumefaciens*, and BatR/BatS from the intracellular zoonotic pathogen *Bartonella* sp. Those orthologous TCSs respond to environmental conditions and regulate the expression of target genes involved in distinct stages of host invasion and intracellular survival (Charles and Nester, 1993; Cheng and Walker, 1998; Batut et al., 2004; Beier and Gross, 2006; Quebatte et al., 2010; Bélanger and Charles, 2013; Heavner et al., 2015; Ratib et al., 2018).

In brucellae, BvrS senses low pH and low nutrient availability, conditions probably encountered when the bacterium is trafficking through the endosomal pathway (Altamirano-Silva et al., 2018, 2021). Following this, BvrS probably auto-phosphorylates and transduces the signal via a phosphate group to BvrR, increasing its affinity for specific chromosomal regions (López-Goñi et al., 2002; Nguyen et al., 2015; Altamirano-Silva et al., 2021). A *B. abortus bvrR* mutant lacks virulence in murine models and does not replicate in cell culture models (Sola-Landa et al., 1998). This mutant differentially expresses outer membrane and periplasmic proteins (Guzman-Verri et al., 2002; Lamontagne et al., 2007; Viadas et al., 2010) and shows a distinctive lipopolysaccharide acylation pattern compared to the wild-type strain (Manterola et al., 2005). Regarding outer membrane proteins, the TCS BvrR/BvrS positively regulates the expression of *omp25* (Guzman-Verri et al., 2002; Lamontagne et al., 2007; Viadas et al., 2010). This gene encodes a major outer-membrane protein of 25 kDa (Omp25) belonging to the Omp25/31 family (Vizcaíno et al., 2001), the most abundant outer-membrane proteins of brucellae (Martín-Martín et al., 2009). In *B. abortus*, although Omp25 is not essential for the invasion, survival, and replication inside RAW macrophages and HeLa cells, it has a structural function in the covalent attachment of the outer membrane to peptidoglycan (Manterola et al., 2007; Godessart et al., 2021).

The TCS BvrR/BvrS also regulates the expression of virulence genes related to intracellular trafficking and cell egress, like the Type IV Secretion System VirB and the quorum-sensing regulator VjbR (Lamontagne et al., 2009; Martínez-Núñez et al., 2010; Viadas et al., 2010; Altamirano-Silva et al., 2018, 2021), and is related to the carbon and nitrogen metabolic fitness according to the encountered environment (Lamontagne et al., 2009; Viadas et al., 2010; Rivas-Solano et al., 2022).

Recently, two DNA binding motifs putatively recognized by BvrR have been reported by *in silico* predictions (Ramírez-González et al., 2019) and experimental approaches (Rivas-Solano et al., 2022).

A direct interaction has been described between BvrR and the upstream region of *omp25*, located between coordinates −159 and + 34 from the start codon (Rivas-Solano et al., 2022). Two transcriptional start sites (TSS) have been independently reported for *omp25*, at positions −131 and − 82 (Suárez-Esquivel et al., 2016; Rivas-Solano et al., 2022).

Here, we characterized the *omp25* transcriptional regulatory region as a prototype of a regulatory element directly controlled by the TCS BvrR/BvrS. Our results suggest that the TCS BvrR/BvrS regulates *omp25* expression directly by binding to up to three regulatory boxes with inverted and non-inverted DNA repeats. The research presented here contributes to understanding how the TCS BvrR/BvrS regulates target genes and might apply to other ortholog TCSs in *Rhizobiales*.

2. Materials and methods

2.1. Bacterial strains and culture conditions

Escherichia coli and *B. abortus* strains (Table 1) were incubated at 37°C at 200 rpm and grown on Luria Bertani Broth (LB) (Sambrook et al., 1989) or Tryptic Soy Broth (TSB) (Suárez-Esquivel et al., 2016). Additionally, culture media were supplemented with antibiotics (kanamycin 30 μg/ml, gentamicin 20 μg/ml, or ampicillin 100 μg/ml) when necessary. All procedures involving live *B. abortus* were performed according to the "Reglamento de Bioseguridad de la CCSS 39975–0," 2012, after the "Decreto Ejecutivo #30965-S," 2002, and research protocol SIA 0652-19, approved by the National University, Costa Rica.

2.2. Construction of transcriptional fusions and β-galactosidase activity assays

The primers used in this study are detailed in Supplementary Table 1. A DNA fragment from the genome of *B. abortus* 2308 W (GenBank Accession ERS568782), encompassing the *omp25* region from −392 to +127 and two smaller ones from −262 to +127 and −151 to +127 (Figure 1A), was amplified by PCR and purified with the QIAquick® Gel Extraction Kit (Qiagen). The amplicons and the pMR15 vector (Table 1) were excised separately with BamHI (10 U/μl) and XbaI (10 U/μl) (Fermentas®) for 18 h at 37°C. The restriction enzymes were inactivated at 80°C for 20 min. The DNA fragments were ligated with the pMR15 vector using T4 DNA ligase (5 U/μl) (Fermentas®) at room temperature overnight to obtain plasmids p392, p262, and p151 (Table 1). Then, the plasmids were electroporated into the *E. coli* strain XL1-Blue to generate the strains E392, E262, and E151 (Table 1) using the Electro Cell Manipulator ECM 630 BTX®. Colonies with the new plasmids were selected using kanamycin and screened using primers omp25lacZF and omp25lacZR (Supplementary Table 1). Plasmid DNA was isolated and electroporated into *B. abortus* using the

TABLE 1 Bacterial strains and plasmids.

Strain	Relevant characteristics	Reference
E. coli		
XL1Blue	*recA1 endA1 gyrA96 thi-1 hsdR17 supE44 relA1 Δ(lac-proAB) [F′ proAB lacIqZΔM15].* Tn*10*(Tet′)	Sambrook et al. (1989)
E392	XL1Blue carrier of p392, Km^r	This study
E262	XL1Blue carrier of p262, Km^r	This study
E151	XL1Blue carrier of p151, Km^r	This study
B. abortus		
2308 W	Wild-type, virulent strain, Nal^r	Suárez-Esquivel et al. (2016)
3aZ	2308 W carrier of transcripcional chromosomal fusion P*omp3a*::*lacZ*, Gm^r Amp^r	Guzman-Verri et al. (2002)
B392	2308 W carrier of p392, Km^r	This study
B262	2308 W carrier of p262, Km^r	This study
B151	2308 W carrier of p151, Km^r	This study
BpMR15	2308 W carrier of pMR15, Kmr	This study
Plasmids		
pMR15	High copy number vector, promoterless *lacZ* gene, Km^r	Gober and Shapiro (1992), Courtesy of M. Roop.
p392	pMR15-derivative with a cloned fragment of 521-bp, 392-bp upstream *omp25*, and the first 127-bp of the coding sequence, Km^r	This study
p262	pMR15-derivative with a cloned fragment of 391-bp, 262-bp upstream *omp25*, and the first 127-bp of the coding sequence, Km^r	This study
p151	pMR15-derivative with a cloned fragment of 280-bp, 151-bp upstream *omp25*, and the first 127-bp of the coding sequence, Km^r	This study

Nal^r, resistance to nalidixic acid; Gm^r, resistance to gentamicin; Amp^r, resistance to ampicillin; Km^r, resistance to kanamycin.

Electro Cell Manipulator ECM 630 BTX® to obtain the strains B392, B262, and B151 (Table 1). The vector pMR15 was also electroporated into *B. abortus* as a non-promoter activity control (strain BpMR15, Table 1). The β-galactosidase assays were performed with modifications (Guzman-Verri et al., 2002). Bacteria were grown until the exponential phase, permeabilized with 0.5% sodium dodecyl sulfate (SDS), 6% chloroform for 10 min at 28°C, and incubated with O-nitrophenyl-β-D-galactopyranoside (ONPG) for 10 min at 28°C. The reaction was stopped with 1 M sodium carbonate, the absorbance was measured at 420 nm, and the specific activity was expressed as nmol of O-nitrophenol produced/min × mg protein (Miller Units). The reported β-galactosidase activity was corrected according to the residual activity obtained from the empty vector strain, BpMR15. A previously constructed *lacZ*:*omp25* chromosomal fusion *B. abortus* strain (3aZ) was used as a positive control of promoter activity (Guzman-Verri et al., 2002; Table 1). A one-way ANOVA statistical analysis followed by Tukey's multiple comparisons test was performed using GraphPad Prism version 8.00 for Windows (Graph Pad, 2019).

2.3. Electrophoretic mobility shift assay (EMSA)

Expression and purification of GST-BvrR were carried out as described (Martínez-Núñez et al., 2010). Before each assay, BvrR was phosphorylated with carbamoyl phosphate as described previously (Altamirano-Silva et al., 2018). DNA probes were labeled using the DIG Gel Shift Kit 2nd Generation (Roche®). Protein and DNA probes were incubated together following the protocol described in the DIG Gel Shift Kit 2nd Generation (Roche®). Protein-DNA mixtures were separated by native polyacrylamide electrophoresis at 150 V at 4°C for 1, 1.5, or 2.5 h, depending on the size of the DNA probe. The gels were electro-blotted into positively charged Nylon membranes, and the results were visualized by an enzymatic immunoassay using anti-digoxigenin-alkaline phosphatase (InvitrogenTM Electrophoretic Mobility Shift Assay Kit). The generated chemiluminescent signals were recorded on an X-ray film. Size and shape are factors that affect the electrophoretic migratory pattern of a molecule (Hellman and Fried, 2007). In our assays, the same protein is used, but the DNA fragments differ, so specific protein-DNA complexes for each DNA fragment run by EMSA were identified based on the following criteria: absence of shifted bands in the lane without P-BvrR, absence of shifted bands in the specificity binding control, P-BvrR concentration-dependent shifted bands, and consistency between independent replicas. If any of these criteria were not met, the shifted band was classified as unspecific (Hellman and Fried, 2007; Altamirano-Silva et al., 2018).

For direct EMSA, two DNA fragments used as probes were obtained by PCR using the following primer pairs: omp25.262 and omp25.152 or omp25.262 and omp25.122 (Supplementary Table 1). Labeled probes at 0.033 μM were incubated with increasing concentrations of phosphorylated BvrR (P-BvrR) (0.1–1.6 μM) for 15 min on ice. Mixtures were electrophoresed for 2.5 h and analyzed as described above. A coding region of the ribosomal protein (*rpIL*) was amplified by PCR with the primers L12.F and L12.R (Supplementary Table 1) and used as a specificity-binding control.

For competitive EMSA, a 193-bp fragment (coordinates −159 to +34 from the *omp25* start codon), previously shown to interact with P-BvrR by EMSA (Rivas-Solano et al., 2022), was amplified by PCR with primers omp25R and omp25F (Supplementary Table 1). The 193-bp labeled probe (0.033 μM) was mixed with P-BvrR

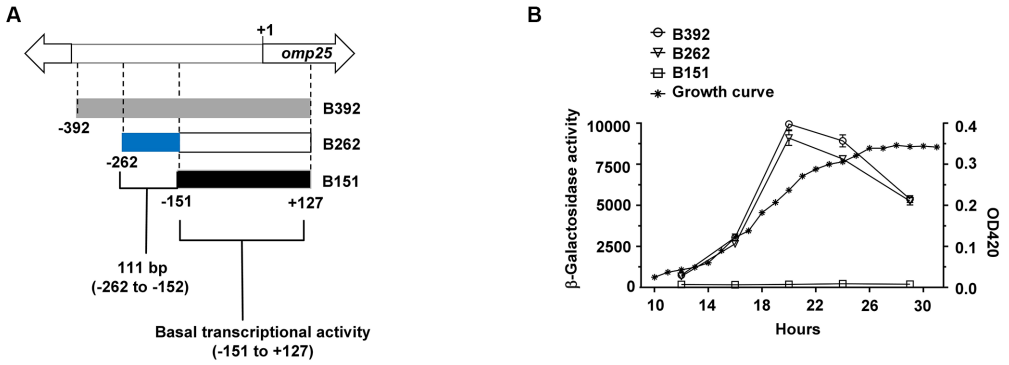

FIGURE 1
A 111-bp fragment upstream of *omp25* is needed for wild-type levels of transcription. **(A)** Schematic representation of the *omp25* upstream region analyzed by constructing three β-galactosidase transcriptional fusions. Gray rectangle = region with wild-type levels of transcription (from −392 to +127), blue rectangle = 111-bp region (from −262 to −152) needed for wild-type levels of transcription, and black rectangle = fragment with basal transcriptional activity. DNA coordinates are given according to the *omp25* adenine in the start codon. **(B)** β-galactosidase results (unfilled figures) and a representative growth curve (asterisks). *B. abortus* 2308 W-derived strains containing the promoterless reporter vector fusions with upstream *omp25* fragments were grown in TSB at 37°C and assayed for β-galactosidase activity at different times of the growth curve. Absorbance was measured at 420 nm at the indicated times. B151 presented significant statistical differences for β-galactosidase activity compared to the rest of the strains. These results are representative of at least three independent experiments. The residual β-galactosidase activity from the empty vector (BpMR15) was removed from each test carried out in the corresponding growth phases (one-way ANOVA followed by Tukey's multiple comparisons test) ($p < 0.05$).

(0.4 μM) and an excess (1,000×) of each nine ~40 pb unlabeled oligonucleotide pairs obtained by chemical synthesis (Supplementary Table 2), encompassing the region covered by the 193-bp probe. The protein-DNA mixtures were incubated as described for direct EMSA, electrophoresed for 1.5 h, and analyzed as described above.

The oligonucleotide pairs that competed with the 193-bp probe for binding to P-BvrR were then labeled and used as probes in another direct EMSA with increasing concentrations of P-BvrR, as described for the direct EMSA above. Mixtures were electrophoresed for 1 h and analyzed as described above. One of the oligonucleotide pairs that did not compete for P-BvrR was used as a specificity-binding control.

2.4. DNase I footprinting

For DNase I footprinting, the same 193-bp region used for competitive EMSA was amplified as described above, labeled with HEX (hexachlorofluorescein) or FAM (5′ 6-carboxyfluorescein), incubated with P-BvrR at 8.32 μM, and proceeded as described for EMSA. The samples were then incubated for 15 min at 15–25°C and placed again in ice. DNAse I (0.05 U) was added, and the samples were incubated for 2 min at 15°C in a thermocycler, followed by 10-min incubation at 75°C. The samples were purified using the Qiagen Qiaquick PCR purification kit and eluted with 30 μl of EB buffer. The samples (10 μl) were run in a 3730 Genetic Analyzer after mixing with 7 μl of HiDi formamide and 0.1 μl of GeneScan 500 Liz size marker and the following running parameters: genotyping module, injection time: 30 s, and injection voltage: 3 kV (Zianni et al., 2006). The Peak Scanner software was used to infer the protected regions by superimposing the electropherograms from digested DNA in the presence of P-BvrR or BSA (3.64 nM). Base pair coordinates of the protected regions were inferred after Sanger sequencing of the 193-bp DNA fragment.

2.5. Fluorescence anisotropy

The fluorescence anisotropy assays were performed as described (Owen and McMurray, 2009) with modifications. Recombinant BvrR was phosphorylated as described for EMSA and serially diluted in a binding buffer (10 mM Tris, 1 mM EDTA, 0.1 M NaCl). The forward oligonucleotide 2 (173.133omp25-O, Supplementary Table 2) was 5′-labeled with FAM and mixed with the non-labeled reverse complementary oligo (173.133omp25-ORC, Supplementary Table 2) at a final concentration of 50 mM. The oligonucleotides Oligo rplL-O (5′-FAM labeled) and the reverse complementary Oligo rplL-ORC (Supplementary Table 2) were used as a negative control at a final concentration of 50 mM. Blank samples without protein were also prepared for background fluorescence estimation. Samples were incubated for 30 min at 37°C inside a CytationTM 3 microplate reader (Biotek, Instruments). Fluorescence anisotropy was measured with the appropriate polarized filters, and the results were graphed following a one-site-specific binding model (Favicchio et al., 2009) using the GraphPad Prism (Hulme and Trevethick, 2010; Graph Pad, 2019).

2.6. Molecular docking analysis of BvrR-DNA interactions

The interactions between BvrR and its three binding sites were explored by molecular docking using the HDOCK server (default parameters) (Yan et al., 2017). The Fasta BvrR sequence (UniProt accession: Q2YQY4) was used as an input receptor molecule, and the sequences Box 1 (TTGTGTAAGGAGAATGCCAT), Box 2 (GATA TGTCACCCCTGTCAGCGCGG), and Box 3 (CTCGACAGAT TATCTCCACACAATGGGGCA) were used as input ligand molecules. Before the free docking, the software selected the crystal structure of the OmpR-like response regulator KdpE from *E. coli* (RCSB PDB: 4KFC) as a modeling template for the BvrR structure (Seq_ID % = 29.4). To ensure the reliability of the model generated by

HDOCK, its quality was analyzed using the QMEANDisCo parameter (Studer et al., 2020) and Ramachandran plots. The model was compared to those generated by SWISS-MODEL (Waterhouse et al., 2018), I-TASSER (Yang et al., 2015), and AlphaFOLD (Jumper et al., 2021; Varadi et al., 2022). The crystal structures of two proteins with DNA-binding domains were used as positive controls for the docking experiments: a *B. abortus* DNA binding protein (RCSB PDB: 4QPJ) and the KdpE protein from *E. coli*. As negative controls, the crystal structures of two proteins lacking DNA-binding domains were used: a *B. suis* 1330 hydrolase (RCSB PDB: 6NQ4) and a *B. abortus* peptidoglycan hydrolase inhibitor (RCSB PDB: 7DPY). For the interpretation, docking scores lower than −200 and confidence scores superior to 0.7 were considered to have good performance and a high likelihood of binding between the analyzed molecules. The NUCPLOT tool (Luscombe et al., 1997) was used to analyze and visualize a 2D interaction coloring scheme of the HDOCK results.

3. Results

3.1. A 111-bp long fragment at position −262 to −152 is needed for transcriptional activity

In *B. abortus* 2308 W, the *omp25* upstream intergenic region comprises 401 nucleotides (Suárez-Esquivel et al., 2016). To characterize the minimal promoter region of *omp25*, we constructed three plasmid-borne *omp25-lacZ* reporter fusions harboring 392-, 262-, and 151-bp upstream of *omp25*, respectively. All three reporter fusions included the first 127-bp of the *omp25* coding sequence (Figure 1A). The resulting plasmids were introduced into *B. abortus* 2308 W-generating strains B392, B262, and B151. Then, we assayed the β-galactosidase activity of each resulting strain at different time points of the growth curve. We used strain 3aZ, carrying a transcriptional chromosomal fusion P*omp3a*::*lacZ*, as the positive control (Table 1). The strain B392 exhibited similar β-galactosidase activity compared to strain 3aZ, except for the late log phase of the growth curve (Supplementary Figure 1; Supplementary Table 3). The strains B392 and B262 reached a peak of β-galactosidase activity at mid-log phase, between 18 and 22 h of growth, without significant statistical differences along the curve (Figure 1B; Supplementary Table 3). However, strain B151, harboring 111-bp less than B262 (Figure 1A), presented significantly reduced β-galactosidase activity compared to B262 and B392. Yet some basal transcriptional activity was observed in this strain at all time points tested, as compared to the empty vector activity (Supplementary Table 3). Therefore, the *omp25* promoter region is located between coordinates −262 and + 127 from the start codon, and the additional 111-bp region in B262 (−262 to −152), as compared to B151, is needed for wild-type transcriptional levels.

3.2. The upstream *omp25* regulatory region displays three BvrR binding sites

In *B. abortus* 2308 W, BvrR positively regulates the expression of *omp25* (Guzman-Verri et al., 2002), and a direct binding to the region between −159 and + 34 from the *omp25* start codon has been demonstrated previously (Rivas-Solano et al., 2022). Therefore, based on the results of the β-galactosidase assay, we tested if P-BvrR could also bind by EMSA to the 111-bp fragment required for optimal transcription (−262 to −152, Figure 2A). However, the 111-bp fragment used as a labeled probe and incubated with increasing concentrations of P-BvrR did not reveal shifted bands as compared to the probe alone or to the binding specificity control using *rplL* (Figure 2B), indicating a lack of interaction. Thus, we tested if a larger fragment of 141-bp (−262 to −122, Figure 2A), which included 30 additional bp from the region known to bind to P-BvrR (−159 to +34) (Rivas-Solano et al., 2022), could bind to P-BvrR by direct EMSA. As a result, the probe incubated with growing concentrations of P-BvrR showed shifted bands as compared to the probe alone and the binding specificity control *rplL* (Figure 2B), indicating a specific protein-DNA interaction with the *omp25* upstream region between coordinates −262 and − 122. Altogether, these two direct EMSA results prompted us to infer a putative P-BvrR binding site between positions −151 and − 122 from the *omp25* start codon.

However, since OmpR has been shown to bind to multiple binding sites on the promoter of its target gene *ompF* (Kenney, 2002), we decided to look for multiple BvrR binding sites in the region from −159 to +34, already known to bind to P-BvrR (Rivas-Solano et al., 2022), including the putatively inferred binding site from −151 to −122. This 193-bp region (−159 to +34) was depicted in nine overlapping sequences of ~40 pb (Figure 3A; Supplementary Table 2). An excess of each non-labeled oligonucleotide was tested in a competitive EMSA with the 193-bp region (−159 to +34) as the labeled probe and P-BvrR at a final concentration of 0.4 μM. As shown in Figure 3B, the oligonucleotides 4 (−100 to −59) and 7 (−39 to +1) outcompeted the 193-bp probe, indicating a specific P-BvrR binding to these oligonucleotides. Additionally, for oligonucleotide 2 (−140 to −100), we observed a less defined lower band that suggested a possible partial competition, although less evident than the one observed for oligonucleotides 4 and 7.

Subsequently, the oligonucleotides 2, 4, and 7 were labeled to perform a direct EMSA with P-BvrR. We also tested the non-competing oligonucleotide 5 (−80 to −39) as a specificity-binding control. As a result, oligonucleotides 2, 4, and 7 showed shifted bands (Figure 4). We did not observe these interactions with the probe in the absence of P-BvrR and with the specificity binding control (oligonucleotide 5), confirming binding specificity to the three oligonucleotides.

To validate and further delimit the P-BvrR binding sites suggested by the competitive and direct EMSA results, we performed a DNase I footprinting analysis using the entire 193-bp fragment (−159 to +34) and P-BvrR. As a result, we found two protected sequences that we called DNA regulatory boxes: one spanning from −18 to +1 (box 1) and the other from −99 to −76 (box 2) (Figure 5A). Boxes 1 and 2 matched oligonucleotides 7 and 4. However, any clear protected sequence matched oligonucleotide 2 (−140 to −100), which was the one that showed a less clear result in the competitive EMSA (Figure 3B), despite showing binding to P-BvrR in the direct EMSA (Figure 4). To further confirm the binding of P-BvrR to oligonucleotide 2 by another experimental approach, we performed a fluorescence anisotropy assay with 5′-FAM-labeled oligonucleotide 2 and increasing concentrations of P-BvrR. In this method, a fluorescent signal is placed on the smaller DNA molecule, and when it binds to the much larger protein, a change in the fluorescence anisotropy is

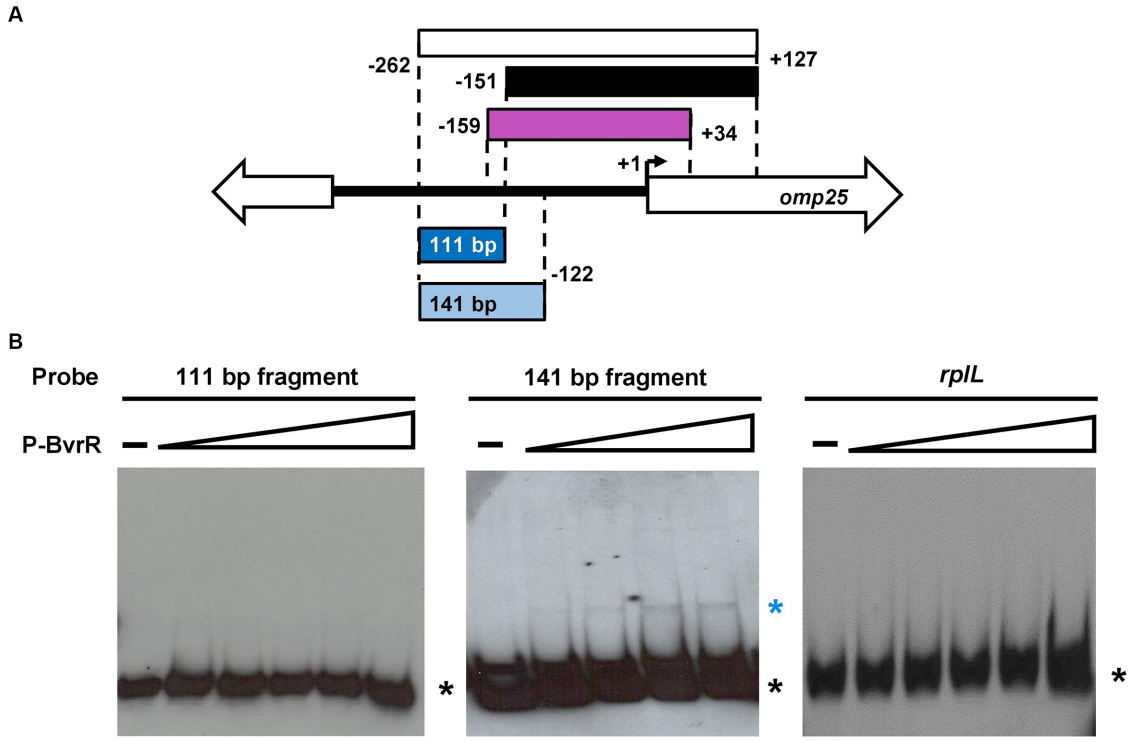

FIGURE 2
A P-BvrR binding site is inferred by EMSA from −152 to −122. **(A)** Schematic representation of the *omp25* intergenic studied region. White rectangle = fragment displaying wild-type levels of transcription (−262 to +127), black rectangle = fragment displaying basal transcriptional activity (−151 to +127), purple rectangle = fragment previously known to bind to P-BvrR by direct EMSA (−159 to +34), blue rectangle = 111-bp fragment (from −262 to −152) needed to enhance transcription and tested as a probe by direct EMSA with P-BvrR, and light blue rectangle = larger fragment of 141-bp (from −262 to −122), comprising 30 additional downstream bp. **(B)** Direct EMSA results were obtained when using increasing concentrations of P-BvrR from 0.1 to 1.6 μM and one of the following labeled probes: the 111-bp fragment from −262 to −152 (left gel) and the 141-bp fragment from −262 to −122 (middle gel). A 290-bp DNA fragment from the coding region of the ribosomal gene *rplL* (right gel) was used as a specificity P-BvrR binding control. Lanes marked as "-" contain the probe without P-BvrR. Blue asterisks = shifted bands (protein-DNA complexes) selected based on the following criteria: absence in the negative control, P-BvrR concentration dependency, and consistency between independent replicas. Black asterisks = bands with the migration pattern of a free probe. These results are representative of at least three independent experiments.

produced, confirming protein-DNA interactions (Owen and McMurray, 2009). As a BvrR specificity binding control, we included a 5′-FAM-labeled oligonucleotide called oligo *rplL* (Supplementary Table 2). The fluorescence anisotropy results showed a positive change in the anisotropy DNA-binding curve for oligonucleotide 2 compared to the specificity binding control (Figure 5B), confirming P-BvrR-DNA-specific interactions with oligonucleotide 2.

Since oligonucleotide 2 (−140 to −100) partially overlaps the first EMSA-inferred binding site between −151 and − 122, these EMSA and fluorescence anisotropy results allowed us to narrow down this third binding site to a 19-bp region between −140 and − 122, which was named box 3.

3.2.1. Molecular docking and sequence alignment of the three DNA regulatory boxes predict BvrR recognition of inverted and non-inverted DNA repeats

To investigate the theoretical interaction between BvrR and the three DNA regulatory boxes confirmed by different experimental approaches including direct and competitive EMSAs, DNase I footprinting, and fluorescence anisotropy, we performed molecular docking using the HDOCK web server. The quality report of the homology modeling showed that the BvrR model falls within the range of low to medium based on the Seq_ID (Supplementary Table 4). However, based on the TMscore, the model demonstrates high quality (Supplementary Figure 2). Similarly, upon comparing HDOCK's BvrR model with models generated by SWISS-MODEL, I-TASSER, and AlphaFold using standard quality parameters, we observed only minimal differences among the models (Supplementary Table 5), suggesting that despite its low identity to the template, the model generated by HDOCK shares similarities with those produced by other widely used software.

The three sequences and the positive controls achieved docking scores lower than −200 (Supplementary Table 6), indicating good performance. Furthermore, BvrR and the positive controls exhibited confidence scores superior to 0.7, suggesting a high likelihood of binding between the molecules, while the negative controls scored more than −200 and their confidence scores were lower than 0.7. These results increase the confidence in the binding of BvrR to its ligands.

The docking results predicted the possibility of hydrogen bonds and non-bonded contacts between 13, 15, and 14 amino acid residues from the C terminal domain (Trans_reg_C) of BvrR and DNA portions from boxes 1 (GTAAGGAGAAT), 2 (ACCCCTGTCA), and 3 (AATGGGGC), respectively, with distances in the appropriate

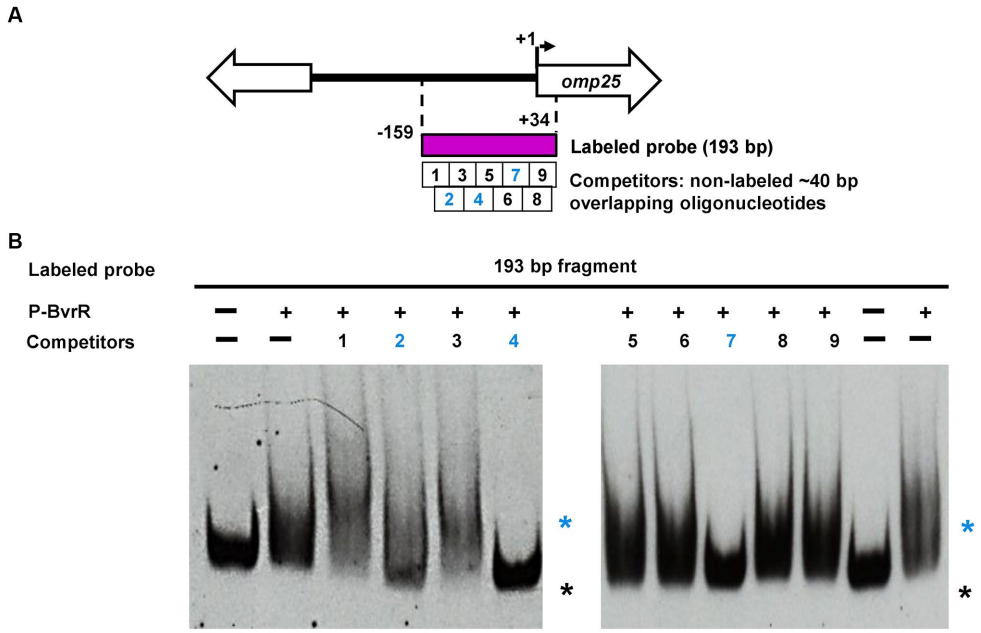

FIGURE 3
Competitive EMSA results suggest the presence of three putative P-BvrR binding sites on the upstream studied region of *omp25*. **(A)** Schematic representation of the DNA fragments from the *omp25* upstream region that were analyzed in competitive EMSA with P-BvrR. The 193-bp region known to bind to P-BvrR by EMSA (purple rectangle) was used as the labeled probe. This fragment was depicted in nine overlapping 40-bp oligonucleotides that were used as non-labeled competitors (white squares). Numbers in blue = competing oligonucleotides, showing the position of the three putative binding sites. **(B)** Competitive EMSA results, using the 193-bp fragment (−159 to +34) as the labeled probe, P-BvrR (0.4 μM), and an excess (1,000×) of the nine different competitors tested. Lanes marked as "−" contain probes without P-BvrR. Blue asterisks = shifted bands (protein-DNA complexes) selected based on the following criteria: absence in the negative control, P-BvrR concentration dependency, and consistency between independent replicas. Black asterisks = bands with the same migration pattern as a free probe. For oligonucleotides 4 and 7, a clear competition was observed. In the case of oligonucleotide 2, a less defined lower band suggested possible competition. These results are representative of at least three independent experiments.

range for these bonds (Figure 6 and Supplementary Figure 3). Regarding the amino acids interacting with DNA, in all three boxes, BvrR utilizes the polar and positively charged amino acids Tyr 230, Thr 228, Arg 213, Lys 210, and Tyr 234 to interact with the DNA molecule through hydrogen bonds. When comparing BvrR with the KdpE template, it becomes apparent that the *E. coli* protein primarily utilizes the Tyr, Ile, Gln, and Arg residues to interact with DNA. However, it is worth noting that the DNA interaction site (TTTATA) differs between BvrR and KdpE (Narayanan et al., 2014).

The sequence alignment of the three boxes (Figure 7A) revealed the presence of the inverted DNA repeat GTAAG – GAATG, separated by two nucleotides (GA) in box 1. In box 2, the non-inverted DNA repeat TGTCA – TGTCA is separated by four nucleotides (CCCC), and nearby in box 3, we found the non-inverted repeat TCTCNACA – TCTCNACA (where N = G or C), separated by five nucleotides (GATTA). Moreover, the sequences of boxes 1 and 3 partially match (83.33 and 66.67%, respectively) a 6-nucleotide long DNA binding motif predicted *in silico* as putatively recognized by BvrR (Ramírez-González et al., 2019). The location of the three boxes is also in agreement with previous P-BvrR ChIP-Seq data, suggesting P-BvrR binding upstream of *omp25* (Rivas-Solano et al., 2022). Since the P-BvrR ChIP-Seq data was used to infer a P-BvrR consensus sequence, it was expected that this region would have some similarity to this sequence. In fact, the three boxes show 78.57 and 71.42% similarity to the 14-bp long consensus sequence (Rivas-Solano et al., 2022).

As shown in Figure 7B, we manually predicted the −35 and −10 elements and the ribosome binding site according to the canonical *E. coli* models. The −35 elements possibly have the sequence GCATTT. This sequence is located at positions −35 to −30 from the first *omp25* TSS, which was described at position −131 from the start codon (Suárez-Esquivel et al., 2016). The sequence GCATTT is also located at positions −41 to −36 from the second TSS described at position −82 from the *omp25* start codon (Rivas-Solano et al., 2022). The −10 elements may have a TATNTC sequence (where N = C or G) located between −10 and −6 and −15 and −10 from the −131 and −82 TSSs, respectively. The ribosome binding sequence is probably TAAGGAG, located at −13 to −7 from the *omp25* start codon. Detailed sequence information is presented in Supplementary Figure 4.

4. Discussion

Despite the crucial role of the TCS BvrR/BvrS in *Brucella*, the DNA-regulatory regions controlled by this TCS are not characterized. Here, we delimited a DNA regulatory region for the gene *omp25*, encoding an outer-membrane protein in *B. abortus* and positively regulated by the TCS BvrR/BvrS (Guzman-Verri et al., 2002). Our results show that a DNA fragment of 380-bp, including 127-bp from the coding region and the first 262-bp upstream of the *omp25* start codon, allows transcription. Additionally, a 111-bp sequence between – 262

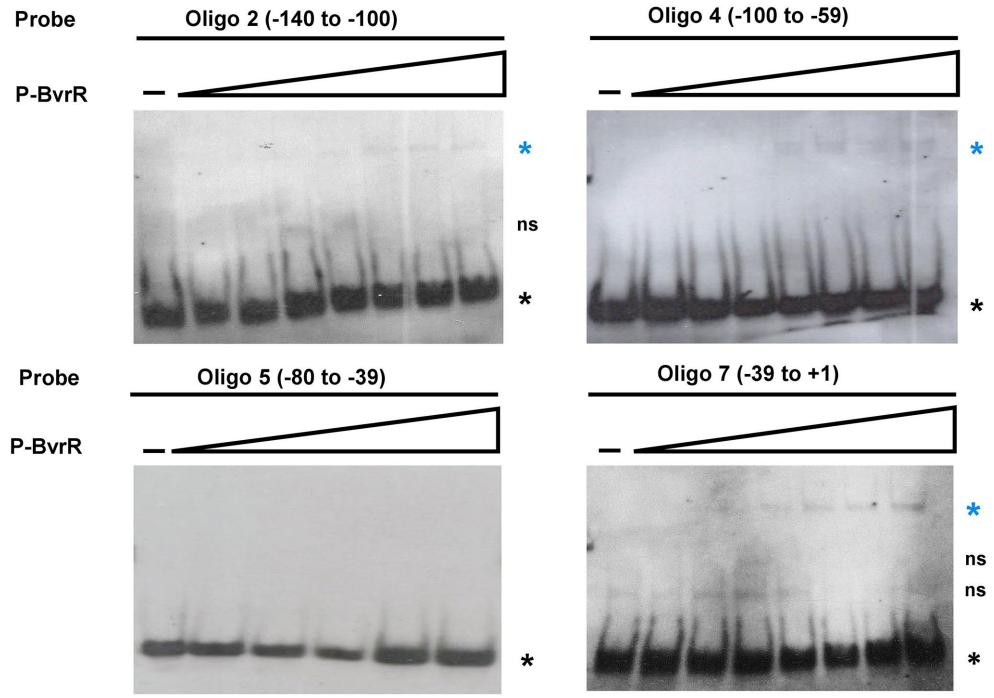

FIGURE 4
Direct EMSA results confirm the presence of three specific P-BvrR binding sites on the upstream region of *omp25*. The competing oligonucleotides 2, 4, and 7, and the non-competing oligonucleotide 5 (specificity control for P-BvrR binding) were labeled and incubated with increasing concentrations of P-BvrR (0.1 to 1.6 μM). Lanes marked as "-" contain probes without P-BvrR. Blue asterisks = shifted bands (protein-DNA complexes) selected based on the following criteria: absence in the negative control, P-BvrR concentration dependency, and consistency between independent replicas. Black asterisks = bands with the same migration pattern as a free probe. "ns" = non-specific bands. These results are representative of at least three independent experiments.

and −151 is required for optimal transcription. P-BvrR binds downstream of this 111-bp sequence in three different boxes. It is possible that binding of P-BvrR to these boxes could recruit other transcription factors to impact *omp25* transcription. Many transcription factors play an architectural role in the genome and remodel DNA structure through bending, kinking, wrapping, or bridging (Dorman et al., 2020). In brucellae, other DNA regulatory regions interplay with different transcription factors (de Jong et al., 2008; Sieira, 2013). For instance, the regulatory region of the *virB* operon displays a complex architecture with binding sites for up to six different types of transcriptional regulators, including BvrR, demonstrating a high versatility in responding to various environmental signals at different stages of the infection process (Sieira, 2013). Small RNAs also seem to influence the expression of the *virB* operon in *B. abortus* at a post-transcriptional level (Caswell et al., 2012). Likewise, the regulatory region of *btaE*, a gene encoding a trimeric autotransporter adhesin relevant for virulence (Ruiz-Ranwez et al., 2013), contains binding sites for three different transcription factors also involved in regulating the expression of the *virB* promoter (Sieira et al., 2017). Thus, it seems possible that other transcription factors could work with BvrR to regulate *omp25* expression. In *B. abortus*, the cell-cycle regulator CtrA, conserved in the *Alphaproteobacteria*, has been implicated in controlling outer membrane composition, particularly the abundance and spatial distribution of Omp25 (Francis et al., 2017; Poncin et al., 2018). The CtrA binding site in the *omp25* upstream region is between positions −389 and −337 (Francis et al., 2017; Figure 7B). Additional transcriptional regulatory mechanisms involved in a BvrR-CtrA interplay remain elusive. In brucellae, mutants in the transcriptional regulators VjbR and GntR display decreased production of Omp25 and altered outer membrane composition (Uzureau et al., 2007; Li et al., 2017). However, the direct interaction between these transcriptional regulators and the regulatory region of *omp25* is currently unknown.

The positions of the BvrR regulatory boxes described here disagree with the canonical *E. coli* models for positive transcriptional regulation. Box 1 (−18 to +1) is next to the *omp25* annotated first codon (Suárez-Esquivel et al., 2016), and box 3 (−140 to −122) includes the transcriptional start site reported for *omp25* at position −131 in brucellae grown to the stationary phase (Suárez-Esquivel et al., 2016), close to −35 and −10 elements. Additionally, another downstream transcription start site at position −82, matching box 2 (−99 to −76) in brucellae grown to the mid-log phase, has recently been reported (Rivas-Solano et al., 2022). How these regions interact deserves further studies. In prokaryotes, a few transcriptional activators are known to bind to unusual regions to induce promoter activity. For example, in *Bacillus subtilis*, PhoP, a response regulator for phosphate starvation response, induces the activation of the gene *pstS* by binding to an upstream region (−40 to −132) and a coding region (+17 to +270) (Liu et al., 1998). The coding region-box has a low affinity for PhoP-P (Liu et al., 1998), suggesting a dynamic DNA-protein binding in which the regulator is required to start transcription but can easily unbind to allow RNA polymerase to proceed. Global regulators like BvrR can bind to a collection of sites, so the regulatory effect on each binding site would depend on the protein concentration and its affinity. Thus, they could have dual roles as activators, repressors, or both

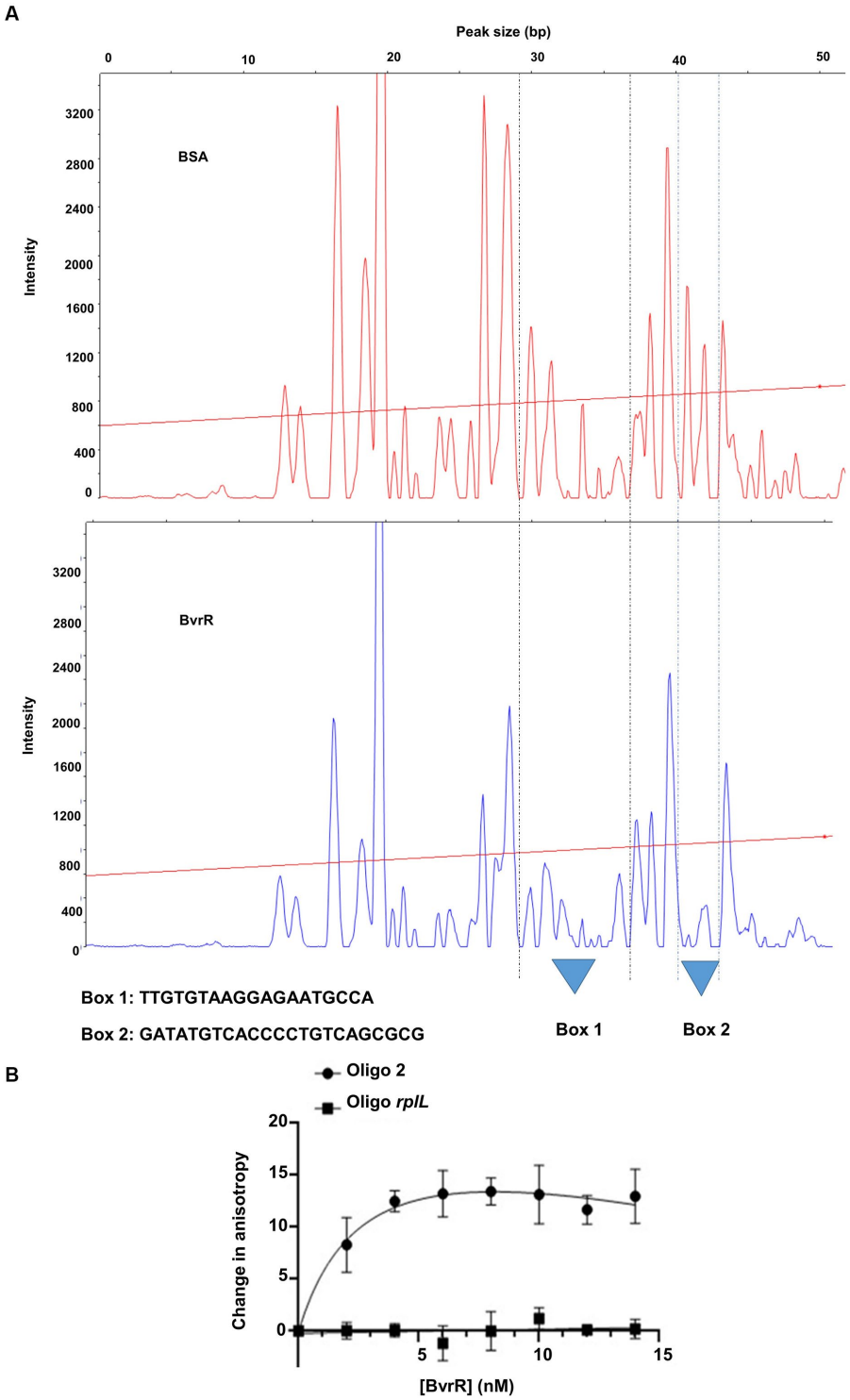

FIGURE 5
Confirmation of BvrR binding sites by additional experimentation. **(A)** DNase I footprinting analysis of the *omp25* upstream fragment (193-bp, –159 to +34). The Peak Scanner software inferred the protected regions by analyzing the electropherograms from digested DNA with 3.64 nM BSA (upper panel) or 8.32 μM P-BvrR (bottom panel). Base pair positions were inferred from the Sanger sequencing of the 193-bp fragment compared to the DNAse I protected regions. Two protected DNA regions of approximately 20 nucleotides between positions –18 to +1 (box 1) and – 99 to –76 (box 2), matching the oligonucleotides 7 and 4, are shown. The straight red line across each electropherogram represents the molecular size calibration obtained with molecular weight markers run together with the samples. **(B)** Fluorescence anisotropy analysis. The oligonucleotide 2 and a smaller fragment of the negative control used for EMSA were labeled with FAM and separately incubated with P-BvrR. The fluorescence anisotropy of each sample was measured, and the obtained curves show a positive change for the oligonucleotide 2 compared to the negative control. This result, combined with the EMSA results shown in Figures 2–4, allowed us to delimit box 3 to the region between –140 and – 122. These results are representative of at least two independent experiments.

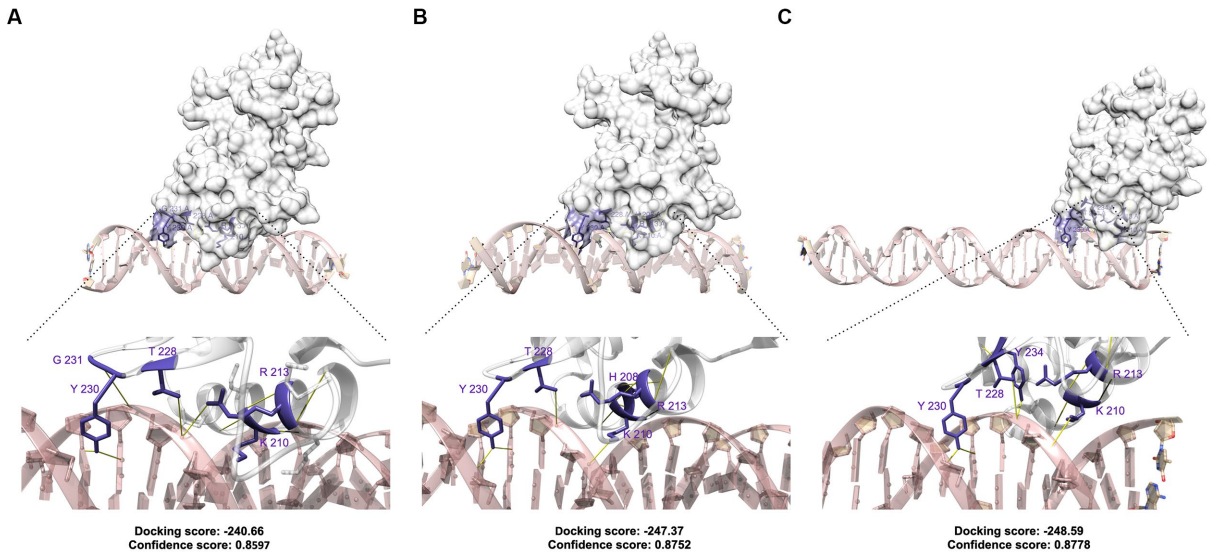

FIGURE 6
Molecular docking of BvrR and its three binding sites on the promoter region of *omp25*. **(A)** Box 1; **(B)** box 2; and **(C)** box 3. The model of BvrR and the docking with its ligands were generated using the HDOCK server. For the protein, the amino acids involved in hydrogen bonds are highlighted in purple. Hydrogen bridges are represented in yellow.

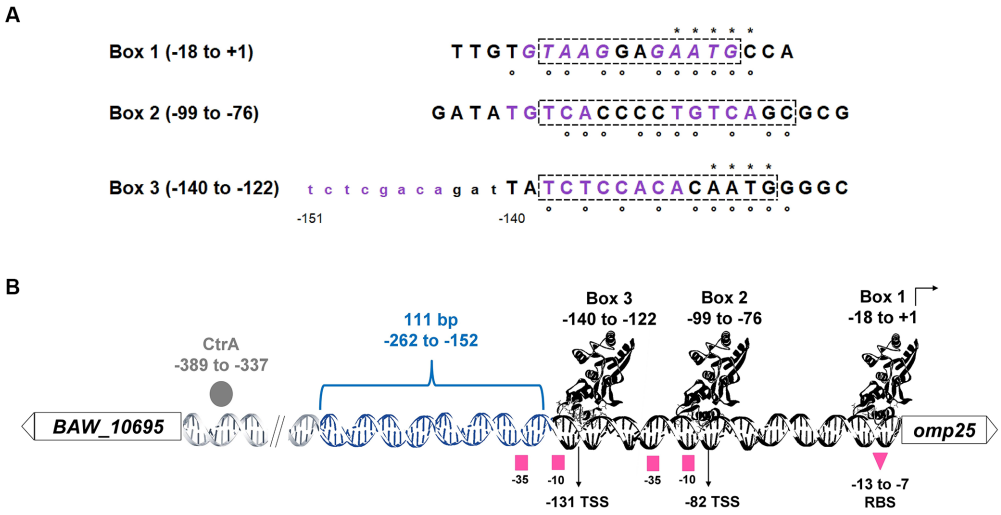

FIGURE 7
B. abortus BvrR regulatory boxes on the regulatory region of *omp25*. **(A)** Nucleotide sequence alignment of the three BvrR regulatory boxes. Dashed squares = nucleotides docked with BvrR. Purple nucleotides = DNA repeats (in italics, the inverted ones in box 1). The 12 upstream nucleotides in lowercase letters next to box 3 (from −151 to −141) were added to show the presence of the repeat. Asterisks = nucleotides matching a 6-nucleotide-long DNA binding motif predicted *in silico* as putatively recognized by BvrR (Ramírez-González et al., 2019). White circles = nucleotides matching a 14-nucleotide-long consensus sequence predicted and experimentally validated for BvrR (Rivas-Solano et al., 2022). **(B)** Non-scale schematic representation of the *omp25* regulatory region. White rectangles = genes *BAW_10695* and *omp25*; DNA chain = intergenic region. Gray circle = CtrA bound to the region from −389 to −337 (Francis et al., 2017), blue DNA chain = 111-bp region from −262 to −152 needed for transcriptional activity, black DNA chain = significantly reduced transcriptional activity, protein structures cartoons = BvrR bound to its three regulatory boxes, right angle arrow = *omp25* coding region, pink squares = predicted −10 and − 35 regulatory elements, pink triangle = predicted ribosome binding site (RBS), vertical black arrows = transcriptional start sites reported elsewhere at positions −131 and − 82, respectively, in bacteria grown until stationary phase (Suárez-Esquivel et al., 2016) and until mid-log phase (Rivas-Solano et al., 2022). The P-BvrR ChIP-Seq signals previously reported have the following coordinates: −242 to −56, −181 to −40, and −159 to +34 (Rivas-Solano et al., 2022).

(Martínez-Antonio and Collado-Vides, 2003; Lozada-Chávez et al., 2008; Balleza et al., 2009). The *E. coli* global response regulator OmpR regulates the expression of the gene *ompF* by binding to four sites with different affinities. At low osmolarity, OmpR concentration is low, and the regulator binds to the four boxes, which promotes OmpF expression. At high osmolarity, OmpR concentration increases, and new interactions of OmpR with a distant box (−380 to −350) repress *ompF* transcription (Huang et al., 1994; Kenney, 2002).

Although hydrogen bonds may vary *in vivo*, hydrogen bond formation capability, the docking scores, and the protein-DNA binding position suggest that BvrR has a binding affinity for the three boxes in the Trans_reg_C domain. The DNA-sequence alignment of the three boxes revealed the presence of inverted and non-inverted repeats separated by variable distances, suggesting that variations in the recognition sequences may influence BvrR affinity for a differential regulation of its target genes. The effector domains of some OmpR-like regulators are known to bind tandem sequences or, more rarely, to inverted repeats for the regulation of transcription. The recognition site in the DNA ranges from 18 to 23-bp, with binding sites between 6 and 10-bp separated by 2 to 5-bp of the intervening sequence (Harlocker et al., 1995; Blanco et al., 2002; He and Wang, 2014). However, the regulator ChvI from *S. meliloti* recognizes an 11-bp-long motif sequence present at least once in the analyzed sequences (Chen et al., 2009). Therefore, the target promoters of the OmpR-like response regulators contain multiple binding sites that vary in nucleotide frequency, position, and relative binding affinities. As a result, cooperativity and differential binding are critical components of the transcriptional regulation exerted by the OmpR-like response regulators.

In brucellae, the current model postulates that the TCS BvrR/BvrS senses environmental conditions and regulates gene expression accordingly (Lamontagne et al., 2007; Viadas et al., 2010; Altamirano-Silva et al., 2018, 2021). Based on the results described here, we conclude that (i) A 111-bp region upstream of BvrR binding boxes is needed for wild-type transcriptional levels at different times of the growth curve, suggesting that additional regulators are binding to this region; (ii) P-BvrR could differentially regulate *omp25* expression by direct binding to three DNA regulatory boxes. Whether a particular condition such as phosphorylation or oligomerization affects BvrR binding remains elusive, as well as how many sites are bound simultaneously or independently; and (iii) BvrR possibly recognizes repeated sequences as has been described for other OmpR-like response regulators, and their influence on BvrR binding affinity and preferences remains to be clarified. The oligonucleotides predicted to bind to BvrR by molecular docking could be mutated and tested by EMSA or fluorescence anisotropy with P-BvrR, to prove the impact of each nucleotide on binding affinity. Additionally, crystallography studies of BvrR and BvrR-DNA complexes could also contribute to revealing the mechanistic insights of the binding of BvrR to the regulatory boxes identified here. The results presented here are observations that contribute to a better understanding of the gene regulation mediated by a TCS conserved in *Rhizobiales*, an essential component for environmental adaptation and host–microbe interactions in these organisms. Additional studies should be performed to elucidate the *omp25* transcriptional regulation.

Data availability statement

The original contributions presented in the study are included in the article/Supplementary material, further inquiries can be directed to the corresponding author.

Author contributions

AC-Z: conceptualization, formal analysis, investigation, methodology, validation, visualization, roles and writing—original draft, writing—review and editing. OR-S: conceptualization, formal analysis, funding acquisition, investigation, methodology, validation, visualization, roles and writing—original draft, writing—review and editing. FV-R: conceptualization, formal analysis, investigation, methodology, resources, writing—review and editing. OG-E: conceptualization, formal analysis, methodology, resources, writing—review and editing. EM: conceptualization, funding acquisition, supervision, writing—review and editing. EC-O: conceptualization, funding acquisition, resources, supervision, writing—review and editing. CG-V: conceptualization, formal analysis, funding acquisition, investigation, methodology, project administration, resources, supervision, validation, visualization, roles and writing—original draft, writing—review and editing. All authors contributed to the article and approved the submitted version.

Funding

This study has been funded by grants from "Fondos del Sistema FEES/CONARE" (FS-CN-02-2020 to CG-V), "Fondos FIDA, Universidad Nacional" (SIA 0047-17 to CG-V), and ICGBE (contract CRP/21/005 to CG-V). OR-S holds a Ph.D. scholarship from "Instituto Tecnológico de Costa Rica," contract number 15-15-D, and from "PINN-MICITT," contract number PND-137-15-1.

Acknowledgments

We would like to thank Laura Monturiol-Gross from Instituto Clodomiro Picado for providing access to the laboratory equipment and facilities to perform the fluorescence anisotropy assays and Reynaldo Pereira-Reyes for his technical assistance with recombinant BvrR purification, EMSA, and DNase I footprinting assays.

Conflict of interest

The authors declare that the research was conducted in the absence of any commercial or financial relationships that could be construed as a potential conflict of interest.

Publisher's note

Supplementary material

The Supplementary material for this article can be found online at: https://www.frontiersin.org/articles/10.3389/fmicb.2023.1241143/full#supplementary-material

References

Altamirano-Silva, P., Cordero-Serrano, M., Méndez-Montoya, J., Chacón-Díaz, C., Guzmán-Verri, C., Moreno, E., et al. (2021). Intracellular passage triggers a molecular response in *Brucella abortus* that increases its infectiousness. *Infect. Immun.* 89:e0000421. doi: 10.1128/IAI.00004-21

Altamirano-Silva, P., Meza-Torres, J., Castillo-Zeledón, A., Ruiz-Villalobos, N., Zuñiga-Pereira, A. M., Chacón-Díaz, C., et al. (2018). *Brucella abortus* senses the intracellular environment through the BvrR/BvrS two-component system, which allows *B. abortus* to adapt to its replicative niche. *Infect. Immun.* 86:e00713-17. doi: 10.1128/IAI.00713-17

Balleza, E., López-Bojorquez, L. N., Martínez-Antonio, A., Resendis-Antonio, O., Lozada-Chávez, I., Balderas-Martínez, Y. I., et al. (2009). Regulation by transcription factors in bacteria: beyond description. *FEMS Microbiol. Rev.* 33, 133–151. doi: 10.1111/j.1574-6976.2008.00145.x

Batut, J., Andersson, S. G. E., and O'Callaghan, D. (2004). The evolution of chronic infection strategies in the α-proteobacteria. *Nat. Rev. Microbiol.* 2, 933–945. doi: 10.1038/nrmicro1044

Beier, D., and Gross, R. (2006). Regulation of bacterial virulence by two-component systems. *Curr. Opin. Microbiol.* 9, 143–152. doi: 10.1016/j.mib.2006.01.005

Bélanger, L., and Charles, T. C. (2013). Members of the *Sinorhizobium meliloti* ChvI regulon identified by a DNA binding screen. *BMC Microbiol.* 13:132. doi: 10.1186/1471-2180-13-132

Blanco, A. G., Sola, M., Gomis-Rüth, F. X., and Coll, M. (2002). Tandem DNA recognition by PhoB, a two-component signal transduction transcriptional activator. *Structure* 10, 701–713. doi: 10.1016/S0969-2126(02)00761-X

Caswell, C. C., Gaines, J. M., and Roop, R. M. II. (2012). The RNA chaperone Hfq independently coordinates expression of the VirB type IV secretion system and the LuxR-type regulator BabR in *Brucella abortus* 2308. *J. Bacteriol.* 194, 3–14. doi: 10.1128/JB.05623-11

Charles, T. C., and Nester, E. W. (1993). A chromosomally encoded two-component sensory transduction system is required for virulence of *Agrobacterium tumefaciens*. *J. Bacteriol.* 175, 6614–6625. doi: 10.1128/jb.175.20.6614-6625.1993

Chen, E. J., Fisher, R. F., Perovich, V. M., Sabio, E. A., and Long, S. R. (2009). Identification of direct transcriptional target genes of ExoS/ChvI two-component signaling in *Sinorhizobium meliloti*. *J. Bacteriol.* 191, 6833–6842. doi: 10.1128/JB.00734-09

Cheng, H. P., and Walker, G. C. (1998). Succinoglycan production by *Rhizobium meliloti* is regulated through the ExoS-ChvI two-component regulatory system. *J. Bacteriol.* 180, 20–26. doi: 10.1128/jb.180.1.20-26.1998

De Jong, M. F., Sun, Y. H., Den Hartigh, A. B., Van Dijl, J. M., and Tsolis, R. M. (2008). Identification of VceA and VceC, two members of the VjbR regulon that are translocated into macrophages by the *Brucella* type IV secretion system. *Mol. Microbiol.* 70, 1378–1396. doi: 10.1111/j.1365-2958.2008.06487.x

Dorman, C. J., Schumacher, M. A., Bush, M. J., Brennan, R. G., and Buttner, M. J. (2020). When is a transcription factor a NAP? *Curr. Opin. Microbiol.* 55, 26–33. doi: 10.1016/j.mib.2020.01.019

Favicchio, R., Dragan, A. I., Kneale, G. G., and Read, C. M. (2009). Fluorescence spectroscopy and anisotropy in the analysis of DNA-protein interactions. *Methods Mol. Biol.* 543, 589–611. doi: 10.1007/978-1-60327-015-1_35

Francis, N., Poncin, K., Fioravanti, A., Vassen, V., Willemart, K., Ong, T. A. P., et al. (2017). CtrA controls cell division and outer membrane composition of the pathogen *Brucella abortus*. *Mol. Microbiol.* 103, 780–797. doi: 10.1111/mmi.13589

Gober, J. W., and Shapiro, L. (1992). A developmentally regulated Caulobacter flagellar promoter is activated by 3′ enhancer and IHF binding elements. *Mol. Biol. Cell* 3, 913–926. doi: 10.1091/mbc.3.8.913

Godessart, P., Lannoy, A., Dieu, M., Van der Verren, S. E., Soumillion, P., Collet, J. F., et al. (2021). β-Barrels covalently link peptidoglycan and the outer membrane in the α-proteobacterium *Brucella abortus*. *Nat. Microbiol.* 6, 27–33. doi: 10.1038/s41564-020-00799-3

Graph Pad (2019). *Home-Graph Pad*. Available at: https://www.graphpad.com/ (Accessed September 20, 2021).

Guzman-Verri, C., Manterola, L., Sola-Landa, A., Parra, A., Cloeckaert, A., Garin, J., et al. (2002). The two-component system BvrR/BvrS essential for *Brucella abortus* virulence regulates the expression of outer membrane proteins with counterparts in members of the Rhizobiaceae. *Proc. Natl. Acad. Sci. U. S. A.* 99, 12375–12380. doi: 10.1073/pnas.192439399

Harlocker, S. L., Bergstrom, L., and Inouye, M. (1995). Tandem binding of six OmpR proteins to the ompF upstream regulatory sequence of *Escherichia coli*. *J. Biol. Chem.* 270, 26849–26856. doi: 10.1074/JBC.270.45.26849

He, X., and Wang, S. (2014). DNA consensus sequence motif for binding response regulator PhoP, a virulence regulator of *Mycobacterium tuberculosis*. *Biochemistry* 53, 8008–8020. doi: 10.1021/bi501019u

Heavner, M. E., Qiu, W. G., and Cheng, H. P. (2015). Phylogenetic co-occurrence of ExoR, ExoS, and ChvI, components of the RSI bacterial invasion switch, suggests a key adaptive mechanism regulating the transition between free-living and host-invading phases in rhizobiales. *PLoS One* 10:e0135655. doi: 10.1371/journal.pone.0135655

Hellman, L. M., and Fried, M. G. (2007). Electrophoretic mobility shift assay (EMSA) for detecting protein–nucleic acid interactions. *Nat. Protoc.* 2, 1849–1861. doi: 10.1038/nprot.2007.249

Huang, K.-J., Schieberl, J. L., and Igo, M. M. (1994). A distant upstream site involved in the negative regulation of the *Escherichia coli* ompF gene. *J. Bacteriol.* 176, 1309–1315. doi: 10.1128/jb.176.5.1309-1315.1994

Hulme, E. C., and Trevethick, M. A. (2010). Ligand binding assays at equilibrium: validation and interpretation. *Br. J. Pharmacol.* 161, 1219–1237. doi: 10.1111/j.1476-5381.2009.00604.x

Jumper, J., Evans, R., Pritzel, A., Green, T., Figurnov, M., Ronneberger, O., et al. (2021). Highly accurate protein structure prediction with AlphaFold. *Nature* 596, 583–589. doi: 10.1038/s41586-021-03819-2

Kenney, L. (2002). Structure/function relationships in OmpR and other winged-helix transcription factors. *Curr. Opin. Microbiol.* 5, 135–141. doi: 10.1016/S1369-5274(02)00310-7

Lamontagne, J., Butler, H., Chaves-Olarte, E., Hunter, J., Schirm, M., Paquet, C., et al. (2007). Extensive cell envelope modulation is associated with virulence in *Brucella abortus*. *J. Proteome Res.* 6, 1519–1529. doi: 10.1021/pr060636a

Lamontagne, J., Forest, A., Marazzo, E., Denis, F., Butler, H., Michaud, J. F., et al. (2009). Intracellular adaptation of *Brucella abortus*. *J. Proteome Res.* 8, 1594–1609. doi: 10.1021/pr800978p

Li, Z. Q., Zhang, J. L., Xi, L., Yang, G. L., Wang, S. L., Zhang, X. G., et al. (2017). Deletion of the transcriptional regulator GntR down regulated the expression of genes related to virulence and conferred protection against wild-type *Brucella* challenge in BALB/c mice. *Mol. Immunol.* 92, 99–105. doi: 10.1016/j.molimm.2017.10.011

Liu, W., Qi, Y., and Hulett, F. M. (1998). Sites internal to the coding regions of phoA and pstS bind PhoP and are required for full promoter activity. *Mol. Microbiol.* 28, 119–130. doi: 10.1046/J.1365-2958.1998.00779.X

López-Goñi, I., Guzmán-Verri, C., Manterola, L., Sola-Landa, A., Moriyón, I., and Moreno, E. (2002). Regulation of *Brucella* virulence by the two-component system BvrR/BvrS. *Vet. Microbiol.* 90, 329–339. doi: 10.1016/S0378-1135(02)00218-3

Lozada-Chávez, I., Angarica, V. E., Collado-Vides, J., and Contreras-Moreira, B. (2008). The role of DNA-binding specificity in the evolution of bacterial regulatory networks. *J. Mol. Biol.* 379, 627–643. doi: 10.1016/j.jmb.2008.04.008

Luscombe, N. M., Laskowski, R. A., and Thornton, J. M. (1997). NUCPLOT: a program to generate schematic diagrams of protein-nucleic acid interactions. *Nucleic Acids Res.* 25, 4940–4945. doi: 10.1093/nar/25.24.4940

Manterola, L., Guzmán-Verri, C., Chaves-Olarte, E., Barquero-Calvo, E., de Miguel, M.-J., Moriyón, I., et al. (2007). BvrR/BvrS-controlled outer membrane proteins Omp3a and Omp3b are not essential for *Brucella abortus* virulence. *Infect. Immun.* 75, 4867–4874. doi: 10.1128/IAI.00439-07

Manterola, L., Moriyón, I., Moreno, E., Sola-Landa, A., Weiss, D. S., Koch, M. H. J., et al. (2005). The lipopolysaccharide of *Brucella abortus* BvrS/BvrR mutants contains lipid a modifications and has higher affinity for bactericidal cationic peptides. *J. Bacteriol.* 187, 5631–5639. doi: 10.1128/JB.187.16.5631-5639.2005

Martínez-Antonio, A., and Collado-Vides, J. (2003). Identifying global regulators in transcriptional regulatory networks in bacteria. *Curr. Opin. Microbiol.* 6, 482–489. doi: 10.1016/J.MIB.2003.09.002

Martínez-Núñez, C., Altamirano-Silva, P., Alvarado-Guillén, F., Moreno, E., Guzmán-Verri, C., and Chaves-Olarte, E. (2010). The two-component system BvrR/BvrS regulates the expression of the type IV secretion system VirB in *Brucella abortus*. *J. Bacteriol.* 192, 5603–5608. doi: 10.1128/JB.00567-10

Martín-Martín, A. I., Caro-Hernández, P., Sancho, P., Tejedor, C., Cloeckaert, A., Fernández-Lago, L., et al. (2009). Analysis of the occurrence and distribution of the Omp25/Omp31 family of surface proteins in the six classical *Brucella* species. *Vet. Microbiol.* 137, 74–82. doi: 10.1016/j.vetmic.2008.12.003

Moreno, E. (2021). The one hundred year journey of the genus *Brucella* (Meyer and Shaw 1920). *FEMS Microbiol. Rev.* 45, 1–22. doi: 10.1093/femsre/fuaa045

Narayanan, A., Kumar, S., Evrard, A. N., Paul, L. N., and Yernool, D. A. (2014). An asymmetric heterodomain interface stabilizes a response regulator–DNA complex. *Nat. Com.* 5:3282. doi: 10.1038/ncomms4282

Nguyen, M. P., Yoon, J. M., Cho, M. H., and Lee, S. W. (2015). Prokaryotic 2-component systems and the Ompr/Phob superfamily. *Can. J. Microbiol.* 61, 799–810. doi: 10.1139/cjm-2015-0345

Owen, B., and McMurray, C. (2009). Rapid method for measuring DNA binding to protein using fluorescence anisotropy. *Protoc. Exch.* doi: 10.1038/NPROT.2009.80

Poncin, K., Gillet, S., and De Bolle, X. (2018). Learning from the master: targets and functions of the CtrA response regulator in *Brucella abortus* and other alpha-proteobacteria. *FEMS Microbiol. Rev.* 42, 500–513. doi: 10.1093/femsre/fuy019

Quebatte, M., Dehio, M., Tropel, D., Basler, A., Toller, I., Raddatz, G., et al. (2010). The BatR/BatS two-component regulatory system controls the adaptive response of *Bartonella henselae* during human endothelial cell infection. *J. Bacteriol.* 192, 3352–3367. doi: 10.1128/JB.01676-09

Ramírez-González, E. A., Moreno-Lafont, M. C., Méndez-Tenorio, A., Cancino-Díaz, M. E., Estrada-García, I., and López-Santiago, R. (2019). Prediction of structure and molecular interaction with DNA of BvrR, a virulence-associated regulatory protein of *Brucella*. *Molecules* 24, 1–15. doi: 10.3390/molecules24173137

Ratib, N. R., Sabio, E. Y., Mendoza, C., Barnett, M. J., Clover, S. B., Ortega, J. A., et al. (2018). Genome-wide identification of genes directly regulated by ChvI and a consensus sequence for ChvI binding in *Sinorhizobium meliloti*. *Mol. Microbiol.* 110, 596–615. doi: 10.1111/mmi.14119

Rivas-Solano, O., Van der Henst, M., Castillo-Zeledón, A., Suárez-Esquivel, M., Muñoz-Vargas, L., Capitan-Barrios, Z., et al. (2022). The regulon of *Brucella abortus* two-component system BvrR/BvrS reveals the coordination of metabolic pathways required for intracellular life. *PLoS One* 17:e0274397. doi: 10.1371/journal.pone.0274397

Roop, R. M., Barton, I. S., Hopersberger, D., and Martin, D. W. (2021). Uncovering the hidden credentials of *Brucella* virulence. *Microbiol. Mol. Biol. Rev.* 85:e00021-19. doi: 10.1128/mmbr.00021-19

Ruiz-Ranwez, V., Posadas, D. M., Estein, S. M., Abdian, P. L., Martin, F. A., and Zorreguieta, A. (2013). The BtaF trimeric autotransporter of *Brucella suis* is involved in attachment to various surfaces, resistance to serum and virulence. *PLoS One* 8:e79770. doi: 10.1371/journal.pone.0079770

Sambrook, J., Fritsch, E. F., and Maniatis, T. (1989). *Molecular cloning: A laboratory model*. Cold Spring Harbor, New York Cold Spring Harbor Laboratory Press.

Sieira, R. (2013). Regulation of virulence in *Brucella*: an eclectic repertoire of transcription factors defines the complex architecture of the virB promoter. *Future Microbiol.* 8, 1193–1208. doi: 10.2217/fmb.13.83

Sieira, R., Bialer, M. G., Roset, M. S., Ruiz-Ranwez, V., Langer, T., Arocena, G. M., et al. (2017). Combinatorial control of adhesion of Brucella abortus 2308 to host cells by transcriptional rewiring of the trimeric autotransporter btaE gene. *Mol. Microbiol.* 103, 553–565. doi: 10.1111/MMI.13576

Sola-Landa, A., Pizarro-Cerdá, J., Grilló, M. J., Moreno, E., Moriyón, I., Blasco, J. M., et al. (1998). A two-component regulatory system playing a critical role in plant pathogens and endosymbionts is present in Brucella abortus and controls cell invasion and virulence. *Mol. Microbiol.* 29, 125–138. doi: 10.1046/j.1365-2958.1998.00913.x

Spink, W. W. (1957). The nature of brucellosis. *Q. Rev. Biol.* 32:311. doi: 10.1086/401954

Studer, G., Rempfer, C., Waterhouse, A. M., Gumienny, R., Haas, J., and Schwede, T. (2020). QMEANDisCo—distance constraints applied on model quality estimation. *Bioinformatics* 36, 1765–1771. doi: 10.1093/bioinformatics/btz828

Suárez-Esquivel, M., Ruiz-Villalobos, N., Castillo-Zeledón, A., Jiménez-Rojas, C., Roop, R. M., Comerci, D. J., et al. (2016). *Brucella abortus* strain 2308 Wisconsin genome: importance of the definition of reference strains. *Front. Microbiol.* 7:1557. doi: 10.3389/fmicb.2016.01557

Uzureau, S., Godefroid, M., Deschamps, C., Lemaire, J., De Bolle, X., and Letesson, J. J. (2007). Mutations of the quorum sensing-dependent regulator VjbR lead to drastic surface modifications in *Brucella melitensis*. *J. Bacteriol.* 189, 6035–6047. doi: 10.1128/JB.00265-07

Varadi, M., Anyango, S., Deshpande, M., Nair, S., Natassia, C., Yordanova, G., et al. (2022). AlphaFold protein structure database: massively expanding the structural coverage of protein-sequence space with high-accuracy models. *Nucleic Acids Res.* 50, D439–D444. doi: 10.1093/nar/gkab1061

Viadas, C., Rodríguez, M. C., Sangari, F. J., Gorvel, J. P., García-Lobo, J. M., and López-Goñi, I. (2010). Transcriptome analysis of the *Brucella abortus* BvrR/BvrS two-component regulatory system. *PLoS One* 5, 1–8. doi: 10.1371/journal.pone.0010216

Vizcaíno, N., Cloeckaert, A., Zygmunt, M. S., and Fernández-Lago, L. (2001). Characterization of a Brucella species 25-kilobase DNA fragment deleted from *Brucella abortus* reveals a large gene cluster related to the synthesis of a polysaccharide. *Infect. Immun.* 69, 6738–6748. doi: 10.1128/IAI.69.11.6738-6748.2001

Waterhouse, A., Bertoni, M., Bienert, S., Studer, G., Tauriello, G., Gumienny, R., et al. (2018). T. SWISS-MODEL: homology modelling of protein structures and complexes. *Nucleic Acids Res.* 46, W296–W303. doi: 10.1093/nar/gky427

Yan, Y., Zhang, D., Zhou, P., Li, B., and Huang, S. Y. (2017). HDOCK: a web server for protein-protein and protein-DNA/RNA docking based on a hybrid strategy. *Nucleic Acids Res.* 45, W365–W373. doi: 10.1093/nar/gkx407

Yang, J., Yan, R., Roy, A., Xu, D., Poisson, J., and Zhang, Y. (2015). The I-TASSER Suite: protein structure and function prediction. *Nat. Methods* 12, 7–8. doi: 10.1038/nmeth.3213

Zianni, M., Tessanne, K., Merighi, M., Laguna, R., and Tabita, F. R. (2006). Identification of the DNA bases of a DNase I footprint by the use of dye primer sequencing on an automated capillary DNA analysis instrument. *J. Biomol. Tech.* 17, 103–113.

frontiers | Frontiers in Microbiology

TYPE Original Research
PUBLISHED 20 September 2023
DOI 10.3389/fmicb.2023.1233686

OPEN ACCESS

EDITED BY
Axel Cloeckaert,
Institut National de recherche pour l'agriculture, l'alimentation et l'environnement (INRAE), France

REVIEWED BY
Gilles Vergnaud,
Université Paris-Saclay, France
Jeffrey T. Foster,
Northern Arizona University, United States
Marcela Suárez-Esquivel,
National University of Costa Rica, Costa Rica

*CORRESPONDENCE
Zhiguo Liu
✉ wlcblzg@126.com
Zhenjun Li
✉ lizhenjun@icdc.cn

RECEIVED 02 June 2023
ACCEPTED 25 August 2023
PUBLISHED 20 September 2023

CITATION
Xue H, Zhao Z, Wang J, Ma L, Li J, Yang X, Ren L, Xu L, Liu Z and Li Z (2023) Native circulating *Brucella melitensis* lineages causing a brucellosis epidemic in Qinghai, China. *Front. Microbiol.* 14:1233686. doi: 10.3389/fmicb.2023.1233686

Native circulating *Brucella melitensis* lineages causing a brucellosis epidemic in Qinghai, China

Hongmei Xue[1], Zhijun Zhao[1], Jianling Wang[1], Li Ma[1], Jiquan Li[1], Xuxin Yang[1], Lingling Ren[1], Liqing Xu[1], Zhiguo Liu[2,3]* and Zhenjun Li[2]*

[1]Department of Brucellosis Prevention and Control, Qinghai Institute for Endemic Disease Prevention and Control, Xining, Qinghai, China, [2]National Institute for Communicable Disease Control and Prevention, Chinese Center for Disease Control and Prevention, Beijing, China, [3]Vocational and Technical College, Inner Mongolia Agricultural University, Baotou, China

Since 2010, the cases and incidences of human brucellosis have been increasing annually in Qinghai (QH) Province. Molecular epidemiology and phylogenetic analyses of strains from this region are crucial to better understand the transmission of the disease and the evolutionary patterns of *Brucella* strains. In this study, classical bio-typing assay, multilocus variable-number tandem repeat analysis, and the whole-genome sequencing–single-nucleotide polymorphism approach were used to illustrate the epidemiological and evolutionary patterns of *Brucella melitensis*. A total of 54 *B. melitensis* bv. 3 strains were isolated and molecularly characterized, with all strains belonging to the East Mediterranean lineages. Cross-regional transmission events (i.e., between counties) were caused by common sources of infection, suggesting that predominant circulating genotypes are endemic in different regions. Strengthening surveillance in animal brucellosis and controlling infected animals' cross-border movement are necessary. Two strains isolated from humans and marmots were clustered in the same sub-clade, implying the possible existence of direct and/or indirect contact between sheep (and goats) and wildlife (marmots), but this needs to be verified by further investigations. The global-scale phylogenetic analysis indicated that 54 strains sorted into six subclades, four of which formed independent lineages, suggesting that the increase in the incidence rate of human brucellosis may be caused by local circulating lineages. Further strengthening the serology and pathogen surveillance of animals (wildlife) and humans will contribute to an in-depth understanding of the transmission chain of human brucellosis in this region.

KEYWORDS

***Brucella melitensis*, whole-genome sequencing, MLVA, WGS–SNP, phylogenetic analysis**

Introduction

Brucellosis (Malta fever) is a globally distributed zoonotic disease. It has severe adverse effects on public health and the agriculture field, including population, livestock, and wildlife health. Since David Bruce first isolated the organism (*Micrococcus melitensis*) in 1887 (Godfroid et al., 2005), 12 species have been identified in the genus *Brucella*, that is, six classical and six novel species (Occhialini et al., 2022). *Brucella melitensis* is the most common pathogenic species in humans and

animals, followed by *Brucella abortus* and *Brucella suis* (Xavier et al., 2010). Brucellosis can be transmitted to humans through the food chain or by direct/indirect contact with infected animals, such as consumption of animal raw milk and meat products or aerosol transmission (Minas et al., 2007). For centuries, brucellosis has been critically endangering human health and has led to substantial economic losses (Wareth, 2019). In some industrial countries, brucellosis has been effectively controlled, but it remains a serious public health risk to the majority of the population in developing areas. For example, in China, brucellosis is widely endemic in all 32 provinces (Rossetti et al., 2017).

Qinghai (QH) Province is located in northwestern China, and animal farming is the main source of income for the local population. Because of low development levels, poverty, and poor hygiene conditions, animal and human brucellosis is highly prevalent in this region (Ma et al., 2016). Although a comprehensive control plan for brucellosis was carried out during 2005–2010, which utilized the *Brucella* S2 vaccine for the immunization of ruminants combined with a serology test, and brucellosis-positive animals were eliminated, persistent funding is a great obstacle to control programs. Subsequently, the prevalence of human brucellosis increased annually in QH from 2005 to 2019 (Ma et al., 2020). Since 2010, the epidemic situation of human brucellosis has gradually become severe: the number of cases increased from 3 in 2010 to 756 in 2021, the incidence rate increased from 0.054/100,000 to 12.76/100,000 accordingly, and the affected geographic territory is currently expanding. Based on the national brucellosis surveillance sites, data indicate that the prevalence rate of human brucellosis was 3.35% (54/1,612) in 2019 and 4.77% (80/1,677) in 2020. However, the ability to tailor a cost-based brucellosis control program requires accurate and robust molecular typing tools to investigate the relationships between strains involved in common outbreaks and determine the source of infection and transmission routes (Pelerito et al., 2021). Generally, classical microbiological techniques allow researchers to obtain and bio-type the strains and facilitate molecular epidemiological investigations of the disease. The multilocus variable-number tandem repeat analysis (MLVA) has been used as the gold standard for genotyping *Brucella* strains, with the results combined with epidemiological data to investigate the relationships between the *Brucella* strains (Kiliç et al., 2011; Liu et al., 2017). Furthermore, single-nucleotide polymorphisms (SNPs) based on whole-genome sequencing have excellent power to discriminate strains and allow for the characterization of the phylogenetic relationships of strains from different scales (Janowicz et al., 2018; Abdel-Glil et al., 2022). Importantly, molecular typing tools can not only limit control costs and test time but also, improve the surveillance and evaluation of control measure effects. Therefore, classical bio-typing assay, MLVA, and whole-genome sequencing–SNP (WGS–SNP) were used to illustrate the species/biovars' genetic diversity and the phylogeography pattern of *B. melitensis* from humans in QH to better assess the epidemiology profile and enhance brucellosis surveillance and control.

Methods

Strain source, identification, DNA isolation, MLST, and MLVA typing assay

A total of 54 *B. melitensis* strains were isolated and identified in the present study, of which 52 were recovered from humans, one from the liver of an aborted sheep fetus, and one from a marmot. All of the tested strains were isolated and identified according to the standard *Brucella* spp. bio-typing procedures (Yagupsky et al., 2019). The DNA of all 54 strains was isolated based on a two-step procedure: (1) the strains were heat inactivated at 80°C for 10 min, and (2) a QIAamp DNA kit (Qiagen, Heidelberg, Germany) was used to prepare the DNA of strains according to the manufacturer's protocol. Following extraction, the harvested DNA from each strain was detected by agarose gel electrophoresis, and the DNA concentration was determined using a Qubit® 2.0 Fluorometer (Thermo Fisher Scientific, Waltham, MA, USA). MLST genotypes were deduced from WGS data using the PubMLST database (Jolley et al., 2018).[1] The MLVA genotyping and data analysis of the strains (Supplementary Table S1) were performed as previously described (Liu et al., 2017).

Genome sequence of *Brucella melitensis* strains

The genome sequencing strategy of strains was referenced in a previous study (Li et al., 2020). Briefly, all 54 *B. melitensis* strains were submitted for whole-genome draft sequencing, and the NEBNext® Ultra™ DNA Library Prep Kit for Illumina platform (New England Biolabs [NEB], Ipswich, MA, USA) was used to yield sequencing libraries according to the manufacturer's specifications, as follows: the quality-tested extracted DNA was fragmented using the E210 Covaris instrument (Covaris, Inc., USA), and segments with approximately 350 bp in length were selected in a 3% agarose gel. The selected DNA fragments were then end-repaired, A-tailed, and ligated to Illumina-compatible adaptors (Bio Scientific, Austin, TX, USA) and then PCR-amplified using Illumina adapter-specific primers and Platinum Pfx DNA polymerase (Invitrogen), and the paired-end sequencing library was completed. Then, the draft genomic sequence of 54 strains was determined, and SOAPdenovo software v.2.04 (Li et al., 2010) was used to assemble and integrate good-quality paired reads into several scaffolds.

SNP phylogenetic analysis of *Brucella melitensis* strains on local and global scales

WGS–SNP phylogenetic analysis of 54 *B. melitensis* strains was performed as previously reported (Li et al., 2020). Subsequently, phylogenetic analysis on the global scale of 133 strains was performed, of which 54 strains were from QH and 79 from GenBank (Supplementary Table S2), including 20 strains that were selected from five genotypes in a previous study, which are marked in red in (Supplementary Table 2) (Pisarenko et al., 2018), and 38 strains from

Abbreviations: WGS–SNP, whole-genome-sequencing–single-nucleotide polymorphism; MLVA, multilocus variable-number tandem repeat analysis.

1 https://pubmlst.org/organisms/brucella-spp

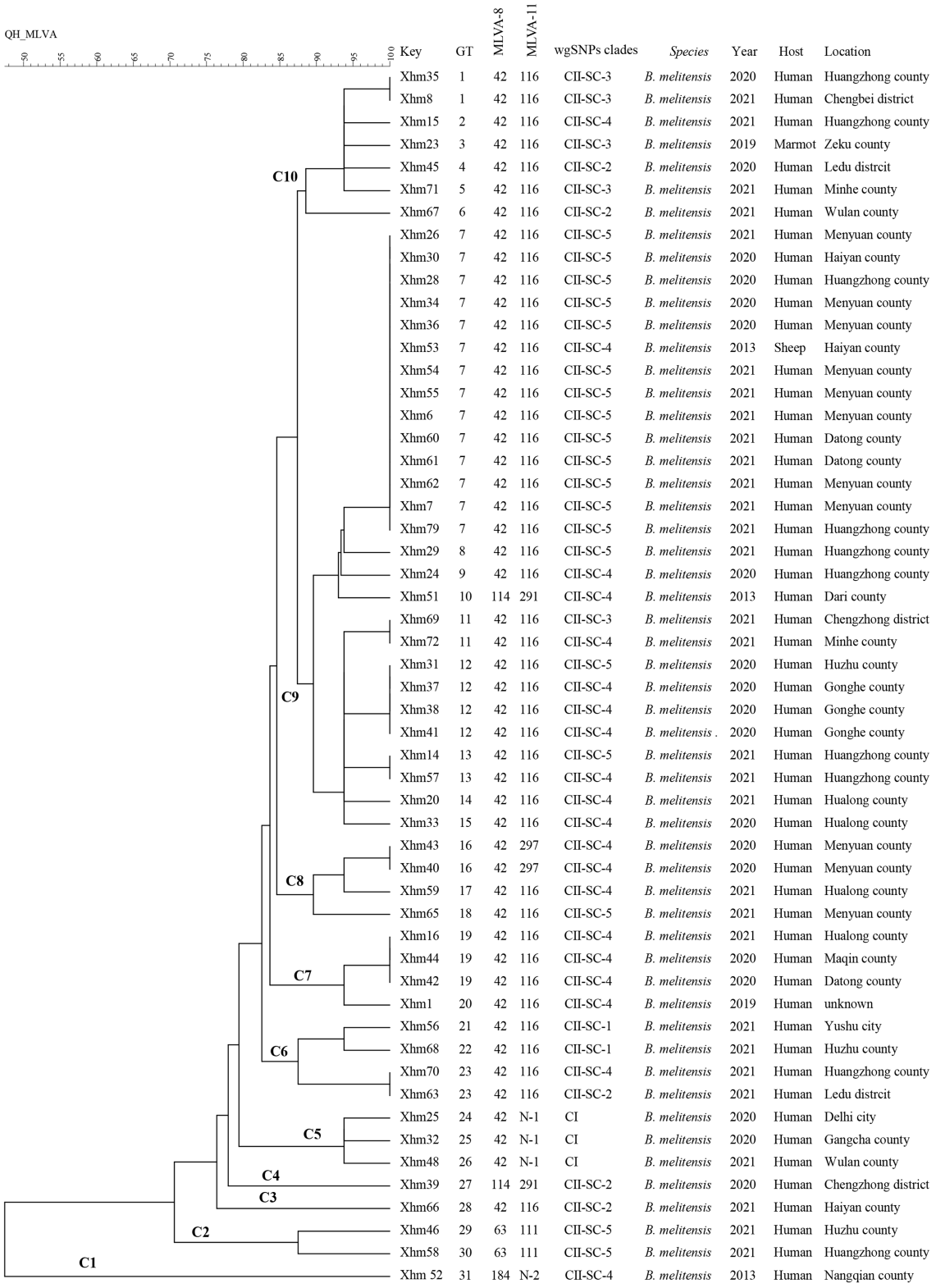

Key	GT	MLVA-8	MLVA-11	wgSNPs clades	*Species*	Year	Host	Location
Xhm35	1	42	116	CII-SC-3	*B. melitensis*	2020	Human	Huangzhong county
Xhm8	1	42	116	CII-SC-3	*B. melitensis*	2021	Human	Chengbei district
Xhm15	2	42	116	CII-SC-4	*B. melitensis*	2021	Human	Huangzhong county
Xhm23	3	42	116	CII-SC-3	*B. melitensis*	2019	Marmot	Zeku county
Xhm45	4	42	116	CII-SC-2	*B. melitensis*	2020	Human	Ledu distrcit
Xhm71	5	42	116	CII-SC-3	*B. melitensis*	2021	Human	Minhe county
Xhm67	6	42	116	CII-SC-2	*B. melitensis*	2021	Human	Wulan county
Xhm26	7	42	116	CII-SC-5	*B. melitensis*	2021	Human	Menyuan county
Xhm30	7	42	116	CII-SC-5	*B. melitensis*	2020	Human	Haiyan county
Xhm28	7	42	116	CII-SC-5	*B. melitensis*	2020	Human	Huangzhong county
Xhm34	7	42	116	CII-SC-5	*B. melitensis*	2020	Human	Menyuan county
Xhm36	7	42	116	CII-SC-5	*B. melitensis*	2020	Human	Menyuan county
Xhm53	7	42	116	CII-SC-4	*B. melitensis*	2013	Sheep	Haiyan county
Xhm54	7	42	116	CII-SC-5	*B. melitensis*	2021	Human	Menyuan county
Xhm55	7	42	116	CII-SC-5	*B. melitensis*	2021	Human	Menyuan county
Xhm6	7	42	116	CII-SC-5	*B. melitensis*	2021	Human	Menyuan county
Xhm60	7	42	116	CII-SC-5	*B. melitensis*	2021	Human	Datong county
Xhm61	7	42	116	CII-SC-5	*B. melitensis*	2021	Human	Datong county
Xhm62	7	42	116	CII-SC-5	*B. melitensis*	2021	Human	Menyuan county
Xhm7	7	42	116	CII-SC-5	*B. melitensis*	2021	Human	Menyuan county
Xhm79	7	42	116	CII-SC-5	*B. melitensis*	2021	Human	Huangzhong county
Xhm29	8	42	116	CII-SC-5	*B. melitensis*	2021	Human	Huangzhong county
Xhm24	9	42	116	CII-SC-4	*B. melitensis*	2020	Human	Huangzhong county
Xhm51	10	114	291	CII-SC-4	*B. melitensis*	2013	Human	Dari county
Xhm69	11	42	116	CII-SC-3	*B. melitensis*	2021	Human	Chengzhong district
Xhm72	11	42	116	CII-SC-4	*B. melitensis*	2021	Human	Minhe county
Xhm31	12	42	116	CII-SC-5	*B. melitensis*	2020	Human	Huzhu county
Xhm37	12	42	116	CII-SC-4	*B. melitensis*	2020	Human	Gonghe county
Xhm38	12	42	116	CII-SC-4	*B. melitensis*	2020	Human	Gonghe county
Xhm41	12	42	116	CII-SC-4	*B. melitensis* .	2020	Human	Gonghe county
Xhm14	13	42	116	CII-SC-5	*B. melitensis*	2021	Human	Huangzhong county
Xhm57	13	42	116	CII-SC-4	*B. melitensis*	2021	Human	Huangzhong county
Xhm20	14	42	116	CII-SC-4	*B. melitensis*	2021	Human	Hualong county
Xhm33	15	42	116	CII-SC-4	*B. melitensis*	2020	Human	Hualong county
Xhm43	16	42	297	CII-SC-4	*B. melitensis*	2020	Human	Menyuan county
Xhm40	16	42	297	CII-SC-4	*B. melitensis*	2020	Human	Menyuan county
Xhm59	17	42	116	CII-SC-4	*B. melitensis*	2021	Human	Hualong county
Xhm65	18	42	116	CII-SC-5	*B. melitensis*	2021	Human	Menyuan county
Xhm16	19	42	116	CII-SC-4	*B. melitensis*	2021	Human	Hualong county
Xhm44	19	42	116	CII-SC-4	*B. melitensis*	2020	Human	Maqin county
Xhm42	19	42	116	CII-SC-4	*B. melitensis*	2020	Human	Datong county
Xhm1	20	42	116	CII-SC-4	*B. melitensis*	2019	Human	unknown
Xhm56	21	42	116	CII-SC-1	*B. melitensis*	2021	Human	Yushu city
Xhm68	22	42	116	CII-SC-1	*B. melitensis*	2021	Human	Huzhu county
Xhm70	23	42	116	CII-SC-4	*B. melitensis*	2021	Human	Huangzhong county
Xhm63	23	42	116	CII-SC-2	*B. melitensis*	2021	Human	Ledu distrcit
Xhm25	24	42	N-1	CI	*B. melitensis*	2020	Human	Delhi city
Xhm32	25	42	N-1	CI	*B. melitensis*	2020	Human	Gangcha county
Xhm48	26	42	N-1	CI	*B. melitensis*	2021	Human	Wulan county
Xhm39	27	114	291	CII-SC-2	*B. melitensis*	2020	Human	Chengzhong district
Xhm66	28	42	116	CII-SC-2	*B. melitensis*	2021	Human	Haiyan county
Xhm46	29	63	111	CII-SC-5	*B. melitensis*	2021	Human	Huzhu county
Xhm58	30	63	111	CII-SC-5	*B. melitensis*	2021	Human	Huangzhong county
Xhm 52	31	184	N-2	CII-SC-4	*B. melitensis*	2013	Human	Nangqian county

FIGURE 1
MLVA dendrogram of 54 strains from this study. The columns show the identification numbers (key), MLVA-16 genotypes (GT), panel 1 genotypes (MLVA-8) and MLVA-11 (panels 1 and 2A) genotypes, wgSNP clades, species-biovar, the year of isolation of the strains, host, and their geographic location. MLVA: multilocus variable-number tandem repeat analysis.

China. The remaining 19 strains were from other countries (such as Italy, Pakistan, Egypt, Afghanistan, Albania, and Iran) with high incidence rates, and *B. melitensis* 16 M (Chromosome accession numbers: NC_003317.1 and NC_003318.1) was used as the reference genome (DelVecchio et al., 2002). Subsequently, the sample genomes were aligned to the reference genomes described above using Nucmer

10.3389/fmicb.2023.1233686

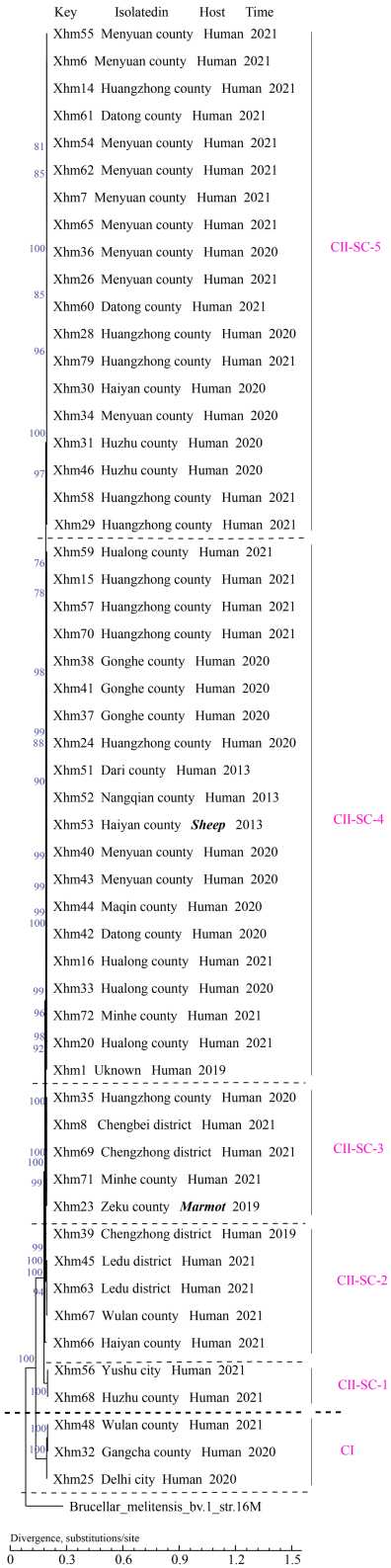

FIGURE 2
Phylogenetic tree of 54 strains from this study based on the WGS–SNP phylogenetic analysis. WGS–SNP, whole-genome sequencing–single-nucleotide polymorphism.

(Kurtz et al., 2004), and the SNP calling and filtering steps were performed using the "show-snps" application (a module of MUMmer with the parameter "-ClrTH") from the MUMmer package (Kurtz et al., 2004). Finally, BLAST (Ye et al., 2006) and RepeatMasker software (Tarailo-Graovac and Chen, 2009) were used to filter SNPs located in repeated regions to obtain reliable SNPs. The nucleotide substitution rate of sequences was used to estimate the phylogenetic relationships of strains. The phylogenetic trees were generated using the maximum likelihood (PHYML) method, with a bootstrap number set to 1,000 with orthologous genes. The phylogenetic tree was further annotated with the top-level clusters identified using RhierBAPS programs via R packages (Tonkin-Hill et al., 2018).

Results

Bio-typing, geographic distribution, hosts, and isolated time of *Brucella melitensis*

Based on the bio-typing approaches, 54 strains were identified, and all strains were identified as *B. melitensis* bv. 3 (Table 1). Furthermore, strains were distributed in all eight regions, with numbers ranging from 2 to 16 (Figure 1; Table 2), namely, 16 in Xining City, 11 in Haidong City, 15 in Haibei Prefecture, 1 in Huangnan Prefecture, 3 in Hainan Prefecture, 2 in Guoluo Prefecture, 2 in Yushu Prefecture, and 3 in Haixi Prefecture. Strains were isolated from three hosts (humans, domestics, and wildlife), namely, 52 humans, 1 sheep, and 1 marmot (Table 2). Moreover, 54 strains spanned the period 2013–2021, that is, 3 in 2013, 2 in 2019, 19 in 2020, and 30 in 2021.

MLST and MLVA genotypes of *Brucella melitensis* isolated from QH

In this study, MLST genotypes were deduced from WGS data using publicly available databases. All 53 *B. melitensis* strains were deduced as being the ST 8 genotype in both the 9-loci and 21-loci MLST approaches, and only one strain (XHM1) was identified as ST 68 (Supplementary Table S3).

Based on the MLVA assay, four MLVA-8 genotypes were identified, that is, 42 ($n = 49$), 63 ($n = 2$), 114 ($n = 2$), and 118 ($n = 1$), whereas six MLVA-11 genotypes were found, that is, four known [111 ($n = 2$), 116 ($n = 44$), 291 ($n = 2$), and 297 ($n = 2$)] and two newly identified (N1 ($n = 3$) and N2 ($n = 1$)), which are all single-locus variants to MLVA-11 genotype 116. These data indicated that all strains belonged to the Eastern Mediterranean lineage (Figure 1).

Based on the MLVA-16 analysis, 54 strains were sorted into 31 genotypes (GT1–31), of which eight genotypes (GT1, GT7, GT11–13, GT16, GT19, and GT23) were each shared by at least two strains (Figure 1). GT7 had the largest shared genotype, and it included 14 strains from different regions in 2013 ($n = 1$), 2020 ($n = 4$), and 2021 ($n = 9$), implying that a major genotype is endemic in these regions, and indicating a lack of control over the spread of this disease between regions. Moreover, XHM53 from GT7 was obtained from the liver of an aborted sheep fetus, and two strains (XHM7 and XHM62) in this shared genotype GT7 were isolated from a couple (husband and wife). Another two strains (XHM42 and XHM44) from the shared genotype GT19 were obtained from a family (father and son) who had a contact history with aborted lambs. These data suggest that each infection event was caused by a common source of infection. The remaining 23

TABLE 1 Bio-typing characteristics of 54 *Brucella melitensis* strains in this study.

Strains	Growth		Dye inhibition test		Monospecific serum		Phage lysis test			No.	Interpretation
	CO_2	H_2S	BF	TH	A	M	Tb	BK_2	Wb		
BA	+	+	+	–	+	–	CL	CL	CL	1	BA bv. 1,544
BM	–	–	+	+	–	+	NL	CL	NL	1	BM bv. 1 16 M
BS	–	++	–	+	+	–	NL	CL	CL	1	MS bv. 11,330
Test strains	–	–	+	+	+	+	NL	CL	NL	54	BM bv. 3

BA, *Brucella abortus*; BM, *B. melitensis*; BS, *Brucella suis*; BF, basic fuchsin; TH, thionin; "+," positive; "–," negative; CL, confluent lysis; NL, no lysis.

genotypes were all singular, and each represented only one strain (Figure 1), suggesting epidemiologically unrelated and sporadic epidemic characteristics of human brucellosis. Remarkably, XHM23 (GT3) was obtained from a marmot blood sample collected in Zeku County (QH) that represented a unique MLVA genotype, but further genomic investigation is needed (Figure 1).

SNP analysis and comparison with MLVA of *Brucella melitensis* strains

All 54 strains were divided into two clusters (I and II) based on the WGS-SNP phylogeny analysis (namely CI and CII), and CII was further sorted into five sub-clusters (CII SC1-5) (Figure 2). Furthermore, the strains with epidemiological links were grouped into the same sub-clusters; this result is consistent with that of the MLVA analysis, suggesting that these cases have a common source of infection. For example, strains from two shared MLVA genotypes with epidemiological links (GT7, XHM42, and XHM44; and GT19, XHM7, and XHM62) were sorted into the same sub-clusters (CII SC-4 and CII SC-5). Additionally, three shared MLVA genotypes (GT1, GT12, and GT16) were clustered into each of the same sub-clades: GT1 (XHM35 and XHM8) was clustered as CII SC-3; GT12 (XHM37, XHM38, and XHM41) clustered as CII SC-4; and GT16 (XHM40 and XHM43) clustered as CII SC-4 (Figure 1). Importantly, all clusters (and sub-clusters) comprised strains from different counties, which implied that multiple *B. melitensis* lineages were circulating in QH, causing the cross-regional human brucellosis epidemic.

SNP phylogenetic analysis of *Brucella melitensis* strains on a global scale

To illustrate the phylogenetic profiles of strains in this study on a global scale, an SNP phylogenetic analysis of 132 *B. melitensis* was performed. The total number of SNPs found in all 132 *B. melitensis* strains ranged from 289 to 2,038 (Supplementary Table S4). These strains were categorized into four clades (CI–CIV) (Figure 3; Supplementary Figure S2; Supplementary Table S1). CI consists of three strains from the present study, CII is GTII, CIII is GTI, and CIV contains three SNP genotypes (GTIII–V), (Figure 3; Supplementary Figure S2). The phylogenetic clades were identified and verified using RhierBAPS programs, supporting the results of this study. Phylogenetic analysis indicated that all 54 strains belonged to the GT II lineage, which corresponds to the East Mediterranean lineages (Figure 1). Furthermore, two strains in QH-2 (XHM56 and XHM68) clustered into GT IIb, and 20 strains from CII-SC-4 clustered into GT IIh. Strains of three sub-clades (CII-SC-1, 4, and 5) clustered into the same sub-lineages with strains from Inner Mongolia, suggesting that there were epidemiological links between strains from Inner Mongolia and QH. The XHM23 isolated from the marmot (marked in bold) (QH-9) and B.m.QH2019001 from humans were clustered into the same sub-clades; both were previously isolated from QH, China. These data suggest that the two cases were caused by a common source of infection (Figure 1). Additionally, the strains in this study formed at least four independent clades (CI and CII-SC-3-5) (Figure 1), implying that these strains were the local-specific epidemic lineages, but further investigations are warranted.

Discussion

In the present study, both classical bio-typing procedures and two molecular tools (MLVA and WGS–SNP) were used to characterize the *B. melitensis* strains from QH, China, to explore the molecular epidemiological relationship. The results of this work provide the crucial evidence necessary to formulate a targeted surveillance and control program. In the present study, the *B. melitensis* species was a predominant pathogen that was isolated from three different host species, and it was widely distributed. In particular, *B. melitensis* was isolated from samples from many hosts, including yaks, sheep, blue sheep, and Tibetan gazelle (Ma et al., 2016; Cao et al., 2018). These data revealed that there was a high diversity of natural reservoir hosts that allowed *B. melitensis* to continue circulating in this province. Indeed, animals are a natural reservoir host for zoonotic organisms and the majority of human brucellosis infections originate from animal hosts (Recht et al., 2020). Sheep and goats are optimal hosts for *B. melitensis*, and they can infect many different hosts such as cattle, swine, and deer (Liu et al., 2020). Thus, brucellosis control in regions with multiple existing hosts is a significant challenge. A targeted and comprehensive control program for infected sheep and goats should be implemented as a priority strategy to curb the spread of this disease to humans. Several further measures should be implemented, such as prohibiting the blind expansion of the breeding industry, strengthening the inspection and quarantine of animals for importation and exportation, widening the wildlife surveillance zone, improving the awareness of disease prevention among practitioners, and banning the circulation of sick animals.

In this present study, four MLVA-8 genotypes and six MLVA-11 genotypes were identified: 42 (MLVA-8) and 116 (MLVA-11) are predominant genotypes, accounting for 90.7% (49/54) and 81.5% (44/54), respectively. These data indicated that all strains were of Eastern Mediterranean lineage. With the use of MLVA-8, the majority of strains (84/105) were genotyped, and

10.3389/fmicb.2023.1233686

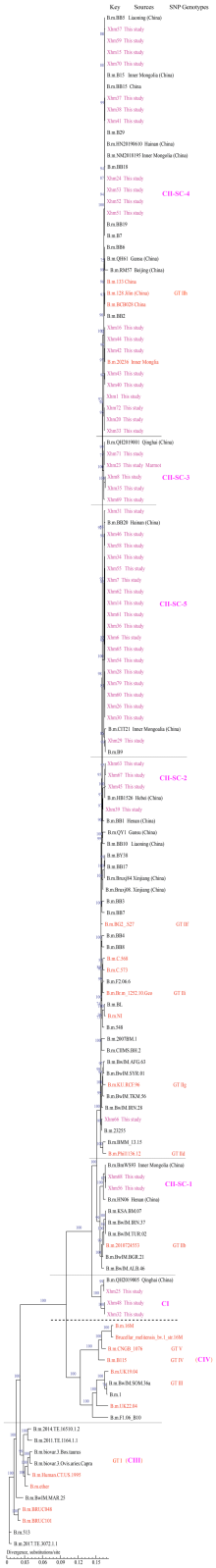

FIGURE 3
WGS–SNP phylogenetic analysis of 133 *Brucella melitensis* strains on a global scale. GT I–V is the same as previously described (Pisarenko et al., 2018) and marker with red, strains from the present study marked with pink, C I and C II from Figure 2 was used to code the clades. WGS–SNP, whole-genome sequencing–single-nucleotide polymorphism. The scale bar indicates the nucleotide sequence divergence.

42 were clustered into the East Mediterranean lineages (Jiang et al., 2011). Furthermore, MLVA-11 genotype 116 is a predominant circulating genotype in China, accounting for 69% (951/1382) (Zhu et al., 2020). Importantly, most *B. melitensis* strains belong to the East Mediterranean group, which comprises strains from Europe, the Middle East, and Asia (Vergnaud et al., 2018). MLVA genotype 116 is predominant in Asian countries (e.g., 86.8% in Kazakhstan) (Shevtsova et al., 2019). Furthermore, MLVA analysis data suggested that epidemiologically related characteristics of *B. melitensis* infection and cross-regional transmission events are caused by common sources of infection, suggesting that the predominant circulating genotype is endemic in different regions; this indicates a lack of control over infected animals' movement and exchange between regions. In the Middle East, uncontrolled animal transportation through "open" borders is a main risk factor for brucellosis spread between some regions (Gwida et al., 2010). We hypothesize that the nomadic lifestyle (which often involves the consumption of raw milk) and production methods (e.g., homemade dairy products) in highland pastoral areas may have caused these infection events, and a detailed field survey is needed to verify the conclusion of this molecular investigation. A nomadic lifestyle may favor the spread of brucellosis among different animals and populations (Liu et al., 2022) because animals and people live in close contact. A 2018 report found that the consumption of raw milk from smuggled sick goats caused human brucellosis epidemics (25 cases) in Douz, Tunisia (Charaa et al., 2022). The purchase and consumption of cheese and milk from non-regulated sources are very common in specific communities among Israeli Arabs, with nearly 41 and 16.1% of respondents consuming cheese and milk, respectively, from non-regulated sources (Baron-Epel et al., 2018). Therefore, ruminant vaccination, control of cross-border animal movements, and control of non-regulated goat milk sales must be strengthened to prevent the spread of brucellosis.

WGS–SNP analysis has proved to be a robust molecular tool for illustrating the phylogenetic patterns of *Brucella* strains (Tan et al., 2015; Georgi et al., 2017). It demonstrated that multiple *B. melitensis* lineages were circulating in QH. Similarly, WGS–SNP phylogenetic analysis resolved Chinese *B. melitensis* strains into five clusters, reflecting the existence of multiple lineages (Sun et al., 2017). In addition, strains from humans and marmots were clustered in the same sub-clades, implying the possible existence of direct and/or indirect contact between sheep (and goats) and wildlife (marmots). Indeed, wildlife has a crucial role in the epidemiology of brucellosis in animals and humans (Galarce et al., 2021). Therefore, strengthening prevention, surveillance, and control of wildlife is recommended.

Global phylogenetic analysis indicated that 54 *B. melitensis* strains were clustered into genotype II (Pisarenko et al., 2018) and further divided into six sub-lineages, revealing the existence of multiple circulating lineages in QH. Additionally, many sub-lineages were shared by strains from this study and strains from Inner Mongolia, Hainan Province, Shandong Province, and Hebei Province, indicating that these strains have a potential phylogenetic relationship (Liu et al., 2020). The cross-border movement and transfer of animals between Côte d'Ivoire and Mali for grazing and/or trade have exacerbated the spread of brucellosis across the region (Oyetola et al., 2021). Therefore, genome sequencing in more strains and building a local genome database are necessary to

TABLE 2 Area distribution and numbers of the 54 *Brucella melitensis* strains* in this study.

City	County/district (no.)	No. of strains
Xining City	Chengzhong District (2), Chengbei District (1), Huangzhong County (10), Datong County (3)	16
Haidong City	Ledu District (2), Minhe County (2), Huzhu County (3), Hualong County (4)	11
Haibei Prefecture	Haiyan County (3), Gangcha County (1), Menyuan County (11)	15
Huangnan Prefecture	Zeku County (1)	1
Hainan Prefecture	Gonghe County (3)	3
Guoluo Prefecture	Maqin County (1), Dari County (1)	2
Yushu Prefecture	Yushu City (1), Nangqian County (1)	2
Haixi Prefecture	Delhi City (1), Wulan County (2)	3

No., number of strains in each region.
*The location of one strain is unknown.

improve the surveillance capacity and control the spread of brucellosis (Liu et al., 2023).

Although we obtained important insight in our investigation, some limitations are worth acknowledging. First, most strains in genome sequencing were obtained over a 2-year period, and more strains involved during a longer period could facilitate a more profound description of the brucellosis epidemiological profile of this region. Second, obtaining field epidemiological data in many cases is challenging. However, these data provide crucial auxiliary support for genome epidemiology.

Conclusion

Brucella melitensis is a predominant species, and its distribution has been widespread in all nine regions in QH. *B. melitensis* strains belonged to the East Mediterranean lineages, and the human brucellosis epidemic in recent years was potentially caused by many native circulating lineages. Strengthening the genome sequencing of strains from a variety of host sources will facilitate the identification of transmission routes and determine potential ongoing outbreaks, which is vital for formulating targeted surveillance and countermeasures.

Data availability statement

The datasets presented in this study can be found in online repositories. The names of the repository/repositories and accession number(s) can be found in the article/Supplementary material.

Ethics statement

The research protocol was reviewed and approved by the Ethics Committees of the Institute for Endemic Disease Control and Prevention of Qinghai (No. 2022006). Informed consent was obtained from all patients. The studies were conducted in accordance with the local legislation and institutional requirements. The participants provided their written informed consent to participate in this study. The animal study was approved by the Ethics Committees of the Institute for Endemic Disease Control and Prevention of Qinghai (No. 2022006). Informed consent was obtained from all patients. The study was conducted in accordance with the local legislation and institutional requirements.

Author contributions

HX performed the strain isolation, collection, and epidemiology data process. ZhiL and ZheL participated in the design of the study, analyzed the sequencing data, and drafted the manuscript. ZZ, JW, LM, JL, XY, and LR participated in the field epidemiology survey. ZhiL, ZheL, and LX critically reviewed the manuscript and managed the project. All authors contributed to the article and approved the submitted version.

Funding

This work was supported by the National Natural Science Foundation of Qinghai, China (No. 81860588). The funders had no role in the study design, data collection and analysis, decision to publish, or preparation of the manuscript.

Conflict of interest

The authors declare that the research was conducted in the absence of any commercial or financial relationships that could be construed as a potential conflict of interest.

Publisher's note

Supplementary material

The Supplementary material for this article can be found online at: https://www.frontiersin.org/articles/10.3389/fmicb.2023.1233686/full#supplementary-material

References

Abdel-Glil, M. Y., Thomas, P., Brandt, C., Melzer, F., Subbaiyan, A., Chaudhuri, P., et al. (2022). Core genome multilocus sequence typing scheme for improved characterization and epidemiological surveillance of pathogenic *Brucella*. *J. Clin. Microbiol.* 60:e0031122. doi: 10.1128/jcm.00311-22

Baron-Epel, O., Bord, S., Cohen-Dar, M., and Obeid, S. (2018). A cross sectional survey assessing knowledge, attitudes and behaviors regarding brucellosis among Arab Israelis. *BMC Public Health* 18:516. doi: 10.1186/s12889-018-5430-9

Cao, X., Li, Z., Liu, Z., Fu, B., Liu, Y., Shang, Y., et al. (2018). Molecular epidemiological characterization of *Brucella* isolates from sheep and yaks in Northwest China. *Transbound. Emerg. Dis.* 65, e425–e433. doi: 10.1111/tbed.12777

Charaa, N., Ghrab, R., Ben Othman, A., Makhlouf, M., Ltaief, H., Ben Alaya, N., et al. (2022). Investigation of a human brucellosis outbreak in Douz, Tunisia, 2018. *Epidemiol. Health* 44:e2022048. doi: 10.4178/epih.e2022048

DelVecchio, V. G., Kapatral, V., Redkar, R. J., Patra, G., Mujer, C., Los, T., et al. (2002). The genome sequence of the facultative intracellular pathogen *Brucella melitensis*. *Proc. Natl. Acad. Sci. U. S. A.* 99, 443–448. doi: 10.1073/pnas.221575398

Galarce, N., de la Fuente, S., Escobar, B., Dettleff, P., Abalos, P., Hormazábal, J. C., et al. (2021). Survey of zoonotic bacterial pathogens in native foxes in Central Chile: first record of *Brucella canis* exposure. *Animals* 11:1980. doi: 10.3390/ani11071980

Georgi, E., Walter, M. C., Pfalzgraf, M. T., Northoff, B. H., Holdt, L. M., Scholz, H. C., et al. (2017). Whole genome sequencing of *Brucella melitensis* isolated from 57 patients in Germany reveals high diversity in strains from Middle East. *PLoS One* 12:e0175425. doi: 10.1371/journal.pone.0175425

Godfroid, J., Cloeckaert, A., Liautard, J. P., Kohler, S., Fretin, D., Walravens, K., et al. (2005). From the discovery of the Malta fever's agent to the discovery of a marine mammal reservoir, brucellosis has continuously been a re-emerging zoonosis. *Vet. Res.* 36, 313–326. doi: 10.1051/vetres:2005003

Gwida, M., Al Dahouk, S., Melzer, F., Rösler, U., Neubauer, H., and Tomaso, H. (2010). Brucellosis – regionally emerging zoonotic disease? *Croat. Med. J.* 51, 289–295. doi: 10.3325/cmj.2010.51.289

Janowicz, A., De Massis, F., Ancora, M., Cammà, C., Patavino, C., Battisti, A., et al. (2018). Core genome multilocus sequence typing and single nucleotide polymorphism analysis in the epidemiology of *Brucella melitensis* infections. *J. Clin. Microbiol.* 56, e00517–18. doi: 10.1128/jcm.00517-18

Jiang, H., Fan, M., Chen, J., Mi, J., Yu, R., Zhao, H., et al. (2011). MLVA genotyping of Chinese human *Brucella melitensis* biovar 1, 2 and 3 isolates. *BMC Microbiol.* 11:256. doi: 10.1186/1471-2180-11-256

Jolley, K. A., Bray, J. E., and Maiden, M. C. J. (2018). Open-access bacterial population genomics: BIGSdb software, the PubMLST.org website and their applications. *Wellcome Open Res* 3:124. doi: 10.12688/wellcomeopenres.14826.1

Kiliç, S., Ivanov, I. N., Durmaz, R., Bayraktar, M. R., Ayaslioglu, E., Uyanik, M. H., et al. (2011). Multiple-locus variable-number tandem-repeat analysis genotyping of human *Brucella* isolates from Turkey. *J. Clin. Microbiol.* 49, 3276–3283. doi: 10.1128/jcm.02538-10

Kurtz, S., Phillippy, A., Delcher, A. L., Smoot, M., Shumway, M., Antonescu, C., et al. (2004). Versatile and open software for comparing large genomes. *Genome Biol.* 5:R12. doi: 10.1186/gb-2004-5-2-r12

Li, Z., Wang, X. M., Zhu, X., Wang, M., Cheng, H., Li, D., et al. (2020). Molecular characteristics of *Brucella* isolates collected from humans in Hainan Province, China. *Front. Microbiol.* 11:452. doi: 10.3389/fmicb.2020.00452

Li, R., Zhu, H., Ruan, J., Qian, W., Fang, X., Shi, Z., et al. (2010). De novo assembly of human genomes with massively parallel short read sequencing. *Genome Res.* 20, 265–272. doi: 10.1101/gr.097261.109

Liu, Z. G., Di, D. D., Wang, M., Liu, R. H., Zhao, H. Y., Piao, D. R., et al. (2017). MLVA genotyping characteristics of human *Brucella melitensis* isolated from Ulanqab of Inner Mongolia, China. *Front. Microbiol.* 8:6. doi: 10.3389/fmicb.2017.00006

Liu, Z., Liu, D., Wang, M., and Li, Z. (2022). Human brucellosis epidemiology in the pastoral area of Hulun Buir city, Inner Mongolia autonomous region, China, between 2003 and 2018. *Transbound. Emerg. Dis.* 69, 1155–1165. doi: 10.1111/tbed.14075

Liu, Z., Wang, M., Shi, Q., Dong, X., Gao, L., and Li, Z. (2023). Original and introduced lineages co-driving the persistence of *Brucella abortus* circulating in West Africa. *Front. Public Health* 11:1106361. doi: 10.3389/fpubh.2023.1106361

Liu, Z., Wang, C., Wei, K., Zhao, Z., Wang, M., Li, D., et al. (2020). Investigation of genetic relatedness of *Brucella* strains in countries along the silk road. *Front. Vet. Sci.* 7:539444. doi: 10.3389/fvets.2020.539444

Ma, J. Y., Wang, H., Zhang, X. F., Xu, L. Q., Hu, G. Y., Jiang, H., et al. (2016). MLVA and MLST typing of *Brucella* from Qinghai, China. *Infect. Dis. Poverty* 5:26. doi: 10.1186/s40249-016-0123-z

Ma, L., Yang, X. X., Xue, H. M., Xu, L. Q., Tian, G. Z., Li, J. Q., et al. (2020). Epidemiological and molecular characteristics of human brucellosis in Qinghai province, 2005–2019. *Zhonghua Liu Xing Bing Xue Za Zhi* 41, 1905–1908. doi: 10.3760/cma.j.cn112338-20200309-00288

Minas, M., Minas, A., Gourgulianis, K., and Stournara, A. (2007). Epidemiological and clinical aspects of human brucellosis in Central Greece. *Jpn. J. Infect. Dis.* 60, 362–366.

Occhialini, A., Hofreuter, D., Ufermann, C. M., Al Dahouk, S., and Köhler, S. (2022). The retrospective on atypical *Brucella* species leads to novel definitions. *Microorganisms* 10:813. doi: 10.3390/microorganisms10040813

Oyetola, W. D., Diallo, K., Kreppel, K., Kone, P. S., Schelling, E., Bonfoh, B., et al. (2021). Factors influencing the transborder transmission of brucellosis in cattle between Côte d'Ivoire and Mali: evidence from literature and current key stakeholders. *Front. Vet. Sci.* 8:630580. doi: 10.3389/fvets.2021.630580

Pelerito, A., Nunes, A., Grilo, T., Isidro, J., Silva, C., Ferreira, A. C., et al. (2021). Genetic characterization of *Brucella* spp.: whole genome sequencing-based approach for the determination of multiple locus variable number tandem repeat profiles. *Front. Microbiol.* 12:740068. doi: 10.3389/fmicb.2021.740068

Pisarenko, S. V., Kovalev, D. A., Volynkina, A. S., Ponomarenko, D. G., Rusanova, D. V., Zharinova, N. V., et al. (2018). Global evolution and phylogeography of *Brucella melitensis* strains. *BMC Genomics* 19:353. doi: 10.1186/s12864-018-4762-2

Recht, J., Schuenemann, V. J., and Sánchez-Villagra, M. R. (2020). Host diversity and origin of zoonoses: the ancient and the new. *Animals* 10:1672. doi: 10.3390/ani10091672

Rossetti, C. A., Arenas-Gamboa, A. M., and Maurizio, E. (2017). Caprine brucellosis: a historically neglected disease with significant impact on public health. *PLoS Negl. Trop. Dis.* 11:e0005692. doi: 10.1371/journal.pntd.0005692

Shevtsova, E., Vergnaud, G., Shevtsov, A., Shustov, A., Berdimuratova, K., Mukanov, K., et al. (2019). Genetic diversity of *Brucella melitensis* in Kazakhstan in relation to world-wide diversity. *Front. Microbiol.* 10:1897. doi: 10.3389/fmicb.2019.01897

Sun, M., Jing, Z., Di, D., Yan, H., Zhang, Z., Xu, Q., et al. (2017). Multiple locus variable-number tandem-repeat and single-nucleotide polymorphism-based *Brucella* typing reveals multiple lineages in *Brucella melitensis* currently endemic in China. *Front. Vet. Sci.* 4:215. doi: 10.3389/fvets.2017.00215

Tan, K. K., Tan, Y. C., Chang, L. Y., Lee, K. W., Nore, S. S., Yee, W. Y., et al. (2015). Full genome SNP-based phylogenetic analysis reveals the origin and global spread of *Brucella melitensis*. *BMC Genomics* 16:93. doi: 10.1186/s12864-015-1294-x

Tarailo-Graovac, M., and Chen, N. (2009). Using RepeatMasker to identify repetitive elements in genomic sequences. *Curr. Protoc. Bioinformatics* Chapter 4:4.10.1. doi: 10.1002/0471250953.bi0410s25

Tonkin-Hill, G., Lees, J. A., Bentley, S. D., Frost, S. D. W., and Corander, J. (2018). RhierBAPS: an R implementation of the population clustering algorithm hierBAPS. *Wellcome Open Res.* 3:93. doi: 10.12688/wellcomeopenres.14694.1

Vergnaud, G., Hauck, Y., Christiany, D., Daoud, B., Pourcel, C., Jacques, I., et al. (2018). Genotypic expansion within the population structure of classical *Brucella* species revealed by MLVA16 typing of 1404 *Brucella* isolates from different animal and geographic origins, 1974–2006. *Front. Microbiol.* 9:1545. doi: 10.3389/fmicb.2018.01545

Wareth, G. (2019). *Brucellosis in the Mediterranean countries: history, prevalence, distribution, current situation and attemps at surveillance and control*. Paris: World Organisation for Animal Health OIE.

Xavier, M. N., Paixão, T., Hartigh, A., Tsolis, R. M., and Santos, R. L. (2010). Pathogenesis of *Brucella* spp. *Open Vet. Sci. J.* 4, 109–118. doi: 10.2174/1874318801004010109

Yagupsky, P., Morata, P., and Colmenero, J. D. (2019). Laboratory diagnosis of human brucellosis. *Clin. Microbiol. Rev.* 33, e00073–19. doi: 10.1128/cmr.00073-19

Ye, J., McGinnis, S., and Madden, T. L. (2006). BLAST: improvements for better sequence analysis. *Nucleic Acids Res.* 34, W6–W9. doi: 10.1093/nar/gkl164

Zhu, X., Zhao, Z., Ma, S., Guo, Z., Wang, M., Li, Z., et al. (2020). *Brucella melitensis*, a latent "travel bacterium," continual spread and expansion from Northern to Southern China and its relationship to worldwide lineages. *Emerg. Microbes Infect.* 9, 1618–1627. doi: 10.1080/22221751.2020.1788995

frontiers | Frontiers in Microbiology

TYPE Original Research
PUBLISHED 04 October 2023
DOI 10.3389/fmicb.2023.1253349

OPEN ACCESS

EDITED BY
Michel Stanislas Zygmunt,
Institut National de Recherche pour l'Agriculture, l'Alimentation et l'Environnement (INRAE), France

REVIEWED BY
Maryam Dadar,
Razi Vaccine and Serum Research Institute, Iran
David W. Pascual,
University of Florida, United States
Paola M. Boggiatto,
National Animal Disease Center, Agricultural Research Service (USDA), United States

*CORRESPONDENCE
Girish Radhakrishnan
girish@niab.org.in

†These authors share first authorship

RECEIVED 06 July 2023
ACCEPTED 12 September 2023
PUBLISHED 04 October 2023

CITATION
Nandini P, Jakka P, Murugan S, Mazumdar V, Kumar D, Prakash R, Barbuddhe SB and Radhakrishnan G (2023) Immuno-profiling of *Brucella* proteins for developing improved vaccines and DIVA capable serodiagnostic assays for brucellosis.
Front. Microbiol. 14:1253349.
doi: 10.3389/fmicb.2023.1253349

Immuno-profiling of *Brucella* proteins for developing improved vaccines and DIVA capable serodiagnostic assays for brucellosis

Prachita Nandini[1,2†], Padmaja Jakka[1†], Subathra Murugan[1†], Varadendra Mazumdar[1,2], Deepak Kumar[1], Richa Prakash[1], Sukhadeo B. Barbuddhe[3] and Girish Radhakrishnan[1*]

[1]National Institute of Animal Biotechnology (NIAB), Hyderabad, India, [2]Regional Centre for Biotechnology (RCB), Faridabad, India, [3]ICAR- National Meat Research Institute, Hyderabad, India

Brucellosis remains a worldwide zoonotic disease with a serious impact on public health and livestock productivity. Controlling brucellosis in livestock is crucial for limiting human infections in the absence of effective human vaccines. Brucellosis control measures are majorly dependent on rigorous monitoring of disease outbreaks and mass vaccination of livestock. Live attenuated vaccines are available for livestock vaccination that play a vital role in brucellosis control programs in many countries. Even though the existing animal vaccines confer protection against brucellosis, they carry some drawbacks, including their infectivity to humans and interference with sero-monitoring. The available serodiagnostic assays for brucellosis depend on detecting anti-LPS antibodies in the serum. Since diagnosis plays a vital role in controlling brucellosis, developing improved serodiagnostic assays with enhanced specificity, sensitivity and DIVA capability is required. Therefore, it is essential to identify novel antigens for developing improved vaccines and serodiagnostic assays for brucellosis. In the present study, we performed a high throughput immunoprofiling of *B. melitensis* protein microarray using brucellosis-positive human and animal serum samples. The screening identified several serodominant proteins of *Brucella* that exhibited common or differential reactivity with sera from animals and humans. Subsequently, we cloned, expressed, and purified ten serodominant proteins, followed by analyzing their potential to develop next-generation vaccines and improved serodiagnostic assays for brucellosis. Further, we demonstrated the protective efficacy of one of the serodominant proteins against the *B. melitensis* challenge in mice. We found that the seroreactive protein, Dps (BMEI1980), strongly reacted with brucellosis-positive serum samples, but it did not react with sera from *B. abortus* S19-vaccinated cattle, indicating DIVA capability. A prototype lateral flow assay and indirect ELISA based on Dps protein exhibited high sensitivity, specificity, and DIVA capability. Thus, the present study identified promising candidates for developing improved vaccines and affordable, DIVA-capable serodiagnostic assays for animal and human brucellosis.

KEYWORDS

***Brucella*, vaccine, DIVA, immunoprofiling, ELISA, serodominant, diagnostics**

Introduction

Brucellosis is one of the major economically important zoonotic diseases worldwide, which is posing a serious threat to both livestock and human health globally (Mcdermott et al., 2013). Besides its impact on economic loss, brucellosis is also associated with high morbidity in many developing countries, both in humans and animals (Rubach et al., 2013). Brucellosis remains endemic in different regions, including Latin America, the Middle East, Africa, Asia, and the Mediterranean basin (Pappas et al., 2006). Brucellosis is caused by the Gram-negative facultative intracellular bacteria, *Brucella* belonging to the class Alphaproteobacteria (Ficht, 2010). Depending on the host preference and pathogenicity, 12 species of *Brucella* have been identified to date, which can infect domestic, wild, and marine animals (Scholz et al., 2016). Four classical *Brucella* species capable of causing severe brucellosis in humans are *B. melitensis*, followed by *B. abortus*, *B. suis*, and *B. canis*. Symptoms of brucellosis in animals are abortions, death of weaker offspring, stillbirth, and sterility in males, while in humans, it mainly causes flu-like symptoms with high fever, headache, weakness, and osteoarticular problems (Godfroid et al., 2011). A severe form of brucellosis could be fatal with cardiac and neurological complications (Solera et al., 1997). Brucellosis in humans is often an occupational hazard directly affecting veterinarians, laboratory technicians, abattoir workers, and farmers (Fiori et al., 2000; Agasthya et al., 2007). Human transmission could mainly occur through direct contact with infected or aborted animals, consuming contaminated dairy products, and inhaling aerosols (Corbel, 1997). There is no human vaccine for brucellosis, and treatment with multiple antibiotic regimens is the only option to treat human brucellosis. However, antibiotic treatment is challenging due to frequent therapeutic failures and relapses (Ariza et al., 2007).

The most plausible way to control brucellosis is early disease diagnosis and mass vaccination of susceptible animals. However, diagnosis of brucellosis is challenging, and the available animal vaccines for brucellosis have many disadvantages despite conferring protection (Schurig et al., 2002; Galińska and Zagórski, 2013). Brucellosis exhibits non-specific clinical manifestations that mimic the symptoms of other infectious or non-infectious diseases (Mantur et al., 2007). Direct culturing of *Brucella* from the tissue specimens is considered the gold standard for diagnosing brucellosis. However, it is often avoided due to its fastidious nature, slow growth, and potential hazard to laboratory personnel (Padilla Poester et al., 2010). Therefore, other diagnostic methods have been developed and practiced over time that require no direct contact and do not require expertise and special equipment (Nielsen and Yu, 2010). Therefore, serological detection of brucellosis is one of the most preferred diagnostic tools since this method addressed most of the challenges stated earlier. The serodiagnosis of brucellosis mainly relies on detecting anti-lipopolysaccharide (LPS) antibodies in the infected serum (Godfroid et al., 2010). However, LPS-based serodiagnostic assays have significant drawbacks, including poor sensitivity, cross-reactivity with several other Gram-negative bacteria, and lack of the capability of Differentiating Infected from Vaccinated Animals (DIVA). Also, the tests fail to detect rough strains of *Brucella*, *viz. B. canis* and *B. ovis*, which lack O-side chains on their LPS (Al Dahouk et al., 2003a,b). Hence it is crucial to identify other serodominant antigens of *Brucella* that are exclusive and capable of addressing major shortcomings of the present serodiagnostic assays.

Among the available animal vaccines, S19 and RB51 are the well-recognized live attenuated vaccines used for cattle (Avila-Calderón et al., 2013). However, there are many disadvantages associated with these vaccines. The immune response induced by the S19 vaccine is still unclear, and it can induce abortion in pregnant animals. *B. abortus* S19 vaccine has no DIVA capability, and most importantly, it is highly infectious to humans (Yang et al., 2013). RB51, a rough live attenuated strain of *B. abortus*, has DIVA capability where the vaccinated cattle can be differentiated from naturally infected animals using routine serodiagnostic tests (Ashford et al., 2004). However, RB51 is rifampicin-resistant and can cause infection in humans. Subunit vaccines using *Brucella* recombinant proteins such as L7/L12 ribosomal protein, Cu-Zn superoxide dismutase, and Outer Membrane Lipoproteins (OMPs) OMP16 and OMP19 have been tested for brucellosis (Oliveira and Splitter, 1996; Bae, 1999; Pasquevich et al., 2009; Sáez et al., 2012). However, no subunit vaccines are currently available to prevent brucellosis in animals and humans. Therefore, the identification and characterization of novel serodominant antigens of *Brucella* are needed for developing improved vaccines and diagnostic assays for brucellosis. Here, we performed a high throughput immunoprofiling of *B. melitensis* antigens using a protein microarray. The screening identified several serodominant proteins of *Brucella* that are uniquely present or shared by various host species. Subsequently, we performed a detailed characterization of 10 serodominant proteins to assess their utility for developing improved vaccines and serodiagnostic assays. Further, we developed a prototype Lateral Flow Assay and indirect ELISA based on one of the serodominant proteins. The assays could detect brucellosis in humans and animals with high sensitivity and specificity and exhibited DIVA capability.

Materials and methods

Ethical statement

Six to eight-week-old female BALB/c mice were procured from the Small Animal Facility of the National Institute of Animal Biotechnology (NIAB). All mice experiments and animal serum collections were approved by the Institutional Biosafety Committee (Approval number: IBSC/2013/NIAB/0001B) and Institutional Animal Ethics Committee (Approval number: IAEC/2019/NIAB/34/GKR & IAEC/2021/NIAB/09/GKR) of NIAB. *In vivo* challenge studies with *B. melitensis* 16 M strain were performed in the BSL-3 laboratory facility of UoH-NIAB (Approval number: IAEC/NIAB/2022/08/GKR). Mice were kept under a standard pathogen-free environment and handled with humane care with free access to food and water throughout the experiment. Serum samples from human subjects were collected by ICAR-National Meat Research Institute with approval from the Institutional Ethics Committee (Approval number: KAMSRC/IEC/04/2018).

High-throughput immunoprobing of the *Brucella melitensis* protein microarray

Brucella melitensis, Bv.1 strain 16 M proteome microarrays with a coverage of 99.5% were commercially procured from Antigen

Discovery, USA (Cat. No. 12-MA-0001). The nitrocellulose microarray slides printed with ~3,000 *Brucella* proteins were analyzed with healthy and brucellosis-positive serum samples. Healthy and brucellosis-positive serum samples were obtained from veterinary diagnostic centers and farms with necessary approvals (Approval number: IBSC/2013/NIAB/0001B). *B. abortus* S19-vaccinated serum samples were obtained from different villages through government agencies as part of the ongoing brucellosis control program in India. Serum samples were primarily screened for the presence of seropositivity using the Rose Bengal Plate Agglutination Test (RBPT) and the presence of anti-*Brucella* antibodies was confirmed using OIE-validated, PrioCHECK™ Brucella Ab 2.0 Strip Kit (Applied Biosystems) and IDEXX Brucellosis Serum X2 Ab Test multi-species ELISA for animal sera. NovaLisa® human IgG and NovaLisa® human IgM kits (Nova Tec, Germany) for screening human sera. To perform RBPT, 25 µL of Rose Bengal *Brucella* antigen and 25 µL of serum sample were added onto the glass slides and mixed, followed by incubation for 5 min and observation for agglutination. Indirect ELISAs were performed with the collected serum samples as per the manufacturer's protocols.

Immunoprobing of protein microarray was performed as per instructions of the manufacturer. Briefly, the printed slides were assembled and blocked with 350 µL of blocking buffer for 1 h at room temperature with gentle agitation. The kit control or test serum samples were diluted at a ratio of 1:100 in the pre-incubation solution (20% *E. coli* lysate in the blocking buffer) and incubated for 30 min before adding onto the microarray slides. Subsequently, 350 µL of diluted sera were added and incubated overnight at 4° C in a humidified airtight container. Next, the slides were washed three times with 1 mL of wash buffer for 5 min each, followed by the addition of 350 µL of diluted secondary antibody (1:1,000) onto the slides and incubated for 1 h at room temperature. The slides were then washed thrice, followed by the addition of 350 µL of diluted tertiary detection antibody and incubated for 1 h at room temperature in the dark. The slides were given a final wash and air-dried before being scanned with the Axon Genepix scanner (Molecular Devices).

The background (true negative) signal was defined as the average signal of the negative control spots on the array. This enabled the comparison of the individual protein signal with the background signal to determine the significant response by protein antigens. The average of replicated spots was measured per sera, and the signal intensities obtained for sera from individual species were analyzed using the Genepix Pro 6.0 software.

Cloning and expression of serodominant proteins of *Brucella*

The genes encoding the identified serodominant protein antigens were amplified from the chromosomal DNA of *B. melitensis* using respective forward and reverse primers harboring *BamH1* and *Xho1* enzymes (Table 1). The PCR amplicons were digested with restriction enzymes and gel eluted. The purified PCR products were cloned into *BamH1* and *Xho1* sites of pET21a(+) in-frame with a 6X Histidine (His) tag at the C-terminus. Subsequently, the clones were confirmed by restriction enzyme digestion and sequencing. The pET21a(+) plasmids harboring the cloned *Brucella* genes were then introduced into BL21 (DE3) *E. coli*. To examine the overexpression of *Brucella* proteins, BL21 cells were induced with 1.0 mM Isopropyl β-D-1-thiogalactopyranoside (IPTG) for 5 h at 37°C, followed by harvesting the cells. The cells were lysed in 2X SDS samples buffer, boiled for 10 min, and analyzed by SDS-PAGE.

TABLE 1 Primers used for amplification of open reading frames of 10 serodominant proteins.

Gene ID	Primer sequence
BMEI1980	F-5′CGCGGATCCGTGCGATCGCCATTT-3′ R-5′CCGCTCGAGATTGCTTTCCTGCACA-3′
BMEI1390	F-5′CGCGGATCCATGACGGCGGGCGC-3′ R-5′CCGCTCGAGGAATGGAGAATCTGGGA-3′
BMEI1513	F-5′CGCGGATCCATGCGCGATCCCTAT-3′ R-5′CCGCTCGAGCACAACCCTGCGTTT-3′
BMEI0063	F-5′CGCGGATCCGTGGGGCAGGGG-3′ R-5′CCGCTCGAGTGTAAAATTAAAGTTTC-3′
BMEI0856	F-5′CGCGGATCCATGCCGATCAATATCACC-3′ R-5′CCGCTCGAGGACCAGCATACCCATC-3′
BMEI0916	F-5′CGCGGATCCATGCGCGACGGCGTA-3′ R-5′CCGCTCGAGGTCGACAATGTCATCG-3′
BMEII1048	F-5′CGCGGATCCATGGCTGCAAAAGAC-3′ R-5′CCGCTCGAGGAAGTCCATGCCGCC-3′
BMEI0855	F-5′ATTTGCGGCCGCATGCCCATAGAAAT-3′ R-5′CCGCTCGAGAGCGGTATAGGTAACG-3′
BMEII0154	F-5′ATTTGCGGCCGCATGAACATTGAG-3′ R-5′CCGCTCGAGTGGCTTGGACTTGAT-3′
BMEI0748	F-5′CGCGGATCCATGGCTGATCTCGCA-3′ R-5′CCGCTCGAGCTTGAGTTCAACCTTGG-3′

Purification of His-tagged serodominant proteins of *Brucella*

The BL21 (DE3) *E. coli* harboring individual *Brucella* protein expression plasmids were grown overnight at 37°C in Lauria Bertini media (LB, Himedia) supplemented with ampicillin (100 µg/mL; Sigma). This starter culture was inoculated into 1 liter of LB broth in 1/100 dilution and incubated at 37°C until the OD at 600 nm reached 0.6. The bacterial cultures were then induced with 1.0 mM IPTG and incubated further for 5 h at 37°C. Subsequently, the bacterial cells were harvested by centrifugation at 6,000 × *g* at 4°C and washed once with PBS. Next, the bacterial cells were lysed in 50 mL of sonication buffer containing 50 mM sodium phosphate buffer with 300 mM NaCl and 10 mM imidazole. The cell lysates were clarified by centrifugation at 16,000 × *g* for 20 min at 4°C, followed by the supernatant collection. Subsequently, the supernatant was passed through the pre-equilibrated column packed with 1 mL of Nickel-NTA Agarose resin (QIAGEN) at a flow rate of 1 mL/min. The Ni-NTA column was then washed with 200 mL of ice-cold wash buffer containing 50 mM sodium phosphate buffer with 300 mM NaCl and 30 mM imidazole. The His-tagged protein immobilized on the Ni-NTA resin, was then eluted with the same buffer containing 300 mM imidazole in various fractions. Next,

SDS-PAGE was performed with the eluted fractions to assess their purity, and the protein-containing fractions were pooled. The residual LPS from the purified proteins was removed using polymyxin-B immobilized columns (Thermo Scientific) as per the manufacturer's protocol. Subsequently, the purified proteins were dialyzed against PBS overnight. After estimating the concentration by Bradford assay (Sigma), the proteins were aliquoted, followed by snap freezing and storing at −80°C for further experiments.

Immunoblot analysis of purified proteins

The protein samples were mixed with 2X Laemmli buffer, followed by boiling for 10 min at 100°C. Next, the samples were resolved on 12% SDS-PAGE gel, followed by the transfer of proteins onto PVDF membranes using a wet tank blotting system (Bio-Rad). The membrane was blocked with 5% skimmed milk in TBST (Cell Signaling Technology) for 1 h, followed by incubation with HRP-conjugated anti-His-tag antibody (R&D Systems) at 1:10,000 dilution overnight at 4°C. Subsequently, the membrane was washed 3 times with TBST and incubated with Super Signal West Pico or Femto chemiluminescent substrate (Pierce). The signals were captured using a chemi-documentation system (Syngene).

To analyze the seroreactivity, the purified recombinant proteins were transferred onto the PVDF membrane as described above. Next, the membranes were blocked with 5% skimmed milk in TBST, followed by incubating with brucellosis positive or negative sera (1:100 dilution) from cattle overnight at 4°C. Next, the membranes were washed 3 times with TBST and incubated with HRP-conjugated anti-bovine IgG at 1:5,000 dilution (ThermoFisher). Subsequently, the membranes were incubated with the chemiluminescent substrate (Pierce), and the signals were captured using a chemi-documentation system (Syngene).

To examine the seroreactivity of Dps protein with brucellosis-positive human and animal sera, Dps protein was resolved on denaturing or native SDS-PAGE gel, followed by immunoblotting. The membranes were blocked with 5% skimmed milk in TBST and incubated with brucellosis-positive human and animal sera (1:100 dilution) overnight at 4°C. Next, the membranes were washed 3 times with TBST and incubated with HRP-conjugated anti-species specific IgG at 1:5,000 dilution (Thermo Fisher), followed by detection of the signal as described before.

To examine the differential recognition of purified recombinant Dps protein by *B. abortus* S19-vaccinated and naturally-infected cattle sera, increasing concentrations of Dps protein along with *B. abortus* and *E. coli* LPS were subjected to 12% SDS-PAGE, followed by immunoblotting as described above. The membranes were incubated with *B. abortus* S19-vaccinated or naturally infected cattle sera. Subsequently, the immunoblots were probed with HRP-conjugated anti-bovine IgG at 1:5,000 dilution (ThermoFisher), followed by detection of the signal as described before.

To assess the seroreactivity of Dps with S19-vaccinated cattle sera after various days post-vaccination, serum samples were collected at 21-, 45-, and 90-days post-vaccination, followed by probing the membrane harboring Dps protein as described before. To examine the expression of Dps protein, total lysates of *B. abortus* and *B. abortus* S19 were resolved by SDS-PAGE, followed by the transfer of the proteins onto the PVDF membrane. The membrane was probed with an anti-Dps antibody (1:5,000), which was generated commercially (GenScript) or serum from L7/L12 immunized mice, followed by detection of the signal as described before.

To examine the reactivity of *S. typhimurium* or *E. coli* lysates with anti-Dps antibody, 40 µg of whole cell lysate of *S. typhimurium, E. coli, B. abortus or* purified Dps protein (10 µg) was resolved on 12% SDS-PAGE gel, followed by transfer of proteins onto PVDF membrane. The membrane was probed with anti-Dps antibody at a dilution of 1:5000 to detect the Dps proteins as described before.

Immunization of mice with purified serodominant proteins

Six to eight-week-old female BALB/c mice were used for analyzing the immunogenicity of purified proteins. Individual animal of each designated group (six mice per group) was intraperitoneally administrated with 40 µg of purified recombinant protein mixed with Freund's complete adjuvant (1:1 ratio). Subsequently, the mice were given a booster dose of 20 µg of protein complexed with Freund's incomplete adjuvant on day 21 (1:1 ratio). The mice injected with recombinant L7/L12 protein of *B. melitensis* were considered the positive control group, and the mice injected with adjuvant alone were considered the negative control group (Oliveira et al., 1994; Oliveira and Splitter, 1994, 1996; Singh et al., 2015). The blood was collected from individual mice from each group on 0, 14, 21, 28, 35, and 45 days after initial immunization through the retro-orbital route. On the 45th day, mice were euthanized, and spleens were removed aseptically to isolate the splenocytes for further immunological assays.

Analyzing the humoral and cell-mediated immune responses in immunized mice

The antibody response against the purified proteins was estimated by iELISA (indirect enzyme-linked immunosorbent assay) in the serum samples collected at various time intervals. Initially, 96-well microtiter plates were coated overnight with respective purified recombinant proteins (100 ng/well) at 4°C. The wells were then washed thrice with 300 µL of 1X phosphate buffered saline—tween 20 (PBST) to remove the unbound proteins and blocked for 1 h at room temperature with 100 µL/ well of 1% BSA prepared in phosphate buffer saline (PBS). The wells were washed thrice with 300 µL of 1X PBST, followed by adding serum samples (100 µL/ well) diluted in 1% BSA at a ratio of 1:100 to the respective wells. The plates were incubated at room temperature for 2 h. Subsequently, the wells were washed again as described earlier, followed by incubation with 100 µL/ well of HRP-conjugated goat anti-mouse IgG1 or IgG2a antibody (Novus Biologicals) at a dilution of 1:10,000 for 1 h at 37° C. Next, the wells were washed and incubated with 50 µL of TMB substrate for 10–15 min, and the reaction was stopped by adding 50 µL of 1 N H_2SO_4. The absorbance of the wells was measured at 450 nm using a microplate reader (PerkinElmer).

To analyze the population of $CD4^+$, $CD8^+$, and IFN-γ producing $CD4^+$ and $CD8^+$ T cells, the spleens were aseptically harvested from immunized mice, followed by homogenization in sterile PBS. Subsequently, a single-cell suspension was prepared by passing the homogenized samples through 70 µm cell strainers (BD

Biosciences). The cells were washed twice with 10 mL of PBS, and residual RBCs were lysed using RBC lysis buffer (Sigma) as per the manufacturer's protocol. The isolated splenocytes were cultured with RPMI 1640 medium containing 10% FBS and 1% penicillin-streptomycin in 6-well plates. Subsequently, the cells in the individual wells were stimulated with 5 μg/mL of purified recombinant proteins for 48 h at 37°C with 5% CO_2. Brefeldin A (5 μg/mL; Sigma) was added to the cells during the last 4 h of culture. Next, the splenocytes were washed with PBS by centrifugation at 300 × *g* for 10 min at 4°C and stained with PerCP-conjugated anti-mouse CD8a, PE-conjugated anti-mouse CD4, and APC-conjugated anti-mouse IFN-γ antibodies (BioLegend) for 1 h at room temperature in the dark. For CD4 and CD8a markers, surface staining was performed while IFN-γ was stained intracellularly. Cells were fixed using ice-cold acetone and methanol in a 1:1 ratio, followed by permeabilization using 0.01 percent of Triton-X 100 (Sigma) in PBS. Subsequently, the cells were subjected to flow cytometry analysis using LSRFortessa (BD Biosciences). The lymphocytes were gated based on the scattering profiles of stains, and the percentage population of CD4 and CD8 positive cells as well as IFN-γ producing cells, were quantified.

Immunization of mice and challenge studies with *Brucella melitensis*

Mice were immunized with serodominant proteins, *viz*. BMEI0856, BMEI0063, BMEI1513, BMEI0748, or adjuvant alone, as described before. The mice injected with recombinant L7/L12 (BMEI0748) protein were considered the positive control group, while the mice injected with adjuvant alone were considered the negative control group. Forty-five days post-immunization, mice were challenged with *B. melitensis* 16 M. *B. melitensis* 16 M was grown in *Brucella* broth at 37° C until the OD reached 1 and resuspended at 2×10^6 CFUs/ml in 100 μL of sterile PBS. Subsequently, mice were administrated intraperitoneally (i.p.) with 2×10^6 CFU of *B. melitensis* 16 M. The mice were euthanized 2 weeks post-challenge, followed by aseptic removal of spleens for the colony forming unit (CFU) enumeration. The harvested spleens were homogenized individually in 1 mL sterile PBS using 1.0 mm zirconium beads (Benchmark Scientifics) for 60 s in a bead beater (Benchmark Scientifics). The homogenized spleens were 10-fold serially diluted and plated on *Brucella* agar plates in triplicates. The plates were incubated at 37°C with 5% CO_2, and the number of CFU was counted after 3 days of incubation. The CFU results were represented as the mean log CFU ± SD per group.

Development of Dps protein-based serodiagnostic assays

To develop Dps protein-based iELISA, the antigen concentration was optimized by performing checkerboard titrations. Various concentrations (10, 5, 2.5, 1.25, 0.625, 0.3125, 0.15625, 0.078125 μg/well) of Dps protein were coated in the 96-well microtiter plates and incubated overnight at 4° C. Subsequently, the coated plates were washed three times with 1 X PBST, followed by blocking with 300 μL of blocking buffer (1% BSA for human sera and 5% BSA for livestock sera) per well. The plates were incubated for 1 h at room temperature and given a wash as described earlier. Next, the brucellosis positive and negative sera (1:100 dilution) were added to the wells, and the plates were incubated for 2 h at room temperature. Next, the plates were washed four times with the wash buffer, and 100 μL of the HRP-conjugated anti-bovine IgG diluted at 1:5,000 (ThermoFisher) was added per well. The plates were incubated for 1 h at room temperature, followed by four washes and the addition of the TMB substrate solution (ThermoFisher). The plates were incubated for 10–15 min, followed by reading absorbance at 450 nm using an ELISA reader (PerkinElmer). For assessing the DIVA capability of Dps-based iELISA, the plates were coated with 100 ng of Dps protein per well, followed by iELISA as described above using serum samples collected at 21, 45, and 90 days post-*B. abortus* S19 vaccination. To evaluate the efficiency of Dps-based iELISA, human and cattle serum samples were screened using Dps-based iELISA, and the results were compared with that of commercially available, validated iELISA for human (NovaLisa) and cattle (PrioCheck) and RBPT. *Brucella*-culture positive/negative sera (bovine and mouse) and OIE-brucellosis positive/negative bovine reference serum samples were also screened using the Dps-based iELISA.

Y. enterocolitica O:9 immune and healthy rabbit serum samples were obtained from the Translational Research Platform for Veterinary Biologicals (TRPVB). Dps-based iELISA was performed with *Y. enterocolitica* O:9 immune and healthy rabbit serum samples as described before and HRP-conjugated anti-rabbit IgG at 1:5000 (CST) dilution was used as the secondary antibody. To perform iELISA with *Salmonella* immune serum, the sera were raised in mice against formalin-inactivated *S. typhimurium*. In brief, 6–8 weeks old female BALB/c mice were injected with 100 μL of inactivated *S.* typhimurium (1×10^5) intraperitoneally. Serum samples were collected on day 21, followed by performing Dps-based iELISA as described before. The HRP-conjugated anti-mouse IgG at a dilution of 1:5,000 (Novus Biologicals) was used as the secondary antibody for iELISA.

To develop the prototype LFA, purified Dps protein and biotinylated bovine serum albumin (Abcam) were dispensed (1.5 mg/mL) as test and control lines, respectively on the nitrocellulose membrane (mdi Membrane Technologies) using a flow dispenser (mdi Membrane Technologies). The protein G-gold (Abcam) and streptavidin-gold (Abcam) conjugates were mixed in a 4:1 ratio and coated on the pre-treated conjugate pad. Various components of LFA were assembled with the help of commercial source. To evaluate the prototype LFA, the serum samples (10 μL) were applied to the sample applicator port, followed by 200 μL of chase buffer to facilitate the sample migration toward the conjugate pad. Antibodies in the sample bound to the protein G-gold continue traveling up the nitrocellulose membrane. Anti-Dps antibodies in the samples were then bound to the Dps protein on the test line, producing a visible test line signal by an accumulation of gold particles on the test line. Streptavidin-gold conjugate bound to BSA-biotin on the control line produced a signal irrespective of the presence of anti-Dps antibodies in the samples. The absorbent pad absorbed excess liquid. The individual test was considered positive when a clear test line was visible or negative when only a control line was observed. To evaluate the LFA, 10 pooled brucellosis positive/negative/S19-vaccinated field serum samples of cattle, goat and humans were tested.

The formula used for the evaluation is given below:

Sensitivity = $a/(a+c) \times 100$.

Specificity = $d/(b+d) \times 100$.

Accuracy = a + d/(a + b + c + d) × 100.

a - Number of serum samples positive both by DPS ELISA and RBPT/iELISA.

b - Number of serum samples negative by RBPT/iELISA, but positive by DPS ELISA.

c - Number of serum samples positive by RBPT/iELISA, but negative by DPS ELISA.

d - Number of serum samples negative both by DPS ELISA and RBPT/iELISA.

Cut-off for commercial LPS based iELISA kit (as per manufacturer's instruction):

Per cent positivity (PP) = ($OD_{45o\ test\ sample}$/mean $OD_{450\ positive\ control}$) × 100.

Per cent positivity (PP) >40% is brucellosis positive.

Per cent positivity (PP) <40% is brucellosis negative.

Cut-off for DPS-based iELISA kit:

Cut-off = (mean OD of confirmed negative samples) ± 3 Standard Deviation.

Statistical analysis

The GraphPad Prism 6.0 software was used for the statistical analysis of experimental data. Data are shown as mean ± SD. Statistical significance was determined by one-way analysis of variance (ANOVA) for analyzing the data that involved more than two samples. FACS data were analyzed using the software FACS Diva (BD Biosciences). The positivity of the serum samples for Dps-based iELISA was determined by the mean OD greater than 2 standard deviations over the mean OD of the negative control. The specificity and sensitivity of Dps-based iELISA were calculated using Bayesian model statistics.

Results

High-throughput immunoprofiling of *Brucella melitensis* protein microarray identified serodominant proteins of *Brucella*

High-throughput immunoprobing of microbial proteins facilitates the identification of serodominant antigens, which can be employed to develop vaccines and serodiagnostic assays. To identify and characterize the serodominant protein antigens of *Brucella*, we performed a high-throughput immunoprobing of the *B. melitensis* protein microarray using serum samples from healthy or brucellosis-positive cattle, goat, and human (Figure 1A). The commercially available full proteome microarray that contains ~3,000 proteins of *B. melitensis* was used for immunoprofiling. The brucellosis-positive serum samples that harbor antibodies against the serodominant proteins of *Brucella* reacted with the respective proteins on the microarray (Figure 1A). The seroreactive proteins were detected by scanning the immunoprobed protein microarrays. The healthy human serum samples did not cross-react with any *Brucella* proteins on the array. However, we observed the reactivity of ELISA and RBPT-negative cattle and goat serum samples with some proteins on the array. Immunoprobing with brucellosis-positive serum samples of human, cattle, and goat detected various proteins on the array (Figure 1B). Subsequently, the scanned images of arrays were analyzed for data acquisition and identification of seroreactive proteins. The antigens with a signal intensity of more than two standard deviations over the mean of signal intensities from negative controls were defined as serodominant antigens (Liang et al., 2010). The high-ranking serodominant proteins from individual species are illustrated as a heat map (Figure 1C). Among the 3,000 antigenic proteins screened, a set of 40, 43, and 120 antigens reacting with human, cattle and goat serum samples, respectively, were identified serodominant (Figure 1D; Tables 2–4). The analysis also identified a set of 9 antigens that were equally seroreactive with all the species (Figure 1D; Table 5).

Cloning, expression, and purification of selected serodominant proteins of *Brucella*

We identified many serodominant proteins of *Brucella* using high-throughput immunoprobing of the *B. melitensis* protein microarray. To characterize these antigens further, we selected 10 serodominant proteins based on their seroreactivity and novelty. These proteins are either shared by brucellosis-positive animals and humans or uniquely expressed by individual species (Table 6). The vaccine and diagnostic potentials of some of these serodominant proteins were not explored before. The coding sequences of respective proteins were amplified from the chromosomal DNA of *B. melitensis*, followed by cloning them into a pET21a(+) prokaryotic expression vector that harbors a C-terminal 6X His tag. Subsequently, the clones were confirmed by restriction enzyme digestion and sequencing. To overexpress serodominant proteins, pET21a(+) harboring the *Brucella* genes were introduced into BL21DE3 *E. coli*. The overexpression of recombinant *Brucella* proteins was induced in *E. coli* using IPTG, followed by analyzing the expression levels by SDS-PAGE (Supplementary Figure S1). Next, the overexpressed *Brucella* proteins were purified using Nickel-NTA-agarose affinity chromatography, and the purity of the proteins was assessed by SDS-PAGE (Figure 2A). Further, we examined the purified *Brucella* proteins by immunoblotting using an anti-His-tag antibody (Figure 2B). The immunoblot showed overexpressed *Brucella* protein of expected size that further confirmed the identity of the recombinant proteins.

Evaluation of the immunogenicity of purified sero-dominant proteins of *Brucella* in mice

The reactivity of *Brucella* proteins with brucellosis-positive serum samples suggests that these proteins are secreted or released by *Brucella* into the circulatory system of the host, resulting in the formation of antibodies against them. Since these proteins are immunogenic, they may induce *Brucella*-specific immune responses other than antibody generation in the host. To examine this, we analyzed the immunogenicity of purified *Brucella* proteins in mice. The mice were immunized with serodominant proteins, followed by the collection of blood samples at various days post-immunization (Figure 3A). We used the immunogenic protein of *Brucella*, L7/L12 (BMEI0748) as the positive control as this antigen has been reported to induce a protective immune response in

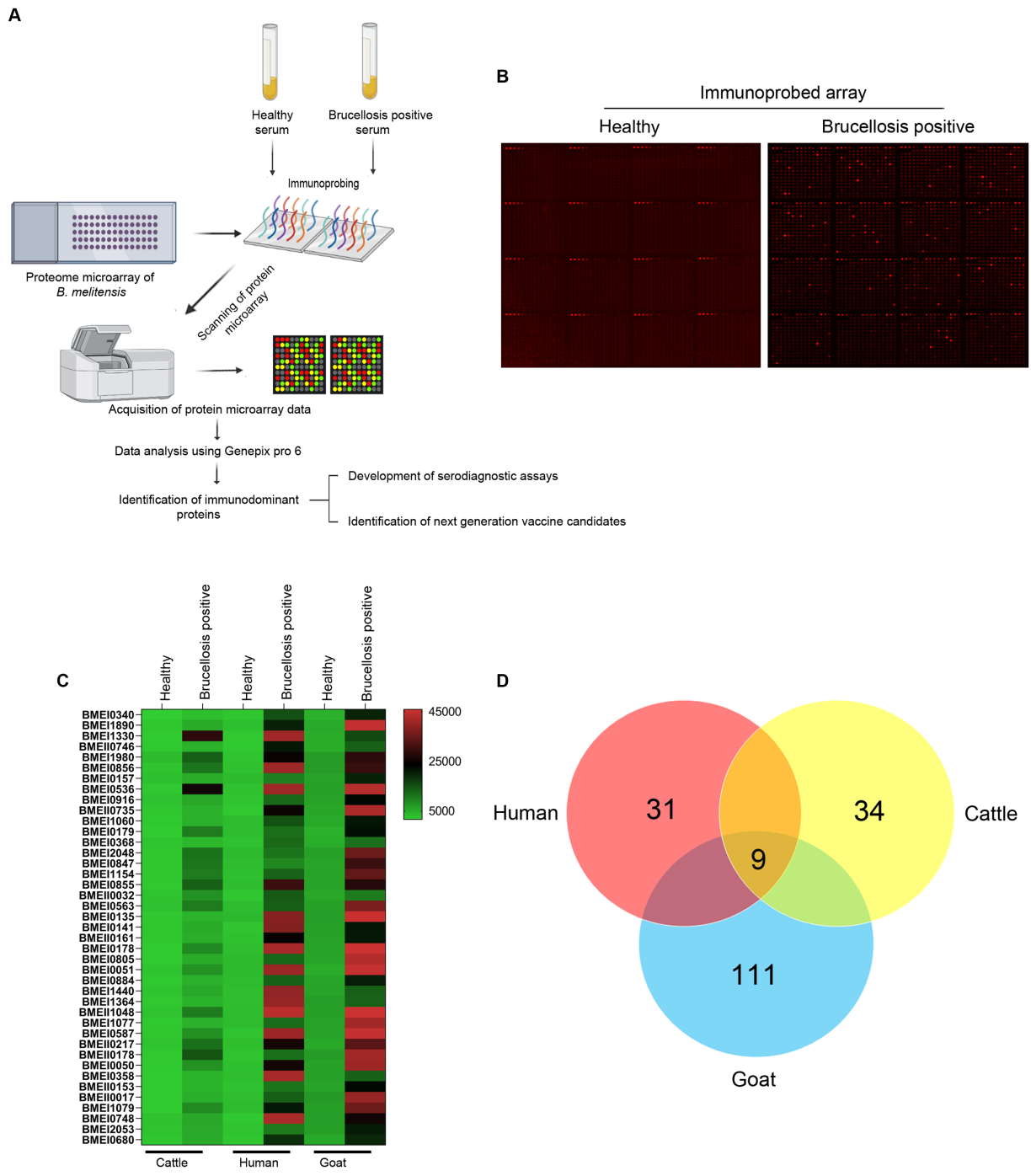

FIGURE 1
(A) A graphical abstract summarizing the identification process of serodominant protein antigens of *Brucella*. **(B)** Representative image of *B. melitensis* protein microarray immunoprobed with healthy or brucellosis-positive serum samples. The red spots on the array probed with healthy serum sample indicate the positive controls. The red spots on the array probed with brucellosis positive serum sample indicate the serodominant proteins that reacted with the respective antibodies in the serum. The intensity of red spots indicates the extent of seropositivity. Confirmed single strong positive or healthy serum samples from cattle, human and goat were utilized for immunoprobing that was performed in triplicates. **(C)** Heat map showing differential detection of serodominant proteins by healthy or brucellosis positive human, cattle and goat serum samples. The seroreactive *Brucella* proteins are mentioned in rows and the columns represent the host species. The seroreactivity of proteins is represented as varying intensity of red (strongest) to bright green (weakest). **(D)** The Venn diagram showing the number of *Brucella* proteins that reacted with serum samples from single or multiple host species. The number of seroreactive proteins detected in each species is shown in individual circle, while the number of proteins that are shared among the different species are shown in the intersection area.

brucellosis (Oliveira et al., 1994; Oliveira and Splitter, 1994, 1996; Singh et al., 2015). The mice were sacrificed at the end of the experiment, followed by analyzing various cell populations to determine the induction of cell-mediated immune responses. Serum samples collected on different days were analyzed for IgG1 and IgG2a levels to estimate the humoral immune response induced by these

TABLE 2 The list of identified serodominat proteins that reacted with human sera.

Peptidoglycan-associated lipoprotein	BMEI0340
Transporter	BMEI1890
Protease Do	BMEI1330
Branched-chain alpha-keto acid dehydrogenase subunit E2	BMEII0746
Isopropylmalate isomerase large subunit	BMEI0157
Immunogenic protein	BMEI0536
Hypothetical protein	BMEI0916
Periplasmic oligopeptide-binding protein precursor	BMEII0735
Hypothetical protein	BMEI1060
Hypothetical protein	BMEI0179
Hypothetical protein	BMEI0368
ATP-dependent protease ATP-binding subunit HslU	BMEI2048
Preprotein translocase subunit SecG	BMEI0847
NADH dehydrogenase subunit E	BMEI1154
Pyruvate dehydrogenase subunit beta	BMEI0855
VirB8	BMEII0032
Hypothetical protein	BMEI0563
Outer membrane lipoprotein	BMEI0135
Dihydrolipoamide succinyltransferase	BMEI0141
Flagellar hook-associated protein FlgL	BMEII0161
Hypothetical protein	BMEI0178
Hypothetical protein	BMEI0805
Hypothetical protein	BMEI0051
DNA gyrase subunit A	BMEI0884
Thiol:disulfide interchange protein DsbA	BMEI1440
Transcriptional regulatory protein MUCR	BMEI1364
Molecular chaperone GroEL	BMEII1048
Hypothetical protein	BMEI1077
COML competence lipoprotein	BMEI0587
Periplasmic dipeptide transport protein precursor	BMEII0217
DNA starvation/stationary phase protection protein Dps	BMEI1980
High-affinity zinc uptake system protein ZNUA	BMEII0178
CobT protein	BMEI0050
Deoxyuridine 5′-triphosphate nucleotidohydrolase	BMEI0358
Hypothetical protein	BMEII0153
Outer membrane lipoprotein	BMEII0017
Lipoprotein NlpD	BMEI1079
50S ribosomal protein L7/L12	BMEI0748
Transporter	BMEI2053
Preprotein translocase subunit SecD/SecF	BMEI0680

antigens (Supplementary Figure S2). We observed a high antibody titer in the immunized mice, indicating that these antigens are potent inducers of the humoral immune response. IgG1 and IgG2a are the markers of Th2 and Th1 responses, respectively, in mice where the Th1 response is reported to be important for protection against brucellosis (Golding et al., 2001; Yingst and Hoover, 2003; Skendros et al., 2011; Vitry et al., 2014). We observed a high titer of IgG2a antibody with BMEI1980, BMEI0063, BMEI0856, BMEI0916, BMEII1048, and BMEI0855 indicating a Th1 specific response (Figure 3C). In contrast, the *Brucella* proteins, BMEI1513, BMEI0748, BMEI1390, and BMEII0154 exhibited induction of IgG1 response, suggesting a Th2 immune response (Figure 3B).

10.3389/fmicb.2023.1253349

TABLE 3 The list of identified serodominant proteins that reacted with goat sera.

Transporter	BMEI1890
30S ribosomal protein S16	BMEI0227
Hypothetical protein	BMEI1866
Immunogenic protein	BMEI0536
Hypothetical protein	BMEI0810
Protease Do	BMEI0613
Type I restriction-modification enzyme S subunit	BMEII0452
Preprotein translocase subunit SecA	BMEI0121
HlyD family secretion protein	BR_1060
Periplasmic oligopeptide-binding protein precursor	BMEII0735
Nucleoside triphosphate pyrophosphohydrolase	BMEI0920
Hypothetical protein	BMEI1847
Hypothetical protein	BMEII0073
Flagellin	BMEII0150
Hypothetical protein	BMEI0699
Cell surface protein	BMEI1872
Riboflavin synthase subunit beta	BMEII0589
Sensory transduction histidine kinase	BMEI0370
2-oxoisovalerate dehydrogenase subunit alpha	BMEII0748
ATP-dependent protease ATP-binding subunit HslU	BMEI2048
ATPase	BMEI1370
Cystine-binding periplasmic protein precursor	BMEII0601
Multidrug resistance protein A	BMEII1118
Leu/Ile/Val-binding protein precursor	BMEII0103
Preprotein translocase subunit SecG	BMEI0847
acyl-CoA hydrolase	BMEI0503
LemA protein	BMEI0228
Electron transfer flavoprotein-ubiquinone oxidoreductase	BMEI1320
NADH dehydrogenase subunit E	BMEI1154
Hypothetical protein	BMEII0924
Sugar-binding protein	BMEII0755
Catalase	BMEII0893
Hypothetical protein	BMEI0563
Hypothetical protein	BMEII0231
Thioredoxin	BMEII0401
trbJ protein	BR_A0368
Outer membrane lipoprotein	BMEI0135
Monovalent cation/H+ antiporter subunit G	BMEII0765
Hypothetical protein	BMEI0973
Colicin V production protein	BMEI1487
Molecular chaperone DnaJ	BMEI1513
Cysteine synthase A	BMEI0101
Alpha-methylacyl-CoA racemase	BMEII1076
Non-motile and phage-resistance protein	BMEI0417
ABC transporter substrate-binding protein	BMEII0338
Superoxide dismutase (Cu-Zn)	BMEII0581
Copper-containing nitrite reductase precursor	BMEII0988
Hemagglutinin	BMEII0717
Hypothetical protein	BMEI1000
Hypothetical protein	BMEI0178

(Continued)

TABLE 3 (Continued)

Transporter	BMEI1890
Hypothetical protein	BMEI0805
Osmotically inducible protein C	BMEII0409
Acetyl-CoA carboxylase biotin carboxyl carrier protein subunit	BMEI1062
Translaldolase	BMEI0244
Dihydroxyacetone kinase	BMEI0397
Dihydrolipoamide dehydrogenase	BMEI0145
Flagellar motor protein MotB	BMEII0154
Oligopeptide-binding protein appa precursor	BMEII0859
Membrane-bound lytic murein transglycosylase B	BMEI0223
Hypothetical protein	BMEI0051
Hypothetical protein	BMEI0063
Alkaline phosphatase	BMEI0790
Hypothetical protein	BMEI1865
tRNA (guanine-N(1)-)-methyltransferase	BMEI0149
Ribosome biogenesis GTP-binding protein YsxC	BMEII0274
Membrane metalloprotease	BMEI0829
Cytoplasmic protein	BMEII0772
D-ribose-binding periplasmic protein precursor	BMEI1390
Molecular chaperone GroEL	BMEII1048
Flagellar motor switch protein FLIM	BMEII1110
ABC transporter periplasmic-binding protein	BMEII0702
Sugar-binding protein	BMEII0590
Hypothetical protein	BMEI1514
Invasion protein B	BMEI1584
Hypothetical protein	BMEI0060
MarR family transcriptional regulator	BMEII0311
Flagellar basal-body rod protein FlgB	BMEII1089
Hypothetical protein	BMEI1077
Oxidoreductase	BMEI1710
Acetylornithine transaminase protein	BMEI1621
Inner membrane protein translocase component YidC	BMEII0275
Flagellar basal body rod modification protein	BMEII0164
D-ribose-binding periplasmic protein precursor	BMEII0435
Hypothetical protein	BMEII0989
COML competence lipoprotein	BMEI0587
Periplasmic protein of efflux system	BMEI0653
ABC transporter substrate-binding protein	BMEI0015
DNA mismatch repair protein MutS	BMEI1801
Translocation protein TolB	BMEI0339
Hypothetical protein	BMEI0186
Hypothetical protein	BMEII0468
3-oxoacyl-ACP synthase	BMEI1112
Stomatin like protein	BMEII0019
Periplasmic dipeptide transport protein precursor	BMEII0217
DNA starvation/stationary phase protection protein Dps	BMEI1980
Ferric uptake regulation protein	BMEI0375
Glycolate oxidase subunit GLCD	BMEI1527
High-affinity zinc uptake system protein ZNUA	BMEII0178
Hypothetical protein	BMEI1724
Leucine- isoleucine- valine- threonine- and alanine-binding protein precursor	BMEI1930

(Continued)

TABLE 3 (Continued)

Transporter	BMEI1890
CobT protein	BMEI0050
AsnC family transcriptional regulator	BMEI0357
Outer membrane lipoprotein	BMEII0017
Hypothetical protein	BMEI0641
ABC transporter substrate-binding protein	BMEI1954
Carnitine operon oxidoreductase CaiA	BMEI0848
Multidrug resistance protein A	BMEI0926
50S ribosomal protein L7/L12	BMEI0748
Hypothetical protein	BMEI0651
Lipoprotein NlpD	BMEI1079
Cell division protein FtsZ	BMEI0585
Dithiobiotin synthetase	BMEII0777
D-3-phosphoglycerate dehydrogenase	BMEII0813
Hypothetical protein	BMEII0895
Glycerol-3-phosphate-binding periplasmic protein precursor	BMEII0625
Hypothetical protein	BMEI0796
Phosphate-binding periplasmic protein	BMEI1989
Hypothetical protein	BMEI1695
Short-chain dehydrogenase/reductase	BMEI1832
Cysteine desulfurase	BMEI1042

Next, we analyzed other indicators of protective immunity against *Brucella,* such as the cell population producing IFN-γ and the levels of $CD4^+$ and $CD8^+$ T cells. The splenocytes isolated from the immunized mice were treated with the respective serodominant proteins for 48 h, followed by staining the cells with PerCP-conjugated anti-mouse CD8a, PE-conjugated anti-mouse CD4, and APC-conjugated anti-mouse IFN-γ antibodies for flow cytometry analysis. A higher percentage of $CD4^+$ and $CD8^+$ T cells population was observed in the mice immunized with BMEI1980, BMEI0063, BMEI0856, BMEI0916, BMEII1048, BMEI0855, BMEII0154, and BMEI0748 compared to the adjuvant alone (Figure 3D). We also observed a high percentage of IFN-γ producing $CD4^+$ and $CD8^+$ T cells in mice immunized with BMEI1390, BMEI0063, BMEI0856, BMEI0916, BMEI0748 and BMEI1980, BMEI1390, BMEI1513, BMEI0063, BMEI0916, BMEII1048, BMEI0855, BMEII0154, BMEI0748, respectively (Figures 3E,F, Supplementary Figure S3).

Evaluation of protective efficacy of serodominant proteins against *Brucella melitensis* challenge

Next, we performed a challenge study with *B. melitensis* using the mice immunized with four serodominant proteins *viz*. BMEI0856, BMEI0063, BMEI1513, and BMEI0748. Our immunogenicity studies revealed that the serodominant proteins, BMEI0856 and BMEI0063, induced a significant level of Th1 type immune response, whereas BMEI1513 induced a Th2 type response. The mice immunized with L7/L12 protein (BMEI0748) and adjuvant alone served as the positive and negative control groups, respectively. The immunized mice were challenged with *B. melitensis*, followed by harvesting the spleen and enumerating bacterial load at 2 weeks post-infection. The protection efficiency of a vaccine candidate is determined by the significant reduction in the number of bacterial colonies in the spleen of immunized mice compared to the control. The mice immunized with BMEI0856 showed a significant reduction of CFU, indicating the protective effect of this protein against *the B. melitensis* challenge (Figure 3G). As reported previously, L7/L12 also exhibited protective efficacy against challenge with *B. melitensis*. Interestingly, BMEI0856 immunized mice showed lesser bacterial load compared to L7/L12. On the other hand, no significant difference in the bacterial load was observed in the mice immunized with the BMEI1513 or BMEI0063 compared to the control groups (Figure 3G).

The serodominant protein, Dps, reacts with brucellosis-positive serum samples and exhibits DIVA capability

The positive signals from the immunoprobed protein array indicated the seroreactivity of serodominant proteins with the respective antibodies in the brucellosis-positive serum samples. To confirm this data further, we examined the seroreactivity of purified serodominant proteins by immunoblotting. The proteins were resolved on SDS-PAGE, followed by transferring them onto the PVDF membrane. Subsequently, the immunoblots were incubated with healthy or brucellosis-positive cattle serum samples. We observed seroreactivity of purified serodominant proteins with varying efficiency where BMEI1980 BMEI0916, BMEI0856, BMEII1048, BMEI0855, and BMEI1513 exhibited strong seroreactivity (Figure 4B). The healthy serum sample did not react with any of the purified proteins that we tested (Figure 4A).

We observed strong reactivity of BMEI1980 with the brucellosis-positive serum samples of cattle and humans. The BMEI1980 encodes

TABLE 4 The list of identified serodominant proteins that reacted with cattle sera.

Protease Do	BMEI1330
bifunctional N-acetylglucosamine-1-phosphate uridyltransferase/glucosamine-1-phosphate acetyltransferase	BMEII0684
Immunogenic protein	BMEI0536
Hypothetical protein	BMEI0810
Protease Do	BMEI0613
tRNA pseudouridine synthase B	BMEI1963
Membrane fusion protein MTRC	BMEI0892
Hypothetical protein	BMEI0179
Cell surface protein	BMEI1872
Riboflavin synthase subunit beta	BMEII0589
2-oxoisovalerate dehydrogenase subunit alpha	BMEII0748
ATP-dependent protease ATP-binding subunit HslU	BMEI2048
Succinyl-CoA synthetase subunit beta	BMEI0138
Aliphatic sulfonates-binding lipoprotein	BMEII0109
Iron(III)-binding periplasmic protein precursor	BMEII1120
Multidrug resistance protein A	BMEII1118
Preprotein translocase subunit SecG	BMEI0847
Hypothetical protein	BMEII0010
Acyl-CoA hydrolase	BMEI0503
Leucine- isoleucine- valine- threonine- and alanine-binding protein precursor	BMEI0263
Cytochrome C-type biogenesis protein CYCH	BMEI1334
Hypothetical protein	BMEII0913
50S ribosomal protein L4	BMEI0758
NADH dehydrogenase subunit E	BMEI1154
Ribosomal-protein-serine acetyltransferase	BMEII0002
Pyruvate dehydrogenase subunit beta	BMEI0855
Hypothetical protein	BMEII0924
Hypothetical protein	BMEI0563
Hypothetical protein	BMEI1033
Molecular chaperone DnaJ	BMEI1513
Hemagglutinin	BMEII0717
Hypothetical protein	BMEI0119
Nitrogen fixation protein FIXG	BMEI1567
Hypothetical protein	BMEI0063
Molecular chaperone GroEL	BMEII1048
ABC transporter periplasmic-binding protein	BMEII0702
Peptidyl-prolyl cis-trans isomerase	BMEI0123
Hypothetical protein	BMEI0443
Periplasmic dipeptide transport protein precursor	BMEII0217
DNA starvation/stationary phase protection protein Dps	BMEI1980
High-affinity zinc uptake system protein ZNUA	BMEII0178
Phosphate-binding periplasmic protein	BMEI1989
Molybdopterin (MPT) converting factor subunit 1	BMEI1253

the DNA-binding protein from starved cells, Dps. A high throughput proteome analysis reported that the Dps protein is expressed only in the *B. abortus* 2,308 compared to the vaccine strain, *B. abortus* S19 (Lamontagne et al., 2009). However, there was no experimental validation of this observation. Therefore, we performed a detailed characterization of Dps protein, intending to develop improved

TABLE 5 The list of identified serodominant antigens that reacted with sera from both animals and humans.

Protease Do	BMEI1330
Immunogenic protein	BMEI0536
ATP-dependent protease ATP-binding subunit HslU	BMEI2048
NADH dehydrogenase subunit E	BMEI1154
Molecular chaperone GroEL	BMEII1048
Periplasmic dipeptide transport protein precursor	BMEII0217
DNA starvation/stationary phase protection protein Dps	BMEI1980
High-affinity zinc uptake system protein ZNUA	BMEII0178
Pyruvate dehydrogenase complex dihydrolipoamide acetyltransferase	BMEI0856

TABLE 6 The list of 10 high-ranking serodominant proteins that were selected for the study.

ID	Gene name
BMEI1980	DNA starvation/ stationary phase protection protein Dps (common in all the species)
BMEI1390	D-ribose-binding periplasmic protein precursor (detected in goat sera)
BMEI1513	J domain-containing protein (detected in goat sera)
BMEI0063	Hypothetical protein (detected only in animal sera)
BMEI0856	Pyruvate dehydrogenase complex dihydrolipoamide acetyltransferase (common in all the species)
BMEI0916	Hypothetical protein (detected in human sera)
BMEII1048	Molecular chaperone GroEL (common in all the species)
BMEI0855	Pyruvate dehydrogenase subunit beta (detected in human and cattle sera)
BMEII0154	MotB family protein (detected in goat sera)
BMEI0748	50S ribosomal protein L7/L12 (detected in human sera and goat sera)

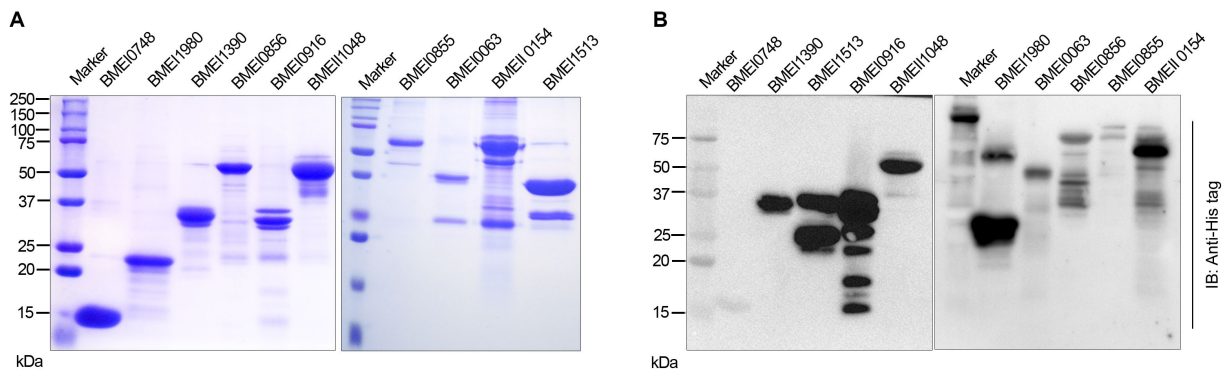

FIGURE 2
(A) SDS-PAGE gel image of purified serodominant proteins. The selected serodominant proteins were cloned and overexpressed in *E. coli* with a C-terminal 6X His-tag. Subsequently, the overexpressed proteins were purified using Ni-NTA affinity chromatography. **(B)** Immunoblot showing the purified serodominant proteins. The blot was probed with HRP-conjugated anti-His antibody to detect the His-tagged proteins.

serodiagnostic assays with DIVA capability. We analyzed the immunoreactivity of purified Dps protein with serum samples from animals and humans. The immunoblots of Dps protein were probed with healthy sera or brucellosis-positive human, goat, cattle, or *B. abortus* S19-vaccinated cattle serum samples. The Dps protein was efficiently detected by brucellosis-positive serum samples from both animals and humans (Figures 5A,B). Further, we found that Dps protein failed to react with the serum sample from *B. abortus* S19-vaccinated cattle. To confirm the differential recognition of Dps protein, we performed immunoprobing of various concentrations of Dps protein with the sera from naturally infected or *B. abortus* S19-vaccinated cattle (Figure 5C). In agreement with previous data, the serum samples from *B. abortus* S19-vaccinated cattle did not detect Dps protein. We used LPS of *E. coli* and *B. abortus* as the negative and positive controls, respectively, for the immunoblots. Next, we probed the Dps blot with cattle serum samples collected at 21, 45, and 90 days post-*B. abortus* S19-vaccination. We did not observe any seroreactivity of Dps protein with serum samples after various days post-vaccination (Figure 5D).

10.3389/fmicb.2023.1253349

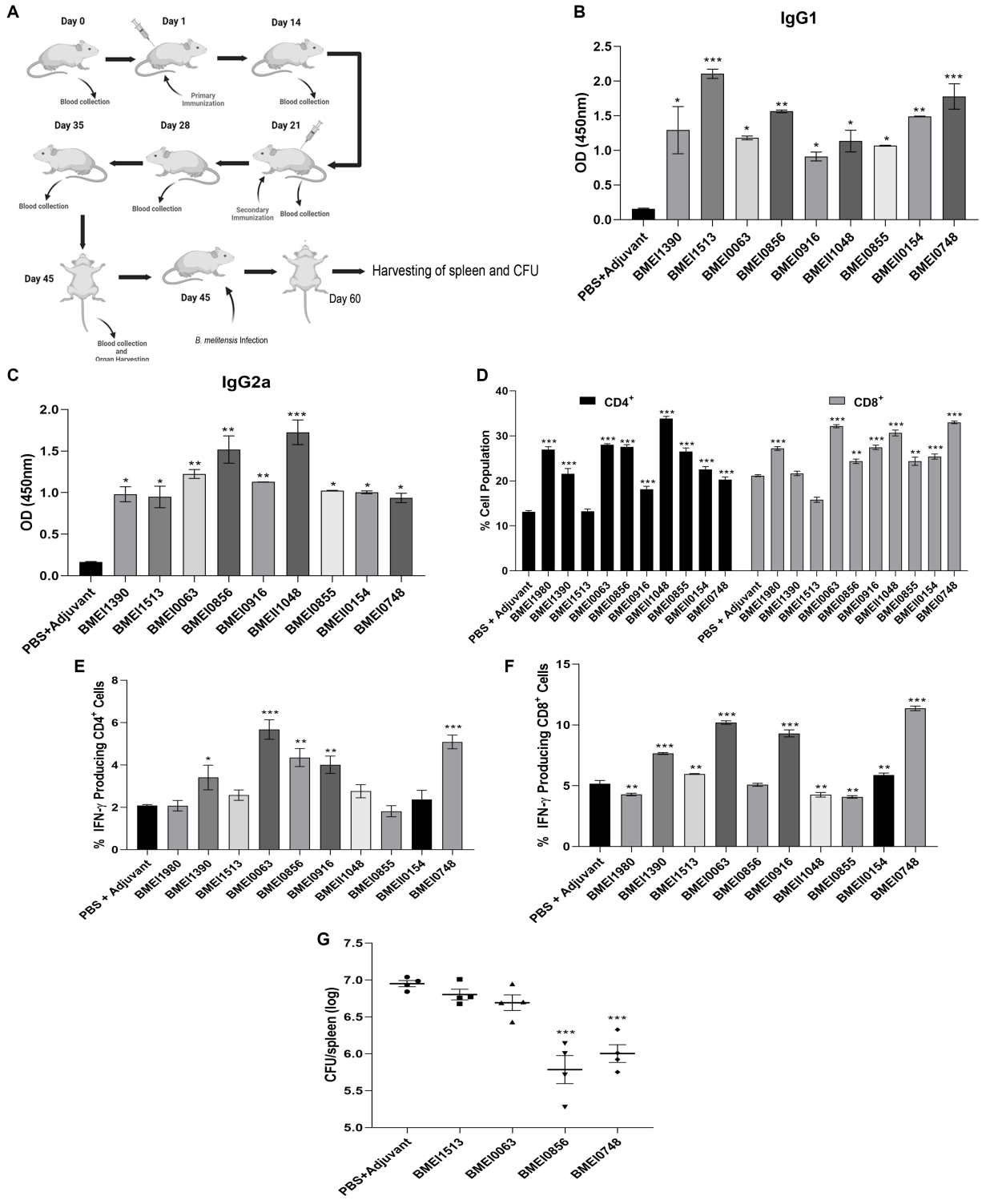

FIGURE 3
(A) A pictographic representation of the study to examine the immunogenicity of purified serodominant proteins of *Brucella*. BALB/c mice were immunized with purified. Recombinant proteins on day 1, followed by administering a booster dose on day 21. Blood samples were collected on day 0, 14, 21, 28, 35, and 45 post-immunization. Mice were euthanized on day 45, followed by collection of spleen. For the challenge studies, the immunized mice were infected with *B. melitensis* on day 45 and euthanized on day 60, followed by collection of spleen for the CFU enumeration. **(B,C)** ELISA showing the levels of IgG1 and IgG2a, respectively in the serum samples. The serum samples collected from immunized mice on day 45 were subjected to ELISA to determine the levels of IgG1 and IgG2a. Mice injected with PBS+Adjuvant and BMEI0748 (L7/L12) were used as the negative and positive controls, respectively. **(D)** Percent cell population of $CD4^+$ and $CD8^+$ T cells, in the immunized or control mice. The splenocytes were isolated from the immunized mice, followed by treating the cells with respective serodominant proteins. Forty-eight hours post-treatment, the cells were stained with anti-CD4, and anti-CD8 antibodies conjugated with fluorescent dyes, followed by FACS analysis. **(E,F)** Showing percent cell population of IFN-γ producing $CD4^+$ and $CD8^+$ T cells in or control mice. The staining procedure was followed as mentioned above followed by staining with

(Continued)

FIGURE 3 (Continued)
anti-CD4, -CD8 and -IFN-γ antibodies conjugated with fluorescent dyes, followed by FACS analysis. **(G)** Bacterial load in the spleen of mice immunized with the serodominant proteins, BMEI0856, BMEI0063, BMEI1513, BMEI0748 (L7/L12) or adjuvant alone. The immunized mice were challenged with 2×10^6 CFUs/ml of *B. melitensis* 16 M, followed by enumeration of CFU at 14 days post-infection. Each data point represents individual mice per group and the bar indicates average of the group. Mice injected with PBS + Adjuvant and BMEI0748 were used as the negative and positive controls, respectively. All the data are presented as mean ± SD. (*$p < 0.05$; **$p < 0.01$; ***$p < 0.001$).

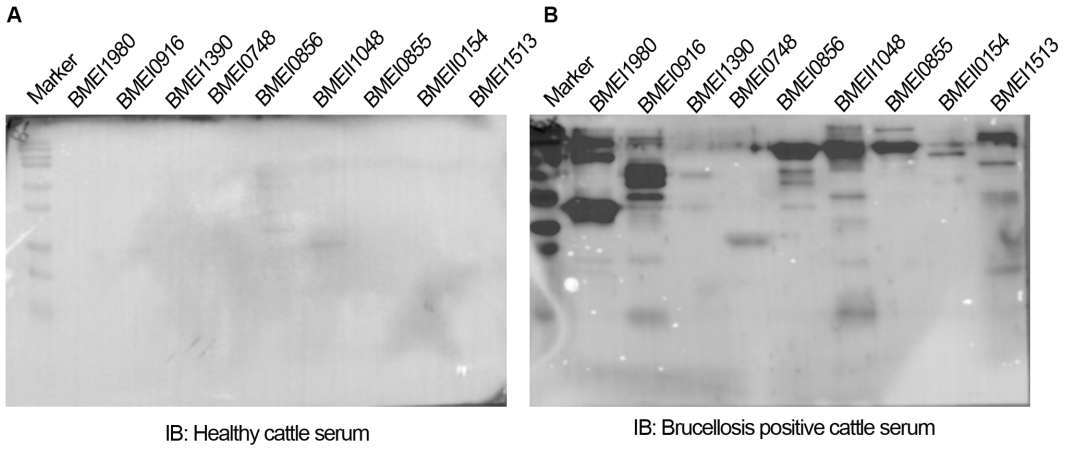

FIGURE 4
(A,B) Immunoblots showing the reactivity of purified serodominant proteins with healthy or brucellosis-positive cattle serum samples, respectively. The purified serodominant proteins were resolved on SDS-PAGE gel, followed by immunoblotting. The membranes were probed with healthy or brucellosis-positive serum samples, followed by HRP-conjugated anti-bovine IgG.

The LPS of *B. abortus* reacted with the sera, which confirms that the serum samples are derived from *B. abortus* S19-vaccinated animals.

Next, we examined the reason behind the non-reactivity of Dps protein with the *B. abortus* S19-vaccinated cattle sera. It is possible that the Dps protein was not expressed in the *B. abortus* S19 vaccine strain, resulting in a lack of antibody production against this protein in the vaccinated animals. To examine this, we performed immunoblotting with total lysates of *B. abortus* and *B. abortus* S19 strain. The membrane was probed with an anti-Dps antibody, which can detect the endogenous level of Dps protein. We used the reported serodominant protein, L7/L12, as the positive control. We observed a diminished level of Dps protein in the *B. abortus* S19 strain in comparison to the wild-type *B. abortus* (Figure 5E). In contrast, we observed a uniform expression of L7/L12 protein in *B. abortus* and *B. abortus* S19 vaccine strains (Figure 5E).

Dps protein-based serodiagnostic assays exhibit DIVA capability and detect brucellosis in animals and humans

Since both the animal and human sera efficiently recognized Dps protein, we wished to develop a lateral flow assay (LFA) and an indirect ELISA (iELISA) based on this protein. Toward developing iELISA, we determined the optimal concentration of Dps protein using the checkerboard titration assays (Figures 6A,B). Various concentrations of Dps protein were titrated against brucellosis-positive or negative human serum samples. The positivity of the serum samples was determined by the mean OD greater than two standard deviations over the mean OD of the negative controls (França et al., 2014). The cut-off value calculated for human serum samples was 0.45. The assay indicated that 1 μg/mL of Dps protein was optimal for developing the iELISA. To develop the assay further, various blocking agents and antibody dilutions were optimized. One percent BSA was found suitable for testing human serum samples, whereas 3% BSA was optimal for cattle serum samples. HRP-conjugated anti-bovine or anti-human antibody at a dilution of 1:5,000 was found optimal for Dps-based iELISA.

Next, the efficiency of Dps-based iELISA was compared with that of commercially available LPS-based iELISA or with RBPT. The validated LPS-based iELISA (NovaLisa) can detect brucellosis with human serum samples. Among the human serum samples tested, 26 sera were found to be positive by Dps protein-based iELISA, and 25 samples were positive by commercial iELISA. In contrast, only 14 samples were found positive by RBPT. A total of 195 samples were declared negative by all three tests. Both ELISAs had an agreement with 25 samples. Out of 207 samples, which were negative with RBPT, 11 samples were found positive by both ELISAs. In the case of one sample, there was a disagreement between the two ELISA (Table 7). The higher number of positive samples in iELISA than RBPT may suggest enhanced sensitivity of ELISA. Our in-house validation assays using human serum samples indicated 99% sensitivity and 98% specificity for the Dps-based iELISA (Table 8).

We have also evaluated the seroreactivity of Dps-based iELISA using *Brucella*-culture positive/negative bovine and mouse sera and OIE-brucellosis positive/negative bovine reference serum samples (Supplementary Figures 4A,B). The assay indicated the detection of anti-Dps antibodies in the brucellosis positive reference serum samples. To examine the DIVA capability of iELISA, cattle serum samples were collected on various days post *B.* abortus S19 vaccination

10.3389/fmicb.2023.1253349

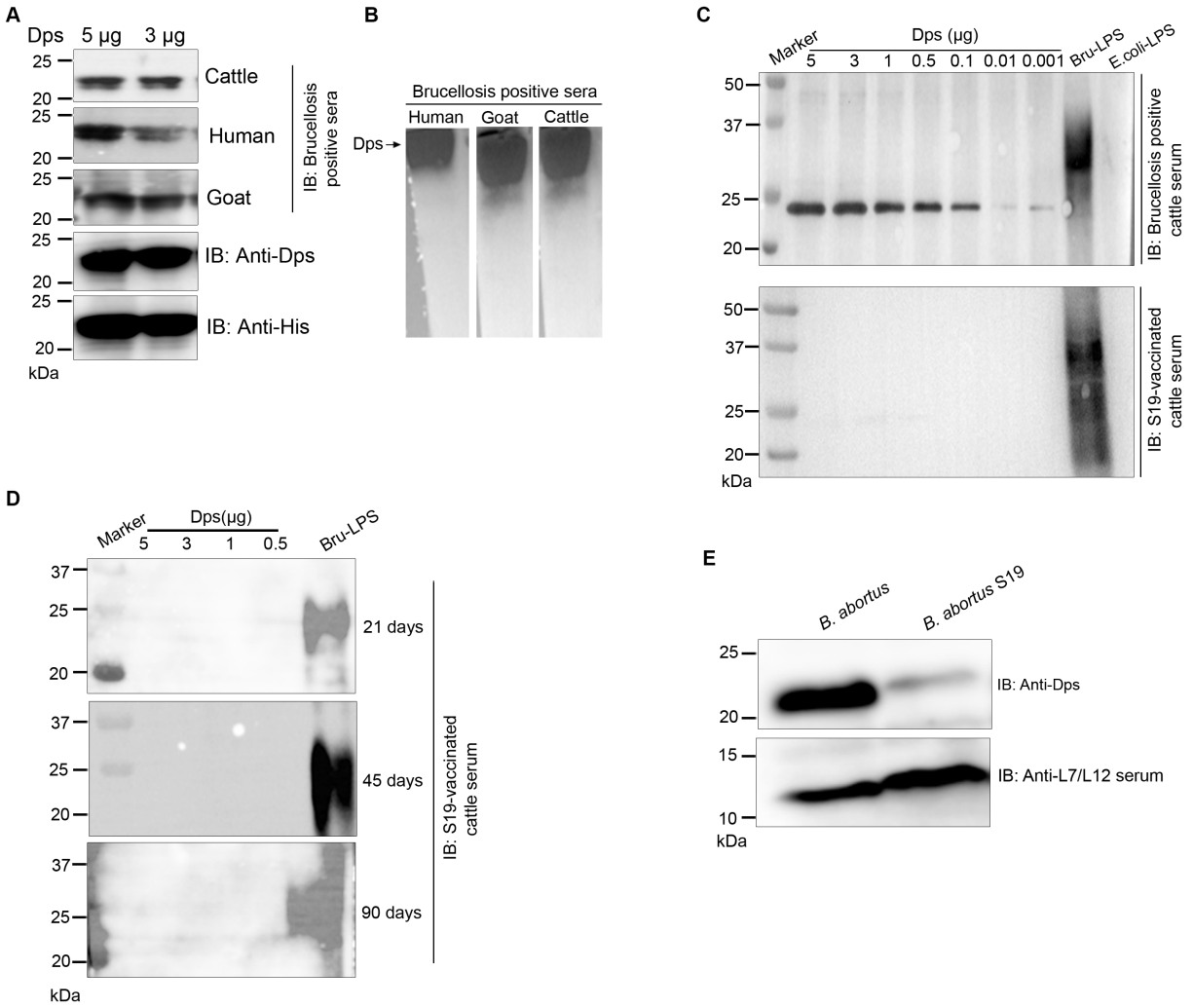

FIGURE 5
Seroreactivity of Dps protein with sera from human and animals. **(A,B)** Purified Dps protein resolved on SDS-PAGE and native-PAGE gel, respectively, followed by immunoblotting. The membrane was probed with 10 pooled healthy or brucellosis-positive serum samples from human, goat and cattle, followed by species-specific HRP-conjugated anti-IgG. The Dps protein was also confirmed by probing the blot with anti-His HRP antibody and anti-Dps antibody. **(C)** Immunoblot showing the reactivity of various concentrations (5, 3, 1, 0.5, 0.1, 0.01, and 0.001 µg) of Dps protein with 10 pooled serum samples from brucellosis-positive cattle or cattle vaccinated with *Brucella abortus* S19 strain. LPS of *B. abortus* S19 and *E. coli* were used as the positive and negative controls, respectively. **(D)** Immunoblot showing various concentrations (5, 3, 1, 0.5 µg) of Dps protein probed with 10 pooled cattle serum samples collected at 21, 45, and 90 days post-vaccination with *Brucella abortus* S19. The LPS of *B. abortus* S19 was used as the positive control. **(E)** Immunoblot showing the levels of Dps protein in *B. abortus* and *B. abortus* S19 strain. The total cell lysates of *B. abortus* or *B. abortus* S19 was subjected to immunoblotting, followed by probing the blot with anti-Dps antibody. The L7/L12 protein was detected on the blot using immunized serum from mice.

(21, 45, and 90 days) and were screened using the Dps-based or LPS-based iELISA. The OD values of the known positive, negative, and *B. abortus* S19-vaccinated serum samples were estimated, and the cut-off values were derived as described before. All the *B. abortus* S19-vaccinated serum samples were seropositive with LPS-based iELISA, whereas these sera showed OD values similar to negative controls with Dps-based iELISA (Figures 6C,D). The assay indicated that the Dps-based iELISA could differentiate *B. abortus* S19-vaccinated from naturally infected cattle.

The LPS-based serodiagnostic assays for brucellosis have been reported to cross-react with the serum samples of animals infected with *Y. enterocolitica* O:9, *S. typhimurium*, and *E. coli* (Al Dahouk et al., 2003a). Therefore, we examined the cross-reactivity of Dps-based iELISA with *Yersinia* and *Salmonella* immune sera. We did not observe any significant cross-reactivity with Dps-based iELISA against the *Yersinia* or *Salmonella* immune serum samples (Figures 6E,F). To further confirm the experimental data, we performed an immunoblot with whole cell lysates of *S. typhimurium*, *E. coli* or *B. abortus*, followed by probing the membrane with *Brucella* anti-Dps antibody. The anti-Dps antibody did not cross-react with any proteins in the lysates of *S. typhimurium* or *E. coli* other than detecting the endogenous Dps protein in the *B. abortus* lysate (Supplementary Figure S5). Collectively, our experimental data indicate that Dps-based iELISA can specifically detect brucellosis positive sera samples without showing any cross-reactivity.

Next, we developed a prototype LFA using Dps protein for pen-site application of this serodiagnostic assay. In the prototype

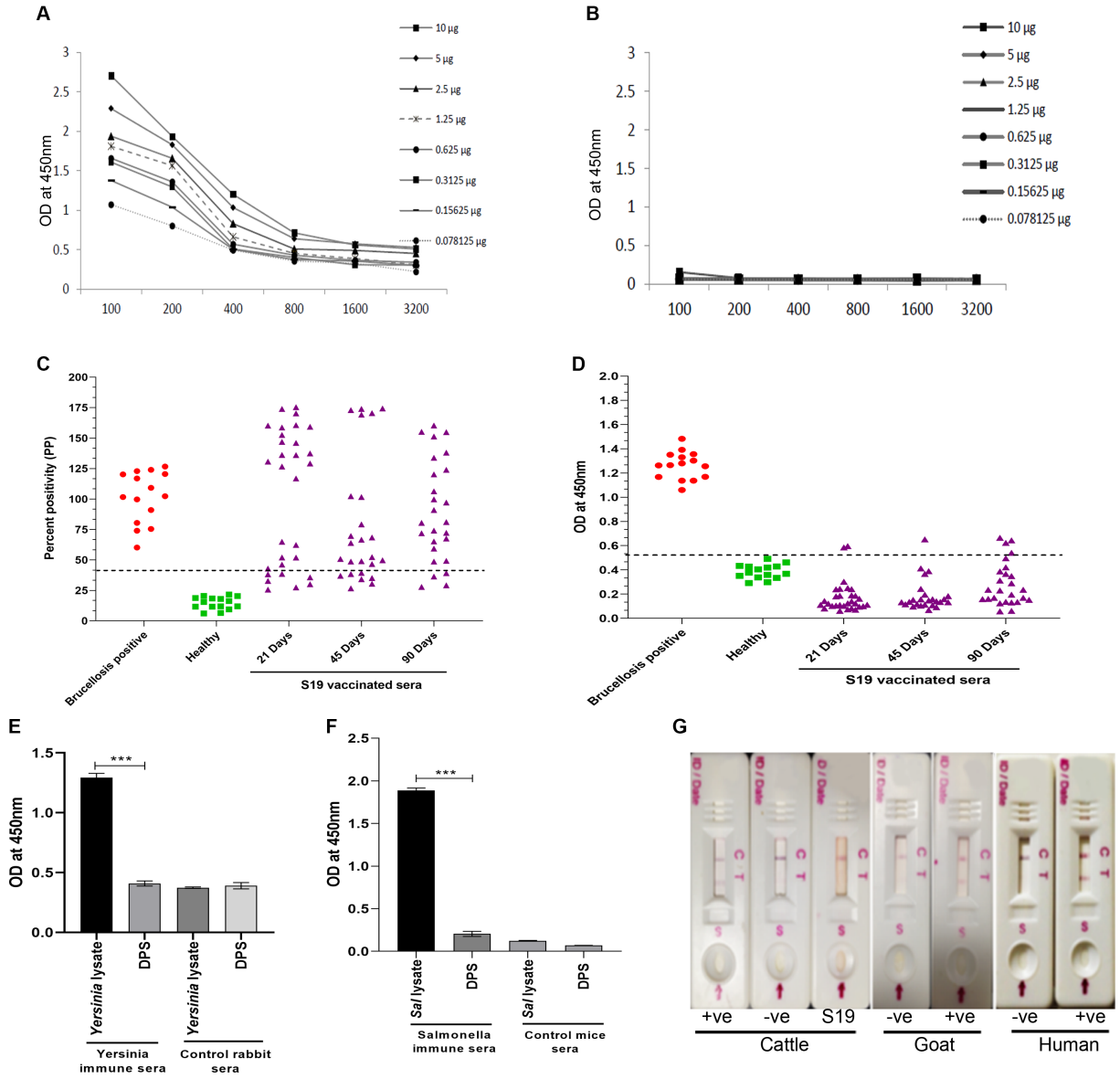

FIGURE 6
Development of Dps-based serodiagnostic assays. **(A,B)** Checkerboard titration analysis using brucellosis positive and healthy human serum samples, respectively, to determine the optimal concentration of Dps protein for ELISA development. **(C)** Percent positivity (PP) of healthy or brucellosis positive or *B. abortus* S19-vaccinated cattle serum samples analyzed using LPS-based iELISA kit (ProCheck). The S19-vaccinated serum samples collected at 21, 45, and 90 days post-vaccination were used for iELISA. Each data point indicates individual serum sample and the horizontal line shows the cut-off for iELISA. Samples with PP value 40% or above were considered positive as per the manufacturer's instructions. **(D)** Dot plot showing OD values of Dps-based iELISA that was performed with brucellosis positive or negative or *B. abortus* S19-vaccinted serum samples. The S19-vaccinated serum samples collected on 21, 45 and 90 days post-vaccination were used for iELISA. The y-axis indicate OD at 450 nm and x-axis indicate number of serum samples screened. The horizontal line indicates the cut-off. Samples with OD values of 0.5 or below were considered negative. **(E)** Evaluation of cross-reactivity of Dps protein with *Yersinia* immune rabbit serum. *Yersinia* immune serum ($n = 2$) or control rabbit serum ($n = 2$) was screened by Dps-based iELISA or iELISA using *Yersinia* whole cell lysate as the antigen. The Y-axis shows the OD values at 450 nm and X-axis indicate the antigens screened with *Yersinia* immune or healthy rabbit serum samples. **(F)** Evaluation of cross-reactivity of Dps protein with *S. typhimurium* immune sera generated in mice. The iELISA was performed with Dps protein or whole cell lysate of *S. typhimurium* as the antigen. The OD values at 450 nm are shown on X-axis and Y-axis indicates the antigens screened using *S. typhimurium* immune serum ($n = 2$) or control mice serum samples ($n = 2$). **(G)** Detection of brucellosis in the animals and humans using Lateral Flow Assay (LFA) based on the Dps protein. The serum samples from healthy or brucellosis positive cattle, goat and human were used for testing the LFA. The absence of test line with serum samples from *B. abortus* S19-vaccinated cattle show the DIVA capability of the assay. C, Control line: T, test line.

LFA, Dps protein was used as the detection agent, while biotinylated bovine serum albumin was employed as the control. To examine the efficiency of LFA, healthy or brucellosis-positive humans, cattle, goat, and *B. abortus* S19-vaccinated cattle were added to the LFA device. A test line could be observed with brucellosis-positive animal and human serum samples (Figure 6G). In agreement with our previous observation, Dps protein did not react with the sera from *B. abortus* S19-vaccinated cattle. The healthy serum samples

TABLE 7 Comparison of results obtained from Dps-based iELISA with RBPT or LPS-based iELISA using human serum samples.

Tests		Dps-based iELISA		
		Positive	Negative	Total
RBPT	Positive	14	0	14
	Negative	12	195	207
	Total	26	195	221
Indirect ELISA	Positive	25	0	25
	Negative	1	195	196
	Total	26	195	221

TABLE 8 Estimates obtained by Bayesian model statistical analysis of Dps-based and LPS-based iELISAs using human serum samples.

Estimates	Values
Sensitivity (%)	100 (86.28–100)
Specificity (%)	99.49 (97.19–99.99)
Accuracy	99.55 (97.50–99.99)
Positive predictive value	96.15 (77.97–99.44)
Negative predictive value	100
Positive likelihood ratio	196 (27.75–1384.52)
Negative likelihood ratio	0

gave no test line indicating no cross-reactivity with the Dps protein (Figure 6G).

Discussion

Brucellosis is an emerging zoonotic disease that seriously impacts human health and livestock productivity (Mcdermott et al., 2013; Rubach et al., 2013). The intracellular niche and the ability to subvert host immune responses enable *Brucella* to cause chronic infection in the host, making treatment options often difficult (Solera et al., 1997; Godfroid et al., 2011). Since there is no human vaccine for brucellosis, controlling the disease in animals through mass vaccination is the only viable option to limit human infections. Early detection and culling/quarantine of infected animals are crucial for controlling the spread of brucellosis in livestock. However, the major drawbacks of available animal vaccines and serodiagnostic assays pose serious hurdles in brucellosis control programs in various countries (Schurig et al., 2002; Galińska and Zagórski, 2013). Therefore, it is essential to identify and characterize novel serodominant antigens of *Brucella* to address major shortcomings of presently available vaccines and serodiagnostic assays.

Compared to other antigens, serodominant proteins are promising targets for developing improved diagnostic assays and vaccines. Once identified, these proteins can be expressed and purified from various expression systems making the process safer and cost-effective as large-scale culturing of the infectious pathogens and extraction of the antigens are not required. Serodiagnostic assays based on these recombinant proteins can provide higher sensitivity, specificity, and DIVA capability (Chaudhuri et al., 2010; Thavaselvam et al., 2010). These recombinant serodominant proteins could also serve as ideal candidates for developing safe and efficient vaccines for animal and human applications. Recent advancements in genomics and proteomics techniques permit large-scale screening for identifying serodominant proteins of pathogenic microorganisms (Liang et al., 2010). We used a full-proteome microarray of *B. melitensis* for the identification of serodominant proteins of *Brucella* from various host species. The immunoprofiling of *B. melitensis* proteins on the microarray yielded 202 potentially immunogenic proteins uniquely present or shared by multiple host species. Our analysis picked up many proteins of *Brucella*, such as BP26, ZunA, Cu-Zn SOD, Omp19, and Omp10, which were previously identified as serodominant and subsequently were used as candidate antigens for the development of either vaccines or serodiagnostic assays (Kim et al., 2004; Pasquevich et al., 2009; Sáez et al., 2012; França et al., 2014). These findings indicate the reliability of the experimental data generated in the present study. Subsequently, we evaluated the vaccine and diagnostic potential of 10 high-ranking immunogenic antigens, excluding previously reported well-characterized proteins.

We cloned, overexpressed, and purified the selected serodominant proteins, followed by analyzing their immunogenic potential to induce Th1 immune response against brucellosis in mice. Th1 type cellular immune response mainly involves generating IFN-γ producing T-cell populations, antigen-specific cytotoxic CD8+ T-cells, and a high titer of IgG2a is reported to confer protection in brucellosis (Golding et al., 2001; Yingst and Hoover, 2003; Skendros et al., 2011; Vitry et al., 2014). Mice immunized with BMEI1980, BMEI1390, BMEI0063, BMEI0856, BMEI0916, BMEII1048, BMEI0855, BMEII0154, and BMEI0748, showed higher percentage of $CD4^+$, $CD8^+$ cell population or IFN-γ producing $CD4^+$, $CD8^+$ cell population. Thus, suggesting a significant induction of Th1-type immune response. These proteins induced a high titer of IgG2a antibody, comparable to the response induced by the reported vaccine candidate, L7/L12 (Oliveira et al., 1994; Oliveira and Splitter, 1994, 1996; Singh et al., 2015). Switching antibody response to the IgG2a type could facilitate antibody-mediated phagocytosis of extracellular *Brucella*, which can enhance bacterial clearance (Ko and Splitter, 2003; Vitry et al., 2014). The identified serodominant protein pyruvate dehydrogenase complex dihydrolipoamide acetyltransferase (BMEI0856) is a part of the Pyruvate Dehydrogenase Complex, which is reported to be involved in protein synthesis during *Brucella* stress response (Teixeira-Gomes et al., 2000; Foth et al., 2005) The D-ribose-binding-periplasmic protein precursor (BMEI1390) is one of the sugar-binding proteins that help in sugar uptake to synthesize complex cell constituents (Wagner et al., 2002). The DNA starvation stationary phase protection (Dps, BMEI1980) is a part of the stress response system that binds non-specifically to DNA during oxidative stress (Martinez and Kolter, 1997; Roop 2nd et al., 2003). BMEII1048 encodes the molecular chaperonin, GroEL, a member of the heat shock protein family that plays a vital role in the structure and folding of other proteins (Abbady et al., 2012). GroEL has been reported to be a potent inducer of host immune responses (Leclerq et al., 2002). The 50S ribosomal protein L7/L12 (BMEI0748) is associated with translation initiation and is critical for ribosomal translocation (Carlson et al., 2017). The protective efficiency of this serodominant protein has been confirmed earlier, therefore L7/L12 was employed as the positive control in this study. BMEI0855 gene encodes the pyruvate dehydrogenase subunit beta of the pyruvate dehydrogenase protein complex that catalyzes the overall conversion of pyruvate to acetyl-CoA and CO_2. The expression

of this protein is reported to be down-regulated under heat stress (Teixeira-Gomes et al., 2000). BMEII0154 codes for MotB family protein that is a part of the stator of the flagellar motor protein complex. MotB mutations have been studied earlier to determine their vital role in establishing chronic infection (Fretin et al., 2005). The genes BMEI0916 and BMEI0063 code for hypothetical proteins where the functions of these proteins are yet to be established.

Our experimental data suggest that these serodominant proteins are potential candidates for developing next-generation vaccines for brucellosis. To validate this, a challenge study was performed to examine the protective efficiency of the serodominant proteins against *B. melitensis* in mice. The serodominant protein, BMEI0856 that induced a Th1 response conferred a significant level of protection against challenge with *B. melitensis*. The protective efficacy of BMEI0856 has appeared to be superior to that of the reported *Brucella* vaccine candidate, L7/L12. Even though we observed induction of Th1 type response by BMEI0063, it did not confer any significant level of protection against *B. melitensis* challenge compared to BME0856 and L7/L12. The serodominant protein, BMEI1513, that induced a Th2 type response failed to confer any protection highlighting the importance of Th1 type immune response for clearance of *Brucella*. The preliminary data obtained from the *in vivo* challenge study indicate that BMEI0856 could serve as an ideal candidate for developing a next-generation vaccine for brucellosis. Our future experiments will examine the utility of other serodominant proteins for vaccine development.

Antigens that induce a robust antibody response can serve as ideal candidates for developing improved serodiagnosis assays. We evaluated the seroreactivity of purified serodominant proteins by immunoblotting with brucellosis-positive and negative serum samples from cattle and humans. Even though all the tested proteins reacted with brucellosis-positive serum samples with different efficiency, Dps protein exhibited strong seroreactivity with both animal and human sera. We did not observe any cross-reactivity of Dps protein with serum samples from healthy animals or humans. The Dps protein is a part of Proteobacteria's σE1 stress response system and is reported to play a crucial role in the stress survival and chronic infection of *Brucella* (Kim et al., 2013). A recent study demonstrated that *Brucella* secretes Dps protein in the infected macrophages that mediate ferritinophagy activation and host cell necrosis to facilitate the egress and bacterial dissemination (Hop et al., 2023). This may release Dps into the circulatory system to generate a potent antibody response in the *Brucella*-infected host.

A DIVA-capable serodiagnostic assay is essential when a whole-cell vaccine is used for administration. The principle of DIVA is eliciting an antibody response against the pathogen that is different from the response induced due to vaccination. Thus, distinguishing an infected animal from the vaccinated in a serological analysis is based on the antigen lacking in the vaccine candidate. DIVA vaccines may lack one or more immunological protein antigens that are present in the natural form of a pathogen. A previous study had identified many proteins, including Dps that were differentially expressed in the *B. abortus* and *B. abortus* S19 vaccine strain (Lamontagne et al., 2009). However, no experimental validation of this data was performed to examine the serodiagnostic potential of Dps protein for developing improved sero-monitoring assays with DIVA capability. Since our screening also identified Dps protein and showed robust immunogenicity in mice, we sought to examine its potential to serve as a candidate for developing improved serodiagnostic assays. Detailed immunoprobing of purified Dps protein with serum samples from naturally infected or *B. abortus* S19-vaccinated cattle indicated that Dps exhibits DIVA capability where it reacted only with the sera from naturally infected cattle and not with the serum samples from *B. abortus* S19-vaccinated animals. Further, no seroreactivity was observed when Dps protein was probed with sera from cattle after various days of *B. abortus* S19 vaccination. These data imply that the S19 vaccine strain of *B. abortus* may not express Dps protein. However, the Dps gene is present on chromosome I of *B. abortus* S19, similar to its parent strain, *B. abortus* (Pajuaba et al., 2012). Therefore, we examined whether Dps protein is expressed in the *B. abortus* S19 strain. Our subsequent immunoblotting experiments indicated a minimal expression of Dps protein in the *B. abortus* S19 strain compared to the wild-type *B. abortus*. Since the expression of Dps is low in the *B. abortus* S19 strain, it appears that the antibody response in the vaccinated animals is undetectable, which provides the DIVA capability.

Given that Dps protein reacted with brucellosis-positive serum samples from animals and humans and exhibited DIVA capability, we wished to develop Dps-based serodiagnostic assays. A prototype LFA based on the Dps protein efficiently detected brucellosis-positive serum samples from animals and humans indicating its utility in point-of-care applications. Further, the LFA could differentiate vaccinated from naturally infected cattle. Toward developing the iELISA, we optimized various assay parameters such as Dps concentration, blocking agent, and optimal serum and secondary antibody dilutions. Subsequently, we prepared the iELISA kits and compared their efficiency with the commercially available brucellosis detection kits. An in-house assay validation with human sera samples showed 99% sensitivity and 98% specificity for the Dps protein-based iELISA. Further, the Dps-based iELISA and LFA showed DIVA capability with bovine serum samples where the vaccinated cattle were assay negative compared to the naturally infected animals. The cross-reactivity with the immune sera of Gram-negative bacteria, especially *Y. enterocolitica* O:9, *S. typhimurium*, and *E. coli* is a major drawback of existing LPS-based serodiagnostic assays for brucellosis. Our experimental data indicate that Dps-based iELISA does not exhibit any cross-reactivity with the immune sera of *Y. enterocolitica* O:9 or *S. typhimurium*. Collectively, our studies suggest that Dps-based LFA and iELISA could serve as ideal diagnostic tools for brucellosis control programs where assays with high sensitivity, specificity, and DIVA capabilities are required.

Conclusion

Our high throughput immunoprobing of *B. melitensis* protein microarray identified many potential candidates for developing improved vaccines and serodiagnostic assays for animal and human brucellosis. Some of the serodominant proteins induced a robust Th1-type response indicating their potential to serve as ideal candidates for developing next-generation vaccines. In accordance with this, BMEI0856 conferred protection against challenge with *B. melitensis* in mice. Among the identified serodominant proteins, Dps exhibited robust seroreactivity with brucellosis-positive sera from both humans and animals except with *B. abortus* S19-vaccinated cattle sera. The Dps-based LFA and iELISA exhibited high sensitivity, specificity, and DIVA capability. The recombinant Dps protein, peptides from Dps, or anti-Dps antibodies could be used for

developing other sensitive point-of-care diagnostic assays and biosensors for the detection of animal and human brucellosis in a cost-effective manner.

Data availability statement

The original contributions presented in the study are included in the article/Supplementary material, further inquiries can be directed to the corresponding author.

Ethics statement

The studies involving serum samples from human subjects were approved and collected by ICAR-National Meat Research Institute, Hyderabad, Inida with approval from the Institutional Ethics Committee (Approval number: KAMSRC/IEC/04/2018). The studies were conducted in accordance with the local legislation and institutional requirements. The participants provided their written informed consent to participate in this study. All the animal studies were approved by the Institutional Biosafety Committee (Approval number: IBSC/2013/NIAB/0001B) and Institutional Animal Ethics Committee (Approval number: IAEC/2019/NIAB/34/GKR & IAEC/2021/NIAB/09/GKR) of NIAB. *In vivo* challenge studies with *B. melitensis* 16M strain were performed in the BSL-3 laboratory facility of UoH-NIAB (Approval number: IAEC/NIAB/2022/08/GKR). The study was conducted in accordance with the local legislation and institutional requirements.

Author contributions

PN: Formal analysis, Investigation, Methodology, Validation, Writing – original draft, Writing – review & editing. PJ: Investigation, Methodology, Validation, Writing – review & editing. SM: Investigation, Methodology, Writing – review & editing. VM: Formal analysis, Investigation, Methodology, Validation, Writing – review & editing. DK: Investigation, Methodology, Writing – review & editing. RP: Investigation, Methodology, Writing – review & editing. SB: Resources, Writing – review & editing. GR: Conceptualization, Funding acquisition, Investigation, Resources, Supervision, Visualization, Writing – original draft, Writing – review & editing.

Acknowledgments

We thank the National Institute of Animal Biotechnology (Project code: C0008) for funding and experimental facilities. We thank the Department of Biotechnology (DBT), Ministry of Science and Technology, Government of India (Grant number: BT/PR36546/ADV/90/284/2020) for additional funding. PN acknowledges a research fellowship from the Council of Scientific and Industrial Research (CSIR). We also acknowledge Telangana State Veterinary Biological and Research Institute and ICAR- National Meat Research Institute for providing animal and human serum samples. We thank Prince and Rama Devi for assistance in flow cytometry, Raju for assisting with mice experiments, and Kiranmai Joshi for her input on writing the manuscript.

Conflict of interest

The authors declare that the research was conducted in the absence of any commercial or financial relationships that could be construed as a potential conflict of interest.

Publisher's note

Supplementary material

The Supplementary material for this article can be found online at: https://www.frontiersin.org/articles/10.3389/fmicb.2023.1253349/full#supplementary-material

References

Abbady, A. Q., Al-Daoude, A., Al-Mariri, A., Zarkawi, M., and Muyldermans, S. (2012). Chaperonin GroEL a brucella immunodominant antigen identified using nanobody and MALDI-TOF-MS technologies. *Vet. Immunol. Immunopathol.* 146, 254–263. doi: 10.1016/j.vetimm.2012.01.015

Agasthya, A. S., Isloor, S., and Prabhudas, K. (2007). Brucellosis in high risk group individuals. *Indian J. Med. Microbiol.* 25, 28–31. doi: 10.4103/0255-0857.31058

Al Dahouk, S., Tomaso, H., Nöckler, K., Neubauer, H., and Frangoulidis, D. (2003a). Laboratory-based diagnosis of brucellosis--a review of the literature. Part I: techniques for direct detection and identification of Brucella spp. *Clin. Lab.* 49, 487–505.

Al Dahouk, S., Tomaso, H., Nöckler, K., Neubauer, H., and Frangoulidis, D. (2003b). Laboratory-based diagnosis of brucellosis--a review of the literature. Part II: serological tests for brucellosis. *Clin. Lab.* 49, 577–589.

Ariza, J., Bosilkovski, M., Cascio, A., Colmenero, J. D., Corbel, M. J., Falagas, M. E., et al. (2007). Perspectives for the treatment of brucellosis in the 21st century: the Ioannina recommendations. *PLoS Med.* 4:e317. doi: 10.1371/journal.pmed.0040317

Ashford, D. A., di Pietra, J., Lingappa, J., Woods, C., Noll, H., Neville, B., et al. (2004). Adverse events in humans associated with accidental exposure to the livestock brucellosis vaccine RB51. *Vaccine* 22, 3435–3439. doi: 10.1016/j.vaccine.2004.02.041

Avila-Calderón, E. D., Lopez-Merino, A., Sriranganathan, N., Boyle, S. M., and Contreras-Rodríguez, A. (2013). A history of the development of brucella vaccines. *Biomed. Res. Int.* 2013:743509. doi: 10.1155/2013/743509

Bae, J. E. (1999). *Generation of baculovirus-Brucella abortus heat shock protein recombinants; mice immune responses against the recombinants, and B. abortus superoxide dismutase and L7/L12 recombinant proteins*. Blacksburg, VA, USA: Virginia Polytechnic Institute and State University. Available at: https://citeseerx.ist.psu.edu/document?repid=rep1&type=pdf&doi=27bcfd0eb6e7e92077a4e9032a4a2c31034b841b

Carlson, M. A., Haddad, B. G., Weis, A. J., Blackwood, C. S., Shelton, C. D., Wuerth, M. E., et al. (2017). Ribosomal protein L7/L12 is required for GTPase translation factors EF-G, RF3, and IF2 to bind in their GTP state to 70S ribosomes. *FEBS J.* 284, 1631–1643. doi: 10.1111/febs.14067

Chaudhuri, P., Prasad, R., Kumar, V., and Gangaplara, A. (2010). Recombinant OMP28 antigen-based indirect ELISA for serodiagnosis of bovine brucellosis. *Mol. Cell. Probes* 24, 142–145. doi: 10.1016/j.mcp.2009.12.002

Corbel, M. J. (1997). Brucellosis: an overview. *Emerg. Infect. Dis.* 3, 213–221. doi: 10.3201/eid0302.970219

Ficht, T. (2010). Brucella taxonomy and evolution. *Future Microbiol.* 5, 859–866. doi: 10.2217/fmb.10.52

Fiori, P. L., Mastrandrea, S., Rappelli, P., and Cappuccinelli, P. (2000). *Brucella abortus* infection acquired in microbiology laboratories. *J. Clin. Microbiol.* 38, 2005–2006. doi: 10.1128/jcm.38.5.2005-2006.2000

Foth, B. J., Stimmler, L. M., Handman, E., Crabb, B. S., Hodder, A. N., and McFadden, G. I. (2005). The malaria parasite plasmodium falciparum has only one pyruvate dehydrogenase complex, which is located in the apicoplast. *Mol. Microbiol.* 55, 39–53. doi: 10.1111/j.1365-2958.2004.04407.x

França, S. A., Mol, J. P. S., Costa, E. A., Silva, A. P. C., Xavier, M. N., Tsolis, R. M., et al. (2014). Indirect ELISA for diagnosis of *Brucella ovis* infection in rams. *Arquivo Brasileiro de Medicina Veterinária e Zootecnia* 66, 1695–1702. doi: 10.1590/1678-6767

Fretin, D., Fauconnier, A., Köhler, S., Halling, S., Léonard, S., Nijskens, C., et al. (2005). The sheathed flagellum of *Brucella melitensis* is involved in persistence in a murine model of infection. *Cell. Microbiol.* 7, 687–698. doi: 10.1111/j.1462-5822.2005.00502.x

Galińska, E. M., and Zagórski, J. (2013). Brucellosis in humans--etiology, diagnostics, clinical forms. *Ann. Agricult. Environ. Med.* 20, 233–238.

Godfroid, J., Nielsen, K., and Saegerman, C. (2010). Diagnosis of brucellosis in livestock and wildlife. *Croat. Med. J.* 51, 296–305. doi: 10.3325/cmj.2010.51.296

Godfroid, J., Scholz, H. C., Barbier, T., Nicolas, C., Wattiau, P., Fretin, D., et al. (2011). Brucellosis at the animal/ecosystem/human interface at the beginning of the 21st century. *Prev. Vet. Med.* 102, 118–131. doi: 10.1016/j.prevetmed.2011.04.007

Golding, B., Scott, D. E., Scharf, O., Huang, L. Y., Zaitseva, M., Lapham, C., et al. (2001). Immunity and protection against *Brucella abortus*. *Microb. Infect. Institut Pasteur.* 3, 43–48. doi: 10.1016/s1286-4579(00)01350-2

Hop, H. T., Huy, T. X. N., Lee, H. J., and Kim, S. (2023). Intracellular growth of brucella is mediated by Dps-dependent activation of ferritinophagy. *EMBO Rep.* 24:e55376. doi: 10.15252/embr.202255376

Kim, H. S., Caswell, C. C., Foreman, R., Roop, R. M. 2nd, and Crosson, S. (2013). The *Brucella abortus* general stress response system regulates chronic mammalian infection and is controlled by phosphorylation and proteolysis. *J. Biol. Chem.* 288, 13906–13916. doi: 10.1074/jbc.M113.459305

Kim, S., Watanabe, K., Shirahata, T., and Watarai, M. (2004). Zinc uptake system (znuA locus) of *Brucella abortus* is essential for intracellular survival and virulence in mice. *J. Vet. Med. Sci. Japanese Soc. Vet. Sci.* 66, 1059–1063. doi: 10.1292/jvms.66.1059

Ko, J., and Splitter, G. A. (2003). Molecular host-pathogen interaction in brucellosis: current understanding and future approaches to vaccine development for mice and humans. *Clin. Microbiol. Rev.* 16, 65–78. doi: 10.1128/CMR.16.1.65-78.2003

Lamontagne, J., Forest, A., Marazzo, E., Denis, F., Butler, H., Michaud, J. F., et al. (2009). Intracellular adaptation of *Brucella abortus*. *J. Proteome Res.* 8, 1594–1609. doi: 10.1021/pr800978p

Leclerq, S., Harms, J. S., Rosinha, G. M. S., Azevedo, V., and Oliveira, S. C. (2002). Induction of a th1-type of immune response but not protective immunity by intramuscular DNA immunisation with *Brucella abortus* GroEL heat-shock gene. *J. Med. Microbiol.* 51, 20–26. doi: 10.1099/0022-1317-51-1-20

Liang, L., Leng, D., Burk, C., Nakajima-Sasaki, R., Kayala, M. A., Atluri, V. L., et al. (2010). Large scale immune profiling of infected humans and goats reveals differential recognition of *Brucella melitensis* antigens. *PLoS Negl. Trop. Dis.* 4:e673. doi: 10.1371/journal.pntd.0000673

Mantur, B. G., Amarnath, S. K., and Shinde, R. S. (2007). Review of clinical and laboratory features of human brucellosis. *Indian J. Med. Microbiol.* 25, 188–202. doi: 10.1016/S0255-0857(21)02105-8

Martinez, A., and Kolter, R. (1997). Protection of DNA during oxidative stress by the nonspecific DNA-binding protein Dps. *J. Bacteriol.* 179, 5188–5194. doi: 10.1128/jb.179.16.5188-5194.1997

Mcdermott, J. J., Grace, D., and Zinsstag, J. (2013). Economics of brucellosis impact and control in low-income countries. *Rev. Sci. Tech.* 32, 249–261. doi: 10.20506/rst.32.1.2197

Nielsen, K., and Yu, W. L. (2010). Serological diagnosis of brucellosis. Prilozi / Makedonska akademija na naukite i umetnostite, Oddelenie za bioloski i medicinski nauki = contributions / Macedonian Academy of Sciences and arts. *Section Biol. Med. Sci.* 31, 65–89. doi: 10.3325/cmj.2010.51.306

Oliveira, S. C., and Splitter, G. A. (1994). Subcloning and expression of the *Brucella abortus* L7/L12 ribosomal gene and T-lymphocyte recognition of the recombinant protein. *Infect. Immun.* 62, 5201–5204. doi: 10.1128/iai.62.11.5201-5204.1994

Oliveira, S. C., and Splitter, G. A. (1996). Immunization of mice with recombinant L7/L12 ribosomal protein confers protection against *Brucella abortus* infection. *Vaccine* 14, 959–962. doi: 10.1016/0264-410x(96)00018-7

Oliveira, S. C., Zhu, Y., and Splitter, G. A. (1994). Recombinant L7/L12 ribosomal protein and gamma-irradiated *Brucella abortus* induce a T-helper 1 subset response from murine $CD4^+$ T cells. *Immunology* 83, 659–664.

Padilla Poester, F., Nielsen, K., Ernesto Samartino, L., and WL, Y. (2010). Diagnosis of brucellosis. *Open Vet. Sci. J.* 4, 46–60. doi: 10.2174/1874318801004010046

Pajuaba, A. C., Silva, D. A., Almeida, K. C., Cunha-Junior, J. P., Pirovani, C. P., Camillo, L. R., et al. (2012). Immunoproteomics of *Brucella abortus* reveals differential antibody profiles between S19-vaccinated and naturally infected cattle. *Proteomics* 12, 820–831. doi: 10.1002/pmic.201100185

Pappas, G., Papadimitriou, P., Akritidis, N., Christou, L., and Tsianos, E. V. (2006). The new global map of human brucellosis. *Lancet Infect. Dis.* 6, 91–99. doi: 10.1016/s1473-3099(06)70382-6

Pasquevich, K. A., Estein, S. M., Garcia Samartino, C., Zwerdling, A., Coria, L. M., Barrionuevo, P., et al. (2009). Immunization with recombinant brucella species outer membrane protein Omp16 or Omp19 in adjuvant induces specific $CD4^+$ and $CD8^+$ T cells as well as systemic and oral protection against *Brucella abortus* infection. *Infect. Immun.* 77, 436–445. doi: 10.1128/iai.01151-08

Roop, R. M. 2nd, Gee, J. M., Robertson, G. T., Richardson, J. M., Ng, W. L., and Winkler, M. E. (2003). Brucella stationary-phase gene expression and virulence. *Annu. Rev. Microbiol.* 57, 57–76. doi: 10.1146/annurev.micro.57.030502.090803

Rubach, M. P., Halliday, J. E., Cleaveland, S., and Crump, J. A. (2013). Brucellosis in low-income and middle-income countries. *Curr. Opin. Infect. Dis.* 26, 404–412. doi: 10.1097/QCO.0b013e3283638104

Sáez, D., Fernández, P., Rivera, A., Andrews, E., and Oñate, A. (2012). Oral immunization of mice with recombinant *Lactococcus lactis* expressing cu, Zn superoxide dismutase of *Brucella abortus* triggers protective immunity. *Vaccine* 30, 1283–1290. doi: 10.1016/j.vaccine.2011.12.088

Scholz, H. C., Revilla-Fernández, S., Dahouk, S. A., Hammerl, J. A., Zygmunt, M. S., Cloeckaert, A., et al. (2016). *Brucella vulpis* sp. nov., isolated from mandibular lymph nodes of red foxes (*Vulpes vulpes*). *Int. J. Syst. Evol. Microbiol.* 66, 2090–2098. doi: 10.1099/ijsem.0.000998

Schurig, G. G., Sriranganathan, N., and Corbel, M. J. (2002). Brucellosis vaccines: past, present and future. *Vet. Microbiol.* 90, 479–496. doi: 10.1016/s0378-1135(02)00255-9

Singh, D., Goel, D., and Bhatnagar, R. (2015). Recombinant L7/L12 protein entrapping PLGA (poly lactide-co-glycolide) micro particles protect BALB/c mice against the virulent *B. abortus* 544 infection. *Vaccine* 33, 2786–2792. doi: 10.1016/j.vaccine.2015.04.030

Skendros, P., Pappas, G., and Boura, P. (2011). Cell-mediated immunity in human brucellosis. *Microb. infect. Institut Pasteur.* 13, 134–142. doi: 10.1016/j.micinf.2010.10.015

Solera, J., Martínez-Alfaro, E., and Espinosa, A. (1997). Recognition and optimum treatment of brucellosis. *Drugs* 53, 245–256. doi: 10.2165/00003495-199753020-00005

Teixeira-Gomes, A. P., Cloeckaert, A., and Zygmunt, M. S. (2000). Characterization of heat, oxidative, and acid stress responses in *Brucella melitensis*. *Infect. Immun.* 68, 2954–2961. doi: 10.1128/iai.68.5.2954-2961.2000

Thavaselvam, D., Kumar, A., Tiwari, S., Mishra, M., and Prakash, A. (2010). Cloning and expression of the immunoreactive *Brucella melitensis* 28 kDa outer-membrane protein (Omp28) encoding gene and evaluation of the potential of Omp28 for clinical diagnosis of brucellosis. *J. Med. Microbiol.* 59, 421–428. doi: 10.1099/jmm.0.017566-0

Vitry, M. A., Hanot Mambres, D., De Trez, C., Akira, S., Ryffel, B., Letesson, J. J., et al. (2014). Humoral immunity and $CD4^+$ Th1 cells are both necessary for a fully protective immune response upon secondary infection with *Brucella melitensis*. *J. Immunol. (Baltimore, Md: 1950)* 192, 3740–3752. doi: 10.4049/jimmunol.1302561

Wagner, M. A., Eschenbrenner, M., Horn, T. A., Kraycer, J. A., Mujer, C. V., Hagius, S., et al. (2002). Global analysis of the *Brucella melitensis* proteome: identification of proteins expressed in laboratory-grown culture. *Proteomics* 2, 1047–1060. doi: 10.1002/1615-9861(200208)2:8<1047::Aid-prot1047>3.0.Co;2-8

Yang, X., Skyberg, J. A., Cao, L., Clapp, B., Thornburg, T., and Pascual, D. W. (2013). Progress in Brucella vaccine development. *Front. Biol.* 8, 60–77. doi: 10.1007/s11515-012-1196-0

Yingst, S., and Hoover, D. L. (2003). T cell immunity to brucellosis. *Crit. Rev. Microbiol.* 29, 313–331. doi: 10.1080/713608012

frontiers | Frontiers in Microbiology

TYPE Original Research
PUBLISHED 29 November 2023
DOI 10.3389/fmicb.2023.1287046

OPEN ACCESS

EDITED BY
Jason K. Blackburn,
University of Florida, United States

REVIEWED BY
Gamal Wareth,
Friedrich Loeffler Institut, Germany
Mostafa Y. Abdel-Glil,
Friedrich Loeffler Institut, Germany
Ana Cristina Ferreira,
National Institute for Agricultural and Veterinary Research (INIAV), Portugal
Maryam Dadar,
Razi Vaccine and Serum Research Institute, Iran
Antonio Battisti,
Institute of Experimental Zooprophylactic of the Lazio and Tuscany Regions (IZSLT), Italy

*CORRESPONDENCE
Jeffrey T. Foster
✉ jeff.foster@nau.edu

†PRESENT ADDRESSES
Nicolette R. Janke,
PacBio, Menlo Park, CA, United States
Kevin P. Drees,
Lonza Biologics, Portsmouth, NH, United States

‡These authors have contributed equally to this work

RECEIVED 01 September 2023
ACCEPTED 06 November 2023
PUBLISHED 29 November 2023

CITATION
Janke NR, Williamson CHD, Drees KP, Suárez-Esquivel M, Allen AR, Ladner JT, Quance CR, Robbe-Austerman S, O'Callaghan D, Whatmore AM and Foster JT (2023) Global phylogenomic diversity of *Brucella abortus*: spread of a dominant lineage.
Front. Microbiol. 14:1287046.
doi: 10.3389/fmicb.2023.1287046

Global phylogenomic diversity of *Brucella abortus*: spread of a dominant lineage

Nicolette R. Janke[1†‡], Charles H. D. Williamson[1‡], Kevin P. Drees[1†‡], Marcela Suárez-Esquivel[2], Adrian R. Allen[3], Jason T. Ladner[1], Christine R. Quance[4], Suelee Robbe-Austerman[4], David O'Callaghan[5,6], Adrian M. Whatmore[7] and Jeffrey T. Foster[1*]

[1]Pathogen and Microbiome Institute, Northern Arizona University, Flagstaff, AZ, United States, [2]Escuela de Medicina Veterinaria, Universidad Nacional, Heredia, Costa Rica, [3]Department of Bacteriology, Agri-Food and Biosciences Institute, Belfast, United Kingdom, [4]USDA-APHIS, National Veterinary Services Laboratories, Ames, IA, United States, [5]VBIC, INSERM U1047, Université de Montpellier, Nîmes, France, [6]CNR Brucella, Laboratoire de Microbiologie, CHU Nîmes, Nîmes, France, [7]WOAH/FAO Reference Laboratory for Brucellosis, Animal and Plant Health Agency, Addlestone, United Kingdom

Brucella abortus is a globally important zoonotic pathogen largely found in cattle hosts and is typically transmitted to humans through contaminated dairy products or contact with diseased animals. Despite the long, shared history of cattle and humans, little is known about how trade in cattle has spread this pathogen throughout the world. Whole genome sequencing provides unparalleled resolution to investigate the global evolutionary history of a bacterium such as *B. abortus* by providing phylogenetic resolution that has been unobtainable using other methods. We report on large-scale genome sequencing and analysis of *B. abortus* collected globally from cattle and 16 other hosts from 52 countries. We used single nucleotide polymorphisms (SNPs) to identify genetic variation in 1,074 *B. abortus* genomes and using maximum parsimony generated a phylogeny that identified four major clades. Two of these clades, clade A (median date 972 CE; 95% HPD, 781–1142 CE) and clade B (median date 150 BCE; 95% HPD, 515 BCE–164 CE), were exceptionally diverse for this species and are exclusively of African origin where provenance is known. The third clade, clade C (median date 949 CE; 95% HPD, 766–1102 CE), had most isolates coming from a broad swath of the Middle East, Europe, and Asia, also had relatively high diversity. Finally, the fourth major clade, clade D (median date 1467 CE; 95% HPD, 1367–1553 CE) comprises the large majority of genomes in a dominant but relatively monomorphic group that predominantly infects cattle in Europe and the Americas. These data are consistent with an African origin for *B. abortus* and a subsequent spread to the Middle East, Europe, and Asia, probably through the movement of infected cattle. We hypothesize that European arrival to the Americas starting in the 15th century introduced *B. abortus* from Western Europe through the introduction of a few common cattle breeds infected with strains from clade D. These data provide the foundation of a comprehensive global phylogeny of this important zoonotic pathogen that should be an important resource in human and veterinary epidemiology.

KEYWORDS

brucellosis, phylogeny, *Brucella abortus*, cattle, infectious disease, evolution

Introduction

Despite having limited motility, bacterial pathogens have an uncanny ability to move on continental scales. Human history can in fact be traced using phylogenetic analyses of our associated bacteria, from our emergence out of Africa to our global diaspora, including *Helicobacter pylori* moving with us in our stomachs (Linz et al., 2007), *Vibrio cholerae* in our intestines (Mutreja et al., 2011), *Mycobacterium tuberculosis* in our lungs (Comas et al., 2013; Liu et al., 2018) and *Burkholderia pseudomallei* in trade (Chewapreecha et al., 2017). Bacteria can also disperse with us in animals such as *Bacillus anthracis* in hides and/or hunted animals (Kenefic et al., 2009), *Yersinia pestis* in commensal rodents (Morelli et al., 2010), and *Brucella melitensis* in domesticated goats (Tan et al., 2015). Thus, phylogeographic reconstructions of pathogens can inform us about past human movements and activities and in turn allow us to better understand patterns of disease transmission, dispersal, and host interactions (Keim and Wagner, 2009; Grad and Lipsitch, 2014; Sintchenko and Holmes, 2015).

Brucella abortus is one of the world's most successful pathogens, causing widespread disease in wildlife, livestock, and humans on a global scale (Pappas et al., 2006; Whatmore, 2009). Brucellosis is endemic to much of the world, but the burden of the disease is particularly borne by people and livestock in developing countries (Moreno, 2014). Substantial production losses in cattle occur due to reproductive complications such as abortion, infertility, and decreased milk output (Carvalho Neta et al., 2010). Humans typically contract the disease through contaminated dairy products although occupational exposure occurs in veterinarians, slaughterhouse personnel, and workers involved in animal husbandry. Health impacts on humans are widespread and pronounced, with new brucellosis infections likely in the millions of cases each year and with large sections of the globe, particularly Africa and Asia, poorly sampled but likely containing many undiagnosed cases (Laine et al., 2022). Although *B. abortus* has a broad host range that includes many ruminants such as elk (*Cervus elaphus*) and bison (*Bison bison*) (Schumaker, 2013), swine (*Sus scrofa*) (WOAH, 2023), and goats (*Capra hircus*) (McDermott and Arimi, 2002), domestic cattle remain the most common host (WOAH, 2023). Indeed, this close host-pathogen relationship of *B. abortus* with cattle and its high prevalence in unmanaged herds suggests that the evolutionary history of *B. abortus* may provide unique insights into the history of cattle movements. Then by comparing these genetic patterns in *B. abortus* to cattle genetics, breeding practices, and livestock movements (Pitt et al., 2019; Verdugo et al., 2019; Xia et al., 2023), we can understand how socioeconomic forces and cultural practices have spread this pathogen.

Initial attempts to characterize *B. abortus* involved microbiological and biochemical testing that grouped isolates into eight biovars (bv. 1–7 and 9). However, subsequent work, including the results presented here, indicates that the biovars do not always correspond with distinct genetic groups (Whatmore et al., 2016). Low amounts of genetic diversity have traditionally hampered genetic characterization of *Brucella* taxa (Whatmore, 2009). Fragment based methods such as variable number tandem repeat (VNTR) analysis and multi-locus sequencing have been fundamental to our understanding of the phylogenetic relationships among species and biovars of the genus (Le Fleche et al., 2006; Whatmore et al., 2007). However, homoplasy, lack of resolution at branch tips, and ambiguity at deeper nodes due to limited phylogenetic characters using these methods (Pearson et al., 2009b), suggest a more in-depth approach is required. Comparative approaches using whole genome sequencing provide this needed resolution and form the basis for better understanding evolutionary, epidemiological, and host relationships in *Brucella* (Foster et al., 2009; Wattam et al., 2009, 2014; Audic et al., 2011; Kamath et al., 2016). Early phylogeographic studies in bacteria used a limited number of loci and various genetic approaches that assessed variation within only portions of the genome. Whole genome analyses have become the new standard, particularly in clonal and low diversity bacteria where many loci are required for sufficient power and resolution (Rokas et al., 2003; Pearson et al., 2009b). Single nucleotide polymorphism (SNP) loci are valuable characters for phylogenetic reconstructions due to their evolutionary stability, exhibited by low mutation rates and minimal homoplasy in clonal bacteria (Keim et al., 2004; Achtman, 2008). SNPs have been successfully utilized in phylogeographic comparisons to draw conclusions about the evolutionary history and global dispersal of a variety of pathogens and their diseases e.g., (e.g., Holt et al., 2008; Harris et al., 2010). These studies exhibit the power of whole genome analysis to characterize global diversity in highly clonal bacteria and potentially link the overlapping histories of their host populations.

In this study, we use comparative genomics to interrogate 1,074 genomes of *B. abortus* to determine its evolutionary history and better understand its global movements in cattle and other hosts. Most genomes came from cattle, although at least 16 other animal species, mostly ruminants, were sampled. The large sample size and wide range of locations involved provides a breadth of scope not previously explored in *B. abortus* and an unparalleled opportunity to catalog the extant diversity and phylogeography of this important zoonotic pathogen. Moreover, these data constitute a phylogenetic framework that will be useful in determining the evolutionary significance of new isolates and their relationship to the current phylogenetic framework, and in disease outbreak investigations in an era of global human and animal movement.

Materials and methods

Sampling

The 1,074 isolates analyzed in this study came from 52 countries across 6 continents (**Figure 1** and **Supplementary Table 1**). Whole genome sequencing data for *B. abortus* isolates were downloaded on June 23, 2023. Paired-end Illumina sequencing data were downloaded from the Sequence Read Archive (Leinonen et al., 2010). Genome assemblies were downloaded from GenBank (Benson et al., 2012) and the Bacterial and Viral Bioinformatics Resource Center (BVBRC).[1] Genomes were removed from the data set if they aligned poorly to the reference genome (quality breadth <80% in program NASP), were identified as poor quality by

1 https://www.bv-brc.org/

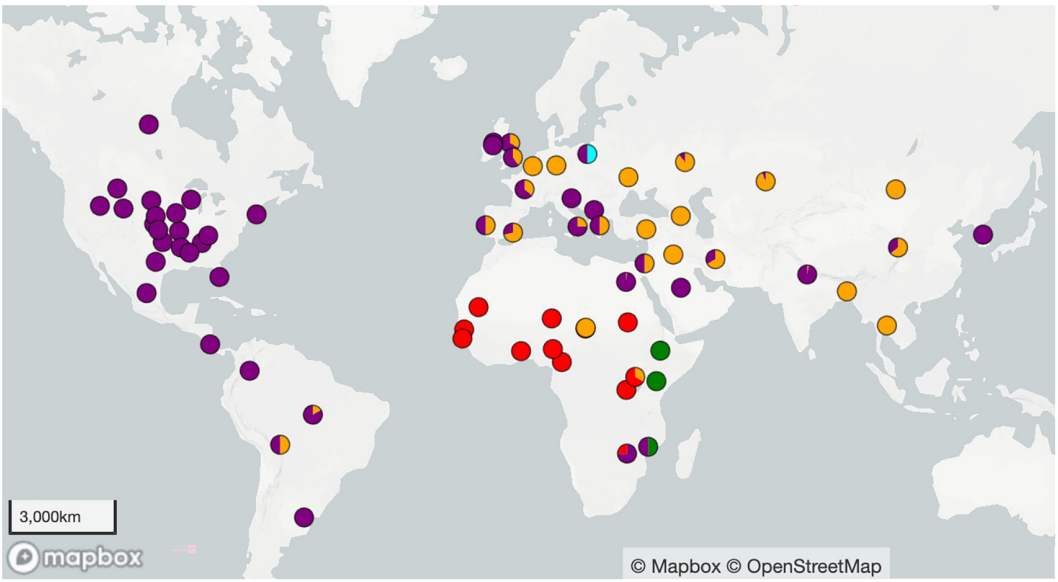

FIGURE 1
Geographic locations of the 1074 *Brucella abortus* genomes used to construct the phylogenies in **Figures 2**, **3**. Country or state centroid is given except when more specific location information was known. Colors refer to the four clades: clade A is green, B is red, C is orange, D is purple, and light blue is undetermined.

BVBRC, or were outliers (i.e., other *Brucella* species). We removed obvious duplicate genomes from the dataset, but retained potential duplicates when we could not determine which genome should take priority. These duplicate genomes served as a doublecheck of our analysis methods, which was confirmed, as all duplicates were identical or highly similar to each other.

The United States (US) was the origin of the largest number of genomes within this study (n = 365), with a majority from the Greater Yellowstone Ecosystem (n = 264). The United Kingdom (UK) had a relatively large number of isolates (n = 93), although as a central repository for strains that have been collected globally, some of these isolates likely originated elsewhere. Ireland, India, Russia, Kazakhstan, Brazil, Egypt, Italy, and Costa Rica were the source of 26–94 isolates each, while the remaining countries were the origin of 1–15 isolates each. The origins of genomes in each lineage and sub-lineage of our phylogeny and basic metadata such as GenBank accession, strain ID, country and collection location, year of collection, host, and phylogenetic lineage are detailed in **Supplementary Table 1**. Isolates were primarily collected from cattle, but the 16 other hosts included bison (*Bison bison*), elk (*Cervus canadensis*), humans (*Homo sapiens*), water buffalo (*Bubalus bubalis*), goats (*Capra hircus*), swine (*Sus domesticus*), yak (*Bos grunniens*), dog (*Canis lupus familiaris*), camel (*Camelus dromedarius*), llama (*Lama glama*), reindeer (*Rangifer tarandus*), sheep (*Ovis aries*), chamois (*Rupicapra rupicapra*), red fox (*Vulpes vulpes*), cat (*Felis catus*), and mouse (*Mus musculus*). Genomes come from sampling across a wide range of time, spanning 1925 to 2022. Of the genomes in this study, 106 were sequenced in the Brucella II initiative at the Broad Institute (broadinstitute.org), with isolate DNA supplied by the Animal Health and Veterinary Laboratories Agency (AHVLA) [now Animal and Plant Health Agency (APHA)] of the UK, the US Centers for Disease Control and Prevention, or Northern Arizona University. A total of 67 isolates were sequenced by Translational Genomics Research Institute North or the Environmental Genetics and Genomics Laboratory from isolates supplied by US Geological Survey and its collaborators, and 281 samples were sequenced by the collaborations of US Department of Agriculture–National Veterinary Services Laboratory (USDA-NSVL). The remaining genomes were sequenced by various other institutes.

SNP discovery

Core-genome single nucleotide polymorphisms (SNPs) were called within NASP (Sahl et al., 2016) using paired-end Illumina reads as input. For genome assemblies, paired-end Illumina sequencing data were simulated from publicly-available genome assemblies with ART (MountRainier) (Huang et al., 2012). Reads were aligned to *B. abortus* strain 2308 (GCA_000054005.1) as the reference genome using BWA-MEM (Li, 2013) and SNPs were called with the Unified Genotyper method in GATK (McKenna et al., 2010; DePristo et al., 2011). Positions were removed from the analysis if the depth of coverage was less than ten or if the allele proportion was less than 0.9 for a genome. Duplicated regions of the reference genome were identified with self-alignments using NUCmer (Delcher et al., 2002; Kurtz et al., 2004) and removed from the analysis. A maximum parsimony phylogeny was generated from high-quality, core-genome SNPs (bestsnp.fasta) with the R package phangorn (Schliep, 2011). A consistency index (excluding parsimony uninformative SNPs) and retention index were calculated with phangorn. The consistency index allows one to determine the amount of homoplasy that is occurring within the genetic markers being used in the phylogeny, with values close to 1 indicating limited amounts of homoplasy. To determine the root of the *B. abortus* tree, we first generated a phylogeny that included

B. melitensis strain 16M (GCA_000740415.1) as an outgroup due to this taxon being sister to *B. abortus* (Wattam et al., 2014). The core genome in these analyses was estimated with the quality breadth metric in NASP (Sahl et al., 2016).

Bayesian time-structured coalescent analysis

We plotted the divergence of each tip from the root against the date of sampling (a root-to-tip plot) in the program TempEST. Thus, this temporal signal allowed us to construct a time-structured phylogeny. For the molecular clock estimation, BEAST v1.10.1 (Suchard et al., 2018) was used to generate a time-structured phylogeny including only a subset (n = 607) of the GenBank genomes with known isolation year. For this analysis, NASP was run again, as described above, to generate a core SNP matrix specific for this subset of isolates. The matrix included only variable positions, but the BEAST XML input file was modified to specify the number of invariant sites, by nucleotide, in the *B. abortus* genomes. Six different combinations of molecular clock and coalescent models were evaluated using path-sampling and stepping-stone marginal likelihood estimation approaches (Lartillot and Philippe, 2006; Fan et al., 2011; Xie et al., 2011). Each model combination was run in duplicate, with one billion Markov chain Monte Carlo steps, and sampling parameters and trees assessed every 100,000 generations to ensure independent convergence of the chains. The log files were combined with LogCombiner v1.10.1 and assessed with Tracer v1.7.1. The first 50,000,000 iterations were discarded as burn-in. As the relaxed clock models did not converge, even when using a subset of the genomes, model selection was based only on strict clock model results, in which all the tree models' effective sample sizes (ESS) were ≥236. The best fit model combination was a strict molecular clock, along with the Bayesian Coalescent Skyline tree prior with 10 categories (Drummond, 2005).

Results

The first phylogenetic tree illustrates the genomic comparisons of all *B. abortus* genomes and is rooted with the outgroup (*B. melitensis* 16M) (**Figure 2**). A total of 2,053 SNPs separated *B. melitensis* 16M from the *B. abortus* isolates. The core genome in this analysis was 1,619,280 nucleotide positions, with SNPs at 13,723 positions. Homoplasy was low, with a consistency index (excluding parsimony uninformative SNPs) of 0.96, and a retention index of 0.99. We then analyzed only the *B. abortus* genomes, which involved 1,629,697 nucleotide positions in the core genome, SNPs at 11,797 positions, a consistency index (excluding parsimony uninformative SNPs) of 0.97, and a retention index of 0.99.

The phylogeny revealed what we consider as four major clades of *B. abortus*, with two clades (A and B) composed almost entirely of isolates of African origin. For isolates with known origin, 52 of 53 came from African countries (**Figure 3**), the sole exception being an isolate from Saudi Arabia, which has an established connection to Africa from infected livestock with brucellosis via historical trade (Foster et al., 2018). The most notable member of these two African clades is the biovar 3 reference strain Tulya, which was isolated from a Ugandan cow in 1958. The distribution of biovars within the African clades is also striking, with biovars 3, 6, and the previously classified biovar 7 predominating [biovar 7 is no longer in usage (Garin-Bastuji et al., 2014)]; these biovars account for nearly all of the African isolates where biovar is known. Despite containing only a small fraction of the total genomes in our analysis, more genetic variation exists in the 56 genomes from the African clades than exists in all of the other *B. abortus* genomes, as indicated by the relatively long branch lengths to and within these clades (**Figures 2**, **3**).

The third major lineage, identified as clade C (corresponding to C2 of MLSA) (Whatmore et al., 2016; Shevtsov et al., 2023), contained isolates of diverse origins but came almost entirely from Europe and Asia (**Figure 4**). Relative to the diversity within the African clades, the *B. abortus* genomes from clade C exhibited minimal genetic diversity but were substantially more diverse than the relatively monomorphic clade D (see below). Clade C can be divided into two broad subclades, with one subclade containing notable isolates such as the reference strains for biovar 5 (strain B3196), biovar 6 (strain 870), and biovar 9 (strain C68). In contrast, the other subclade contains no reference strains but does include a large number of isolates predominantly from Asia, particularly countries with extensive sampling such as Kazakhstan, Russia, and China, and to a lesser extent countries such as Brazil, Italy, Mongolia, and Georgia. The diversity and geographic distributions of clade C have been previously described and molecular dating indicates the arrival of this subclade into Kazakhstan in the 19th or early 20th century (Shevtsov et al., 2023). One unusual finding from Italy is that despite strains sharing a common host, water buffalo, Italian herds are infected with strains from both clades C and D, suggesting two separate introductions and two distinct lineages have remained despite control efforts (Garofolo et al., 2013, 2017). Clade C seems likely to have been imported with infected water buffalo from Asia and clade D was likely acquired locally from infected cattle as the two species interact on some farms. Of note, when extensive sampling has been conducted for a study focused on a single location over a short time frame, those genomes will generally cluster together and are depicted as triangles for the collapsed branches (**Figure 4**).

Clade D contains the largest number of genomes (n = 837) from six continents but surprisingly little genetic diversity and is largely composed of biovars 1, 2, and 4 (**Figures 2**, **5**). Clade D contains multiple subclades, several with striking geographic localization of closely related genomes, as was also seen in clade C. These clusters were associated with sampling of infected livestock (primarily cattle herds and water buffalo) and included five clusters associated with the Yellowstone region (Kamath et al., 2016), and additional clusters from Costa Rica (Suarez-Esquivel et al., 2020), Northern Ireland (Allen et al., 2020), Brazil (Pereira et al., 2023), Texas (this study), and Italy (Garofolo et al., 2017). This geographic clustering of closely related strains demonstrates the low diversity of most brucellosis outbreaks. Interestingly, some of these clusters contain isolates that were collected over several decades, indicating that limited differentiation and circulation occurs over these time scales. Interspersed among these clusters were samples from other US states (26 states sampled) and diverse international locations such as the South American countries of Argentina, Bolivia, Brazil, and Trinidad and Tobago, European countries including France, Kosovo, Poland, Portugal, Spain, and the UK, as well as Mexico, New Zealand, and Zimbabwe. The overall global pattern for clade D is the spread of this lineage over the past several centuries followed by limited and local

FIGURE 2
Maximum parsimony phylogeny of 1074 *Brucella abortus* genomes rooted with *B. melitensis* 16M outgroup. We define four major lineages A, B, C, D, which correspond to the four main MLST groups of Whatmore et al. (2016), but as A, B, C2, and C1, respectively. Full details of isolate origins and other metadata are found in **Supplementary Table 1**.

differentiation. However, the connectedness of global trade allows for some isolates to spread between distant locations. Finer scale details for all genomes in this study can be found online: https://microreact.org/project/t3oxnHhmZrAhtuw6mamutc-b-abortusglobal-phylogenomic-diversity.

Our results indicate that the most recent common ancestor (MRCA) of *B. abortus* as a species occurred approximately 3726 BCE (median estimate date 3683 BCE, 95% HPD 4657–2871 BCE; **Table 1**), with an estimated mean substitution (subs) rate of 6.49×10^{-8} subs/sites/year. This rate is highly similar to a rate estimate for *B. melitensis* of 9.3×10^{-8} subs/sites/year (Long et al., 2023) as well as our rate estimates from *B. abortus* spread in Costa Rica of 8.28×10^{-8} subs/sites/year (95% HPD interval: 2.8×10^{-8}–1.7×10^{-7} (Suarez-Esquivel et al., 2020), which was estimated with an uncorrelated relaxed clock model and a skyline tree. This shows consistency in the estimation of the substitution rate for *Brucella* in general despite the model used for the analysis. The B clade, which includes genomes from Africa, is predicted as the oldest *B. abortus* clade based on the available sequences, followed by clades C, A and D (**Figure 6**). Nonetheless, both clades A and B are poorly sampled and unsampled diversity likely remains that would make these divergence times earlier.

Discussion

Homoplasy was minimal within our trees, increasing confidence in the topologies. Homoplasy can be the consequence of directional selection or horizontal gene transfer, and the low levels seen here in *B. abortus* are indicative a largely clonal population of organisms undergoing minimal recombination or convergent evolution (as also occurs in *Mycobacterium tuberculosis*; (Comas et al., 2013) and where nearly all genetic variation is created by mutations. This is consistent with *B. abortus* being a clonal intracellular pathogen that has had limited genetic exchange with other bacteria in its recent evolution.

African origin of *B. abortus*

We posit that Africa is the likely origin of *B. abortus*. Clades C and D are nested within clades A and B containing the African strains. We note that this differs from the "basal clade" interpretation often mistaken as indicative of a species' origin or for clades containing ancestral traits, which is an especially common misconception in trees with poorly sampled taxa in a sister group

10.3389/fmicb.2023.1287046

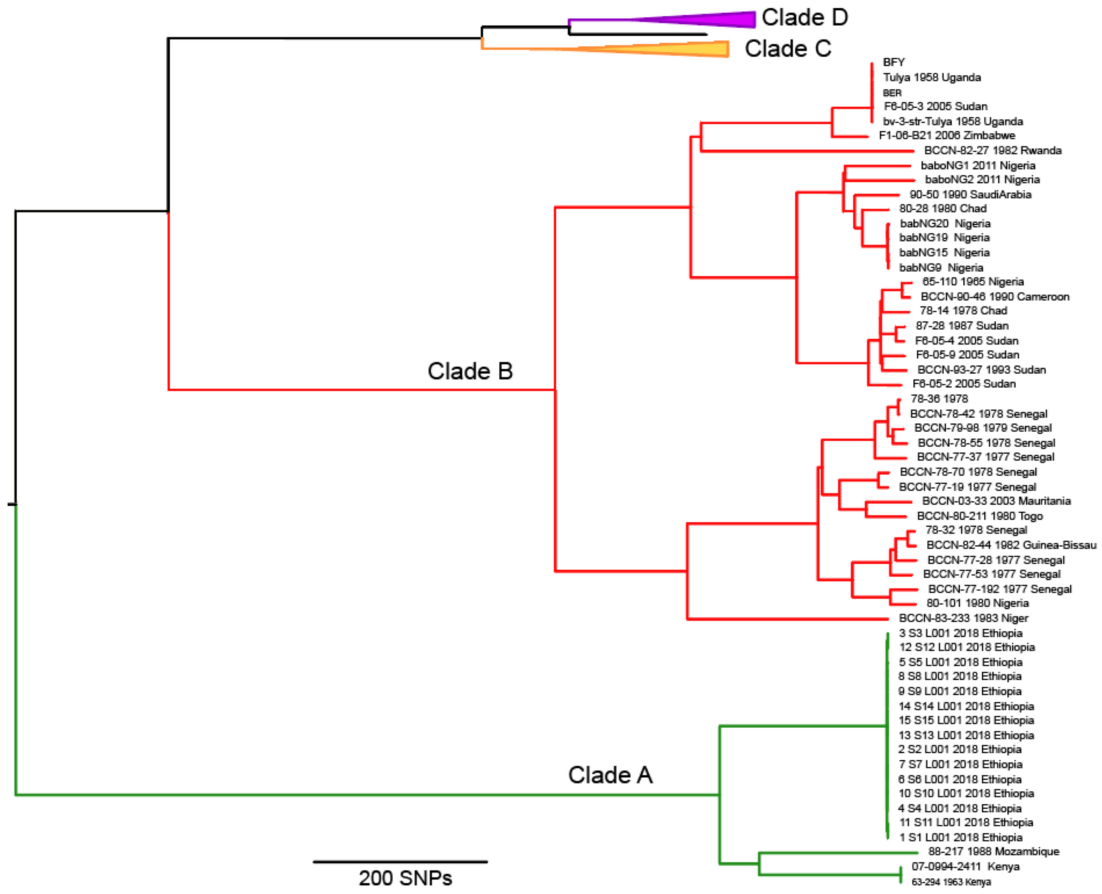

FIGURE 3
Maximum parsimony phylogeny of 56 *Brucella abortus* genomes from clades A and B, all but one have African origins, including the strain Tulya from Uganda, the reference strain for biovar 3. Clades C and D have been collapsed to allow for details of clades A and B to be visualized.

(Crisp and Cook, 2005). Also supporting an African origin is that strains from clades A and B have the highest amounts of genetic diversity within the species, and high levels of genetic diversity often indicate a species' geographic origin (Pearson et al., 2009a). Similar phylogeographic findings have supported an African origin for another important bacterial taxon of zoonotic pathogens—the *Mycobacterium tuberculosis* complex (Comas et al., 2013). If *B. abortus* has had a limited number of hosts and similar selective pressures, one would not expect substantial differences in substitution rates among lineages of *B. abortus*. Moreover, all of the genomes in our analyses came from contemporary samples within the past few decades. We are thus left trying to explain the relatively long branches for clades A and B; it is likely that substantial diversity remains to be discovered within these two clades and that missing diversity is most likely in Africa. These findings suggest the emergence of *B. abortus* in Africa and from there an expansion into Europe and Asia (clade C), and later to the Americas (clade D).

Understanding the relationship between *B. abortus* and cattle and their mutual global spread is a complex issue, complicated by imprecise estimates of the timing of both cattle and *Brucella* evolution. Furthermore, matching our proposed African origin of *B. abortus* with cattle evolution on the continent is made more challenging by the uncertain timing and spread of cattle in Africa. Taurine (*Bos taurus*) cattle domestication occurred in the Fertile Crescent in roughly 8500 BCE, along with the domestication of goats, sheep, and pigs slightly earlier (Zeder, 2008). A second cattle domestication event, the zebu or indicine species (*Bos indicus*) occurred in the Indus Valley in roughly 6500 BCE (Loftus et al., 1994). Although the archeological and molecular evidence are much debated, both cattle species subsequently spread to Africa and interbred with each other as well as with wild aurochs (*Bos primigenius*) (Felius et al., 2014; Pitt et al., 2019; Verdugo et al., 2019). As a result, African cattle are genetically diverse (Troy et al., 2001; Hanotte, 2002; Decker et al., 2014) but also provide numerous opportunities and timepoints for *B. abortus* to emerge. Brucellosis in African cattle, particularly in sub-Saharan Africa, is widespread and remains a substantial burden for animal production (McDermott and Arimi, 2002; Ducrotoy et al., 2017). Sampling and genotyping of strains from these animals will better inform the movement and history of *B. abortus* on this continent and we are likely only seeing a small proportion of its diversity. Khames et al. (2017) described new diversity within *B. abortus* isolates from Algeria, although we are not certain where these samples would fall within our phylogenies as the genomes are not yet available. We are cautious, however, about overinterpreting the phylogenetic data with respect to geography (Crisp et al., 2011). Relating phylogenetic patterns with biogeographic patterns is even

10.3389/fmicb.2023.1287046

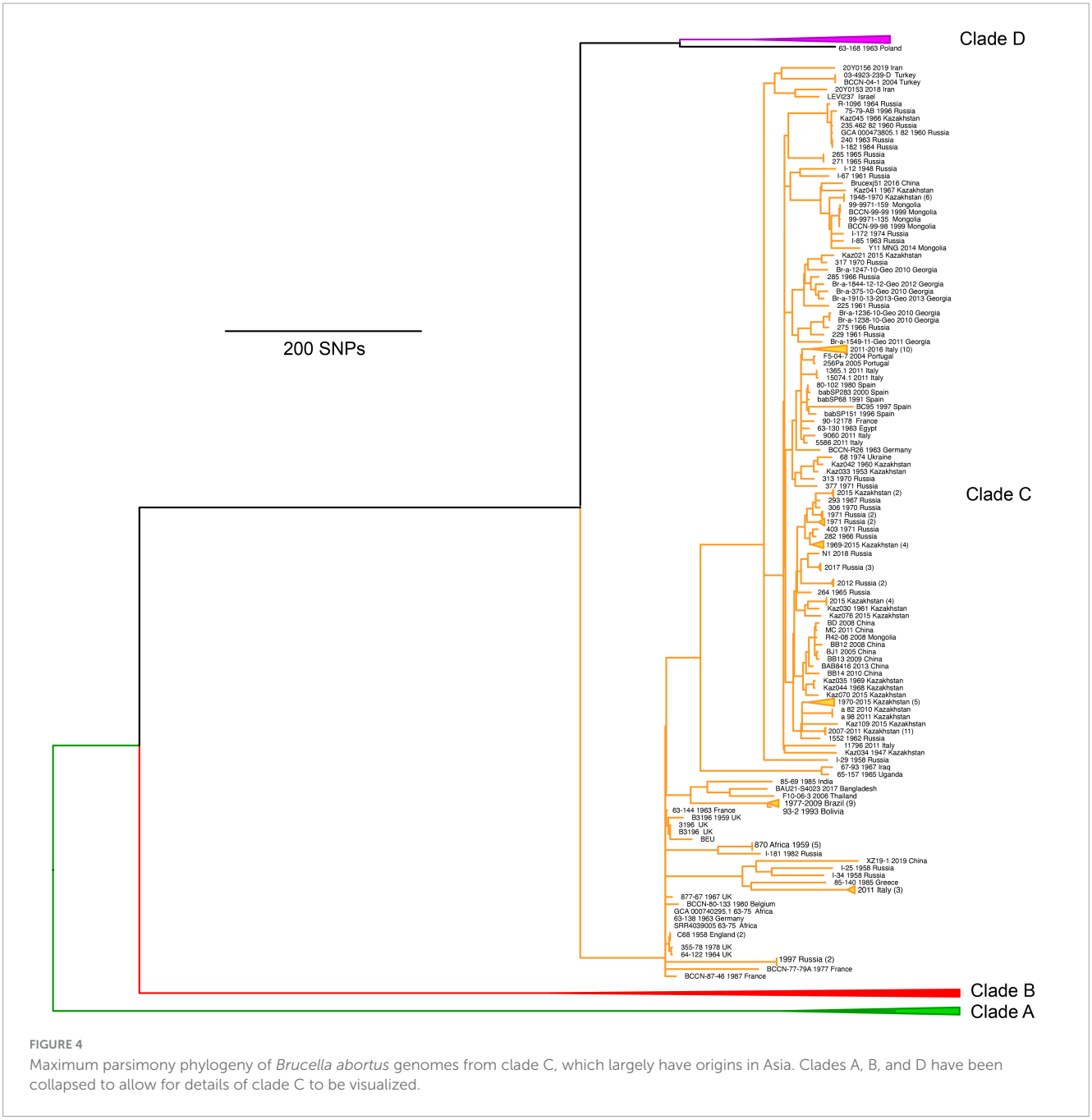

FIGURE 4
Maximum parsimony phylogeny of *Brucella abortus* genomes from clade C, which largely have origins in Asia. Clades A, B, and D have been collapsed to allow for details of clade C to be visualized.

more difficult to disentangle in *B. abortus* and other intracellular pathogens because of the essential host-pathogen relationship, the potential effects of domestication and human transport of livestock, complex cattle and human histories, and the ability of pathogens to switch hosts. A broad range of ungulates and other wildlife species are suitable hosts for *B. abortus*, although most sampling to date has found genotypes from clade D (Simpson et al., 2021).

Moreno et al. (2002) proposed that the *Brucella* genus began to diverge 20–25 million years ago concurrent with speciation of ovine, caprine and bovine hosts from their ancestors. However, results from Foster et al. (2009) using rough approximations of mutation rates indicated that while the divergence of species within the *Brucella* genus is more recent, although we must note, estimated this divergence far earlier than our present study. Our molecular dating presented here suggest even more recent emergence of the core/classical *Brucella* (Whatmore and Foster, 2021). It is tempting to speculate that animal domestication in the Middle East allowed for the emergence of several *Brucella* species in livestock. Long et al. (2023) used molecular dating of *B. melitensis* and concluded that this species diverged from *B. abortus* early in the domestication of sheep and goats. Our results from *B. abortus* are consistent with these findings but are not certain as to the exact timing of when and where *B. abortus* diverged from *B. melitensis*. Our time-based reconstruction indicates that clade B diverged from the *B. abortus* common ancestor sometime from 515 BC to 164 AD. Taken with the findings we describe herein, it seems plausible therefore that wild ancestors of domesticated bovines or other ruminants in Africa were afflicted by brucellosis and

10.3389/fmicb.2023.1287046

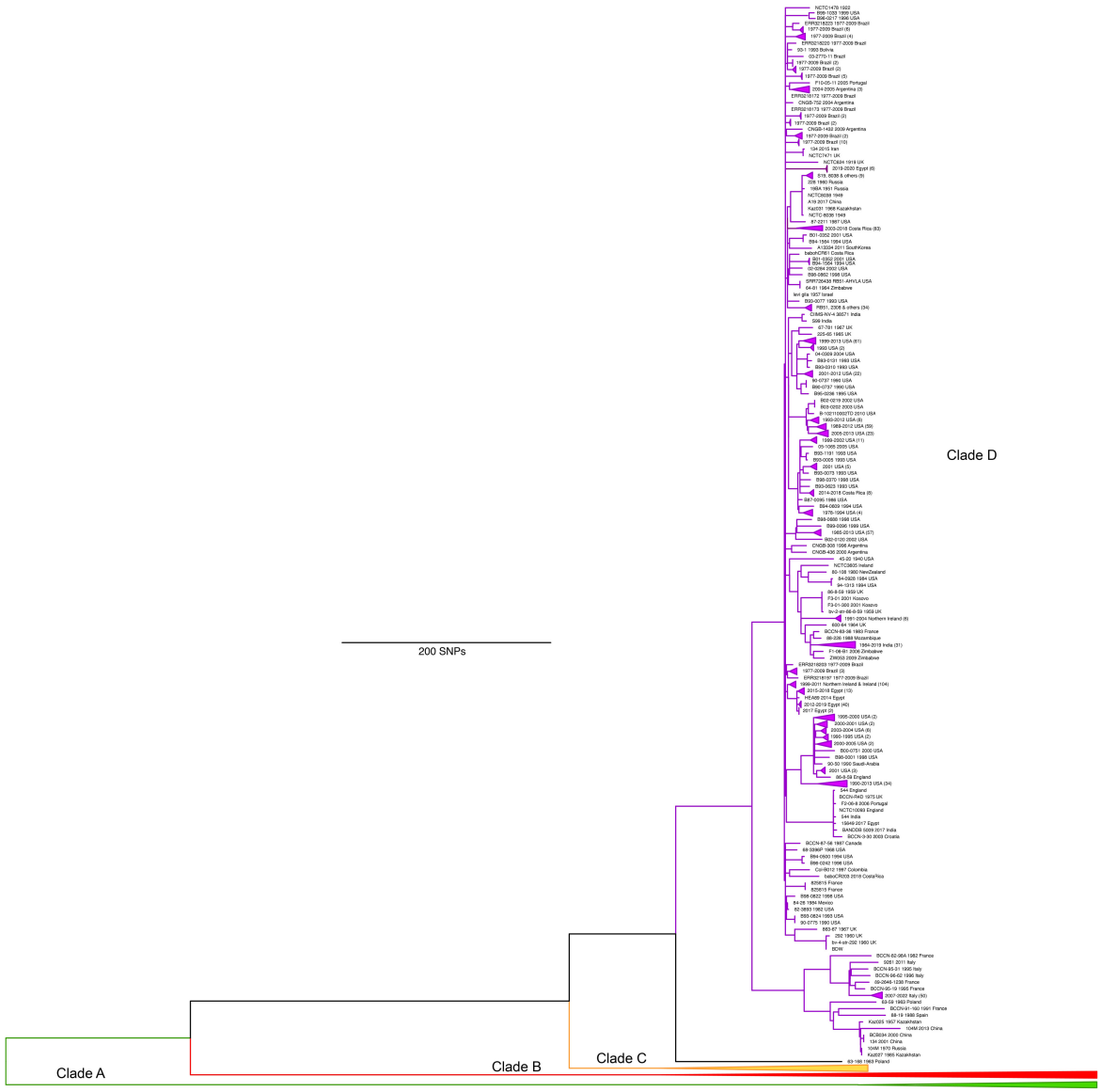

FIGURE 5
Maximum parsimony phylogeny of *Brucella abortus* genomes from clade D, which largely have origins in W. Europe, and North and South America. Clades A, B, and C have been collapsed to allow for details of clade D to be visualized.

that host specific evolution of *B. abortus* and its subsequent diversification predated domestication. However, to adequately address this question would require a denser sampling of both wildlife and wild and domesticated bovine species infected with *B. abortus*, and ideally, generating genomes from ancient DNA from bones from animals or humans infected with brucellosis (Kay et al., 2014; Long et al., 2023).

Movement of *B. abortus* out of Africa

Our trees do not inform us as to the likely path of movement of *B. abortus* out of Africa but based on current distributions it appears that the lineages went in two directions. Clade C originated roughly in 972 CE (range 766–1102 CE), spread primarily into the Middle East and then into the rest of Asia, with some movement into Europe as well. The spread into Asia may have occurred along the Silk Road, as has been proposed for *B. melitensis* (Pisarenko et al., 2018), although Shevtsov et al. (2023) suggest that movement into Kazakhstan might have been much more recent, in the past 100–200 years. Clade C is well distributed across

TABLE 1 Time of most recent common ancestor of *Brucella abortus* and clades from BEAST analysis.

	Mean	Median	95% HPD* interval
TMCRA	3727 BCE	3683 BCE	4657 BCE, 2871 BCE
Clade A	965 CE	972 CE	781 CE, 1142 CE
Clade B	164 BCE	150 BCE	516 BCE, 164 BCE
Clade C	941 CE	949 CE	766 CE, 1102 CE
Clade D	1464 CE	1468 CE	1367 CE, 1553 CE

*HPD, high posterior density, a Bayesian version of a confidence interval. Tree topology and clade branching depicted in **Figure 6**.

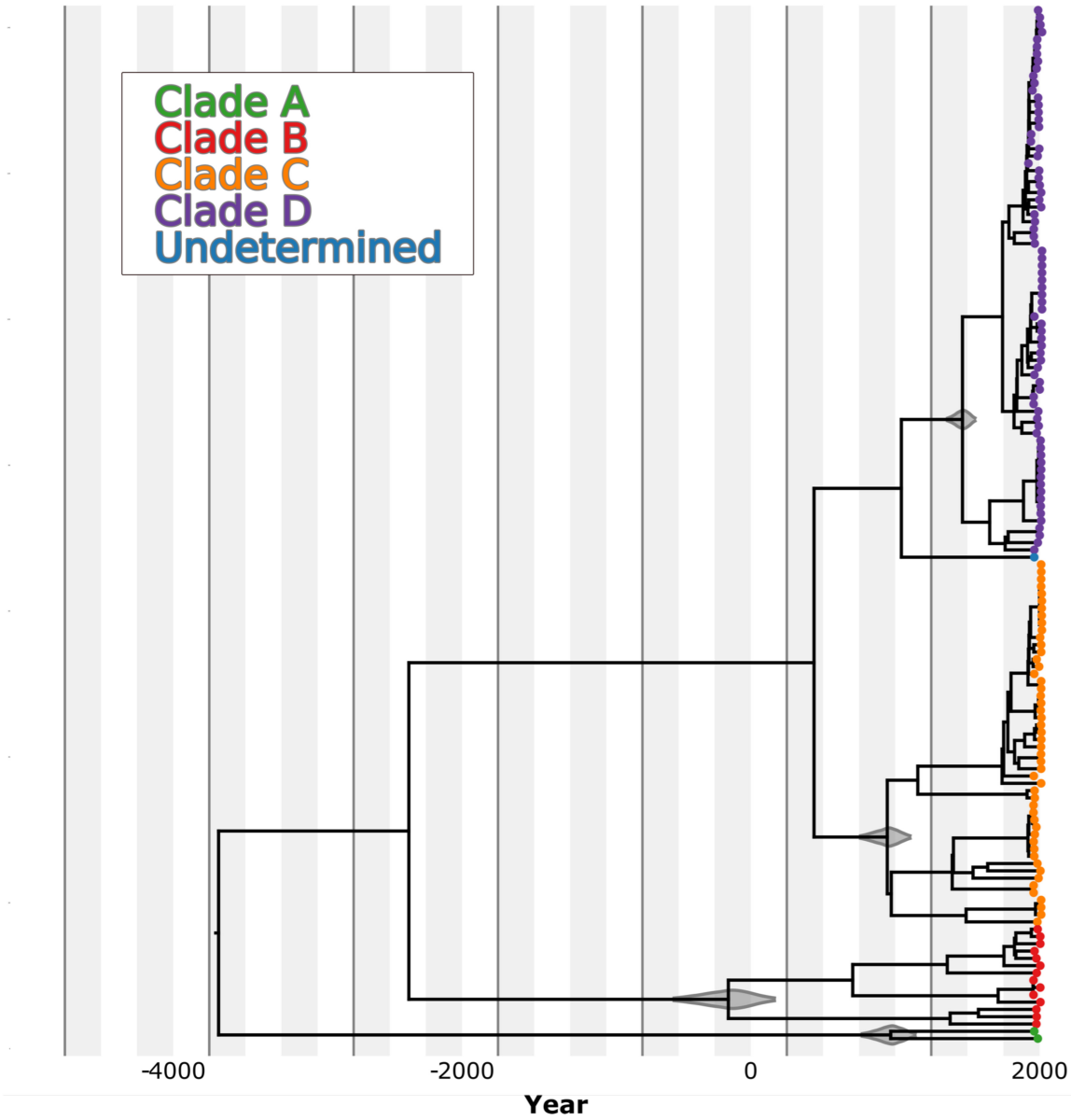

FIGURE 6
Time-structured maximum clade credibility (MCC) phylogenetic tree of 607 *B. abortus* genomes. The branches are color-coded according to the MLST clade clustering pattern, which also corresponds to the grouping based on the geographic origin of the genomes. The violin plots over the nodes show the 95% highest posterior distribution of the time to the most common recent ancestor (MRCA) from each one of the clusters.

Eurasia, from present day western Europe to China, but represents considerably lower amounts of genetic diversity compared to the African lineages. This reduced diversity may result from a variety of factors. Sampling bias and a reduced number of available genomes may underestimate the true diversity, although the 60 genomes from this clade are dispersed over a large extent of Eurasia, which should aid in capturing a representative level of the extant diversity. Additionally, our data on the major African lineages is indicative that even small sample numbers from a specific geographic region can provide useful information on pathogen genetic diversity relative to other regions. We speculate that the movement of *B. abortus* across Eurasia may be tied to the domestication of wild aurochs into taurine cattle in the Middle East around 10,000 years ago (Zeder, 2008) and the subsequent spread of agriculture—and infected animals—across these two continents (Achilli et al., 2008; Decker et al., 2014). More recent movements of livestock out of Africa and into the Middle East have been connected to Arab trade in the region (Foster et al., 2018; Holzer et al., 2021), and may also be connected to animal importation into Saudi Arabia during the Hajj each year. It is plausible that non-domesticated animals could have aided the movement of *B. abortus* across Eurasia, but we are unaware of likely hosts to have allowed for this wide dispersal. Modern reports of the spread of zoonotic disease also indicate that human mediated movement of infected animals underpins much of disease spread (Christley et al., 2005; Bigras-Poulin et al., 2006; Rautureau et al., 2010).

In contrast to the diversity and widespread distribution of clade C, clade D is largely restricted to Western Europe and

the Americas. Despite the many inconsistencies with biovars and frequent lack of correspondence to genetic groupings (Whatmore, 2009), biovars 3, 6, 7, and 9 comprise clades A, B, and C, and clade D is comprised of biovars 1, 2, and 4. The latter may potentially be attributed to the difficulty of transporting cattle across oceans in the past and that this was done solely by European colonists, a historical fact given additional molecular credence by the finding that greater than 50% of cattle mtDNA variation can be partitioned among the continents (Bradley et al., 1996). Along with the presence of genomes from the US in clade D, these biovar data hint as to how *B. abortus* reached the Americas (detailed below). The spread of clade D as a dominant lineage is similar to the clonal expansions of other notable pathogens such as *Bacillus anthracis*, *Yersinia pestis*, and *Francisella tularensis* (Keim and Wagner, 2009).

The New World

The majority of the genomes found in clade D are from the Americas, principally from the US; although sampling bias in our isolate collection undoubtedly plays a role. When biotyped, nearly all of these samples are from biovars 1, 2, and 4, although isolates from these three biovars do not always group together. Despite the 837 genomes and many subclades within this lineage, the branching is shallow and overall SNP variation with these genomes is very limited compared to the rest of *B. abortus*. This suggests a relatively recent introduction of genetically monomorphic *B. abortus* strains into the Americas from Western Europe, which is consistent with our molecular dating estimates of the emergence of clade D of ~1467 AD. Tellingly, embedded within this mainly American group of genomes and sub-lineages includes closely related genomes from Europe. We hypothesize that the historical events that likely lie at the root of this bacterial movement are the introduction of infected livestock into the Americas by European colonists as early as the 15th and 16th centuries. More European isolates as well as historic isolates would allow us to more conclusively address this question, however it is striking to observe the close genetic relationship between genomes from North America and the UK and South America and Portugal/Spain. Given the past colonial histories of these territories, we believe the latter observations strengthen our hypothesis. Furthermore, this same pattern of associations between European countries and their colonies appears to be occurring in *B. melitensis* in goats and sheep with the introduction of the Americas clade into the Western hemisphere, likely soon after the colonization of the New World (Al Dahouk et al., 2007; Tan et al., 2015; Pisarenko et al., 2018).

A wider diaspora beyond the Americas?

We have presented larger patterns in our trees that suggest wide-ranging movement of *B. abortus* globally. We do not go into all of the details of every genome and its origin, but it is worth noting that many have complex histories. The continued global movement of people, animals, and goods, and in fact the greater global connectivity allows for widespread movement of pathogens such as *B. abortus*. Embedded within clade D are genomes from diverse locations such as India, Mozambique, New Zealand, Saudi Arabia, and Zimbabwe. This suggests that the spread of *B. abortus* out of Europe to the Americas was part of a wider diaspora involving global trade from Europe with many other territories or that these strains were introduced from American sources at later dates. A similar pattern of worldwide spread was observed for another important zoonotic veterinary pathogen, *Mycobacterium bovis*, where the central role of Britain in trading cattle globally during the expansion of the British Empire underpinned the spread of this disease (Smith et al., 2011). Moreover, British farmers played a leading role in developing many modern cattle breeds (Decker et al., 2009). The Hereford breed in particular has been an important genetic stock used in the foundation and improvement of many beef cattle breeds across North and South America, Australia and New Zealand (Porter, 1991).

Within the United States

Within clade D, we observe at least eight sub-clades that are specific to particular regions or outbreaks (**Figure 5**). Five of these sub-clades are linked to the Yellowstone area, with isolates originating from both domestic and wildlife species (Kamath et al., 2016)—a complex multi-host epidemiology that has been previously noted in traditional veterinary and molecular based studies (Higgins et al., 2012; Cross et al., 2013). Three of these sub-clades also contain samples from outside this region, reflecting the connection of infected cattle throughout the country with Yellowstone as the recipient or source of infected animals. The three other subclades containing mostly US genomes have some geographic localization such as clusters of samples in Arkansas, Kansas, Missouri, Texas, and Mississippi, but the overall pattern is a homogenized population throughout the country apparently spread by the cattle trade.

Conclusion

Whole genome phylogenetic analysis of global *B. abortus* genomes suggests Africa as the origin of *B. abortus*. Subsequent movement out of Africa likely went in two directions, one into Western Europe and the other into Asia. Strains in the Americas appear to have originated from the introduction of a limited genetic stock of bacteria, likely originating in cattle from Europe during the period of European colonization of the North and South American continents.

The large number of isolates from the US serves to illustrate the potential usefulness of genome sequencing to further understand the dynamics of disease spread within territories. In particular, the observation that the Greater Yellowstone Area has been subject to at least five separate pathogen introductions affecting multiple animal hosts illustrates the power of this method to provide novel and meaningful epidemiological insights. With denser sampling of animals over longer time periods, there is the potential to gain even greater understanding of local epidemics using a phylodynamic approach such as has been illustrated before with a variety of human and animal pathogens (Volz et al., 2009; Biek et al., 2012; Harris et al., 2013).

Having a global phylogeny such as the one we present here is also of great potential use in determining likely infection sources

for new outbreaks in an age of globalization and long-distance livestock transport. What we present herein is a foundation on which to build more detailed surveys of other locales to expand the usefulness of this resource. Increasing the collection of isolates and genomes so that future phylogenies are more representative of the global distribution of *B. abortus* is essential to our understanding the movement and evolution of these important bacteria as well as for taking One Health actions for animal and human health.

Data availability statement

The datasets presented in this study can be found in online repositories. The names of the repository/repositories and accession number(s) can be found in the article/ **Supplementary material**.

Author contributions

NJ: Formal analysis, Writing – original draft. CW: Data curation, Formal analysis, Methodology, Writing – review and editing. KD: Data curation, Formal analysis, Methodology, Writing – original draft. MS-E: Data curation, Formal analysis, Visualization, Writing – review and editing. AA: Formal analysis, Methodology, Writing – review and editing. JL: Formal analysis, Methodology, Writing – review and editing. CQ: Data curation, Resources, Writing – review and editing. SR-A: Data curation, Resources, Writing – review and editing. DO'C: Conceptualization, Funding acquisition, Investigation, Resources, Writing – review and editing. AW: Conceptualization, Funding acquisition, Investigation, Resources, Writing – review and editing. JF: Conceptualization, Data curation, Formal analysis, Funding acquisition, Investigation, Methodology, Project administration, Resources, Supervision, Visualization, Writing – original draft, Writing – review and editing.

Funding

The author(s) declare financial support was received for the research, authorship, and/or publication of this article. JF was supported by funding from the US Department of Defense–Defense Threat Reduction Agency (Grant HDTRA1-2010028).

Acknowledgments

We thank Broad Institute staff Doyle Ward, Sinead Chapman, and Susanna Hamilton for their sequencing efforts. AA was funded for this work by a scholarship from the US-UK Fulbright Commission.

Conflict of interest

The authors declare that the research was conducted in the absence of any commercial or financial relationships that could be construed as a potential conflict of interest.

Publisher's note

Supplementary material

The Supplementary Material for this article can be found online at: https://www.frontiersin.org/articles/10.3389/fmicb.2023.1287046/full#supplementary-material

SUPPLEMENTARY TABLE 1
Summary data for genomes making up major clades A–D, including GenBank Accession Number or SRA identifier for sequencing data. Genome information including strain name, country of origin, year of collection, and host largely come from the National Center for Biotechnology Information (NCBI) GenBank BioSample Attributes metadata fields.

References

Achilli, A., Olivieri, A., Pellecchia, M., Uboldi, C., Colli, L., Al-Zahery, N., et al. (2008). Mitochondrial genomes of extinct aurochs survive in domestic cattle. *Curr. Biol.* 18, R157–R158. doi: 10.1016/j.cub.2008.01.019

Achtman, M. (2008). Evolution, population structure, and phylogeography of genetically monomorphic bacterial pathogens. *Annu. Rev. Microbiol.* 62, 53–70. doi: 10.1146/annurev.micro.62.081307.162832

Al Dahouk, S., Le Fleche, P., Nockler, K., Jacques, I., Grayon, M., Scholz, H. C., et al. (2007). Evaluation of *Brucella* MLVA typing for human brucellosis. *J. Microbiol. Methods* 69, 137–145. doi: 10.1016/j.mimet.2006.12.015

Allen, A. R., Milne, G., Drees, K., Presho, E., Graham, J., Mcadam, P., et al. (2020). Genomic epizootiology of a *Brucella abortus* outbreak in Northern Ireland (1997–2012). *Infect. Genet. Evol.* 81:104235. doi: 10.1016/j.meegid.2020.104235

Audic, S., Lescot, M., Claverie, J.-M., Cloeckaert, A., and Zygmunt, M. (2011). The genome sequence of Brucella pinnipedialis B2/94 sheds light on the evolutionary history of the genus Brucella. *BMC Evol. Biol.* 11:200. doi: 10.1186/1471-2148-11-200

Benson, D. A., Cavanaugh, M., Clark, K., Karsch-Mizrachi, I., Lipman, D. J., Ostell, J., et al. (2012). GenBank. *Nucleic Acids Res.* 41, D36–D42. doi: 10.1093/nar/gkr1202

Biek, R., O'Hare, A., Wright, D., Mallon, T., Mccormick, C., Orton, R. J., et al. (2012). Whole genome sequencing reveals local transmission patterns of *Mycobacterium bovis* in sympatric cattle and badger populations. *PLoS Pathog.* 8:e1003008. doi: 10.1371/journal.ppat.1003008

Bigras-Poulin, M., Thompson, R. A., Chriel, M., Mortensen, S., and Greiner, M. (2006). Network analysis of Danish cattle industry trade patterns as an evaluation of risk potential for disease spread. *Preventive Vet. Med.* 76, 11–39. doi: 10.1016/j.prevetmed.2006.04.004

Bradley, D. G., Machugh, D. E., Cunningham, P., and Loftus, R. T. (1996). Mitochondrial diversity and the origins of African and European cattle. *Proc. Natl. Acad. Sci. U.S.A.* 93, 5131–5135. doi: 10.1073/pnas.93.10.5131

Carvalho Neta, A. V., Mol, J. P. S., Xavier, M. N., Paixão, T. A., Lage, A. P., and Santos, R. L. (2010). Pathogenesis of bovine brucellosis. *Vet. J.* 184, 146–155. doi: 10.1016/j.tvjl.2009.04.010

Chewapreecha, C., Holden, M. T. G., Vehkala, M., Välimäki, N., Yang, Z., Harris, S. R., et al. (2017). Global and regional dissemination and evolution of *Burkholderia pseudomallei*. *Nat. Microbiol.* 2:16263. doi: 10.1038/nmicrobiol.2016.263

Christley, R. M., Robinson, S. E., Lysons, R., and French, N. P. (2005). "Network analysis of cattle movement in Great Britain," in *Proceedings of a meeting held at Nairn, Inverness*, Scotland.

Comas, I., Coscolla, M., Luo, T., Borrell, S., Holt, K. E., Kato-Maeda, M., et al. (2013). Out-of-Africa migration and Neolithic coexpansion of *Mycobacterium tuberculosis* with modern humans. *Nat. Genet.* 45, 1176–1182. doi: 10.1038/ng.2744

Crisp, M. D., and Cook, L. G. (2005). Do early branching lineages signify ancestral traits? *Trends Ecol. Evol.* 20, 122–128. doi: 10.1016/j.tree.2004.11.010

Crisp, M. D., Trewick, S. A., and Cook, L. G. (2011). Hypothesis testing in biogeography. *Trends Ecol. Evol.* 26, 66–72. doi: 10.1016/j.tree.2010.11.005

Cross, P. C., Maichak, E. J., Brennan, A., Scurlock, B. M., Henningsen, J., and Luikart, G. (2013). An ecological perspective on *Brucella abortus* in the western United States. *Rev. Sci. Tech.* 32, 79–87. doi: 10.20506/rst.32.1.2184

Decker, J. E., Mckay, S. D., Rolf, M. M., Kim, J., Molina Alcalá, A., Sonstegard, T. S., et al. (2014). Worldwide patterns of ancestry, divergence, and admixture in domesticated cattle. *PLoS Genet.* 10:e1004254. doi: 10.1371/journal.pgen.1004254

Decker, J. E., Pires, J. C., Conant, G. C., Mckay, S. D., Heaton, M. P., Chen, K., et al. (2009). Resolving the evolution of extant and extinct ruminants with high-throughput phylogenomics. *Proc. Natl. Acad. Sci. U.S.A.* 106, 18644–18649. doi: 10.1073/pnas.0904691106

Delcher, A. L., Phillippy, A., Carlton, J., and Salzberg, S. L. (2002). Fast algorithms for large-scale genome alignment and comparison. *Nucleic Acids Res.* 30, 2478–2483. doi: 10.1093/nar/30.11.2478

DePristo, M. A., Banks, E., Poplin, R., Garimella, K. V., Maguire, J. R., Hartl, C., et al. (2011). A framework for variation discovery and genotyping using next-generation DNA sequencing data. *Nat. Genet.* 43, 491–498. doi: 10.1038/ng.806

Drummond, A. J. (2005). Bayesian coalescent inference of past population dynamics from molecular sequences. *Mol. Biol. Evol.* 22, 1185–1192. doi: 10.1093/molbev/msi103

Ducrotoy, M., Bertu, W. J., Matope, G., Cadmus, S., Conde-Álvarez, R., Gusi, A. M., et al. (2017). Brucellosis in Sub-Saharan Africa: Current challenges for management, diagnosis and control. *Acta Trop.* 165, 179–193. doi: 10.1016/j.actatropica.2015.10.023

Fan, Y., Wu, R., Chen, M.-H., Kuo, L., and Lewis, P. O. (2011). Choosing among partition models in Bayesian phylogenetics. *Mol. Biol. Evol.* 28, 523–532. doi: 10.1093/molbev/msq224

Felius, M., Beerling, M.-L., Buchanan, D. S., Theunissen, B., Koolmees, P. A., and Lenstra, J. A. (2014). On the history of cattle genetic resources. *Diversity* 6, 705–750.

Foster, J. T., Beckstrom-Sternberg, S. M., Pearson, T., Beckstrom-Sternberg, J. S., Chain, P. S. G., Roberto, F. F., et al. (2009). Whole genome-based phylogeny and divergence of the genus *Brucella*. *J. Bacteriol.* 191, 2864–2870. doi: 10.1128/JB.01581-08

Foster, J. T., Walker, F. M., Rannals, B. D., Hussain, M. H., Drees, K. P., Tiller, R. V., et al. (2018). African lineage *Brucella melitensis* isolates from Omani livestock. *Front. Microbiol.* 8:2702. doi: 10.3389/fmicb.2017.02702

Garin-Bastuji, B., Mick, V., Le Carrou, G., Allix, S., Perrett, L. L., Dawson, C. E., et al. (2014). Examination of taxonomic uncertainties surrounding *Brucella abortus* bv. 7 by phenotypic and molecular approaches. *Appl. Environ. Microbiol.* 80, 1570–1579. doi: 10.1128/AEM.03755-13

Garofolo, G., Di Giannatale, E., De Massis, F., Zilli, K., Ancora, M., Camma, C., et al. (2013). Investigating genetic diversity of *Brucella abortus* and *Brucella melitensis* in Italy with MLVA-16. *Infect. Genet. Evol.* 19, 59–70. doi: 10.1016/j.meegid.2013.06.021

Garofolo, G., Di Giannatale, E., Platone, I., Zilli, K., Sacchini, L., Abass, A., et al. (2017). Origins and global context of *Brucella abortus* in Italy. *BMC Microbiol.* 17:28. doi: 10.1186/s12866-017-0939-0

Grad, Y. H., and Lipsitch, M. (2014). Epidemiologic data and pathogen genome sequences: a powerful synergy for public health. *Genome Biol.* 15:538. doi: 10.1186/s13059-014-0538-4

Hanotte, O. (2002). African pastoralism: genetic imprints of origins and migrations. *Science* 296, 336–339. doi: 10.1126/science.1069878

Harris, S. R., Cartwright, E. J. P., Török, M. E., Holden, M. T. G., Brown, N. M., Ogilvy-Stuart, A. L., et al. (2013). Whole-genome sequencing for analysis of an outbreak of meticillin-resistant Staphylococcus aureus: a descriptive study. *Lancet Infect. Dis.* 13, 130–136. doi: 10.1016/S1473-3099(12)70268-2

Harris, S. R., Feil, E. J., Holden, M. T. G., Quail, M. A., Nickerson, E. K., Chantratita, N., et al. (2010). Evolution of MRSA during hospital transmission and intercontinental spread. *Science* 327, 469–474.

Higgins, J., Stuber, T., Quance, C., Edwards, W. H., Tiller, R. V., Linfield, T., et al. (2012). Molecular epidemiology of *Brucella abortus* isolates from cattle, elk, and bison in the United States, 1998 to 2011. *Appl. Environ. Microbiol.* 78, 3674–3684. doi: 10.1128/AEM.00045-12

Holt, K. E., Parkhill, J., Mazzoni, C. J., Roumagnac, P., Weill, F. X., Goodhead, I., et al. (2008). High-throughput sequencing provides insights into genome variation and evolution in *Salmonella* Typhi. *Nat. Genet.* 40, 987–993. doi: 10.1038/ng.195

Holzer, K., El-Diasty, M., Wareth, G., Abdel-Hamid, N. H., Hamdy, M. E. R., Moustafa, S. A., et al. (2021). Tracking the Distribution of Brucella abortus in Egypt Based on Core Genome SNP Analysis and In Silico MLVA-16. *Microorganisms* 9:1942. doi: 10.3390/microorganisms9091942

Huang, W., Li, L., Myers, J. R., and Marth, G. T. (2012). ART: A next-generation sequencing read simulator. *Bioinformatics* 28, 593–594.

Kamath, P. L., Foster, J. T., Drees, K. P., Luikart, G., Quance, C., Anderson, N. J., et al. (2016). Genomics reveals historic and contemporary transmission dynamics of a bacterial disease among wildlife and livestock. *Nat. Commun.* 7:11448. doi: 10.1038/ncomms11448

Kay, G. L., Sergeant, M. J., Giuffra, V., Bandiera, P., Milanese, M., Bramanti, B., et al. (2014). Recovery of a medieval *Brucella melitensis* genome using shotgun metagenomics. *mBio* 5, e1337–e1314. doi: 10.1128/mBio.01337-14

Keim, P., Van Ert, M. N., Pearson, T., Vogler, A. J., Huynh, L. Y., and Wagner, D. M. (2004). Anthrax molecular epidemiology and forensics: using the appropriate marker for different evolutionary scales. *Infect. Genet. Evol.* 4, 205–213. doi: 10.1016/j.meegid.2004.02.005

Keim, P. S., and Wagner, D. M. (2009). Humans and evolutionary and ecological forces shaped the phylogeography of recently emerged diseases. *Nat. Rev. Microbiol.* 7, 813–821. doi: 10.1038/nrmicro2219

Kenefic, L. J., Pearson, T., Okinaka, R. T., Schupp, J. M., Wagner, D. M., Ravel, J., et al. (2009). Pre-columbian origins for North American anthrax. *PLoS One* 4:e4813. doi: 10.1371/journal.pone.0004813

Khames, M., Mick, V., De Miguel, M. J., Girault, G., Conde-Álvarez, R., Khelef, D., et al. (2017). The characterization of *Brucella* strains isolated from cattle in Algeria reveals the existence of a *B. abortus* lineage distinct from European and Sub-Saharan Africa strains. *Vet. Microbiol.* 211, 124–128. doi: 10.1016/j.vetmic.2017.10.008

Kurtz, S., Phillippy, A., Delcher, A. L., Smoot, M., Shumway, M., Antonescu, C., et al. (2004). Versatile and open software for comparing large genomes. *Genome Biol.* 5, R12.

Laine, C. G., Scott, H. M., and Arenas-Gamboa, A. M. (2022). Human brucellosis: Widespread information deficiency hinders an understanding of global disease frequency. *PLoS Negl. Trop. Dis.* 16:e0010404. doi: 10.1371/journal.pntd.0010404

Lartillot, N., and Philippe, H. (2006). Computing Bayes factors using thermodynamic integration. *Syst. Biol.* 55, 195–207.

Le Fleche, P., Jacques, I., Grayon, M., Al Dahouk, S., Bouchon, P., Denoeud, F., et al. (2006). Evaluation and selection of tandem repeat loci for a *Brucella* MLVA typing assay. *BMC Microbiol.* 6:9. doi: 10.1186/1471-2180-6-9

Leinonen, R., Sugawara, H., Shumway, M., and International Nucleotide Sequence Database Collaboration. (2010). The Sequence Read Archive. *Nucleic Acids Res.* 39, D19–D21.

Li, H. (2013). Aligning sequence reads, clone sequences and assembly contigs with BWA-MEM. *arXiv* [Preprint]. doi: 10.48550/arXiv.1303.3997

Linz, B., Balloux, F., Moodley, Y., Manica, A., Liu, H., Roumagnac, P., et al. (2007). An African origin for the intimate association between humans and *Helicobacter* pylori. *Nature* 445, 915–918. doi: 10.1038/nature05562

Liu, Q., Ma, A., Wei, L., Pang, Y., Wu, B., Luo, T., et al. (2018). China's tuberculosis epidemic stems from historical expansion of four strains of *Mycobacterium tuberculosis*. *Nat. Ecol. Evol.* 2, 1982–1992. doi: 10.1038/s41559-018-0680-6

Loftus, R. T., Machugh, D. E., Bradley, D. G., Sharp, P. M., and Cunningham, P. (1994). Evidence for two independent domestications of cattle. *Proc. Natl. Acad. Sci.* 91, 2757–2761.

Long, G. S., Hider, J., Duggan, A. T., Klunk, J., Eaton, K., Karpinski, E., et al. (2023). A 14th century CE *Brucella melitensis* genome and the recent expansion of the Western Mediterranean clade. *PLoS Pathog.* 19:e1011538. doi: 10.1371/journal.ppat.1011538

McDermott, J. J., and Arimi, S. M. (2002). Brucellosis in sub-Saharan Africa: epidemiology, control and impact. *Vet. Microbiol.* 90, 111–134.

McKenna, A., Hanna, M., Banks, E., Sivachenko, A., Cibulskis, K., Kernytsky, A., et al. (2010). The Genome Analysis Toolkit: a MapReduce framework for analyzing next-generation DNA sequencing data. *Genome Res.* 20, 1297–1303. doi: 10.1101/gr.107524.110

Morelli, G., Song, Y., Mazzoni, C. J., Eppinger, M., Roumagnac, P., Wagner, D. M., et al. (2010). *Yersinia pestis* genome sequencing identifies patterns of global phylogenetic diversity. *Nat. Genet.* 42, 1140–1143. doi: 10.1038/ng.705

Moreno, E. (2014). Retrospective and prospective perspectives on zoonotic brucellosis. *Front. Microbiol.* 5:213–213. doi: 10.3389/fmicb.2014.00213

Moreno, E., Cloeckaert, A., and Moriyon, I. (2002). *Brucella* evolution and taxonomy. *Vet. Microbiol.* 90, 209–227. doi: 10.1016/s0378-1135(02)00210-9

Mutreja, A., Kim, D. W., Thomson, N. R., Connor, T. R., Lee, J. H., Kariuki, S., et al. (2011). Evidence for several waves of global transmission in the seventh cholera pandemic. *Nature* 477, 462–465. doi: 10.1038/nature10392

Pappas, G., Papadimitriou, P., Akritidis, N., Christou, L., and Tsianos, E. V. (2006). The new global map of human brucellosis. *Lancet Infect. Dis.* 6, 91–99.

Pearson, T., Giffard, P., Beckstrom-Sternberg, S., Auerbach, R., Hornstra, H., Tuanyok, A., et al. (2009a). Phylogeographic reconstruction of a bacterial species with high levels of lateral gene transfer. *BMC Biol.* 7:78. doi: 10.1186/1741-7007-7-78

Pearson, T., Okinaka, R. T., Foster, J. T., and Keim, P. (2009b). Phylogenetic understanding of clonal populations in an era of whole genome sequencing. *Infect. Genet. Evol.* 9, 1010–1019. doi: 10.1016/j.meegid.2009.05.014

Pereira, C. R., Neia, R. C., Silva, S. B., Williamson, C. H. D., Gillece, J. D., O'callaghan, D., et al. (2023). Comparison of *Brucella abortus* population structure based on genotyping methods with different levels of resolution. *J. Microbiol. Methods* 211:106772. doi: 10.1016/j.mimet.2023.106772

Pisarenko, S. V., Kovalev, D. A., Volynkina, A. S., Ponomarenko, D. G., Rusanova, D. V., Zharinova, N. V., et al. (2018). Global evolution and phylogeography of *Brucella melitensis* strains. *BMC Genomics* 19:353. doi: 10.1186/s12864-018-4762-2

Pitt, D., Sevane, N., Nicolazzi, E. L., Machugh, D. E., Park, S. D. E., Colli, L., et al. (2019). Domestication of cattle: Two or three events? *Evol. Applic.* 12, 123–136.

Porter, V. (1991). *Cattle - A handbook to the breeds of the world*. London: A & C Black Ltd.

Rautureau, S., Dufour, B., and Durand, B. (2010). Vulnerability of animal trade networks to the spread of infectious diseases: A methodological approach applied to evaluation and emergency control strategies in cattle, France, 2005. *Transbound. Emerg. Dis.* 58, 110–120. doi: 10.1111/j.1865-1682.2010.01187.x

Rokas, A., Williams, B. L., King, N., and Carroll, S. B. (2003). Genome-scale approaches to resolving incongruence in molecular phylogenies. *Nature* 425, 798–804.

Sahl, J. W., Lemmer, D., Travis, J., Schupp, J. M., Gillece, J. D., Aziz, M., et al. (2016). NASP: an accurate, rapid method for the identification of SNPs in WGS datasets that supports flexible input and output formats. *Microb. Genom.* 2, e000074. doi: 10.1099/mgen.0.000074

Schliep, K. P. (2011). phangorn: phylogenetic analysis in R. *Bioinformatics* 27, 592–593. doi: 10.1093/bioinformatics/btq706

Schumaker, B. (2013). Risks of *Brucella abortus* spillover in the Greater Yellowstone area. *Rev. Sci. Tech.* 32, 71–77. doi: 10.20506/rst.32.1.2185

Shevtsov, A., Cloeckaert, A., Berdimuratova, K., Shevtsova, E., Shustov, A. V., Amirgazin, A., et al. (2023). Brucella abortus in Kazakhstan, population structure and comparison with worldwide genetic diversity. *Front. Microbiol.* 14:1106994. doi: 10.3389/fmicb.2023.1106994

Simpson, G., Thompson, P. N., Saegerman, C., Marcotty, T., Letesson, J. J., De Bolle, X., et al. (2021). Brucellosis in wildlife in Africa: a systematic review and meta-analysis. *Sci. Rep.* 11:5960. doi: 10.1038/s41598-021-85441-w

Sintchenko, V., and Holmes, E. C. (2015). The role of pathogen genomics in assessing disease transmission. *BMJ* 350, h1314.

Smith, N. H., Berg, S., Dale, J., Allen, A., Rodriguez, S., Romero, B., et al. (2011). European 1: A globally important clonal complex of *Mycobacterium bovis*. *Infect. Genet. Evol.* 11, 1340–1351. doi: 10.1016/j.meegid.2011.04.027

Suarez-Esquivel, M., Hernandez-Mora, G., Ruiz-Villalobos, N., Barquero-Calvo, E., Chacon-Diaz, C., Ladner, J. T., et al. (2020). Persistence of *Brucella abortus* lineages revealed by genomic characterization and phylodynamic analysis. *PLoS Negl. Trop. Dis.* 14:e0008235. doi: 10.1371/journal.pntd.0008235

Suchard, M. A., Lemey, P., Baele, G., Ayres, D. L., Drummond, A. J., and Rambaut, A. (2018). Bayesian phylogenetic and phylodynamic data integration using BEAST 1.10. *Virus Evol.* 4, vey016. doi: 10.1093/ve/vey016

Tan, K.-K., Tan, Y.-C., Chang, L.-Y., Lee, K. W., Nore, S. S., Yee, W.-Y., et al. (2015). Full genome SNP-based phylogenetic analysis reveals the origin and global spread of *Brucella melitensis*. *BMC Genomics* 16:93. doi: 10.1186/s12864-015-1294-x

Troy, C. S., Machugh, D. E., Bailey, J. F., Magee, D. A., Loftus, R. T., Cunningham, P., et al. (2001). Genetic evidence for near eastern origins of European cattle. *Nature* 410, 1088–1091. doi: 10.1038/35074088

Verdugo, M. P., Mullin, V. E., Scheu, A., Mattiangeli, V., Daly, K. G., Maisano Delser, P., et al. (2019). Ancient cattle genomics, origins, and rapid turnover in the Fertile Crescent. *Science* 365, 173–176. doi: 10.1126/science.aav1002

Volz, E. M., Kosakovsky Pond, S. L., Ward, M. J., Leigh Brown, A. J., and Frost, S. D. W. (2009). Phylodynamics of infectious disease epidemics. *Genetics* 183, 1421–1430.

Wattam, A. R., Foster, J. T., Mane, S. P., Beckstrom-Sternberg, S. M., Beckstrom-Sternberg, J. M., Dickerman, A. W., et al. (2014). Comparative phylogenomics and evolution of the Brucellae reveal a path to virulence. *J. Bacteriol.* 196, 920–930. doi: 10.1128/JB.01091-13

Wattam, A. R., Williams, K. P., Snyder, E. E., Almeida, N. F. Jr., Shukla, M., Dickerman, A. W., et al. (2009). Analysis of ten *Brucella* genomes reveals evidence for horizontal gene transfer despite a preferred intracellular lifestyle. *J. Bacteriol.* 191, 3569–3579. doi: 10.1128/JB.01767-08

Whatmore, A. M. (2009). Current understanding of the genetic diversity of *Brucella*, an expanding genus of zoonotic pathogens. *Infect. Genet. Evol.* 9, 1168–1184. doi: 10.1016/j.meegid.2009.07.001

Whatmore, A. M., and Foster, J. T. (2021). Emerging diversity and ongoing expansion of the genus *Brucella*. *Infect. Genet. Evol.* 92:104865. doi: 10.1016/j.meegid.2021.104865

Whatmore, A. M., Koylass, M. S., Muchowski, J., Edwards-Smallbone, J., Gopaul, K. K., and Perrett, L. L. (2016). Extended multilocus sequence analysis to describe the global population structure of the genus *Brucella*: phylogeography and relationship to biovars. *Front. Microbiol.* 7:2049. doi: 10.3389/fmicb.2016.02049

Whatmore, A. M., Perrett, L. L., and Macmillan, A. P. (2007). Characterisation of the genetic diversity of *Brucella* by multilocus sequencing. *BMC Microbiol.* 7:34. doi: 10.1186/1471-2180-7-34

WOAH (2023). *Manual of Diagnostic Tests and Vaccines for Terrestrial Animals*, 12th Edn. Paris: World Organization for Animal Health.

Xia, X., Qu, K., Wang, Y., Sinding, M.-H. S., Wang, F., Hanif, Q., et al. (2023). Global dispersal and adaptive evolution of domestic cattle: a genomic perspective. *Stress Biol.* 3:8. doi: 10.1007/s44154-023-00085-2

Xie, W., Lewis, P. O., Fan, Y., Kuo, L., and Chen, M.-H. (2011). Improving marginal likelihood estimation for Bayesian phylogenetic model selection. *Syst. Biol.* 60, 150–160.

Zeder, M. A. (2008). Domestication and early agriculture in the Mediterranean Basin: Origins, diffusion, and impact. *Proc. Natl. Acad. Sci. U.S.A.* 105, 11597–11604. doi: 10.1073/pnas.0801317105

Frontiers in Microbiology

Explores the habitable world and the potential of microbial life

The largest and most cited microbiology journal which advances our understanding of the role microbes play in addressing global challenges such as healthcare, food security, and climate change.

Discover the latest Research Topics

See more →

Frontiers

Avenue du Tribunal-Fédéral 34
1005 Lausanne, Switzerland
frontiersin.org

Contact us

+41 (0)21 510 17 00
frontiersin.org/about/contact